Guidance and Control of Ocean Vehicles

THOR I. FOSSEN

Guidance and Control of Ocean Vehicles

Thor I. Fossen
University of Trondheim
Norway

JOHN WILEY & SONS
Chichester · New York · Brisbane · Toronto · Singapore

Baffins Lane, Chichester
West Sussex PO19 1UD, England
National Chichester (0243) 779777
International (+44) 243 779777

Reprinted December 1995

Reprinted May 1998

Reprinted March 1999

Other Wiley Editorial Offices

John Wiley & Sons, Inc., 605 Third Avenue,
New York, NY 10158-0012, USA

Jacaranda Wiley Ltd, 33 Park Road, Milton,
Queensland 4064, Australia

John Wiley & Sons (Canada) Ltd, 22 Worcester Road,
Rexdale, Ontario M9W 1L1, Canada

John Wiley & Sons (SEA) Pte Ltd, 37 Jalan Pemimpin #05-04,
Block B, Union Industrial Building, Singapore 2057

British Library Cataloguing in Publication Data

A catalogue record for this book is available from the British Library

ISBN 0 471 94113 1

Produced from camera-ready copy supplied by the author using LaTeX.
Printed and bound in Great Britain by Antony Rowe Ltd, Chippenham, Wiltshire

This book is dedicated
to
Heidi and Sindre

Contents

Preface

My first interest for offshore technology and marine vehicles started during my "sivilingeniør" (MSc) study at the Department of Marine Systems Design at The Norwegian Institute of Technology (NIT). This interest was my main motivation for a doctoral study in Engineering Cybernetics at the Faculty of Electrical Engineering and Computer Sciences (NIT) and my graduate studies in flight control at the Department of Aeronautics and Astronautics, University of Washington, Seattle. Consequently, much of the material and inspiration for the book has evolved from this period. Writing this book, is an attempt to draw the disciplines of engineering cybernetics and marine engineering together.

Systems for Guidance and Control have been taught by the author since 1991 for MSc students in Engineering Cybernetics at the Faculty of Electrical Engineering and Computer Science (NIT). The book is intended as a textbook for senior and graduate students with some background in control engineering and calculus. Some basic knowledge of linear and nonlinear control theory, vector analysis and differential equations is required. The objective of the book is to present and apply advanced control theory to marine vehicles like remotely operated vehicles (ROVs), surface ships, high speed crafts and floating offshore structures. The reason for applying more sophisticated autopilots for steering and dynamic positioning of marine vehicles is mainly due to fuel economy, improved reliability and performance enhancement. Since 1973, the rapid increase in oil prices has contributed to this trend. This justifies the use of more advanced mathematical models and control theory in guidance and control applications.

Ass. Professor Thor I. Fossen
University of Trondheim
The Norwegian Institute of Technology
Department of Engineering Cybernetics
N-7034 Trondheim, Norway

Acknowledgments

It is impossible to mention everyone who has contributed with ideas, suggestions and examples, but I owe you all my deepest thanks. I am particularly grateful to Dr. Svein I. Sagatun (ABB Industry, Oslo) and Dr. Asgeir Sørensen (ABB Corporate Research, Oslo) for their comments and useful suggestions. Dr. Sørensen should also be thanked for his sincere help in writing Section 7.1 on surface effect ships.

I acknowledge the help of Professor Mogens Blanke (Department of Control Engineering, Aalborg University) for his help in writing Section 6.2 on ship propulsion and speed control while Dr. Erling Lunde (consultant for Dynamica AS, Trondheim) and Mr. William C. O'Neill (consultant for Advanced Marine Vehicles, 852 Goshen Road, Newtown Square, PA 19073) should be thanked for their sincere help in writing Section 7.2 on foilborne catamarans. I am also grateful to Professor Olav Egeland (Department of Engineering Cybernetics, NIT) for his valuable comments to Sections 2.1 to 2.3 and to Professor Anthony J. Healey (Mechanical Engineering Department, Naval Postgraduate School, Monterey) for contributing with lecture notes and the underwater vehicle models in Appendix E.2.

I want to express my gratitude to ABB Industry (Oslo), Robertson Tritech A/S (Egersund), the Norwegian Defence Research Establishment (Kjeller) and the Ulstein Group (Ulsteinvik) for contributing with full scale experimental results.

Furthermore, Mr. Stewart Clark, Senior Consultant (NIT) and doctoral students Alf G. Bringaker and Erling Johannessen (Department of Engineering Cybernetics, NIT) should be thanked for their careful proofreading and comments to the final manuscript.

The author is also grateful to his doctoral student Ola-Erik Fjellstad and Astrid Egeland for their useful comments and suggestions. Morten Brekke, Geir Edvin Hovland, Trygve Lauvdal and Kjetil Røe should be thanked for their help with illustrations, examples and computer simulations. The book also greatly benefits from students who took the course in guidance and control at NIT from 1991 to 1993. They have all helped me to reduce the number of typographical errors to an acceptable level. Finally, I want to thank Ms. Laura Denny and Mr. Stuart Gale (John Wiley & Sons Ltd.) who have provided me with technical and editorial comments to the final manuscript.

Thor I. Fossen
January 1994

Chapter 1

Introduction

The subject of this textbook is *guidance and control of ocean vehicles*. This title covers control systems design for all types of marine vehicles like submarines, torpedoes, unmanned and manned underwater vehicles, conventional ships, high speed crafts and semi-submersibles. Examples of such systems are:

- control systems for forward speed control
- autopilots for course-keeping and diving
- turning controllers
- track-keeping systems
- dynamic positioning (DP)
- rudder-roll stabilization (RRS)
- fin control systems
- wave-induced vibration damping

For practical purposes the discussion will concentrate on three vehicle categories: small unmanned underwater vehicles, surface ships and high speed craft.

Guidance and Control

The terms *guidance* and *control* can be defined so that:

GUIDANCE is the action of determining the course, attitude and speed of the vehicle, relative to some reference frame (usually the earth), to be followed by the vehicle.

CONTROL is the development and application to a vehicle of appropriate forces and moments for operating point control, tracking and stabilization. This involves designing the feedforward and feedback control laws.

The ... will be used to illustrate these definitions.

Example 1.1 (Automatic Weather Routing)
The design of an automatic weather routing system for a ship requires insight in both advanced modeling and optimal control theory. Moreover, we need an accurate model of the ship and the environmental forces (wind, waves and currents) to describe the speed loss of the ship in bad weather. Based on the speed loss computations we can compute a fuel optimal route. Finally, we have to design an optimal track-keeping controller (autopilot) to ensure that this route is followed by the ship.

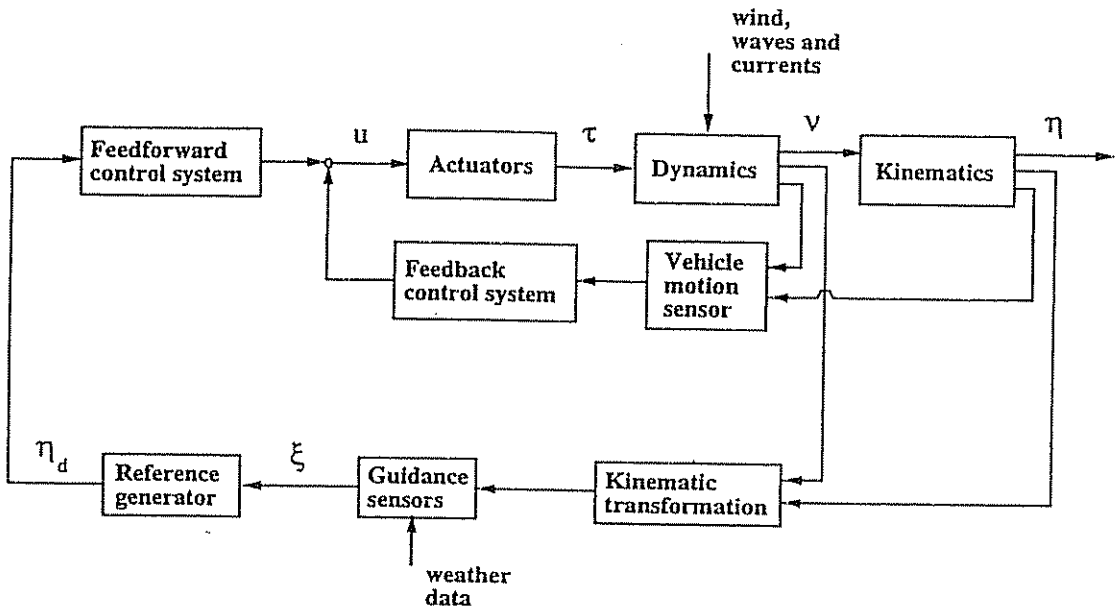

Figure 1.1: Guidance and control system for automatic weather routing of ships.

A guidance and control system for automatic weather routing of a ship is shown in Figure 1.1. This system uses weather data measurements to compute a fuel optimal route for the ship which is fed forward to the control system through a block denoted as the "feedforward control system". In addition to this, feedback is provided in an optimal manner from velocity ν and position/attitude η through the block "feedback control system". The control force and moment vector τ is provided by the actuator via the control variable u, which may be interpreted as the sum of the feedforward and feedback control action.

We also notice that the reference generator η_d may use weather data ξ (wind speed, wind direction, wave height etc.) together with the ship states (ν, η) to compute the optimal route. This is usually done by including constraints for fuel consumption, actuator saturation, forward speed, restricted areas for ship maneuvering etc.

□

An Overview of the Book

This book deals mainly with modeling and control of unmanned untethered underwater vehicles (remotely operated vehicles and autonomous underwater vehicles), surface ships (cargo ships, tankers etc.) and high speed craft (surface effect ships and foilborne catamarans).

The design of modern marine vehicle guidance and control systems requires knowledge of a broad field of disciplines. Some of these are vectorial kinematics and dynamics, hydrodynamics, navigation systems and control theory. To be able to design a high performance control system it is evident that a good mathematical model of the vehicle is required for simulation and verification of the design. As a result of this, the book contains a large number of mathematical models intended for this purpose. The different topics in the book are organized according to:

MODELING: marine vehicle kinematics and dynamics in 6 degrees of freedom (Chapter 2) and environmental disturbances in terms of wind, waves and currents (Chapter 3).

UNDERWATER VEHICLES: stability and control system design for small unmanned underwater vehicles (Chapter 4).

SURFACE SHIPS: ship dynamics, stability and maneuvering (Chapter 5) and ship control system design (Chapter 6).

HIGH SPEED CRAFT: control system design for surface effect ships (SES) and foilcats (Chapter 7).

It is recommended that one should read Chapter 2 before Chapters 3–7 since these chapters use basic results from vectorial kinematics and dynamics.

Chapter 2

Modeling of Marine Vehicles

Modeling of marine vehicles involves the study of *statics* and *dynamics*. Statics is concerned with the equilibrium of bodies at rest or moving with constant velocity, whereas dynamics is concerned with bodies having accelerated motion. Statics is the oldest of the engineering sciences. In fact, important contributions were made over 2000 years ago by Archimedes (287–212 BC) who derived the basic law of hydrostatic buoyancy. This result is the foundation for static stability analyses of marine vessels.

The study of dynamics started much later since accurate measurements of time are necessary to perform dynamic experiments. One of the first time-measuring instruments, a "water clock", was designed by Leonardo da Vinci (1452–1519). This simple instrument exploited the fact that the interval between the falling drops of water could be considered constant. The scientific basis of dynamics was provided by Newton's laws published in 1687. It is common to divide the study of dynamics into two parts: *kinematics*, which treats only geometrical aspects of motion, and *kinetics*, which is the analysis of the forces causing the motion.

Table 2.1: Notation used for marine vehicles.

DOF		forces and moments	linear and angular vel.	positions and Euler angles
1	motions in the x-direction (surge)	X	u	x
2	motions in the y-direction (sway)	Y	v	y
3	motions in the z-direction (heave)	Z	w	z
4	rotation about the x-axis (roll)	K	p	ϕ
5	rotation about the y-axis (pitch)	M	q	θ
6	rotation about the z-axis (yaw)	N	r	ψ

This study discusses the motion of marine vehicles in 6 *degrees of freedom* (DOF) since 6 independent coordinates are necessary to determine the position and orientation of a rigid body. The first three coordinates and their time derivatives correspond to the position and translational motion along the x-, y-, and

z-axes, while the last 3 coordinates and time derivatives are used to describe orientation and rotational motion. For marine vehicles, the 6 different motion components are conveniently defined as: *surge, sway, heave, roll, pitch* and *yaw*, see Table 2.1.

2.1 Kinematics

COORDINATE FRAMES

When analyzing the motion of marine vehicles in 6 DOF it is convenient to define two coordinate frames as indicated in Figure 2.1. The moving coordinate frame $X_0Y_0Z_0$ is conveniently fixed to the vehicle and is called the body-fixed reference frame. The origin O of the body-fixed frame is usually chosen to coincide with the center of gravity (CG) when CG is in the principal plane of symmetry or at any other convenient point if this is not the case.

For marine vehicles, the body axes X_0, Y_0 and Z_0 coincide with the *principal axes of inertia*, and are usually defined as:

- X_0 - longitudinal axis (directed from aft to fore)
- Y_0 - transverse axis (directed to starboard)
- Z_0 - normal axis (directed from top to bottom)

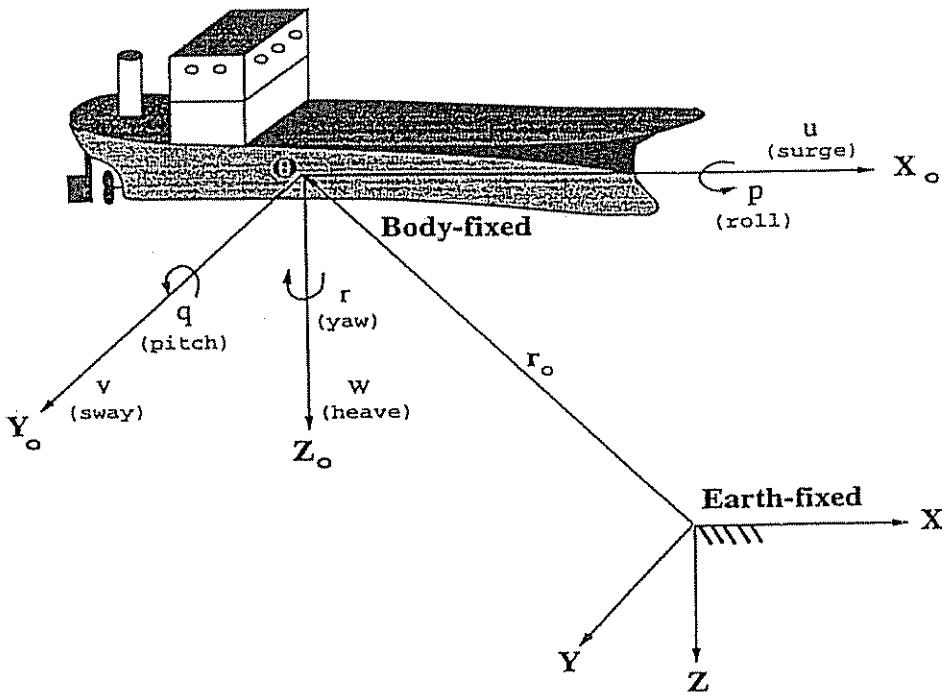

Figure 2.1: Body-fixed and earth-fixed reference frames.

The motion of the body-fixed frame is described relative to an inertial reference frame. For marine vehicles it is usually assumed that the accelerations of a point on the surface of the Earth can be neglected. Indeed, this is a good approximation since the motion of the Earth hardly affects low speed marine vehicles. As a result of this, an earth-fixed reference frame XYZ can be considered to be inertial. This suggests that the position and orientation of the vehicle should be described relative to the inertial reference frame while the linear and angular velocities of the vehicle should be expressed in the body-fixed coordinate system. The different quantities are defined according to the SNAME (1950) notation as indicated in Table 2.1. Based on this notation, the general motion of a marine vehicle in 6 DOF can be described by the following vectors:

$$\eta = [\eta_1^T, \eta_2^T]^T; \qquad \eta_1 = [x, y, z]^T; \qquad \eta_2 = [\phi, \theta, \psi]^T$$

$$\nu = [\nu_1^T, \nu_2^T]^T; \qquad \nu_1 = [u, v, w]^T; \qquad \nu_2 = [p, q, r]^T$$

$$\tau = [\tau_1^T, \tau_2^T]^T; \qquad \tau_1 = [X, Y, Z]^T; \qquad \tau_2 = [K, M, N]^T$$

Here η denotes the position and orientation vector with coordinates in the earth-fixed frame, ν denotes the linear and angular velocity vector with coordinates in the body-fixed frame and τ is used to describe the forces and moments acting on the vehicle in the body-fixed frame. In marine guidance and control systems, orientation is usually represented by means of Euler angles or quaternions. In the next sections the kinematic equations relating the body-fixed reference frame to the earth-fixed reference frame will be derived.

2.1.1 Euler Angles

The vehicle's flight path relative to the earth-fixed coordinate system is given by a velocity transformation:

$$\dot{\eta}_1 = J_1(\eta_2)\, \nu_1 \tag{2.1}$$

where $J_1(\eta_2)$ is a transformation matrix which is related through the functions of the Euler angles: roll (ϕ), pitch (θ) and yaw (ψ). The inverse velocity transformation will be written:

$$\nu_1 = J_1^{-1}(\eta_2)\, \dot{\eta}_1 \tag{2.2}$$

We will now derive the expression for the transformation matrix $J_1(\eta_2)$. Consider the following definition:

Definition 2.1 (Simple Rotation)
A motion of a rigid body or reference frame $\mathcal{B}$ relative to a rigid body or reference frame $\mathcal{A}$ is called a simple rotation of $\mathcal{B}$ in $\mathcal{A}$ if there exists a line L, called an axis of rotation, whose orientation relative to both $\mathcal{A}$ and $\mathcal{B}$ remains unaltered throughout the motion.

Based on this definition Euler stated in 1776 the following theorem for rotation of two rigid bodies or reference frames.

Theorem 2.1 (Euler's Theorem on Rotation)
Every change in the relative orientation of two rigid bodies or reference frames $\mathcal{A}$ and $\mathcal{B}$ can be produced by means of a simple rotation of $\mathcal{B}$ in $\mathcal{A}$.
□

Let $\boldsymbol{a}$ be a vector fixed in $\mathcal{A}$ and $\boldsymbol{b}$ be a vector fixed in $\mathcal{B}$. Hence, the vector $\boldsymbol{b}$ can be expressed in terms of the vector $\boldsymbol{a}$, the unit vector $\lambda = [\lambda_1, \lambda_2, \lambda_3]^T$ parallel to L (the axis of rotation) which $\mathcal{B}$ is rotated about and β the angle frame $\mathcal{B}$ is rotated. The rotation is described by (see Hughes (1986) or Kane, Likins and Levinson (1983)):

$$\boldsymbol{b} = \cos\beta\, \boldsymbol{a} + (1 - \cos\beta)\, \lambda\lambda^T\, \boldsymbol{a} - \sin\beta\, \lambda \times \boldsymbol{a} \tag{2.3}$$

Consequently, the rotation sequence from $\boldsymbol{a}$ to $\boldsymbol{b}$ can be written as:

$$\boldsymbol{b} = \boldsymbol{C}\, \boldsymbol{a} \tag{2.4}$$

where $\boldsymbol{C}$ can be interpreted as a *rotation matrix* which simply is an operator taking a fixed vector $\boldsymbol{a}$ and rotating it to a new vector $\boldsymbol{Ca}$. From (2.3) we obtain the following expression for $\boldsymbol{C}$:

$$\boxed{\boldsymbol{C} = \cos\beta\, \boldsymbol{I} + (1 - \cos\beta)\, \lambda\lambda^T - \sin\beta\, \boldsymbol{S}(\lambda)} \tag{2.5}$$

where $\boldsymbol{I}$ is the 3×3 identity matrix and $\boldsymbol{S}(\lambda)$ is a skew-symmetric matrix (see Definition 2.2) defined such that $\lambda \times \boldsymbol{a} \triangleq \boldsymbol{S}(\lambda)\boldsymbol{a}$, that is:

$$\boldsymbol{S}(\lambda) = \begin{bmatrix} 0 & -\lambda_3 & \lambda_2 \\ \lambda_3 & 0 & -\lambda_1 \\ -\lambda_2 & \lambda_1 & 0 \end{bmatrix} \tag{2.6}$$

Definition 2.2 (Skew-Symmetry of a Matrix)
A matrix $\boldsymbol{S}$ is said to be skew-symmetrical if:

$$\boldsymbol{S} = -\boldsymbol{S}^T$$

This implies that the off-diagonal matrix elements of $\boldsymbol{S}$ satisfy $s_{ij} = -s_{ji}$ for $i \neq j$ while the matrix diagonal consists of zero elements.
□

The set of all 3×3 skew-symmetric matrices is denoted by $SS(3)$ while the set of all 3×3 rotation matrices is usually referred to by the symbol $SO(3)$[1].

[1]Special Orthogonal group of order 3.

Another useful interpretation of $C \in SO(3)$ is as a *coordinate transformation matrix* giving the orientation of a transformed coordinate frame with respect to a fixed (inertial) coordinate frame. This interpretation is particularly useful in guidance and control applications where we are concerned with motion variables in the inertial and body-fixed reference frames.

Expanding (2.5) yields the following expressions for the matrix elements C_{ij}:

$$\begin{aligned}
C_{11} &= (1-\cos\beta)\,\lambda_1^2 + \cos\beta \\
C_{22} &= (1-\cos\beta)\,\lambda_2^2 + \cos\beta \\
C_{33} &= (1-\cos\beta)\,\lambda_3^2 + \cos\beta \\
C_{12} &= (1-\cos\beta)\,\lambda_1\lambda_2 + \lambda_3 \sin\beta \\
C_{21} &= (1-\cos\beta)\,\lambda_2\lambda_1 - \lambda_3 \sin\beta \\
C_{23} &= (1-\cos\beta)\,\lambda_2\lambda_3 + \lambda_1 \sin\beta \\
C_{32} &= (1-\cos\beta)\,\lambda_3\lambda_2 - \lambda_1 \sin\beta \\
C_{31} &= (1-\cos\beta)\,\lambda_3\lambda_1 + \lambda_2 \sin\beta \\
C_{13} &= (1-\cos\beta)\,\lambda_1\lambda_3 - \lambda_2 \sin\beta
\end{aligned} \tag{2.7}$$

Principal Rotations

The principal rotation matrices can be obtained by setting $\lambda = [1,0,0]^T$, $\lambda = [0,1,0]^T$ and $\lambda = [0,0,1]^T$, respectively, in the general formula for C. This yields the following transformation matrices:

$$C_{x,\phi} = \begin{bmatrix} 1 & 0 & 0 \\ 0 & \mathrm{c}\phi & \mathrm{s}\phi \\ 0 & -\mathrm{s}\phi & \mathrm{c}\phi \end{bmatrix} \quad C_{y,\theta} = \begin{bmatrix} \mathrm{c}\theta & 0 & -\mathrm{s}\theta \\ 0 & 1 & 0 \\ \mathrm{s}\theta & 0 & \mathrm{c}\theta \end{bmatrix} \quad C_{z,\psi} = \begin{bmatrix} \mathrm{c}\psi & \mathrm{s}\psi & 0 \\ -\mathrm{s}\psi & \mathrm{c}\psi & 0 \\ 0 & 0 & 1 \end{bmatrix} \tag{2.8}$$

where $\mathrm{s}\cdot = \sin(\cdot)$ and $\mathrm{c}\cdot = \cos(\cdot)$. The notation $C_{i,\alpha}$ denotes a rotation angle α about the i-axis. Notice that all $C_{i,\alpha}$ satisfy the following property:

Property 2.1 (Coordinate Transformation Matrix)
A coordinate transformation matrix $C \in SO(3)$ satisfies:

$$CC^T = C^TC = I; \qquad \det C = 1$$

which implies that C is orthogonal. As a consequence of this, the inverse coordinate transformation matrix (rotation matrix) can be computed as: $C^{-1} = C^T$.
□

Linear Velocity Transformation

It is customary to describe $J_1(\eta_2)$ by three rotations. Note that the order in which these rotations is carried out is not arbitrary. In guidance and control applications it is common to use the xyz-convention specified in terms of Euler angles for the rotations

Let $X_3Y_3Z_3$ be the coordinate system obtained by translating the earth-fixed coordinate system XYZ parallel to itself until its origin coincides with the origin of the body-fixed coordinate system. Then, the coordinate system $X_3Y_3Z_3$ is rotated a *yaw* angle ψ about the Z_3 axis. This yields the coordinate system $X_2Y_2Z_2$. The coordinate system $X_2Y_2Z_2$ is rotated a *pitch* angle θ about the Y_2 axis. This yields the coordinate system $X_1Y_1Z_1$. Finally, the coordinate system $X_1Y_1Z_1$ is rotated a *bank* or *roll* angle ϕ about the X_1 axis. This yields the body-fixed coordinate system $X_0Y_0Z_0$, see Figure 2.2. The rotation sequence is written as:

$$\boldsymbol{J}_1(\boldsymbol{\eta}_2) = \boldsymbol{C}_{z,\psi}^T \boldsymbol{C}_{y,\theta}^T \boldsymbol{C}_{x,\phi}^T \tag{2.9}$$

which implies that the inverse transformation can be written:

$$\boldsymbol{J}_1^{-1}(\boldsymbol{\eta}_2) = \boldsymbol{J}_1^T(\boldsymbol{\eta}_2) = \boldsymbol{C}_{x,\phi} \boldsymbol{C}_{y,\theta} \boldsymbol{C}_{z,\psi} \tag{2.10}$$

Here we have used the result of Property 2.1. Expanding this expression yields:

$$\boldsymbol{J}_1(\boldsymbol{\eta}_2) = \begin{bmatrix} \mathrm{c}\psi\mathrm{c}\theta & -\mathrm{s}\psi\mathrm{c}\phi + \mathrm{c}\psi\mathrm{s}\theta\mathrm{s}\phi & \mathrm{s}\psi\mathrm{s}\phi + \mathrm{c}\psi\mathrm{c}\phi\mathrm{s}\theta \\ \mathrm{s}\psi\mathrm{c}\theta & \mathrm{c}\psi\mathrm{c}\phi + \mathrm{s}\phi\mathrm{s}\theta\mathrm{s}\psi & -\mathrm{c}\psi\mathrm{s}\phi + \mathrm{s}\theta\mathrm{s}\psi\mathrm{c}\phi \\ -\mathrm{s}\theta & \mathrm{c}\theta\mathrm{s}\phi & \mathrm{c}\theta\mathrm{c}\phi \end{bmatrix} \tag{2.11}$$

Angular Velocity Transformation

The body-fixed angular velocity vector $\boldsymbol{\nu}_2 = [p, q, r]^T$ and the Euler rate vector $\dot{\boldsymbol{\eta}}_2 = [\dot{\phi}, \dot{\theta}, \dot{\psi}]^T$ are related through a transformation matrix $\boldsymbol{J}_2(\boldsymbol{\eta}_2)$ according to:

$$\dot{\boldsymbol{\eta}}_2 = \boldsymbol{J}_2(\boldsymbol{\eta}_2)\, \boldsymbol{\nu}_2 \tag{2.12}$$

It should be noted that the angular body velocity vector $\boldsymbol{\nu}_2 = [p, q, r]^T$ cannot be integrated directly to obtain actual angular coordinates. This is due to the fact that $\int_0^t \boldsymbol{\nu}_2(\tau)\, d\tau$ does not have any immediate physical interpretation. However, the vector $\boldsymbol{\eta}_2 = [\phi, \theta, \psi]^T$ will represent proper generalized coordinates. The orientation of the body-fixed reference frame with respect to the inertial reference frame is given by:

$$\boldsymbol{\nu}_2 = \begin{bmatrix} \dot{\phi} \\ 0 \\ 0 \end{bmatrix} + \boldsymbol{C}_{x,\phi} \begin{bmatrix} 0 \\ \dot{\theta} \\ 0 \end{bmatrix} + \boldsymbol{C}_{x,\phi} \boldsymbol{C}_{y,\theta} \begin{bmatrix} 0 \\ 0 \\ \dot{\psi} \end{bmatrix} = \boldsymbol{J}_2^{-1}(\boldsymbol{\eta}_2)\, \dot{\boldsymbol{\eta}}_2 \tag{2.13}$$

This relationship is verified by inspection of Figure 2.2. Expanding (2.13) yields:

$$\boldsymbol{J}_2^{-1}(\boldsymbol{\eta}_2) = \begin{bmatrix} 1 & 0 & -\mathrm{s}\theta \\ 0 & \mathrm{c}\phi & \mathrm{c}\theta\mathrm{s}\phi \\ 0 & -\mathrm{s}\phi & \mathrm{c}\theta\mathrm{c}\phi \end{bmatrix} \quad \Longrightarrow \quad \boldsymbol{J}_2(\boldsymbol{\eta}_2) = \begin{bmatrix} 1 & \mathrm{s}\phi\mathrm{t}\theta & \mathrm{c}\phi\mathrm{t}\theta \\ 0 & \mathrm{c}\phi & -\mathrm{s}\phi \\ 0 & \mathrm{s}\phi/\mathrm{c}\theta & \mathrm{c}\phi/\mathrm{c}\theta \end{bmatrix} \tag{2.14}$$

where $\mathrm{s}\cdot = \sin(\cdot)$, $\mathrm{c}\cdot = \cos(\cdot)$ and $\mathrm{t}\cdot = \tan(\cdot)$.

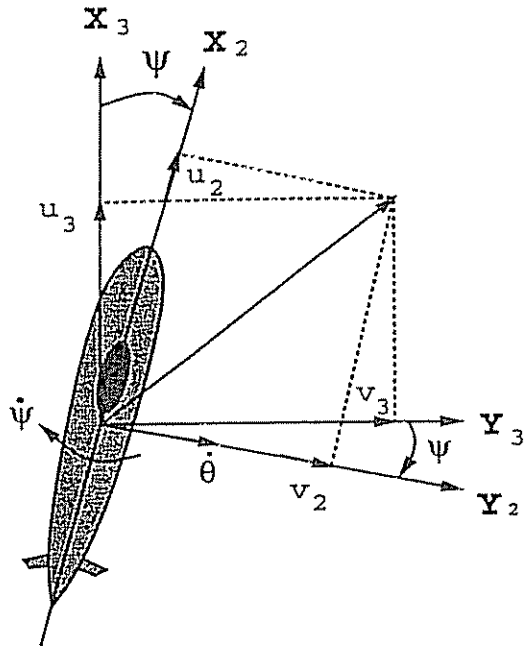

(1) Rotation over heading angle ψ about Z_3
Note that $w_3 = w_2$

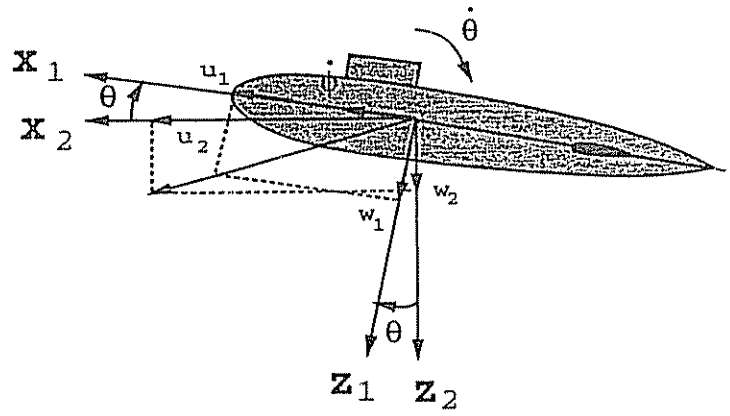

(2) Rotation over pitch angle θ about Y_2
Note that $v_2 = v_1$

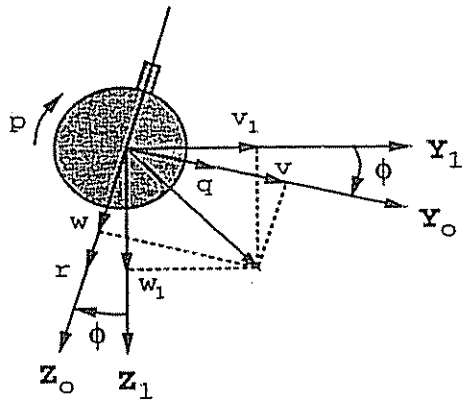

(3) Rotation over roll angle ϕ about X_1
Note that $u_1 = u_2$

Figure 2.2: The rotation sequence according to the xyz-convention showing both the linear (u, v, w) and angular (p, q, r) velocities.

Notice that $J_2(\eta_2)$ is undefined for a pitch angle of $\theta = \pm 90^o$ and that $J_2(\eta_2)$ does not satisfy Property 2.1. Consequently, $J_2^{-1}(\eta_2) \neq J_2^T(\eta_2)$. For surface vessels this is not a problem whereas both underwater vehicles and aircraft may operate close to this singularity. In that case, the kinematic equations can be described by two Euler angle representations with different singularities. Another possibility is to use a quaternion representation. This is the topic of the next section. Summarizing the results from this section, the kinematic equations can be expressed in vector form as:

$$\begin{bmatrix} \dot{\eta}_1 \\ \dot{\eta}_2 \end{bmatrix} = \begin{bmatrix} J_1(\eta_2) & 0_{3\times3} \\ 0_{3\times3} & J_2(\eta_2) \end{bmatrix} \begin{bmatrix} \nu_1 \\ \nu_2 \end{bmatrix} \quad \Longleftrightarrow \quad \boxed{\dot{\eta} = J(\eta)\,\nu} \tag{2.15}$$

2.1.2 Euler Parameters

An alternative to the Euler angle representation is a four-parameter method based on unit quaternions. Consider the following definitions:

Definition 2.3 (Quaternion)
A quaternion q is defined as a complex number (Chou 1992):

$$q = q_1\, i + q_2\, j + q_3\, k + q_4 \tag{2.16}$$

formed by four units $(i, j, k, 1)$ by means of the real parameters q_i $(i = 1, 2, 3, 4)$, where i, j and k are three orthogonal unit vectors.
□

Consequently, a quaternion q may be viewed as a linear combination of a scalar q_4 and a vector $q_0 = [q_1, q_2, q_3]^T$, that is:

$$q = q_0 + q_4 \tag{2.17}$$

If $q_4 = 0$, q is a purely imaginary number and is called a *vector quaternion*. Similarly, q is called a *scalar quaternion* if $q_0 = 0$. By applying quaternions, we will show that we can describe the motion of the body-fixed reference frame relative to the inertial frame.

Unit Quaternions (Euler Parameters)

From (2.5) we have:

$$C = \cos\beta\, I + (1 - \cos\beta)\, \lambda\lambda^T - \sin\beta\, S(\lambda) \tag{2.18}$$

The Euler parameters or unit quaternions are defined as:

$$\boxed{\varepsilon = [\varepsilon_1, \varepsilon_2, \varepsilon_3]^T = \lambda\, \sin\tfrac{\beta}{2}} \tag{2.19}$$

$$\boxed{\eta = \cos\tfrac{\beta}{2}} \tag{2.20}$$

where the unit vector $\lambda = [\lambda_1, \lambda_2, \lambda_3]^T$ is:

$$\lambda = \pm \frac{\varepsilon}{\sqrt{\varepsilon^T \varepsilon}}; \qquad \sqrt{\varepsilon^T \varepsilon} \neq 0 \tag{2.21}$$

Consequently, the Euler parameters can be expressed in the form:

$$e = \begin{bmatrix} \varepsilon_1 \\ \varepsilon_2 \\ \varepsilon_3 \\ \eta \end{bmatrix} = \begin{bmatrix} \lambda \sin \frac{\beta}{2} \\ \cos \frac{\beta}{2} \end{bmatrix}; \qquad 0 \leq \beta \leq 2\pi \tag{2.22}$$

This parameterization implies that the Euler parameters satisfy the constraint $e^T e = 1$, that is:

$$\boxed{\varepsilon_1^2 + \varepsilon_2^2 + \varepsilon_3^2 + \eta^2 = 1} \tag{2.23}$$

From (2.18) with (2.19) and (2.20), we obtain the following coordinate transformation matrix for the Euler parameters:

$$\boxed{C = (\eta^2 - \varepsilon^T \varepsilon)\, I + 2\varepsilon\varepsilon^T - 2\eta\, S(\varepsilon)} \tag{2.24}$$

Linear Velocity Transformation

The transformation relating the linear velocity vector in the inertial reference frame to the velocity in the body-fixed reference frame can be expressed as:

$$\boxed{\dot{\eta}_1 = E_1(e)\, \nu_1} \tag{2.25}$$

where $E_1 = C^T$ with C defined in (2.24) is the rotation matrix. Hence,

$$E_1(e) = \begin{bmatrix} 1 - 2(\varepsilon_2^2 + \varepsilon_3^2) & 2(\varepsilon_1\varepsilon_2 - \varepsilon_3\eta) & 2(\varepsilon_1\varepsilon_3 + \varepsilon_2\eta) \\ 2(\varepsilon_1\varepsilon_2 + \varepsilon_3\eta) & 1 - 2(\varepsilon_1^2 + \varepsilon_3^2) & 2(\varepsilon_2\varepsilon_3 - \varepsilon_1\eta) \\ 2(\varepsilon_1\varepsilon_3 - \varepsilon_2\eta) & 2(\varepsilon_2\varepsilon_3 + \varepsilon_1\eta) & 1 - 2(\varepsilon_1^2 + \varepsilon_2^2) \end{bmatrix} \tag{2.26}$$

As for the Euler angle representation, Property 2.1 implies that the inverse transformation matrix satisfies $E_1^{-1}(e) = E_1^T(e)$.

Angular Velocity Transformation

The angular velocity transformation can be derived by differentiating:

$$C(t)C^T(t) = I \tag{2.27}$$

with respect to time, which yields:

$$\dot{C}(t)C^T(t) + C(t)\dot{C}^T(t) = 0 \tag{2.28}$$

Let us define the matrix $S(t)$ as:

$$\boldsymbol{S}(t) = \boldsymbol{C}(t)\,\dot{\boldsymbol{C}}^T(t) \tag{2.29}$$

Hence, it follows from (2.28) that:

$$\boldsymbol{S}^T(t) + \boldsymbol{S}(t) = \boldsymbol{0} \tag{2.30}$$

This shows that the matrix $\boldsymbol{S}(t)$ is skew-symmetrical. Postmultiplying all elements in (2.28) with $\boldsymbol{C}(t)$ and using the fact $\boldsymbol{C}^T(t)\boldsymbol{C}(t) = \boldsymbol{I}$, yields:

$$\boxed{\dot{\boldsymbol{C}}(t) + \boldsymbol{S}(t)\,\boldsymbol{C}(t) = \boldsymbol{0}} \tag{2.31}$$

Since $\boldsymbol{S}(t)$ is skew-symmetrical it can be represented as:

$$\boldsymbol{S}(\boldsymbol{\omega}(t)) = \begin{bmatrix} 0 & -\omega_3(t) & \omega_2(t) \\ \omega_3(t) & 0 & -\omega_1(t) \\ -\omega_2(t) & \omega_1(t) & 0 \end{bmatrix} \tag{2.32}$$

where $\boldsymbol{\omega}(t)$ is a unique vector defined as the *angular velocity* of the body-fixed rotating frame with respect to the earth-fixed frame at time t. Introducing the notation $\boldsymbol{\omega}(t) = [p, q, r]^T$, we obtain from (2.31)

$$\begin{bmatrix} \dot{C}_{11} & \dot{C}_{12} & \dot{C}_{13} \\ \dot{C}_{21} & \dot{C}_{22} & \dot{C}_{23} \\ \dot{C}_{31} & \dot{C}_{32} & \dot{C}_{33} \end{bmatrix} = \begin{bmatrix} r\,C_{21} - q\,C_{31} & r\,C_{22} - q\,C_{32} & r\,C_{23} - q\,C_{33} \\ p\,C_{31} - r\,C_{11} & p\,C_{32} - r\,C_{12} & p\,C_{33} - r\,C_{13} \\ q\,C_{11} - p\,C_{21} & q\,C_{12} - p\,C_{22} & q\,C_{13} - p\,C_{23} \end{bmatrix} \tag{2.33}$$

Substituting the expressions for C_{ij} from (2.24) into this expression, some calculation yields:

$$\boxed{\dot{\boldsymbol{e}} = \boldsymbol{E}_2(\boldsymbol{e})\,\boldsymbol{\nu}_2} \tag{2.34}$$

where $\boldsymbol{\nu}_2 = [p, q, r]^T$ and

$$\boldsymbol{E}_2(\boldsymbol{e}) = \frac{1}{2}\begin{bmatrix} \eta & -\varepsilon_3 & \varepsilon_2 \\ \varepsilon_3 & \eta & -\varepsilon_1 \\ -\varepsilon_2 & \varepsilon_1 & \eta \\ -\varepsilon_1 & -\varepsilon_2 & -\varepsilon_3 \end{bmatrix} \qquad \boldsymbol{E}_2^T(\boldsymbol{e})\boldsymbol{E}_2(\boldsymbol{e}) = \frac{1}{4}\boldsymbol{I}_{3\times 3} \tag{2.35}$$

Consequently, the kinematic equations of motion can be expressed as:

$$\begin{bmatrix} \dot{\boldsymbol{\eta}}_1 \\ \dot{\boldsymbol{e}} \end{bmatrix} = \begin{bmatrix} \boldsymbol{E}_1(\boldsymbol{e}) & \boldsymbol{0}_{3\times 3} \\ \boldsymbol{0}_{4\times 3} & \boldsymbol{E}_2(\boldsymbol{e}) \end{bmatrix} \begin{bmatrix} \boldsymbol{\nu}_1 \\ \boldsymbol{\nu}_2 \end{bmatrix} \quad \Longleftrightarrow \quad \boxed{\dot{\boldsymbol{\eta}}_E = \boldsymbol{E}(\boldsymbol{\eta}_E)\,\boldsymbol{\nu}} \tag{2.36}$$

where $\boldsymbol{\eta}_E = [x, y, z, \varepsilon_1, \varepsilon_2, \varepsilon_3, \eta]^T$.

Implementation Considerations

In the implementation of Formula (2.36), a normalization procedure should be used to ensure that the constraint:

$$e^T e = \varepsilon_1^2 + \varepsilon_2^2 + \varepsilon_3^2 + \eta^2 = 1 \tag{2.37}$$

is satisfied in the presence of measurement noise and numerical round-off errors. For this purpose, the following simple discrete-time algorithm can be applied:

Algorithm 2.1 (Computation of Euler Parameters)

1. $k = 0$. *Compute initial values of* $\eta_1(k)$ *and* $e(k)$
2. *Euler Integration (see Section B.2):*

$$\begin{aligned} \eta_1(k+1) &= \eta_1(k) + h\, \boldsymbol{E}_1(e(k))\, \nu_1(k) \\ e(k+1) &= e(k) + h\, \boldsymbol{E}_2(e(k))\, \nu_2(k) \end{aligned}$$

   Here h *is the sampling time.*

3. *Normalization:*

$$e(k+1) = \frac{e(k+1)}{\|e(k+1)\|}$$

4. $k = k + 1$. *Return to 2.*

Transformation Between Euler Angles and Euler Parameters

If the Euler angles are known and therefore the expression for the rotation matrix $\boldsymbol{J}_1 = \{J_{ij}\}$, a singularity free extraction procedure can be used to compute the corresponding Euler parameters. For instance, the initial values of the Euler parameters corresponding to step 1 of Algorithm 2.1 can be computed by means of the following scheme proposed by Shepperd (1978):

Algorithm 2.2 (Quaternion From Rotation Matrix)

1. *Assume that the Euler angles* ϕ, θ *and* ψ *are given. Hence, the transformation matrix* $\boldsymbol{J}_1$ *corresponding to these values can be written:*

$$\boldsymbol{J}_1 = \begin{bmatrix} J_{11} & J_{12} & J_{13} \\ J_{21} & J_{22} & J_{23} \\ J_{31} & J_{32} & J_{33} \end{bmatrix}$$

2. *The trace of* J_1 *is computed according to:*

$$J_{44} = \mathrm{tr}\,(J_1) = \sum_{j=1}^{3} J_{jj}$$

3. *Let* $1 \leq i \leq 4$ *be the index corresponding to:*

$$J_{ii} = \max(J_{11}, J_{22}, J_{33}, J_{44})$$

4. *Define:*

$$|p_i| = \sqrt{1 + 2J_{ii} - J_{44}}$$

where the sign ascribed to p_i *can be chosen either plus or minus.*

5. *Compute the other three p-values from:*

$$\begin{aligned} p_4\, p_1 &= J_{32} - J_{23} & \qquad p_2\, p_3 &= J_{32} + J_{23} \\ p_4\, p_2 &= J_{13} - J_{31} & \qquad p_3\, p_1 &= J_{13} + J_{31} \\ p_4\, p_3 &= J_{21} - J_{12} & \qquad p_1\, p_2 &= J_{21} + J_{12} \end{aligned}$$

by simply dividing the three equations containing the component p_i *with* p_i *on both sides.*

6. *Compute the Euler parameters* $\boldsymbol{e} = [e_1, e_2, e_3, e_4]^T = [\varepsilon_1, \varepsilon_2, \varepsilon_3, \eta]^T$*:*

$$e_j = p_j/2 \qquad (j = 1...4)$$

Transformation Between Euler Parameters and Euler Angles

The relationship between the Euler angles ϕ, θ and ψ (xyz-convention) and the Euler parameters e_i ($i = 1...4$) can be established by requiring that the rotation matrices of the two kinematic representations are equal. Moreover:

$$\boldsymbol{J}_1(\phi, \theta, \psi) \triangleq \boldsymbol{E}_1(e) \tag{2.38}$$

Let the elements of $\boldsymbol{E}_1$ be denoted by E_{ij} where the superscripts i and j denote the i-th row and j-th column of $\boldsymbol{E}_1$. Writing expression (2.38) in component form yields a system of 9 equations with 3 unknowns (ϕ, θ and ψ), that is:

$$\begin{bmatrix} \mathrm{c}\psi\mathrm{c}\theta & -\mathrm{s}\psi\mathrm{c}\phi + \mathrm{c}\psi\mathrm{s}\theta\mathrm{s}\phi & \mathrm{s}\psi\mathrm{s}\phi + \mathrm{c}\psi\mathrm{c}\phi\mathrm{s}\theta \\ \mathrm{s}\psi\mathrm{c}\theta & \mathrm{c}\psi\mathrm{c}\phi + \mathrm{s}\phi\mathrm{s}\theta\mathrm{s}\psi & -\mathrm{c}\psi\mathrm{s}\phi + \mathrm{s}\theta\mathrm{s}\psi\mathrm{c}\phi \\ -\mathrm{s}\theta & \mathrm{c}\theta\mathrm{s}\phi & \mathrm{c}\theta\mathrm{c}\phi \end{bmatrix} \triangleq \begin{bmatrix} E_{11} & E_{12} & E_{13} \\ E_{21} & E_{22} & E_{23} \\ E_{31} & E_{32} & E_{33} \end{bmatrix} \tag{2.39}$$

One solution to (2.39) is:

$$\theta = -\text{asin}(E_{31}); \qquad \theta \neq \pm 90^o \tag{2.40}$$

$$\phi = \text{atan2}(E_{32}, E_{33}) \tag{2.41}$$

$$\psi = \text{atan2}(E_{21}, E_{11}) \tag{2.42}$$

where $\text{atan2}(y, x)$ is the four quadrant arctangent of the real elements of x and y, defined as:

$$\alpha = \text{atan2}(y, x) = \begin{cases} 2\,\pi - \text{acos}(x) & \text{if } y \leq 0 \\ \text{acos}(x) & \text{if } y > 0 \end{cases} \tag{2.43}$$

where $-\pi \leq \alpha \leq \pi$. Precautions must be taken against computational errors in the vicinity of $\theta = \pm 90^o$. Also, a convention for choosing the signs of the Euler angles should be adopted.

2.1.3 Euler–Rodrigues Parameters

A related three parameter description, the so-called Euler–Rodrigues parameters $\rho = [\rho_1, \rho_2, \rho_3]^T$, is defined in terms of Euler parameters as follows:

$$\rho = \frac{1}{\eta}\,\epsilon = \lambda\,\tan\frac{\beta}{2} \qquad \beta \neq \pi \tag{2.44}$$

For this particular choice, the coordinate transformation matrix takes the form:

$$C = I + \frac{2}{1 + \rho^T\,\rho}\,S(\rho)\,[S(\rho) - I] \tag{2.45}$$

where $S(\rho)$ is defined in (2.6). This representation presents a singularity at $\beta = \pi$, that is $\eta = 0$. Application of Euler–Rodrigues parameters suggests that the position and attitude vector should be chosen as $\eta_R = [x, y, z, \rho_1, \rho_2, \rho_3]^T$.

2.1.4 Comments on Parameter Alternatives

In the previous sections, Euler angles, Euler parameters and Rodrigues parameters have been suggested as candidates to describe the orientation of marine vehicles. It is attractive to use the Euler angle representation since this is a three-parameter set corresponding to well known quantities like the roll, pitch and yaw angle of the vehicle. However, no continuous three-parameter description can be both global and without singularities. In fact, the roll-pitch-yaw representation is not defined for a pitch angle of $\theta = \pm 90$ degrees. However, during practical operations with marine vehicles, the parameter region of $\theta = \pm 90$ degrees is not likely to be entered. This is due to the metacentric restoring forces. Another problem with the Euler angle representation is the so-called "wraparound" problem which implies that the Euler angles may be integrated up to values outside

the normal $\pm 90^o$ range of pitch and $\pm 180^o$ range of roll and yaw. This problem requires that some normalization procedure is adopted.

One way to avoid singularities and "wraparound" problems is by applying a four-parameter description based on Euler parameters. Another advantage with the Euler parameters is their representation and computational efficiency. The Euler angles are computed by numerical integration of a set of nonlinear differential equations. This procedure involves computation of a large number of trigonometric functions. For infinitesimal analyses this solution is quite accurate but problems arise for arbitrary displacements.

The Rodrigues parameter representation is also computationally effective but this representation has one singularity. Although it is dangerous to generalize, computational efficiency and accuracy suggests that Euler parameters are the best choice. However, Euler angles are more intuitive and therefore more used.

2.2 Newtonian and Lagrangian Mechanics

In the following sections, we will show that the 6 DOF nonlinear dynamic equations of motion can be conveniently expressed as:

$$M\dot{\nu} + C(\nu)\,\nu + D(\nu)\,\nu + g(\eta) = \tau \tag{2.46}$$

where

M	= inertia matrix (including added mass)
$C(\nu)$	= matrix of Coriolis and centripetal terms (including added mass)
$D(\nu)$	= damping matrix
$g(\eta)$	= vector of gravitational forces and moments
τ	= vector of control inputs

Before we derive the 6 DOF dynamic equations of motion, we will briefly review some principles from *Newtonian* and *Lagrangian* mechanics.

2.2.1 Newton–Euler Formulation

The *Newton–Euler formulation* is based on *Newton's Second Law* which relates mass m, acceleration $\dot{v}_C$ and force f_C according to:

$$m\,\dot{v}_C = f_C \tag{2.47}$$

If no force is acting ($f_C = 0$) then the body is moving with constant speed ($v_C = constant$) or the body is at rest ($v_C = 0$). This result is actually known as *Newton's First Law*. These laws were published in 1687 by Isaac Newton (1643–1727) in "Philosophia Naturalis Principia Mathematica".

Euler's First and Second Axioms

Leonhard Euler (1707–1783) suggested expressing *Newton's Second Law* in terms of conservation of both linear p_C and angular momentum h_C ("Novi Commentarii Academiae Scientarium Imperialis Petropolitane"). These results are known as *Euler's First and Second Axioms*, respectively.

$$\dot{p}_C \triangleq f_C\,; \qquad p_C \triangleq m\,v_C \tag{2.48}$$

$$\dot{h}_C \triangleq m_C\,; \qquad h_C \triangleq I_C\,\omega \tag{2.49}$$

Here f_C and m_C are the forces and moments referred to the body's center of gravity, ω is the angular velocity vector and I_C is the inertia tensor about the body's center of gravity (to be defined later). The application of these equations is often referred to as *vectorial mechanics* since both conservation laws are expressed in terms of vectors.

2.2.2 Lagrangian Formulation

An alternative approach to the Newton–Euler formulation is to apply Lagrangian mechanics. The Lagrangian approach involves three basic steps. First, we need to formulate a suitable expression for the vehicle's kinetic and potential energy, denoted T and V, respectively. Then we can compute the Lagrangian L according to:

$$L = T - V \tag{2.50}$$

Finally, we apply the *Lagrange equation*:

$$\frac{d}{dt}\left(\frac{\partial L}{\partial \dot{\eta}}\right) - \frac{\partial L}{\partial \eta} = J^{-T}(\eta)\,\tau \tag{2.51}$$

which in component form corresponds to a set of 6 second-order differential equations. From the above formula it is seen that the Lagrangian mechanics describes the system's dynamics in terms of energy. It will be shown in Section 2.5.3 that the nonlinear equations of motion can be derived by simple means when L is given. It should be noted that the Lagrange equation is valid regardless of the number of masses considered. Furthermore, Formula (2.51) is valid in any reference frame, inertial and body-fixed as long as *generalized coordinates* are used.

For a vehicle not subject to any motion constraints, the number of independent (generalized) coordinates will be equal to the number of DOF. The generalized coordinates are chosen as:

$$\eta = [x, y, z, \phi, \theta, \psi]^T \tag{2.52}$$

for a vehicle moving in 6 DOF. It should be noted that the alternative representation $\eta_E = [x, y, z, \varepsilon_1, \varepsilon_2, \varepsilon_3, \eta]^T$ using Euler parameters cannot be used in a

Lagrangian approach since this representation is defined by 7 parameters. Hence, these parameters cannot be viewed as *generalized coordinates*. Often it is advantageous to formulate the equations of motion in a body-fixed reference frame. Unfortunately, the body-fixed velocity vector:

$$\nu = [u, v, w, p, q, r]^T \tag{2.53}$$

cannot be integrated to yield a set of generalized coordinates in terms of position and orientation. In fact, $\int_0^t \nu \, d\tau$ has no immediate physical interpretation. As a consequence of this, we cannot use the Lagrange equation directly to formulate the equations of motion in the body-fixed coordinate system. However, this problem can be circumvented by applying Kirchhoff's equations of motion or the so-called *Quasi-Lagrangian* approach.

2.2.3 Kirchhoff's Equations of Motion

Lagrange's equations of motion in terms of *generalized velocities*, usually the body-fixed velocities (u, v, w, p, q, r), can be obtained from the ordinary Lagrange equations. The derivation is laborious and mathematically involved and will thus be omitted here. The interested reader is advised to consult Meirovitch and Kwak (1989) and references therein. The main results are summarized below:

Kirchhoff's Equations in Vector Form (Kirchhoff 1869)

Consider a vehicle with body-fixed linear velocity $\nu_1 = [u, v, w]^T$ and angular velocity $\nu_2 = [p, q, r]^T$. Hence, the force τ_1 and moment τ_2 are related to the kinetic energy:

$$T = \frac{1}{2} \nu^T M \nu \tag{2.54}$$

by the vector equations:

$$\frac{d}{dt}\left(\frac{\partial T}{\partial \nu_1}\right) + \nu_2 \times \frac{\partial T}{\partial \nu_1} = \tau_1 \tag{2.55}$$

$$\frac{d}{dt}\left(\frac{\partial T}{\partial \nu_2}\right) + \nu_2 \times \frac{\partial T}{\partial \nu_2} + \nu_1 \times \frac{\partial T}{\partial \nu_1} = \tau_2 \tag{2.56}$$

Kirchhoff's equations will prove to be very useful in the derivation of the expression for added inertia in Section 2.4.1. Notice that Kirchhoff's equations do not include the gravitational forces. If gravitation is important, the following representation of the Lagrange equations can be used.

Quasi-Lagrange Equations of Motion (Meirovitch 1990)

The *quasi-Lagrange equations* is a more general version of Kirchhoff's equations where the Lagrangian $L = T - V$ is used instead of the kinetic energy T. This implies that gravitational forces can be included as well (see page 42 of Meirovitch 1990). These equations are:

$$\frac{d}{dt}\left(\frac{\partial L}{\partial \nu_1}\right) + \nu_2 \times \frac{\partial L}{\partial \nu_1} - \boldsymbol{J}_1^T(\eta_2)\frac{\partial L}{\partial \eta_1} = \tau_1 \qquad (2.57)$$

$$\frac{d}{dt}\left(\frac{\partial L}{\partial \nu_2}\right) + \nu_2 \times \frac{\partial L}{\partial \nu_2} + \nu_1 \times \frac{\partial L}{\partial \nu_1} - \boldsymbol{J}_2^T(\eta_2)\frac{\partial L}{\partial \eta_2} = \tau_2 \qquad (2.58)$$

2.3 Rigid-Body Dynamics

In this section we will apply Euler's first and second axioms to derive the rigid-body equations of motion. Consider a body-fixed coordinate system $X_0Y_0Z_0$ rotating with an angular velocity $\omega = [\omega_1, \omega_2, \omega_3]^T$ about an earth-fixed coordinate system XYZ, see Figure 2.3. The body's inertia tensor $\boldsymbol{I}_0$ referred to an arbitrary body-fixed coordinate system $X_0Y_0Z_0$ with origin O in the body-fixed frame is defined as:

$$\boldsymbol{I}_0 \triangleq \begin{bmatrix} I_x & -I_{xy} & -I_{xz} \\ -I_{yx} & I_y & -I_{yz} \\ -I_{zx} & -I_{zy} & I_z \end{bmatrix}; \qquad \boldsymbol{I}_0 = \boldsymbol{I}_0^T > 0 \qquad (2.59)$$

Here I_x, I_y and I_z are the moments of inertia about the X_0, Y_0 and Z_0-axes and $I_{xy} = I_{yx}, I_{xz} = I_{zx}$ and $I_{yz} = I_{zy}$ are the products of inertia defined as:

$$\begin{array}{ll} I_x = \int_V (y^2 + z^2)\, \rho_A dV; & I_{xy} = \int_V xy\, \rho_A dV = \int_V yx\, \rho_A dV = I_{yx} \\ I_y = \int_V (x^2 + z^2)\, \rho_A dV; & I_{xz} = \int_V xz\, \rho_A dV = \int_V zx\, \rho_A dV = I_{zx} \\ I_z = \int_V (x^2 + y^2)\, \rho_A dV; & I_{yz} = \int_V yz\, \rho_A dV = \int_V zy\, \rho_A dV = I_{zy} \end{array}$$

with ρ_A as the mass density of the body. Consequently, we can represent the inertia tensor $\boldsymbol{I}_0$ in vectorial form as:

$$\boldsymbol{I}_0\, \omega = \int_V \boldsymbol{r} \times (\omega \times \boldsymbol{r})\, \rho_A\, dV \qquad (2.60)$$

Another useful definition of $\boldsymbol{I}_0$ is:

$$\boldsymbol{I}_0 = -\int_V \boldsymbol{S}(\boldsymbol{r})\, \boldsymbol{S}(\boldsymbol{r})\, \rho_A\, dV = \int_V (\boldsymbol{r}^T\boldsymbol{r}\, \boldsymbol{I} - \boldsymbol{r}\boldsymbol{r}^T)\, \rho_A\, dV \qquad (2.61)$$

Furthermore the mass of the body is defined as:

$$m = \int_V \rho_A\, dV \qquad (2.62)$$

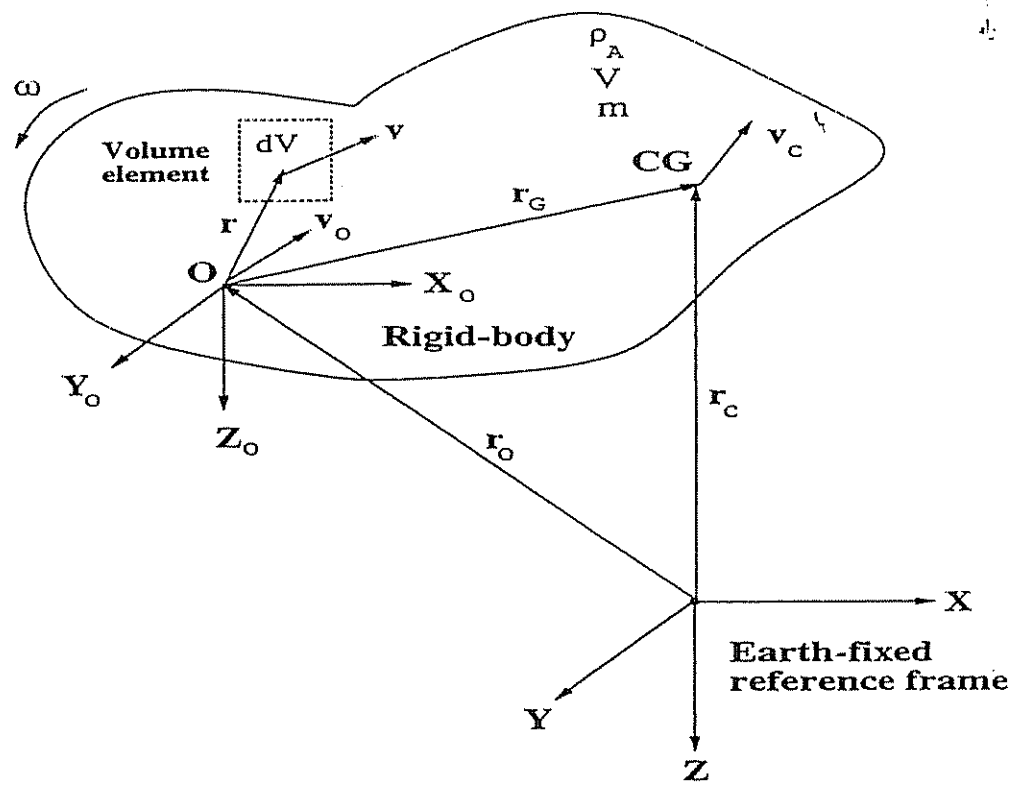

Figure 2.3: The inertial, earth-fixed non-rotating reference frame XYZ and the body-fixed rotating reference frame $X_0Y_0Z_0$.

It will be assumed that the mass is constant in time ($\dot{m} = 0$). For a rigid body satisfying this the distance from the origin O of the body-fixed coordinate system to the vehicle's center of gravity can be defined as:

$$r_G = \frac{1}{m} \int_V r \, \rho_A \, dV \tag{2.63}$$

For marine vehicles it is desirable to derive the equations of motion for an arbitrary origin in a local body-fixed coordinate system to take advantage of the vehicle's geometrical properties. Since the hydrodynamic and kinematic forces and moments are given in the body-fixed reference frame we will formulate Newton's laws in the body-fixed reference frame.

When deriving the equations of motion it will be assumed that: (1) the vehicle is rigid and (2) the earth-fixed reference frame is inertial. The first assumption eliminates the consideration of forces acting between individual elements of mass while the second eliminates forces due to the Earth's motion relative to a star-fixed reference system. In guidance and control applications in space it is usual to use a star-fixed reference frame or a reference frame rotating with the Earth, while marine vehicles usually are related to an earth-fixed reference frame. To derive the equations of motion for an arbitrary origin in a local body-fixed rotating coordinate system we need the formula:

$$\dot{c} = \mathring{c} + \omega \times c \tag{2.64}$$

which relates the time derivatives of an arbitrary vector c in XYZ and $X_0Y_0Z_0$. Here $\dot{c}$ is the time derivative in the earth-fixed reference frame XYZ and $\mathring{c}$ is the time derivative in the moving reference frame $X_0Y_0Z_0$. Notice that this simple relation yields:

$$\dot{\omega} = \mathring{\omega} + \omega \times \omega = \mathring{\omega} \tag{2.65}$$

which simply states that the angular acceleration is equal in the body-fixed and earth-fixed reference frames.

Translational Motion

The translational motion of a marine vehicle is described by (2.48). From Figure 2.3 it is seen that:

$$r_C = r_0 + r_G \tag{2.66}$$

Hence, the velocity of the center of gravity is:

$$v_C = \dot{r}_C = \dot{r}_0 + \dot{r}_G \tag{2.67}$$

By using the fact $v_0 = \dot{r}_0$ and $\mathring{r}_G = 0$ for a rigid body,

$$\dot{r}_G = \mathring{r}_G + \omega \times r_G = \omega \times r_G \tag{2.68}$$

Hence,

$$v_C = v_0 + \omega \times r_G \tag{2.69}$$

The acceleration vector can be found as:

$$\dot{v}_C = \dot{v}_0 + \dot{\omega} \times r_G + \omega \times \dot{r}_G \tag{2.70}$$

which yields

$$\dot{v}_C = \mathring{v}_0 + \omega \times v_0 + \mathring{\omega} \times r_G + \omega \times (\omega \times r_G) \tag{2.71}$$

Substituting this expression into (2.48) finally yields

$$\boxed{m\left(\mathring{v}_0 + \omega \times v_0 + \mathring{\omega} \times r_G + \omega \times (\omega \times r_G)\right) = f_0} \tag{2.72}$$

If the origin of the body-fixed coordinate system $X_0Y_0Z_0$ is chosen to coincide with the vehicle's center of gravity, we have $r_G = [0, 0, 0]^T$. Hence, (2.72) with $f_0 = f_C$ and $v_0 = v_C$, yields:

$$\boxed{m(\mathring{v}_C + \omega \times v_C) = f_C} \tag{2.73}$$

Rotational Motion

A similar approach can be used to obtain the rotational equations of motion referred to the origin O in Figure 2.3. The absolute angular momentum about O is defined as:

$$\boldsymbol{h}_0 \triangleq \int_V \boldsymbol{r} \times \boldsymbol{v}\, \rho_A\, dV \tag{2.74}$$

Differentiating this expression with respect to time yields:

$$\dot{\boldsymbol{h}}_0 = \int_V \boldsymbol{r} \times \dot{\boldsymbol{v}}\, \rho_A\, dV + \int_V \dot{\boldsymbol{r}} \times \boldsymbol{v}\, \rho_A\, dV \tag{2.75}$$

The first term on the right-hand side is the moment vector:

$$\boldsymbol{m}_0 \triangleq \int_V \boldsymbol{r} \times \dot{\boldsymbol{v}}\, \rho_A\, dV \tag{2.76}$$

From Figure 2.3 we see that:

$$\boldsymbol{v} = \dot{\boldsymbol{r}}_0 + \dot{\boldsymbol{r}} \qquad \Longrightarrow \qquad \dot{\boldsymbol{r}} = \boldsymbol{v} - \boldsymbol{v}_0 \tag{2.77}$$

Substituting (2.77) and (2.76) into the expression for $\dot{\boldsymbol{h}}_0$ and using the fact that $\boldsymbol{v} \times \boldsymbol{v} = \boldsymbol{0}$, yields

$$\dot{\boldsymbol{h}}_0 = \boldsymbol{m}_0 - \boldsymbol{v}_0 \times \int_V \boldsymbol{v}\, \rho_A\, dV \tag{2.78}$$

or equivalently

$$\dot{\boldsymbol{h}}_0 = \boldsymbol{m}_0 - \boldsymbol{v}_0 \times \int_V (\boldsymbol{v}_0 + \dot{\boldsymbol{r}})\, \rho_A\, dV = \boldsymbol{m}_0 - \boldsymbol{v}_0 \times \int_V \dot{\boldsymbol{r}}\, \rho_A\, dV \tag{2.79}$$

This expression can be rewritten by differentiating (2.63) with respect to time, that is:

$$m\dot{\boldsymbol{r}}_G = \int_V \dot{\boldsymbol{r}}\, \rho_A\, dV \tag{2.80}$$

Since $\dot{\boldsymbol{r}}_G = \boldsymbol{\omega} \times \boldsymbol{r}_G$, Equation (2.80) can be expressed as

$$\int_V \dot{\boldsymbol{r}}\, \rho_A\, dV = m(\boldsymbol{\omega} \times \boldsymbol{r}_G) \tag{2.81}$$

Substituting this result into (2.79) yields

$$\dot{\boldsymbol{h}}_0 = \boldsymbol{m}_0 - m\boldsymbol{v}_0 \times (\boldsymbol{\omega} \times \boldsymbol{r}_G) \tag{2.82}$$

The next step is to write the absolute angular momentum (2.74) as

$$\boldsymbol{h}_0 = \int_V \boldsymbol{r} \times \boldsymbol{v}\, \rho_A\, dV = \int_V \boldsymbol{r} \times \boldsymbol{v}_0\, \rho_A\, dV + \int_V \boldsymbol{r} \times (\boldsymbol{\omega} \times \boldsymbol{r})\, \rho_A\, dV \tag{2.83}$$

The first term on the right-hand side of this expression can be rewritten by using the definition (2.63), that is:

$$\int_V r \times v_0 \, \rho_A \, dV = (\int_V r \, \rho_A \, dV) \times v_0 = m \, r_G \times v_0 \tag{2.84}$$

The second term is recognized as the definition (2.60). Hence, (2.83) reduces to:

$$h_0 = I_0 \, \omega + m \, r_G \times v_0 \tag{2.85}$$

Differentiating this expression according to (2.64) (assuming that I_0 is constant with respect to time), yields

$$\dot{h}_0 = I_0 \mathring{\omega} + \omega \times (I_0 \, \omega) + m \, (\omega \times r_G) \times v_0 + m \, r_G \times (\mathring{v}_0 + \omega \times v_0) \tag{2.86}$$

Using the relation $(\omega \times r_G) \times v_0 = -v_0 \times (\omega \times r_G)$ and eliminating $\dot{h}_0$ from (2.82) and (2.86) finally yields

$$\boxed{I_0 \mathring{\omega} + \omega \times (I_0 \omega) + m r_G \times (\mathring{v}_0 + \omega \times v_0) = m_0} \tag{2.87}$$

If the origin O of the body-fixed coordinate system $X_0 Y_0 Z_0$ is chosen to coincide with the vehicle's center of gravity, equation (2.87) simplifies to:

$$\boxed{I_C \mathring{\omega} + \omega \times (I_C \, \omega) = m_C} \tag{2.88}$$

The rotational equations of motion are often referred to as the *Euler equations*.

2.3.1 6 DOF Rigid-Body Equations of Motion

In the previous sections we have shown how the rigid-body dynamics can be derived by applying the *Newtonian* and *Lagrangian* formalism. In this section we will discuss useful properties of the nonlinear equations of motion and show how these properties considerably simplify the representation of the nonlinear model.

General 6 DOF Rigid-Body Equations of Motion

Equations (2.72) and (2.87) are usually written in component form according to the SNAME (1950) notation, that is:

f_0	$=$	τ_1	$=$	$[X, Y, Z]^T$	external forces
m_0	$=$	τ_2	$=$	$[K, M, N]^T$	moment of external forces about O
v_0	$=$	ν_1	$=$	$[u, v, w]^T$	linear velocity of $X_0 Y_0 Z_0$
ω	$=$	ν_2	$=$	$[p, q, r]^T$	angular velocity of $X_0 Y_0 Z_0$
r_G			$=$	$[x_G, y_G, z_G]^T$	center of gravity

Applying this notation to (2.72) and (2.87) yields:

$$
\begin{aligned}
m\left[\dot{u} - vr + wq - x_G(q^2 + r^2) + y_G(pq - \dot{r}) + z_G(pr + \dot{q})\right] &= X \\
m\left[\dot{v} - wp + ur - y_G(r^2 + p^2) + z_G(qr - \dot{p}) + x_G(qp + \dot{r})\right] &= Y \\
m\left[\dot{w} - uq + vp - z_G(p^2 + q^2) + x_G(rp - \dot{q}) + y_G(rq + \dot{p})\right] &= Z \\
I_x\dot{p} + (I_z - I_y)qr - (\dot{r} + pq)I_{xz} + (r^2 - q^2)I_{yz} + (pr - \dot{q})I_{xy} & \\
+m\left[y_G(\dot{w} - uq + vp) - z_G(\dot{v} - wp + ur)\right] &= K \qquad (2.89) \\
I_y\dot{q} + (I_x - I_z)rp - (\dot{p} + qr)I_{xy} + (p^2 - r^2)I_{zx} + (qp - \dot{r})I_{yz} & \\
+m\left[z_G(\dot{u} - vr + wq) - x_G(\dot{w} - uq + vp)\right] &= M \\
I_z\dot{r} + (I_y - I_x)pq - (\dot{q} + rp)I_{yz} + (q^2 - p^2)I_{xy} + (rq - \dot{p})I_{zx} & \\
+m\left[x_G(\dot{v} - wp + ur) - y_G(\dot{u} - vr + wq)\right] &= N
\end{aligned}
$$

The three first equations represent the translational motion while the three last equations represent the rotational motion.

Vectorial Representation of the 6 DOF Rigid-Body Equations of Motion

These equations can be expressed in a more compact form as:

$$\boxed{M_{RB}\,\dot{\nu} + C_{RB}(\nu)\,\nu = \tau_{RB}} \qquad (2.90)$$

Here $\nu = [u, v, w, p, q, r]^T$ is the body-fixed linear and angular velocity vector and $\tau_{RB} = [X, Y, Z, K, M, N]^T$ is a generalized vector of external forces and moments.

Property 2.2 (M_{RB})
The parameterization of the rigid-body inertia matrix M_{RB} is unique and it satisfies:

$$M_{RB} = M_{RB}^T > 0; \qquad \dot{M}_{RB} = 0$$

where

$$M_{RB} = \begin{bmatrix} mI_{3\times3} & -mS(r_G) \\ mS(r_G) & I_0 \end{bmatrix} = \begin{bmatrix} m & 0 & 0 & 0 & mz_G & -my_G \\ 0 & m & 0 & -mz_G & 0 & mx_G \\ 0 & 0 & m & my_G & -mx_G & 0 \\ 0 & -mz_G & my_G & I_x & -I_{xy} & -I_{xz} \\ mz_G & 0 & -mx_G & -I_{yx} & I_y & -I_{yz} \\ -my_G & mx_G & 0 & -I_{zx} & -I_{zy} & I_z \end{bmatrix} \qquad (2.91)$$

Here $I_{3\times3}$ is the identity matrix, $I_0 = I_0^T > 0$ is the inertia tensor with respect to O and $S(r_G) \in SS(3)$ is defined in (2.6).
□

On the contrary, it is possible to find a large number of parameterizations for the C_{RB} matrix which consists of the Coriolis vector term $\omega \times v$ and the centripetal vector term $\omega \times (\omega \times r_G)$. We will use Kirchhoff's equations to derive a *skew-symmetric* representation of C_{RB}.

Theorem 2.2 (Coriolis and Centripetal Matrix from Inertia Matrix)
Let $M > 0$ be an 6×6 inertia matrix defined as:

$$M = \begin{bmatrix} M_{11} & M_{12} \\ M_{21} & M_{22} \end{bmatrix} \tag{2.92}$$

Hence, we can always parameterize the Coriolis and centripetal matrix such that $C(\nu) = -C^T(\nu)$ by defining:

$$C(\nu) = \begin{bmatrix} 0_{3\times 3} & -S(M_{11}\,\nu_1 + M_{12}\,\nu_2) \\ -S(M_{11}\,\nu_1 + M_{12}\,\nu_2) & -S(M_{21}\,\nu_1 + M_{22}\,\nu_2) \end{bmatrix} \tag{2.93}$$

Proof: *The kinetic energy T can be written as a quadratic form:*

$$T = \frac{1}{2}\nu^T M \nu \tag{2.94}$$

Expanding this expression yields:

$$T = \frac{1}{2}\left(\nu_1^T M_{11}\nu_1 + \nu_1^T M_{12}\nu_2 + \nu_2^T M_{21}\nu_1 + \nu_2^T M_{22}\nu_2\right) \tag{2.95}$$

Hence, we obtain:

$$\frac{\partial T}{\partial \nu_1} = M_{11}\,\nu_1 + M_{12}\,\nu_2 \tag{2.96}$$

$$\frac{\partial T}{\partial \nu_2} = M_{21}\,\nu_1 + M_{22}\,\nu_2 \tag{2.97}$$

From Kirchhoff's equations (2.55) and (2.56) we recognize that:

$$C(\nu)\,\nu \triangleq \begin{bmatrix} \nu_2 \times \frac{\partial T}{\partial \nu_1} \\ \nu_2 \times \frac{\partial T}{\partial \nu_2} + \nu_1 \times \frac{\partial T}{\partial \nu_1} \end{bmatrix} = \begin{bmatrix} 0_{3\times 3} & -S(\frac{\partial T}{\partial \nu_1}) \\ -S(\frac{\partial T}{\partial \nu_1}) & -S(\frac{\partial T}{\partial \nu_2}) \end{bmatrix} \begin{bmatrix} \nu_1 \\ \nu_2 \end{bmatrix}$$

which after substitution of (2.96) and (2.97) proves (2.93). This result was first proven by Sagatun and Fossen (1991).

Property 2.3 (C_{RB})
According to Theorem 2.2 the rigid-body Coriolis and centripetal matrix $C_{RB}(\nu)$ can always be parameterized such that $C_{RB}(\nu)$ is skew-symmetrical, that is:

$$C_{RB}(\nu) = -C_{RB}^T(\nu) \quad \forall \quad \nu \in \mathbb{R}^6$$

□

Application of Theorem 2.2 with $M = M_{RB}$ yields the following expression for $C_{RB}(\nu)$:

$$C_{RB}(\nu) = \begin{bmatrix} 0_{3\times 3} & -mS(\nu_1) - mS(S(\nu_2)r_G) \\ -mS(\nu_1) - mS(S(\nu_2)r_G) & mS(S(\nu_1)r_G) - S(I_0\,\nu_2) \end{bmatrix} \quad (2.98)$$

Notice that $S(\nu_1)\nu_1 = 0$ in this expression. Three other useful skew-symmetric representations can be derived from this expression (Fossen and Fjellstad 1994):

$$C_{RB}(\nu) = \begin{bmatrix} 0_{3\times 3} & -mS(\nu_1) - mS(\nu_2)S(r_G) \\ -mS(\nu_1) + mS(r_G)S(\nu_2) & -S(I_0\,\nu_2) \end{bmatrix} \quad (2.99)$$

$$C_{RB}(\nu) = \begin{bmatrix} mS(\nu_2) & -mS(\nu_2)S(r_G) \\ mS(r_G)S(\nu_2) & -S(I_0\,\nu_2) \end{bmatrix} \quad (2.100)$$

$$C_{RB}(\nu) = \begin{bmatrix} mS(\nu_2) & -mS(S(\nu_2)r_G) \\ -mS(S(\nu_2)r_G) & mS(S(\nu_1)r_G) - S(I_0\,\nu_2) \end{bmatrix} \quad (2.101)$$

The first of these three expressions can be written in component form according to (Fossen 1991):

$$C_{RB}(\nu) \triangleq \begin{bmatrix} 0 & 0 & 0 \\ 0 & 0 & 0 \\ 0 & 0 & 0 \\ -m(y_G q + z_G r) & m(y_G p + w) & m(z_G p - v) \\ m(x_G q - w) & -m(z_G r + x_G p) & m(z_G q + u) \\ m(x_G r + v) & m(y_G r - u) & -m(x_G p + y_G q) \end{bmatrix}$$
$$\begin{bmatrix} m(y_G q + z_G r) & -m(x_G q - w) & -m(x_G r + v) \\ -m(y_G p + w) & m(z_G r + x_G p) & -m(y_G r - u) \\ -m(z_G p - v) & -m(z_G q + u) & m(x_G p + y_G q) \\ 0 & -I_{yz}q - I_{xz}p + I_z r & I_{yz}r + I_{xy}p - I_y q \\ I_{yz}q + I_{xz}p - I_z r & 0 & -I_{xz}r - I_{xy}q + I_x p \\ -I_{yz}r - I_{xy}p + I_y q & I_{xz}r + I_{xy}q - I_x p & 0 \end{bmatrix} \quad (2.102)$$

It will be shown in a later section that the design of a nonlinear control system can be quite simple if the dynamic properties (symmetry, skew-symmetry, positiveness etc.) of the nonlinear equations of motion are exploited.

Simplified 6 DOF Rigid-Body Equations of Motion

The general rigid-body equations of motion can be simplified by choosing the origin of the body-fixed coordinate system according to the following criteria:

(1) Origin O Coincides with the Center of Gravity

This implies that $r_G = [0, 0, 0]^T$. The simplest form of the equations of motion is obtained when the body axes coincide with the principal axes of inertia. This implies that $I_C = \mathrm{diag}\{I_{x_C}, I_{y_C}, I_{z_C}\}$. If this is not the case, the body-fixed coordinate system $X_C Y_C Z_C$ can be rotated about its axes to obtain a diagonal inertia tensor by simply performing a *principal axis transformation*. The eigenvalues λ_i (i=1...3) of the inertia matrix I_C are found from the characteristic equation:

$$\det(\lambda\, I_{3\times3} - I_C) = \lambda^3 + a_2\lambda^2 + a_1\lambda + a_0 = 0 \tag{2.103}$$

where $I_{3\times3}$ is the identity matrix. Hence, the modal matrix $H = [h_1, h_2, h_3]$ is obtained by calculating the right eigenvectors h_i from:

$$(\lambda_i\, I_{3\times3} - I_C)\, h_i = 0; \qquad (i = 1, 2, 3) \tag{2.104}$$

Consequently, the coordinate system $X_CY_CZ_C$ should be rotated about its axes to form a new coordinate system $X'_CY'_CZ'_C$ with unit vectors:

$$e'_x = He_x; \qquad e'_y = He_y; \qquad e'_z = He_z \tag{2.105}$$

Here e_x, e_y and e_z are the unit vectors corresponding to $X_CY_CZ_C$. This in turn implies that the new inertia tensor I'_C will be diagonal, that is:

$$I'_C = \text{diag}\{I'_{x_C}, I'_{y_C}, I'_{z_C}\} = \text{diag}\{\lambda_1, \lambda_2, \lambda_3\} \tag{2.106}$$

The disadvantage with this approach is that the new coordinate system will differ from the longitudinal, lateral and normal symmetry axes of the vehicle. This can be compensated for in the control design by transforming the desired state trajectory to the $X'_CY'_CZ'_C$ system. Applying these results to (2.89) yields the following simple representation:

$$\begin{array}{rclrcl} m(\dot{u} - vr + wq) &=& X; & I_{x_C}\dot{p} + (I_{z_C} - I_{y_C})qr &=& K \\ m(\dot{v} - wp + ur) &=& Y; & I_{y_C}\dot{q} + (I_{x_C} - I_{z_C})rp &=& M \\ m(\dot{w} - uq + vp) &=& Z; & I_{z_C}\dot{r} + (I_{y_C} - I_{x_C})pq &=& N \end{array} \tag{2.107}$$

(2) Origin O Chosen such that I_0 is Diagonal

If it is often convenient to let the body axes coincide with the principal axes of inertia or the longitudinal, lateral and normal symmetry axes of the vehicle, the origin of the body-fixed coordinate system can then be chosen such that the inertia tensor of the body-fixed coordinate system will be diagonal, that is $I_0 = \text{diag}\{I_x, I_y, I_z\}$, by applying the following theorem:

Theorem 2.3 (Parallel Axes Theorem)
The inertia tensor I_0 about an arbitrary origin O is defined as:

$$I_0 = I_C - m\, S(r_G)\, S(r_G) = I_C - m(r_G r_G^T - r_G^T r_G\, I_{3\times3}) \tag{2.108}$$

where $I_{3\times3}$ is the identity matrix, I_C is the inertia tensor about the body's center of gravity and $S(r_G)$ is defined in (2.6).
□

Expanding (2.108) with $I_0 = \text{diag}\{I_x, I_y, I_z\}$, yields the following set of equations:

$$
\begin{aligned}
I_x &= I_{x_C} + m(y_G^2 + z_G^2) \\
I_y &= I_{y_C} + m(x_G^2 + z_G^2) \\
I_z &= I_{z_C} + m(x_G^2 + y_G^2)
\end{aligned} \tag{2.109}
$$

where x_G, y_G and z_G must be chosen such that:

$$
\begin{aligned}
m I_{y_C z_C}\, x_G^2 &= -I_{x_C y_C} I_{x_C z_C} \\
m I_{x_C z_C}\, y_G^2 &= -I_{x_C y_C} I_{y_C z_C} \\
m I_{x_C y_C}\, z_G^2 &= -I_{x_C z_C} I_{y_C z_C}
\end{aligned} \tag{2.110}
$$

are satisfied. The proof is left as an exercise. Hence, the rigid-body equations of motion can be expressed as:

$$
\begin{aligned}
m\left[\dot{u} - vr + wq - x_G(q^2 + r^2) + y_G(pq - \dot{r}) + z_G(pr + \dot{q})\right] &= X \\
m\left[\dot{v} - wp + ur - y_G(r^2 + p^2) + z_G(qr - \dot{p}) + x_G(qp + \dot{r})\right] &= Y \\
m\left[\dot{w} - uq + vp - z_G(p^2 + q^2) + x_G(rp - \dot{q}) + y_G(rq + \dot{p})\right] &= Z \\
I_x\dot{p} + (I_z - I_y)qr + m\left[y_G(\dot{w} - uq + vp) - z_G(\dot{v} - wp + ur)\right] &= K \\
I_y\dot{q} + (I_x - I_z)rp + m\left[z_G(\dot{u} - vr + wq) - x_G(\dot{w} - uq + vp)\right] &= M \\
I_z\dot{r} + (I_y - I_x)pq + m\left[x_G(\dot{v} - wp + ur) - y_G(\dot{u} - vr + wq)\right] &= N
\end{aligned} \tag{2.111}
$$

This representation ensures that the X_0, Y_0 and Z_0 axes will correspond to the longitudinal, lateral and normal direction of the vehicle, respectively.

2.4 Hydrodynamic Forces and Moments

In basic hydrodynamics it is common to assume that the hydrodynamic forces and moments on a rigid body can be linearly superposed by considering two sub-problems (see Faltinsen 1990).

Sub-Problem 1 (Radiation-Induced Forces)

Forces on the body when the body is forced to oscillate with the wave excitation frequency and there are no incident waves.

The radiation-induced forces and moments can be identified as the sum of three new components:

(1) *Added mass* due to the inertia of the surrounding fluid.

(2) *Radiation-induced potential damping* due to the energy carried away by generated surface waves.

(3) *Restoring forces* due to Archimedes (weight and buoyancy).

The contribution from these three components can be expressed mathematically as:

$$\tau_R = -\underbrace{M_A\,\dot{\nu} - C_A(\nu)\,\nu}_{\text{added mass}} - \underbrace{D_P(\nu)\,\nu}_{\text{potential damping}} - \underbrace{g(\eta)}_{\text{restoring forces}} \tag{2.112}$$

In addition to radiation-induced potential damping we have to include other damping effects like skin friction, wave drift damping and damping due to vortex shedding, that is:

$$\tau_D = -\underbrace{D_S(\nu)\,\nu}_{\substack{\text{skin friction}}} - \underbrace{D_W(\nu)\,\nu}_{\substack{\text{wave drift}\\ \text{damping}}} - \underbrace{D_M(\nu)\,\nu}_{\substack{\text{damping due to}\\ \text{vortex shedding}}} \tag{2.113}$$

This implies that the hydrodynamic forces and moments τ_H can be written as the sum of τ_R and τ_D, that is:

$$\tau_H = -M_A\,\dot{\nu} - C_A(\nu)\,\nu - D(\nu)\,\nu - g(\eta) \tag{2.114}$$

where the total hydrodynamic damping matrix $D(\nu)$ is defined as:

$$D(\nu) \triangleq D_P(\nu) + D_S(\nu) + D_W(\nu) + D_M(\nu) \tag{2.115}$$

Sub-Problem 2 (Froude-Kriloff and Diffraction Forces)

Forces on the body when the body is restrained from oscillating and there are incident regular waves.

Froude-Kriloff and diffraction forces will be treated separately in Chapter 3 where environmental forces are discussed in the context of waves, wind and currents. A more general discussion on marine hydrodynamics is found in Faltinsen (1990), Newman (1977) and Sarpkaya (1981).

Model Representation Used in This Text

The right-hand side vector term of (2.89) and (2.90) represents the external forces and moments acting on the vehicle. These forces can be classified according to:

- Radiation-induced forces (Sections 2.4.1 to 2.4.3)
  - added inertia
  - hydrodynamic damping
  - restoring forces

- Environmental forces (Sections 3.1 to 3.4):
  - ocean currents
  - waves
  - wind
- Propulsion forces (Sections 4.1, 5.4, 6.2, 7.1 and 7.2):
  - thruster/propeller forces
  - control surfaces/rudder forces

We will restrict our treatment to a nonlinear model representation of the dynamic equations of motion similar to that of Fossen (1991), that is:

$$M_{RB}\,\dot{\nu} + C_{RB}(\nu)\,\nu = \tau_{RB} \tag{2.116}$$

$$\tau_{RB} = \tau_H + \tau_E + \tau \tag{2.117}$$

Here τ_H is defined in (2.114), τ_E is used to describe the *environmental* forces and moments acting on the vehicle and τ is the *propulsion* forces and moments. Substitution of (2.117) into (2.116) together with (2.114) yields the following representation of the 6 DOF dynamic equations of motion:

$$\boxed{M\,\dot{\nu} + C(\nu)\,\nu + D(\nu)\,\nu + g(\eta) = \tau_E + \tau} \tag{2.118}$$

where

$$M \triangleq M_{RB} + M_A; \qquad C(\nu) \triangleq C_{RB}(\nu) + C_A(\nu)$$

We will now be discussing the terms in (2.118) in more detail.

2.4.1 Added Mass and Inertia

In the previous section, we have shown that the rigid body dynamics of a marine vehicle can be derived by applying the *Newtonian* formalism. As for the rigid-body dynamics, it is desirable to separate the added mass forces and moments in terms which belong to an added inertia matrix M_A and a matrix of hydrodynamic Coriolis and centripetal terms denoted $C_A(\nu)$. To derive the expressions for these two matrices we will use an *energy approach* in terms of Kirchhoff's equations.

The concept of added mass is usually misunderstood to be a finite amount of water connected to the vehicle such that the vehicle and the fluid represents a new system with mass larger than the original system. This is *not* true since the vehicle motion will force the whole fluid to oscillate with different fluid particle amplitudes in phase with the forced harmonic motion of the vehicle. However, the amplitudes will decay far away from the body and may therefore be negligible. Added (virtual) mass should be understood as pressure-induced forces and moments due to a forced harmonic motion of the body which are proportional to the acceleration of the body. Consequently, the added mass forces and the acceleration will be 180 degrees out of phase to the forced harmonic motion.

Fluid Kinetic Energy

For completely submerged vehicles we will assume that the added mass coefficients are constant and thus independent of the wave circular frequency. Together with this assumption, we will use the concept of fluid kinetic energy to derive the added mass terms. Moreover, any motion of the vehicle will induce a motion in the otherwise stationary fluid. In order to allow the vehicle to pass through the fluid, the fluid must move aside and then close behind the vehicle. As a consequence, the fluid passage possesses kinetic energy that it would lack if the vehicle was not in motion.

The expression for the fluid kinetic energy T_A, see Lamb (1932), can be written as a quadratic form of the body axis velocity vector components, that is:

$$T_A = \frac{1}{2}\boldsymbol{\nu}^T \boldsymbol{M}_A \boldsymbol{\nu} \tag{2.119}$$

Here $\boldsymbol{M}_A$ is a 6×6 added inertia matrix defined as:

$$\boldsymbol{M}_A = \begin{bmatrix} \boldsymbol{A}_{11} & \boldsymbol{A}_{12} \\ \boldsymbol{A}_{21} & \boldsymbol{A}_{22} \end{bmatrix} \triangleq -\begin{bmatrix} X_{\dot{u}} & X_{\dot{v}} & X_{\dot{w}} & X_{\dot{p}} & X_{\dot{q}} & X_{\dot{r}} \\ Y_{\dot{u}} & Y_{\dot{v}} & Y_{\dot{w}} & Y_{\dot{p}} & Y_{\dot{q}} & Y_{\dot{r}} \\ Z_{\dot{u}} & Z_{\dot{v}} & Z_{\dot{w}} & Z_{\dot{p}} & Z_{\dot{q}} & Z_{\dot{r}} \\ K_{\dot{u}} & K_{\dot{v}} & K_{\dot{w}} & K_{\dot{p}} & K_{\dot{q}} & K_{\dot{r}} \\ M_{\dot{u}} & M_{\dot{v}} & M_{\dot{w}} & M_{\dot{p}} & M_{\dot{q}} & M_{\dot{r}} \\ N_{\dot{u}} & N_{\dot{v}} & N_{\dot{w}} & N_{\dot{p}} & N_{\dot{q}} & N_{\dot{r}} \end{bmatrix} \tag{2.120}$$

The notation of SNAME (1950) is used in this expression; for instance the hydrodynamic added mass force Y_A along the y-axis due to an acceleration $\dot{u}$ in the x-direction is written as:

$$Y_A = Y_{\dot{u}}\dot{u} \quad \text{where} \quad Y_{\dot{u}} \triangleq \frac{\partial Y}{\partial \dot{u}} \tag{2.121}$$

In some textbooks the notation $A_{ij} = -\{M_A\}_{ij}$ is used instead. This implies that $A_{21} = -Y_{\dot{u}}$ in the example above. It should be noted that the hydrodynamic derivatives $A_{11} = -X_{\dot{u}}, A_{22} = -Y_{\dot{v}}, A_{33} = -Z_{\dot{w}}, A_{44} = -K_{\dot{p}}, A_{55} = -M_{\dot{q}}$ and $A_{66} = -N_{\dot{r}}$ corresponding to the diagonal of the added inertia matrix, will all be positive for most applications. However for certain frequencies negative added mass values have been documented for catamarans, bulb sections and submerged body sections close to the free surface. For completely submerged vehicles $\boldsymbol{M}_A$ will always be strictly positive, that is $\boldsymbol{M}_A > \boldsymbol{0}$.

Property 2.4 ($\boldsymbol{M}_A$)
For a rigid-body at rest ($U \approx 0$) under the assumption of an ideal fluid, no incident waves, no sea currents and frequency independence the added inertia matrix is positive definite:

$$\boldsymbol{M}_A = \boldsymbol{M}_A^T > \boldsymbol{0}$$

Proof: *Newman (1977).*

Remark 1: *In a real fluid the 36 elements of $\boldsymbol{M}_A$ may all be distinct but still $\boldsymbol{M}_A > \mathbf{0}$. Experience has shown that the numerical values of the added mass derivatives in a real fluid are usually in good agreement with those obtained from ideal theory (see Wendel 1956). Hence, $\boldsymbol{M}_A = \boldsymbol{M}_A^T > \mathbf{0}$ is a good approximation.*

Remark 2: *It should be noted that for surface ships moving with a speed $U \gg 0$ in waves, Salvesen, Tuck and Faltinsen (1970) have shown by applying strip theory that $\boldsymbol{M}_A(U) \neq \boldsymbol{M}_A^T(U)$. However, for underwater vehicles (ROVs) and foilborne catamarans operating outside the wave-affected zone, symmetry and frequency independence have been shown to be reasonable assumptions. This is also a good approximation for positioned ships ($U \approx 0$).*
□

Consider a symmetrical added inertia matrix (without loss of generality) having 21 distinct hydrodynamic derivatives. The added mass forces and moments can be derived by applying potential theory. The method is based on the assumptions of inviscid fluid, no circulation and that the body is completely submerged in an unbounded fluid. The last assumption is violated at the seabed, near underwater installations and at the surface. However, this is not a practical problem since *double-body* theory can be applied (Faltinsen 1990). Expanding (2.119) under the assumption that $\boldsymbol{M}_A = \boldsymbol{M}_A^T$, yields:

$$\begin{aligned} 2T_A = \; & -X_{\dot{u}}u^2 - Y_{\dot{v}}v^2 - Z_{\dot{w}}w^2 - 2Y_{\dot{w}}vw - 2X_{\dot{w}}wu - 2X_{\dot{v}}uv \\ & -K_{\dot{p}}p^2 - M_{\dot{q}}q^2 - N_{\dot{r}}r^2 - 2M_{\dot{r}}qr - 2K_{\dot{r}}rp - 2K_{\dot{q}}pq \\ & -2p(X_{\dot{p}}u + Y_{\dot{p}}v + Z_{\dot{p}}w) \\ & -2q(X_{\dot{q}}u + Y_{\dot{q}}v + Z_{\dot{q}}w) \\ & -2r(X_{\dot{r}}u + Y_{\dot{r}}v + Z_{\dot{r}}w) \end{aligned} \tag{2.122}$$

Added Mass Forces and Moments

Based on the kinetic energy T_A of the fluid it is straightforward to derive the added mass forces and moments. This usually done by application of *Kirchhoff's equations* (Kirchhoff 1869), which simply relates the fluid energy to the forces and moments acting on the vehicle. Consider *Kirchhoff's equations* in component form (see Milne-Thomson 1968):

$$\begin{aligned} \frac{d}{dt}\frac{\partial T_A}{\partial u} &= r\frac{\partial T_A}{\partial v} - q\frac{\partial T_A}{\partial w} - X_A \\ \frac{d}{dt}\frac{\partial T_A}{\partial v} &= p\frac{\partial T_A}{\partial w} - r\frac{\partial T_A}{\partial u} - Y_A \\ \frac{d}{dt}\frac{\partial T_A}{\partial w} &= q\frac{\partial T_A}{\partial u} - p\frac{\partial T_A}{\partial v} - Z_A \end{aligned}$$

$$\begin{aligned}
\frac{d}{dt}\frac{\partial T_A}{\partial p} &= w\frac{\partial T_A}{\partial v} - v\frac{\partial T_A}{\partial w} + r\frac{\partial T_A}{\partial q} - q\frac{\partial T_A}{\partial r} - K_A \\
\frac{d}{dt}\frac{\partial T_A}{\partial q} &= u\frac{\partial T_A}{\partial w} - w\frac{\partial T_A}{\partial u} + p\frac{\partial T_A}{\partial r} - r\frac{\partial T_A}{\partial p} - M_A \\
\frac{d}{dt}\frac{\partial T_A}{\partial r} &= v\frac{\partial T_A}{\partial u} - u\frac{\partial T_A}{\partial v} + q\frac{\partial T_A}{\partial p} - p\frac{\partial T_A}{\partial q} - N_A
\end{aligned} \tag{2.123}$$

Substituting (2.122) into (2.123) gives the following expressions for the added mass terms (Imlay 1961):

$$\begin{aligned}
X_A &= X_{\dot{u}}\dot{u} + X_{\dot{w}}(\dot{w} + uq) + X_{\dot{q}}\dot{q} + Z_{\dot{w}}wq + Z_{\dot{q}}q^2 \\
&\quad + X_{\dot{v}}\dot{v} + X_{\dot{p}}\dot{p} + X_{\dot{r}}\dot{r} - Y_{\dot{v}}vr - Y_{\dot{p}}rp - Y_{\dot{r}}r^2 \\
&\quad - X_{\dot{v}}ur - Y_{\dot{w}}wr \\
&\quad + Y_{\dot{w}}vq + Z_{\dot{p}}pq - (Y_{\dot{q}} - Z_{\dot{r}})qr \\
Y_A &= X_{\dot{v}}\dot{u} + Y_{\dot{w}}\dot{w} + Y_{\dot{q}}\dot{q} \\
&\quad + Y_{\dot{v}}\dot{v} + Y_{\dot{p}}\dot{p} + Y_{\dot{r}}\dot{r} + X_{\dot{v}}vr - Y_{\dot{w}}vp + X_{\dot{r}}r^2 + (X_{\dot{p}} - Z_{\dot{r}})rp - Z_{\dot{p}}p^2 \\
&\quad - X_{\dot{w}}(up - wr) + X_{\dot{u}}ur - Z_{\dot{w}}wp \\
&\quad - Z_{\dot{q}}pq + X_{\dot{q}}qr \\
Z_A &= X_{\dot{w}}(\dot{u} - wq) + Z_{\dot{w}}\dot{w} + Z_{\dot{q}}\dot{q} - X_{\dot{u}}uq - X_{\dot{q}}q^2 \\
&\quad + Y_{\dot{w}}\dot{v} + Z_{\dot{p}}\dot{p} + Z_{\dot{r}}\dot{r} + Y_{\dot{v}}vp + Y_{\dot{r}}rp + Y_{\dot{p}}p^2 \\
&\quad + X_{\dot{v}}up + Y_{\dot{w}}wp \\
&\quad - X_{\dot{v}}vq - (X_{\dot{p}} - Y_{\dot{q}})pq - X_{\dot{r}}qr \\
K_A &= X_{\dot{p}}\dot{u} + Z_{\dot{p}}\dot{w} + K_{\dot{q}}\dot{q} - X_{\dot{v}}wu + X_{\dot{r}}uq - Y_{\dot{w}}w^2 - (Y_{\dot{q}} - Z_{\dot{r}})wq + M_{\dot{r}}q^2 \\
&\quad + Y_{\dot{p}}\dot{v} + K_{\dot{p}}\dot{p} + K_{\dot{r}}\dot{r} + Y_{\dot{w}}v^2 - (Y_{\dot{q}} - Z_{\dot{r}})vr + Z_{\dot{p}}vp - M_{\dot{r}}r^2 - K_{\dot{q}}rp \\
&\quad + X_{\dot{w}}uv - (Y_{\dot{v}} - Z_{\dot{w}})vw - (Y_{\dot{r}} + Z_{\dot{q}})wr - Y_{\dot{p}}wp - X_{\dot{q}}ur \\
&\quad + (Y_{\dot{r}} + Z_{\dot{q}})vq + K_{\dot{r}}pq - (M_{\dot{q}} - N_{\dot{r}})qr \\
M_A &= X_{\dot{q}}(\dot{u} + wq) + Z_{\dot{q}}(\dot{w} - uq) + M_{\dot{q}}\dot{q} - X_{\dot{w}}(u^2 - w^2) - (Z_{\dot{w}} - X_{\dot{u}})wu \\
&\quad + Y_{\dot{q}}\dot{v} + K_{\dot{q}}\dot{p} + M_{\dot{r}}\dot{r} + Y_{\dot{p}}vr - Y_{\dot{r}}vp - K_{\dot{r}}(p^2 - r^2) + (K_{\dot{p}} - N_{\dot{r}})rp \\
&\quad - Y_{\dot{w}}uv + X_{\dot{v}}vw - (X_{\dot{r}} + Z_{\dot{p}})(up - wr) + (X_{\dot{p}} - Z_{\dot{r}})(wp + ur) \\
&\quad - M_{\dot{r}}pq + K_{\dot{q}}qr \\
N_A &= X_{\dot{r}}\dot{u} + Z_{\dot{r}}\dot{w} + M_{\dot{r}}\dot{q} + X_{\dot{v}}u^2 + Y_{\dot{w}}wu - (X_{\dot{p}} - Y_{\dot{q}})uq - Z_{\dot{p}}wq - K_{\dot{q}}q^2 \\
&\quad + Y_{\dot{r}}\dot{v} + K_{\dot{r}}\dot{p} + N_{\dot{r}}\dot{r} - X_{\dot{v}}v^2 - X_{\dot{r}}vr - (X_{\dot{p}} - Y_{\dot{q}})vp + M_{\dot{r}}rp + K_{\dot{q}}p^2 \\
&\quad - (X_{\dot{u}} - Y_{\dot{v}})uv - X_{\dot{w}}vw + (X_{\dot{q}} + Y_{\dot{p}})up + Y_{\dot{r}}ur + Z_{\dot{q}}wp \\
&\quad - (X_{\dot{q}} + Y_{\dot{p}})vq - (K_{\dot{p}} - M_{\dot{q}})pq - K_{\dot{r}}qr
\end{aligned} \tag{2.124}$$

Imlay (1961) arranged the equations in four lines with longitudinal components on the first line and lateral components on the second line. The third line consists of mixed terms involving u or w as one factor. If one or both of these velocities are large enough to be treated as a constant the third line may be treated as an additional term to the lateral equation of motion. The fourth line

contains mixed terms that usually can be neglected as second order terms. It should be noted that the off-diagonal elements of M_A will be small compared to the diagonal elements for most practical applications. A more detailed discussion on the different added mass derivatives is found in Humphreys and Watkinson (1978).

Property 2.5 (C_A)
For a rigid-body moving through an ideal fluid the hydrodynamic Coriolis and centripetal matrix $C_A(\nu)$ can always be parameterized such that $C_A(\nu)$ is skew-symmetrical, that is:

$$C_A(\nu) = -C_A^T(\nu) \quad \forall \quad \nu \in \mathbb{R}^6$$

by defining:

$$C_A(\nu) = \begin{bmatrix} 0_{3\times 3} & -S(A_{11}\,\nu_1 + A_{12}\,\nu_2) \\ -S(A_{11}\,\nu_1 + A_{12}\,\nu_2) & -S(A_{21}\,\nu_1 + A_{22}\,\nu_2 \end{bmatrix} \tag{2.125}$$

where A_{ij} $(i,j = 1,2)$ are defined in (2.120).

Proof: *Substituting:*

$$M = M_A = \begin{bmatrix} A_{11} & A_{12} \\ A_{21} & A_{22} \end{bmatrix} \tag{2.126}$$

into (2.93) in Theorem 2.2 directly proves (2.125).
□

Formula (2.125) can be written in component form according to:

$$C_A(\nu) = \begin{bmatrix} 0 & 0 & 0 & 0 & -a_3 & a_2 \\ 0 & 0 & 0 & a_3 & 0 & -a_1 \\ 0 & 0 & 0 & -a_2 & a_1 & 0 \\ 0 & -a_3 & a_2 & 0 & -b_3 & b_2 \\ a_3 & 0 & -a_1 & b_3 & 0 & -b_1 \\ -a_2 & a_1 & 0 & -b_2 & b_1 & 0 \end{bmatrix} \tag{2.127}$$

where

$$\begin{aligned} a_1 &= X_{\dot{u}}u + X_{\dot{v}}v + X_{\dot{w}}w + X_{\dot{p}}p + X_{\dot{q}}q + X_{\dot{r}}r \\ a_2 &= X_{\dot{v}}u + Y_{\dot{v}}v + Y_{\dot{w}}w + Y_{\dot{p}}p + Y_{\dot{q}}q + Y_{\dot{r}}r \\ a_3 &= X_{\dot{w}}u + Y_{\dot{w}}v + Z_{\dot{w}}w + Z_{\dot{p}}p + Z_{\dot{q}}q + Z_{\dot{r}}r \\ b_1 &= X_{\dot{p}}u + Y_{\dot{p}}v + Z_{\dot{p}}w + K_{\dot{p}}p + K_{\dot{q}}q + K_{\dot{r}}r \\ b_2 &= X_{\dot{q}}u + Y_{\dot{q}}v + Z_{\dot{q}}w + K_{\dot{q}}p + M_{\dot{q}}q + M_{\dot{r}}r \\ b_3 &= X_{\dot{r}}u + Y_{\dot{r}}v + Z_{\dot{r}}w + K_{\dot{r}}p + M_{\dot{r}}q + N_{\dot{r}}r \end{aligned} \tag{2.128}$$

Surface Ships

For surface ships like tankers, cargo ships, cruise-liners etc. it is common to decouple the surge mode from the steering dynamics. Similarly, the heave, pitch and roll modes are neglected under the assumption that these motion variables are small. This implies that the contribution from the added mass derivatives on a surface ship moving with forward speed $U \gg 0$ and thus $M_A \neq M_A^T$ is:

$$\begin{bmatrix} X_A \\ Y_A \\ N_A \end{bmatrix} = \begin{bmatrix} X_{\dot{u}} & 0 & 0 \\ 0 & Y_{\dot{v}} & Y_{\dot{r}} \\ 0 & N_{\dot{v}} & N_{\dot{r}} \end{bmatrix} \begin{bmatrix} \dot{u} \\ \dot{v} \\ \dot{r} \end{bmatrix} + \begin{bmatrix} 0 & 0 & -Y_{\dot{v}} v - \frac{Y_{\dot{r}}+N_{\dot{v}}}{2} r \\ 0 & 0 & X_{\dot{u}} u \\ Y_{\dot{v}} v + \frac{Y_{\dot{r}}+N_{\dot{v}}}{2} r & -X_{\dot{u}} u & 0 \end{bmatrix} \begin{bmatrix} u \\ v \\ r \end{bmatrix}$$

For ship positioning we have that $U \approx 0$ and therefore $M_A = M_A^T$. Hence, we can replace $N_{\dot{v}}$ with $Y_{\dot{r}}$ in the above expression which yields:

$$\begin{bmatrix} X_A \\ Y_A \\ N_A \end{bmatrix} = \begin{bmatrix} X_{\dot{u}} & 0 & 0 \\ 0 & Y_{\dot{v}} & Y_{\dot{r}} \\ 0 & Y_{\dot{r}} & N_{\dot{r}} \end{bmatrix} \begin{bmatrix} \dot{u} \\ \dot{v} \\ \dot{r} \end{bmatrix} + \begin{bmatrix} 0 & 0 & -(Y_{\dot{v}} v + Y_{\dot{r}} r) \\ 0 & 0 & X_{\dot{u}} u \\ Y_{\dot{v}} v + Y_{\dot{r}} r & -X_{\dot{u}} u & 0 \end{bmatrix} \begin{bmatrix} u \\ v \\ r \end{bmatrix}$$

Underwater Vehicles

In general, the motion of an underwater vehicle moving in 6 DOF at high speed will be highly nonlinear and coupled. However, in many ROV applications the vehicle will only be allowed to move at low speed. If the vehicle also has three planes of symmetry, this suggests that we can neglect the contribution from the off-diagonal elements in the added mass matrix M_A. Hence, the following simple expressions for M_A and C_A are obtained:

$$M_A = -\text{diag}\{ X_{\dot{u}}, Y_{\dot{v}}, Z_{\dot{w}}, K_{\dot{p}}, M_{\dot{q}}, N_{\dot{r}} \} \tag{2.129}$$

$$C_A(\nu) = \begin{bmatrix} 0 & 0 & 0 & 0 & -Z_{\dot{w}} w & Y_{\dot{v}} v \\ 0 & 0 & 0 & Z_{\dot{w}} w & 0 & -X_{\dot{u}} u \\ 0 & 0 & 0 & -Y_{\dot{v}} v & X_{\dot{u}} u & 0 \\ 0 & -Z_{\dot{w}} w & Y_{\dot{v}} v & 0 & -N_{\dot{r}} r & M_{\dot{q}} q \\ Z_{\dot{w}} w & 0 & -X_{\dot{u}} u & N_{\dot{r}} r & 0 & -K_{\dot{p}} p \\ -Y_{\dot{v}} v & X_{\dot{u}} u & 0 & -M_{\dot{q}} q & K_{\dot{p}} p & 0 \end{bmatrix} \tag{2.130}$$

The diagonal structure is highly attractive since off-diagonal elements are difficult to determine from experiments as well as theory. In practice, the diagonal approximation is found to be quite good for many applications. This is due to the fact that the off-diagonal elements of a positive matrix (inertia) will be much smaller than their diagonal counterparts.

Strip Theory

For slender bodies an estimate of the hydrodynamic derivatives can be obtained by applying *strip theory*. The principle of strip theory involves dividing the

submerged part of the vehicle into a number of strips. Hence, two-dimensional hydrodynamic coefficients for added mass can be computed for each strip and summarized over the length of the body to yield the three-dimensional coefficients. The two-dimensional added mass coefficients in surge, sway and roll for some bodies are given in Table 2.2. For a *submerged slender vehicle* we can use the following formulas:

$$A_{11} = -X_{\dot{u}} = \int_{-L/2}^{L/2} A_{11}^{(2D)}(y,z)\,dx \approx 0.10\,m \tag{2.131}$$

$$A_{22} = -Y_{\dot{v}} = \int_{-L/2}^{L/2} A_{22}^{(2D)}(y,z)\,dx \tag{2.132}$$

$$A_{33} = -Z_{\dot{w}} = \int_{-L/2}^{L/2} A_{33}^{(2D)}(y,z)\,dx \tag{2.133}$$

$$A_{44} = -K_{\dot{p}} = \int_{-L/2}^{L/2} A_{44}^{(2D)}(y,z)\,dx \tag{2.134}$$

$$A_{55} = -M_{\dot{q}} = \int_{-L/2}^{L/2} A_{55}^{(2D)}(y,z)\,dx \tag{2.135}$$

$$A_{66} = -N_{\dot{r}} = \int_{-L/2}^{L/2} A_{66}^{(2D)}(y,z)\,dx \tag{2.136}$$

where $A_{22}^{(2D)}(y,z)$, $A_{33}^{(2D)}(y,z)$ and $A_{44}^{(2D)}(y,z)$ are usually approximated with values similar to those of Table 2.2.

Table 2.2: Two-dimensional added mass coefficients $A_{ii}^{(2D)}(y,z)$ for $(i = 2...4)$

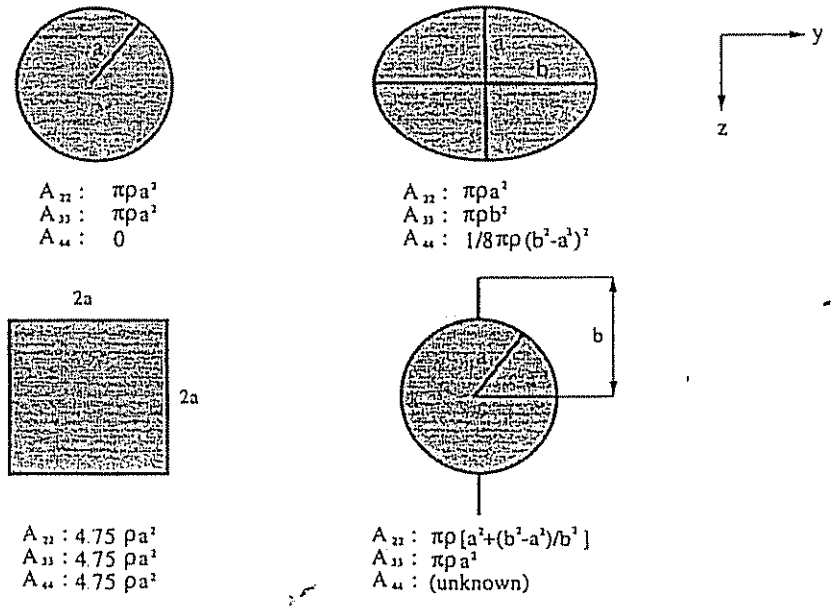

The two-dimensional added inertia moment in roll, pitch and yaw can be rewritten according to:

$$\int_{-L/2}^{L/2} A_{44}^{(2D)}(y,z)\,dx \triangleq \int_{-B/2}^{B/2} y^2\, A_{33}^{(2D)}(x,z)\,dy + \int_{-H/2}^{H/2} z^2\, A_{22}^{(2D)}(x,y)\,dz$$

$$\int_{-L/2}^{L/2} A_{55}^{(2D)}(y,z)\,dx \triangleq \int_{-L/2}^{L/2} x^2\, A_{33}^{(2D)}(y,z)\,dx + \int_{-H/2}^{H/2} z^2\, A_{11}^{(2D)}(x,y)\,dz$$

$$\int_{-L/2}^{L/2} A_{66}^{(2D)}(y,z)\,dx \triangleq \int_{-B/2}^{B/2} y^2\, A_{11}^{(2D)}(x,z)\,dy + \int_{-L/2}^{L/2} x^2\, A_{22}^{(2D)}(y,z)\,dx$$

where L, B and H are the main dimensions of the vehicle. For a rectangle-shaped body Table 2.3 can be used to compute two-dimensional added mass derivatives.

Table 2.3: Two-dimensional added mass for a rectangular cross-section

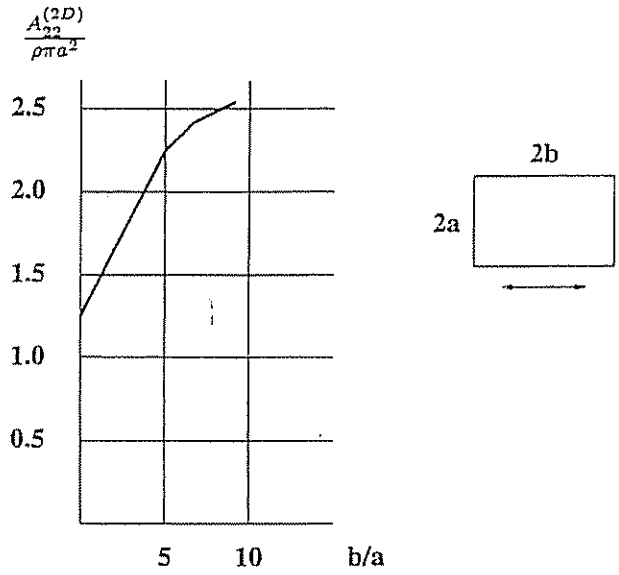

For a *surface ship* we can approximate A_{22} and A_{66} by treating the submerged part of the ship as a *half cylinder* with added mass:

$$A_{22}^{(2D)} = \frac{1}{2}\,\rho\pi D^2(x) \tag{2.137}$$

where the hull draft $D(x)$ is taken to be the cylinder radius and ρ is the water density. Hence, the following set of formulas can be used:

$$A_{11} = -X_{\dot{u}} \approx 0.05\ m \tag{2.138}$$

$$A_{22} = -Y_{\dot{v}} = \frac{1}{2}\int_{-L/2}^{L/2} \rho\pi D^2(x)\,dx \overset{D(x)=D}{=} \frac{1}{2}\rho\pi D^2 L \tag{2.139}$$

$$A_{66} = -N_{\dot{r}} = \frac{1}{2}\int_{-B/2}^{B/2} y^2 \frac{0.1m}{B}\,dy + \frac{1}{2}\int_{-L/2}^{L/2} x^2\,\rho\pi D^2(x)\,dx$$
$$\overset{D(x)=D}{=} \frac{1}{24}(0.1\,m\,B^2 + \rho\pi D^2 L^3) \tag{2.140}$$

Two-dimensional added mass coefficients $A_{22}^{(2D)}$ and $A_{33}^{(2D)}$ as function of the circular frequency of oscillation ω for a circular cylinder is shown in Figure 2.4. Notice that the cylinder approximation in the ship example is based on the assumption that $A_{22}^{(2D)}/(\rho A)$ in Figure 2.4 is equal to one. This is only true for a limited frequency interval.

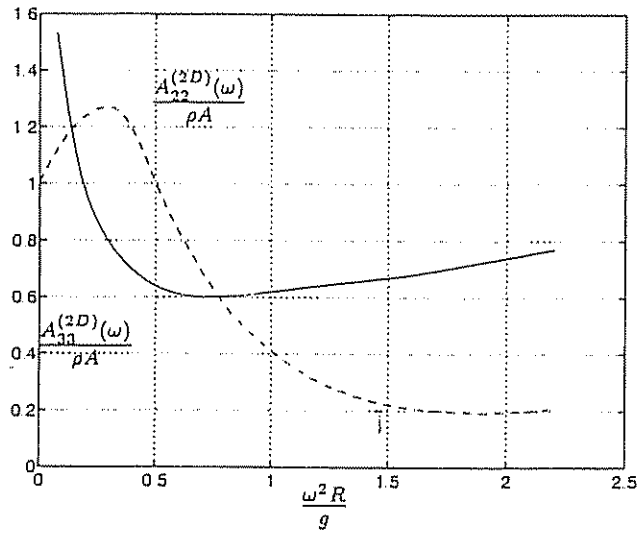

Figure 2.4: Two-dimensional added mass in heave and sway for a circular cylinder (infinite water depth) as a function of wave circular frequency. In the figure $A = 0.5\pi R^2$ where R is the cylinder radius.

Added Mass Derivatives for a Prolate Ellipsoid

Fortunately, many of the added mass derivatives contained in the general expressions for added mass are either zero or mutually related when the body has various symmetries. Consider an ellipsoid totally submerged and with the origin at the center of the ellipsoid, described as:

$$\frac{x^2}{a^2} + \frac{y^2}{b^2} + \frac{z^2}{c^2} = 1 \tag{2.141}$$

Here a, b and c are the semi-axes, see Figure 2.5. A prolate spheroid is obtained by letting $b = c$ and $a > b$. Imlay (1961) gives the following expressions for the

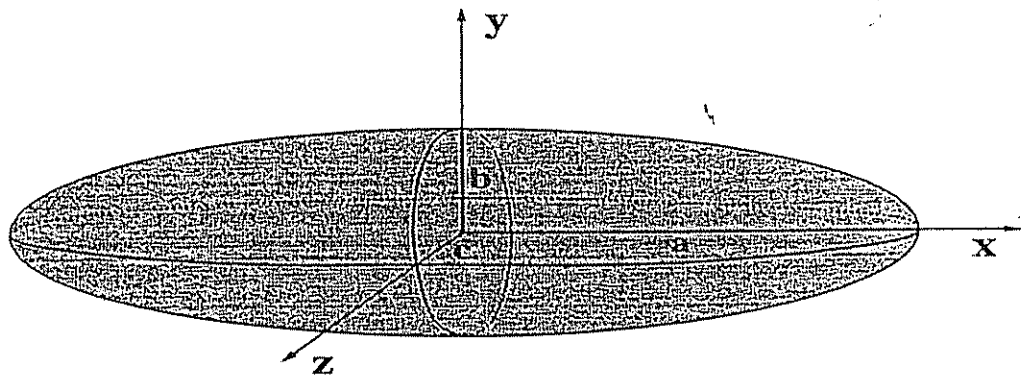

Figure 2.5: Ellipsoid with semi-axes a, b and c.

diagonal added mass derivatives (cross-coupling terms will be zero due to body symmetry about three planes):

$$X_{\dot{u}} = -\frac{\alpha_0}{2-\alpha_0} m \tag{2.142}$$

$$Y_{\dot{v}} = Z_{\dot{w}} = -\frac{\beta_0}{2-\beta_0} m \tag{2.143}$$

$$K_{\dot{p}} = 0 \tag{2.144}$$

$$N_{\dot{r}} = M_{\dot{q}} = -\frac{1}{5} \frac{(b^2-a^2)^2(\alpha_0-\beta_0)}{2(b^2-a^2)+(b^2+a^2)(\beta_0-\alpha_0)} m \tag{2.145}$$

where the mass of the prolate spheroid is:

$$m = \frac{4}{3}\pi\rho ab^2 \tag{2.146}$$

Introduce the eccentricity e defined as:

$$e = 1-(b/a)^2 \tag{2.147}$$

Hence, the constants α_0 and β_0 can be calculated as:

$$\alpha_0 = \frac{2(1-e^2)}{e^3}\left(\frac{1}{2}\ln\frac{1+e}{1-e} - e\right) \tag{2.148}$$

$$\beta_0 = \frac{1}{e^2} - \frac{1-e^2}{2e^3}\ln\frac{1+e}{1-e} \tag{2.149}$$

An alternative representation of these mass derivatives is presented by Lamb (1932) who defines Lamb's k-factors as:

$$k_1 = \frac{\alpha_0}{2-\alpha_0} \tag{2.150}$$

$$k_2 = \frac{\beta_0}{2-\beta_0} \tag{2.151}$$

$$k' = \frac{e^4(\beta_0 - \alpha_0)}{(2-e^2)[2e^2 - (2-e^2)(\beta_0 - \alpha_0)]} \tag{2.152}$$

Hence, the definition of the added mass derivatives simplifies to:

$$X_{\dot{u}} = -k_1\, m \tag{2.153}$$

$$Y_{\dot{v}} = Z_{\dot{w}} = -k_2\, m \tag{2.154}$$

$$N_{\dot{r}} = M_{\dot{q}} = -k'\, I_y \tag{2.155}$$

where the moment of inertia of the prolate spheroid is:

$$I_y = I_z = \frac{4}{15}\pi\rho a b^2(a^2+b^2) \tag{2.156}$$

A more general discussion on added mass derivatives for bodies with various symmetries is found in Imlay (1961). Other useful references discussing methods for computation of the added mass derivatives are Humphreys and Watkinson (1978) and Triantafyllou and Amzallag (1984).

2.4.2 Hydrodynamic Damping

As mentioned in the previous section hydrodynamic damping for ocean vehicles is mainly caused by:

$\boldsymbol{D_P(\nu)}$ = radiation-induced potential damping due to forced body oscillations.

$\boldsymbol{D_S(\nu)}$ = linear skin friction due to laminar boundary layers and quadratic skin friction due to turbulent boundary layers.

$\boldsymbol{D_W(\nu)}$ = wave drift damping.

$\boldsymbol{D_M(\nu)}$ = damping due to vortex shedding (Morison's equation).

Consequently, the total hydrodynamic damping matrix can be written as a sum of these components, that is:

$$\boldsymbol{D(\nu)} \triangleq \boldsymbol{D_P(\nu)} + \boldsymbol{D_S(\nu)} + \boldsymbol{D_W(\nu)} + \boldsymbol{D_M(\nu)} \tag{2.157}$$

where $\boldsymbol{D(\nu)}$ satisfies that following property:

Property 2.6 ($\boldsymbol{D}$)
For a rigid-body moving through an ideal fluid the hydrodynamic damping matrix will be real, non-symmetrical and strictly positive (see Appendix A). Hence:

$$\boldsymbol{D(\nu)} > 0 \quad \forall \quad \boldsymbol{\nu} \in \mathbb{R}^6$$

Proof: *The property is trivial since hydrodynamic damping forces are known to be dissipative. Therefore, the quadratic form:*

$$\nu^T D(\nu)\,\nu > 0 \quad \forall \quad \nu \neq 0$$

□

In practical implementations it is difficult to determine higher order terms as well as the off-diagonal terms in the general expression for $D(\nu)$. This suggests the following approximation of $D(\nu)$:

Surface Ships

For low speed slender ships we can decouple the surge mode from the steering modes (sway and yaw). Hence, the linearized damping forces and moments (neglecting heave, roll and pitch) can be written:

$$D(\nu) = -\begin{bmatrix} X_u & 0 & 0 \\ 0 & Y_v & Y_r \\ 0 & N_v & N_r \end{bmatrix} \tag{2.158}$$

Notice that $Y_r \neq N_v$.

Underwater Vehicles

In general, the damping of an underwater vehicle moving in 6 DOF at high speed will be highly nonlinear and coupled. Nevertheless, one rough approximation could be to assume that the vehicle is performing a non-coupled motion, has three planes of symmetry and that terms higher than second order are negligible. This suggests a diagonal structure of $D(\nu)$ with only linear and quadratic damping terms on the diagonal. Moreover,

$$\begin{aligned} D(\nu) = &-\text{diag}\{X_u, Y_v, Z_w, K_p, M_q, N_r\} \\ &-\text{diag}\{X_{u|u|}\,|u|, Y_{v|v|}\,|v|, Z_{w|w|}\,|w|, K_{p|p|}\,|p|, M_{q|q|}\,|q|, N_{r|r|}\,|r|\} \end{aligned} \tag{2.159}$$

Potential Damping

We recall from the beginning of Section 2.4 that forces on the body when the body is forced to oscillate with the wave excitation frequency and there are no incident waves will result in *added mass, damping* and *restoring* forces and moments. The radiation-induced damping term is usually referred to as *potential damping*. However, the contribution from the potential damping terms compared to other dissipative terms like viscous damping terms are negligible for underwater vehicles operating at great depths. However, for surface vehicles the potential damping effect may be significant. For ships linear theory suggests that the radiation-induced forces and moments can be written according to (see Equation 2.112):

$$\tau_R = -A(\omega)\,\ddot{\eta} - B(\omega)\,\dot{\eta} - C\eta \tag{2.160}$$

where $A = -M_A$ is the added inertia matrix, $B = -D_P$ represents linear potential damping, C represents the linearized restoring forces and moments and ω is the wave circular frequency.

The frequency dependency for the 2D damping coefficients in sway and heave for a floating cylinder is illustrated in Figure 2.6. 3D linear damping coefficients in sway and yaw for a slender ship with length L can thus be estimated by using the value for $B_{22}^{(2D)}$ according to:

$$B_{22} = -Y_v = \frac{1}{2}\int_{-L/2}^{L/2} B_{22}^{(2D)}(y,z)\,dx \tag{2.161}$$

$$B_{66} = -N_r = \frac{1}{2}\int_{-L/2}^{L/2} x^2\, B_{22}^{(2D)}(y,z)\,dx \tag{2.162}$$

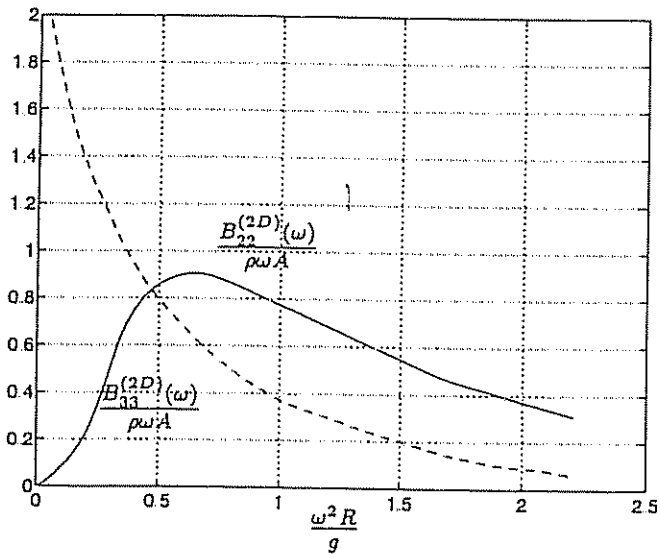

Figure 2.6: Two-dimensional linear damping in heave and sway as a function of wave circular frequency for a circular cylinder (infinite water depth). In the figure $A = 0.5\,\pi R^2$ where R is the cylinder radius.

It should be noted that most ship control systems are based on the assumption that $A(\omega)$ and $B(\omega)$ are frequency-independent ($\omega = 0$) because the control system is only designed to counteract for low-frequency motion components.

Skin Friction

Linear skin friction due to laminar boundary layer theory is important when considering the low-frequency motion of the vehicle. Hence, this effect should

be considered when designing the control system. In addition to linear skin friction there will be a high-frequency contribution due to turbulent boundary layer theory. This is usually referred to as a quadratic or nonlinear skin friction.

Wave Drift Damping

Wave drift damping can be interpreted as added resistance for surface vessels advancing in waves. This type of damping is derived from 2nd-order wave theory. Wave drift damping is the most important damping contribution to surge for higher sea states. This is due to the fact that the wave drift forces are proportional to the square of the significant wave height. Wave drift damping in sway and yaw is small relative to eddy making damping (vortex shedding). A rule of thumb is that 2nd-order wave drift forces are less than 1% of the 1st-order wave forces when the significant wave height is equal to 1 m and 10% when the significant wave height is equal to 10 m.

Damping Due to Vortex Shedding

D'Alambert's paradox states that no hydrodynamic forces act on a solid moving completely submerged with constant velocity in a non-viscous fluid. In a viscous fluid, frictional forces are present such that the system is not conservative with respect to energy. The viscous damping force due to vortex shedding can be modeled as:

$$f(U) = -\frac{1}{2}\rho\, C_D(\mathrm{Rn})\, A\, |U|\, U \tag{2.163}$$

where U is the velocity of the vehicle, A is the projected cross-sectional area, $C_D(\mathrm{Rn})$ is the drag-coefficient based on the representative area and ρ is the water density. This expression is recognized as one of the terms in Morison's equation (see Faltinsen 1990). The drag coefficient $C_D(\mathrm{Rn})$ depends on the *Reynolds number* (see Figure 2.7):

$$\mathrm{Rn} = \frac{U\,D}{\nu} \tag{2.164}$$

where D is the characteristic length of the body and ν is the kinematic viscosity coefficient ($\nu = 1.56 \cdot 10^{-6}$ for salt water at 5^o C with salinity 3.5%), see Appendix F. Quadratic drag in 6 DOF is conveniently expressed as:

$$D_M(\nu)\,\nu = \begin{bmatrix} |\nu|^T\, D_1\, \nu \\ |\nu|^T\, D_2\, \nu \\ |\nu|^T\, D_3\, \nu \\ |\nu|^T\, D_4\, \nu \\ |\nu|^T\, D_5\, \nu \\ |\nu|^T\, D_6\, \nu \end{bmatrix} \tag{2.165}$$

Here D_i $(i = 1...6)$ is 6×6 matrices depending on ρ, C_D and A. Notice that C_D and A will be different for the different matrix elements.

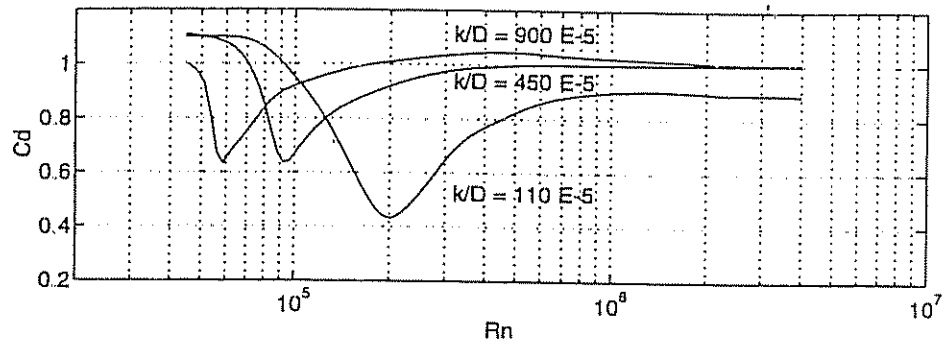

Figure 2.7: Drag coefficient C_D versus Reynolds number Rn for a rough circular cylinder in steady incident flow. Three different surface roughness curves k/D where k is the average height of the surface roughness and D is the cylinder diameter are shown (Faltinsen 1990).

2.4.3 Restoring Forces and Moments

In the hydrodynamic terminology, the gravitational and buoyant forces are called restoring forces. The gravitational force $\boldsymbol{f}_G$ will act through the center of gravity $\boldsymbol{r}_G = [x_G, y_G, z_G]^T$ of the vehicle. Similarly, the buoyant force $\boldsymbol{f}_B$ will act through the center of buoyancy $\boldsymbol{r}_B = [x_B, y_B, z_B]^T$. The restoring forces will have components along the respective body axes.

Underwater Vehicles

Let m be the mass of the vehicle including water in free floating spaces, ∇ the volume of fluid displaced by the vehicle, g the acceleration of gravity (positive downwards) and ρ the fluid density. According to the SNAME (1950) notation, the submerged weight of the body is defined as: $W = mg$, while the buoyancy force is defined as: $B = \rho g \nabla$. By applying the results from Section 2.1.1, the weight and buoyancy force can be transformed to the body-fixed coordinate system with:

$$\boldsymbol{f}_G(\boldsymbol{\eta}_2) = \boldsymbol{J}_1^{-1}(\boldsymbol{\eta}_2) \begin{bmatrix} 0 \\ 0 \\ W \end{bmatrix} \qquad \boldsymbol{f}_B(\boldsymbol{\eta}_2) = -\boldsymbol{J}_1^{-1}(\boldsymbol{\eta}_2) \begin{bmatrix} 0 \\ 0 \\ B \end{bmatrix} \tag{2.166}$$

where $\boldsymbol{J}_1(\boldsymbol{\eta}_2)$ is the Euler angle coordinate transformation matrix defined in Section 2.1.1. According to (2.118), the sign of the restoring forces and moments $\boldsymbol{g}(\boldsymbol{\eta})$ must be changed since this term is included on the left-hand side of Newton's 2nd law. Consequently, the restoring force and moment vector in the body-fixed coordinate system is:

$$g(\eta) = -\begin{bmatrix} f_G(\eta) + f_B(\eta) \\ r_G \times f_G(\eta) + r_B \times f_B(\eta) \end{bmatrix} \tag{2.167}$$

Notice that the z-axis is taken to be positive downwards. Expanding this expression yields:

$$g(\eta) = \begin{bmatrix} & (W-B)\,\mathrm{s}\theta & & \\ - & (W-B)\,\mathrm{c}\theta\mathrm{s}\phi & & \\ - & (W-B)\,\mathrm{c}\theta\mathrm{c}\phi & & \\ - & (y_G W - y_B B)\,\mathrm{c}\theta\mathrm{c}\phi & + & (z_G W - z_B B)\,\mathrm{c}\theta\mathrm{s}\phi \\ & (z_G W - z_B B)\,\mathrm{s}\theta & + & (x_G W - x_B B)\,\mathrm{c}\theta\mathrm{c}\phi \\ - & (x_G W - x_B B)\,\mathrm{c}\theta\mathrm{s}\phi & - & (y_G W - y_B B)\,\mathrm{s}\theta \end{bmatrix} \tag{2.168}$$

Equation (2.168) is the Euler angle representation of the hydrostatic forces and moments. An alternative representation can be found by applying quaternions. Then $\boldsymbol{E}_1(e)$ replaces $\boldsymbol{J}_1(\eta_2)$ in (2.166), see Section 2.1.2. A neutrally buoyant underwater vehicle will satisfy:

$$W = B \tag{2.169}$$

Let the distance between the center of gravity CG and the center of buoyancy CB be defined by the vector:

$$\overline{BG} = [\overline{BG}_x,\ \overline{BG}_y,\ \overline{BG}_z]^T = [x_G - x_B,\ y_G - y_B,\ z_G - z_B]^T \tag{2.170}$$

Hence, (2.168) simplifies to:

$$g(\eta) = \begin{bmatrix} 0 \\ 0 \\ 0 \\ -\overline{BG}_y W\,\mathrm{c}\theta\mathrm{c}\phi + \overline{BG}_z W\,\mathrm{c}\theta\mathrm{s}\phi \\ \overline{BG}_z W\,\mathrm{s}\theta + \overline{BG}_x W\,\mathrm{c}\theta\mathrm{c}\phi \\ -\overline{BG}_x W\,\mathrm{c}\theta\mathrm{s}\phi - \overline{BG}_y W\,\mathrm{s}\theta \end{bmatrix} \tag{2.171}$$

Surface Ships

The general expression (2.168) should only be used for completely submerged vehicles. For surface vessels, the restoring forces will depend on the vessel's metacentric height, the location of the center of gravity and the center of buoyancy. Metacentric stability and restoring forces for surface ships are treated separately in Section 5.5.2.

2.5 Equations of Motion

In this section we will discuss different representations and properties of the marine vehicle equations of motion. Moreover, we will show how various body-symmetries can be used to simplify the equations of motion.

2.5.1 Vector Representations

The equations of motion can be represented in both the body-fixed and earth-fixed reference frames. We will discuss both these representations.

Body-Fixed Vector Representation

In Section 2.3 we have already shown that the nonlinear equations of motion in the body-fixed frame can be written as:

$$\boxed{M\,\dot{\nu} + C(\nu)\,\nu + D(\nu)\,\nu + g(\eta) = \tau} \tag{2.172}$$

$$\boxed{\dot{\eta} = J(\eta)\,\nu} \tag{2.173}$$

where

$$M = M_{RB} + M_A \qquad C(\nu) = C_{RB}(\nu) + C_A(\nu) \tag{2.174}$$

$$D(\nu) = D_P(\nu) + D_S(\nu) + D_W(\nu) + D_M(\nu) \tag{2.175}$$

Earth-fixed Vector Representation

The earth-fixed representation is obtained by applying the following kinematic transformations (assuming that $J(\eta)$ is non-singular):

$$\begin{array}{rclcrcl} \dot{\eta} &=& J(\eta)\,\nu & \Longleftrightarrow & \nu &=& J^{-1}(\eta)\,\dot{\eta} \\ \ddot{\eta} &=& J(\eta)\,\dot{\nu} + \dot{J}(\eta)\,\nu & \Longleftrightarrow & \dot{\nu} &=& J^{-1}(\eta)\left[\ddot{\eta} - \dot{J}(\eta)J^{-1}(\eta)\dot{\eta}\right] \end{array} \tag{2.176}$$

to eliminate ν and $\dot{\nu}$ from (2.172). Defining:

$$\begin{aligned} M_\eta(\eta) &= J^{-T}(\eta) M\, J^{-1}(\eta) \\ C_\eta(\nu,\eta) &= J^{-T}(\eta)\left[C(\nu) - MJ^{-1}(\eta)\dot{J}(\eta)\right] J^{-1}(\eta) \\ D_\eta(\nu,\eta) &= J^{-T}(\eta)\, D(\nu)\, J^{-1}(\eta) \\ g_\eta(\eta) &= J^{-T}(\eta)\, g(\eta) \\ \tau_\eta(\eta) &= J^{-T}(\eta)\,\tau \end{aligned} \tag{2.177}$$

yields the earth-fixed vector representation:

$$\boxed{M_\eta(\eta)\,\ddot{\eta} + C_\eta(\nu,\eta)\,\dot{\eta} + D_\eta(\nu,\eta)\,\dot{\eta} + g_\eta(\eta) = \tau_\eta} \tag{2.178}$$

2.5.2 Useful Properties of the Nonlinear Equations of Motion

We have seen that the 6 DOF nonlinear equations of motion, in their most general representation, require that a large number of hydrodynamic derivatives are known. From a practical point of view this is an unsatisfactory situation. However, the number of unknown parameters can be drastically reduced by using body symmetry considerations.

We will first discuss some useful properties of the nonlinear equations of motion and then show how symmetry can be exploited to reduce the complexity of the model.

Properties of the Body-Fixed Vector Representation

The following properties are observed for the body-fixed vector representation:

Property 2.7 (M)
For a rigid body the inertia matrix is strictly positive if and only if $M_A > 0$, that is:

$$M = M_{RB} + M_A > 0$$

If in addition we require that the body is at rest (or at least moves at low speed) under the assumption of an ideal fluid (see Property 2.4) the inertia matrix will also be symmetrical and therefore positive definite, that is:

$$M = M^T > 0$$

Hence, M takes the form:

$$M = \begin{bmatrix} m - X_{\dot{u}} & -X_{\dot{v}} & -X_{\dot{w}} & -X_{\dot{p}} & mz_G - X_{\dot{q}} & -my_G - X_{\dot{r}} \\ -X_{\dot{v}} & m - Y_{\dot{v}} & -Y_{\dot{w}} & -mz_G - Y_{\dot{p}} & -Y_{\dot{q}} & mx_G - Y_{\dot{r}} \\ -X_{\dot{w}} & -Y_{\dot{w}} & m - Z_{\dot{w}} & my_G - Z_{\dot{p}} & -mx_G - Z_{\dot{q}} & -Z_{\dot{r}} \\ -X_{\dot{p}} & -mz_G - Y_{\dot{p}} & my_G - Z_{\dot{p}} & I_x - K_{\dot{p}} & -I_{xy} - K_{\dot{q}} & -I_{xz} - K_{\dot{r}} \\ mz_G - X_{\dot{q}} & -Y_{\dot{q}} & -mx_G - Z_{\dot{q}} & -I_{xy} - K_{\dot{q}} & I_y - M_{\dot{q}} & -I_{yz} - M_{\dot{r}} \\ -my_G - X_{\dot{r}} & mx_G - Y_{\dot{r}} & -Z_{\dot{r}} & -I_{xz} - K_{\dot{r}} & -I_{yz} - M_{\dot{r}} & I_z - N_{\dot{r}} \end{bmatrix}$$

Proof: *$M = M_{RB} + M_A$ is positive definite under the assumptions that M_{RB} and M_A are positive definite matrices.*
□

Property 2.8 (C)
For a rigid body moving through an ideal fluid the Coriolis and centripetal matrix $C(\nu)$ can always be parameterized such that $C(\nu)$ is skew-symmetrical, that is:

$$C(\nu) = -C^T(\nu) \quad \forall \quad \nu \in \mathbb{R}^6$$

Proof: *$C(\nu)$ is skew-symmetrical under the assumptions that $C_{RB}(\nu)$ and $C_A(\nu)$ are skew-symmetrical.*
□

The Assumption of Wave Frequency-Independence

For a marine vehicle, M, C and D will depend on the wave frequency ω and thus the speed of the vehicle (frequency of encounter). This relationship has not been established for a general vehicle in 6 DOF. However, for control systems design asymptotically values can be used since only the low-frequency motion components are of interest. Hence, we will assume that:

$$M = \lim_{\omega \to 0} M(\omega); \qquad C = \lim_{\omega \to 0} C(\omega); \qquad D = \lim_{\omega \to 0} D(\omega) \tag{2.179}$$

in all control system analyses. This assumption implies that $\dot{M} = 0$ (frequency-independent) such that the following holds:

$$s^T \left[\dot{M} - 2C(\nu)\right] s \overset{\dot{M}=0}{=} -2\, s^T\, C(\nu)\, s = 0 \quad \forall \quad s \in \mathbb{R}^6 \tag{2.180}$$

This relationship has its analogy in the dynamic description of robot manipulators where the C matrix can be calculated by using the so-called Christoffel symbols (see Ortega and Spong 1988). Christoffel symbols, however, are not defined for vehicles in terms of body-fixed velocities.

Properties of the Earth-Fixed Vector Representation

As in the body-fixed vector representation it is straightforward to show that:

(1) $M_\eta(\eta) = M_\eta^T(\eta) > 0 \;\; \forall \;\; \eta \in \mathbb{R}^6$

(2) $s^T \left[\dot{M}_\eta(\eta) - 2C_\eta(\nu, \eta)\right] s = 0 \;\; \forall \;\; s \in \mathbb{R}^6, \; \nu \in \mathbb{R}^6, \; \eta \in \mathbb{R}^6$

(3) $D_\eta(\nu, \eta) \; > \; 0 \;\; \forall \;\; \nu \in \mathbb{R}^6, \; \eta \in \mathbb{R}^6$

if $M = M^T > 0$ and $\dot{M} = 0$. The proofs are left as an exercise. It should be noted that $C_\eta(\nu, \eta)$ will not be skew-symmetrical although $C(\nu)$ is skew-symmetrical.

Simplicity Considerations of the Inertia Matrix

The general expression for the inertia matrix M can be considerably simplified by exploiting different body symmetries. It is straightforward to verify the following cases (notice that $m_{ij} = m_{ji}$):

(i) xy-plane of symmetry (bottom/top symmetry).

$$M = \begin{bmatrix} m_{11} & m_{12} & 0 & 0 & 0 & m_{16} \\ m_{21} & m_{22} & 0 & 0 & 0 & m_{26} \\ 0 & 0 & m_{33} & m_{34} & m_{35} & 0 \\ 0 & 0 & m_{43} & m_{44} & m_{45} & 0 \\ 0 & 0 & m_{53} & m_{54} & m_{55} & 0 \\ m_{61} & m_{62} & 0 & 0 & 0 & m_{66} \end{bmatrix}$$

(ii) xz-plane of symmetry (port/starboard symmetry).

$$M = \begin{bmatrix} m_{11} & 0 & m_{13} & 0 & m_{15} & 0 \\ 0 & m_{22} & 0 & m_{24} & 0 & m_{26} \\ m_{31} & 0 & m_{33} & 0 & m_{35} & 0 \\ 0 & m_{42} & 0 & m_{44} & 0 & m_{46} \\ m_{51} & 0 & m_{53} & 0 & m_{55} & 0 \\ 0 & m_{62} & 0 & m_{64} & 0 & m_{66} \end{bmatrix}$$

(iii) yz-plane of symmetry (fore/aft symmetry).

$$M = \begin{bmatrix} m_{11} & 0 & 0 & 0 & m_{15} & m_{16} \\ 0 & m_{22} & m_{23} & m_{24} & 0 & 0 \\ 0 & m_{32} & m_{33} & m_{34} & 0 & 0 \\ 0 & m_{42} & m_{43} & m_{44} & 0 & 0 \\ m_{51} & 0 & 0 & 0 & m_{55} & m_{56} \\ m_{61} & 0 & 0 & 0 & m_{65} & m_{66} \end{bmatrix}$$

(iv) xz- and yz-planes of symmetry (port/starboard and fore/aft symmetries).

$$M = \begin{bmatrix} m_{11} & 0 & 0 & 0 & m_{15} & 0 \\ 0 & m_{22} & 0 & m_{24} & 0 & 0 \\ 0 & 0 & m_{33} & 0 & 0 & 0 \\ 0 & m_{42} & 0 & m_{44} & 0 & 0 \\ m_{51} & 0 & 0 & 0 & m_{55} & 0 \\ 0 & 0 & 0 & 0 & 0 & m_{66} \end{bmatrix}$$

More generally, the resulting inertia matrix for a body with ij- and jk-planes of symmetry is formed by the intersection $M_{ij \cap jk} = M_{ij} \cap M_{jk}$.

(v) xz-, yz- and xy-planes of symmetry (port/starboard, fore/aft and bottom/top symmetries).

$$M = \text{diag}\{\, m_{11},\ m_{22},\ m_{33},\ m_{44},\ m_{55},\ m_{66} \,\}$$

Simplicity Considerations of the Damping Matrix

For the linear time-invariant system:

$$M\,\dot{\nu} + D\,\nu = \tau \tag{2.181}$$

the symmetry properties of the damping matrix D will be equal to those of the inertia matrix M.

Example 2.1 (Horizontal Motion of a Dynamically Positioned Ship)
The horizontal motion of a dynamically positioned ship ($U = 0$) is usually described by the motion components in surge, sway and yaw. Therefore, we choose $\nu = [u, v, r]^T$ and $\eta = [x, y, \psi]^T$. This implies that the dynamics associated with the motion in heave, roll and pitch are neglected, that is $w = p = q = 0$. Furthermore, we assume that the ship has homogeneous mass distribution and xz-plane symmetry. Hence,

$$I_{xy} = I_{yz} = 0 \tag{2.182}$$

Let the coordinate origin be set in the center line of the ship such that: $y_G = 0$. *Under the previously stated assumptions, matrices (2.91) and (2.102) associated with the rigid-body dynamics reduce to:*

$$M_{RB} = \begin{bmatrix} m & 0 & 0 \\ 0 & m & mx_G \\ 0 & mx_G & I_z \end{bmatrix} \quad C_{RB}(\nu) = \begin{bmatrix} 0 & 0 & -m(x_G r + v) \\ 0 & 0 & mu \\ m(x_G r + v) & -mu & 0 \end{bmatrix} \tag{2.183}$$

This motivates the following reduction of (2.120) and (2.127):

$$M_A = \begin{bmatrix} -X_{\dot{u}} & 0 & 0 \\ 0 & -Y_{\dot{v}} & -Y_{\dot{r}} \\ 0 & -Y_{\dot{r}} & -N_{\dot{r}} \end{bmatrix} \quad C_A(\nu) = \begin{bmatrix} 0 & 0 & Y_{\dot{v}} v + Y_{\dot{r}} r \\ 0 & 0 & -X_{\dot{u}} u \\ -Y_{\dot{v}} v - Y_{\dot{r}} r & X_{\dot{u}} u & 0 \end{bmatrix} \tag{2.184}$$

Hence, $M = M^T$ *and* $C(\nu) = -C^T(\nu)$, *that is:*

$$M = \begin{bmatrix} m - X_{\dot{u}} & 0 & 0 \\ 0 & m - Y_{\dot{v}} & mx_G - Y_{\dot{r}} \\ 0 & mx_G - Y_{\dot{r}} & I_z - N_{\dot{r}} \end{bmatrix} \tag{2.185}$$

$$C(\nu) = \begin{bmatrix} 0 & 0 & -(m - Y_{\dot{v}})v - (mx_G - Y_{\dot{r}})r \\ 0 & 0 & (m - X_{\dot{u}})u \\ (m - Y_{\dot{v}})v + (mx_G - Y_{\dot{r}})r & -(m - X_{\dot{u}})u & 0 \end{bmatrix} \tag{2.186}$$

For simplicity, we assume linear damping and that surge is decoupled from sway and yaw. This implies that:

$$D = \begin{bmatrix} -X_u & 0 & 0 \\ 0 & -Y_v & -Y_r \\ 0 & -N_v & -N_r \end{bmatrix} \tag{2.187}$$

A model that is well suited for ship positioning is then obtained by writing:

$$M\,\dot{\nu} + C(\nu)\,\nu + D\,\nu = B\,u \tag{2.188}$$

where B *is the control matrix describing the thruster configuration and* u *is the control vector. During station keeping,* u, v *and* r *are all small which suggests that a further simplification could be to neglect the term* $C(\nu)\nu$.

□

2.5.3 The Lagrangian Versus the Newtonian Approach

One advantage with the Lagrangian approach is that we only have to deal with the two scalar energy functions T and V. The Newtonian approach is vector-oriented since everything is derived from Newton's second law. This often leads to a more cumbersome derivation of the equations of motion. We will illustrate this by applying the *Lagrange equations* of motion to derive the earth-fixed vector representation.

Lagrangian Derivation of the Earth-Fixed Vector Representation

Recall that:

$$\frac{d}{dt}\left(\frac{\partial L}{\partial \dot{\eta}}\right) - \frac{\partial L}{\partial \eta} + \frac{\partial P_d}{\partial \dot{\eta}} = \tau_\eta \tag{2.189}$$

Here we have included an additional term:

$$\frac{\partial P_d}{\partial \dot{\eta}} = D_\eta(\nu, \eta)\, \dot{\eta} \tag{2.190}$$

to describe the dissipative forces. P_d can be interpreted as a power function. The Lagrangian for the *vehicle-ambient water system* is given by:

$$L = T_{RB} + T_A - V \tag{2.191}$$

where T_{RB} is the rigid-body kinetic energy, T_A is the fluid kinetic energy and V is the potential energy defined implicit by:

$$\frac{\partial V}{\partial \eta} = g_\eta(\eta) \tag{2.192}$$

Hence, the total kinetic energy can be expressed as:

$$T = T_{RB} + T_A = \frac{1}{2}\, \dot{\eta}^T\, J^{-T}(M_{RB} + M_A)J^{-1}\, \dot{\eta} = \frac{1}{2}\, \dot{\eta}^T\, M_\eta(\eta)\, \dot{\eta} \tag{2.193}$$

Furthermore, we can compute:

$$\frac{\partial L}{\partial \dot{\eta}} = M_\eta(\eta)\, \dot{\eta} - \frac{\partial V}{\partial \dot{\eta}} = M_\eta(\eta)\, \dot{\eta} \tag{2.194}$$

$$\frac{d}{dt}\left(\frac{\partial L}{\partial \dot{\eta}}\right) = M_\eta(\eta)\, \ddot{\eta} + \dot{M}_\eta(\eta)\, \dot{\eta} \tag{2.195}$$

The next step involves computing:

$$\frac{\partial L}{\partial \eta} = \frac{\partial T}{\partial \eta} - \frac{\partial V}{\partial \eta} = \frac{1}{2}\, \dot{\eta}^T\, \frac{\partial M_\eta(\eta)}{\partial \eta}\, \dot{\eta} - g_\eta(\eta) \tag{2.196}$$

Using these results together with:

$$\dot{M}_\eta(\eta) = \dot{\eta}^T\, \frac{\partial M_\eta(\eta)}{\partial \eta} \tag{2.197}$$

implies that (2.189) can be written:

$$M_\eta(\eta)\, \ddot{\eta} + \frac{1}{2}\, \dot{M}_\eta(\eta)\, \dot{\eta} + D_\eta(\nu, \eta)\, \dot{\eta} + g_\eta(\eta) = \tau_\eta \tag{2.198}$$

From this expression, the definition of the Coriolis and centripetal matrix is recognized as:

$$C_\eta(\nu,\eta)\dot{\eta} \triangleq \frac{1}{2}\dot{M}_\eta(\eta)\dot{\eta} \tag{2.199}$$

which has its analogous definition in the skew-symmetric property:

$$x^T\left[\dot{M}_\eta(\eta) - 2C_\eta(\nu,\eta)\right]x = 0 \quad \forall \; x \tag{2.200}$$

Hence, we have shown that:

$$M_\eta(\eta)\,\ddot{\eta} + C_\eta(\nu,\eta)\,\dot{\eta} + D_\eta(\nu,\eta)\,\dot{\eta} + g_\eta(\eta) = \tau_\eta \tag{2.201}$$

by applying the *Lagrange equations* with $\eta = [x, y, z, \phi, \theta, \psi]^T$ as generalized coordinates. A similar derivation can be done in the body-fixed reference frame with $\nu = [u, v, w, p, q, r]^T$ by applying the Quasi-Lagrangian approach described in Section 2.2.3. A more detailed discussion on Lagrangian dynamics and its applications to marine vehicles is found in Sagatun (1992).

2.6 Conclusions

In this chapter, we have used a general framework in terms of the Newtonian and Lagrangian formalism to derive the nonlinear dynamic equations of motion in 6 DOF. The kinematic equations of motion are mainly discussed in terms of the quaternion and Euler angle representation. Emphasis is placed on expressing the multivariable nonlinear equations of motion such that well known properties from mechanical system theory can be extended to the multivariable case. The main motivation for this is that certain nonlinear system properties can be used to simplify the control systems design. In other words, a systematic representation of a complex model is necessary for a good exploitation of the physics and *a priori* information of the system. It should be noted that the resulting mathematical model does not include the contribution of the environmental disturbances like wind, waves and currents. However, environmental modeling will be discussed in the next chapter.

For the interested reader the development of the kinematic equations of motion are found in Kane, Likins and Levinson (1983) and Hughes (1986). Both these references use spacecraft systems for illustration. An alternative derivation of the Euler angle representation in the context of ship steering is given by Abkowitz (1964). An analogy to robot manipulators is given by Craig (1989). A detailed discussion on kinematics is found in Goldstein (1980) while a more recently discussion of quaternions is found in Chou (1992).

The nonlinear model structure presented at the end of this chapter is mainly intended for control systems design in combination with system identification and parameter estimation. Hence, the extensive literature on basic hydrodynamics should be consulted to obtain numerical values for the hydrodynamic derivatives

which are necessary for accurate prediction and computer simulations. Some standard references in hydrodynamics are Faltinsen (1990), Newman (1977) and Sarpkaya (1981). A detailed discussion on Lagrangian and Newtonian dynamics can be found in Goldstein (1980), Hughes (1986), Kane et al. (1983) and Meirovitch (1990), for instance.

2.7 Exercises

2.1 A marine vehicle is moving in the x-direction with a speed $u(t) = 2$ (m/s) and in the y-direction with a speed $v(t) = a \sin(t)$ (m/s). The heading angle is $\psi(t)$ (rad). Assume that the heave, roll and pitch modes can be neglected. Calculate both the body-fixed and earth-fixed acceleration in the x- and y-directions.

2.2 Calculate the inertia moment with respect to the center of gravity for a sphere with radius r and mass density ρ. Show that the sphere's products of inertia are zero.

2.3 Use the parallel axes theorem to prove Expressions (2.109) and (2.110).

2.4 Given a rigid-body with a coordinate frame $X_C Y_C Z_C$ located in the center of gravity. The body's inertia tensor is:

$$\boldsymbol{I}_C = \begin{bmatrix} 3 & 2 & 1 \\ 2 & 4 & 2 \\ 1 & 2 & 5 \end{bmatrix}$$

(a) Rotate the given coordinate system $X_C Y_C Z_C$ such that the axes of the new coordinate system $X'_C Y'_C Z'_C$ coincides with the principal axes of inertia.

(b) Instead of rotating the coordinate system $X_C Y_C Z_C$ find the distance between the coordinate system $X_C Y_C Z_C$ and a new coordinate system $X_0 Y_0 Z_0$ located at a point O such that the inertia tensor $\boldsymbol{I}_0$ becomes diagonal.

2.5 Find a continuous linear approximation to the quadratic damping force:

$$f(t) = -X_{u|u|}\, u(t)|u(t)|$$

where $X_{u|u|} < 0$ and $-u_0 \leq u(t) \leq u_0$.

2.6 Derive the equations of motion for an underwater vehicle in surge, sway, roll and yaw by applying the body-fixed vector representation. Assume linear damping and that all terms including Coriolis and centripetal forces can be neglected. Write the expressions for $\boldsymbol{M}$, $\boldsymbol{D}$, $\boldsymbol{g}$ and $\boldsymbol{J}$ according to the SNAME notation for hydrodynamic derivatives. The control force and moment vector are assumed to be $\boldsymbol{\tau} = [\tau_1, \tau_2, \tau_3, \tau_4]^T$.

2.7 Compute the added inertia matrix for a prolate spheroid with mass m and semi-axes $a = 2r$ and $b = c = r$.

2.8 Given the Euler angles $\phi = 10^o$, $\theta = 60^o$ and $\psi = 48^o$.

(a) Compute the corresponding Euler parameters e_i for $(i = 1...4)$ by applying Algorithm 2.2.

(b) Repeat the computation with $\theta = 89.9^o$ and ϕ and ψ unchanged.

(c) Use the inverse transformation to compute the Euler angles corresponding to the solutions from (a) and (b). Comment on the results.

2.9 Consider a surface ship in surge, sway and yaw with added inertia:

$$M_{\mathrm{A}} = -\begin{bmatrix} X_{\dot{u}} & 0 & 0 \\ 0 & Y_{\dot{v}} & Y_{\dot{r}} \\ 0 & N_{\dot{v}} & N_{\dot{r}} \end{bmatrix}$$

Find an expression for the fluid kinetic energy T_A and use Kirchhoffs' equations to derive a skew-symmetric matrix $C_A(\nu)$ for this system.

2.10 Assume that $M = M^T > 0$ and $D(\nu) > 0 \; \forall \; \nu \neq 0$. Show that:

(a) $M_\eta(\eta) = M_\eta^T(\eta) > 0 \quad \forall \; \eta \in \mathbb{R}^6$

(b) $D_\eta(\nu, \eta) \; > \; 0 \quad \forall \; \nu \in \mathbb{R}^6, \; \eta \in \mathbb{R}^6$

2.11 Compute $Y_{\dot{v}}, N_{\dot{r}}, Y_v$ and N_r for a surface ship with main dimensions $D = 8$ (m) and $L = 100$ (m) at a wave circular frequency $\omega = 1.0$ (rad/s) by applying strip theory.

2.12 Derive (2.98) and (2.99) from (2.72) and (2.87) by using the formulas:

$$\begin{aligned} a \times (b \times c) &= S(a)S(b)c \\ (a \times b) \times c &= S(S(a)b)c \end{aligned}$$

where $S(a)S(b) \neq S(S(a)b)$. Another useful formula is the *Jacobi identity*:

$$a \times (b \times c) + b \times (c \times a) + c \times (a \times b) = 0$$

which can be expressed in terms of the skew-symmetric operator $S(\cdot) \in SS(3)$ according to:

$$S(a)S(b)c + S(b)S(c)a + S(c)S(a)b = 0$$

Finally show that (2.100) and (2.101) can be derived from (2.98) and (2.99).

2.13 Derive the nonlinear body-fixed vector representation for a marine vehicle moving in 6 DOF by applying the Quasi-Lagrangian approach. All terms should be expressed by matrices and vectors.

Chapter 3

Environmental Disturbances

In the previous chapter a general model structure for marine vehicles was derived. In this chapter we will look further into details on the modeling aspects in terms of environmental disturbance models. Moreover, the following type of environmental disturbances will be considered:

- Waves (wind generated)
- Wind
- Ocean currents

In general these disturbances will be both additive and multiplicative to the dynamic equations of motion. However, in this chapter we will assume that the principle of superposition can be applied. For most marine control applications this is a good approximation.

3.1 The Principle of Superposition

The previous chapter has shown that the nonlinear dynamic equations of motion could be written:

$$[M_{RB} + M_A]\,\dot{\nu} + [C_{RB}(\nu) + C_A(\nu)]\,\nu + D(\nu)\,\nu + g(\eta) = \tau_E + \tau \qquad (3.1)$$

In the analysis below it is convenient to write the damping matrix as a sum of the radiation-induced potential damping matrix $D_P(\nu)$ and a viscous damping matrix $D_V(\nu) = D_S(\nu) + D_W(\nu) + D_M(\nu)$ containing the remaining damping terms. Hence we can write:

$$D(\nu) = D_P(\nu) + D_V(\nu) \qquad (3.2)$$

Based on this model we will apply the principle of superposition to derive the linear and nonlinear equations of motion in terms of environmental disturbances.

Linear Equations of Motion

Linearization of the Coriolis and centripetal forces $C_{RB}(\nu)\nu$ and $C_A(\nu)\nu$ about zero angular velocity ($p = q = r = 0$) implies that the Coriolis and centripetal terms can be removed from the above expressions, that is $C_{RB}(\nu)\nu = C_A(\nu)\nu = 0$. If we also linearize $D(\nu)\nu$ about zero angular velocity, and $u = u_0$, $v = v_0$ and $w = w_0$, we can write (3.1) as:

$$[M_{RB} + M_A]\,\dot{\nu} + [N_P + N_V]\,\nu + G\,\eta = \tau_E + \tau \tag{3.3}$$

where N_P, N_V and G are three *constant* matrices given by:

$$N_P = \left.\frac{\partial[D_P(\nu)\nu]}{\partial\nu}\right|_{\nu=\nu_0} \qquad N_V = \left.\frac{\partial[D_V(\nu)\nu]}{\partial\nu}\right|_{\nu=\nu_0} \qquad G = \left.\frac{\partial g(\eta)}{\partial\eta}\right|_{\eta=\eta_0} \tag{3.4}$$

Linear Equations of Motion Including the Environmental Disturbances

Furthermore, the principle of superposition suggests that the environmental disturbances can be added to the right-hand side of (3.3) to yield:

$$M_{RB}\,\dot{\nu} + N_V\,\nu + \underbrace{M_A\,\dot{\nu} + N_P\,\nu + G\,\eta}_{\text{radiation-induced forces}} = \underbrace{\tau_{\text{wave}} + \tau_{\text{wind}} + \tau_{\text{current}}}_{\text{environmental forces}} + \tau \tag{3.5}$$

In the previous chapter the *radiation-induced forces* were referred to as *sub-problem one*, Section 2.4. In this chapter *sub-problem two* is considered. Moreover, we want to find the forces on the body when the body is restrained from oscillating, and there are incident regular waves. These forces are recognized as the *Froude-Kriloff* and *diffraction forces*. Generally, the forces of sub-problem two are computed by integrating the pressure induced by the undisturbed waves and the pressure created by the vehicle when the waves are reflected from the vehicle over the wet body surface (Faltinsen 1990). Since this procedure is mathematically involved and not to well suited to control systems design, we will restrict our treatment to the following approximate solution for the Froude-Kriloff and diffraction forces.

Approximate Solution for the Froude-Kriloff and Diffraction Forces

If the body is totally submerged, has a *small volume* and the whole body surface is wetted, a special solution to sub-problem two exists. By *small volume* we mean that a characteristic cross-sectional dimension of the body is small relative to the wavelength λ. For a vertical cylinder *small volume* means that $\lambda > 5D$, where D is the cylinder diameter. ROVs are usually within this limit. Let the fluid velocity vector be defined by $\nu_c = [u_c, v_c, w_c, 0, 0, 0]^T$ where the last three fluid motion components are zero (assuming irrotational fluid) we can write (Faltinsen 1990):

$$\tau_{\text{current}} = \underbrace{M_{FK}\,\dot{\nu}_c}_{\text{Froude-Kriloff}} + \underbrace{M_A\,\dot{\nu}_c + N_P\,\nu_c}_{\text{diffraction forces}} + \underbrace{N_V\,\nu_c}_{\text{viscous forces}} \tag{3.6}$$

where M_{FK} may be interpreted as the *Froude-Kriloff inertia matrix*, that is the inertia matrix of the displaced fluid. Moreover, let ∇ be the volume of the displaced fluid and ρ the fluid density, hence the mass of the displaced fluid can be written:

$$\overline{m} = \rho\,\nabla \tag{3.7}$$

The moments and products of the inertia of the displaced fluid are:

$$\begin{array}{ll} \overline{I}_x = \int_\nabla (y^2+z^2)\rho d\nabla & \overline{I}_{xy} = \int_\nabla xy\rho d\nabla \\ \overline{I}_y = \int_\nabla (x^2+z^2)\rho d\nabla & \overline{I}_{xz} = \int_\nabla xz\rho d\nabla \\ \overline{I}_z = \int_\nabla (x^2+y^2)\rho d\nabla & \overline{I}_{yz} = \int_\nabla yz\rho d\nabla \end{array} \tag{3.8}$$

We can now establish the concept of displaced fluid inertia for a completely submerged body by defining the FK-inertia matrix $M_{FK} = M_{FK}^T > 0$ similar to M_{RB} (see Section 2.3.1). Moreover,

$$M_{FK} = \begin{bmatrix} mI_{3\times 3} & -mS(r_B) \\ mS(r_B) & \overline{I}_0 \end{bmatrix} = \begin{bmatrix} \overline{m} & 0 & 0 & 0 & \overline{m}z_B & -\overline{m}y_B \\ 0 & \overline{m} & 0 & -\overline{m}z_B & 0 & \overline{m}x_B \\ 0 & 0 & \overline{m} & \overline{m}y_B & -\overline{m}x_B & 0 \\ 0 & -\overline{m}z_B & \overline{m}y_B & \overline{I}_x & -\overline{I}_{xy} & -\overline{I}_{xz} \\ \overline{m}z_B & 0 & -\overline{m}x_B & -\overline{I}_{xy} & \overline{I}_y & -\overline{I}_{yz} \\ -\overline{m}y_B & \overline{m}x_B & 0 & -\overline{I}_{xz} & -\overline{I}_{yz} & \overline{I}_z \end{bmatrix} \tag{3.9}$$

where $r_B = [x_B, y_B, z_B]^T$ is the center of buoyancy.

Linear Equations of Relative Motion

If we assume that $M_{FK} = M_{RB}$, that is the vehicle is neutrally buoyant and the mass is homogeneously distributed, the linear equations of motion can be combined to give:

$$\underbrace{[M_{RB} + M_A]}_{M}\,\dot{\nu}_r + \underbrace{[N_P + N_V]}_{N}\,\nu_r + G\,\eta = \tau_{\text{wave}} + \tau_{\text{wind}} + \tau \tag{3.10}$$

where $\nu_r = \nu - \nu_c$ can be interpreted as the relative velocity vector. In this case ν_c should contain the contribution from the currents.

Nonlinear Equations of Relative Motion

For underwater vehicles, an extension to the nonlinear case could be to write (Fossen 1991):

$$M\,\dot{\nu}_r + C(\nu_r)\,\nu_r + D(\nu_r)\,\nu_r + g(\eta) = \tau_{\text{wave}} + \tau_{\text{wind}} + \tau \tag{3.11}$$

Often this approximation is also used for ships due to its intuitive and simple way of treating slowly-varying currents in terms of relative velocity. In the next sections we will discuss mathematical models for ν_c, τ_{wave} and τ_{wind}.

3.2 Wind-Generated Waves

The process of wave generation due to wind starts with small wavelets appearing on the water surface. This increases the drag force which in turn allows short waves to grow. These short waves continue to grow until they finally break and their energy is dissipated. It is observed that a *developing sea* or storm starts with high frequencies creating a spectrum with peak at a relative high frequency. A storm which has been blowing for a long time is said to create a *fully developed sea*. After the wind has stopped blowing, low frequency decaying sea or swell is being formed. These long waves form a wave spectrum with a low peak frequency[1]. If the swell from one storm interacts with the waves from another storm, a wave spectrum with two peak frequencies may be observed. For simplicity we will only consider wave spectra with one peak frequency, see Figure 3.1. Wind-generated waves are usually represented as a sum of a large number of wave components. The wave amplitude A_i of wave component i is related to the wave spectral density function $S(\omega_i)$ as (Newman 1977):

$$A_i^2 = 2S(\omega_i)\,\Delta\omega \tag{3.12}$$

where ω_i is the wave frequency of wave component i and $\Delta\omega$ is a constant difference between successive frequencies.

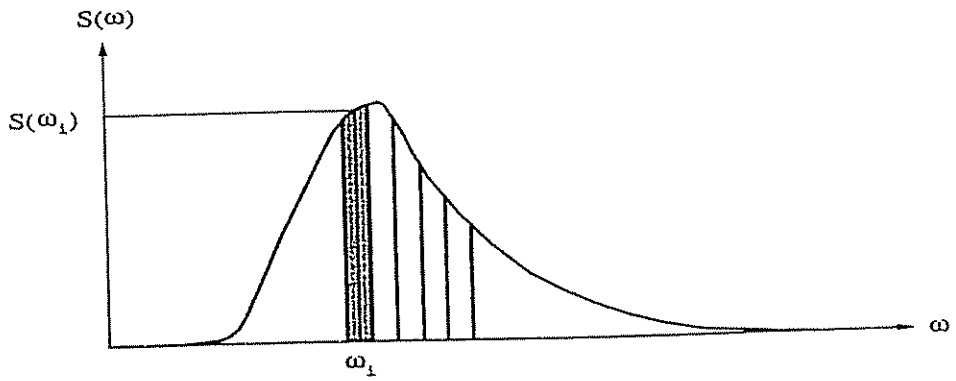

Figure 3.1: Figure showing wave spectrum with one peak. ω_i is chosen as a random frequency in the frequency interval $\Delta\omega$.

Let the *wave number* of one single wave component be denoted by k_i. Hence,

$$k_i = \frac{2\pi}{\lambda_i} \tag{3.13}$$

[1]The peak frequency of the wave spectrum is often referred to as the *modal frequency*.

where λ_i is the wave length, see Figure 3.2. The wave elevation $\zeta(x,t)$ of a long-crested irregular sea propagating along the positive x-axis can be written as a sum of wave components (Newman 1977):

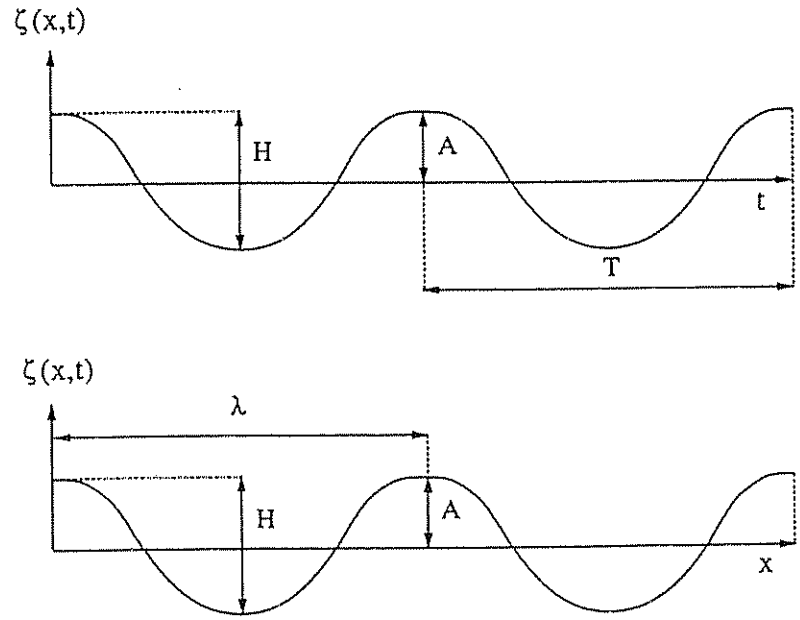

Figure 3.2: Characteristics of a wave traveling with speed $c = \lambda/T = \omega/k$. In the figure λ = wave length, H = wave height, A = wave amplitude, T = wave period and ζ = wave elevation.

$$\begin{aligned}\zeta(x,t) &= \sum_{i=1}^{N} A_i \cos(\omega_i t - k_i x + \phi_i) \\ &+ \sum_{i=1}^{N} \frac{1}{2} k_i A_i^2 \cos 2(\omega_i t - k_i x + \phi_i) + O(A_i^3) \end{aligned} \tag{3.14}$$

where ϕ_i is a random phase angle uniformly distributed and constant with time in $[0\ 2\pi\rangle$. From regular wave theory it can be shown that the connection between the wave number k_i and the circular frequency: $\omega_i = 2\pi/T_i$ is:

$$\omega_i^2 = k_i\, g\, \tanh(k_i\, d) \tag{3.15}$$

Here d is used to denote the water depth. This relationship is often referred to as the *dispersion relation*. For infinite water depth, that is $d/\lambda_i > 1/2$, the dispersion relation reduces to $\omega_i^2 = k_i\, g$ since $\tanh(k_i\, d) \to 1$ as $d/\lambda_i \to \infty$.

Unfortunately, Expression (3.14) repeats itself after a time $2\pi/\Delta\omega$. This suggests that a large number of wave components should be used, typically $N = 1000$. However, this problem can be circumvented by simply choosing ω_i as a random frequency in the frequency interval $\Delta\omega$.

Linear wave theory or *Airy,theory* represents a 1st-order approximation of the wave elevation $\zeta(x,t)$. This corresponds to the first term A_i in Formula (3.14). Furthermore, *2nd-order theory* implies that an additional term $1/2\, k_i\, A_i^2$ is included in the expression for $\zeta(x,t)$. This is done by applying a so-called *Stoke's expansion* to solve the wave theory problem up to second order. Similarly, forces caused by these terms are usually referred to as *1st-order* and *2nd-order wave forces*, respectively. 2nd-order theory is usually sufficient to describe the response of most marine vehicles in a seaway. 1st-order wave disturbances will describe the oscillatoric motion of the vehicle while the 2nd-order term represents the wave drift forces. The next section shows how to compute $S(\omega_i)$ and thus A_i in (3.12).

3.2.1 Standard Wave Spectra

The earliest spectral formulation is due to Neumann (1952) who proposed the *one-parameter* spectrum:

$$S(\omega) = C\,\omega^{-6}\,\exp\left(-2g^2\,\omega^{-2}\,V^{-2}\right) \quad (\mathrm{m^2s}) \tag{3.16}$$

where C is an empirical constant, V is the wind speed and g is the acceleration of gravity. More recently, the tendency has gone towards another class of spectra motivated by the early work of Phillips (1958) who showed that the high frequency form of the sea spectrum was asymptotically limited by ($\omega \gg 1$):

$$S(\omega) \quad \longrightarrow \quad \alpha\, g^2\, \omega^{-5} \tag{3.17}$$

where α is a positive constant. We will concentrate our discussion on this type of spectra.

Table 3.1: Description of wind, p. 162 of Price and Bishop (1974). Reproduced by permission of Chapman and Hall, Ltd.

Beaufort number	Description of wind	Wind speed (knots)
0	Calm	0-1
1	Light air	2-3
2	Light breeze	4-7
3	Gentle breeze	8-11
4	Moderate breeze	12-16
5	Fresh breeze	17-21
6	Strong breeze	22-27
7	Moderate gale	28-33
8	Fresh gale	34-40
9	Strong gale	41-48
10	Whole gale	49-56
11	Storm	57-65
12	Hurricane	More than 65

Bretschneider Spectrum

A more sophisticated spectrum than the Neumann spectrum has been proposed by Bretschneider (1959). The two-parameter *Bretschneider spectrum* is written:

$$S(\omega) = \frac{1.25}{4}\,\frac{\omega_0^4}{\omega^5}\,H_s^2\;\exp\left(-1.25\,(\omega_0/\omega)^4\right) \qquad (\mathrm{m^2s}) \tag{3.18}$$

where ω_0 is the *modal frequency* and H_s is the *significant wave height*[2] (mean of the one-third highest waves). This spectrum was developed for the North Atlantic, for unidirectional seas, infinite depth, no swell and unlimited fetch.

Pierson–Moskowitz Spectrum

Independently of this work Pierson and Moskowitz (1963) developed a wave spectral formulation for fully developed wind-generated seas from analyses of wave spectra in the North Atlantic Ocean. The *Pierson–Moskowitz (PM) spectrum* is written:

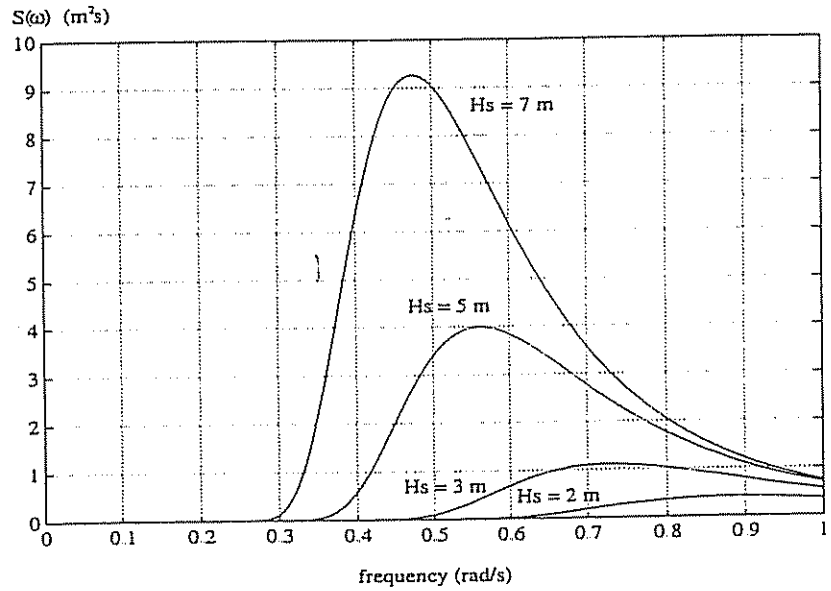

Figure 3.3: Figure showing the PM-spectrum for different values of H_s.

$$S(\omega) = A\,\omega^{-5}\;\exp\left(-B\omega^{-4}\right) \qquad (\mathrm{m^2s}) \tag{3.19}$$

where

$$A = 8.1\cdot 10^{-3}\,g^2 \tag{3.20}$$

$$B = 0.74\left(\frac{g}{V}\right)^4 \tag{3.21}$$

[2] In some textbooks the significant wave height is denoted by $H_{1/3}$.

Here V is the wind speed at a height of 19.4 m over the sea surface and g is the gravity constant. By assuming that the waves can be represented by Gaussian random processes and that $S(\omega)$ is narrow-banded, the PM-spectrum can be reformulated in terms of significant wave height, that is:

$$A = 8.1 \cdot 10^{-3}\, g^2 \tag{3.22}$$

$$B = 0.0323 \left(\frac{g}{H_s}\right)^2 = \frac{3.11}{H_s^2} \tag{3.23}$$

Table 3.2: Description of sea, p. 147 of Price and Bishop (1974). Reproduced by permission of Chapman and Hall, Ltd. Notice that the percentage probability for sea state code 0, 1 and 2 is summarized.

			Percentage probability		
Sea state code	Description of sea	Wave height observed (m)	World wide	North Atlantic	Northern North Atlantic
0	Calm (glassy)	0			
1	Calm (rippled)	0-0.1	11.2486	8.3103	6.0616
2	Smooth (wavelets)	0.1-0.5			
3	Slight	0.5-1.25	31.6851	28.1996	21.5683
4	Moderate	1.25-2.5	40.1944	42.0273	40.9915
5	Rough	2.5-4.0	12.8005	15.4435	21.2383
6	Very rough	4.0-6.0	3.0253	4.2938	7.0101
7	High	6.0-9.0	0.9263	1.4968	2.6931
8	Very high	9.0-14.0	0.1190	0.2263	0.4346
9	Phenomenal	Over 14.0	0.0009	0.0016	0.0035

A description of significant wave height with percentage probability is given in Table 3.2. This implies that the wind speed V and significant wave height H_s will be related through:

$$H_s = 0.21 \frac{V^2}{g} \tag{3.24}$$

This relationship is plotted in Figure 3.4. The *modal frequency* ω_0 for the PM-spectrum is found by requiring that:

$$\left(\frac{dS(\omega)}{d\omega}\right)_{\omega=\omega_0} = 0 \tag{3.25}$$

Straightforward computation yields:

$$\omega_0 = \sqrt[4]{\frac{4B}{5}} \tag{3.26}$$

$$T_0 = 2\pi \sqrt[4]{\frac{5}{4B}} \tag{3.27}$$

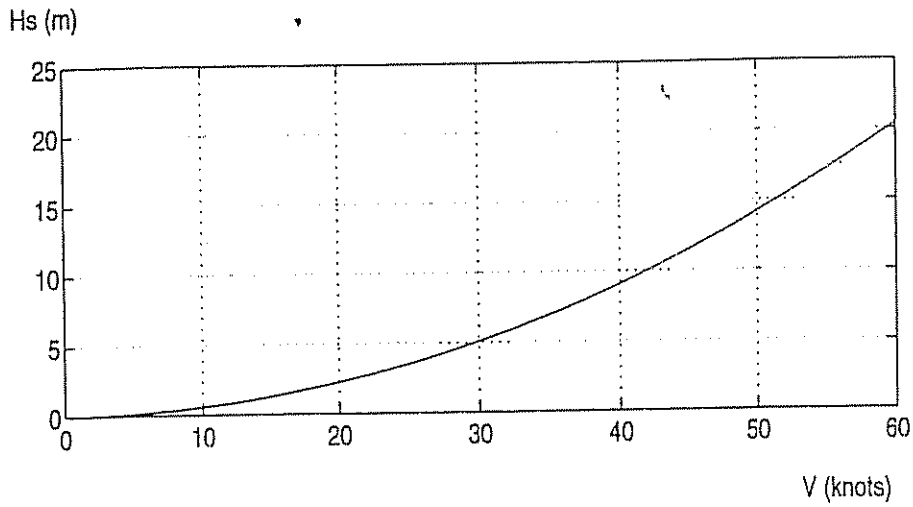

Figure 3.4: Significant wave height $H_s = 0.21\,V^2/g$ (m) versus wind speed V (knots). (1 knot = 0.51 m/s).

where T_0 is the *modal period*. Substituting the values for A and B into (3.26), yields:

$$\omega_0 = 0.88\,\frac{g}{V} = 0.40\,\sqrt{\frac{g}{H_s}} \tag{3.28}$$

Hence, the maximum value of $S(\omega)$ is:

$$S_{\max}(\omega) = S(\omega_0) = \frac{5A}{4B\omega_0}\exp\left(-5/4\right) \tag{3.29}$$

The Bretschneider spectrum is described by two parameters H_s and ω_0 and is thus referred to as a *two-parameter* spectrum. Notice that if ω_0 is chosen as $0.40\,\sqrt{g/H_s}$ the Bretschneider spectrum reduces to the *one-parameter* PM-spectrum.

Wave Spectrum Moments

The different wave spectra can be classified by means of so-called *wave spectrum moments* to illustrate some of the statistical properties of their parameterization. The spectrum moments are defined as:

$$m_k = \int_0^\infty \omega^k\,S(\omega)\,d\omega \qquad\qquad (k = 0...N) \tag{3.30}$$

For $k = 0$, we obtain:

$$m_0 = \int_0^\infty S(\omega)\,d\omega = \frac{A}{4B} \tag{3.31}$$

This simply states that the instantaneous wave elevation is Gaussian-distributed with zero mean and variance $\sigma^2 = A/4B$. Hence, $\sqrt{m_0}$ can be interpreted as the RMS-value of the spectrum. Furthermore, we obtain:

$$m_1 = 0.306\frac{A}{B^{3/4}} \tag{3.32}$$

$$m_2 = \frac{\sqrt{\pi}}{4}\frac{A}{\sqrt{B}} \tag{3.33}$$

For the PM-spectrum the *average wave period* is defined as:

$$T_1 = 2\pi\frac{m_0}{m_1} \tag{3.34}$$

while the *average zero-crossings period* is defined as:

$$T_z = 2\pi\sqrt{\frac{m_0}{m_2}} \tag{3.35}$$

Furthermore, by assuming that the wave height is Rayleigh distributed it can be shown that (Price and Bishop 1974):

$$H_s = 4\sqrt{m_0} \tag{3.36}$$

Modified Pierson–Moskowitz (MPM) Spectrum

For prediction of responses of marine vehicles and offshore structures in open sea, the International Ship and Offshore Structures Congress, 2nd ISSC (1964), and the International Towing Tank Conference, 12th ITTC (1969b) and 15th ITTC (1978) have recommended the use of a modified version of the PM-spectrum, that is:

$$S(\omega) = \frac{4\,\pi^3 H_s^2}{T_z^4\omega^5}\exp\left(\frac{-16\,\pi^3}{T_z^4\omega^4}\right) \quad (\mathrm{m^2s}) \tag{3.37}$$

This representation of the PM-spectrum has two parameters H_s and T_z. Alternatively, we can substitute:

$$T_z = 0.710\,T_0 = 0.921\,T_1 \tag{3.38}$$

if T_0 and T_1 are more convenient to use. This representation of $S(\omega)$ should only be used for a fully developed sea with infinite depth, no swell and unlimited fetch. For non-fully developed seas the following spectrum has been proposed by the ITTC.

JONSWAP Spectrum

In 1968 and 1969 an extensive measurement program was carried out in the North Sea, between the island Sylt in Germany and Iceland. The measurement program is known as the *Joint North Sea Wave Project* (JONSWAP) and the results from these investigations have been adopted as an ITTC standard by the 17th ITTC (1984). Since the JONSWAP spectrum is used to describe *non-fully developed seas*, the spectral density function will be more peaked than the those for the fully developed spectra. The proposed spectral formulation is representative for wind-generated waves under the assumption of finite water depth and limited fetch. The spectral density function is written:

$$S(\omega) = 155\,\frac{H_s^2}{T_1^4\,\omega^5}\exp\left(\frac{-944}{T_1^4\,\omega^4}\right)(\gamma)^Y \tag{3.39}$$

where Hasselmann et al. (1973) suggest that $\gamma = 3.3$ and:

$$Y = \exp\left[-\left(\frac{0.191\,\omega\,T_1 - 1}{\sqrt{2}\,\sigma}\right)^2\right] \tag{3.40}$$

where

$$\sigma = \begin{cases} 0.07 & \text{for } \omega \leq 5.24/T_1 \\ 0.09 & \text{for } \omega > 5.24/T_1 \end{cases} \tag{3.41}$$

This formulation can be used with other characteristic periods like T_0 and T_z by substituting:

$$T_1 = 0.834\,T_0 = 1.073\,T_z \tag{3.42}$$

The peak value of the JONSWAP spectrum can be related to the PM-spectrum by the ratio:

$$\gamma = \frac{S(\omega_0)_{JONSWAP}}{S(\omega_0)_{PM}} \tag{3.43}$$

This value is usually between 1 and 7.

Example 3.1 (Experimental Wave Spectrum Results)
A full-scale experiment was performed west of Bergen in order to measure the motion components in surge, sway, heave, roll, pitch and yaw for a moving supply vessel (Far Scandia). Both time-series and power spectral density functions $P(\omega)$ are shown in Figure 3.5. The motion components corresponding to the figures are:

$\dot{u}$	=	*surge acceleration* (m/s^2)	ϕ	=	*roll angle (deg)*
$\dot{v}$	=	*sway acceleration* (m/s^2)	θ	=	*pitch angle (deg)*
$\dot{w}$	=	*heave acceleration* (m/s^2)	ψ	=	*yaw angle (deg)*

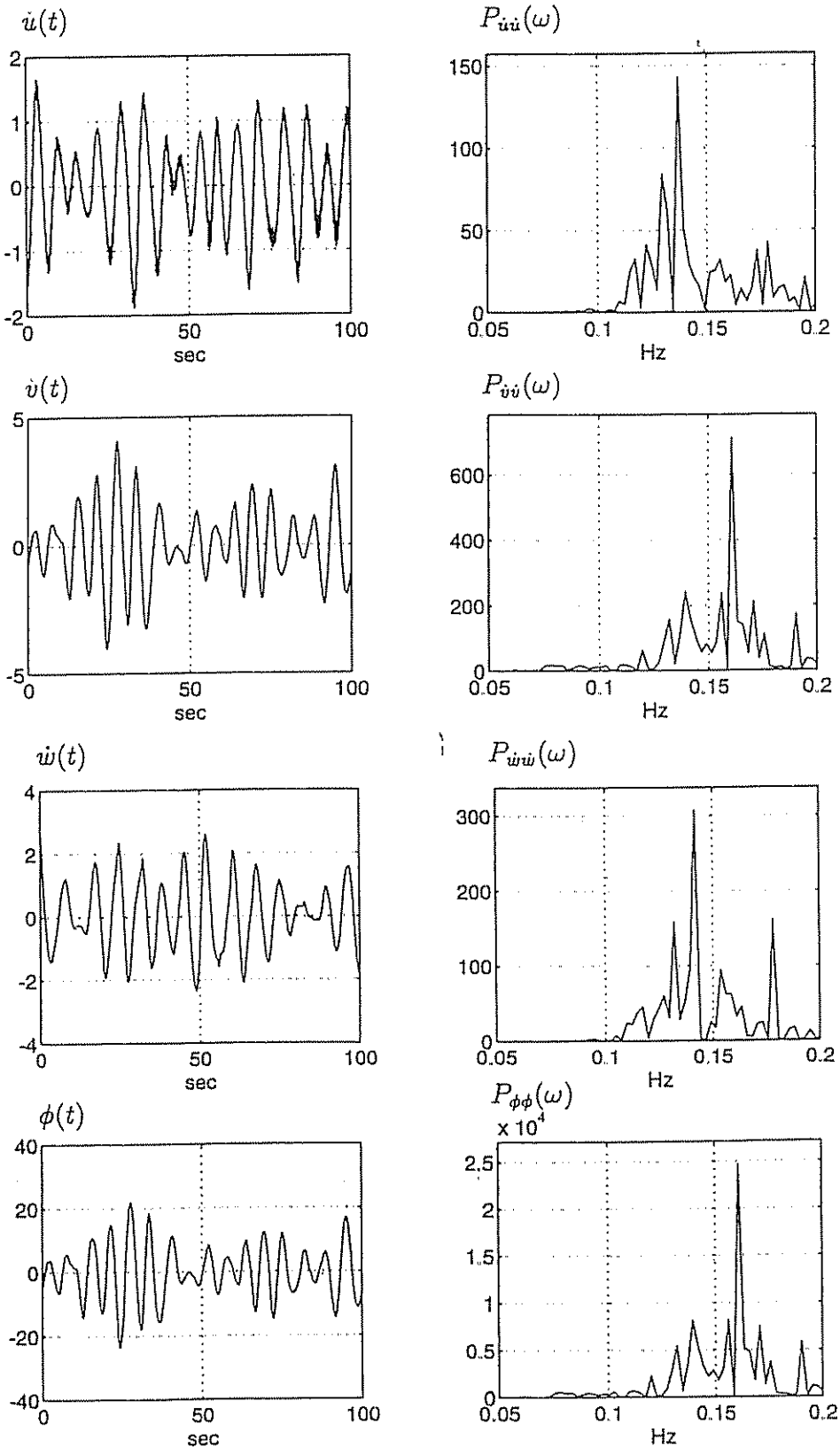
$\dot{u}(t)$
$P_{\dot{u}\dot{u}}(\omega)$
$\dot{v}(t)$
$P_{\dot{v}\dot{v}}(\omega)$
$\dot{w}(t)$
$P_{\dot{w}\dot{w}}(\omega)$
$\phi(t)$
$P_{\phi\phi}(\omega)$
x 10^4
sec
Hz

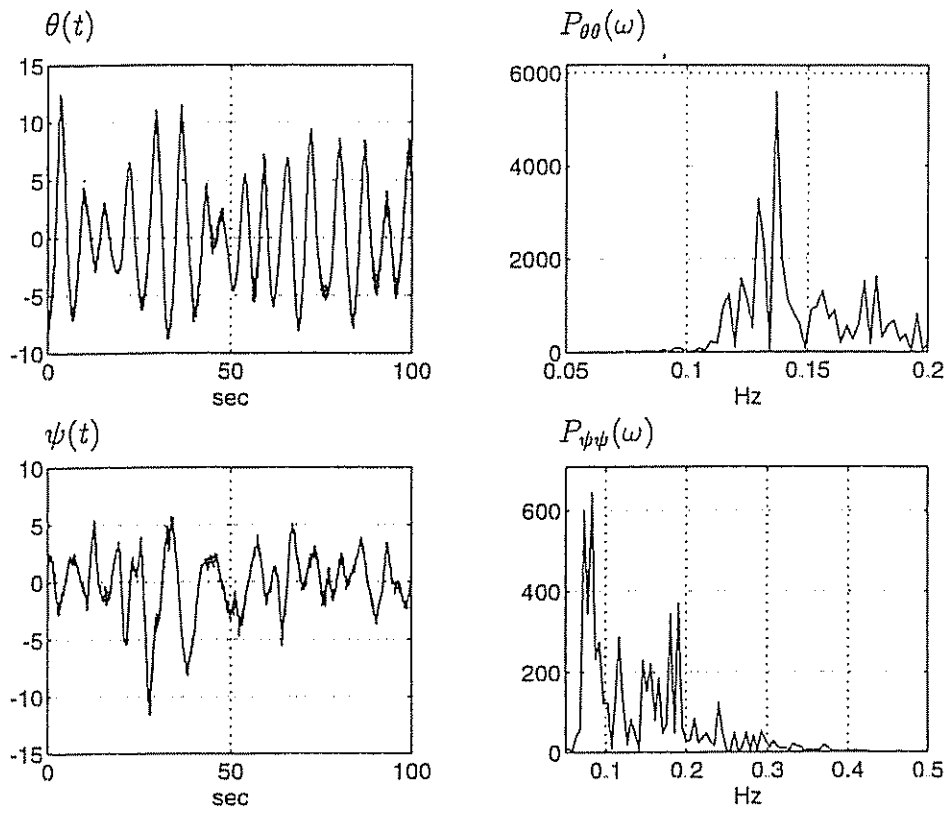

Figure 3.5: Experimental time-series and wave spectra in 6 DOF for a moving ship in sea state code 8 (measured with a Seatex MRU sensor unit). Notice that the yaw signal is highly affected by the feedback signal from the autopilot. Reproduced by permission of ABB Industry in Oslo.

3.2.2 Linear Approximations to the Wave Spectra

A linear approximation to the PM spectral density function $S(\omega)$ can be found by writing the output $y(s)$ from the wave model as:

$$y(s) = h(s)\, w(s) \tag{3.44}$$

where $w(s)$ is a zero-mean Gaussian white noise process with power spectrum:

$$P_{ww}(\omega) = 1.0 \tag{3.45}$$

and $h(s)$ is a transfer function to be determined. Hence, the power spectral density (PSD) function for $y(s)$ can be computed as:

$$P_{yy}(\omega) = |h(j\omega)|^2\, P_{ww}(\omega) = |h(j\omega)|^2 \tag{3.46}$$

The ultimate goal is to design an approximation $P_{yy}(\omega)$ to $S(\omega)$, for instance by means of linear regression, such that $P_{yy}(\omega)$ reflects the energy distribution of $S(\omega)$ in the actual frequency range. We will in the forthcoming discuss some linear approximations well suited for this purpose.

2nd-Order Wave Transfer Function Approximation

Linear wave model approximations are usually preferred by ship control systems engineers, owing to their simplicity and applicability. The first applications were reported in 1976 by Balchen, Jenssen and Sælid (1976) who proposed to model the high-frequency motion of a dynamically positioned ship in surge, sway and yaw by three harmonic oscillators without damping. Later Sælid, Jenssen and Balchen (1983) introduced a damping term in the wave model to better fit the shape of the PM-spectrum. This model is written:

$$h(s) = \frac{K_w\, s}{s^2 + 2\,\zeta\,\omega_0\, s + \omega_0^2} \tag{3.47}$$

where it is convenient to define the gain constant according to:

$$K_w = 2\,\zeta\,\omega_0\,\sigma_w \tag{3.48}$$

Here σ_w is a constant describing the wave intensity, ζ is a damping coefficient while ω_0 is the dominating wave frequency. Hence, substituting $s = j\omega$ yields:

$$h(j\omega) = \frac{j\,2(\zeta\,\omega_0\,\sigma_w)\,\omega}{(\omega_0^2 - \omega^2) + j\,2\,\zeta\,\omega_0\,\omega} \tag{3.49}$$

This in turn implies that:

$$|h(j\omega)| = \frac{2\,(\zeta\,\omega_0\,\sigma_w)\,\omega}{\sqrt{(\omega_0^2 - \omega^2)^2 + 4\,(\zeta\,\omega_0\,\omega)^2}} \tag{3.50}$$

From (3.46) we recall that:

$$P_{yy}(\omega) = |h(jw)|^2 = \frac{4\,(\zeta\,\omega_0\,\sigma_w)^2\omega^2}{(\omega_0^2 - \omega^2)^2 + 4\,(\zeta\,\omega_0\,\omega)^2} \tag{3.51}$$

This expression for $P_{yy}(\omega)$ is shown in Figure 3.6. From this it is seen that the maximum value of $|P_{yy}(\omega)|$ is obtained for $\omega = \omega_0$, that is:

$$\max_{\omega} P_{yy}(\omega) = P_{yy}(\omega_0) = \sigma_w^2 \tag{3.52}$$

State-Space Model

A linear state-space model can be obtained from (3.47) by transforming this expression to the time-domain by:

$$\ddot{y}(t) + 2\,\zeta\,\omega_0\,\dot{y}(t) + \omega_0^2\,y(t) = K_w\,\dot{w}(t) \tag{3.53}$$

Defining $\dot{x}_{h1} = x_{h2}$ and $x_{h2} = y_h$ as state variables, this implies that the state-space model can be written:

$$\dot{x}_H = A_H\, x_H + E_H\, w_H \tag{3.54}$$
$$y_H = C_H\, x_H \tag{3.55}$$

where w_H is a zero-mean white noise process. Writing this expression in component form, yields:

$$\begin{bmatrix} \dot{x}_{h1} \\ \dot{x}_{h2} \end{bmatrix} = \begin{bmatrix} 0 & 1 \\ -\omega_0^2 & -2\,\zeta\,\omega_0 \end{bmatrix} \begin{bmatrix} x_{h1} \\ x_{h2} \end{bmatrix} + \begin{bmatrix} 0 \\ K_w \end{bmatrix} w_h \tag{3.56}$$

$$y_h = \begin{bmatrix} 0 & 1 \end{bmatrix} \begin{bmatrix} x_{h1} \\ x_{h2} \end{bmatrix} \tag{3.57}$$

This model is highly applicable for control systems design due to its simplicity. Applications will be discussed in later chapters.

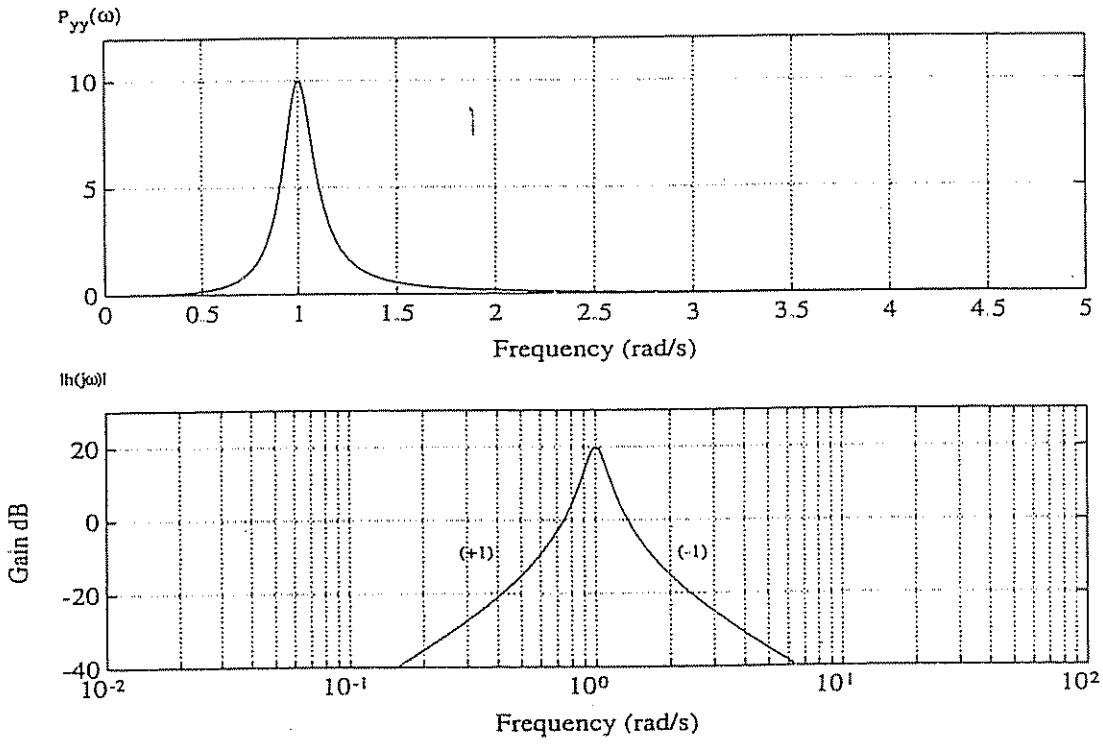

Figure 3.6: Power spectral density $P_{yy}(\omega)$ and amplitude $|h(j\omega)|$ as a function of frequency for the linear wave spectrum ($\omega_0 = 1.0$, $\zeta = 0.1$ and $\sigma_w^2 = 10$).

Higher-Order Wave Transfer Function Approximations

An alternative wave transfer function based on five parameters has been proposed by Grimble, Patton and Wise (1980a) and Fung and Grimble (1983). This model is written:

$$h(s) = \frac{K_w s^2}{s^4 + a_1 s^3 + a_2 s^2 + a_3 s + a_4} \tag{3.58}$$

where a_i (i = 1...4) are four parameters. Hence, four differential equations are required to describe the wave model. Moreover,

$$\begin{bmatrix} \dot{x}_{h1} \\ \dot{x}_{h2} \\ \dot{x}_{h3} \\ \dot{x}_{h4} \end{bmatrix} = \begin{bmatrix} 0 & 1 & 0 & 0 \\ 0 & 0 & 1 & 0 \\ 0 & 0 & 0 & 1 \\ -a_4 & -a_3 & -a_2 & -a_1 \end{bmatrix} \begin{bmatrix} x_{h1} \\ x_{h2} \\ x_{h3} \\ x_{h4} \end{bmatrix} + \begin{bmatrix} 0 \\ 0 \\ 0 \\ K_w \end{bmatrix} w_h \tag{3.59}$$

$$y_h = \begin{bmatrix} 0 & 0 & 1 & 0 \end{bmatrix} \begin{bmatrix} x_{h1} \\ x_{h2} \\ x_{h3} \\ x_{h4} \end{bmatrix} \tag{3.60}$$

The number of unknown parameters can be reduced by assuming that the denominator can be factorized according to:

$$h(s) = \frac{K_w s^2}{(s^2 + 2\,\zeta\,\omega_0\,s + \omega_0^2)^2} \tag{3.61}$$

More recently, Triantafyllou, Bodson and Athans (1983) have shown by applying a rational approximation to the Bretschneider spectrum that a satisfactory approximation of the high-frequency ship motion can be obtained by using the transfer function:

$$h(s) = \frac{K_w s^2}{(s^2 + 2\,\zeta\,\omega_0\,s + \omega_0^2)^3} \tag{3.62}$$

which only has three unknown parameters ζ, ω_0 and K_w. The advantage of the higher order models to the simple 2nd-order system (3.47) is that they will represent a more precise approximation to the wave spectrum. The disadvantage, of course, is higher model complexity and often more parameters to determine.

3.2.3 Frequency of Encounter

For a ship moving with forward speed U, the wave frequency ω_0 will be modified according to:

$$\omega_e(U, \omega_0, \beta) = \omega_0 - \frac{\omega_0^2}{g}\,U\,\cos\beta \tag{3.63}$$

where $\omega_0^2 = k\,g$ (assuming deep water) and:

ω_e = encounter frequency (rad/s)
ω_0 = wave frequency (rad/s)
g = acceleration of gravity (m/s^2)
U = total speed of ship (m/s)
β = the angle between the heading and the direction of the wave (rad)

Notice that the encounter frequency can be negative for large values of U. The definition of the encounter angle β is shown in Figure 3.7.

This suggests that the wave spectrum for a heading-controlled ship moving at speed $U > 0$ should be modified to incorporate the frequency of encounter. For instance, we can rewrite (3.47) as:

$$h(s) = \frac{K_w\, s}{s^2 + 2\,\zeta\,\omega_e\, s + \omega_e^2} \tag{3.64}$$

However, it should be noted that the wave frequency of a dynamic positioned ship can be perfectly described by $\omega_e = \omega_0$ since U is close to or equal to zero.

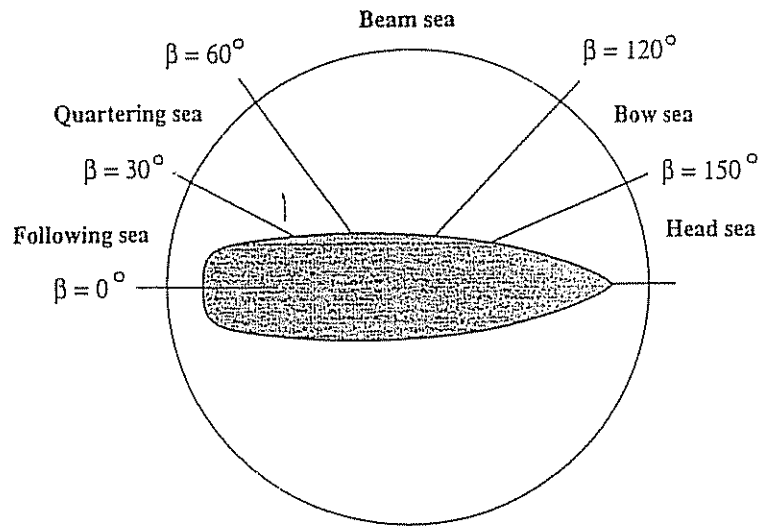

Figure 3.7: Definition of ship's heading (encounter) angle (Reid et al. 1984).

3.2.4 Wave-Induced Forces and Moments

In order to simulate the motion of ocean vehicles in the presence of irregular waves we will consider the effect of 1st- and 2nd-order wave disturbances.

Superposition in Terms of 1st- and 2nd-Order Wave Disturbances

The responses of an ocean vehicle in a seaway are usually computed by applying the principle of *superposition*. Assume that the 1st-order wave disturbances can

be described by the damped oscillator (3.54)–(3.57). Alternatively, y_H can be computed by using the spectral density function $S(\omega)$. Furthermore, we assume that 2nd-order wave drift forces in the x-, y- and z-directions can be modelled by three slowly-varying parameters: $d = [d_1, d_2, d_3]^T$. Hence,

$$\begin{array}{lll} \textit{1st-order wave disturbances} & \dot{x}_H = A_H\, x_H + E_H\, w_H \\ \textit{(oscillatoric motion)} & y_H = C_H\, x_H \\ \textit{2nd-order wave drift} & \dot{d} = w_d \end{array} \tag{3.65}$$

Here w_d is a vector of zero mean Gaussian white noise processes. Moreover, the principle of superposition suggests that the vehicle dynamics and the 2nd-order wave disturbances can be combined to yield:

$$M\,\nu + C(\nu)\,\nu + D(\nu)\,\nu + g(\eta) = d + \tau \tag{3.66}$$

$$\dot{\eta} = J(\eta)\,\nu \tag{3.67}$$

The measurement equation is modified to include the 1st-order wave induced motion, that is:

$$y = y_L + y_H \tag{3.68}$$

where the low-frequency position and attitude components usually are given by $y_L = \eta$. Notice that we have included the wave drift forces in the dynamic equation of motion (process noise) while the oscillatoric motion is added to the model output (colored measurement noise). In many practical operations like ship steering and positioning this simple model is sufficient.

A more intuitive and physical approach would be to model 1st-order wave forces and moments as process noise as well. This can be done by applying the following model description.

1st-Order Wave Forces and Moment on a Block-Shaped Ship

Consider the expression $\zeta_i(x,t)$ in (3.14) for the wave elevation. The wave slope s_i for wave component i is defined as:

$$s_i(x,t) = \frac{d\zeta_i(x,t)}{dx} = A_i\, k_i\, \sin(\omega_i t - k_i x + \phi_i) + O(A_i^2) \tag{3.69}$$

The wave elevation and wave slope can be expressed in terms of ω_e for a moving ship. For simplicity, we assume that $x = 0$ and that higher order terms can be neglected. Hence,

$$\zeta_i(t) = \zeta_i(0,t) = A_i\, \cos(\omega_{ei} t + \phi_i) \tag{3.70}$$

This implies that the wave slope can be computed according to:

$$s_i(t) = s_i(0,t) = A_i\ k_i\ \sin(\omega_{ei}t + \phi_i) \tag{3.71}$$

Here ω_{ei} is the encounter frequency corresponding to wave component i. Based on these expressions we can derive the forces and moments:

$$\tau_{\text{wave}} = [X_{\text{wave}}, Y_{\text{wave}}, N_{\text{wave}}]^T \tag{3.72}$$

induced by a regular sea on a block-shaped ship. To do this Zuidweg (1970) makes the following assumptions: (1) the forces and moments only result from water pressure acting on the wetted surface, (2) the wave field is not disturbed by the ship and (3) the influence of the waves is accounted for by assuming a fluctuating pressure distribution below the water surface, whereas the water surface itself is assumed to be undisturbed. Moreover, the principle of superposition suggests that:

$$M\,\dot{\nu} + C(\nu)\,\nu + D(\nu)\,\nu + g(\eta) = \tau_{\text{wave}} + \tau \tag{3.73}$$

For a ship where the wetted part is a rectangular parallelepiped with length L, breadth B and draft T, we obtain the following formulas for the 1st-order wave disturbances (Källström 1979):

$$X_{\text{wave}}(t) = \sum_{i=1}^{N} \rho\, g\, BLT \cos\beta\ s_i(t) \tag{3.74}$$

$$Y_{\text{wave}}(t) = \sum_{i=1}^{N} -\rho\, g\, BLT \sin\beta\ s_i(t) \tag{3.75}$$

$$N_{\text{wave}}(t) = \sum_{i=1}^{N} \frac{1}{24}\,\rho\, g\, BL(L^2 - B^2)\ \sin 2\beta\ s_i^2(t) \tag{3.76}$$

where β is defined in Figure 3.7. These equations will only hold if the ship is small compared to the wavelength and the water surface across the hull can be approximated as a plane surface. An alternative approach, removing the assumption of the plane water surface, can be derived by assuming that $(k_i\, L)$, $(k_i\, B)$ and $(k_i\, T)$ are small. This results in the same expressions for X_{wave} and Y_{wave} while N_{wave} is modified to:

$$N_{\text{wave}}(t) = \sum_{i=1}^{N} \frac{1}{24}\,\rho\, g\, BL(L^2 - B^2)\, T\, k_i^2\ \sin 2\beta\ \zeta_i(t) \tag{3.77}$$

More detailed analyses of wave forces and moments are found in Zuidweg (1970). In order to implement the above formulas we can use the following algorithm to compute the wave elevation ζ_i and slope s_i.

Algorithm 3.1 (Wave Elevation and Wave Slope)

1. Divide the spectral density function $S(\omega)$ into N intervals with length $\Delta\omega$, see Figure 3.1.
2. Pick a random frequency ω_i in each of the frequency intervals and compute $S(\omega_i)$.
3. Compute the wave amplitude $A_i = \sqrt{2S(\omega_i)\,\Delta\omega}$ and the wave number $k_i = \omega_i^2/g$ for $(i = 1...N)$.
4. Compute ζ_i and s_i by applying Formulas (3.70) and (3.71).

3.3 Wind

Wind forces and moments on a vessel can usually be described in terms of a mean wind speed in combination with a wind spectrum describing the variation of the wind speed (gusting). We will first describe some standard wind spectra for this purpose and then relate the wind speed and direction to the forces and moments acting on the vehicle.

3.3.1 Standard Wind Spectra

One the most used spectral formulations for wind gust is the Davenport (1961) spectrum:

$$S_w(\omega) = k\,\frac{916700\,\omega}{[1+(191\,\omega/V_w(10))^2]^{4/3}} \tag{3.78}$$

where

k	=	0.05 (turbulence factor)
$V_w(10)$	=	average wind speed at a level of 10 m above the water surface (knots)
ω	=	frequency of the wind oscillations (rad/s)

Another attractive spectral formulation is the so-called Harris (1971) spectrum which is written:

$$S_w(\omega) = k\,\frac{5286\,V_w(10)}{[1+(286\,\omega/V_w(10))^2]^{5/6}} \tag{3.79}$$

These spectra are based on land-based measurements. More recently Ochi and Shin (1988) presented a spectral formulation relying on wind speed measurements carried out at sea. This spectrum is written in non-dimensional form according to:

$$S(f_*) = \begin{cases} 583\,f_* & \text{for } 0 \le f_* < 0.003 \\ \frac{420\,f_*^{0.75}}{(1+f_*^{0.35})^{11.5}} & \text{for } 0.003 \le f_* \le 0.1 \\ \frac{838\,f_*}{(1+f_*^{0.35})^{11.5}} & \text{for } f_* > 0.1 \end{cases} \tag{3.80}$$

where

$$\begin{array}{rcl} f_* & = & 10\, f/V_w(10) \\ S(f_*) & = & f \cdot S(f)/C_{10} \cdot V_w^2(10) \\ f & = & \text{frequency of oscillation (Hz)} \\ C_{10} & = & \text{surface drag coefficient, see Ochi and Shin (1988)} \\ S(f) & = & \text{spectral density} \end{array}$$

Other useful spectral formulations are Hino (1971), Kaimal et al. (1972), Simiu and Leigh (1983) and Kareem (1985); see the 10th ISSC (1988) pp. 15–18 and references therein.

Linear Approximation to the Harris Spectrum

The above wind spectra are nonlinear approximations. A linear 1st-order approximation for the Harris spectrum is:

$$h(s) = \frac{K}{1+Ts} \tag{3.81}$$

which implies that:

$$S_w(\omega) \approx |h(j\omega)|^2 = \frac{K^2}{1+(\omega T)^2} \tag{3.82}$$

Hence, we can choose the time and gain constant according to:

$$K = \sqrt{5286\, k\, V_w(10)}; \qquad T = \sqrt{286/V_w(10)} \tag{3.83}$$

Wind Velocity Profile

In order to determine the local velocity z (m) above the sea surface we can use the boundary-layer profile (see Bretschneider 1969):

$$V_w(z) = V_w(10) \cdot (z/10)^{1/7} \tag{3.84}$$

where $V_w(10)$ is the relative wind velocity 10 (m) above the sea surface.

3.3.2 Wind Forces and Moments

As mentioned in the previous section the total wind speed will contain a slowly-varying component (average wind speed) and a high-frequency component (wind gust). The resultant wind forces and moment acting on a surface vessel are usually defined in terms of relative wind speed V_R (knots) and angle γ_R (deg) according to:

$$V_R = \sqrt{u_R^2 + v_R^2} \qquad \gamma_R = \tan^{-1}(v_R/u_R) \tag{3.85}$$

where the components of V_R in the x- and y-directions are:

$$u_R = V_w \cos(\gamma_R) - u + u_c \quad (3.86)$$
$$v_R = V_w \sin(\gamma_R) - v + v_c \quad (3.87)$$

Here (u, v) and (u_c, v_c) are the ship and current velocity components while $\gamma_R = \psi_w - \psi$ is the angle of relative wind of the ship bow, see Figure 3.8.

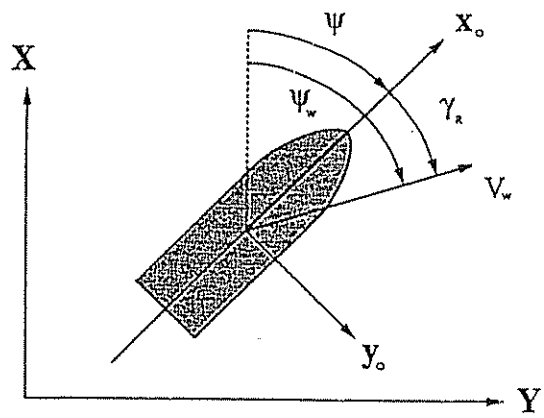

Figure 3.8: Definition of wind speed and direction.

We can simulate time-series for V_w and ψ_w by adding a *mean* and a *turbulent* component according to:

$$\dot{x}_1 = w_1 \qquad \dot{x}_3 = w_3$$
$$\dot{x}_2 = -\tfrac{1}{T}(x_2 - K\, w_2) \qquad \dot{x}_4 = -\tfrac{1}{T}(x_4 - K\, w_4)$$

$$V_w = x_1 + x_2 \qquad \psi_w = x_3 + x_4$$

where w_i (i = 1...4) are zero-mean Gaussian white noise processes and T and K are the time and gain constants of the Harris spectrum, for instance.

For most ships the wind gust cannot be compensated for by the control system since the dynamics of the ship is too slow compared with the gusts. However, slowly-varying wind forces can be fed forward to the controller by measuring the average wind speed and direction. This requires the wind force and moment coefficients to be known with sufficient accuracy. We will now describe two attractive methods for computation of the wind force and moment vector:

$$\tau_{\text{wind}} = [X_{\text{wind}},\ Y_{\text{wind}},\ N_{\text{wind}}]^T \quad (3.88)$$

acting on a surface ship.

Wind Resistance of Merchant Ships (Isherwood 1972).

Isherwood (1972) suggested that one write the wind forces (surge and sway) and moment (yaw) according to:

$$X_{\text{wind}} = \frac{1}{2} C_X(\gamma_R)\, \rho_w\, V_R^2\, A_T \quad \text{(N)} \tag{3.89}$$

$$Y_{\text{wind}} = \frac{1}{2} C_Y(\gamma_R)\, \rho_w\, V_R^2\, A_L \quad \text{(N)} \tag{3.90}$$

$$N_{\text{wind}} = \frac{1}{2} C_N(\gamma_R)\, \rho_w\, V_R^2\, A_L\, L \quad \text{(Nm)} \tag{3.91}$$

where C_X and C_Y are the force coefficients and C_N is the moment coefficient, and where ρ_w is the density of air in kg/m^3, A_T and A_L are the transverse and lateral projected areas in m^2 and L is the overall length of the ship in m. Notice that V_R is given in knots.

Based on these equations measured data were analyzed by multiple regression techniques in terms of the following 8 parameters:

L	=	length overall
B	=	beam
A_L	=	lateral projected area
A_T	=	transverse projected area
A_{SS}	=	lateral projected area of superstructure
S	=	length of perimeter of lateral projection of model excluding waterline and slender bodies such as masts and ventilators
C	=	distance from bow of centroid of lateral projected area
M	=	number of distinct groups of masts or kingposts seen in lateral projection; kingposts close against the bridge front are not included

Moreover, Isherwood found that the data were best fitted to the following three equations:

$$C_X = A_0 + A_1\frac{2A_L}{L^2} + A_2\frac{2A_T}{B^2} + A_3\frac{L}{B} + A_4\frac{S}{L} + A_5\frac{C}{L} + A_6 M \tag{3.92}$$

$$C_Y = B_0 + B_1\frac{2A_L}{L^2} + B_2\frac{2A_T}{B^2} + B_3\frac{L}{B} + B_4\frac{S}{L} + B_5\frac{C}{L} + B_6\frac{A_{SS}}{A_L} \tag{3.93}$$

$$C_N = C_0 + C_1\frac{2A_L}{L^2} + C_2\frac{2A_T}{B^2} + C_3\frac{L}{B} + C_4\frac{S}{L} + C_5\frac{C}{L} \tag{3.94}$$

where A_i and B_i ($i = 0...6$) and C_j ($j = 0...5$) are tabulated below together with the residual standard errors (S.E.).

Table 3.3: Surge induced wind force parameters (Isherwood 1972).

γ_R (deg)	A_0	A_1	A_2	A_3	A_4	A_5	A_6	$S.E.$
0	2.152	−5.00	0.243	−0.164	–	–	–	0.086
10	1.714	−3.33	0.145	−0.121	–	–	–	0.104
20	1.818	−3.97	0.211	−0.143	–	–	0.033	0.096
30	1.965	−4.81	0.243	−0.154	–	–	0.041	0.117
40	2.333	−5.99	0.247	−0.190	–	–	0.042	0.115
50	1.726	−6.54	0.189	−0.173	0.348	–	0.048	0.109
60	0.913	−4.68	–	−0.104	0.482	–	0.052	0.082
70	0.457	−2.88	–	−0.068	0.346	–	0.043	0.077
80	0.341	−0.91	–	−0.031	–	–	0.032	0.090
90	0.355	–	–	–	−0.247	–	0.018	0.094
100	0.601	–	–	–	−0.372	–	−0.020	0.096
110	0.651	1.29	–	–	−0.582	–	−0.031	0.090
120	0.564	2.54	–	–	−0.748	–	−0.024	0.100
130	−0.142	3.58	–	0.047	−0.700	–	−0.028	0.105
140	−0.677	3.64	–	0.069	−0.529	–	−0.032	0.123
150	−0.723	3.14	–	0.064	−0.475	–	−0.032	0.128
160	−2.148	2.56	–	0.081	–	1.27	−0.027	0.123
170	−2.707	3.97	−0.175	0.126	–	1.81	–	0.115
180	−2.529	3.76	−0.174	0.128	–	1.55	–	0.112
							Mean S.E.	0.103

Table 3.4: Sway induced wind force parameters (Isherwood 1972).

γ_R (deg)	B_0	B_1	B_2	B_3	B_4	B_5	B_6	$S.E.$
10	0.096	0.22	–	–	–	–	–	0.015
20	0.176	0.71	–	–	–	–	–	0.023
30	0.225	1.38	–	0.023	–	−0.29	–	0.030
40	0.329	1.82	–	0.043	–	−0.59	–	0.054
50	1.164	1.26	0.121	–	−0.242	−0.95	–	0.055
60	1.163	0.96	0.101	–	−0.177	−0.88	–	0.049
70	0.916	0.53	0.069	–	–	−0.65	–	0.047
80	0.844	0.55	0.082	–	–	−0.54	–	0.046
90	0.889	–	0.138	–	–	−0.66	–	0.051
100	0.799	–	0.155	–	–	−0.55	–	0.050
110	0.797	–	0.151	–	–	−0.55	–	0.049
120	0.996	–	0.184	–	−0.212	−0.66	0.34	0.047
130	1.014	–	0.191	–	−0.280	−0.69	0.44	0.051
140	0.784	–	0.166	–	−0.209	−0.53	0.38	0.060
150	0.536	–	0.176	−0.029	−0.163	–	0.27	0.055
160	0.251	–	0.106	−0.022	–	–	–	0.036
170	0.125	–	0.046	−0.012	–	–	–	0.022
							Mean S.E.	0.044

Table 3.5: Yaw induced wind moment parameters (Isherwood 1972).

γ_R (deg)	C_0	C_1	C_2	C_3	C_4	C_5	$S.E.$
10	0.0596	0.061	–	–	–	−0.074	0.0048
20	0.1106	0.204	–	–	–	−0.170	0.0074
30	0.2258	0.245	–	–	–	−0.380	0.0105
40	0.2017	0.457	–	0.0067	–	−0.472	0.0137
50	0.1759	0.573	–	0.0118	–	−0.523	0.0149
60	0.1925	0.480	–	0.0115	–	−0.546	0.0133
70	0.2133	0.315	–	0.0081	–	−0.526	0.0125
80	0.1827	0.254	–	0.0053	–	−0.443	0.0123
90	0.2627	–	–	–	–	−0.508	0.0141
100	0.2102	–	−0.0195	–	0.0335	−0.492	0.0146
110	0.1567	–	−0.0258	–	0.0497	−0.457	0.0163
120	0.0801	–	−0.0311	–	0.0740	−0.396	0.0179
130	−0.0189	–	−0.0488	0.0101	0.1128	−0.420	0.0166
140	0.0256	–	−0.0422	0.0100	0.0889	−0.463	0.0162
150	0.0552	–	−0.0381	0.0109	0.0689	−0.476	0.0141
160	0.0881	–	−0.0306	0.0091	0.0366	−0.415	0.0105
170	0.0851	–	−0.0122	0.0025	–	−0.220	0.0057
						Mean S.E.	0.0127

Wind Resistance of Very Large Crude Carriers (OCIMF 1977).

Wind loads on very large crude carriers (VLCCs), that is vessels in the 150 000 to 500 000 (dwt) class, can be computed by applying the following approach.

$$X_{\text{wind}} = C_{Xw}(\gamma_R)\,\frac{\rho_a}{7.6}\,V_R^2\,A_T \quad \text{(N)} \tag{3.95}$$

$$Y_{\text{wind}} = C_{Yw}(\gamma_R)\,\frac{\rho_a}{7.6}\,V_R^2\,A_L \quad \text{(N)} \tag{3.96}$$

$$N_{\text{wind}} = C_{Nw}(\gamma_R)\,\frac{\rho_a}{7.6}\,V_R^2\,A_L L \quad \text{(Nm)} \tag{3.97}$$

Here the non-dimensional force and moment coefficients C_{Xw}, C_{Yw} and C_{Nw} are given as a function of γ_R in Figures 3.9–3.11. ρ_a is the density of air in kg/m^3, see Appendix F, while 7.6 is a conversion factor. For ships that are not too asymmetrical with respect to the xz- and yz-planes, we can approximate:

$$C_{Xw}(\gamma_R) \approx \hat{C}_{Xw}\cos(\gamma_R) \tag{3.98}$$

$$C_{Yw}(\gamma_R) \approx \hat{C}_{Yw}\sin(\gamma_R) \tag{3.99}$$

$$C_{Nw}(\gamma_R) \approx \hat{C}_{Nw}\sin(2\gamma_R) \tag{3.100}$$

Figures 3.9–3.11 indicate that $\hat{C}_{Xw} \in \{-1.0,\ -0.8\}$, $\hat{C}_{Yw} \in \{-1.0,\ -0.7\}$ and $\hat{C}_{Nw} \in \{-0.2,\ -0.05\}$. However, the figures also indicate that these approximations should be used with care.

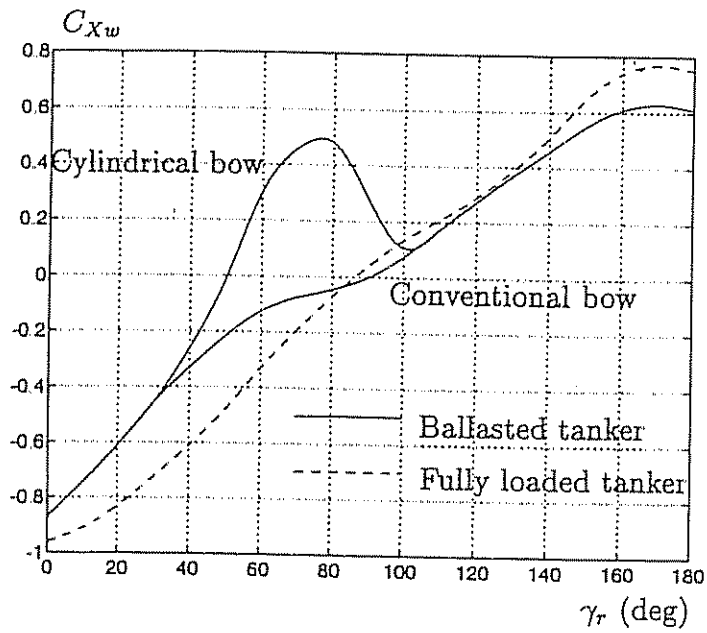

Figure 3.9: Longitudinal wind force coefficient C_{Xw} as a function of relative wind angle of attack γ_R (OCIMF 1977).

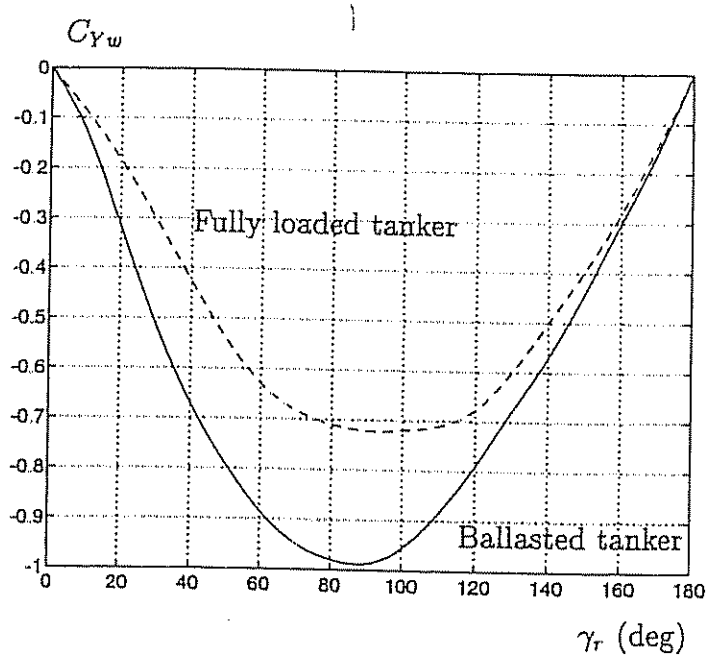

Figure 3.10: Lateral wind force coefficient C_{Yw} as a function of relative wind angle of attack γ_R (OCIMF 1977).

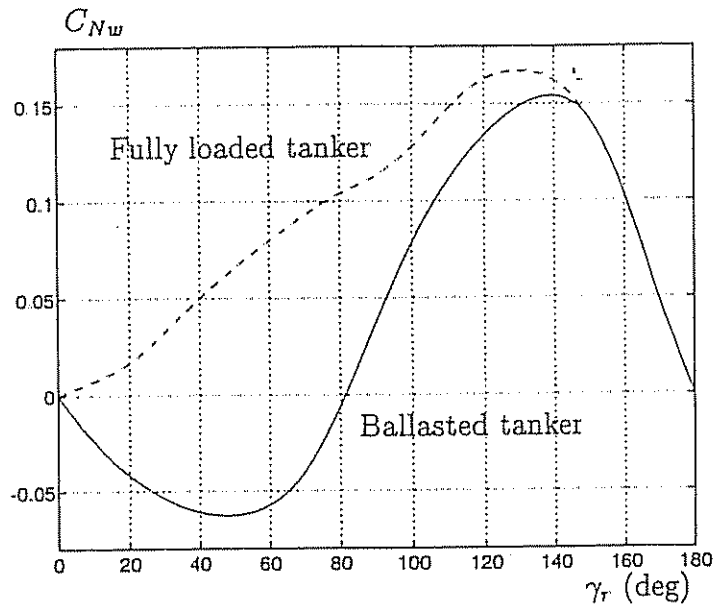

Figure 3.11: Wind yaw moment coefficient C_{Nw} as a function of relative wind angle of attack γ_R (OCIMF 1977).

The following example adopted from OCIMF (1977) illustrates how the wind forces and moment on a 280 000 (dwt) tanker with cylindrical bow configuration can be computed.

Example 3.2 (Wind Load Calculations for a 280 000 dwt Tanker)
Consider a tanker in fully loaded condition with:

$$A_T = 3160 \ (m^2) \qquad A_L = 1130 \ (m^2) \qquad L = 325 \ (m)$$

From Figures 3.9–3.11 for a wind angle of 30 *(deg) we obtain:*

$$C_{Xw} = -0.73; \qquad C_{Yw} = -0.31; \qquad C_{Nw} = 0.032$$

Assume that the wind speed at a 20 *(m) elevation is* $V_w(20) = 66$ *(knots). Hence, we can compute (see Equation (3.84)):*

$$V_w(10) = V_w(20)(10/20)^{1/7} = 60 \ (knots)$$

which according to Formulas (3.95)–(3.97) with $V_R = V_w(10)$ *results in:*

$$\begin{aligned} X_{wind} &= -0.73 \cdot (1.224/7.6) \cdot 60^2 \cdot 1130 \approx -478 \ (kN) \\ Y_{wind} &= -0.31 \cdot (1.224/7.6) \cdot 60^2 \cdot 3160 \approx -568 \ (kN) \\ N_{wind} &= 0.032 \cdot (1.223/7.6) \cdot 60^2 \cdot 3160 \cdot 325 \approx 19054 \ (kNm) \end{aligned}$$

Here the density of air is taken to be $\rho_w = 1.224$ (kg/m^3) corresponding to 20° (C), see Appendix F. If the ship's heading is changed, the above calculations must be repeated for the new incident wind angle γ_R.
□

Another useful reference discussing wind resistance on large tankers in the 100 000 to 500 000 (dwt) class is Van Berlekom, Trägårdh and Dellhag (1974). For medium sized ships of the order 600 to 50 000 (dwt) it is advised to consult Wagner (1967). Finally, an excellent reference for moored ships is De Kat and Wichers (1991).

3.4 Ocean Currents

Currents in the upper layers of the ocean are mainly generated by the atmospheric wind system over the sea surface; see pp. 38–44 of 10th ISSC (1988). Besides *wind-generated currents*, the heat exchange at the sea surface together with the salinity changes develop an additional sea current component, usually referred to as *thermohaline currents*. This process also explains why varying water types are observed in different climatic regions. The oceans are conveniently divided into two water spheres, the cold and warm water sphere, which again are separated by the 8° C isotherm. Since the earth is rotating, the Coriolis force will try to turn the major currents to the right in the northern hemisphere and opposite in the southern hemisphere. Finally, the major ocean circulations will also have a tidal component arising from planetary interactions like gravity. In coastal regions and fjords tidal components can obtain very high speeds, in fact speeds of 2 to 3 m/s or more can be measured. A world map showing most major ocean surface currents is found in Defant (1961).

3.4.1 Current Velocity

The 10th ISSC (1988) proposed that one write the surface current velocity V_c as a sum of the following velocity components:

$$V_c = V_t + V_{lw} + V_s + V_m + V_{set-up} + V_d \tag{3.101}$$

where

V_t = tidal component
V_{lw} = component generated by local wind.
V_s = component generated by nonlinear waves (Stokes drift).
V_m = component from major ocean circulation (e.g. Gulf Stream).
V_{set-up} = component due to set-up phenomena and storm surges.
V_d = local density driven current components governed by strong density jumps in the upper ocean.

Tidal Component

Let the vertical component z (m) be measured positive downwards. Hence, the velocity profile of the tidal component can be written:

$$V_t(z) = \begin{cases} V_t(0) & \text{for} \quad 0 \leq z \leq d-10 \\ V_t(0)\ \log_{10}\left(1+\frac{9z}{d-10}\right) & \text{for} \quad d-10 < z < d \end{cases} \tag{3.102}$$

Here $V_t(0)$ (m/s) is the surface speed of the tidal and $d > 10$ (m) is the water depth.

Component Generated by Nonlinear Waves (Stokes Drift)

As mentioned in Section 3.2, 2nd-order wave disturbances or so-called wave drift forces can be treated as an additional current component. The contribution to the surface drift (Stokes theory) resulting from the irrotational properties of the waves is written:

$$V_s(z) = \sum_{i=1}^{N} k_i\,\omega_i\,A_i^2\,\exp(-2\,k_i\,z) = \sum_{i=1}^{N} \frac{4\,\pi^2\,A_i^2}{T_i\lambda_i}\,\exp(-4\,\pi\,z/\lambda_i) \tag{3.103}$$

The derivation of this expression is found in Sarpkaya (1981).

Component Generated by Local Wind

The component generated by the local wind is written:

$$V_{lw}(z) = \begin{cases} V_{lw}(0)\,\frac{d_0-z}{d_0} & \text{for} \quad 0 \leq z \leq d_0 \\ 0 & \text{for} \quad d_0 < z \end{cases} \tag{3.104}$$

Here d_0 is the reference depth for the wind-generated current usually taken to be 50 (m). Collar (1986) has shown that $V_{lw}(0)$ can be approximated as:

$$V_{lw}(0) = 0.02\,V_{10} \tag{3.105}$$

where V_{10} (m/s) is the wind velocity measured 10 (m) above sea level.

3.4.2 Current-Induced Forces and Moments

This section shows that the current-induced forces and moments can be included in the dynamic equations of motion by two methods. Both methods are based on the assumption that the equations of motion can be represented in terms of the relative velocity:

$$\nu_r = \nu - \nu_c \tag{3.106}$$

where $\nu_c = [u_c, v_c, w_c, 0, 0, 0]^T$ is a vector of irrotational body-fixed current velocities.

Method 1:

Section 2.1.1 has already shown that the earth-fixed linear velocity could be transformed to body-fixed linear velocities by applying the principal rotation matrices. Let the earth-fixed current velocity vector be denoted by $[u_c^E, v_c^E, w_c^E]$. Hence, we can compute the body-fixed components as:

$$\begin{bmatrix} u_c \\ v_c \\ w_c \end{bmatrix} = J_1^T(\phi, \theta, \psi) \begin{bmatrix} u_c^E \\ v_c^E \\ w_c^E \end{bmatrix} \tag{3.107}$$

where

$$J_1(\phi, \theta, \psi) = \begin{bmatrix} \mathrm{c}\psi\mathrm{c}\theta & -\mathrm{s}\psi\mathrm{c}\phi + \mathrm{c}\psi\mathrm{s}\theta\mathrm{s}\phi & \mathrm{s}\psi\mathrm{s}\phi + \mathrm{c}\psi\mathrm{c}\phi\mathrm{s}\theta \\ \mathrm{s}\psi\mathrm{c}\theta & \mathrm{c}\psi\mathrm{c}\phi + \mathrm{s}\phi\mathrm{s}\theta\mathrm{s}\psi & -\mathrm{c}\psi\mathrm{s}\phi + \mathrm{s}\theta\mathrm{s}\psi\mathrm{c}\phi \\ -\mathrm{s}\theta & \mathrm{c}\theta\mathrm{s}\phi & \mathrm{c}\theta\mathrm{c}\phi \end{bmatrix} \tag{3.108}$$

Let us assume that body-fixed current velocity is constant or at least slowly-varying such that the following holds:

$$\dot{\nu}_c = 0 \quad \Longrightarrow \quad \dot{\nu}_r = \dot{\nu} \tag{3.109}$$

Hence, the nonlinear relative equations of motion (3.11) take the form:

$$\boxed{M\,\dot{\nu} + C(\nu_r)\,\nu_r + D(\nu_r)\,\nu_r + g(\eta) = \tau} \tag{3.110}$$

$$\boxed{\dot{\eta} = J(\eta)\,\nu} \tag{3.111}$$

Notice that this model representation is based on the state variables (ν, ν_c, η) with $\nu_r = \nu - \nu_c$.

Method 2:

An alternative representation of the nonlinear equations of motion is obtained by defining (ν_r, ν_c^E, η) as the state variables. Moreover, from (3.11) we have that:

$$\boxed{M\,\dot{\nu}_r + C(\nu_r)\,\nu_r + D(\nu_r)\,\nu_r + g(\eta) = \tau} \tag{3.112}$$

Furthermore, we can write:

$$\dot{\eta} = J(\eta)\,\nu = J(\eta)\,(\nu_r + \nu_c) \tag{3.113}$$

We recall that:

$$\nu_c^E = J(\eta)\,\nu_c \tag{3.114}$$

where $\nu_c^E = [u_c^E, v_c^E, w_c^E, 0, 0, 0]^T$. Hence,

$$\begin{bmatrix} u_c^E \\ v_c^E \\ w_c^E \end{bmatrix} = J_1(\eta) \begin{bmatrix} u_c \\ v_c \\ w_c \end{bmatrix} \tag{3.115}$$

Next, the kinematic equations can be modified to include the new state variable ν_r and a vector ν_c^E describing the earth-fixed current velocity, that is:

$$\boxed{\dot{\eta} = J(\eta)\,\nu_r + \nu_c^E} \tag{3.116}$$

Three-Dimensional Current Model (Submerged Body)

If the vertical velocity profile $V_z(z)$ is known, the average current velocity V_c over the draft of the vehicle can be computed as:

$$V_c = \frac{1}{T}\int_0^T V_z(z)\,dz \tag{3.117}$$

where T is the hull draft. The earth-fixed fluid velocity components (u_c^E, v_c^E, w_c^E) can be related to V_c by defining two angles α (angle of attack) and β (sideslip angle) describing the orientation of V_c about the y- and z-axis, respectively (see Figure 3.12).

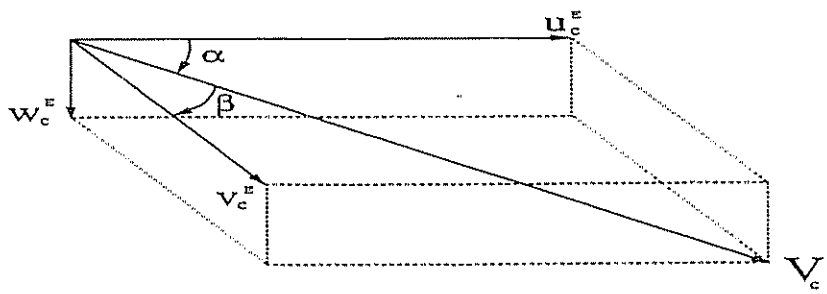

Figure 3.12: Orientation of average current velocity with earth-fixed X, Y, and Z axes.

Using the results from Section 2.1.1, we can write:

$$\begin{bmatrix} u_c^E \\ v_c^E \\ w_c^E \end{bmatrix} = C_{y,\alpha}\, C_{z,-\beta} \begin{bmatrix} V_c \\ 0 \\ 0 \end{bmatrix} \tag{3.118}$$

where $C_{i,j}$ is the transformation matrix defined in (2.8) and V_c is the average current velocity in the earth-fixed reference frame. Expanding this expression yields:

$$u_c^E = V_c \cos\alpha \cos\beta \tag{3.119}$$
$$v_c^E = V_c \sin\beta \tag{3.120}$$
$$w_c^E = V_c \sin\alpha \cos\beta \tag{3.121}$$

Two-Dimensional Current Model (Surface Vessel)

For the 2-D case, the earth-fixed current components can be described by two parameters only, that is average current speed V_c and direction of current β. Consequently, the above 3-D expressions reduce to:

$$u_c^E = V_c \cos\beta \tag{3.122}$$
$$v_c^E = V_c \sin\beta \tag{3.123}$$

Since we are considering the horizontal motion of the vehicle, we can assume that both ϕ and θ are zero which implies that (u_c, v_c) can be computed from (3.107) as:

$$\begin{bmatrix} u_c \\ v_c \end{bmatrix} = \begin{bmatrix} \cos\psi & \sin\psi \\ -\sin\psi & \cos\psi \end{bmatrix} \begin{bmatrix} u_c^E \\ v_c^E \end{bmatrix} \tag{3.124}$$

Substituting the expressions for u_c^E and v_c^E into (3.124) finally yields[3],

$$u_c = V_c \cos(\beta - \psi) \tag{3.125}$$
$$v_c = V_c \sin(\beta - \psi) \tag{3.126}$$

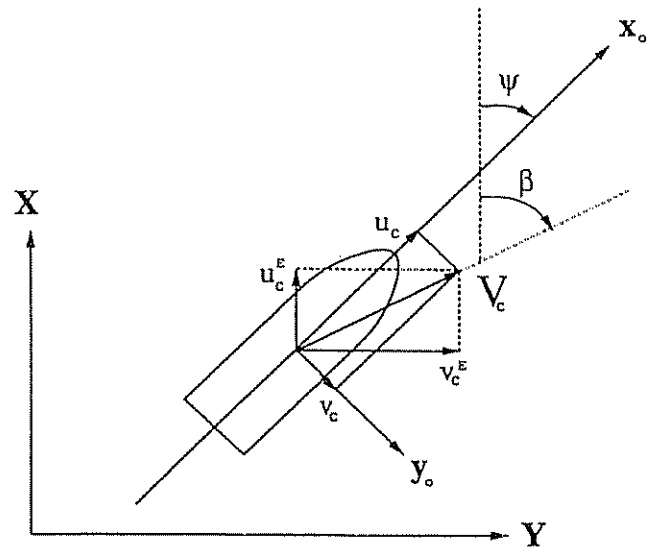

Figure 3.13: Definition of average velocity V_c and direction β of the current for a surface vessel.

[3]Here we have used the trigonometric formulas: (1) $\cos(a-b) = \cos a \cos b + \sin a \sin b$ and (2) $\sin(a-b) = \sin a \cos b - \cos a \sin b$.

Generation of Ocean Currents

For computer simulations the average current velocity can be generated by using a 1st-order *Gauss-Markov Process*. For instance $V_c(t)$ can be described by the following differential equation:

$$\dot{V}_c(t) + \mu_0 V_c(t) = w(t) \tag{3.127}$$

where $w(t)$ is a zero mean Gaussian white noise sequence and $\mu_0 \geq 0$ is a constant. In many cases it is sufficient to choose $\mu_0 = 0$ which simply corresponds to a *random walk*, that is time integration of *white noise*. For details on Gaussian processes see Gelb, Kasper, Jr., Nash, Jr., Price and Sutherland, Jr. (1988).

This process must be limited such that $V_{\min} \leq V_c(t) \leq V_{\max}$ in order to simulate realistic ocean currents. The following algorithm utilizing Euler integration and a simple limiter can be used for this purpose:

Algorithm 3.2 (Current Generator)

1. Initial value: $V_c(0) = 0.5\,(V_{\max} + V_{\min})$.
2. Euler Integration with sampling time h (see Appendix B.2):

$$V_c(k+1) = V_c(k) + h\,\dot{V}_c(k)$$

3. Limiter: *if* $(V_c(k+1) > V_{\max})$ *or* $(V_c(k+1) < V_{\min})$ then

$$V_c(k+1) = V_c(k) - h\,\dot{V}_c(k)$$

4. $k = k+1$, *return to step 2.*

□

Similar algorithms for $\alpha(t)$ and $\beta(t)$ can be used to simulate time-varying directions. We will now show how current disturbances and 1st-order wave disturbances can be included in the ship steering equations of motion.

Example 3.3 (Augmented Model for Ship Steering)

The linear sway-yaw dynamics of a ship with single screw propeller can be written in terms of (see Section 5.3.1):

$$\begin{bmatrix} \dot{v}_L \\ \dot{r}_L \\ \dot{\psi}_L \end{bmatrix} = \begin{bmatrix} a_{11} & a_{12} & 0 \\ a_{21} & a_{22} & 0 \\ 0 & 1 & 0 \end{bmatrix} \begin{bmatrix} v_L - v_c \\ r_L \\ \psi_L \end{bmatrix} + \begin{bmatrix} b_1 \\ b_2 \\ 0 \end{bmatrix} \delta \tag{3.128}$$

where v_L is the sway velocity, r_L is the yaw rate, ψ_L is the heading angle, δ is the rudder angle and v_c is a parameter representing slowly-varying currents (see Equation 3.126). The subscript L is used to denote the low-frequency motion components. The high-frequency oscillatoric motion ψ_H of the waves can then be

added to the model by simply augmenting (3.128) to the linear wave model (3.56) and (3.57), which yields:

$$\begin{bmatrix} \dot{v}_L \\ \dot{r}_L \\ \dot{\psi}_L \\ \dot{V}_c \\ \dot{\psi}_H \\ \dot{\xi}_H \end{bmatrix} = \begin{bmatrix} a_{11} & a_{12} & 0 & -a_{11}\sin(\beta-\psi_L-\psi_H) & 0 & 0 \\ a_{21} & a_{22} & 0 & -a_{21}\sin(\beta-\psi_L-\psi_H) & 0 & 0 \\ 0 & 1 & 0 & 0 & 0 & 0 \\ 0 & 0 & 0 & -\mu_0 & 0 & 0 \\ 0 & 0 & 0 & 0 & -\omega_e^2 & -2\zeta\omega_e \\ 0 & 0 & 0 & 0 & 1 & 0 \end{bmatrix} \begin{bmatrix} v_L \\ r_L \\ \psi_L \\ V_c \\ \psi_H \\ \xi_H \end{bmatrix} + \begin{bmatrix} b_1 \\ b_2 \\ 0 \\ 0 \\ 0 \\ 0 \end{bmatrix} \delta + \begin{bmatrix} 0 & 0 \\ 0 & 0 \\ 0 & 0 \\ 1 & 0 \\ 0 & K_w \\ 0 & 0 \end{bmatrix} \begin{bmatrix} w_1 \\ w_2 \end{bmatrix} + \begin{bmatrix} Y_{wind} \\ N_{wind} \\ 0 \\ 0 \\ 0 \\ 0 \end{bmatrix} \tag{3.129}$$

where w_1 and w_2 are zero mean Gaussian white noise processes and Y_{wind} and N_{wind} are two additional terms used to describe the wind force and moment in sway and yaw. For this system the compass measurement equation is written:

$$\psi = \psi_L + \psi_H + v \tag{3.130}$$

where v is zero mean Gaussian white noise process. This particular way of modeling the ship-wave interactions is attractive for control systems design and state estimation.

□

3.5 Conclusions

In this chapter, we have discussed simple models for wave, wind and current-induced forces and moments in terms of the 6 DOF marine vehicle equations of motion. This is done by applying spectral formulations of wind and waves whereas currents are modelled as random walks.

The models discussed in this chapter are mainly intended for simulation and design of model-based control systems. Consequently, accurate prediction of marine vehicles in the presence of wind, waves and currents require more advanced modeling techniques. A more detailed discussion on regular and irregular Airy (linear) wave theory can be found in Newman (1977) and Faltinsen (1990) while a detailed discussion on 2nd- and 5th-order Stokes theory is given by Sarpkaya (1981). In addition to this, it is recommended that one consults Ochi and Bales (1977) for a comparison and discussion of different wave spectra.

Some standard references on wave, wind and current models with application to ship control are Zuidweg (1970), Källström (1979), Jenssen (1980) and Blanke (1981); De Kat and Wichers (1991) and references therein is an excellent reference for moored ships.

3.6 Exercises

3.1 Plot the wave frequency ω as a function of depth d for a wave with wave length $\lambda = 100$ m. Show that if the ratio d/λ is large enough, ω will approach $\sqrt{k\,g}$, where g is the acceleration of gravity. This result should also be verified theoretically.

3.2 Show that:

$$\omega_0 = \sqrt[4]{\frac{4B}{5}} \tag{3.131}$$

is the modal frequency for the Pierson–Moskowitz spectrum. Find an analytical expression for the peak frequency of the JONSWAP and the modified Pierson–Moskowitz (MPM) spectrum.

3.3 Plot the spectral density function for the Harris spectrum together with a linear approximation of the same spectrum in a dB-$\log_{10}(\omega)$ diagram for $V_w(10) \in \{10$ (knots), 20 (knots), 50 (knots) $\}$. Is the linear approximation valid for the whole frequency range ?

3.4 Compare the spectral formulations for the Harris, Davenport and, Ochi and Shin spectra by plotting $S(\omega)$ versus ω in a dB-$\log_{10}(\omega)$ diagram. Comment on the results.

3.5 Plot the frequency of encounter as a function of negative and positive speeds U with $\beta = 0$ and $\omega_0 = 0.6$ (rad/s). Repeat the computation with $U = 1$ (m/s) and $\beta \in [0^o\ 360^o\rangle$. Comment on the results.

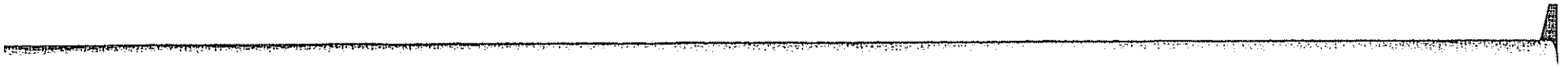

Chapter 4

Stability and Control of Underwater Vehicles

Conventional autopilot design based on linear theory starts with the assumption that the 6 DOF underwater vehicle equations of motion can be described as a linear model linearized around a point of equilibrium. This may be a rough approximation for many control applications. Indeed, underwater vehicles performing coupled maneuvers at some speed are known to be highly nonlinear in their dynamics and kinematics. In such cases autopilots based on linear control theory can yield poor performance.

It is a common assumption that linear control design is much simpler than its nonlinear counterpart. However, exploiting the structure of the nonlinear equations of motion often yields a relatively simple and intuitive nonlinear autopilot design. This will clearly be shown in this chapter which emphasizes the following topics:

- Remotely operated vehicle (ROV) equations of motion
- Stability of underwater vehicles
- Conventional and nonlinear autopilot design of PID-type
- Linear quadratic optimal autopilot design
- Decoupled autopilot design
- Sliding mode control
- Feedback linearization
- Nonlinear tracking
- Adaptive autopilot design

This involves the design of automatic speed control systems, systems for dynamic positioning and tracking, as well as autopilot systems for automatic steering and depth control.

4.1 ROV Equations of Motion

This section discusses different representations of the linear and nonlinear ROV equations of motion.

4.1.1 Thruster Model

Bilinear Thruster Model

In the general case, the thruster force and moment vector will be a complicated function depending on the vehicle's velocity vector $\nu \in \mathbb{R}^6$ and the control variable $n \in \mathbb{R}^p$ $(p \geq 6)$. This relationship can be expressed as:

$$\boxed{\tau = b(\nu, n)} \tag{4.1}$$

where $b(\cdot)$ is a nonlinear vector function. A 1st-order approximation of the developed thrust T and torque Q for a single-screw propeller can be derived from lift force calculations (see Blanke 1981). Let n denote the propeller revolution, D the propeller diameter, ρ the water density and V_a the advance speed at the propeller (speed of the water going into the propeller). Hence the following expressions for the propeller thrust can be established:

$$T = \rho D^4 K_T(J_0)\,|n|n \tag{4.2}$$

where $J_0 = V_a/(nD)$ is the *advance number* and K_T is the *thrust coefficient*; see Section 6.2.1 for details. In the general case K_T will be a four quadrant nonlinear function as shown in Figure 4.1.

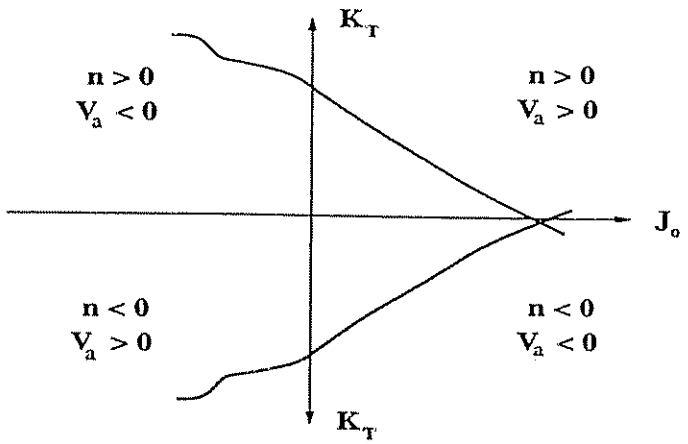

Figure 4.1: Four quadrant positive K_T curve as a function of J_0. For positive values of J_0 experiments verify that K_T is approximately linear in J_0 while the results for negative J_0-values often show a nonlinear behavior; see Van Lammern et al. (1969) and Fossen (1991), pp. 45–47.

In the general case the forward and backward thrusts will be non-symmetrical. However, many ROV thruster systems are designed to give symmetrical thrust. Furthermore, K_T usually shows linear behavior in J_0 such that the following approximation holds:

$$K_T = \alpha_1 + \alpha_2 \frac{V_a}{nD} \tag{4.3}$$

where α_1 and α_2 are two constants given by the curves shown in Figure 4.1. This implies that the thruster force (4.2) can be written:

$$T(n, V_a) = T_{|n|n}\, |n|n + T_{|n|V_a} |n|\, V_a \tag{4.4}$$

where $T_{|n|n} > 0$ and $T_{|n|V_a} < 0$. By using a similar approach it can be shown that the thruster torque can be written:

$$Q(n, V_a) = Q_{|n|n}\, |n|n + Q_{|n|V_a} |n|\, V_a \tag{4.5}$$

Here $Q_{|n|n} > 0$ and $Q_{|n|V_a} < 0$ are design parameters depending on propeller diameter, shape of the duct, water density etc.

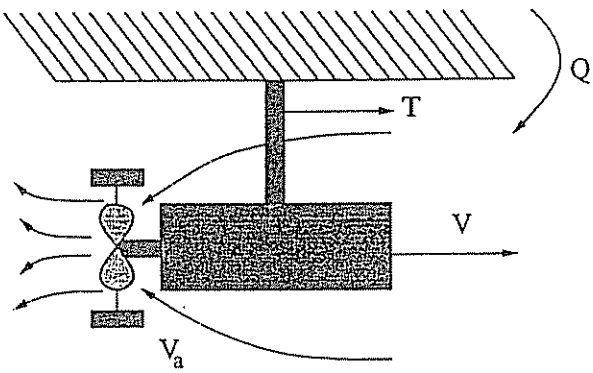

Figure 4.2: Schematic drawing of propeller.

The above coefficients will also depend on n and V_a since (4.4) and (4.5) are only first-order approximations to a more general expression. However, experiments have shown that this dependency can be neglected for most practical conditions of operation. The advance speed V_a is related through the speed of the vehicle V according to (see Figure 4.2):

$$V_a = (1 - w)\, V \tag{4.6}$$

where w is the wake fraction number (typically: 0.1–0.4). Using the result, (4.4) implies that the propeller force developed by a single propeller can be described by the nonlinear function:

$$\tau = b_1\, |n|n - b_2\, |n|\, \nu \tag{4.7}$$

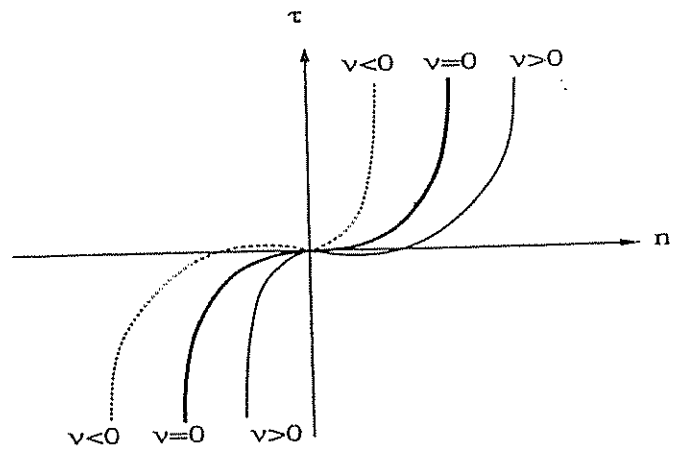

Figure 4.3: Propeller force τ as a function of propeller revolution n and speed of the vehicle ν.

where $b_1 = T_{|n|n} > 0$, $b_2 = -T_{|n|V_a}(1-w) > 0$ and $\nu = V$. An extension to the multivariable case could be to write:

$$\boxed{\tau = B_1\, u - B_2(u)\, \nu} \tag{4.8}$$

where B_1 and $B_2(u)$ are two matrices of appropriate dimensions and $u \in \mathbb{R}^p$ is a new control variable defined as:

$$u_i = |n_i|\, n_i \qquad (i = 1 \ldots p) \tag{4.9}$$

A similar discussion on propeller forces can be made for ships, see Section 6.2.1.

Affine Thruster Model

In many practical applications the *bilinear* model can be approximated by an *affine* model, that is a system which is linear in its input. For instance, we can approximate (4.8) as:

$$\boxed{\tau = B\, u} \tag{4.10}$$

by letting $B = B_1$ and:

$$B_2(u)\, \nu \approx 0 \tag{4.11}$$

Notice that for zero velocity, that is $\nu = 0$, this will always be true. Moreover, this implies that the propeller force in the i-th DOF developed by the j-th propeller can be described by:

$$\tau_i = B_{ij}\, u_j; \qquad B_{ij} = T_{|n|n} \tag{4.12}$$

In the rest of this chapter, we will mainly consider *affine* systems since the theory of non-affine control systems is quite limited. In fact, this is still an active area

of research. However, regulation of non-affine systems will be discussed briefly in Section 4.3.3.

Actuator Dynamics

Most thruster systems are driven by small DC motors designed for underwater operating conditions. The dynamic model of a speed-controlled DC motor can be written:

$$L_a \frac{di_a}{dt} = -R_a\, i_a - 2\pi K_M\, n + u_a \tag{4.13}$$

$$2\pi J_m \frac{dn}{dt} = K_M\, i_a - Q(n, V_a) \tag{4.14}$$

where L_a is the armature inductance, R_a is the armature resistance, u_a is the armature voltage, K_M is the motor torque constant, J_m is the moment of inertia of motor and thruster, n is the velocity of the motor in revolutions per second and $Q(n, V_a)$ is the load from the propeller defined in (4.5).

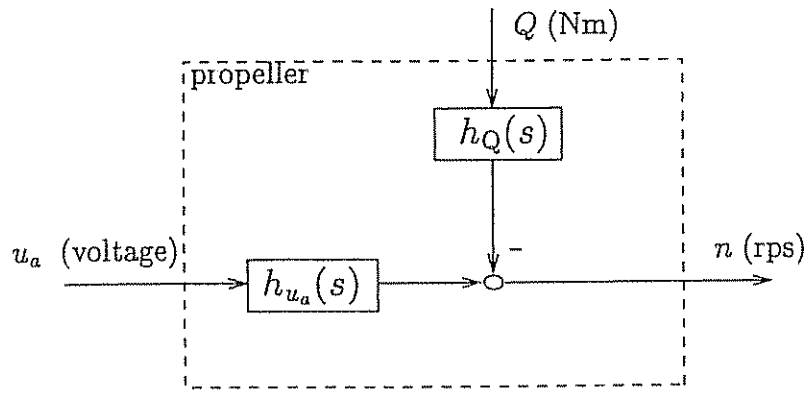

Figure 4.4: Propeller transfer functions

Due to physical limitations of the DC motor, hard nonlinearities like actuator saturation, Coulomb friction, dead-zones and hysteresis should also be included in the complete model. Neglecting these effects, implies that we can apply Laplace's transformation to (4.13) and (4.14). Moreover,

$$n(s) = h_{u_a}(s)\, u_a(s) - h_Q(s)\, Q(s) \tag{4.15}$$

where s is the Laplace variable and:

$$h_{u_a}(s) = \frac{K_1}{(1+T_1 s)(1+T_2 s)}; \qquad h_Q(s) = \frac{K_2(1+T_3 s)}{(1+T_1 s)(1+T_2 s)} \tag{4.16}$$

Here K_i $(i = 1, 2)$ are two gain constants and T_i $(i = 1, 2, 3)$ are three time constants depending on the parameters in (4.13) and (4.14).

Optimal Distribution of Propulsion and Control Forces

For underwater vehicles where the control matrix $\boldsymbol{B}$ is non-square and $p \geq n$, that is there are equal or more control inputs than controllable DOF, it is possible to find an "optimal" distribution of control energy, for each DOF (Fossen and Sagatun 1991a). Consider the quadratic energy cost function:

$$J = \frac{1}{2}\boldsymbol{u}^T\boldsymbol{W}\boldsymbol{u} \tag{4.17}$$

which can be minimized subject to:

$$\boldsymbol{\tau} - \boldsymbol{B}\boldsymbol{u} = 0 \tag{4.18}$$

Here $\boldsymbol{W}$ is a positive definite matrix, usually diagonal, weighting the control energy. For underwater vehicles which have both control surfaces and thrusters, the elements in $\boldsymbol{W}$ should be selected such that using the control surfaces is much more inexpensive than using the thrusters, that is providing a means of saving battery energy. Define the Lagrangian:

$$L(\boldsymbol{u}, \boldsymbol{\lambda}) = \frac{1}{2}\boldsymbol{u}^T\boldsymbol{W}\boldsymbol{u} + \boldsymbol{\lambda}^T(\boldsymbol{\tau} - \boldsymbol{B}\boldsymbol{u}) \tag{4.19}$$

where $\boldsymbol{\lambda}$ denotes the Lagrange multipliers. Hence, differentiating the Lagrangian L with respect to $\boldsymbol{u}$ yields:

$$\frac{\partial L}{\partial \boldsymbol{u}} = \boldsymbol{W}\boldsymbol{u} - \boldsymbol{B}^T\boldsymbol{\lambda} = 0 \tag{4.20}$$

From this expression we obtain:

$$\boldsymbol{u} = \boldsymbol{W}^{-1}\boldsymbol{B}^T\boldsymbol{\lambda} \tag{4.21}$$

By using the fact that:

$$\boldsymbol{\tau} = \boldsymbol{B}\boldsymbol{u} = \boldsymbol{B}\boldsymbol{W}^{-1}\boldsymbol{B}^T\boldsymbol{\lambda} \tag{4.22}$$

and assuming that $\boldsymbol{B}\boldsymbol{W}^{-1}\boldsymbol{B}^T$ is non-singular, we find the following optimal solution for the Lagrange multiplicators:

$$\boldsymbol{\lambda} = (\boldsymbol{B}\boldsymbol{W}^{-1}\boldsymbol{B}^T)^{-1}\boldsymbol{\tau} \tag{4.23}$$

Substituting this result into (4.21) yields the *generalized inverse*:

$$\boxed{\boldsymbol{B}_{\boldsymbol{W}}^{\dagger} = \boldsymbol{W}^{-1}\boldsymbol{B}^T(\boldsymbol{B}\boldsymbol{W}^{-1}\boldsymbol{B}^T)^{-1}} \tag{4.24}$$

which suggests that $\boldsymbol{u}$ can be computed as:

$$\boldsymbol{u} = \boldsymbol{B}_{\boldsymbol{W}}^{\dagger}\,\boldsymbol{\tau} \tag{4.25}$$

In the case when all inputs are equality weighted, that is $\boldsymbol{W} = \boldsymbol{I}$, (4.24) simplifies to:

$$\boxed{B^{\dagger} = B^T(BB^T)^{-1}} \tag{4.26}$$

This simplified result is known as the *Moore–Penrose pseudo inverse*. Notice that for the square case ($p = n$), $B^{\dagger}$ is simply equal to B^{-1}.

4.1.2 Nonlinear ROV Equations of Motion

The nonlinear ROV equations of motion can be represented both in the body-fixed and the earth-fixed reference frames. This has already been shown in Section 2.5. The body-fixed and earth-fixed vector representations are as follows:

Body-Fixed Vector Representation

$$\boxed{M\,\dot{\nu} + C(\nu)\,\nu + D(\nu)\,\nu + g(\eta) = \tau} \tag{4.27}$$

$$\boxed{\dot{\eta} = J(\eta)\,\nu} \tag{4.28}$$

Earth-Fixed Vector Representation

$$\boxed{M_{\eta}(\eta)\,\ddot{\eta} + C_{\eta}(\nu,\eta)\,\dot{\eta} + D_{\eta}(\nu,\eta)\,\dot{\eta} + g_{\eta}(\eta) = J^{-T}(\eta)\,\tau} \tag{4.29}$$

The state vectors are $\nu = [u, v, w, p, q, r]^T$ and $\eta = [x, y, z, \phi, \theta, \psi]^T$. The different matrices and their properties are discussed more closely in Section 2.5.

4.1.3 Linear ROV Equations of Motion

The linear equations of motion are obtained by linearization of the general expressions (4.27) and (4.28) about a time-varying reference trajectory or an equilibrium point, for instance:

$$\nu_0(t) = [u_0(t), v_0(t), w_0(t), p_0(t), q_0(t), r_0(t)]^T \tag{4.30}$$
$$\eta_0(t) = [x_0(t), y_0(t), z_0(t), \phi_0(t), \theta_0(t), \psi_0(t)]^T \tag{4.31}$$

6 DOF Perturbed Equations of Motion

Let the perturbations from the reference trajectory $\nu_0(t)$ and $\eta_0(t)$ be described by the differentials:

$$\Delta\nu(t) = \nu(t) - \nu_0(t); \quad \Delta\eta(t) = \eta(t) - \eta_0(t); \quad \Delta\tau(t) = \tau(t) - \tau_0(t) \tag{4.32}$$

Introducing the following vector notation:

$$f_c(\nu) = C(\nu)\,\nu; \qquad f_d(\nu) = D(\nu)\,\nu \tag{4.33}$$

implies that (4.27) can be linearized according to:

$$M\,\Delta\dot{\nu} + \left.\frac{\partial f_c(\nu)}{\partial \nu}\right|_{\nu_0} \Delta\nu + \left.\frac{\partial f_d(\nu)}{\partial \nu}\right|_{\nu_0} \Delta\nu + \left.\frac{\partial g(\eta)}{\partial \eta}\right|_{\eta_0} \Delta\eta = \Delta\tau \tag{4.34}$$

Perturbating (4.28) yields:

$$\dot{\eta}_0 + \Delta\dot{\eta} = J(\eta_0 + \Delta\eta)\,[\nu_0 + \Delta\nu] \tag{4.35}$$

Substituting $\dot{\eta}_0 = J(\eta_0)\,\nu_0$ into this expression implies that:

$$\Delta\dot{\eta} = J(\eta_0 + \Delta\eta)\,\Delta\nu + [J(\eta_0 + \Delta\eta) - J(\eta_0)]\,\nu_0 \tag{4.36}$$

Linear theory implies that 2nd-order terms ($\Delta\eta_i\,\Delta\nu_j \approx 0$) can be neglected. Hence,

$$\boxed{\Delta\dot{\eta} = J(\eta_0)\,\Delta\nu + J^*(\nu_0, \eta_0)\,\Delta\eta} \tag{4.37}$$

Here we have rearranged the last term in (4.36) according to:

$$[J(\eta_0 + \Delta\eta) - J(\eta_0)]\,\nu_0 \triangleq J^*(\nu_0, \eta_0)\,\Delta\eta \tag{4.38}$$

The following two special cases of (4.37) are particularly useful:

$$\begin{array}{lll} (1) & \nu_0 = 0 & \longrightarrow \quad \Delta\dot{\eta} = J(\eta_0)\,\Delta\nu \\ (2) & \nu_0 = \eta_0 = 0 & \longrightarrow \quad \Delta\dot{\eta} = \Delta\nu \end{array}$$

Linear Time-Varying ROV Equations of Motion

Defining $x_1 = \Delta\nu$ and $x_2 = \Delta\eta$, yields the following linear time-varying model:

$$M\,\dot{x}_1 + C(t)\,x_1 + D(t)\,x_1 + G(t)\,x_2 \;=\; \tau \tag{4.39}$$

$$\dot{x}_2 = J(t)\,x_1 + J^*(t)\,x_2 \tag{4.40}$$

where

$$\begin{aligned} C(t) &= \left.\frac{\partial f_c(\nu)}{\partial \nu}\right|_{\nu_0(t)} & G(t) &= \left.\frac{\partial g(\eta)}{\partial \eta}\right|_{\eta_0(t)} & J(t) &= J(\eta_0(t)) \\ D(t) &= \left.\frac{\partial f_d(\nu)}{\partial \nu}\right|_{\nu_0(t)} & J^*(t) &= J^*(\nu_0(t), \eta_0(t)) \end{aligned} \tag{4.41}$$

Defining $x = [x_1^T,\, x_2^T]^T$ and $u = \tau$, we obtain the following state-space model:

$$\begin{bmatrix} \dot{x}_1 \\ \dot{x}_2 \end{bmatrix} = \begin{bmatrix} -M^{-1}[C(t) + D(t)] & -M^{-1}G(t) \\ J(t) & J^*(t) \end{bmatrix} \begin{bmatrix} x_1 \\ x_2 \end{bmatrix} + \begin{bmatrix} M^{-1} \\ 0 \end{bmatrix} u \tag{4.42}$$

which can be written in abbreviated form as:

$$\dot{x} = A(t)\, x + B(t)\, u \tag{4.43}$$

Linear Time-Invariant ROV Equations of Motion

In many ROV applications it is reasonable to assume that the ROV is moving in the longitudinal plane with non-zero velocity components u_0 and w_0 in the x- and z-directions, respectively. Furthermore, let us assume that the steady-state linear and angular velocity components: $v_0 = p_0 = q_0 = r_0 = 0$ and that the equilibrium point is defined by the zero roll and pitch angles, that is: $\phi_0 = \theta_0 = 0$. Hence, the time-varying matrices in (4.42) simplify to the following constant matrices:

$$M = \begin{bmatrix} m - X_{\dot{u}} & -X_{\dot{v}} & -X_{\dot{w}} & -X_{\dot{p}} & mz_G - X_{\dot{q}} & -my_G - X_{\dot{r}} \\ -X_{\dot{v}} & m - Y_{\dot{v}} & -Y_{\dot{w}} & -mz_G - Y_{\dot{p}} & -Y_{\dot{q}} & mx_G - Y_{\dot{r}} \\ -X_{\dot{w}} & -Y_{\dot{w}} & m - Z_{\dot{w}} & my_G - Z_{\dot{p}} & -mx_G - Z_{\dot{q}} & -Z_{\dot{r}} \\ -X_{\dot{p}} & -mz_G - Y_{\dot{p}} & my_G - Z_{\dot{p}} & I_x - K_{\dot{p}} & -I_{xy} - K_{\dot{q}} & -I_{xz} - K_{\dot{r}} \\ mz_G - X_{\dot{q}} & -Y_{\dot{q}} & -mx_G - Z_{\dot{q}} & -I_{xy} - K_{\dot{q}} & I_y - M_{\dot{q}} & -I_{yz} - M_{\dot{r}} \\ -my_G - X_{\dot{r}} & mx_G - Y_{\dot{r}} & -Z_{\dot{r}} & -I_{xz} - K_{\dot{r}} & -I_{yz} - M_{\dot{r}} & I_z - N_{\dot{r}} \end{bmatrix}$$

$$D = -\begin{bmatrix} X_u & X_v & X_w & X_p & X_q & X_r \\ Y_u & Y_v & Y_w & Y_p & Y_q & Y_r \\ Z_u & Z_v & Z_w & Z_p & Z_q & Z_r \\ K_u & K_v & K_w & K_p & K_q & K_r \\ M_u & M_v & M_w & M_p & M_q & M_r \\ N_u & N_v & N_w & N_p & N_q & N_r \end{bmatrix} \qquad C = \begin{bmatrix} 0 & C_{12} \\ -C_{12}^T & C_{22} \end{bmatrix}$$

$$C_{12} = \begin{bmatrix} 0 & -X_{\dot{w}}u_0 + (m - Z_{\dot{w}})w_0 & X_{\dot{v}}u_0 + Y_{\dot{w}}w_0 \\ X_{\dot{w}}u_0 - (m - Z_{\dot{w}})w_0 & 0 & (m - X_{\dot{u}})u_0 - X_{\dot{w}}w_0 \\ -X_{\dot{v}}u_0 - Y_{\dot{w}}w_0 & -(m - X_{\dot{u}})u_0 + X_{\dot{w}}w_0 & 0 \end{bmatrix}$$

Assuming that $x_G = y_G = z_G = 0$ see Eq. (2.102)

$$C_{22} = \begin{bmatrix} 0 & -(X_{\dot{r}}u_0 + Z_{\dot{r}}w_0) & X_{\dot{q}}u_0 + Z_{\dot{q}}w_0 \\ X_{\dot{r}}u_0 + Z_{\dot{r}}w_0 & 0 & -(X_{\dot{p}}u_0 + Z_{\dot{p}}w_0) \\ -(X_{\dot{q}}u_0 + Z_{\dot{q}}w_0) & X_{\dot{p}}u_0 + Z_{\dot{p}}w_0 & 0 \end{bmatrix}$$

$$G = \begin{bmatrix} 0 & 0 & 0 & 0 & (W - B) & 0 \\ 0 & 0 & 0 & -(W - B) & 0 & 0 \\ 0 & 0 & 0 & 0 & 0 & 0 \\ 0 & 0 & 0 & (z_G W - z_B B) & 0 & 0 \\ 0 & 0 & 0 & 0 & (z_G W - z_B B) & 0 \\ 0 & 0 & 0 & -(x_G W - x_B B) & -(y_G W - y_B B) & 0 \end{bmatrix} \tag{4.44}$$

If we assume that $\psi_0 = \text{constant}$ and $\phi_0 = \theta_0 = 0$, the kinematic transformation matrix J takes the form:

$$J = \begin{bmatrix} J_1 & 0 \\ 0 & I \end{bmatrix}; \qquad J_1 = \begin{bmatrix} \cos\psi_0 & -\sin\psi_0 & 0 \\ \sin\psi_0 & \cos\psi_0 & 0 \\ 0 & 0 & 1 \end{bmatrix} \tag{4.45}$$

whereas $J^* = 0$. Consequently, the linear time-invariant model can be written as:

$$\dot{x} = A\, x + B\, u \tag{4.46}$$

$$\Updownarrow$$

$$\begin{bmatrix} \dot{x}_1 \\ \dot{x}_2 \end{bmatrix} = \begin{bmatrix} -M^{-1}[C + D] & -M^{-1}G \\ J & 0 \end{bmatrix} \begin{bmatrix} x_1 \\ x_2 \end{bmatrix} + \begin{bmatrix} M^{-1} \\ 0 \end{bmatrix} u \tag{4.47}$$

where A and B are constant matrices. Notice that C will be zero if we require that $u_0 = w_0 = 0$ in addition to $v_0 = 0$.

4.2 Stability of Underwater Vehicles

Stability of an underwater vehicle can be defined as the ability of returning to an equilibrium state of motion after a disturbance without any corrective action, such as use of thruster power or control surfaces. Hence, maneuverability can be defined as the capability of the vehicle to carry out specific maneuvers. Excessive stability implies that the control effort will be excessive while a marginally stable vehicle is easy to control. Thus, a compromise between stability and maneuverability must be made. Furthermore, it makes sense to distinguish between *controls-fixed* and *controls-free* stability. The essential difference between these terms is that:

- **Controls-fixed stability** implies investigating the vehicle's stability when the control surfaces are fixed and when the thrust from all the thrusters is constant.
- **Controls-free stability** refers to the case when both the control surfaces and the thruster power are allowed to vary. This implies that the dynamics of the control system must also be considered in the stability analysis.

These terms will be described more closely in the next sections.

4.2.1 Open-Loop Stability

Open-loop (controls-fixed) stability analysis of marine vehicles concerns the problem of finding static stability criteria based on the hydrodynamic derivatives. For linear models this is quite simple thanks to the well known techniques of Routh and Hurwitz. This section shows that an alternative approach based on Lyapunov's direct method can be applied in the nonlinear case. For marine vehicles the Lyapunov function V can be chosen to represent the system's total mechanical energy. Consider the Lyapunov function candidate

$$V(\eta, \dot{\eta}) = \frac{1}{2}\, \dot{\eta}^T\, M_\eta(\eta)\, \dot{\eta} + \int_0^\eta g_\eta^T(z)\, dz \tag{4.48}$$

where M_η and g_η are defined in Chapter 2. Here V can be interpreted as the sum of the kinetic and potential energy of the vehicle. Hence, zero energy corresponds to the equilibrium point $\eta = 0$ and $\dot{\eta} = 0$. Instability corresponds to a growth in mechanical energy while asymptotic stability ensures the convergence of mechanical energy to zero. Differentiating V with respect to time (assuming $M_\eta = M_\eta^T > 0$) yields:

$$\dot{V} = \dot{\eta}^T\, [M_\eta(\eta)\ddot{\eta} + g_\eta(\eta)] + \frac{1}{2}\, \dot{\eta}^T\, \dot{M}_\eta\, \dot{\eta} \tag{4.49}$$

Hence the expression for $\dot{V}$ can be rewritten as:

$$\dot{V} = \dot{\eta}^T \left[M_\eta(\eta)\ddot{\eta} + C_\eta(\nu,\eta)\dot{\eta} + g_\eta(\eta) \right] + \frac{1}{2}\dot{\eta}^T \left[\dot{M}_\eta - 2C_\eta(\nu,\eta) \right] \dot{\eta} \tag{4.50}$$

Applying the skew-symmetric property: $\dot{\eta}^T \left(\dot{M}_\eta - 2C_\eta \right) \dot{\eta} = 0 \ \forall \ \dot{\eta}$, yields

$$\dot{V} = \dot{\eta}^T \left[M_\eta \ddot{\eta} + C_\eta(\nu,\eta)\dot{\eta} + g_\eta(\eta) \right] \tag{4.51}$$

In controls-fixed stability analyses, the dynamics of the control inputs is neglected. Hence, we simply consider the system:

$$M_\eta(\eta)\ddot{\eta} + C_\eta(\nu,\eta)\dot{\eta} + D_\eta(\nu,\eta)\dot{\eta} + g_\eta(\eta) = 0 \tag{4.52}$$

Applying this equation to the expression for $\dot{V}$, finally yields:

$$\dot{V} = -\dot{\eta}^T D_\eta \dot{\eta} = -\nu^T D \nu \tag{4.53}$$

Theorem 4.1 (Controls-Fixed Stability)
According to Lyapunov stability theory, Appendix C.1, sufficient conditions for controls-fixed stability are:

(i) $V > 0$ *for all* $\dot{\eta}, \eta \in \mathbb{R}^n$ *whereas* $\dot{\eta} \neq 0$ *and* $\eta \neq 0$. *Hence:*

$$\dot{\eta}^T M_\eta(\eta)\, \dot{\eta} = \nu^T M \nu > 0 \qquad \nu \neq 0 \tag{4.54}$$

if and only if the inertia matrix:

$$M > 0 \tag{4.55}$$

Notice that $J^{-1}(\eta)$ *is defined for all* $\eta \in \mathbb{R}^n$ *while* $J(\eta)$ *is undefined for* $\theta = \pm 90^o$.

(ii) $\dot{V} < 0$ *for all* $\nu \in \mathbb{R}^n$ *if and only if the damping matrix:*

$$D(\nu) > 0 \ \forall \ \nu \in \mathbb{R}^n \tag{4.56}$$

(iii) $V \to \infty$ *as* $\|\eta\| \to \infty$ *and* $\|\dot{\eta}\| \to \infty$. *This is satisfied for (4.48).*

□

The first condition simply states that the inertia including hydrodynamic added mass must be strictly positive. For underwater vehicles we can assume constant added mass (independent of the wave frequency) which implies that $\dot{M} = 0$ and $M = M^T > 0$. The second condition simply states that the system must be

dissipative which is also true for an uncontrolled undisturbed ROV. Moreover, energy should not be generated by the system itself.

The uncontrolled system above is said to be *autonomous* since it does not explicitly depend on time t. Hence, we can apply *Lyapunov's direct method* to prove stability (see Appendix C.1.1). If tracking of a time-varying reference trajectory is of interest, the new dynamics associated with the tracking error will be *non-autonomous*. By non-autonomous we mean a system with state equation:

$$\dot{\boldsymbol{x}} = \boldsymbol{f}(\boldsymbol{x}, t) \tag{4.57}$$

where the nonlinear function $\boldsymbol{f}(\boldsymbol{x}, t)$ explicitly depends on time. In order to prove convergence or stability of this system non-autonomous theory must be applied.

4.2.2 Closed-Loop Tracking Control

In this section, it will be shown how *Barbălat's lemma* can be used to derive a non-autonomous tracking control law. The design methodology is best illustrated by considering a simple example.

Example 4.1 (Velocity Tracking Control)
Assume that we want to control the vehicle's linear and angular velocities. Let the error dynamics be denoted by $\tilde{\boldsymbol{\nu}}(t) = \boldsymbol{\nu}(t) - \boldsymbol{\nu}_d(t)$ *where* $\boldsymbol{\nu}_d(t)$ *is the desired state vector. For marine vehicles as well as mechanical systems in general, we can define a Lyapunov function candidate:*

$$V(\tilde{\boldsymbol{\nu}}, t) = \frac{1}{2}\, \tilde{\boldsymbol{\nu}}^T \boldsymbol{M} \tilde{\boldsymbol{\nu}} \tag{4.58}$$

which can be interpreted as the "pseudo-kinetic" energy of the vehicle. Differentiating V *with respect to time (assuming* $\boldsymbol{M} = \boldsymbol{M}^T$ *and* $\dot{\boldsymbol{M}} = \boldsymbol{0}$*) yields:*

$$\dot{V} = \tilde{\boldsymbol{\nu}}^T\, \boldsymbol{M}\, \dot{\tilde{\boldsymbol{\nu}}} \tag{4.59}$$

Substituting (4.27) into the expression for $\dot{V}$ *yields:*

$$\dot{V} = \tilde{\boldsymbol{\nu}}^T[\boldsymbol{\tau} - \boldsymbol{M}\dot{\boldsymbol{\nu}}_d - \boldsymbol{C}(\boldsymbol{\nu})\boldsymbol{\nu}_d - \boldsymbol{D}(\boldsymbol{\nu})\boldsymbol{\nu}_d - \boldsymbol{g}(\boldsymbol{\eta})] - \tilde{\boldsymbol{\nu}}^T \boldsymbol{D}(\boldsymbol{\nu})\tilde{\boldsymbol{\nu}} \tag{4.60}$$

Here we have used the skew-symmetric property: $\tilde{\boldsymbol{\nu}}^T \boldsymbol{C}(\boldsymbol{\nu})\tilde{\boldsymbol{\nu}} = 0 \;\; \forall \;\; \tilde{\boldsymbol{\nu}} \in \mathbb{R}^n$. *This suggests that the control law could be be selected as*[1]*:*

$$\boldsymbol{\tau} = \boldsymbol{M}\dot{\boldsymbol{\nu}}_d + \boldsymbol{C}(\boldsymbol{\nu})\boldsymbol{\nu}_d + \boldsymbol{D}(\boldsymbol{\nu})\boldsymbol{\nu}_d + \boldsymbol{g}(\boldsymbol{\eta}) - \boldsymbol{K}_d\tilde{\boldsymbol{\nu}} \tag{4.61}$$

where $\boldsymbol{K}_d$ *is a positive regulator gain matrix of appropriate dimension. Hence:*

$$\dot{V} = -\tilde{\boldsymbol{\nu}}^T\, [\boldsymbol{D}(\boldsymbol{\nu}) + \boldsymbol{K}_d]\, \tilde{\boldsymbol{\nu}} \;\leq\; 0 \tag{4.62}$$

[1]This type of control action is usually referred to as the Slotine and Li algorithm in robotics (Slotine and Li 1987). However, in this case the special structure of the underwater vehicle dynamics is exploited in the design.

Notice that $\dot{V} \leq 0$ implies that $V(t) \leq V(0) \quad \forall\ t \geq 0$, and therefore that $\tilde{\nu}$ is bounded. This in turn implies that $\ddot{V}$ is bounded. Hence, $\dot{V}$ must be uniformly continuous. Finally, application of Barbălat's lemma (see Appendix C.1) shows that $\dot{V} \to 0$ which implies that $\tilde{\nu} \to 0$ as $t \to \infty$.

□

4.3 Conventional Autopilot Design

This section starts with a brief review of PID-control design before we discuss extensions to nonlinear control theory.

4.3.1 Joy-Stick Control Systems Design

It is common to classify control systems into two fundamental types, *open-loop* and *closed-loop* (feedback) control systems. Figure 4.5 shows an *open-loop* ROV autopilot system where the commanded feedforward force and moment vector τ_c is generated by the ROV pilot. The output from the joy-stick system u is computed by applying the generalized inverse $B_W^{\dagger}$ of the input matrix. Open-loop systems work satisfactory if the environmental disturbances are not too large and if the numerical expression for B is known with sufficient accuracy.

Improved robustness and performance in the presence of environmental disturbances can be obtained by applying a *closed-loop* control system of PID-type (proportional, derivative and integral) instead, see Figure 4.5 In this case, the pilot joy-stick is used to generate the commanded position and attitude η_c (or alternatively linear and angular velocity). *Closed-loop* control requires that sensor/navigation data are available for feedback.

In Figure 4.5 a reference pre-filter is included to smooth out the commanded input. This is done to avoid saturation in the actuator as a result of large tracking errors caused by steps in the commanded input. For a second-order system, the reference pre-filter is usually chosen as:

$$\ddot{\eta}_d + 2\,\Lambda\,\Omega\,\dot{\eta}_d + \Omega^2\,\eta_d = \Omega^2\,\eta_c \tag{4.63}$$

where $\eta_d \in \mathbb{R}^6$ is the desired output from the pre-filter, $\eta_c \in \mathbb{R}^6$ is the commanded input, $\Lambda = \text{diag}\{\zeta_1, ..., \zeta_6\}$ is the desired damping ratios and $\Omega = \text{diag}\{\omega_1, ..., \omega_6\}$ is the desired natural frequencies. The design of the PID-control law for tracking of the desired state η_d is the topic for the next section.

4.3.2 Multivariable PID-Control Design for Nonlinear Systems

Most existing ROV-systems use a series of single-input single-output (SISO) controllers of PID-type where each controller is designed for the control of one DOF. This implies that the control matrices K_p, K_d and K_i in the PID-control law:

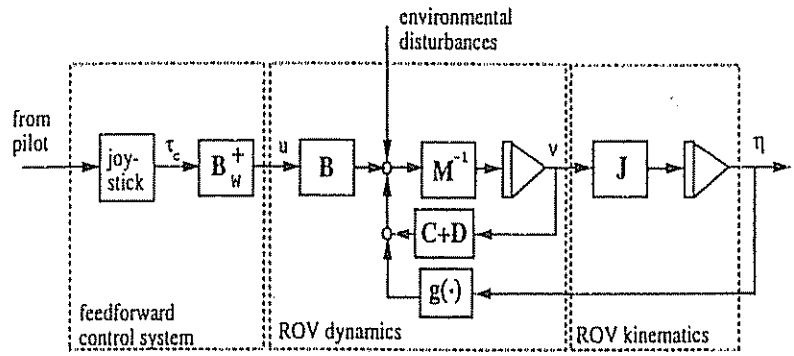

A Open-loop (feedforward) force/moment control

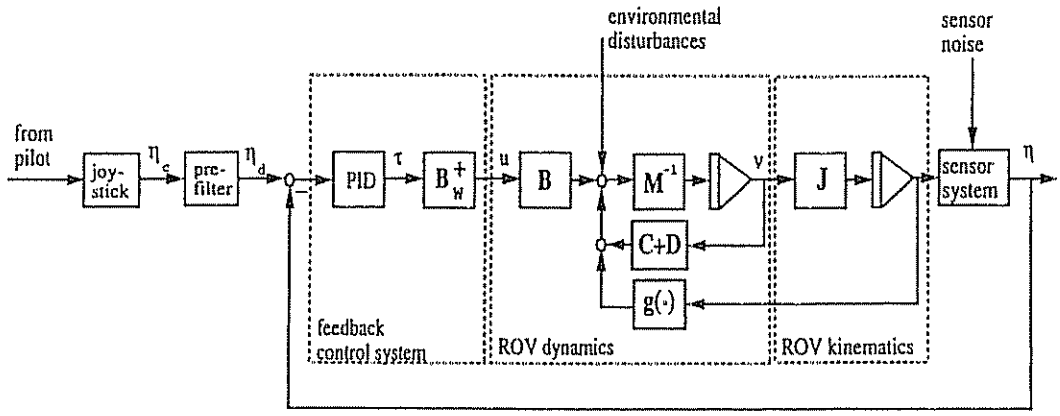

B Closed-loop (feedback) position/attitude control

Figure 4.5: Open-loop and closed-loop ROV control systems design.

$$\tau_{PID} = \boldsymbol{K}_p\, \boldsymbol{e}(t) + \boldsymbol{K}_d\, \dot{\boldsymbol{e}}(t) + \boldsymbol{K}_i \int_0^t \boldsymbol{e}(\tau)\, d\tau \tag{4.64}$$

should be chosen positive and diagonal. Here $\boldsymbol{e} = \boldsymbol{\eta}_d - \boldsymbol{\eta}$ is the tracking error. However, most ROV systems for offshore applications use only simple P- and PI-controllers for automatic heading and depth control since it is difficult to measure (estimate) the velocity vector $\boldsymbol{\nu}$. A standard PID-control design can be improved by using the vehicle kinematics together with gravity compensation. Moreover, we will show that perfect set-point regulation can be achieved in terms of Lyapunov stability theory if τ_{PID} is transformed according to:

$$\tau = \boldsymbol{J}^T(\boldsymbol{\eta})\, \tau_{PID} + \boldsymbol{g}(\boldsymbol{\eta}) \tag{4.65}$$

In addition, we will assume that the control input vector is related to the thruster

forces and moments according to (4.10). Hence, the inverse mapping:

$$u = B_W^{\dagger}\, \tau \tag{4.66}$$

where $B_W^{\dagger}$ is the generalized inverse (see Section 4.1.1), can be used to calculate the desired controls u.

In the next section we will also show that excellent performance can be obtained for the whole flight envelope by including the vehicle kinematics and restoring forces in the PID-control design. Moreover, it is not necessary to perform a gain-scheduling technique to counteract the time-varying behavior of the dynamics and kinematics. However, precautions against saturation and integral wind-up should be made. This is illustrated in Figure 4.6 where the PID-control law of the EAVE-EAST vehicle at the University of New-Hampshire is shown. This design is performed under the assumptions (without loss of generality) η_d = constant, $J(\eta) = I$ and $g(\eta) = 0$.

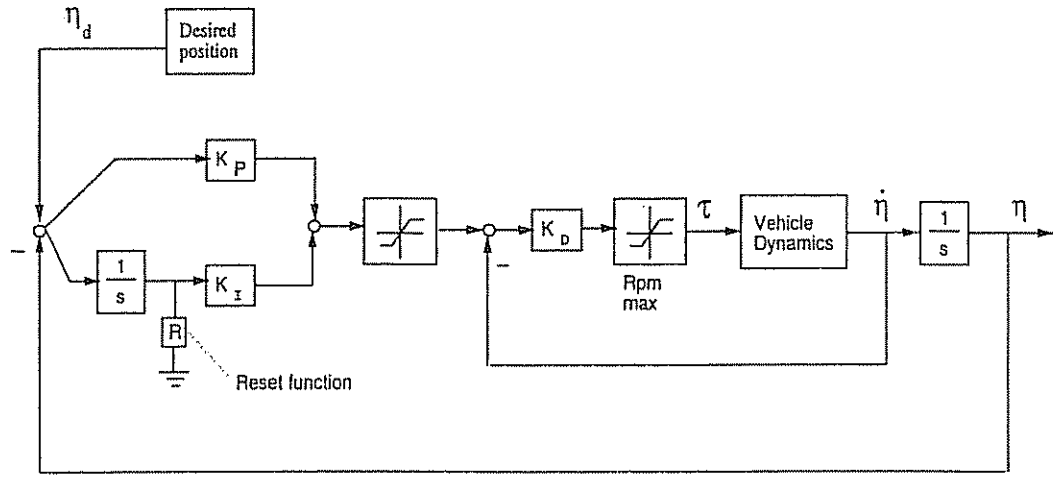

Figure 4.6: The EAVE-EAST Proportional Integral Derivative Controller (Venkatachalam et al. 1985)

4.3.3 PID Set-Point Regulation in Terms of Lyapunov Stability

In this section, we will investigate the closed-loop dynamics of the control law (4.64) and (4.65) under the assumption that the desired state vector:

$$\eta_d = \text{constant} \tag{4.67}$$

This control problem will be referred to as *regulation* as the opposite of *tracking control* which involves the design of a feedback and feedforward controller for tracking of a time-varying smooth reference trajectory $\eta_d(t)$. Consider an affine ROV-model:

$$M\,\dot{\nu} + C(\nu)\,\nu + D(\nu)\,\nu + g(\eta) = B\,u \tag{4.68}$$

where $\eta \in \mathbb{R}^n$, $\nu \in \mathbb{R}^n$ and $u \in \mathbb{R}^r$. Let us assume that the input matrix B and gravitational forces $g(\eta)$ are *known* whereas M, C and D are *unknown*. Hence, the following considerations may be done:

PD-Control of Nonlinear Square System (r = n)

Assume that B is invertible and let the control law be chosen as a PD-control law where the term $g(\eta)$ is included to compensate for gravity and buoyancy, that is:

$$\boxed{u = B^{-1}\left[J^T(\eta)\,K_p\,e - K_d^*\,\nu + g(\eta)\right]} \tag{4.69}$$

Notice that (4.64) and (4.65) are equivalent to (4.69) if $K_d^* = J^T K_d J > 0$ and $K_i = 0$. This control law is motivated from time differentiation of a Lyapunov function candidate:

$$V(\nu, e) = \frac{1}{2}\left(\nu^T\,M\,\nu + e^T K_p\,e\right) \tag{4.70}$$

which yields

$$\dot{V} = \nu^T\,\left[M\dot{\nu} - J^T(\eta)\,K_p\,e\right] \tag{4.71}$$

Here we have used the fact that $\dot{e} = -\dot{\eta} = -J(\eta)\,\nu$. Substituting (4.68) into this expression for $\dot{V}$, yields:

$$\dot{V} = \nu^T\,\left[B\,u - D(\nu)\,\nu - g(\eta) - J^T(\eta)\,K_p\,e\right] \tag{4.72}$$

Notice that $\nu^T\,C(\nu)\,\nu = 0$ for all $\nu \in \mathbb{R}^n$. From this it is seen that the proposed PD-control law with appropriate choices of $K_p = K_P^T > 0$ and $K_d^* > 0$ ensures that:

$$\dot{V} = -\nu^T\,[D(\nu) + K_d^*]\,\nu \leq 0 \tag{4.73}$$

This means that the power is dissipated passively by the damping matrix D and actively by the virtual damping matrix K_d^*. We now only have to check that the system cannot get "stuck" at $\dot{V}$ equal to zero, whenever $e \neq 0$. From (4.73) we see that $\dot{V} = 0$ implies that $\nu = 0$. Hence, (4.68) with (4.69) yields:

$$\dot{\nu} = M^{-1}\,J^T(\eta)\,K_p\,e \tag{4.74}$$

Consequently $\dot{\nu}$ will be non-zero if $e \neq 0$ and $\dot{V} = 0$ only if $e = 0$. Therefore the system cannot get "stuck" and the system state vector η will always converge to η_d in view of $V \to 0$.

This result was first proven by Tagegaki and Arimoto (1981) who applied the result to robot manipulator control. However, nonlinear control of underwater

vehicles in terms of *Euler angle* feedback was first discussed by Fossen and Sagatun (1991b). Later this work has been extended to *quaternion* feedback regulation in terms of *vector quaternion*, *Euler rotation* and *Rodrigues parameter* feedback by Fjellstad and Fossen (1994b).

PID-Control of Nonlinear Square System (r = n)

Arimoto and Miyazaki (1984) have shown that the results above can be generalized to include integral action. Let:

$$p = M_\eta \, \dot{\eta} \tag{4.75}$$

denote the generalized momentum of the vehicle. Hence, it can be shown by time differentiation of a Lyapunov function candidate:

$$V(x) = \frac{1}{2} x^T \begin{bmatrix} M_\eta^{-1} & \alpha I & 0 \\ \alpha I & K_p & K_i \\ 0 & K_i & \alpha K_i \end{bmatrix} x \tag{4.76}$$

where α is small positive constant and

$$x = [p, \, \eta, \, \int_0^t e(\tau) \, d\tau]^T \tag{4.77}$$

that $\dot{V} \leq 0$ and that η converges to η_d = constant. This is based on the assumption that the PID-control law is taken to be:

$$u = B^{-1} \left[J^T(\eta) \left(K_p \, e + K_i \int_0^t e(\tau) \, d\tau - K_d \dot{\eta} \right) + g(\eta) \right] \tag{4.78}$$

where K_p, K_i and K_d are matrices satisfying:

$$K_d > M_\eta \tag{4.79}$$

$$K_i > 0 \tag{4.80}$$

$$K_p > K_d + \frac{2}{\alpha} K_i \tag{4.81}$$

where α is a small positive constant chosen so small that:

$$\frac{1}{2}(1-\alpha) K_d - \alpha M_\eta + \frac{\alpha}{2} \sum_{i=1}^{6} (\eta_i - \eta_{id}) \frac{\partial M_\eta}{\partial \eta_i} > 0 \tag{4.82}$$

It should be noted that this solution only guarantees local stability in a limited region about the origin. For details on the proof see Arimoto and Miyazaki (1984).

Overdetermined System (r > n)

If we have more control inputs than states to be controlled, we showed that B^{-1} could be replaced by the generalized inverse $B_W^{\dagger}$ defined in Section 4.1.1. Hence, it is straightforward to show that the above results are valid for the non-square case $r > n$.

Non-Affine Systems (r > n)

For the regulation problem it is straightforward to extend the above results to non-affine systems where the control input is given by (see (4.8)):

$$\tau = B_1\, u - B_2(u)\, \nu \tag{4.83}$$

In fact the nonlinear control law:

$$\boxed{u = B_1^{\dagger}\left[J^T(\eta)\, K_p\, e - K_d^*\, \nu + g(\eta)\right]} \tag{4.84}$$

applied to (4.68) implies that $\dot{V}$ can be written:

$$\dot{V} = -\nu^T \left[D(\nu) + B_2(u) + K_d^*\right] \nu \tag{4.85}$$

where $K_d^* > 0$ must be chosen such that this expression becomes negative. Notice that the additional coupling term $B_2(u)\nu$ only contributes to the system damping if $B_2(u) > 0$. If $B_2(u) < 0$ we must choose $K_d^* > -B_2(u)$ to ensure stability.

Perfect Collocation (r = m)

In some cases, we can design an output feedback control law that overcomes the problem that all states must be measured. This design is based on the assumption that the number of inputs $u \in \mathbb{R}^r$ are equal to the number of measured outputs $y \in \mathbb{R}^m$. To do this, we will apply *passivity theory*; see Appendix C.3 for details. This suggest that the plant and control system can be described by two blocks according to Figure 4.7.

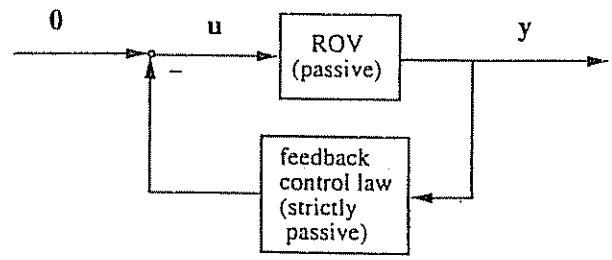

Figure 4.7: Passive and strictly passive block.

For simplicity, we will assume that the ROV can represented by a linear model which is quite realistic if only positioning is of concern. The model is:

$$M\,\dot{\nu} + N\,\nu + G\,\eta = B\,u \tag{4.86}$$

$$\dot{\eta} = \nu \tag{4.87}$$

Here the inertia matrix M, Coriolis, centripetal and damping matrix $N = C+D$, gravitational matrix G and input matrix B are assumed to be constant (the earth-fixed coordinate system is orientated such that $J(\eta) = I$ whenever the ROV is perfectly positioned). Hence, we can write the above system in state-space form as:

$$\dot{x} = A\,x + B\,u \tag{4.88}$$

where $x = [\nu^T, \eta^T]^T$ and A and B are given in (4.47). Consider the Lyapunov function candidate:

$$V = \frac{1}{2}\,x^T\,P\,x \tag{4.89}$$

with $P = P^T > 0$. Hence

$$\dot{V} = \frac{1}{2}\,x^T(A^TP + PA)x + x^TPBu \tag{4.90}$$

Let us assume that the sensors and actuators can be located such that:

$$y = C\,x \tag{4.91}$$

where C is a constant known matrix defined by:

$$\boxed{C = B^T\,P} \tag{4.92}$$

and P satisfies the Lyapunov equation:

$$\boxed{A^TP + PA = -Q} \tag{4.93}$$

with $Q = Q^T \geq 0$. Hence:

$$\dot{V} = y^Tu - \frac{1}{2}\,x^TQx \tag{4.94}$$

This is referred to as *perfect collocation* between the sensors and actuators. This result is also known as the *Kalman–Yakubovich lemma* (see Appendix C.3) which is used to check if a system is *positive real*. For linear causal systems positive realness is equivalent with passivity.

We now turn our attention to the last block representing the output feedback control law. According to Appendix C.3 a system is strictly passive if and only if there exists a scalar $\alpha > 0$ and some constant β such that:

$$\langle y|u\rangle_T \quad \geq \quad \alpha\,\|u_T\|_2 + \beta \tag{4.95}$$

For a linear output feedback control law:

$$\boxed{u = -H(s)\, y} \tag{4.96}$$

where $H(s) = \text{diag}\{h_i(s)\}$ $(i = 1...r)$ to be *strictly passive* the transfer functions $h_i(s)$ must satisfy:

$$\text{Re}\{h_i(s - \sigma)\} \geq 0 \quad \forall \quad \omega \geq 0 \tag{4.97}$$

for some $\sigma > 0$ and:

$$\angle h_i(j\omega) < 90^\circ \quad \forall \quad \omega \geq 0 \tag{4.98}$$

This is satisfied, for instance, if $h_i(s)$ is chosen as a PID-control law with limited derivative and integral action, that is:

$$h_i(s) = K_p\, \beta\, \frac{1 + T_i\, s}{1 + \beta\, T_i s}\, \frac{1 + T_d\, s}{1 + \alpha\, T_d s} \tag{4.99}$$

Here $K_p > 0$, $T_i > T_d$, $\alpha < 1$ and $\beta > 1$. Finally, Definition C.8 ensures that $y \in L_2^m$. It should be noted that it is straightforward to generalize these results to a nonlinear ROV model by using the general framework of passivity. A related work on collocation is found in Sørensen (1993) who has applied this design methodology to control high-speed surface effect ships (see Section 7.1).

4.3.4 Linear Quadratic Optimal Control

Linear quadratic (LQ) optimal control design is based on minimization of a linear quadratic performance index representing the control objective. Consider the linear state-space model:

$$\dot{x} = Ax + Bu + Ew \tag{4.100}$$
$$y = Cx \tag{4.101}$$

where x is the state vector, u is the input vector, w is the disturbance vector and y is used to describe the control objective. Let J be a performance index weighting the tracking error vector against the control power, that is:

$$\min\, J = \frac{1}{2} \int_0^T (\tilde{y}^T Q \tilde{y} + u^T P u)\, d\tau \tag{4.102}$$

Here $P > 0$ and $Q \geq 0$ are the weighting matrices and $\tilde{y} = y - y_d$ is the tracking error vector. The commanded input vector is denoted y_d. An approximate optimal solution to the tracking problem (4.102) for $0 \ll T < \infty$ is given in Athans and Falb (1966) as:

$$\boxed{u = G_1\, x + G_2\, y_d + G_3 w} \tag{4.103}$$

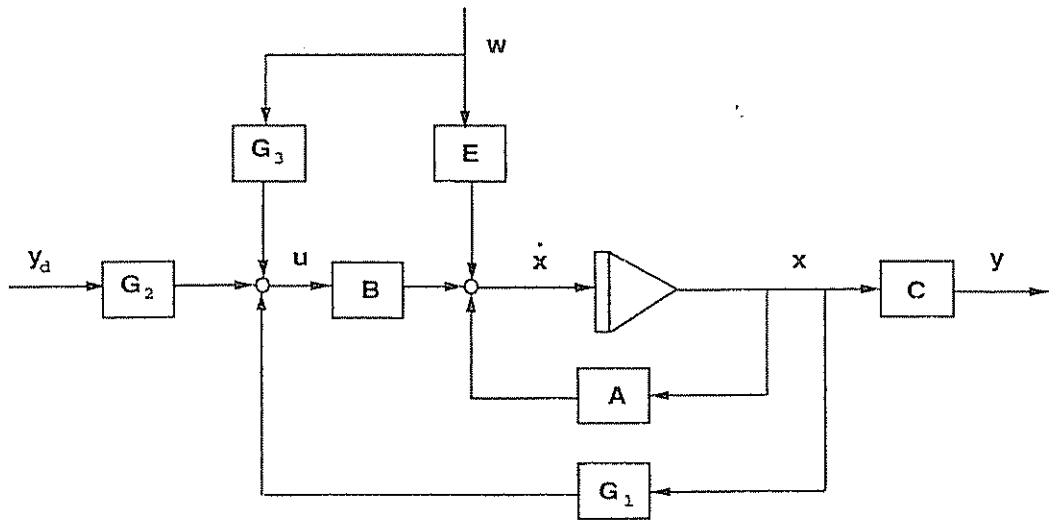

Figure 4.8: Linear Quadratic Optimal Autopilot

A block diagram of the control system is shown in Figure 4.8. Under the assumption that y_d = constant and w = constant, the following steady-state solution is obtained; see Appendix D for details:

$$G_1 = -P^{-1}B^T R_\infty \tag{4.104}$$
$$G_2 = -P^{-1}B^T(A+BG_1)^{-T}C^T Q \tag{4.105}$$
$$G_3 = P^{-1}B^T(A+BG_1)^{-T}R_\infty E \tag{4.106}$$

Here R_∞ is the steady-state solution of the matrix algebraic Riccati equation:

$$R_\infty A + A^T R_\infty - R_\infty B P^{-1} B^T R_\infty + C^T Q C = 0 \tag{4.107}$$

Optimal state estimation (Kalman filtering) can be used to realize the autopilot in the case when not all states are measured. For instance, the LQG/LTR (Loop Transfer Recovery) design methodology have been applied to underwater vehicles by Milliken (1984) and Triantafyllou and Grosenbaugh (1991). Loop shaping techniques like the LQG/LTR design methodology allow the designer to deal with robustness issues in a systematic manner. Moreover, robust stability (RS) can be guaranteed if bounds on the uncertainties are known. On the contrary, robust performance (RP) is still an unsolved problem. A linear controller design can be checked for RP by performing a structured singular value analysis. This technique is often referred to as the *μ-analysis* technique in the technical literature (see e.g. Maciejowski 1990). Nevertheless, the design of a so-called μ-optimal controller is still an active area for research.

4.4 Decoupled Control Design

Healey and Marco (1992) suggest that the 6 DOF linear equations of motion can be divided into three non-interacting (or lightly interacting) subsystems for speed control, steering and diving. Each systems consists of the state variables:

1) **Speed system state:** $u(t)$.

2) **Steering system states:** $v(t), r(t)$ and $\psi(t)$.

3) **Diving system states:** $w(t), q(t), \theta(t)$ and $z(t)$.

The rolling mode, that is $p(t)$ and $\phi(t)$ is left passive in this approach. This decomposition is motivated by the slender form of the Naval Postgraduate School (NPS) AUV (see Figure 4.9).

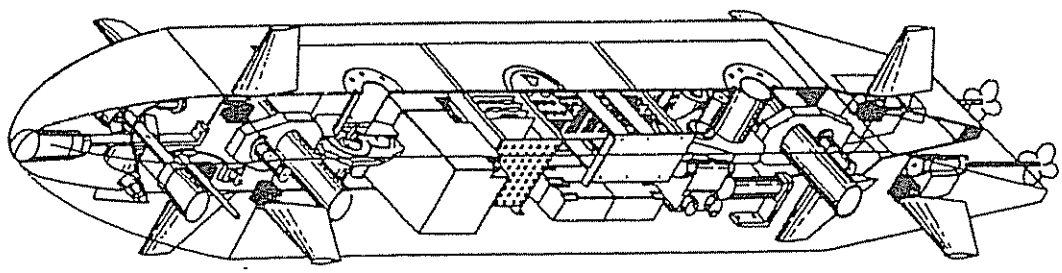

Figure 4.9: Schematic drawing of the NPS AUV II (Healey and Lienhard 1993). The mathematical model and specifications of the vehicle are given in Appendix E.2.

Healey and Lienard (1993) have applied the theory of *sliding regimes* to control the NPS AUV II. This control system has been successfully implemented and tested at the NPS in Monterey. A related work discussing the problems on adaptive sliding mode control in the dive plane is found in Cristi, Papoulias and Healey (1990). We will discuss this design methodology in a later section.

The above configuration suggests that the three subsystems can be controlled by means of two single-screw propellers with revolution $n(t)$, a rudder with deflection $\delta_R(t)$ and a stern plane with deflection $\delta_S(t)$. This particular choice of actuators is inspired by those used in flight and submarine control. Of course other combinations of control surfaces, thrusters etc. can be used to control the above subsystems. Nevertheless, we will use this simple actuator configuration to illustrate how a decoupled control design can be performed in terms of: (1) proportional, derivative and integral control and (2) sliding mode control.

The AUV examples in this section are based on the NDRE-AUV (see Figure 4.10). This is a test vehicle designed by the Norwegian Defence Research Establishment where the main purpose has been to test a propulsion system using sea water batteries (Jalving and Størkersen 1994).

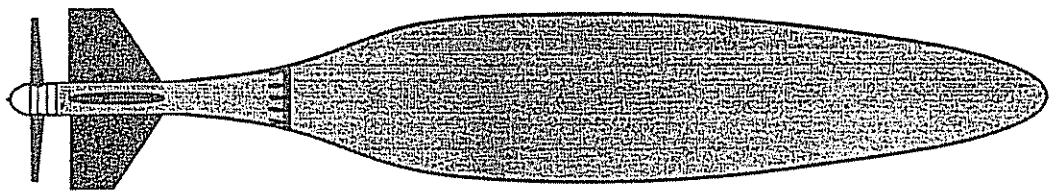

Figure 4.10: Schematic drawing of the NDRE-AUV (Jalving and Størkersen 1994). Specifications: length of hull = 4.3 m, maximum hull diameter = 0.7 m, propeller diameter = 0.6 m, cruise speed = 2.0 m/s and hull contour displacement = 1.0 m^3.

4.4.1 Forward Speed Control

Neglecting the interactions from sway, heave, roll, pitch and yaw suggests that the speed equation can be written as:

$$(m - X_{\dot{u}})\,\dot{u} = X_{|u|u}\,|u|u + (1-t)\,T + X_{\text{ext}} \tag{4.108}$$

Here we have assumed that quadratic damping is the dominating dissipative effect. Furthermore n represents the propeller revolution, u is the surge velocity, X_{ext} is external disturbances due to waves and currents and t is the thrust deduction number t. Recall that the thruster force T and moment Q can be written:

$$T = T_{|n|n}\,|n|n + T_{|n|V_a}\,|n|V_a; \qquad Q = Q_{|n|n}\,|n|n + Q_{|n|V_a}\,|n|V_a \tag{4.109}$$

For simplicity, we will assume that $T_{|n|V_a} = 0$ (affine system). Introducing, the notation $X_{|n|n|} = (1-t)T_{|n|n}$, finally yields:

$$\boxed{(m - X_{\dot{u}})\,\dot{u} = X_{|u|u}\,|u|u + X_{|n|n}\,|n|n + X_{\text{ext}}} \tag{4.110}$$

We will now demonstrate how a speed control system can be designed for this model.

Inner Loop PI Control System

The propeller revolution $n(s)$ can be measured with a pulse counter or a tachogenerator. Hence, an inner loop feedback control system can be designed by applying a PI-controller (see Figure 4.11).

$$h_{pi}(s) = \frac{u_a(s)}{n_d(s) - n(s)} = \frac{K_p(1 + T_i s)}{T_i s} \tag{4.111}$$

Here $n_d(s)$ is the desired propeller revolution and $u_a(s)$ is the armature voltage (see Section 4.1.1). This implies that (4.15) can be written:

$$n(s) = \frac{h_{u_a}(s)h_{pi}(s)}{1 + h_{u_a}(s)h_{pi}(s)} n_d(s) - \frac{h_Q(s)}{1 + h_{u_a}(s)h_{pi}(s)} Q(s) \tag{4.112}$$

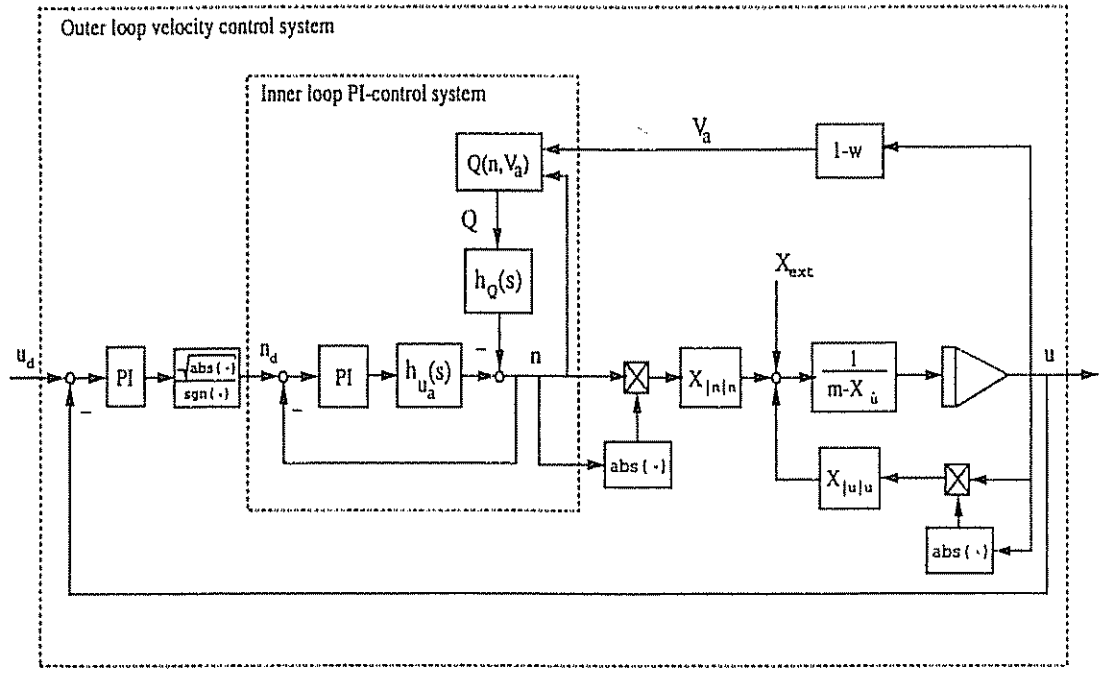

Figure 4.11: Speed Control System

where

$$h_{u_a}(s) = \frac{K_1}{(1+T_1 s)(1+T_2 s)}; \qquad h_Q(s) = \frac{K_2(1+T_3 s)}{(1+T_1 s)(1+T_2 s)} \tag{4.113}$$

Proper tuning of the PI-control parameters will ensure that $n(s)$ tracks the desired propeller revolution $n_d(s)$. The main advantages with an inner servo loop is that sensitivity to varying load conditions $Q(s)$, nonlinear actuator dynamics and hysteresis are reduced. The desired forward speed u_d corresponding to the propeller revolution n_d can be solved from (4.110) under the assumption that $X_{ext} = 0$ and that all model parameters are known. Unfortunately, it is quite obvious that this result will be uncertain. If accurate speed is important, an outer loop control system must be design in addition to the inner servo loop.

Outer Loop Velocity Control System

If u is measured or at least estimated, an outer velocity servo loop can be designed for proper tracking of the desired velocity u_d. This is illustrated in Figure 4.11, where the nonlinear term $|n|n$ is generated by a PI-control law under the assumption that n tracks n_d perfectly, that is:

$$|n|n = G_1\,\tilde{u} + G_2 \int_0^t \tilde{u}(\tau)\,d\tau \tag{4.114}$$

Here $\tilde{u} = u_d - u$ is the tracking error and $G_1 > 0$ and $G_2 > 0$ are the regulator proportional and integral gains, respectively.

Example 4.2 (The NDRE-AUV Speed Control System)
The performance of the inner-loop speed controller, Equation (4.111), has been demonstrated by NDRE[2] who has designed a long-range AUV for testing of new battery technology and advanced control theory, Figure 4.10. The NDRE-AUV has a low drag hull and a battery capable of delivering energy for a long mission. In May 1993 the NDRE-AUV was successfully tested in the open sea between Norway and Denmark. It then traveled a distance of 109 nautical miles.

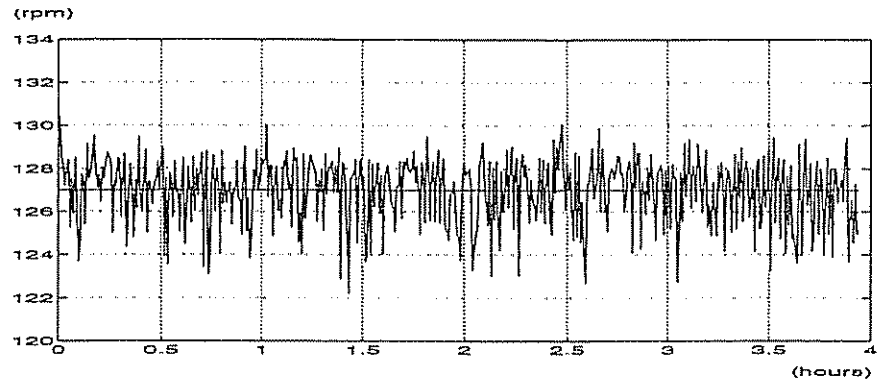

Figure 4.12: Desired and actual propeller revolution versus time for the NDRE-AUV.

The propeller revolution n for a typical mission is shown in Figure 4.12 where the desired propeller revolution is held constant at $n_d = 127$ rpm.
□

4.4.2 Automatic Steering

Automatic steering or heading control can be done by means of a rudder or a pair of thrusters. In the next section we will show how a rudder control system can be designed for course-changing maneuvers and then illustrate the performance of the control system by considering a small example.

Steering Equations of Motion

According to (4.44), the linear steering equations of motion can be expressed in a compact form as:

$$\begin{bmatrix} m - Y_{\dot{v}} & mx_G - Y_{\dot{r}} & 0 \\ mx_G - N_{\dot{v}} & I_z - N_{\dot{r}} & 0 \\ 0 & 0 & 1 \end{bmatrix} \begin{bmatrix} \dot{v} \\ \dot{r} \\ \dot{\psi} \end{bmatrix} + \begin{bmatrix} -Y_v & mu_0 - Y_r & 0 \\ -N_v & mx_G u_0 - N_r & 0 \\ 0 & -1 & 0 \end{bmatrix} \begin{bmatrix} v \\ r \\ \psi \end{bmatrix} = \begin{bmatrix} Y_\delta \\ N_\delta \\ 0 \end{bmatrix} \delta_R \tag{4.115}$$

[2]The Norwegian Defence Research Establishment, Kjeller, Norway.

where v is the sway velocity, r is the angular velocity in yaw, ψ is the heading angle and δ_R is the rudder deflection. Rearranging this expression into state-space form, yields:

$$\dot{\boldsymbol{x}} = \boldsymbol{A}\,\boldsymbol{x} + \boldsymbol{b}\,\delta_R \tag{4.116}$$

$$y = \boldsymbol{c}^T\,\boldsymbol{x} \tag{4.117}$$

where $\boldsymbol{x} = [v, r, \psi]^T$ and $y = \psi$. Moreover,

$$\begin{bmatrix} \dot{v} \\ \dot{r} \\ \dot{\psi} \end{bmatrix} = \begin{bmatrix} a_{11} & a_{12} & 0 \\ a_{21} & a_{22} & 0 \\ 0 & 1 & 0 \end{bmatrix} \begin{bmatrix} v \\ r \\ \psi \end{bmatrix} + \begin{bmatrix} b_1 \\ b_2 \\ 0 \end{bmatrix} \delta_R \tag{4.118}$$

where the choices of a_{ij} and b_i should be quite obvious. Consequently, the transfer function between ψ and δ_R is obtained as:

$$\frac{\psi}{\delta_R}(s) = \boldsymbol{c}^T(s\boldsymbol{I} - \boldsymbol{A})^{-1}\boldsymbol{b} = \frac{(a_{21}b_1 - a_{11}b_2) + b_2 s}{s[s^2 - (a_{11} + a_{22})s + a_{11}a_{22} - a_{12}a_{21}]} \tag{4.119}$$

or equivalently:

$$\frac{\psi}{\delta_R}(s) = \frac{K(1 + T_3 s)}{s(1 + T_1 s)(1 + T_2 s)} \tag{4.120}$$

where K is a gain constant and T_j $(j = 1, 2, 3)$ are three time constants.

Autopilot Design

The heading control system can be designed by applying a PID-control law:

$$\delta_R(s) = K_p \frac{1 + T_i s}{T_i s} \frac{1 + T_d s}{1 + T_f s} [\psi_d(s) - \psi(s)] \tag{4.121}$$

where K_p (controller gain), T_i (integral time constant), T_d (derivative time constant) and $T_f \approx 0.1\,T_d$ (low-pass filter time constant). The loop transfer function is:

$$l(s) = \frac{K K_p}{T_i s^2} \frac{(1 + T_i s)(1 + T_d s)(1 + T_3 s)}{(1 + T_f s)(1 + T_1 s)(1 + T_2 s)} \tag{4.122}$$

Hence, the closed-loop dynamics is described by:

$$\psi(s) = \frac{l(s)}{1 + l(s)} \psi_d(s) \tag{4.123}$$

It is seen from the final value theorem that the yaw angle will converge to the desired value for a step response: $\psi_d(s) = \psi_0/s$, that is:

$$\lim_{t \to \infty} \psi(t) = \lim_{s \to 0} s\psi(s) = \lim_{s \to 0} \frac{l(s)}{1 + l(s)} \psi_0 = \psi_0 \tag{4.124}$$

The yaw angle can be measured by a compass while rate measurements usually are obtained by a rate gyro or a rate sensor. If the compass measurements are of good quality, rate estimates can be obtained from numerical differentiation or state estimation (Kalman filtering).

Example 4.3 (The NDRE-AUV Heading Control System)
A simplified version of (4.121) without integral action has shown to perform satisfactory for the NDRE-AUV. This control law is simply taken to be:

$$\delta_R = K_p\,(\psi_d - \psi) - K_d\,r \tag{4.125}$$

where K_p and K_d are the proportional and derivative gain, respectively. Hence, steady-state errors due to environmental disturbances and neglected dynamics cannot be compensated for.

The main reason for omitting integral action is that the rudder servo has an on-off or relay nonlinearity which would cause a limit-cycle (chattering) if integral action is added. However, the magnitude of the steady-state errors, 1–2 degrees, was in the same order as the accuracy of the flux-gate compass. Consequently, there is not much gained by including integral action. For the PD-control law the loop-transfer function (4.122) reduces to:

$$l(s) = \frac{K(K_p + K_d s)(1 + T_3 s)}{s(1 + T_1 s)(1 + T_2 s)} \tag{4.126}$$

Hence, tuning of the yaw controller (4.125) in terms of the controller parameters K_p and K_d can easily be done by plotting $l(j\omega)$ in a Bode-diagram.

The performance of the autopilot is shown in Figure 4.13 for a long time mission where the course is changed in steps of 10 degrees each 10 minutes. A typical step response is shown in Figure 4.14 where the heading angle is changed from 195 to 185 degrees.
□

4.4.3 Combined Pitch and Depth Control

In this section we will design a control system for decoupled pitch and depth control. This design will also be based on a linearized model of the vehicle.

Diving Equations of Motion

The diving equations of motion should include the heave velocity w, the angular velocity in pitch q, the pitch angle θ, the depth z and the stern plane deflection δ_S. Assume that the forward speed is constant and that the sway and yaw modes can be neglected. Hence, the pitch and heave kinematics can be perturbed according to:

$$(\dot{\theta}_0 + \Delta\dot{\theta}) = \cos(\phi_0 + \Delta\phi)\,(q_0 + \Delta q) \tag{4.127}$$

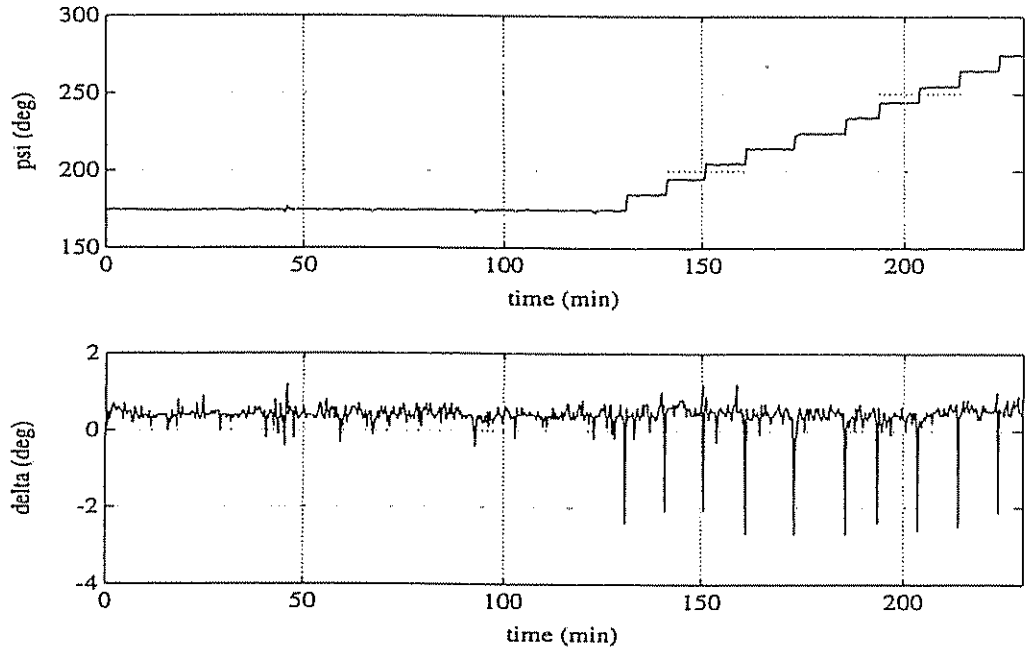

Figure 4.13: Long time mission for the NDRE-AUV where the heading is changed in steps of 10 degrees each 10 minutes.

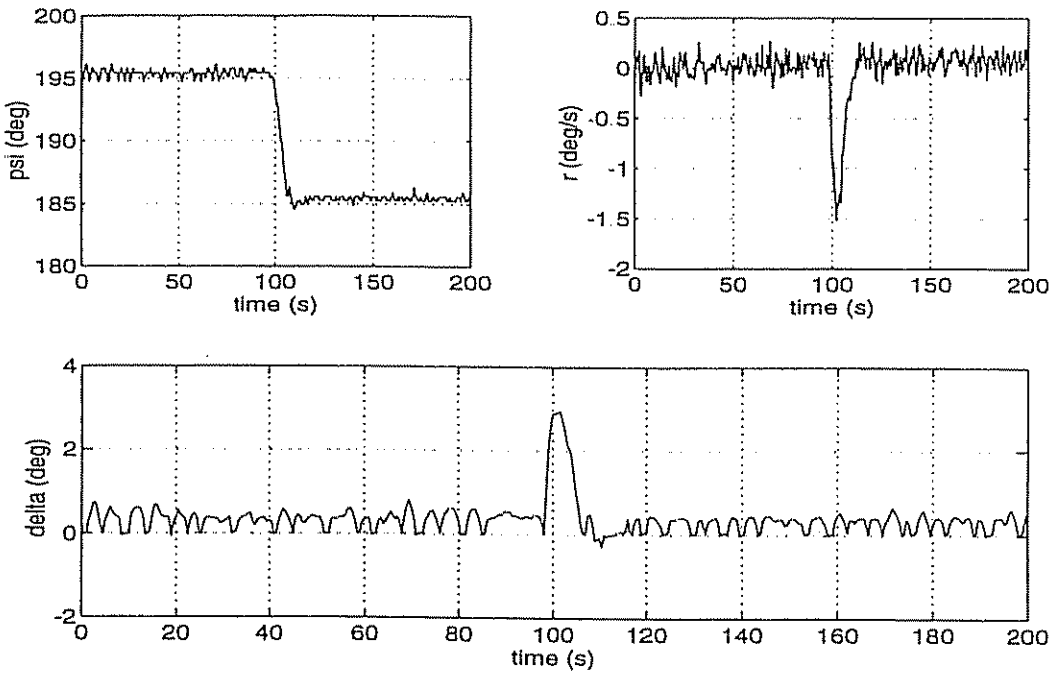

Figure 4.14: Full-scale experiment showing one typical step response for the NDRE-AUV. The heading angle is changed 10 degrees from 195 to 185 degrees.

In steady-state we have that $\theta_0 = \text{constant}$, $q_0 = 0$ and $\phi_0 = 0$. Hence:

$$\boxed{\Delta\dot{\theta} = \cos\Delta\phi\,\Delta q \approx \Delta q} \tag{4.128}$$

for small $\Delta\phi$. Similarly, the perturbed heave dynamics is:

$$(\dot{z}_0+\Delta\dot{z}) = -\sin(\theta_0+\Delta\theta)(u_0+\Delta u)+\cos(\theta_0+\Delta\theta)\cos(\phi_0+\Delta\phi)(w_0+\Delta w) \tag{4.129}$$

Using the trigonometric formulas:

$$\sin(\theta_0+\Delta\theta) = \sin\theta_0\,\cos\Delta\theta+\cos\theta_0\,\sin\Delta\theta \approx \sin\theta_0+\cos\theta_0\,\Delta\theta \tag{4.130}$$
$$\cos(\theta_0+\Delta\theta) = \cos\theta_0\,\cos\Delta\theta-\sin\theta_0\,\sin\Delta\theta \approx \cos\theta_0-\sin\theta_0\,\Delta\theta \tag{4.131}$$

together with $\phi_0 = 0$ yields:

$$(\dot{z}_0+\Delta\dot{z}) = -(\sin\theta_0+\cos\theta_0\Delta\theta)(u_0+\Delta u)+(\cos\theta_0-\sin\theta_0\Delta\theta)(w_0+\Delta w) \tag{4.132}$$

Applying the steady-state condition:

$$\dot{z}_0 = -\sin\theta_0\,u_0+\cos\theta_0\,w_0 \tag{4.133}$$

to this expression together with the assumption that 2nd-order terms in Δ can be neglected, finally yields:

$$\boxed{\Delta\dot{z} = -\sin\theta_0\,\Delta u-\cos\theta_0\,u_0\Delta\theta+\cos\theta_0\,\Delta w-\sin\theta_0\,w_0\Delta\theta} \tag{4.134}$$

This suggests the following linear model (dropping the Δ-notation for notational simplicity):

$$\begin{bmatrix}\dot{u}\\ \dot{w}\\ \dot{q}\\ \dot{\theta}\\ \dot{z}\end{bmatrix} = \begin{bmatrix}\alpha_{11} & \alpha_{12} & \alpha_{13} & 0 & 0\\ \alpha_{21} & \alpha_{22} & \alpha_{23} & \alpha_{24} & 0\\ \alpha_{31} & \alpha_{32} & \alpha_{33} & \alpha_{34} & 0\\ 0 & 0 & 1 & 0 & 0\\ -\mathrm{s}\theta_0 & \mathrm{c}\theta_0 & 0 & -(\mathrm{s}\theta_0 w_0+\mathrm{c}\theta_0 u_0) & 0\end{bmatrix}\begin{bmatrix}u\\ w\\ q\\ \theta\\ z\end{bmatrix}+\begin{bmatrix}\beta_1\\ \beta_2\\ \beta_3\\ 0\\ 0\end{bmatrix}\delta_S \tag{4.135}$$

where α_{ij} is found from the general expression for the 6 DOF linear equations of motion and β_i should be determined for the actual stern plane.

Simplified Diving Equations of Motion (Zero Pitch Angle)

A further reduction could be to assume zero pitch ($\theta_0 = 0$) constant forward speed ($u_0 = \text{constant}$). Hence, the above state-space model reduces to:

$$\begin{bmatrix} \dot{w} \\ \dot{q} \\ \dot{\theta} \\ \dot{z} \end{bmatrix} = \begin{bmatrix} a_{11} & a_{12} & a_{13} & 0 \\ a_{21} & a_{22} & a_{23} & 0 \\ 0 & 1 & 0 & 0 \\ 1 & 0 & -u_0 & 0 \end{bmatrix} \begin{bmatrix} w \\ q \\ \theta \\ z \end{bmatrix} + \begin{bmatrix} b_1 \\ b_2 \\ 0 \\ 0 \end{bmatrix} \delta_S \tag{4.136}$$

with obvious definitions of a_{ij} and b_i. Alternatively, we can write this model in terms of the hydrodynamic derivatives as:

$$\begin{bmatrix} m - Z_{\dot{w}} & mx_G - Z_{\dot{q}} & 0 & 0 \\ mx_G - M_{\dot{w}} & I_y - M_{\dot{q}} & 0 & 0 \\ 0 & 0 & 1 & 0 \\ 0 & 0 & 0 & 1 \end{bmatrix} \begin{bmatrix} \dot{w} \\ \dot{q} \\ \dot{\theta} \\ \dot{z} \end{bmatrix} + \begin{bmatrix} -Z_w & mu_0 - Z_q & 0 & 0 \\ -M_w & mx_G u_0 - M_q & \overline{BG}_z W & 0 \\ 0 & -1 & 0 & 0 \\ -1 & 0 & u_0 & 0 \end{bmatrix} \begin{bmatrix} w \\ q \\ \theta \\ z \end{bmatrix} = \begin{bmatrix} Z_\delta \\ M_\delta \\ 0 \\ 0 \end{bmatrix} \delta_S \tag{4.137}$$

Here $\overline{BG}_z = z_G - z_B$ is used to denote the vertical distance between the center of buoyancy and center of gravity.

Pitch-Depth Control Design

The pitch-depth controller can be designed with background in the linear model (4.136), by simply choosing $y = z$. Hence:

$$\dot{\boldsymbol{x}} = \boldsymbol{A}\,\boldsymbol{x} + \boldsymbol{b}\,\delta_S \tag{4.138}$$

$$y = \boldsymbol{c}^T \boldsymbol{x} \tag{4.139}$$

where:

$$\boldsymbol{c}^T = [0\,0\,0\,1] \tag{4.140}$$

Applying the Laplace transformation to this model yields the transfer function:

$$\frac{z}{\delta_S}(s) = \frac{b_1 s^2 + (b_2 a_{12} - b_1 a_{22} - b_2 u_0)s + (b_2 u_0 a_{11} - b_1 a_{21} u_0 - b_1 a_{23} + b_2 a_{13})}{s[s^3 - (a_{11} + a_{22})s^2 + (a_{11}a_{22} - a_{23} - a_{21}a_{12})s + (a_{11}a_{23} - a_{21}a_{13})]} \tag{4.141}$$

For simplicity, we will assume that the heave velocity during diving is small and that $x_G = 0$. This is quite realistic since most small underwater vehicles move slowly in the vertical direction. This assumption implies that the linear model (4.137) reduces to:

$$\begin{bmatrix} \dot{q} \\ \dot{\theta} \\ \dot{z} \end{bmatrix} = \begin{bmatrix} \frac{M_q}{I_y - M_{\dot{q}}} & -\frac{(z_G - z_B)W}{I_y - M_{\dot{q}}} & 0 \\ 1 & 0 & 0 \\ 0 & -u_0 & 0 \end{bmatrix} \begin{bmatrix} q \\ \theta \\ z \end{bmatrix} + \begin{bmatrix} \frac{M_\delta}{I_y - M_{\dot{q}}} \\ 0 \\ 0 \end{bmatrix} \delta_S \tag{4.142}$$

Consequently, the transfer functions θ/δ_S and z/δ_S are obtained as follows:

$$\frac{\theta}{\delta_S}(s) = \frac{K_\theta}{s^2 + 2\,\zeta_\theta\,\omega_\theta\,s + \omega_\theta^2}; \qquad \frac{z}{\delta_S}(s) = -\frac{u_0}{s}\,\frac{\theta(s)}{\delta_S(s)} \tag{4.143}$$

where the gain constant is $K_\theta = M_\delta/(I_y - M_{\dot{q}})$. The *natural frequency* ω_θ and *relative damping ratio* ζ_θ for the pure pitching motion are defined as:

$$\omega_\theta = \sqrt{\frac{\overline{BG}_z W}{I_y - M_{\dot{q}}}}; \qquad \zeta_\theta = \frac{-M_q}{2\sqrt{\overline{BG}_z W (I_y - M_{\dot{q}})}} \tag{4.144}$$

Consequently, the *natural period* in pitch is:

$$T_\theta = \frac{2\pi}{\omega_\theta} = 2\pi\sqrt{\frac{I_y - M_{\dot{q}}}{\overline{BG}_z W}} \tag{4.145}$$

From this expression it is seen that a reduction in the moment of inertia $(I_y - M_{\dot{q}})$ or an increase of the vertical distance between the center of gravity and the center of buoyancy $\overline{BG}_z$, and the vehicle's weight W, will reduce the natural pitch period.

The terms $M_q q$ and $\overline{BG}_z W\theta$ are often referred to as *passive* damping and restoring forces, respectively, since modifications of these parameters require the vehicle to be redesigned. Similar effects can be obtained by designing an *active* feedback control system of PID-type for combined pitch and depth control. For instance, the control law:

$$\delta_S = G_1(z_d - z) + G_2\int_0^t [z_d - z(\tau)]d\tau + G_3(\theta_d - \theta) - G_4 q + G_5\int_0^t [\theta_d - \theta(\tau)]d\tau \tag{4.146}$$

allows the designer to modify the damping and the restoring forces through the derivative and proportional action in the controller, that is, adjusting the controller gains G_i $(i = 1...5)$. Notice that feedback from w is omitted since this state is not usually measured.

In the implementation of the controller, the depth z can be measured by a pressure meter, the pitch angle θ can be measured by an inclinometer while the pitch rate q requires a rate gyro or a rate sensor. If heave velocity w is measured in addition, the more complex model (4.137) can be used in the control design instead. One way to obtain velocity measurement in the vertical plane is by simply combining a pressure meter with an accelerometer to form a velocity state estimator. Kalman filter algorithms are well suited for this purpose. A more expensive solution is using a Doppler log for directly obtaining velocity measurements.

Example 4.4 (The NDRE-AUV Depth Control System)
The NDRE-AUV depth controller was designed without integral action according to:

$$\delta_S = G_1\,(z_d - z) - G_3\,\theta - G_4\,q \tag{4.147}$$

We also notice that $\theta_d = 0$ in this implementation. Substituting this expression into (4.143) yields:

$$[s^2 + (2\zeta_\theta\omega_\theta + K_\theta G_4)\,s + (\omega_\theta^2 + K_\theta G_3)]\,\theta(s) = K_\theta\,G_1\,[z_d(s) - z(s)] \tag{4.148}$$

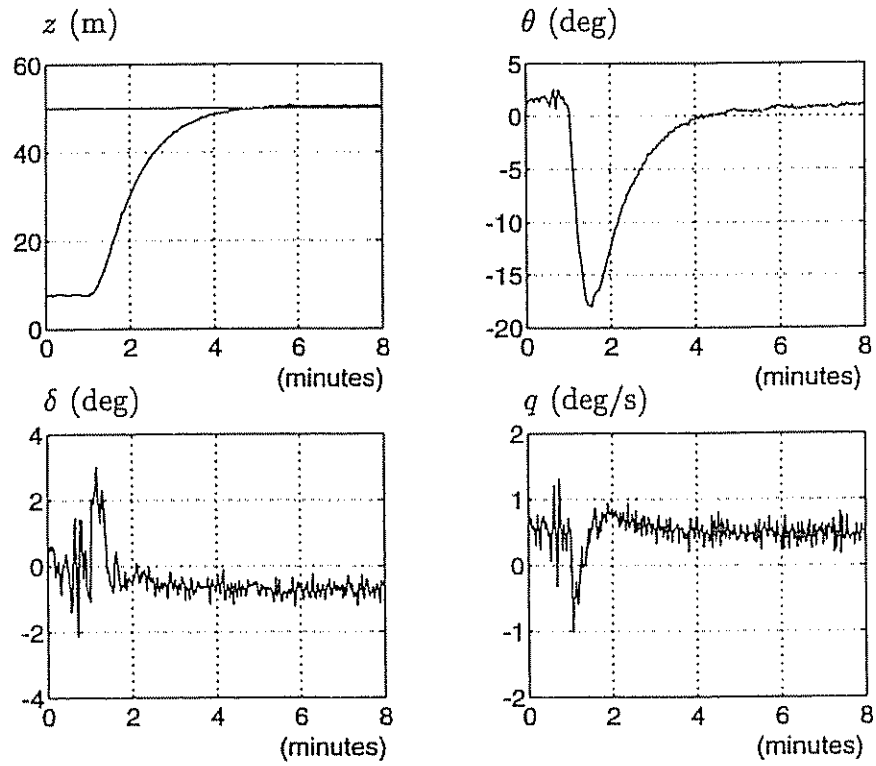

Figure 4.15: Full-scale depth changing maneuver for the NDRE-AUV. The bias in the pitch rate time series is due to a small off-set in the rate sensor.

Hence, we can choose G_3 and G_4 such that the closed-loop pitch dynamics is stable. Next, we can use the relationship:

$$z(s) = -\frac{u_0}{s}\,\theta(s) \tag{4.149}$$

to tune G_1. Moreover, the cubic characteristic equation:

$$[s^3 + (2\zeta_\theta\omega_\theta + K_\theta G_4)\,s^2 + (\omega_\theta^2 + K_\theta G_3)\,s - u_0 K_\theta G_1]\,z(s) = -u_0 K_\theta G_1\,z_d(s) \tag{4.150}$$

must have all its roots strictly in the left half-plane to ensure that ($z = z_d$ = constant) in steady-state. However, environmental disturbances can cause steady-state errors for this approach since integral action is omitted. A full-scale depth changing maneuver for the NDRE-AUV is shown in Figure 4.15.
□

4.5 Advanced Autopilot Design for ROVs

4.5.1 Sliding Mode Control

Sliding control has been applied successfully in the control of underwater vehicles by Yoerger and Slotine (1984, 1985) who propose to use a series of single-input single-output (SISO) continuous time controllers. Recent work by Yoerger and Slotine (1991) discusses how adaptive sliding control can be applied to underwater vehicles. Cristi et al. (1990) have applied an adaptive sliding mode controller to control an AUV in the dive plane. Sliding mode controllers have been successfully implemented for the JASON vehicle, Woods Hole Oceanographic Institution by Yoerger, Newman and Slotine (1986) and the MUST vehicle at Martin Marietta, Baltimore by Dougherty, Sherman, Woolweaver and Lovell (1988) and Dougherty and Woolweaver (1990). Besides this, successful implementations have been reported for the NPS AUV II at the Naval Postgraduate School, Monterey by Marco and Healey (1992) and Healey and Lienard (1993). All these experiments show that sliding mode controllers have significant advantages to traditional linear control theory.

Single-Input Single-Output (SISO) Affine Systems

Yoerger and co-authors propose to use a simplified ROV model:

$$M_{ii}\dot{\nu}_i + n_i(\nu_i) = \tau_i \quad \text{and} \quad \dot{\eta}_i = \nu_i \quad (i = 1...6) \tag{4.151}$$

where all kinematic and dynamic cross-coupling terms terms are neglected. Here, τ_i is the input, M_{ii} is the diagonal element of the inertia matrix M and n_i corresponds to the quadratic damping term in the nonlinear vector n, that is:

$$M = \begin{bmatrix} m - X_{\dot{u}} & 0 & 0 & 0 & 0 & 0 \\ 0 & m - Y_{\dot{v}} & 0 & 0 & 0 & 0 \\ 0 & 0 & m - Z_{\dot{w}} & 0 & 0 & 0 \\ 0 & 0 & 0 & Ix - K_{\dot{p}} & 0 & 0 \\ 0 & 0 & 0 & 0 & Iy - M_{\dot{q}} & 0 \\ 0 & 0 & 0 & 0 & 0 & Iz - N_{\dot{r}} \end{bmatrix} \tag{4.152}$$

$$n(\nu) = -[\, X_{|u|u}\,|u|u,\; Y_{|v|v}\,|v|v,\; Z_{|w|w}\,|w|w,\; K_{|p|p}\,|p|p,\; M_{|q|q}\,|q|q,\; N_{|r|r}\,|r|r \,]^T \tag{4.153}$$

Uncertainties in the model are compensated for in the control design. For notational simplicity, let us write the ROV model according to:

$$m\ddot{x} + d\,|\dot{x}|\dot{x} = \tau \quad \text{where} \quad m > 0; \quad d > 0 \tag{4.154}$$

Here $x = \eta_i$, $\tau = \tau_i$, $m = M_{ii}$ and $d\,|\dot{x}|\dot{x} = n_i(\nu_i)$. We also assume that both $\dot{x}$ and x are measured.

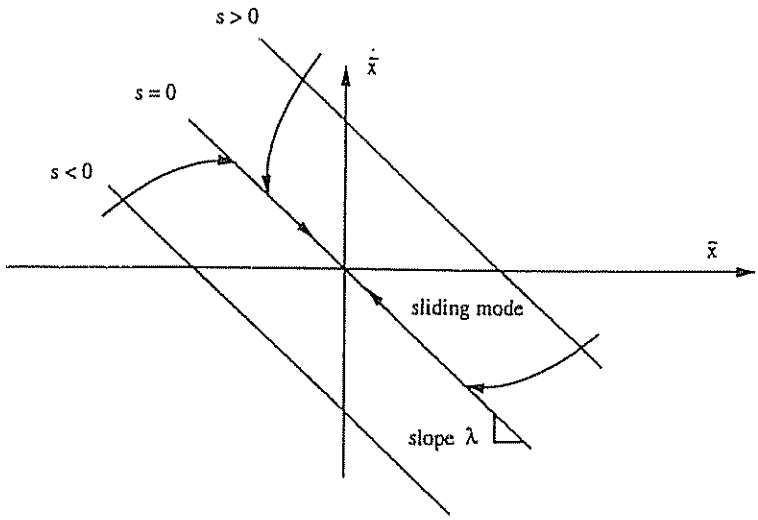

Figure 4.16: Graphical interpretation of the sliding surface.

Define a scalar measure of tracking:

$$\boxed{s = \dot{\tilde{x}} + \lambda\tilde{x}} \tag{4.155}$$

where $\tilde{x} = x - x_d$ is the tracking error and $\lambda > 0$ is the control bandwidth. For $s = 0$ this expression describes a *sliding surface* with exponential dynamics:

$$\tilde{x}(t) = \exp(-\lambda(t - t_0))\,\tilde{x}(t_0) \tag{4.156}$$

which ensures that the tracking error $\tilde{x}(t)$ converges to zero in finite time when $s = 0$ (sliding mode). In fact, the error trajectory will reach the time-varying sliding surface in finite time for any initial condition $\tilde{x}(t_0)$ and then slide along the surface towards $\tilde{x}(t) = 0$ exponentially. Hence, the control objective is reduced to finding a nonlinear control law which ensures that:

$$\lim_{t\to\infty} s(t) = 0 \tag{4.157}$$

A graphical interpretation of the *sliding surface* is given in Figure 4.16. In the design of the sliding control law, it is convenient to define a virtual reference x_r satisfying:

$$\dot{x}_r = \dot{x}_d - \lambda\tilde{x} \quad \Rightarrow \quad s = \dot{x} - \dot{x}_r \tag{4.158}$$

Hence, the following expression for $m\,\dot{s}$ is obtained:

$$\begin{aligned} m\,\dot{s} &= m\,\ddot{x} - m\,\ddot{x}_r = (\,\tau - d\,|\dot{x}|\dot{x}\,) - m\ddot{x}_r \\ &= -d\,|\dot{x}|s + (\tau - m\ddot{x}_r - d\,|\dot{x}|\dot{x}_r) \end{aligned} \tag{4.159}$$

Consider the scalar Lyapunov-like function candidate:

$$V(s,t) = \frac{1}{2} m\, s^2 \quad , \quad m > 0 \tag{4.160}$$

Differentiating V with respect to time (assuming $\dot{m} = 0$) yields

$$\dot{V} = m\,\dot{s}\,s = -d\,|\dot{x}|s^2 + s\,(\tau - m\ddot{x}_r - d\,|\dot{x}|\dot{x}_r) \tag{4.161}$$

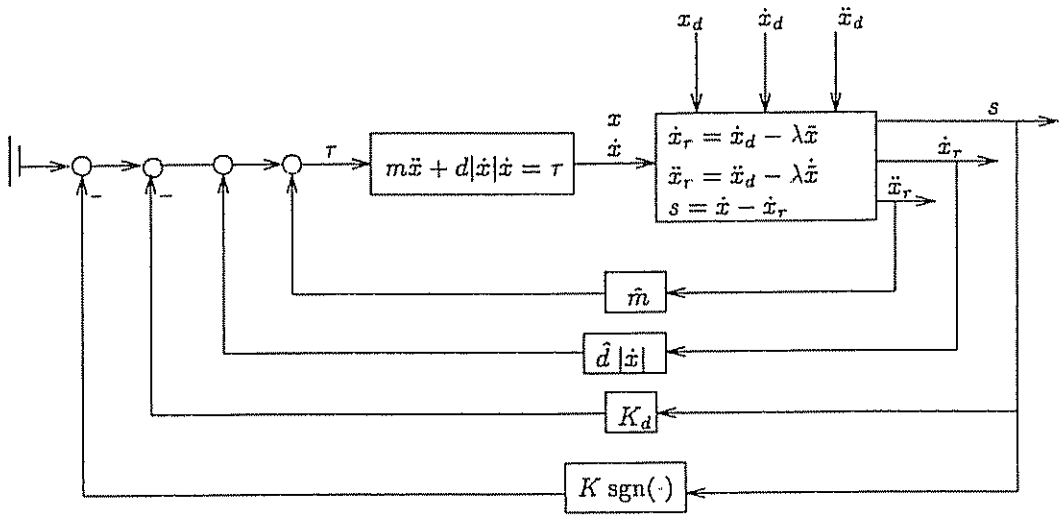

Figure 4.17: SISO sliding control applied to underwater vehicles

Taking the control law to be:

$$\boxed{\tau = \hat{m}\ddot{x}_r + \hat{d}\,|\dot{x}|\dot{x}_r - K_d\,s - K\,\mathrm{sgn}(s)} \qquad K_d \geq 0 \tag{4.162}$$

where $\hat{m}$ and $\hat{d}$ are the estimates of m and d, respectively, and:

$$\mathrm{sgn}(s) = \begin{cases} 1 & \text{if } s > 0 \\ 0 & \text{if } s = 0 \\ -1 & \text{otherwise} \end{cases} \tag{4.163}$$

yields:

$$\dot{V} = -(\,K_d + d\,|\dot{x}|\,)\,s^2 + (\,\tilde{m}\ddot{x}_r + \tilde{d}\,|\dot{x}|\dot{x}_r\,)\,s - K\,|s| \tag{4.164}$$

Here $\tilde{m} = \hat{m} - m$ and $\tilde{d} = \hat{d} - d$. Conditions on the switching gain K are found by requiring that $\dot{V} \leq 0$. The particular choice:

$$\boxed{K \geq |\tilde{m}\ddot{x}_r + \tilde{d}\,|\dot{x}|\,\dot{x}_r| + \eta} \tag{4.165}$$

with $\eta > 0$ implies that:

$$\dot{V} \leq -(\,K_d + d\,|\dot{x}|\,)\,s^2 - \eta\,|s| \leq 0 \tag{4.166}$$

This is due to the fact that $(\,K_d + d\,|\dot{x}|\,) > 0 \quad \forall\, \dot{x}$. Notice that, $\dot{V} \leq 0$ implies that $V(t) \leq V(0)$, and therefore that s is bounded. This in turn implies that $\ddot{V}$ is bounded. Hence $\dot{V}$ must be uniformly continuous. Finally, application of Barbălat's lemma then shows that $s \to 0$ and thus $\tilde{x} \to 0$ as $t \to \infty$.

Chattering

It is well known that the switching term $K\,\mathrm{sgn}(s)$ can lead to chattering. Chattering must be eliminated for the controller to perform properly. Slotine and Li (1991) suggest smoothing out the control law discontinuity inside a boundary layer by replacing the sgn(·) function in the control law with:

$$\mathrm{sat(s}/\phi) = \begin{cases} \mathrm{sgn}(s) & \text{if } |s/\phi| > 1 \\ s/\phi & \text{otherwise} \end{cases} \tag{4.167}$$

where ϕ should be interpreted as the boundary layer thickness. This substitution will in fact assign a low-pass filter structure to the dynamics of the sliding surface s inside the boundary layer (see below). Moreover, replacing the $K\,\mathrm{sgn}(s)$ term in (4.162) with $K\,\mathrm{sat}(s/\phi)$ yields the following expressions for the s-dynamics and $\dot{V}$.

- **Inside the boundary layer:**

$$m\,\dot{s} + (\,K_d + d\,|\dot{x}| + \frac{K}{\phi}\,)\,s = \tilde{m}\ddot{x}_r + \tilde{d}\,|\dot{x}|\dot{x}_r \tag{4.168}$$

$$\dot{V} \leq -(\,K_d + d\,|\dot{x}| + \frac{\eta}{\phi}\,)\,s^2 \tag{4.169}$$

- **Outside the boundary layer:**

$$m\,\dot{s} + (\,K_d + d\,|\dot{x}|\,)\,s + K\,\mathrm{sgn}(s) = \tilde{m}\ddot{x}_r + \tilde{d}\,|\dot{x}|\dot{x}_r \tag{4.170}$$

$$\dot{V} \leq -(\,K_d + d\,|\dot{x}|\,)\,s^2 - \eta\,|s| \tag{4.171}$$

The boundary layer thickness can also be made time-varying to exploit the maximum control bandwidth available. See Slotine and Li (1991) for a closer description on time-varying boundary layers.

Example 4.5 (Sliding Mode Control Applied to ROVs)
Consider the simplified model of an underwater vehicle in surge:

$$m\,\ddot{x} + d\,|\dot{x}|\dot{x} = \tau \tag{4.172}$$

with $m = 200$ kg and $d = 50$ kg/m. The SISO sliding controller can be computed as:

$$\boxed{\tau = \hat{m}\,\ddot{x}_r + \hat{d}\,|\dot{x}|\dot{x}_r - K_d\,s - K\,\mathrm{sat}(s/\phi)} \tag{4.173}$$

where $K_d \geq 0$. The following two cases were studied:

(1) PD-Controller:

$$\begin{aligned} \hat{m} &= 0 & K_d &= 500 \\ \hat{d} &= 0 & K &= 0 \end{aligned}$$

Notice that this simply corresponds to the PD control law:

$$\tau = -K_d\,s = -K_d\,\dot{\tilde{x}} - \lambda\,K_d\,\tilde{x} \tag{4.174}$$

(2) Sliding Mode Controller:

$$\begin{aligned} \hat{m} &= 0.6\,m & \tilde{m} &\leq 0.5\,m \\ \hat{d} &= 1.5\,d & \tilde{d} &\leq 0.5\,d \\ K &= \left|\,(\tilde{m}\,\ddot{x}_r + \tilde{d}\,|\dot{x}|\,\dot{x}_r)\,\right| + 0.1 & K_d &= 200 \end{aligned}$$

In the simulation study the closed-loop bandwidth was chosen as $\lambda = 1$ for both controllers. The boundary layer thickness was chosen as $\phi = \pm\ 0.35$ for the sliding controller while the sampling frequency was set at 10 Hz.

It is seen from Figures 4.18 and 4.19 that the performance of the sliding controller is superior the performance of the PD-controller. Note that the control input for the sliding controller is relatively smooth due to the low-pass filter structure of the boundary layer.

□

Single-Input Multiple-States (SIMS) Affine Systems

For coupled maneuvers where the modes are highly coupled an alternative approach where the sliding surface is based on the state variable errors rather than the output errors can be used. We will briefly review the main results of Healey and Marco (1992) and Healey and Lienard (1993) who define the sliding surface as:

$$\sigma(\tilde{x}) = h^T\,\tilde{x} \tag{4.175}$$

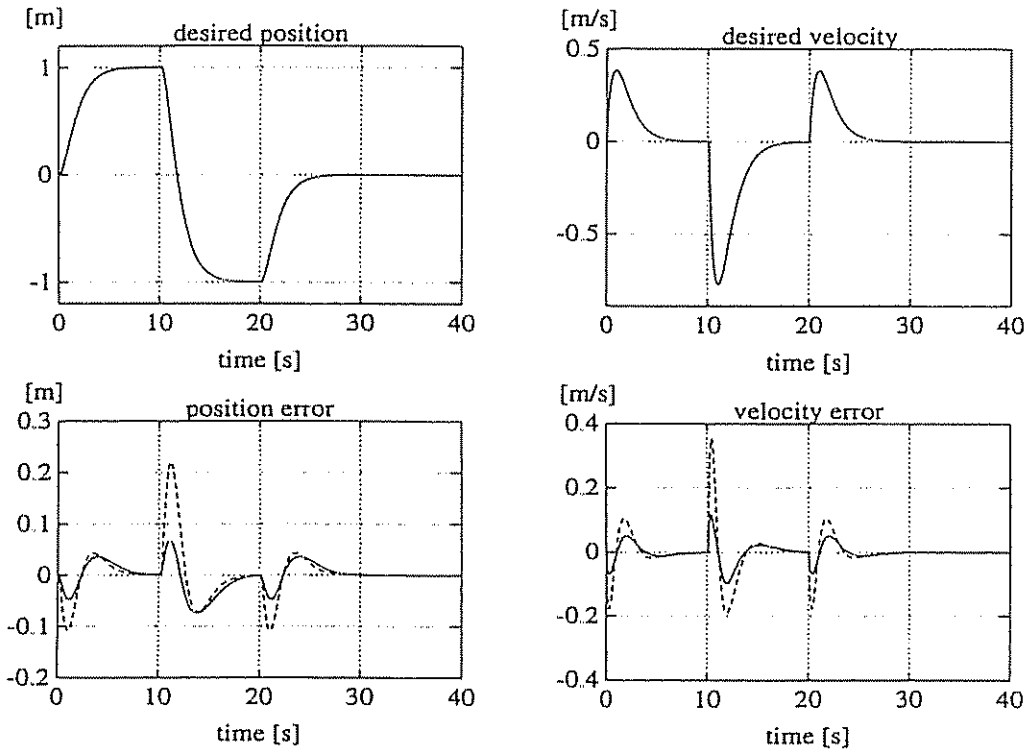

Figure 4.18: Performance study of the sliding controller (solid) and the PD-controller (dotted).

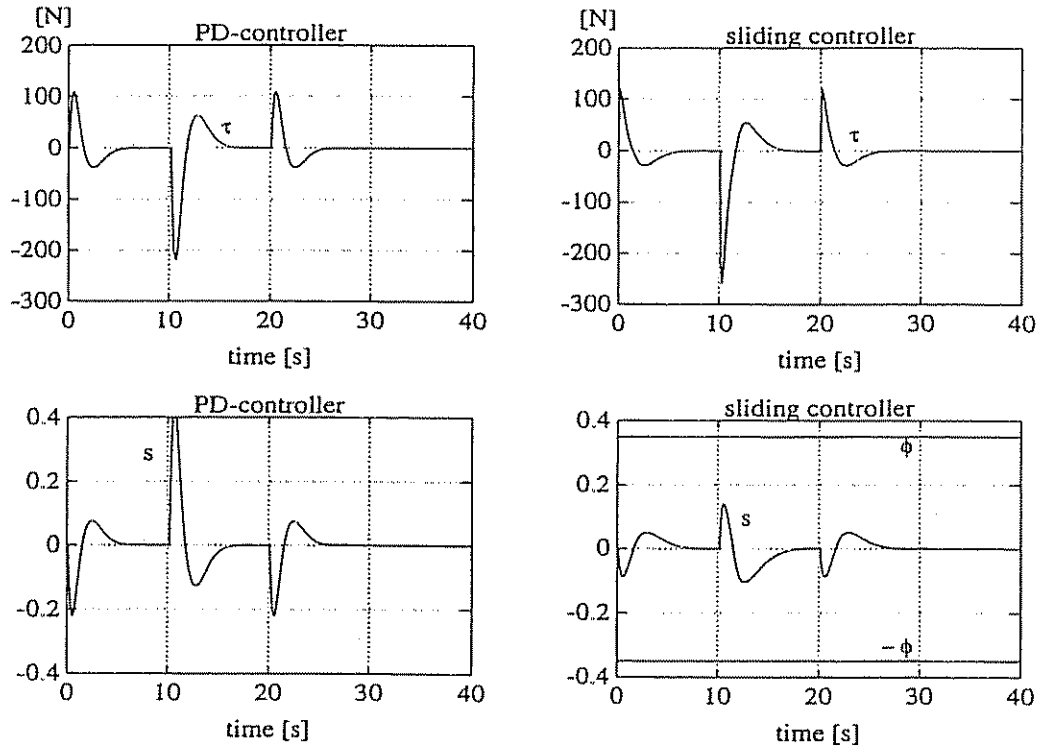

Figure 4.19: Control input and measure of tracking for the PD-controller and the sliding controller.

where $\tilde{x} = x - x_d$ is the state tracking error and $h \in \mathbb{R}^n$ is a vector of known coefficients to be interpreted later. It is important that the sliding surface is defined such that convergence of $\sigma(\tilde{x}) \rightarrow 0$ implies convergence of the state tracking error $\tilde{x} \rightarrow 0$.

Assume that we can write the dynamic and kinematic model as a SIMS linear model:

$$\dot{x} = A\,x + b\,u + f(x) \tag{4.176}$$

where $x \in \mathbb{R}^n$ and $u \in \mathbb{R}$. $f(x)$ should be interpreted as a nonlinear function describing the deviation from linearity in terms of disturbances and unmodelled dynamics. The experiments of Healey and co-authors show that this model can be used to describe a large number of ROV flight conditions. The feedback control law is composed of two parts:

$$u = \hat{u} + \overline{u} \tag{4.177}$$

where the nominal part is chosen as:

$$\hat{u} = -k^T\,x \tag{4.178}$$

Here k is the feedback gain vector. Substituting these expressions into (4.176) yields the closed-loop dynamics:

$$\dot{x} = A_c\,x + b\,\overline{u} + f(x); \qquad A_c = A - b\,k^T \tag{4.179}$$

Hence, the feedback gain vector k can be computed by means of pole-placement by first specifying the closed-loop state matrix A_c. In order to determine the nonlinear part of the feedback control law we first pre-multiply (4.179) with h^T and then subtract $h^T\dot{x}_d$ from both sides. Hence the following expression is obtained:

$$\dot{\sigma}(\tilde{x}) = h^T\,A_c\,x + h^T\,b\,\overline{u} + h^T\,f(x) - h^T\dot{x}_d \tag{4.180}$$

Choosing $\overline{u}$ (assuming that $h^T\,b \neq 0$) as:

$$\overline{u} = (h^T\,b)^{-1}[h^T\dot{x}_d - h^T\,\hat{f}(x) - \eta\,\mathrm{sgn}(\sigma)] \qquad \eta > 0 \tag{4.181}$$

where $\hat{f}(x)$ is an estimate of $f(x)$, yields the σ-dynamics:

$$\dot{\sigma}(\tilde{x}) = h^T\,A_c\,x - \eta\,\mathrm{sgn}(\sigma(\tilde{x})) + h^T\,\Delta f(x) \tag{4.182}$$

where $\Delta f(x) = f(x) - \hat{f}(x)$. We now turn to the choice of h. A nonzero vector $m \in \mathbb{R}^n$ that satisfies:

$$A\,m = \lambda\,m \tag{4.183}$$

where $\lambda \in \lambda(A)$ is an *eigenvalue* of A is said to be a *right eigenvector* of A for λ. Hence, if one of the eigenvalues of A_c is specified to be zero, the term

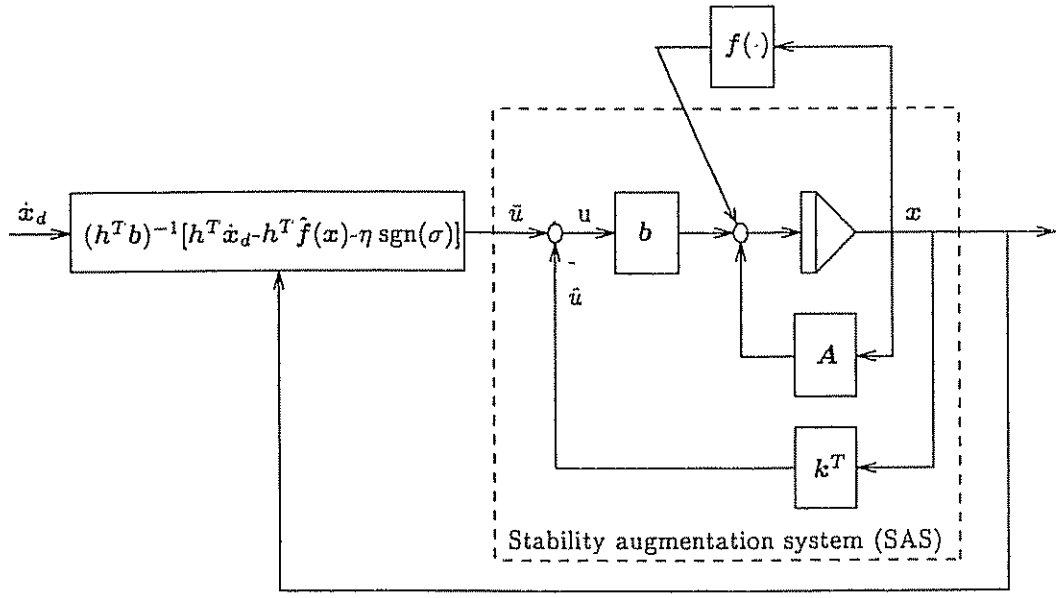

Figure 4.20: Single-input multiple-states (SIMS) sliding mode control law.

$h^T A_c x = (A_c^T h)^T x$ in (4.182) can be made equal to zero by choosing h as the *right eigenvector* of A_c^T for $\lambda = 0$, that is:

$$A_c^T h = 0 \iff h \text{ is a right eigenvector of } A_c^T \text{ for } \lambda = 0 \tag{4.184}$$

With this choice of h, the σ-dynamics reduces to:

$$\dot{\sigma}(\tilde{x}) = -\eta\,\mathrm{sgn}(\sigma(\tilde{x})) + h^T \Delta f(x) \tag{4.185}$$

which can be made globally convergent, by selecting η as:

$$\eta > \| h \| \cdot \| \Delta f(x) \| \tag{4.186}$$

This is easily seen by applying the Lyapunov function candidate:

$$V(\sigma) = \frac{1}{2}\sigma^2 \tag{4.187}$$

Differentiation of V with respect to time yields:

$$\dot{V} = \sigma\,\dot{\sigma} = -\eta\,\sigma\,\mathrm{sgn}(\sigma) + \sigma\,h^T \Delta f(x) = -\eta\,|\sigma| + \sigma\,h^T \Delta f(x) \tag{4.188}$$

Choosing η according to (4.186) ensures that $\dot{V} \leq 0$. Hence, by application of Barbălat's lemma σ converges to zero in finite time if η is chosen large enough to overcome the destabilizing effects of the unmodelled dynamics $\Delta f(x)$. The choice of η will be a trade-off between robustness and performance.

Implementation Considerations

In practical implementations, chattering should be removed by replacing $\text{sgn}(\sigma)$ with $\text{sat}(\sigma/\phi)$ in (4.181) where the design parameter ϕ is the sliding surface boundary layer thickness. Alternatively, the discontinuous function $\text{sat}(\sigma/\phi)$ could be replaced by the continuous function $\tanh(\sigma/\phi)$; see the upper plot of Figure 4.21.

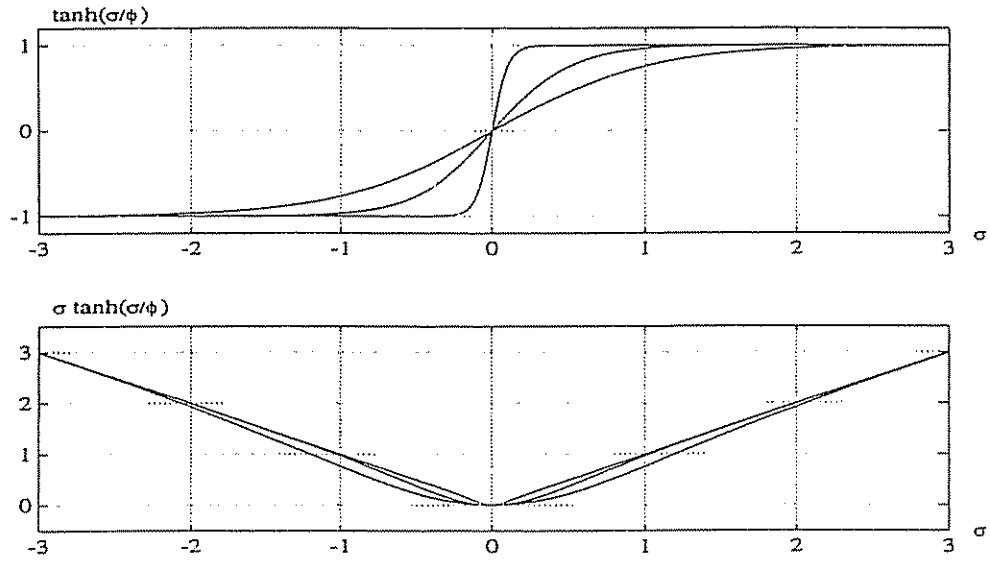

Figure 4.21: Diagram showing $\tanh(\sigma/\phi)$ and $\sigma\tanh(\sigma/\phi)$ as a function of the boundary layer thickness $\phi \in \{0.1, 0.5, 1.0\}$.

This suggests the modified control laws:

$$u = -k^T x + (h^T b)^{-1}[h^T \dot{x}_d - h^T \hat{f}(x) - \eta\,\text{sat}(\sigma/\phi)] \quad (4.189)$$

$$u = -k^T x + (h^T b)^{-1}[h^T \dot{x}_d - h^T \hat{f}(x) - \eta\tanh(\sigma/\phi)] \quad (4.190)$$

These substitutions imply that:

$$\dot{V} = -\eta\,\sigma\tanh(\sigma/\phi) + \sigma\,h^T\Delta f$$

$$\dot{V} = -\eta\,\sigma\,\text{sat}(\sigma/\phi) + \sigma\,h^T\Delta f = \begin{cases} -\eta\,|\sigma| + \sigma\,h^T\Delta f & \text{if } |\sigma/\phi| > 1 \\ -\eta\,\sigma^2/\phi + \sigma\,h^T\Delta f & \text{otherwise} \end{cases}$$

where the product $\sigma\tanh(\sigma/\phi)$ is shown in the lower plot of Figure 4.21. It should be noted that the proposed feedback control with a predescribed η usually yields a conservative estimate of the necessary control action required to stabilize the plant. This suggests that η should be treated as a tunable parameter.

Example 4.6 (Forward Speed Control)
Again consider the speed equation (4.110) in the form:

$$(m - X_{\dot{u}})\,\dot{u} + \frac{1}{2}\rho\, C_D\, A\, |u|u = X_{|n|n}\, |n|n + f(u,n) \tag{4.191}$$

where $m - X_{\dot{u}}$ is the mass of the vehicle including hydrodynamic added mass, ρ is the water density, C_D is the drag coefficient, A is the projected area, $X_{|n|n}$ is the propeller force coefficient and $f(u,n)$ represents the unmodelled dynamics. Since the speed dynamics is of first order and completely decoupled from the other state variables, we can select $\boldsymbol{h} = 1$ so that:

$$\sigma = \tilde{u} = u - u_d \tag{4.192}$$

The desired σ-dynamics is obtained for the following feedback control law:

$$|n|n = \frac{1}{X_{|n|n}}\left[(m - X_{\dot{u}})\,\dot{u}_d + \frac{1}{2}\rho\, C_D\, A\, |u|u - (m - X_{\dot{u}})\,\eta\, \tanh(\sigma/\phi)\right] \tag{4.193}$$

Hence, n is computed as the signed square root of the right-hand side of (4.193).
□

Example 4.7 (Steering Autopilot)
Consider the linear steering equations of motion in the form:

$$\begin{bmatrix} \dot{v} \\ \dot{r} \\ \dot{\psi} \end{bmatrix} = \begin{bmatrix} a_{11} & a_{12} & 0 \\ a_{21} & a_{22} & 0 \\ 0 & 1 & 0 \end{bmatrix} \begin{bmatrix} v \\ r \\ \psi \end{bmatrix} + \begin{bmatrix} b_1 \\ b_2 \\ 0 \end{bmatrix} \delta_R - \begin{bmatrix} a_{11} \\ a_{21} \\ 0 \end{bmatrix} \cdot V_c \sin(\pi/2 - \psi) \tag{4.194}$$

where V_c is an unknown sinusoidal disturbance defined as:

$$V_c = 0.5\, \sin(0.2\, t) \tag{4.195}$$

It is practical to specify the desired sway velocity during steering as $v_d = 0$ while the desired yaw rate and heading angle are denoted by r_d and ψ_d, respectively. Let us define the sliding surface as:

$$\sigma = h_1\, v + h_2\, (r - r_d) + h_3\, (\psi - \psi_d) \tag{4.196}$$

where h_i for (i=1...3) are the components of $\boldsymbol{h}$. To stabilize the sway-yaw dynamics, we choose $\boldsymbol{k} = [k_1, k_2, 0]^T$ such that:

$$\boldsymbol{A}_c = \boldsymbol{A} - \boldsymbol{b}\boldsymbol{k}^T = \begin{bmatrix} a_{11} - b_1\, k_1 & a_{12} - b_1\, k_2 & 0 \\ a_{21} - b_2\, k_1 & a_{22} - b_2\, k_2 & 0 \\ 0 & 1 & 0 \end{bmatrix} \tag{4.197}$$

Notice that $k_3 = 0$, *or in other words* linear feedback *from* ψ *is not necessary to stabilize the sway-yaw dynamics. Hence, two of the closed-loop eigenvalues* $\lambda_{1,2}$ *will simply be given by the upper-left* 2×2 *submatrix of* $\boldsymbol{A}_c$, *that is:*

$$(a_{11} - b_1\, k_1 - \lambda)(a_{22} - b_2\, k_2 - \lambda) - (a_{21} - b_2\, k_1)(a_{12} - b_1\, k_2) = 0 \tag{4.198}$$

This expression can be solved to yield k_1 *and* k_2 *for any values of* $\lambda_{1,2}$. *Alternatively, a pole placement algorithm or optimal control theory can be used to compute* k_1 *and* k_2. *The last eigenvalue* λ_3 *is zero due to the pure integration in the yaw channel* ($\dot{\psi} = r$). *This in turn implies that* $\boldsymbol{h}$ *can be computed as the right eigenvector of* $\boldsymbol{A}_c^T$ *for* $\lambda_3 = 0$. *Furthermore, let us define:*

$$\beta_0 = \boldsymbol{h}^T \boldsymbol{b} = h_1\, b_1 + h_2\, b_2 \neq 0 \tag{4.199}$$

then the steering control law δ_R *becomes:*

$$\delta_R = -k_1\, v - k_2\, r + \frac{1}{\beta_0}[h_2\, \dot{r}_d + h_3\, r_d - \eta\, \tanh(\sigma/\phi)] \tag{4.200}$$

During course-keeping $\psi_d = constant$, *which again implies that* $\dot{r}_d = r_d = 0$. *Consider the numerical example:* $a_{11} = -0.25, a_{12} = -0.87, a_{21} = -0.012, a_{22} = -0.23, b_1 = 0.22$ *and* $b_2 = -0.043$. *Choosing:* $\lambda_1 = -0.5, \lambda_2 = -0.32$ *and* $\lambda_3 = 0$ *by pole placement, yields:*

$$\boldsymbol{k} = [0.3623, -6.0534, 0]^T \tag{4.201}$$

Hence,

$$\boldsymbol{A}_c = \boldsymbol{A} - \boldsymbol{b}\boldsymbol{k}^T = \begin{bmatrix} -0.3297 & 0.4618 & 0 \\ 0.0036 & -0.4903 & 0 \\ 0 & 1.0000 & 0 \end{bmatrix} \tag{4.202}$$

Solve the right eigenvector $\boldsymbol{h}$ *of* $\boldsymbol{A}_c^T$ *corresponding to* $\lambda_3 = 0$, *that is:*

$$\boldsymbol{A}_c^T \boldsymbol{h} = 0 \quad \Longrightarrow \quad \boldsymbol{h} = [h_1, h_2, h_3]^T = [0.0098, 0.8996, 0.4366]^T \tag{4.203}$$

Furthermore, we have that:

$$\beta_0 = \boldsymbol{h}^T \boldsymbol{b} = -0.0365 \tag{4.204}$$

$$\eta > \| \boldsymbol{h} \| \cdot \| -[a_{11}, a_{12}, 0]^T\, V_c \| = 0.1251 \tag{4.205}$$

The simulation results for this system with reference model:

$$\begin{bmatrix} \dot{\psi}_d \\ \dot{r}_d \end{bmatrix} = \begin{bmatrix} 0 & 1 \\ -\omega_n^2 & -2\zeta\omega_n \end{bmatrix} \begin{bmatrix} \psi_d \\ r_d \end{bmatrix} + \begin{bmatrix} 0 \\ \omega_n^2 \end{bmatrix} \psi_c \tag{4.206}$$

where $\zeta = 0.8$ *and* $\omega_n = 0.1$ *are shown in Figure 4.22. All simulations were performed with a sampling time of 0.1 (s) and boundary layer thickness* $\phi = 0.1$.

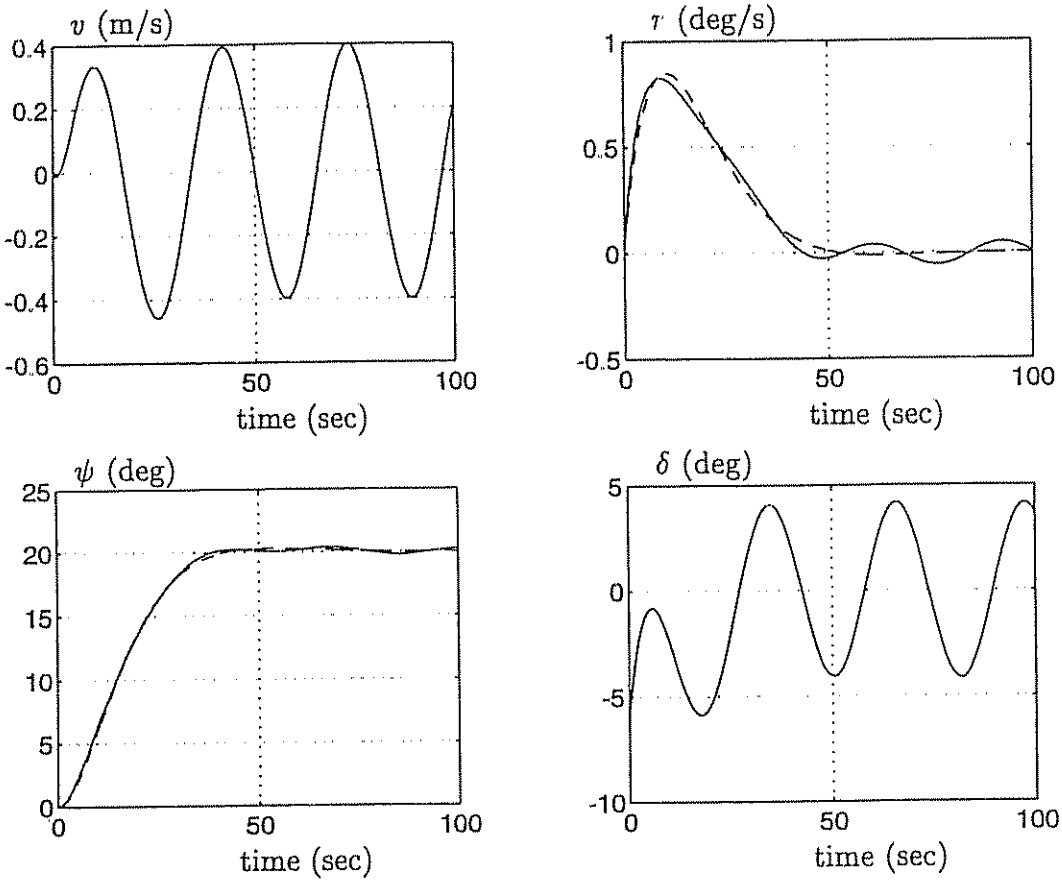

Figure 4.22: Step response $\psi_c = 20$ (deg) with sinusoidal disturbance V_c. Dotted lines denote ψ_d and r_d.

From this figure it is seen that the sinusoidal disturbance does not affect the tracking performance or the stability of the control law. This will not be the case if a simple PID-control law is applied to this system.
□

Example 4.8 (Combined Pitch/Depth Control)

Consider the simplified diving equations of motion in the form:

$$\begin{bmatrix} \dot{w} \\ \dot{q} \\ \dot{\theta} \\ \dot{z} \end{bmatrix} = \begin{bmatrix} a_{11} & a_{12} & 0 & 0 \\ a_{21} & a_{22} & a_{23} & 0 \\ 0 & 1 & 0 & 0 \\ 1 & 0 & -u_0 & 0 \end{bmatrix} \begin{bmatrix} w \\ q \\ \theta \\ z \end{bmatrix} + \begin{bmatrix} b_1 \\ b_2 \\ 0 \\ 0 \end{bmatrix} \delta_S \tag{4.207}$$

We now define the sliding surface as:

$$\sigma = h_1 (w - w_d) + h_2 (q - q_d) + h_3 (\theta - \theta_d) + h_4 (z - z_d) \tag{4.208}$$

where h_i for (i=1...4) are the components of $\boldsymbol{h}$. As in the previous example $\boldsymbol{k} = [k_1, k_2, k_3, k_4]^T$ must be solved from the specified closed-loop dynamics via

eigenvalue specifications. Since there is one pure integration in the pitch channel this mode can be removed from A_c by selecting $k_3 = 0$. Hence, we can compute h by solving: $\lambda(A_c) = \lambda(A - bk^T)$ such that $A_c^T h = 0$ for $\lambda_3 = 0$ which is simply a 3rd-order pole-placement problem. Finally,

$$\beta_0 = h^T b = h_1\, b_1 + h_2\, b_2 \neq 0 \tag{4.209}$$

and

$$\delta_S = -k_1\, w - k_2\, q - k_4\, z + \frac{1}{\beta_0}[h_1\, \dot{w}_d + h_2\, \dot{q}_d + h_3\, \theta_d + h_4\, z_d - \eta\, \tanh(\sigma/\phi)] \tag{4.210}$$

□

4.5.2 State Feedback Linearization

The basic idea with feedback linearization is to transform the nonlinear systems dynamics into a linear system (Freund 1973). Conventional control techniques like pole placement and linear quadratic optimal control theory can then be applied to the linear system. In robotics, this technique is commonly referred to as *computed torque* control.

Adaptive computed torque control has been applied to robot manipulators by Horowitz and Tomizuka (1986) and to underwater vehicles by Fossen (1991). Feedback linearization is easily applicable to underwater vehicles. We will discuss applications to both the body-fixed and earth-fixed reference frames.

Decoupling in the Body-Fixed Reference Frame (Velocity Control)

The control objective is to transform the vehicle dynamics into a linear system $\dot{\nu} = a_\nu$, where a_ν can be interpreted as a commanded acceleration vector. The body-fixed vector representation should be used to control the vehicle's linear and angular velocities. Consider the nonlinear ROV dynamics (4.27) which can be compactly expressed as:

$$M\, \dot{\nu} + n(\nu, \eta) = \tau \tag{4.211}$$

Here η and ν are assumed to be measured and n is the nonlinear vector:

$$n(\nu, \eta) = C(\nu)\nu + D(\nu)\nu + g(\eta) \tag{4.212}$$

The nonlinearities can be canceled out by simply selecting the control law as

$$\boxed{\tau = M\, a_\nu + n(\nu, \eta)} \tag{4.213}$$

where the commanded acceleration vector a_ν can be chosen by e.g. pole placement or linear quadratic optimal control theory. Let λ be the control bandwidth,

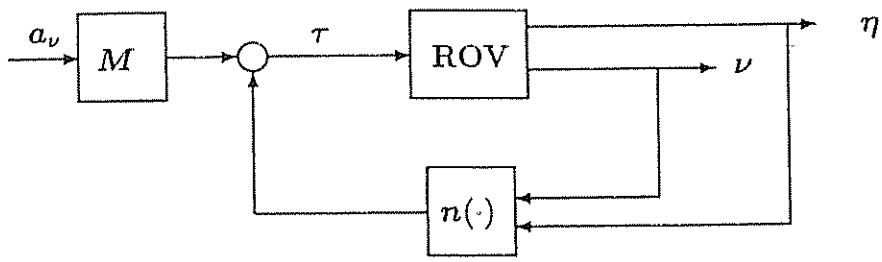

Figure 4.23: Nonlinear decoupling

ν_d the desired linear and angular velocity vector and $\tilde{\nu} = \nu - \nu_d$ the velocity tracking error. Then the commanded acceleration vector:

$$\boxed{a_\nu = \dot{\nu}_d - \lambda\tilde{\nu}} \tag{4.214}$$

yields the 1st-order error dynamics:

$$M\,(\dot{\tilde{\nu}} - a_\nu) = M\,(\dot{\tilde{\nu}} + \lambda\tilde{\nu}) = 0 \tag{4.215}$$

The calculation of the commanded acceleration vector is shown in Figure 4.24.

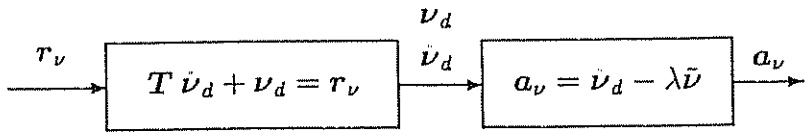

Figure 4.24: Calculation of the commanded acceleration (body-fixed)

The reference model is simply chosen as a first-order model with time constants $T = \mathrm{diag}\{T_1, T_2, ..., T_6\}$ and r_ν as the commanded input vector. Note that in steady-state:

$$\lim_{t\to\infty} \nu_d(t) = r_\nu \tag{4.216}$$

Example 4.9 (Surge Velocity Control System)
Consider a simplified model of an ROV in surge, that is:

$$m\,\dot{u} + d\,|u|\,u = \tau \tag{4.217}$$

The commanded acceleration is calculated as:

$$a_\nu = \dot{u}_d - \lambda(u - u_d) \tag{4.218}$$

This suggests that the control law should be computed as:

$$\tau = m\left[\dot{u}_d - \lambda(u - u_d)\right] + d\,|u|\,u \tag{4.219}$$

□

Decoupling in the Earth-Fixed Reference Frame (Position and Attitude)

In the earth-fixed vector representation the vehicle's dynamics and kinematics are decoupled into the earth-fixed reference frame i.e. $\ddot{\eta} = a_\eta$ where a_η can be interpreted as the earth-fixed commanded acceleration. Consider the ROV dynamics and kinematics in the form:

$$M\dot{\nu} + n(\nu, \eta) = \tau \tag{4.220}$$

$$\dot{\eta} = J(\eta)\,\nu \tag{4.221}$$

where $J(\eta)$ is the kinematic transformation matrix and where both η and ν are assumed measured. Differentiation of the kinematic equation with respect to time yields:

$$\dot{\nu} = J^{-1}(\eta)\left[\ddot{\eta} - \dot{J}(\eta)\nu\right] \tag{4.222}$$

The nonlinear control law:

$$\boxed{\tau = Ma_\nu + n(\nu, \eta)} \tag{4.223}$$

applied to the ROV equations of motion, yields:

$$M\left(\dot{\nu} - a_\nu\right) = MJ^{-1}(\eta)\left[\ddot{\eta} - \dot{J}(\eta)\,\nu - J(\eta)\,a_\nu\right] = 0 \tag{4.224}$$

Defining

$$M_\eta = J^{-T}(\eta)MJ^{-1}(\eta) \quad \text{and} \quad a_\eta = \dot{J}(\eta)\nu + J(\eta)a_\nu \tag{4.225}$$

yields the linear decoupled system:

$$M_\eta(\ddot{\eta} - a_\eta) = 0 \tag{4.226}$$

This suggests that the commanded acceleration a_η should be chosen as:

$$\boxed{a_\eta = \ddot{\eta}_d - K_d\,\dot{\tilde{\eta}} - K_p\,\tilde{\eta}} \tag{4.227}$$

where K_p and K_d are two positive definite matrices chosen such that the error dynamics:

$$\ddot{\tilde{\eta}} + K_d\,\dot{\tilde{\eta}} + K_p\,\tilde{\eta} = 0 \tag{4.228}$$

is stable. In the implementation of the control law (4.223) the commanded acceleration in the body-fixed reference frame is calculated as:

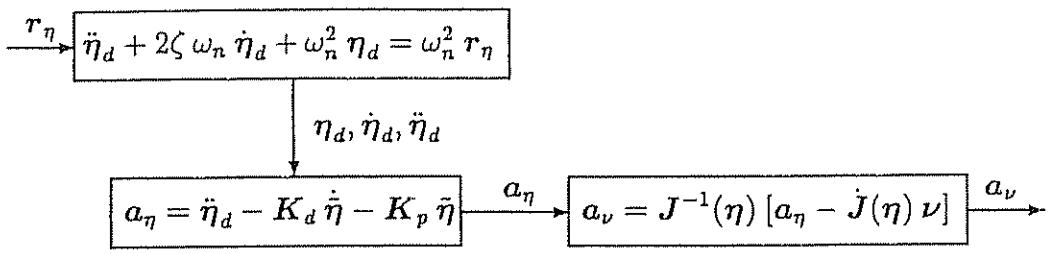

Figure 4.25: Calculation of commanded acceleration (earth-fixed).

$$\boxed{a_\nu = J^{-1}(\eta)\,[a_\eta - \dot{J}(\eta)\,\nu]} \tag{4.229}$$

This is shown in Figure 4.25. The reference model is chosen such that the commanded input vector r_η is equal to the steady-state reference vector, that is $\eta_d(\infty) = r_\eta$.

Example 4.10 (Heading Control System)
Consider the simplified model of an underwater vehicle in yaw:

$$m\,\dot{r} + d\,|r|\,r = \tau; \qquad \dot{\psi} = r \tag{4.230}$$

Hence, the commanded acceleration can be calculated as:

$$a_\eta = \dot{r}_d - K_d\,(r - r_d) - K_p\,(\psi - \psi_d) \tag{4.231}$$

where r_d is the desired angular velocity and ψ_d is the desired heading angle. For this particular example $a_\nu = a_\eta$, which yields the decoupling control law:

$$\tau = m\,[\dot{r}_d - K_d\,(r - r_d) - K_p\,(\psi - \psi_d)] + d\,|r|\,r \tag{4.232}$$

To illustrate the robustness of the control system, we investigated the performance of the heading control system for perturbations in m and d. These results are shown in Figure 4.26. The sampling time in the simulation study was chosen as 0.1 (s). The nominal model parameters are $m = 200$ and $d = 50$. Furthermore, we designed the control law according to $K_p = 2\lambda$ and $K_d = \lambda^2$ with "bandwidth" $\lambda = 1$ (rad/s). The mass and damping estimates are denoted by m_0 and d_0, respectively. Moreover:

$$\tau = m_0\,[\dot{r}_d - 2.0\,(r - r_d) - 1.0\,(\psi - \psi_d)] + d_0\,|r|\,r \tag{4.233}$$

□

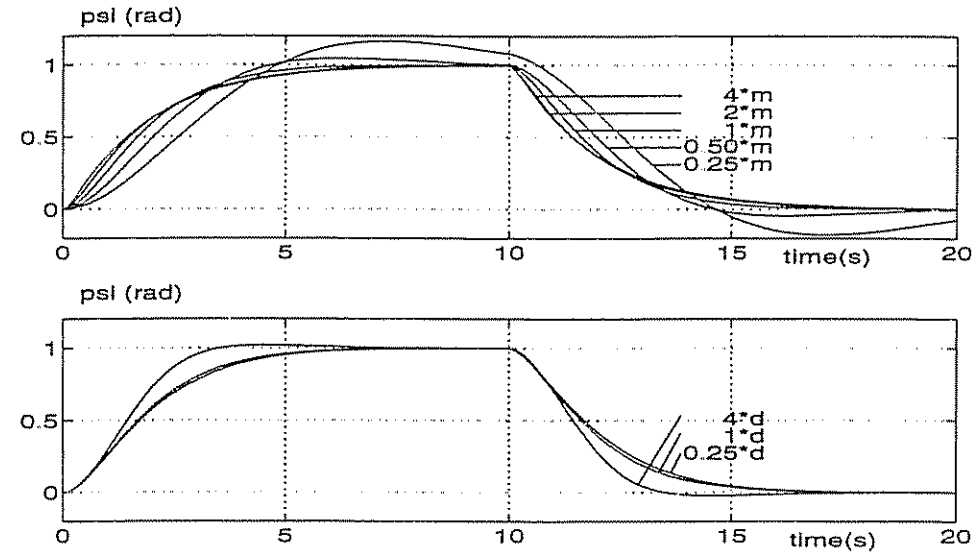

Figure 4.26: Computer simulation showing the robustness and performance of the control law where $d_0 = \alpha \cdot d$ (upper plot) and $m_0 = \beta \cdot m$ (lower plot) are allowed to vary according to $\alpha \in \{0.25, 0.50, 1, 2, 4\}$ and $\beta \in \{0.25, 1, 4\}$.

Computation of Desired States by Means of the Vehicle Kinematics

The decoupled reference models:

$$\ddot{\eta}_d + 2\zeta\omega_n \dot{\eta}_d + \omega_n^2 \eta_d = \omega_n^2 r_\eta \tag{4.234}$$

can result in unrealistic maneuvers of the vehicle. A better approach is to take advantage of the vehicle kinematics when designing the desired state trajectories. For instance, we can compute ν_d and η_d from:

$$\dot{\nu}_d + \Lambda \nu_d + J^T(\eta_d)\, \Omega\, \eta_d = J^T(\eta_d)\, \Omega\, r_\eta \tag{4.235}$$

$$\dot{\eta}_d = J(\eta_d)\, \nu_d \tag{4.236}$$

where r_η is a constant (slowly-varying) commanded input. Hence, we can show by applying Lyapunov stability analysis that:

$$\lim_{t\to\infty} \nu_d(t) = 0; \qquad \lim_{t\to\infty} \eta_d(t) = r_\eta \tag{4.237}$$

The proof is based on time differentiation of a Lyapunov function candidate:

$$V = \frac{1}{2}\left(\nu_d^T \nu_d + (\eta_d - r_\eta)^T \Omega (\eta_d - r_\eta)\right) \tag{4.238}$$

which after substitution of the reference model dynamics yields:

$$\dot{V} = -\nu_d^T\, \Lambda\, \nu_d \leq 0 \tag{4.239}$$

The only design parameters in the reference model are the matrices $\Lambda > 0$ and $\Omega = \Omega^T > 0$ describing the preferred damping and stiffness of the system. Λ and Ω are usually chosen as diagonal matrices with positive entries on the diagonal.

Extensions to Systems which are Nonlinear in their Input

Both feedback linearization and sliding control can be applied to the more general model class (Fossen and Foss 1991):

$$M\dot{\nu} + n(\nu, \eta) = b(\nu, u) \tag{4.240}$$

$$\dot{\eta} = J(\eta)\,\nu \tag{4.241}$$

which is nonlinear in the input u. Time differentiating of the first expression with respect to time, yields:

$$M\ddot{\nu} + \frac{\partial n(\nu,\eta)}{\partial \nu}\dot{\nu} + \frac{\partial n(\nu,\eta)}{\partial \eta}\dot{\eta} = \frac{\partial b(\nu,u)}{\partial \nu}\dot{\nu} + \frac{\partial b(\nu,u)}{\partial u}\dot{u} \tag{4.242}$$

Substituting the kinematic equation of motion into this expression, yields:

$$M\ddot{\nu} + \left(\frac{\partial n(\nu,\eta)}{\partial \nu} - \frac{\partial b(\nu,u)}{\partial \nu}\right)\dot{\nu} + \left(\frac{\partial n(\nu,\eta)}{\partial \eta}J(\eta)\right)\nu = \frac{\partial b(\nu,u)}{\partial u}\dot{u} \tag{4.243}$$

Introducing the notation:

$$n^*(\dot{\nu}, \nu, \eta, u) = \left(\frac{\partial n(\nu,\eta)}{\partial \nu} - \frac{\partial b(\nu,u)}{\partial \nu}\right)\dot{\nu} + \left(\frac{\partial n(\nu,\eta)}{\partial \eta}J(\eta)\right)\nu \tag{4.244}$$

$$B^*(\nu, u) = \frac{\partial b(\nu,u)}{\partial u} \tag{4.245}$$

yields the more compact representation:

$$\boxed{M\ddot{\nu} + n^*(\dot{\nu}, \nu, \eta, u) = B^*(\nu, u)\,\dot{u}} \tag{4.246}$$

Let the control law be chosen as:

$$\boxed{\dot{u} = (B^*(\nu, u))^{\dagger}\left[Ma_{\nu}^* + n^*(\dot{\nu}, \nu, \eta, u)\right]} \tag{4.247}$$

Hence, the error dynamics is:

$$M(\ddot{\nu} - a_{\nu}^*) = 0 \tag{4.248}$$

For velocity control, the *commanded jerk* a_{ν}^* (the time derivative of acceleration) could be chosen as:

$$a_{\nu}^* = \ddot{\nu}_d - 2\,\lambda\dot{\tilde{\nu}} - \lambda^2\,\tilde{\nu} \tag{4.249}$$

to yield the asymptotically stable velocity error dynamics:

$$\left(\frac{d}{dt} + \lambda\right)^2 \tilde{\nu} = 0 \tag{4.250}$$

A position and attitude scheme is derived by first differentiating (4.241) twice with respect to time, to yield:

$$\eta^{(3)} = J(\eta)\,\ddot{\nu} + 2\dot{J}(\eta)\,\dot{\nu} + \ddot{J}(\eta)\,\nu \tag{4.251}$$

Consequently, we can rewrite the error dynamics (4.248) as:

$$M\,J^{-1}(\eta)[\eta^{(3)} - 2\dot{J}(\eta)\,\dot{\nu} - \ddot{J}(\eta)\,\nu - J(\eta)\,a_\nu^*] = 0 \tag{4.252}$$

This in turn suggests that the body-fixed commanded jerk a_ν^* should be computed by means of the earth-fixed commanded jerk a_η^* according to:

$$\boxed{a_\nu^* = J^{-1}(\eta)[a_\eta^* - 2\,\dot{J}(\eta)\,\dot{\nu} - \ddot{J}(\eta)\,\nu]} \tag{4.253}$$

where a_η^* must be chosen such that the closed-loop error dynamics:

$$M_\eta\,(\eta^{(3)} - a_\eta^*) = 0 \tag{4.254}$$

is asymptotically stable. Notice that in the implementation of the *"non-affine"* controller, acceleration measurements are required in addition to velocity and position measurements, whereas acceleration measurements are not necessary for the *affine* model. A similar approach can be applied to the sliding control scheme discussed in the previous section. A more detailed discussion on sliding control for MIMO nonlinear systems is found in Fossen and Foss (1991).

4.5.3 Adaptive Feedback Linearization

So far we have only discussed feedback linearization under the assumption that all model parameters are *known*. In this section we will derive a *parameter adaptation law* to be used together with the previous control laws. Consider the nonlinear equations of motion (4.211). Taking the control law to be:

$$\boxed{\tau = \hat{M} a_\nu + \hat{n}(\nu, \eta)} \tag{4.255}$$

where the hat denotes the adaptive parameter estimates, yields the error dynamics:

$$M\,[\dot{\nu} - a_\nu] = [\hat{M} - M]\,a_\nu + [\hat{n}(\nu, \eta) - n(\nu, \eta)] \tag{4.256}$$

If the underwater vehicle equations of motion are linear in a parameter vector θ, the following parameterization can be applied:

$$[\hat{M} - M]\,a_\nu + [\hat{n}(\nu, \eta) - n(\nu, \eta)] \triangleq \Phi(a_\nu, \nu, \eta)\,\tilde{\theta} \tag{4.257}$$

Here $\tilde{\theta} = \hat{\theta} - \theta$ is the *unknown* parameter error vector and $\Phi(a_\nu, \nu, \eta)$ is a *known* matrix function of measured signals usually referred to as the *regressor matrix*.

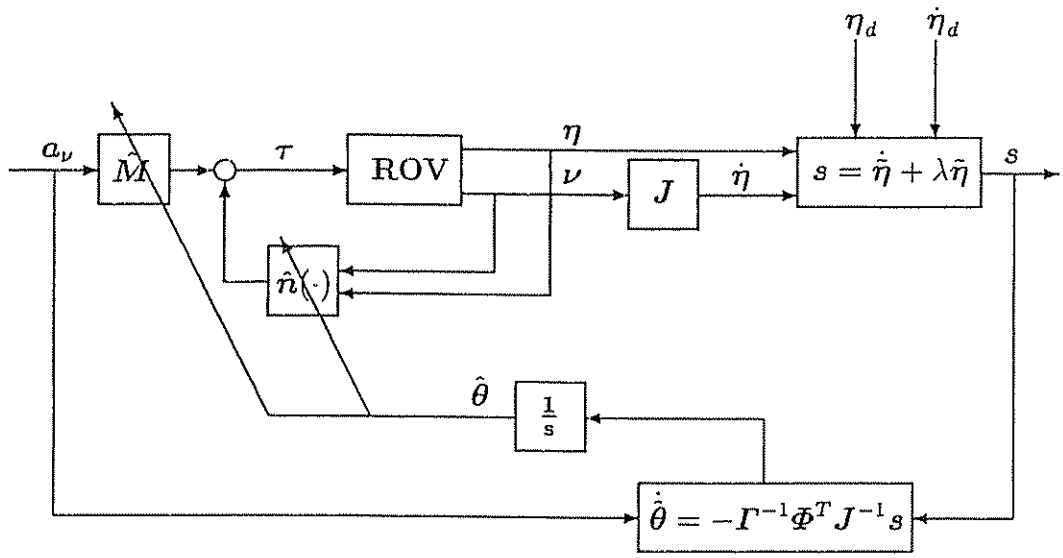

Figure 4.27: Adaptive feedback linearization applied to the nonlinear ROV equations of motion.

Using the result $a_\eta = \dot{J}(\eta)\nu + J(\eta)a_\nu$, yields:

$$M J^{-1}(\eta)\left[\ddot{\eta} - a_\eta\right] = \Phi(a_\nu, \nu, \eta)\,\tilde{\theta} \tag{4.258}$$

Premultiplying this expression with $J^{-T}(\eta)$ and letting $M_\eta(\eta) = J^{-T}(\eta) M J^{-1}(\eta)$ yields the earth-fixed error dynamics:

$$M_\eta(\eta)\left[\ddot{\eta} - a_\eta\right] = J^{-T}(\eta)\,\Phi(a_\nu, \nu, \eta)\,\tilde{\theta} \tag{4.259}$$

Furthermore, let the commanded acceleration be chosen as:

$$\boxed{a_\eta = \ddot{\eta}_d - K_d\,\dot{\tilde{\eta}} - K_p\,\tilde{\eta}} \tag{4.260}$$

where $K_p > 0$ and $K_d > 0$. Hence we can express the error dynamics according to:

$$M_\eta(\eta)\left[\ddot{\tilde{\eta}} + K_d\,\dot{\tilde{\eta}} + K_p\,\tilde{\eta}\right] = J^{-T}(\eta)\,\Phi(a_\nu, \nu, \eta)\,\tilde{\theta} \tag{4.261}$$

Writing this expression in state-space form, yields:

$$\dot{x} = A\,x + B\,J^{-T}(\eta)\,\Phi(a_\nu, \nu, \eta)\,\tilde{\theta} \tag{4.262}$$

where $x = [\tilde{\eta},\ \dot{\tilde{\eta}}]^T$ and

$$A = \begin{bmatrix} 0 & I \\ -K_p & -K_d \end{bmatrix} \qquad B = \begin{bmatrix} 0 \\ M_\eta^{-1} \end{bmatrix} \tag{4.263}$$

Convergence of $\tilde{\eta}$ to zero can be proven by defining:

$$V(x,\tilde{\theta},t) = x^T P x + \tilde{\theta}^T \Gamma^{-1} \tilde{\theta}; \qquad P = P^T > 0 \tag{4.264}$$

Differentiating V with respect to time and substituting the error dynamics into the expression for $\dot{V}$, yields:

$$\dot{V} = x^T(\dot{P} + PA + A^T P)x + 2\,(x^T P B J^{-T} \Phi + \dot{\tilde{\theta}}^T \Gamma^{-1})\tilde{\theta} \tag{4.265}$$

where $\Gamma = \Gamma^T > 0$ is a positive definite weighting matrix of appropriate dimension. This suggests the parameter update law (assuming $\dot{\theta} = 0$):

$$\boxed{\dot{\hat{\theta}} = -\Gamma\, \Phi^T(a_\nu, \nu, \eta)\, J^{-1}(\eta)\, y} \tag{4.266}$$

where we have introduced a new signal vector y defined as

$$y = C\,x \qquad C = B^T P \tag{4.267}$$

In order to prove that $\dot{V} \leq 0$ we can choose:

$$C = [c_0 I \;\; c_1 I] \tag{4.268}$$

where $c_0 > 0$ and $c_1 > 0$ are two positive scalars to be interpreted later. Furthermore we choose:

$$PA + A^T P = -Q; \qquad Q = Q^T > 0 \tag{4.269}$$

where P and Q are defined according to Asare and Wilson (1986):

$$P = \begin{bmatrix} c_0 M_\eta K_d + c_1 M_\eta K_p & c_0 M_\eta \\ c_0 M_\eta & c_1 M_\eta \end{bmatrix} \tag{4.270}$$

$$Q = \begin{bmatrix} 2c_0 M_\eta K_p & 0 \\ 0 & 2(c_1 M_\eta K_d - c_0 M_\eta) \end{bmatrix} \tag{4.271}$$

If in addition, we use the fact that $z^T M_\eta z$ is bounded, we can establish: $(z \in \mathbb{R}^3)$

$$x^T \dot{P} x \leq \alpha\, x^T x \implies x^T \dot{P} x \leq \beta\, x^T \begin{bmatrix} M_\eta & 0 \\ 0 & M_\eta \end{bmatrix} x \tag{4.272}$$

where $\alpha > 0$ and $\beta > 0$ are two positive constants. Hence, we can choose $c_0 > 0$, $c_1 > 0$ and:

$$x^T Q x > \beta\, x^T \begin{bmatrix} M_\eta & 0 \\ 0 & M_\eta \end{bmatrix} x \tag{4.273}$$

such that $P = P^T > 0$ and:

$$\dot{V} = x^T\,(\dot{P} - Q)x \leq 0 \tag{4.274}$$

by requiring:

$$\begin{array}{ll} (1) & (c_0 K_d + c_1 K_p)\, c_1 > c_0^2 I \\ (2) & 2c_0 K_p > \beta I \\ (3) & 2(c_1 K_d - c_0 I) > \beta I \end{array}$$

Here β usually is taken to be a small positive constant while $K_p > 0$ and $K_d > 0$ can be chosen as diagonal matrices. Consequently, convergence of $\tilde{\eta}$ to zero is guaranteed by applying Barbălat's lemma. We also notice that the parameter vector $\tilde{\theta}$ will be bounded. Hence, PE is not required to guarantee the tracking error to converge to zero. Robustness due to actuator dynamics and saturation are discussed by Fjellstad, Fossen and Egeland (1992).

4.5.4 Nonlinear Tracking (The Slotine and Li Algorithm)

An adaptive control law exploiting the skew-symmetric property of robot manipulators was first derived by Slotine and Li (1987). Later, extensions of this work was made to the 3 DOF spacecraft attitude control problem in terms of *Rodrigues parameters* by Slotine and Benedetto (1990) together with Fossen (1993a). These results have been extended to 6 DOF (position and attitude) in terms of *Euler angles* by Fossen and Sagatun (1991a, 1991b) who used their control law to control an underwater vehicle in 6 DOF. More recently Fjellstad and Fossen (1994a) have shown that *Euler parameters* (vector quaternion, Euler rotation and Rodrigues parameters) can be used in the 6 DOF tracking control problem as well. We will exclusively discuss the work of Fossen and Sagatun (1991b) in this section.

Reference Trajectory Definitions

Let the desired earth-fixed position and attitude be described by a smooth time-varying reference trajectory $\ddot{\eta}_d$, $\dot{\eta}_d$ and η_d where:

$$\eta_d = [x_d, y_d, z_d, \phi_d, \theta_d, \psi_d]^T \tag{4.275}$$

Furthermore, let $\tilde{\eta} = \eta - \eta_d$ denote the tracking error. The control law will be designed such that the following measure of tracking converges to zero:

$$s = \dot{\tilde{\eta}} + \lambda \tilde{\eta} \tag{4.276}$$

Here λ is a positive constant which may be interpreted as the control bandwidth. Hence convergence of s to zero implies that the tracking error $\tilde{\eta}$ converges to zero. For notational simplicity, it is convenient to rewrite (4.276) in term of a *virtual reference* trajectory η_r defined according to:

$$s = \dot{\eta} - \dot{\eta}_r \quad \Longrightarrow \quad \dot{\eta}_r = \dot{\eta}_d - \lambda \tilde{\eta} \tag{4.277}$$

We can transform η_r to the body-fixed reference frame by using (Niemeyer and Slotine 1991):

$$\dot{\eta}_r = J(\eta)\,\nu_r \tag{4.278}$$

Hence, the body-fixed virtual reference vectors ν_r and $\dot{\nu}_r$ can be computed according to:

$$\nu_r = J^{-1}(\eta)\dot{\eta}_r \tag{4.279}$$

$$\dot{\nu}_r = J^{-1}(\eta)\,[\ddot{\eta}_r - \dot{J}(\eta)J^{-1}(\eta)\,\dot{\eta}_r] \tag{4.280}$$

Adaptive Position and Attitude Control

Consider the following nonlinear model describing an ROV in 6 DOF:

$$M_\eta(\eta)\,\ddot{\eta} + C_\eta(\nu,\eta)\,\dot{\eta} + D_\eta(\nu,\eta)\,\dot{\eta} + g_\eta(\eta) = J^{-T}(\eta)\,\tau \tag{4.281}$$

Let V be a Lyapunov function candidate:

$$V(s,\tilde{\theta},t) = \frac{1}{2}\,(s^T M_\eta s + \tilde{\theta}^T \Gamma^{-1}\tilde{\theta}); \qquad M_\eta = M_\eta^T > 0 \tag{4.282}$$

where Γ is a positive definite weighting matrix of appropriate dimension and $\tilde{\theta} = \hat{\theta} - \theta$ is the parameter estimation error. Differentiating V with respect to time, yields:

$$\dot{V}(s,\tilde{\theta},t) = \frac{1}{2}\,(s^T M_\eta \dot{s} + \dot{s}^T M_\eta s + s^T \dot{M}_\eta s) + \dot{\tilde{\theta}}^T \Gamma^{-1}\tilde{\theta} \tag{4.283}$$

Since $s^T M_\eta \dot{s} = \dot{s}^T M_\eta s$ and:

$$s^T[\dot{M}_\eta(\eta) - 2C_\eta(\nu,\eta)]\,s = 0 \;\;\forall\;\; s,\nu,\eta \in \mathbb{R}^n \tag{4.284}$$

we can write:

$$\dot{V} = s^T(M_\eta \dot{s} + C_\eta s) + \dot{\tilde{\theta}}^T \Gamma^{-1}\tilde{\theta} \tag{4.285}$$

The application of the virtual reference trajectory in (4.277) together with (4.281), yields:

$$\dot{V} = -s^T D_\eta s + \dot{\tilde{\theta}}^T \Gamma^{-1}\tilde{\theta} + s^T(J^{-T}\tau - M_\eta \ddot{\eta}_r - C_\eta \dot{\eta}_r - D_\eta \dot{\eta}_r - g_\eta) \tag{4.286}$$

Transforming the earth-fixed virtual reference trajectory to body-fixed coordinates, see (4.279) and (4.280), implies that the last term in the expression for $\dot{V}$ can be written:

$$\begin{aligned} &M_\eta(\eta)\,\ddot{\eta}_r + C_\eta(\nu,\eta)\,\dot{\eta}_r + D_\eta(\nu,\eta)\,\dot{\eta}_r + g_\eta(\eta) \\ &\quad = J^{-T}(\eta)\,[M\,\dot{\nu}_r + C(\nu)\,\nu_r + D(\nu)\,\nu_r + g(\eta)] \end{aligned} \tag{4.287}$$

Assuming that $M, C(\nu), D(\nu)$ and $g(\eta)$ are linear in their parameters, this suggests that we can use the following parameterization (Fossen 1993a):

$$M\,\dot{\nu}_r + C(\nu)\,\nu_r + D(\nu)\,\nu_r + g(\eta) \triangleq \Phi(\dot{\nu}_r, \nu_r, \nu, \eta)\,\theta \tag{4.288}$$

where θ is an *unknown* parameter vector and $\Phi(\dot{\nu}_r, \nu_r, \nu, \eta)$ is a *known* regression matrix of appropriate dimension. By using ν_r instead of η_r in the parameterization, the transformation matrix (kinematics) $J(\eta)$ does not enter into the regression matrix. This yields:

$$\dot{V} = -s^T D_\eta(\nu,\eta)s + [J^{-1}(\eta)s]^T\,[\tau - \Phi(\dot{\nu}_r, \nu_r, \nu, \eta)\,\theta] + \tilde{\theta}^T \Gamma^{-1}\dot{\tilde{\theta}} \tag{4.289}$$

Let the control law be chosen as:

$$\boxed{\tau = \Phi(\dot{\nu}_r, \nu_r, \nu, \eta)\,\hat{\theta} - J^T(\eta)\,K_d\,s} \tag{4.290}$$

where $\hat{\theta}$ is the estimated parameter vector and K_d is a symmetric positive regulator gain matrix of appropriate dimension. Hence,

$$\dot{V} = -s^T\,[K_d + D_\eta(\nu,\eta)]\,s + \tilde{\theta}^T\,[\Phi^T(\dot{\nu}_r, \nu_r, \nu, \eta)\,J^{-1}(\eta)s + \Gamma^{-1}\,\dot{\hat{\theta}}] \tag{4.291}$$

Then, the parameter update law (assuming $\dot{\theta} = 0$):

$$\boxed{\dot{\hat{\theta}} = -\Gamma\,\Phi^T(\dot{\nu}_r, \nu_r, \nu, \eta)\,J^{-1}(\eta)\,s} \tag{4.292}$$

cancels out the last term in the expression for $\dot{V}$, such that:

$$\dot{V} = -s^T\,[K_d + D_\eta(\nu,\eta)]\,s \leq 0 \quad \forall\,\nu \in \mathbb{R}^n,\ \eta \in \mathbb{R}^n \tag{4.293}$$

Hence, convergence of s to zero except for the singular point $\theta = \pm 90^o$ is guaranteed by applying Barbălat's lemma. This in turn implies that s converges to zero and that $\tilde{\theta}$ is bounded.

Non-Adaptive Position and Attitude Control

If the model parameters are known with some accuracy the following non-adaptive nonlinear control law can be applied:

$$\boxed{\tau = M\,\dot{\nu}_r + C(\nu)\,\nu_r + D(\nu)\,\nu_r + g(\eta) - J^T(\eta)\,K_d\,s} \tag{4.294}$$

where ν_r and $\dot{\nu}_r$ are defined in (4.279) and (4.280), respectively. It should be noted that implementation of the non-adaptive version of the control law often is advantageous since the parameter adaptation law can be sensitive to measurement noise. This control law can also be written in terms of *Euler parameters*; see Fjellstad and Fossen (1994a) for details.

Example 4.11 (ROV Position and Attitude Control System)
The motion of a metacenter stable (roll and pitch stabilized) ROV can be described by the following simplified model in surge, sway, heave and yaw:

$$M = \text{diag}\{m - X_{\dot{u}},\ m - Y_{\dot{v}},\ m - Z_{\dot{w}},\ I_z - N_{\dot{r}}\}$$

$$C(\nu) = \begin{bmatrix} 0 & -mr & 0 & Y_{\dot{v}}v \\ mr & 0 & 0 & -X_{\dot{u}}u \\ 0 & 0 & 0 & 0 \\ -Y_{\dot{v}}v & X_{\dot{u}}u & 0 & 0 \end{bmatrix} \qquad g(\eta) = [\ 0 \quad 0 \quad 0 \quad 0\ ]^{\mathrm{T}}$$

$$D(\nu) = -\text{diag}\{X_u + X_{|u|u}|u|, Y_u + Y_{|v|v}|v|, Z_w + Z_{|w|w}|w|, N_r + N_{|r|r}|r|\}$$

For the non-adaptive case we compute the control force and moment vector according to:

$$\tau = M\,\dot{\nu}_r + C(\nu)\,\nu_r + D(\nu)\,\nu_r + g(\eta) - J^T(\eta)\,K_d\,s \tag{4.295}$$

Finally, these forces and moments can be distributed to the different thrusters and control surfaces by:

$$u = B^{\dagger}\,\tau \tag{4.296}$$

where B is the control matrix.
□

Velocity Control

An adaptive velocity controller can be derived for the system:

$$M\,\dot{\nu} + C(\nu)\,\nu + D(\nu)\,\nu + g(\eta) = \tau \tag{4.297}$$

by simply letting $J(\eta) = I$ and $s = \tilde{\nu}$ in (4.290) and (4.292), that is:

$$\boxed{\tau = \Phi(\dot{\nu}_r, \nu_r, \nu, \eta)\,\hat{\theta} - K_d\,\tilde{\nu}} \tag{4.298}$$

$$\boxed{\dot{\hat{\theta}} = -\Gamma\,\Phi^T(\dot{\nu}_r, \nu_r, \nu, \eta)\,\tilde{\nu}} \tag{4.299}$$

Here, $\nu_r = \nu_d$. Hence, it can be shown that:

$$\dot{V} = -\tilde{\nu}^T\,[K_d + D(\nu)]\,\tilde{\nu} \leq 0 \quad \forall\,\nu \in \mathbb{R}^n \tag{4.300}$$

Integral Action

Although the above tracking controllers are of PD-type (position/attitude) and P-type (velocity), integral action can be obtained by redefining the measure of tracking according to:

$$\boxed{s_I = s + \lambda \int_0^t s(\tau)\, d\tau} \tag{4.301}$$

while the parameters are updated by means of:

$$\boxed{\dot{\hat{\theta}} = -\Gamma\, \Phi^T(\dot{\nu}_r, \nu_r, \nu, \eta)\, J^{-1}(\eta)\, s_I} \tag{4.302}$$

More generally, it can be proven that this substitution can be made without affecting the previous stability results by defining:

- **Position and attitude scheme**

$$s_I = \dot{\tilde{\eta}} + 2\lambda\, \tilde{\eta} + \lambda^2 \int_0^t \tilde{\eta}(\tau)\, d\tau \tag{4.303}$$

The virtual reference trajectory is modified accordingly as:

$$\dot{\eta}_r = \dot{\eta} - s_I = \dot{\eta}_d - 2\lambda\, \tilde{\eta} - \lambda^2 \int_0^t \tilde{\eta}(\tau)\, d\tau \tag{4.304}$$

while ν_r and $\dot{\nu}_r$ are calculated through (4.279) and (4.280). For the position/attitude scheme, this substitution implies that:

$$\tau = \Phi(\dot{\nu}_r, \nu_r, \nu, \eta)\, \hat{\theta} - J^T(\eta)\, [\underbrace{K_d}_{D}\, \dot{\tilde{\eta}} + \underbrace{2\,\lambda\, K_d}_{P}\, \tilde{\eta} + \underbrace{\lambda^2\, K_d}_{I} \int_0^t \tilde{\eta}(\tau)\, d\tau] \tag{4.305}$$

where P, D and I are the proportional, derivative and integral gains, respectively.

- **Velocity scheme**

$$s_I = \tilde{\nu} + \lambda \int_0^t \tilde{\nu}(\tau)\, d\tau \tag{4.306}$$

which suggests that the virtual reference trajectory should be computed as:

$$\nu_r = \nu - s_I = \nu_d - \lambda \int_0^t \tilde{\nu}(\tau)\, d\tau \tag{4.307}$$

Hence, we obtain the PI-control law:

$$\tau = \Phi(\dot{\nu}_r, \nu_r, \nu, \eta)\, \hat{\theta} - \underbrace{K_p}_{P}\, \tilde{\nu} + + \underbrace{\lambda\, K_d}_{I} \int_0^t \tilde{\nu}(\tau)\, d\tau \tag{4.308}$$

4.5.5 Nonlinear Tracking (The Sadegh and Horowitz Algorithm)

It is well known that the adaptive control law of Slotine and Li is sensitive to velocity measurement noise (Berghuis 1993). For a marine vehicle body-fixed velocities are usually obtained by model-based state estimation through noisy position measurements. This implies that the velocity estimates can be contaminated with a significant amount of noise. In such cases the adaptive control law of Slotine and Li can go unstable due to drift in the parameter estimates. However, precautions against parameter drift can be taken by small modifications of the adaptive scheme (see Section 4.5.8).

In this section we will briefly extend the results of Sadegh and Horowitz (1990) to marine vehicle control. This control scheme is less sensitive to velocity measurement (estimation) noise. The main idea of Sadegh and Horowitz (1990) is to replace the actual position and velocity in the regressor by the desired state trajectories. This is usually referred to as the *desired compensation adaptive law* (DCAL). In the original work of Sadegh and Horowitz (1990) the kinematic equations of motion are omitted since they use the DCAL to control a robot manipulator. An extension of this work to marine vehicle control in terms of Euler angle feedback has been made by Fossen and Fjellstad (1995). This results is based on the assumption that the desired state trajectories can be computed according to the following scheme:

Reference Trajectory Definitions

The desired state vectors ν_d and η_d must be computed from:

$$\dot{\nu}_d + \Lambda\,\nu_d + J^T(\eta)\,\Omega\,\eta_d = J^T(\eta)\,\Omega\,r \tag{4.309}$$

$$\dot{\eta}_d = J(\eta)\,\nu_d \tag{4.310}$$

where r is a constant (slowly-varying) commanded input, $\Omega = \Omega^T > 0$ and $\Lambda > 0$. Hence, $\nu_d(\infty) = 0$ and $\eta_d(\infty) = r$. Notice that $J(\eta)$ is a function of the actual Euler angles. This is not a problem since (ϕ, θ, ψ) are easy to measure with good accuracy. The reason for this is that the representation of the control law is considerably simplified if $J(\eta)$ is used instead of $J(\eta_d)$. Moreover, this assumption implies that it is possible to formulate the control law in terms of M, C, D and g instead of the earth-fixed quantities M_η, C_η, D_η and g_η.

Modified DCAL (Fossen and Fjellstad 1995)

Parameterization:
$$M\,\dot{\nu}_d + C(\nu_d)\,\nu_d + D(\nu_d)\,\nu_d + g(\eta_d) \triangleq \Phi(\dot{\nu}_d, \nu_d, \eta_d)\,\theta$$

Control law:
$$\tau = \hat{M}\,\dot{\nu}_d + \hat{C}(\nu_d)\,\nu_d + \hat{D}(\nu_d)\,\nu_d + \hat{g}(\eta_d) - J^T(\eta)\,[K_p\tilde{\eta} + K_d\dot{\tilde{\eta}} + K_f \parallel \tilde{\eta} \parallel^2 s] \tag{4.311}$$

Adaptation law:
$$\dot{\hat{\theta}} = -\Gamma\,\Phi^T(\dot{\nu}_d, \nu_d, \eta_d)J^{-1}(\eta)s$$

where $K_p = K_p^T > 0$, $K_d > 0$, $K_f > 0$, $\Gamma = \Gamma^T > 0$ and $s = J(\eta)\tilde{\nu} + \lambda\tilde{\eta}$. The stability proof is a straightforward generalization of Sadegh and Horowitz (1990).

4.5.6 Cascaded Adaptive Control (ROV and Actuator Dynamics)

The adaptive sliding controller discussed in the previous section is based on the assumption that the actuator dynamics can be neglected. Hence, parameter drift and robustness of the adaptive controller can be a severe problem for vehicles where this is not the case. Van Amerongen (1982, 1984) shows that this problem can be circumvented to some extent by using *ad-hoc* modifications of the reference model. This is done by including a low-pass structure in the reference model to smooth out the reference trajectory: $\ddot{\eta}_d$, $\dot{\eta}_d$ and η_d (see Section 6.4).

An extension to this work is found in Butler, Honderd and Van Amerongen (1991) who present a more systematic approach, the so-called reference model decomposition (RMD) technique, to compensate for the unmodelled dynamics. Furthermore, the RMD has been applied to underwater vehicles by Fjellstad et al. (1992). The main disadvantage with these methods is that global stability and therefore boundness of the parameter estimates cannot be proven. A solution to this problem has been proposed by Fossen and Fjellstad (1993). We will now briefly review the main results from this method.

Actuator Dynamics

For simplicity, let us consider a MIMO linear actuator model:

$$T\dot{u} + u = u_c \tag{4.312}$$

where $u \in \mathbb{R}^p$ ($p \geq 6$) is a vector of actual control inputs, $u_c \in \mathbb{R}^p$ is a vector of commanded actuator inputs and $T = \text{diag}\{T_i\}$ is a $p \times p$ diagonal matrix of positive unknown actuator time constants ($T_i > 0$). Moreover T_i can be understood as the effective time lag in a PI-controlled DC motor, that is:

$$h_{DC}(s) = \frac{K}{(1+\tau_1 s)(1+\tau_2 s)} \qquad \text{(DC-motor)} \tag{4.313}$$

where τ_1 and τ_2 are the motor time constants and K is the motor gain. Furthermore,

$$h_{PI}(s) = \frac{K_p(1+\tau_i s)}{\tau_i s} \qquad \text{(PI-controller)} \tag{4.314}$$

where τ_i is the integral time constant K_p is the proportional gain constant. Hence, the resulting closed-loop transfer function is $l(s) = h_{DC}(s)h_{PI}(s)$ which implies that:

$$\frac{u}{u_c}(s) = \frac{l(s)}{1+l(s)} \approx \frac{1}{1+T_i s} \tag{4.315}$$

where T_i is the effective time lag of the closed-loop system.

Theorem 4.2 (Cascaded Adaptive Velocity Control)
Let the adaptive control law be described by:

$$u_c = u + \hat{T}\,\dot{u}_d - B^T(\nu)\tilde{\nu} - K_u\,\tilde{u} \tag{4.316}$$

The desired control input u_d is computed from:

$$u_d = B^+(\nu)[\Phi(\dot{\nu}_d, \nu_d, \nu, \eta)\,\hat{\theta} - K_\nu\,\tilde{\nu}] \tag{4.317}$$

with parameter adaptation laws:

$$\dot{\hat{\theta}} = -\Gamma\,\Phi^T(\dot{\nu}_d, \nu_d, \nu, \eta)\,\tilde{\nu} \tag{4.318}$$

$$\dot{\hat{T}}_i = -\alpha_i\,\tilde{u}_i\,\dot{u}_{di}, \qquad \alpha_i > 0 \tag{4.319}$$

Here $K_u > 0$, $K_\nu \geq 0$ and $\Gamma = \Gamma^T > 0$. It can be shown that (Fossen and Fjellstad 1993):

$$\dot{V} = -\tilde{\nu}^T\,[K_\nu + D(\nu)]\,\tilde{\nu} - \tilde{u}^T\,K_u\,\tilde{u} \leq 0 \tag{4.320}$$

Then the signals $\tilde{\theta}$ and $\tilde{T}$ remain bounded and $\tilde{u}$ and $\tilde{\nu}$ converge to zero as $t \to \infty$.

$$\dot{V} = -\tilde{\nu}^T\,[K_\nu + D(\nu)]\,\tilde{\nu} - \tilde{u}^T\,K_u\,\tilde{u} \leq 0 \tag{4.321}$$

□

It seems reasonable to choose the maximum singular values of the gain matrices K_u and K_ν according to:

$$\overline{\sigma}(K_u) > \overline{\sigma}(K_\nu) \tag{4.322}$$

where $\overline{\sigma}(\cdot)$ is the maximum singular value, to ensure that the bandwidth of the inner servo loop (actuator dynamics) will be higher than the bandwidth of the outer loop (vehicle dynamics).

Theorem 4.3 (Cascaded Adaptive Position and Attitude Control)
Consider the system (4.281) and (4.312) together with the control law:

$$u_c = u + \hat{T}\,\dot{u}_d - B^T(\nu)J^{-1}(\eta)\,s - K_u\,\tilde{u}; \qquad K_u > 0 \tag{4.323}$$

where $\tilde{u} = u - u_d$ and $\dot{u}_d$ is computed by time differentiation of:

$$u_d = B^+(\nu)[\Phi(\dot{\nu}_r, \nu_r, \nu, \eta)\,\hat{\theta} - J^T(\eta)\,K_\eta\,s]; \qquad K_\eta \geq 0 \tag{4.324}$$

The parameter estimates $\hat{\theta}$ and $\hat{T}$ are updated through to the differential equations:

$$\dot{\hat{\theta}} = -\Gamma\, \Phi^T(\dot{\nu}_r, \nu_r, \nu, \eta)\, J^{-1}(\eta)\, s; \qquad \Gamma > 0 \qquad (4.325)$$

$$\dot{\hat{T}}_i = -\alpha_i\, \tilde{u}_i\, \dot{u}_{di}; \qquad \alpha_i > 0 \quad (i = 1...6) \qquad (4.326)$$

Then the signals $\tilde{\theta}$ and $\tilde{T}$ remain bounded and $\tilde{u}$ and s converge asymptotically to zero as $t \to \infty$. This in turn implies that $\tilde{\eta}$ converge to zero as $t \to \infty$.

Proof: *Consider the Lyapunov function candidate:*

$$V = \frac{1}{2}\,[s^T\, M_\eta\, s + \tilde{u}^T\, T\, \tilde{u} + \tilde{\theta}^T\, \Gamma^{-1}\, \tilde{\theta} + \sum_{i=1}^{6} \frac{1}{\alpha_i}\, \tilde{T}_i^2] \qquad (4.327)$$

where $\tilde{T}_i = \hat{T}_i - T_i$ and $\alpha_i > 0$ is constant. Differentiating V with respect to time and using $M_\eta(\eta) = M_\eta^T(\eta) > 0 \;\; \forall \;\; \eta \in \mathbb{R}^6$ and $s^T \left[\dot{M}_\eta(\eta) - 2C_\eta(\nu, \eta)\right] s = 0 \;\; \forall \;\; s \in \mathbb{R}^6$, yields:

$$\dot{V} = s^T[M_\eta(\eta)\dot{s} + C_\eta(\nu, \eta)s] + \tilde{u}^T T \dot{\tilde{u}} + \dot{\tilde{\theta}}^T\, \Gamma^{-1}\, \tilde{\theta} + \sum_{i=1}^{6} \frac{1}{\alpha_i}\, \dot{\tilde{T}}_i \tilde{T}_i \qquad (4.328)$$

Substituting the system equation (4.281), (4.312) into this expression and using the definition (2.177) together with (4.277), (4.279) and (4.280) yields:

$$\begin{aligned} \dot{V} \;=\; & -s^T D_\eta(\nu, \eta) s \\ & + [J^{-1}(\eta)s]^T [B(\nu)u - M_\eta(\eta)\dot{\nu}_r - C_\eta(\nu, \eta)\nu_r - D_\eta(\nu, \eta)\nu_r - g_\eta(\eta)] \\ & + \dot{\tilde{\theta}}^T\, \Gamma^{-1}\, \tilde{\theta} + \tilde{u}^T[u_c - u - T\dot{u}_d] + \sum_{i=1}^{6} \frac{1}{\alpha_i}\, \dot{\tilde{T}}_i \tilde{T}_i \end{aligned} \qquad (4.329)$$

Since $s^T J^{-T}(\eta) B(\nu) \tilde{u} = \tilde{u}^T B^T(\nu) J^{-1}(\eta) s$, we can subtract $B(\nu)\tilde{u} = B(\nu)u - B(\nu)u_d$ from the first bracket and add $B^T(\nu)J^{-1}(\eta)s$ to the second bracket. Applying the parameterization (4.288) yields:

$$\begin{aligned} \dot{V} \;=\; & -s^T D_\eta(\nu, \eta) s + [J^{-1}(\eta)s]^T [B(\nu)u_d - \Phi(\dot{\nu}_r, \nu_r, \nu, \eta)\, \theta] + \dot{\tilde{\theta}}^T\, \Gamma^{-1}\, \tilde{\theta} \\ & + \tilde{u}^T[u_c - u - T\dot{u}_d + B^T(\nu)J^{-1}(\eta)s] + \sum_{i=1}^{6} \frac{1}{\alpha_i}\, \dot{\tilde{T}}_i \tilde{T}_i \end{aligned} \qquad (4.330)$$

Substituting the control law (4.323) and (4.324) into this expression yields:

$$\begin{aligned} \dot{V} \;=\; & -s^T[K_\eta + D_\eta(\nu, \eta)]s + [s^T J^{-T}(\eta)\Phi(\dot{\nu}_r, \nu_r, \nu, \eta) + \dot{\tilde{\theta}}^T\, \Gamma^{-1}]\tilde{\theta} \\ & - \tilde{u}^T K_u \tilde{u} + \sum_{i=1}^{6} (\frac{1}{\alpha_i}\, \dot{\tilde{T}}_i + \tilde{u}_i \dot{u}_{di})\, \tilde{T}_i \end{aligned} \qquad (4.331)$$

Finally, assuming that $\dot{\theta} = 0$ *and* $\dot{T} = 0$, *suggests that the parameter adaptation laws should be chosen as (4.325) and (4.326) to obtain:*

$$\dot{V} = -s^T[K_\eta + D_\eta(\nu, \eta)]s - \tilde{u}^T K_u \tilde{u} \leq 0 \tag{4.332}$$

□

Notice that convergence to zero is guaranteed even for $K_\eta = 0$ since the quadratic form $x^T D_\eta(\nu, \eta)x > 0 \; \forall \; \eta, \nu, x \in \mathbb{R}^6, \; x \neq 0$. Also notice that in the implementation of the control law, acceleration $\dot{\nu}$, velocity ν, position/attitude η and control input u are required measured.

Example 4.12 (Cascaded Adaptive Velocity Control)
Consider an ROV speed system described by:

$$m\,\dot{\nu} + d(\nu)\,\nu = u; \quad d(\nu) = d_0\,|\nu| \tag{4.333}$$

$$T\,\dot{u} + u = u_c \tag{4.334}$$

A normalized system with parameters $m = 4$, $d_0 = 1$ *and a sampling time of 0.1 s was used in the computer simulations. The tracking errors* $\tilde{\nu}$ *and* $\tilde{u}$ *of the adaptive velocity controller (Theorem 4.2) are shown in Figure 4.28. The parameter estimates* $\hat{m}$, $\hat{d}_0$ *and* $\hat{T}$ *and their true values are shown in Figure 4.29. We see from the simulation results that* $\tilde{\nu} \to 0$, $\tilde{u} \to 0$ *and that* $\hat{m}$, $\hat{d}$ *and* $\hat{T}$ *converge to their true values in less than 50 seconds.*
□

Extension to Nonlinear Actuator Models

It is straightforward to extend the adaptive control scheme to a more general nonlinear actuator model:

$$\dot{u} + f(u) = G(u)\,u_c \tag{4.335}$$

where $f(u)$ and $G(u)$ are two *unknown* functions. To prove global stability, we must in addition require that both functions are linear in their parameters. Hence, stability for the nonlinear actuator model can be proven by small modifications in the proof of Theorem 4.3.

4.5.7 Unified Passive Adaptive Control Design

The adaptive controller discussed in the previous section can be view as a special case of a more general class of *passive* adaptive control laws, see Ortega and Spong (1988) and Brogliato and Landau (1991), all exploiting the skew-symmetric property of $\dot{M}_\eta(\eta) - 2C_\eta(\nu)$. By *passive*, we mean that a system with input u and output y satisfies the inequality (see Appendix C.3):

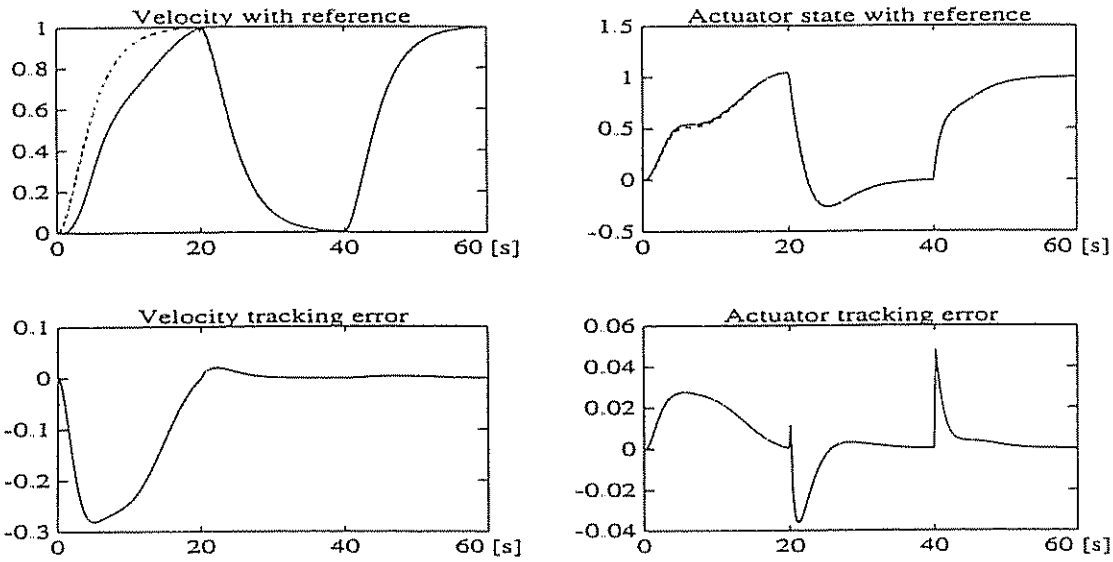

Figure 4.28: Upper plot shows the surge velocity $\nu(t)$ and actuator state $u(t)$ together with their desired values $\nu_d(t)$ and $u_d(t)$ while the lower plot shows their corresponding tracking errors $\tilde{\nu}(t)$ and $\tilde{u}(t)$ as a function of time.

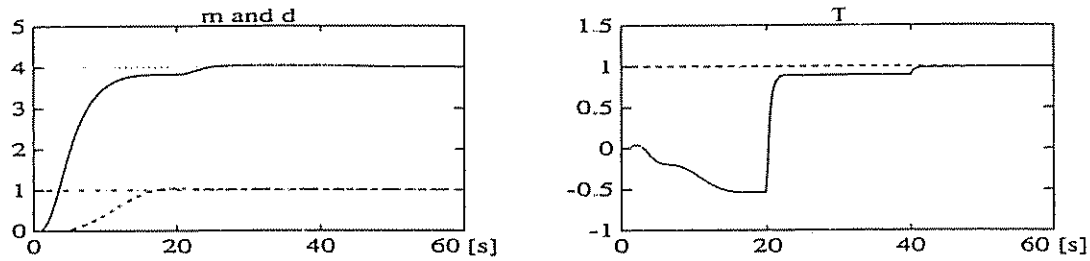

Figure 4.29: Normalized parameter estimates $\hat{m}(t)$, $\hat{d}_0(t)$ and $\hat{T}(t)$ and their true values $m = 4.0$, $d_0 = 1.0$ and $T = 1.0$ as a function of time.

$$\int_0^T \boldsymbol{y}^T(\tau)\boldsymbol{u}(\tau)\, d\tau \geq \beta \tag{4.336}$$

for all $\boldsymbol{u} \in L_{2e}^r$, all $T \geq 0$ and some constant $\beta > -\infty$. Furthermore, we say that the system is *input strictly passive* if (and only if) there exists an $\alpha > 0$ and some constant β such that:

$$\int_0^T \boldsymbol{y}^T(\tau)\boldsymbol{u}(\tau)\, d\tau \quad \geq \quad \alpha \left\|\boldsymbol{u}_T\right\|_2 + \beta \tag{4.337}$$

To apply the passivity formalism in the control design, we will use a general framework where the system dynamics is represented by three subsystems B1, B2 and B3, see Figure 4.30:

- B1: closed-loop equation (strictly passive)
- B2: vehicle dynamics (passive)
- B3: adaptation algorithm (passive)

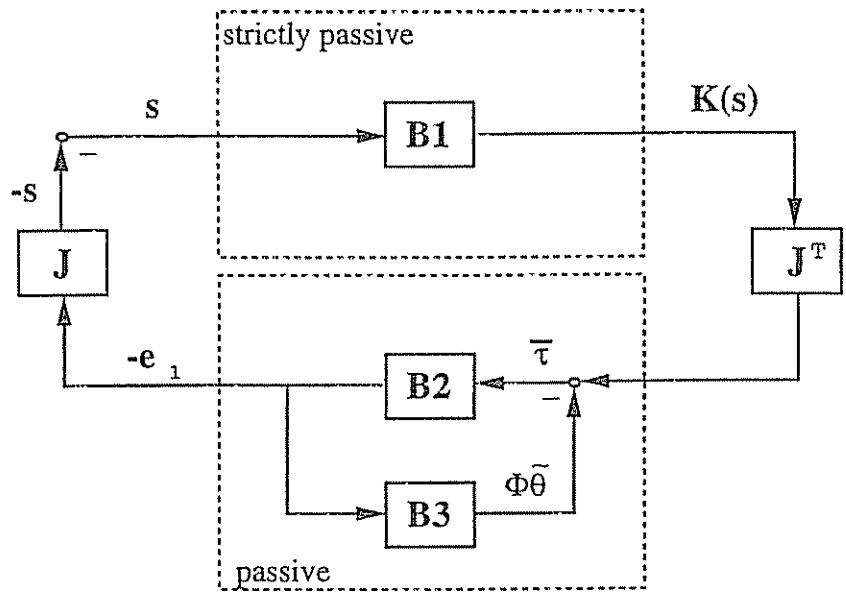

Figure 4.30: Closed-loop equivalent system, adopted from Brogliato and Landau (1991). Notice that stability according to this figure is based on the assumption that J is non-singular.

Hence, the following theorem, see Appendix C.3, ensures that the measure of tracking e_1 converges to zero in finite time.

Theorem 4.4 (Feedback L_2-Stability)
Assume that B1 is a strictly passive system and B2 and B3 are passive blocks, then:

$$e_1(t) \in L_2^m \tag{4.338}$$

Proof: *See Desoer and Vidyasagar (1975) page 182.*
□

We will now apply this theorem in the control design. Let us consider the following control law:

$$\tau = \Phi(\dot{\nu}_r, \nu_r, \nu, \eta)\,\hat{\theta} - J^T(\eta)\,K(s) \tag{4.339}$$

where $K(s)$ is a vector function describing the closed-loop dynamics; see block B1 in Figure 4.30.

Block B1

The closed-loop dynamics $K(s)$ is always chosen to be *strictly passive*, independent on what type of adaptation algorithm we use. For instance, the adaptive scheme of Section 4.5.4 is obtained by choosing the compensator $K(s)$ according to:

$$K(s) = K_d\, s; \qquad K_d > 0 \tag{4.340}$$

which clearly is *strictly passive*.

Block B2

We know turn our attention to block B2, representing the vehicle dynamics. First, we notice that the signal, $\overline{\tau}$ in Figure 4.30 can be written:

$$\begin{aligned}
\overline{\tau} &= J^T(\eta)\, K(s) - \Phi(\dot{\nu}_r, \nu_r, \nu, \eta)\, (\hat{\theta} - \theta) \\
&= \Phi(\dot{\nu}_r, \nu_r, \nu, \eta)\, \theta - \tau \\
&= M\, \dot{\nu}_r + C(\nu)\, \nu_r + D(\nu)\, \nu_r + g(\eta) - \tau \\
&= J^T(\eta)\, [M_\eta\, \ddot{\eta}_r + C_\eta(\nu)\, \dot{\eta}_r + D_\eta(\nu)\, \dot{\eta}_r + g_\eta(\eta)] - \tau
\end{aligned} \tag{4.341}$$

Using the fact $\dot{\eta}_r = \dot{\eta} - s$ and

$$M_\eta\, \ddot{\eta} + C_\eta(\nu)\, \dot{\eta} + D_\eta(\nu)\, \dot{\eta} + g_\eta(\eta) = J^{-T}(\eta)\, \tau \tag{4.342}$$

yields:

$$\overline{\tau} = -J^T(\eta)\, [M_\eta\, \dot{s} + C_\eta\, s + D_\eta\, s] \tag{4.343}$$

Let $e_1 = J^{-1}(\eta)\, s$, then

$$\begin{aligned}
\langle \overline{\tau}, -e_1 \rangle_T &= \int_0^T -[J^{-1}\, s]^T\, \overline{\tau}\, d\tau = \int_0^T s^T\, [M_\eta\, \dot{s} + C_\eta\, s + D_\eta\, s]\, d\tau \\
&= \int_0^T \left[\frac{1}{2} \frac{d}{dt} \left[s^T\, M_\eta\, s \right] - \frac{1}{2} s^T \left[\dot{M}_\eta - 2C_\eta \right]\, s + s^T\, D_\eta\, s \right]\, d\tau
\end{aligned}$$

Since the rate of energy dissipated from the system satisfies:

$$s^T\, D_\eta\, s > 0 \quad \forall \quad s \neq 0 \tag{4.344}$$

and skew-symmetry implies that

$$s^T \left[\dot{M}_\eta - 2C_\eta \right]\, s = 0 \quad \forall \quad s \tag{4.345}$$

we have that

$$\langle \overline{\tau}, -e_1 \rangle_T \geq -\frac{1}{2} s^T(0)\, M_\eta(\eta(0))\, s(0) \tag{4.346}$$

This shows that the mapping $\overline{\tau} \rightarrow -e_1$ is *passive*.

Block B3

Finally, we want to show that the mapping represented by block B3 is *passive*. The update law is given by:

$$\dot{\tilde{\theta}} = -\Gamma\, \Phi^T(\dot{\nu}_r, \nu_r, \nu, \eta)\, e_1; \qquad \Gamma = \Gamma^T > 0 \tag{4.347}$$

Hence,

$$\begin{aligned} \left\langle -e_1, \Phi\, \tilde{\theta} \right\rangle_T &= \int_0^T -e_1^T\, \Phi\, \tilde{\theta}\, d\tau \\ &= \int_0^T \dot{\tilde{\theta}}\, \Gamma^{-1}\, \tilde{\theta}\, d\tau \geq -\frac{1}{2}\tilde{\theta}^T(0)\, \Gamma^{-1}\, \tilde{\theta}(0) \end{aligned} \tag{4.348}$$

This shows that the mapping $-e_1 \rightarrow \Phi\, \tilde{\theta}$ is *passive*.

4.5.8 Parameter Drift due to Bounded Disturbances

It is well known that external disturbances may cause parameter drift. Consider the nonlinear model:

$$M\, \dot{\nu}(t) + C(\nu)\, \nu(t) + D(\nu)\, \nu(t) + g(\eta) = \tau(t) + \gamma(t) \tag{4.349}$$

where $\gamma(t)$ is a bounded disturbance with $|\gamma(t)| \leq \gamma_0$. Hence, the control law:

$$\tau = \hat{M}\, \dot{\nu} + \hat{C}(\nu)\, \nu + \hat{D}(\nu)\, \nu + \hat{g}(\eta) - J^T(\eta)\, K_d\, s \tag{4.350}$$

yields the error dynamics:

$$M_\eta\, \dot{s} + [C_\eta(\nu) + D_\eta(\nu) + K_d]s = J^{-T}(\eta)\, \Phi(\dot{\nu}_r, \nu_r, \nu, \eta)\, \tilde{\theta} + J^{-T}(\eta)\, \gamma \tag{4.351}$$

We recall that the parameter adaptation law for this system was chosen as:

$$\dot{\tilde{\theta}} = -\Gamma\, \Phi^T(\dot{\nu}_r, \nu_r, \nu, \eta)\, e_1; \qquad e_1 = J^{-1}(\eta)\, s \tag{4.352}$$

which yields the following expression for $\dot{V}$:

$$\dot{V} = -s^T\, [K_d + D_\eta(\nu, \eta)]\, s + \gamma^T\, e_1 \tag{4.353}$$

Hence, integration of the error dynamics to yield s and e_1 in the parameter adaptation law, clearly shows that the resulting parameter estimate $\hat{\theta}$ will be sensitive to the time-varying noise term γ. We also see that $\dot{V}$ no longer can be guaranteed to be non-increasing since γ is unknown.

Precautions for bounded disturbances can be taken in several ways by small modifications of the adaptation law. We will discuss four standard methods.

Dead-Zone Technique

Peterson and Narendra (1982) propose stopping the adaptation when the output error e_1 becomes smaller than a prescribed value Δ by introducing a dead-zone in the adaptation law. This is due the fact that small tracking errors mainly contain noise and disturbances. This suggests that:

$$\dot{\hat{\theta}} = \begin{cases} -\Gamma \Phi^T(\dot{\nu}_r, \nu_r, \nu, \eta)\, e_1 & \|e_1\| \geq \Delta \\ 0 & \|e_1\| < \Delta \end{cases} \tag{4.354}$$

Hence, by choosing Δ sufficient large V becomes non-increasing outside the dead-zone. The choice $d\hat{\theta}/dt = 0$ inside the dead-zone implies that the cancellation in (4.291)–(4.293) no longer is satisfied. As a result of this, V may grow inside the dead-zone. Hence, asymptotic convergence of the plant output to the desired trajectory no longer can be guaranteed even when no disturbances are present.

The choice of Δ should be seen as a trade-off between robustness and performance. A large value for Δ implies that the parameter adaptation is less sensitive for plant disturbances while a low Δ yields better performance but increased possibility for parameter drift. Still, mainly because of its simplicity and effectiveness, this method is highly attractive to use.

Bound on the Parameters

If bounds on the desired parameter vector θ are known, instability due to parameter errors can be avoided by a simple modification of the adaptive law. This problem has been addressed by Kresselmeier and Narendra (1982) who assume that a bound θ_{max} on the parameter vector is known such that:

$$\|\theta\| \leq \theta_{max}; \qquad 0 < \theta_{max} < \infty \tag{4.355}$$

The adaptive law is modified as:

$$\dot{\hat{\theta}} = -\Gamma \Phi^T(\dot{\nu}_r, \nu_r, \nu, \eta)\, e_1 - \hat{\theta} \left(1 - \frac{\|\hat{\theta}\|}{\theta_{max}}\right)^2 f(\hat{\theta}) \tag{4.356}$$

where

$$f(\hat{\theta}) = \begin{cases} 1 & \text{if } \|\hat{\theta}\| > \theta_{max} \\ 0 & \text{otherwise} \end{cases} \tag{4.357}$$

σ-Modification

The two previous schemes assume that a bound on the disturbance vector γ or the parameter vector θ is known. A popular robust adaptive control scheme where this *a priori* information is not necessary was proposed by Ioannou and Kokotovic (1983). This scheme is usually referred to as the σ-modification scheme. To avoid

the parameters growing unbounded in the presence of bounded disturbances an additional stabilizing term $-\sigma\,\hat{\theta}$ is used in the adaptive law, that is:

$$\dot{\hat{\theta}} = -\sigma\,\hat{\theta} - \Gamma\,\Phi^T(\dot{\nu}_r, \nu_r, \nu, \eta)\,e_1 \tag{4.358}$$

where $\sigma > 0$. However, introduction of the term $-\sigma\,\hat{\theta}$ implies that the origin is no longer the equilibrium point. This implies that the parameter estimates will not converge to their true values even for a PE reference input or the case when all external disturbances are removed.

e_1-Modification

To overcome the limitations of the σ-modification scheme Narendra and Annaswamy (1987) proposed a slight modification of the above scheme, that is:

$$\dot{\hat{\theta}} = -\alpha\,\|e_1\|\,\hat{\theta} - \Gamma\,\Phi^T(\dot{\nu}_r, \nu_r, \nu, \eta)\,e_1 \tag{4.359}$$

where $\alpha > 0$. This method is referred to as the e_1-modification. The motivation for using the gain $\|e_1\|$ instead of σ is that this proportional term tends to zero with the tracking error e_1. Hence, parameter convergence to the true parameter values under the assumption of PE can be obtained when there are no external disturbances present.

A more detailed discussion on convergence properties, stability and implementation considerations are found in Narendra and Annaswamy (1989). This text also includes stability proofs for the above mentioned schemes.

4.6 Conclusions

A model-based control system design requires proper modeling of both the dynamics and kinematics of the vehicle. In this chapter we have shown how different mathematical models can be derived for this purpose. In addition to this, emphasis is put on showing how simple controllers of PID-type can be designed for ROV systems with unknown and partially known dynamics and kinematics. These results are highly applicable in most practical applications.

The last part of the chapter discusses advanced nonlinear and adaptive control theory utilizing the nonlinear model structure of Chapter 2. Moreover, it is shown how the nonlinear ROV equations of motion can be decoupled both in the body-fixed and earth-fixed reference frames to obtain a linear control problem, which is usually solved by applying a simple control law of PID-type. In addition to *feedback linearization* techniques, alternative design methods based on *sliding mode control* and *passivity* are applied to control the ROV. These methods are highly suited for high performance tracking of time-varying reference trajectories in 6 DOF. Extensions to adaptive control theory are done both for the feedback linearization and passivity-based schemes.

Mathematical models for underwater vehicle simulation are proposed by numerous authors. The mathematical model for the UNH-EAVE Autonomous Underwater Vehicle is discussed by Humphreys and Watkinson (1982) while the control system design is found in Venkatachalam, Limbert and Jalbert (1985). Modeling of ROVs is also discussed by Goheen (1986), Kalske (1989), Lewis, Lipscombe and Thomasson (1984) and Yuh (1990). Nonlinear models for ROV and AUV simulation are proposed by Fossen (1991) and Sagatun (1992). For the interested reader mathematical models for ROV and AUV simulation are found in Appendix E.

Other useful references in the field of ROV and AUV control are: Cristi et al. (1990), Dougherty et al. (1988), Dougherty and Woolweaver (1990), Fjellstad et al. (1992), Fjellstad and Fossen (1994a, 1994b), Fossen and Sagatun (1991a, 1991b), Gallardo (1986), Healey, Papoulias and Cristi (1989), Healey and Marco (1992), Healey and Lienard (1993), Jalving and Størkersen (1994), Mahesh, Yuh and Lakshmi (1991), Marco and Healey (1992), Triantafyllou and Grosenbaugh (1991), Yoerger and Slotine (1984, 1985), Yoerger et al. (1986), Yoerger, Cooke and Slotine (1990), Yoerger and Slotine (1991) to mention some.

The interested reader is recommended to consult the proceedings of the *International Symposium on Unmanned Untethered Submersible Technology* which is arranged on a biannual basis at the University of New Hampshire, Durham, and the IEEE *Symposium on Autonomous Underwater Vehicle Technology*. Other useful publications are the proceedings of the *ROV Conference*, the *Ocean Conference* and the *International Offshore and Polar Engineering Conference*.

Prediction of hydrodynamic coefficients for underwater vehicles from geometric parameters is discussed by Humphreys and Watkinson (1978). Triantafyllou and Amzallag (1984) discuss the design of unmanned tethered submersibles for operations at large depths while Allmendinger (1990) is an excellent reference for submersible vehicle system design in the more general context. Operational guidelines for ROVs can be found in MTS (1986).

We have not discussed modeling and control of submarines in this chapter. However, for the interested reader a standard model for submarine simulation and control is proposed by Gertler and Hagen (1967). A revised version of this model is found in Feldman (1979). Submarine control applications utilizing the LQG/LTR design methodology are discussed by Milliken (1984) whereas H_∞ control is discussed by Williams and Marshfield (1990, 1991), Grimble, Van der Molen and Liceaga-Castro (1993) and Marshfield (1991). An application of sliding mode control to submarines is found in McGookin (1993).

4.7 Exercises

4.1 Consider the ROV yaw dynamics in the form:

$$m\dot{r} + d_1 r + d_2 |r| r = \delta$$

where r is the yaw rate, δ is the rudder angle and m, d_1 and d_2 are three parameters. Let the kinematics be given by $\dot{\psi} = r$ while the actuator dynamics is written:

$$T\,\dot{\delta} + \delta = \delta_c$$

where T is the time constant and δ_c is the commanded rudder angle.

(a) Assume that ψ and r are measured. Derive a feedback linearization control law for δ under the assumption that m, d_1 and d_2 are known and that $\delta_c = \delta$.

(b) Assume that m, d_1 and d_2 are unknown. Derive an adaptive feedback linearization scheme such that these parameters can be estimated on-line.

(c) Extend the results from (b) to incorporate the actuator dynamics. Assume that only the actuator time constant T is known. Prove global stability for the yaw control system with actuator dynamics. Both $\dot{r}$ and δ are assumed measured.

(d) Suggest a more practical solution than the solution under (c) not depending on yaw acceleration measurements $\dot{r}$. (Hint: Design a cascaded control system with two servo loops.)

4.2 Consider an ROV described by:

$$M\,\dot{\nu} + n(\nu, \eta_E) = \tau$$

where $\nu = [u, v, w, p, q, r]^T$. Let the kinematics of the vehicle be described by unit quaternions (Euler parameter representation), see (2.36),

$$\dot{\eta}_E = E(\eta_E)\,\nu$$

where $\eta_E = [x, y, z, \varepsilon_1, \varepsilon_2, \varepsilon_3, \eta]^T$. Derive a position and velocity control scheme for this system by applying the theory of feedback linearization. Assume that M and n are perfectly known. The error dynamics of the linear system shall be pole-placed in terms of a PID control law with acceleration feedforward.

4.3 Consider the horizontal motion of an ROV.

(a) Under which assumptions can we express the dynamic equations of motion by:

$$M\dot{\nu} + C(\nu)\,\nu + D\,\nu = \tau$$

where $\nu = [u, v, r]^T$ is the state vector, τ is the control variable and:

$$M = \begin{bmatrix} m - X_{\dot{u}} & 0 & 0 \\ 0 & m - Y_{\dot{v}} & mx_G - Y_{\dot{r}} \\ 0 & mx_G - N_{\dot{v}} & I_z - N_{\dot{r}} \end{bmatrix} \quad D = \begin{bmatrix} -X_u & 0 & 0 \\ 0 & -Y_v & -Y_r \\ 0 & -N_v & -N_r \end{bmatrix}$$

Find a skew-symmetric representation of $C(\nu)$. What is the kinematic equations of motion for this case if position and heading are the desired state variables ?

(b) Assume that M, C and D are known. Derive a controller for tracking of a smooth reference trajectory $x_d(t)$, $y_d(t)$ and $\psi_d(t)$ by applying the Slotine and Li, and Sadegh and Horowitz algorithms.

(c) Assume that $Y_{\dot{r}}$, $N_{\dot{v}}$, Y_r and N_v are unknown. Design a parameter adaptation law for these coefficients which can be used together with the above tracking control laws.

4.4 Consider a deep submergence rescue vehicle (DSRV) given by the following non-dimensional data (Healey 1992):

I'_x	=	0.000118	$M'_{\dot{q}}$	=	−0.001573	Z'_q	=	−0.017455
I'_z	=	$I'_y = 0.001925$	M'_w	=	0.011175	$Z'_{\dot{q}}$	=	−0 000130
m'	=	0.036391	$M'_{\dot{w}}$	=	−0.000146	Z'_w	=	−0.043938
u_0	=	13.5 (ft/s)	M_δ	=	−0.012797	Z'_δ	=	−0.027695
M'_q	=	−0.01131	M'_θ	=	$-0.156276/U^2$	$Z'_{\dot{w}}$	=	−0.031545

Here the non-dimensional hydrodynamic derivatives are defined according to Prime-system I in Table 5.1 with u_0 in (ft/s) and L in (ft); see Section 5.3.3 (1 ft = 0.30 m). Assume that $x'_G = 0$. Notice that $M_\theta = -\overline{BG}_z\, W$.

(a) Write down the linear equations of motion for maneuvers in the vertical plane. The only control input used for depth changing maneuvers is the stern plane δ_S. Find a state-space model for the DSRV.

(b) Find and plot the characteristic equation roots versus total speed:

$$U = \sqrt{(u_0 + \Delta u)^2 + (v_0 + \Delta v)^2 + (w_0 + \Delta w)^2} = \sqrt{u_0^2 + (\Delta w)^2}$$

in the range 1–8 knots (1 knot = 1.68 ft/s). Is the DSRV open-loop stable ?

(c) A dive maneuver is attempted at 8 knots by holding a 5 degrees angle on the stern planes for a time of 5 non-dimensional seconds. Simulate the depth change response and find out how long the vehicle takes to regain the level pitch condition and the resulting final change in depth.

(d) Design a depth control system for the DSRV.

4.5 Consider a swimmer delivery vehicle (SDV) given by the following non-dimensional data (Healey 1992):

I'_x		= 0.000949	Y'_v	=	$-1.0 \cdot 10^{-1}$	$Y'_{\dot{v}}$	=	$-5.5 \cdot 10^{-2}$
I'_z	$= I'_y$	= 0.006326	Y'_r	=	$3.0 \cdot 10^{-2}$	$Y'_{\dot{r}}$	=	0
m'		= 0.1415	N'_v	=	$-7.4 \cdot 10^{-3}$	$N'_{\dot{v}}$	=	0
u_0		= 13.5 (ft/s)	N'_r	=	$-1.6 \cdot 10^{-2}$	$N'_{\dot{r}}$	=	$-3.4 \cdot 10^{-3}$
W'	$= B'$	= 0.2175	Y'_δ	=	$2.7 \cdot 10^{-2}$	N'_δ	=	$-1.3 \cdot 10^{-2}$

Notice that the non-dimensional hydrodynamic derivatives are defined according to Prime-system I in Table 5.1 with u_0 in (ft/s) and L in (ft); see Section 5.3.3. In addition to this, we have $x_G = y_G = 0$ and $z_G = 0.2$ (ft). The length of the vehicle is $L = 17.4$ (ft).

(a) Write down the linear steering equations of motion and find a state-space model for the SDV. Simulate turning response to a sudden application of 15 degrees of rudder δ_R in a turn to starboard (negative rudder). Include the kinematic equations of motion for x, y and ψ and plot x versus y and sideslip angle:

$$\beta = \sin^{-1}(\Delta v/U)$$

versus time. The total speed of the SDV is:

$$U = \sqrt{(u_0 + \Delta u)^2 + (v_0 + \Delta v)^2 + (w_0 + \Delta w)^2} = \sqrt{u_0^2 + (\Delta v)^2}$$

Perform the analysis in non-dimensional format.

(b) Repeat the analysis under (a) but this time by including the roll mode, that is:

$$\begin{array}{llll} K'_{\dot{p}} = -1.0 \cdot 10^{-3} & K'_p = -1.1 \cdot 10^{-2} & K'_{\dot{v}} = 1.3 \cdot 10^{-4} & K'_v = 3.1 \cdot 10^{-3} \\ K'_{\dot{r}} = -3.4 \cdot 10^{-5} & K'_r = -8.4 \cdot 10^{-4} & K'_\delta = 0 & N'_{\dot{p}} = K'_{\dot{r}} \end{array}$$

What is the steady-state roll angle developed by the turn ? Does the SDV exhibit non-minimum phase behavior in response to the rudder input ? Verify your statement by computing all poles and zeros.

(c) Design a course controller for the SDV with and without roll angle feedback ?

Chapter 5

Dynamics and Stability of Ships

This chapter discusses state-of-the-art linear and nonlinear modeling techniques for ships. These include standard ship steering equations of motion (with and without the roll mode), models of the speed system, the sensor system and the environmental disturbances, see Figure 5.1. These models can be written:

$$\begin{array}{lrcl} \text{Ship dynamics:} & \dot{x} & = & f(x,u,w) \\ \text{Actuator dynamics:} & \dot{u} & = & g(x,u,u_c) \\ \text{Sensor system:} & z & = & h(x,v) \end{array}$$

where $f(\cdot)$, $g(\cdot)$ and $h(\cdot)$ are three nonlinear functions to be interpreted in this chapter. Automatic control systems design for ships applying these models will be discussed in the next chapter.

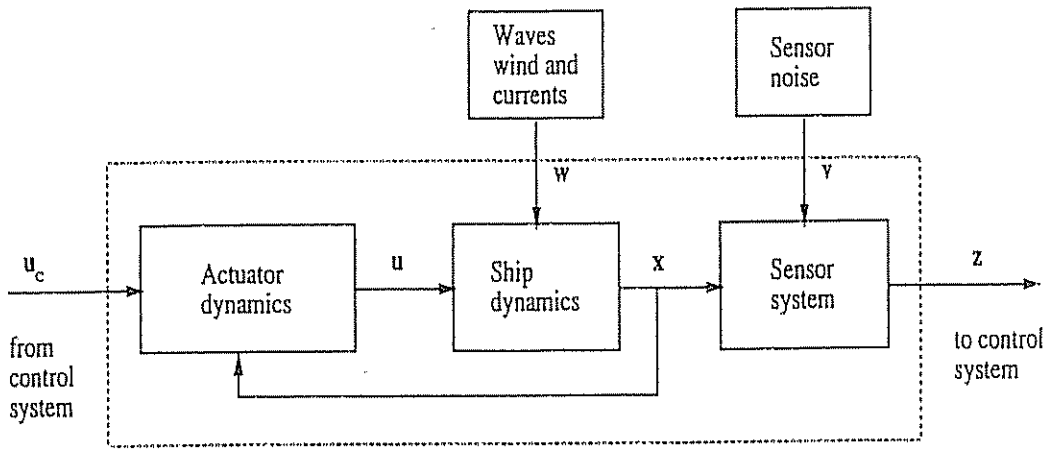

Figure 5.1: Diagram showing actuator dynamics, ship dynamics, sensor system and environmental disturbances.

Besides ship modeling special attention is paid to ship maneuvering and stability. An evaluation of the ship's maneuvering properties before designing the control system often leads to significant information about the ship's performance limitations and the degree of stability.

5.1 Rigid-Body Ship Dynamics

Nonlinear Ship Equations of Motion

Equation (2.110) suggests that the coordinate origin should be set in the center line of the ship, that is $y_G = 0$. In addition to this, the speed and ship steering equations of motion are based on the following assumptions:

(i) Homogeneous mass distribution and xz-plane symmetry ($I_{xy} = I_{yz} = 0$).

(ii) The heave, roll and pitch modes can be neglected ($w = p = q = \dot{w} = \dot{p} = \dot{q} = 0$).

Applying these assumptions to (2.111) yields:

$$\begin{array}{lrcl} \text{Surge:} & m(\dot{u} - vr - x_G r^2) & = & X \\ \text{Sway:} & m(\dot{v} + ur + x_G \dot{r}) & = & Y \\ \text{Yaw:} & I_z \dot{r} + m x_G (\dot{v} + ur) & = & N \end{array} \tag{5.1}$$

Perturbed Ship Equations of Motion

The perturbed equations of motion are based on an additional assumption:

(iii) The sway velocity v, the yaw rate r and the rudder angle δ are small.

This implies that the surge mode can be decoupled from the sway and yaw modes by assuming that the mean forward speed u_0 is constant for constant thrust. Similarly, we assume that the mean velocities in sway and yaw are $v_0 = r_0 = 0$. Consequently,

$$\begin{array}{lllllll} u & = & u_0 + \Delta u; & v & = & \Delta v; & r & = & \Delta r \\ X & = & X_0 + \Delta X; & Y & = & \Delta Y; & N & = & \Delta N \end{array} \tag{5.2}$$

where Δu, Δv and Δr are small perturbations from the nominal values u_0, v_0 and r_0, and ΔX, ΔY and ΔN are small perturbations from the nominal values X_0, Y_0 and N_0.

Assuming that higher order perturbations can be neglected, the nonlinear equations of motion can be expressed as:

$$\begin{array}{lcl} m\Delta\dot{u} & = & X_0 + \Delta X \\ m(\Delta\dot{v} + u_0 \Delta r + x_G \Delta\dot{r}) & = & \Delta Y \\ I_z \Delta\dot{r} + m x_G (\Delta\dot{v} + u_0 \Delta r) & = & \Delta N \end{array} \tag{5.3}$$

Notice that the steering equations of motion are completely decoupled from the speed equation. Applying Expression (5.2) to the steering equations finally yields:

$$\begin{array}{lrcl} \text{Speed equation:} & m\dot{u} & = & X \\ \text{Steering equations:} & m(\dot{v} + u_0 r + x_G \dot{r}) & = & Y \\ & I_z \dot{r} + m x_G (\dot{v} + u_0 r) & = & N \end{array} \tag{5.4}$$

The assumption that the mean forward speed is constant implies that this model is only valid for small rudder angles.

Hydrodynamic Forces and Moment

In the forthcoming sections we will discuss the choices of X, Y and N. We will restrict our treatment to formulas that are functions of:

$$\begin{aligned} X &= X(u, v, r, \dot{u}, \delta, T) \\ Y &= Y(v, r, \dot{v}, \dot{r}, \delta) \\ N &= N(v, r, \dot{v}, \dot{r}, \delta) \end{aligned} \tag{5.5}$$

Here T is the propeller thrust corresponding to one single-screw propeller. Ships having more than one propeller can be described by simply adding additional terms to the surge equation X.

5.2 The Speed Equation

The speed equation relates the propeller thrust T to the forward speed u.

5.2.1 Nonlinear Speed Equation

From (5.1) and (5.5), we obtain the following nonlinear expression for the surge equation:

$$m(\dot{u} - vr - x_G r^2) = X(u, v, r, \dot{u}, \delta, T) \tag{5.6}$$

Here X is a nonlinear function describing the hydrodynamic surge force. Blanke (1981) proposes the following expression for the surge force:

$$X = X_{\dot{u}}\,\dot{u} + X_{vr}\,vr + X_{|u|u}\,|u|u + X_{rr}\,r^2 + (1-t)\,T + X_{cc\delta\delta}\,c^2\,\delta^2 + X_{\text{ext}} \tag{5.7}$$

The hydrodynamic derivatives in this expression are defined below. Substituting (5.7) into (5.6), yields:

$$\boxed{(m - X_{\dot{u}})\dot{u} = X_{|u|u}|u|u + (1-t)\,T + T_{\text{loss}}} \tag{5.8}$$

with

$$\boxed{T_{\text{loss}} = (m + X_{vr})\,vr + X_{cc\delta\delta}\,c^2\,\delta^2 + (X_{rr} + mx_G)\,r^2 + X_{\text{ext}}} \tag{5.9}$$

where

$X_{\dot{u}}$	=	added mass in surge
$X_{\|u\|u}$	=	drag force coefficient surge (resistance)
t	=	thrust deduction number
$X_{cc\delta\delta}$	=	resistance due to rudder deflection
T	=	propeller thrust
c	=	flow velocity past the rudder
T_{loss}	=	loss term or added resistance
$(m + X_{vr})$	=	excessive drag force due to combined sway and yaw motions
$(X_{rr} + mx_G)$	=	excessive drag force in yaw
X_{ext}	=	external force due to wind and waves

It should be noted that the resistance and the propeller thrust will outbalance each other in steady state, when the loss term $T_{\text{loss}} = 0$. The flow past the rudder is of course strongly influenced by the propeller-induced flow. A theoretical framework showing this relationship is included in Blanke (1981). This is based on the experiments of Van Berlekom (1975) that suggest that the square velocity past the rudder can be modelled as:

$$c^2 = V_a^2 + C_T^2\, T \tag{5.10}$$

where an average C_T-value for the rudder profile is:

$$C_T \approx 0.8\alpha\frac{8}{\pi\rho D^2} \tag{5.11}$$

Here α is the ratio between the screw diameter and the height of the rudder and D is the propeller diameter. V_a is the advance speed at the propeller (speed of the water going into the propeller).

5.2.2 Linear Speed Equation

A linear approximation to (5.8) is obtained by introducing the following perturbations:

$$u = u_0 + \Delta u; \qquad T = T_0 + \Delta T; \qquad T_{\text{loss}} = (T_{\text{loss}})_0 + \Delta T_{\text{loss}} \tag{5.12}$$

where Δu, ΔT and ΔT_{loss} are small perturbations from the nominal values u_0, T_0 and $(T_{\text{loss}})_0$. Hence,

$$\boxed{(m - X_{\dot{u}})\Delta\dot{u} = X_u \Delta u + (1-t)\,\Delta T + \Delta T_{\text{loss}}} \tag{5.13}$$

where $X_u = 2u_0\, X_{u|u|}$ is the linear damping derivative in surge. The "balance condition" corresponding to steady state is:

$$(m - X_{\dot{u}})u_0 = X_{|u|u}|u_0|u_0 + (1-t)T_0 + (T_{\text{loss}})_0 = 0 \tag{5.14}$$

which yields:

$$|u_0|u_0 = \frac{1}{-X_{|u|u}}[(1-t)T_0 + (T_{\text{loss}})_0] \tag{5.15}$$

5.3 The Linear Ship Steering Equations

The ship steering equations of motion usually include the state variables v, r, ψ and the control input δ.

5.3.1 The Model of Davidson and Schiff (1946)

Consider the linear steering dynamics (5.4) in the form:

$$\begin{aligned} m(\dot{v} + u_0\, r + x_G\, \dot{r}) &= Y \\ I_z\, \dot{r} + m\, x_G(\dot{v} + u_0\, r) &= N \end{aligned} \tag{5.16}$$

Linear theory suggests that the hydrodynamic force and moment can be modeled as, Davidson and Schiff (1946):

$$\begin{aligned} Y &= Y_{\dot{v}}\, \dot{v} + Y_{\dot{r}}\, \dot{r} + Y_v\, v + Y_r\, r + Y_\delta\, \delta_R \\ N &= N_{\dot{v}}\, \dot{v} + N_{\dot{r}}\, \dot{r} + N_v\, v + N_r\, r + N_\delta\, \delta_R \end{aligned} \tag{5.17}$$

Hence we can write the equations of motion according to:

$$\boxed{M\dot{\nu} + N(u_0)\,\nu = b\,\delta_R} \tag{5.18}$$

where $\nu = [v, r]^T$ is the state vector, δ_R is the rudder angle and:

$$M = \begin{bmatrix} m - Y_{\dot{v}} & mx_G - Y_{\dot{r}} \\ mx_G - N_{\dot{v}} & I_z - N_{\dot{r}} \end{bmatrix} \quad N(u_0) = \begin{bmatrix} -Y_v & mu_0 - Y_r \\ -N_v & mx_G u_0 - N_r \end{bmatrix} \quad b = \begin{bmatrix} Y_\delta \\ N_\delta \end{bmatrix} \tag{5.19}$$

Notice that the matrix $N(u_0)$ is obtained by summation of linear damping D and Coriolis and centripetal terms $C(u_0)$ (additional terms mu_0 and $mx_G u_0$), that is:

$$N(u_0) = C(u_0) + D \tag{5.20}$$

Also notice that we have chosen the inertia matrix such that $M \neq M^T$. The corresponding state-space model is obtained by letting $x = [v, r]^T$ be the state vector and $u = \delta_R$. Hence,

$$\boxed{\dot{x} = A\,x + b_1\,u} \tag{5.21}$$

with

$$A = -M^{-1}N = \begin{bmatrix} a_{11} & a_{12} \\ a_{21} & a_{22} \end{bmatrix} \qquad b_1 = M^{-1}b = \begin{bmatrix} b_1 \\ b_2 \end{bmatrix} \tag{5.22}$$

The coefficients are defined as:

$$\begin{aligned}
a_{11} &= \frac{(I_z - N_{\dot{r}})Y_v - (mx_G - Y_{\dot{r}})N_v}{\det(M)} \\
a_{12} &= \frac{(I_z - N_{\dot{r}})(Y_r - mu_0) - (mx_G - Y_{\dot{r}})(N_{\dot{r}} - mx_G u_0)}{\det(M)} \\
a_{21} &= \frac{(m - Y_{\dot{v}})N_v - (mx_G - N_{\dot{v}})Y_v}{\det(M)} \\
a_{22} &= \frac{(m - Y_{\dot{v}})(N_r - mx_G u_0) - (mx_G - N_{\dot{v}})(Y_r - mu_0)}{\det(M)} \\
b_1 &= \frac{(I_z - N_{\dot{r}})Y_\delta - (mx_G - Y_{\dot{r}})N_\delta}{\det(M)} \\
b_2 &= \frac{(m - Y_{\dot{v}})N_\delta - (mx_G - N_{\dot{v}})Y_\delta}{\det(M)}
\end{aligned} \tag{5.23}$$

where $\det(M)$ is the determinant of the inertia matrix.

5.3.2 The Models of Nomoto (1957)

Two alternative representations of the model of Davidson and Schiff (1946) were proposed by Nomoto, Taguchi, Honda and Hirano (1957). These models are obtained by eliminating the sway velocity v from (5.18) to obtain the Nomoto transfer function between r and δ_R, that is:

$$\frac{r}{\delta_R}(s) = \frac{K_R\,(1 + T_3 s)}{(1 + T_1 s)(1 + T_2 s)} \tag{5.24}$$

The parameters of the transfer functions are related to the hydrodynamic derivatives as:

$$\begin{aligned}
T_1 T_2 &= \frac{\det(M)}{\det(N)} \\
T_1 + T_2 &= \frac{n_{11}m_{22} + n_{22}m_{11} - n_{12}m_{21} - n_{21}m_{12}}{\det(N)} \\
K_R &= \frac{n_{21}b_1 - n_{11}b_2}{\det(N)} \\
K_R T_3 &= \frac{m_{21}b_1 - m_{11}b_2}{\det(N)}
\end{aligned} \tag{5.25}$$

where the elements m_{ij}, n_{ij} and b_i ($i = 1, 2$ and $j = 1, 2$) are defined in (5.19). The determinants of the inertia and damping matrices are calculated as:

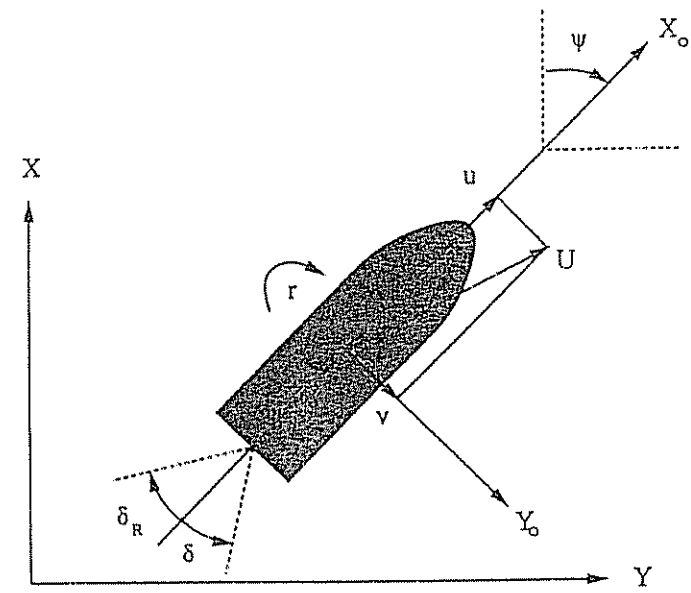

Figure 5.2: Variables used to describe the motion in the horizontal plane.

$$\det(M) = (m - Y_{\dot{v}})(I_z - N_{\dot{r}}) - (mx_G - N_{\dot{v}})(mx_G - Y_{\dot{r}}) \quad (5.26)$$

$$\det(N) = Y_v(N_r - mx_G u_0) - N_v(Y_r - mu_0) \quad (5.27)$$

It is often convenient to redefine the rudder deflection and the Nomoto gain constant according to:

$$\delta_R \triangleq -\delta; \qquad K_R \triangleq -K \quad (5.28)$$

such that a positive rudder deflection $\delta > 0$ corresponds to a positive turning rate $r > 0$. Positive rudder angle, turning rate, and surge and sway velocities are defined according to Figure 5.2. From (2.14) we see that in absence of the roll and pitch modes ($\phi = \theta = 0$), the yawing rate is defined as:

$$\dot{\psi} = r \quad (5.29)$$

Hence, we can classify the Nomoto models in the time as well as the frequency domain according to their order[1].

Nomoto's 2nd-Order Model

Nomoto's 2nd-order model relates the yaw angle ψ to the rudder angle δ according to:

- Time-domain:

$$T_1 T_2 \psi^{(3)} + (T_1 + T_2)\ddot{\psi} + \dot{\psi} = K(\delta + T_3\dot{\delta})$$

[1]The order n of the Nomoto models refers to the order of the transfer function between $r(s)$ and $\delta(s)$. Consequently, the transfer function between $\psi(s)$ and $\delta(s)$ will be of order $n+1$.

- Transfer function:

$$\frac{\psi}{\delta}(s) = \frac{K(1+T_3 s)}{s\,(1+T_1 s)(1+T_2 s)}$$

Since $r(s) = s\,\psi(s)$, the transfer function representation can also be written:

$$\frac{r}{\delta}(s) = \frac{K(1+T_3 s)}{(1+T_1 s)(1+T_2 s)} \tag{5.30}$$

In addition to the Nomoto model relating $r(s)$ to $\delta(s)$, we can express the sway velocity $v(s)$ in a similar manner by:

$$\frac{v}{\delta}(s) = \frac{K_v(1+T_v s)}{(1+T_1 s)(1+T_2 s)} \tag{5.31}$$

where K_v and T_v are the gain and time constants describing the sway mode.

Nomoto's 1st-Order Model

A 1st-order approximation is obtained by letting the effective time constant be equal to: $T = T_1 + T_2 - T_3$.

- Time-domain:

$$T\ddot{\psi} + \dot{\psi} = K\delta$$

- Transfer function:

$$\frac{\psi}{\delta}(s) = \frac{K}{s\,(1+Ts)}$$

The 1st-order Nomoto model should only be used for low frequencies. This is illustrated in the following example where the frequency response of Nomoto's 1st- and 2nd-order models is compared in an amplitude–phase diagram.

Example 5.1 (Nomoto's 1st- and 2nd-Order Models)

In this example we will consider a stable cargo ship and an unstable oil tanker.

	Cargo ship (Mariner class) Chislett and Strøm-Tejsen (1965a)	Oil tanker (full loaded) Dyne and Trägårdh (1975)
L (m)	161	350
u_0 (m/s)	7.7	8.1
∇ (dwt)	16622	389100
K (1/s)	0.185	−0.019
T_1 (s)	118.0	−124.1
T_2 (s)	7.8	16.4
T_3 (s)	18.5	46.0

An amplitude–phase diagram can be generated by the following MATLAB program:

```
% ------------------------------------------------------------------
% MAIN PROGRAM
% ------------------------------------------------------------------

T1 = 118; T2 = 7.8; T3 = 18.5; K = 0.185;
wc = nomoto(T1,T2,T3,K), pause

T1 = -124.1; T2 = 16.4; T3 = 46.0; K = -0.019;
wc = nomoto(T1,T2,T3,K)

% ------------------------------------------------------------------
% FUNCTION NOMOTO
% ------------------------------------------------------------------

function wc = nomoto(T1,T2,T3,K)
% NOMOTO(T1,T2,T3,K)
%
%                K                          K (1+T3s)
%  H1(s) = ----------       H2(s) = --------------------
%           (1+Ts)s                    s(1+T1s)(1+T2s)

T = T1+T2-T3;
d1 = [T 1 0];
n1 = K;
d2 = [T1*T2 T1+T2 1 0];
n2 = K*[T3 1];

[mag1,phase1,w1] = bode(n1,d1);
[mag2,phase2,w2] = bode(n2,d2);

if K < 0,
  phase1 = phase1-360;
  phase2 = phase2-360;
end

clg,subplot(211),semilogx(w1,20*log10(mag1)),grid
xlabel('Frequency [rad/s]'),title('Gain [dB]')
hold on,semilogx(w2,20*log10(mag2),'--'),hold off
subplot(212),semilogx(w1,phase1),grid
xlabel('Frequency [rad/s]'),title('Phase [deg]')
hold on,semilogx(w2,phase2,'--'),hold off
```

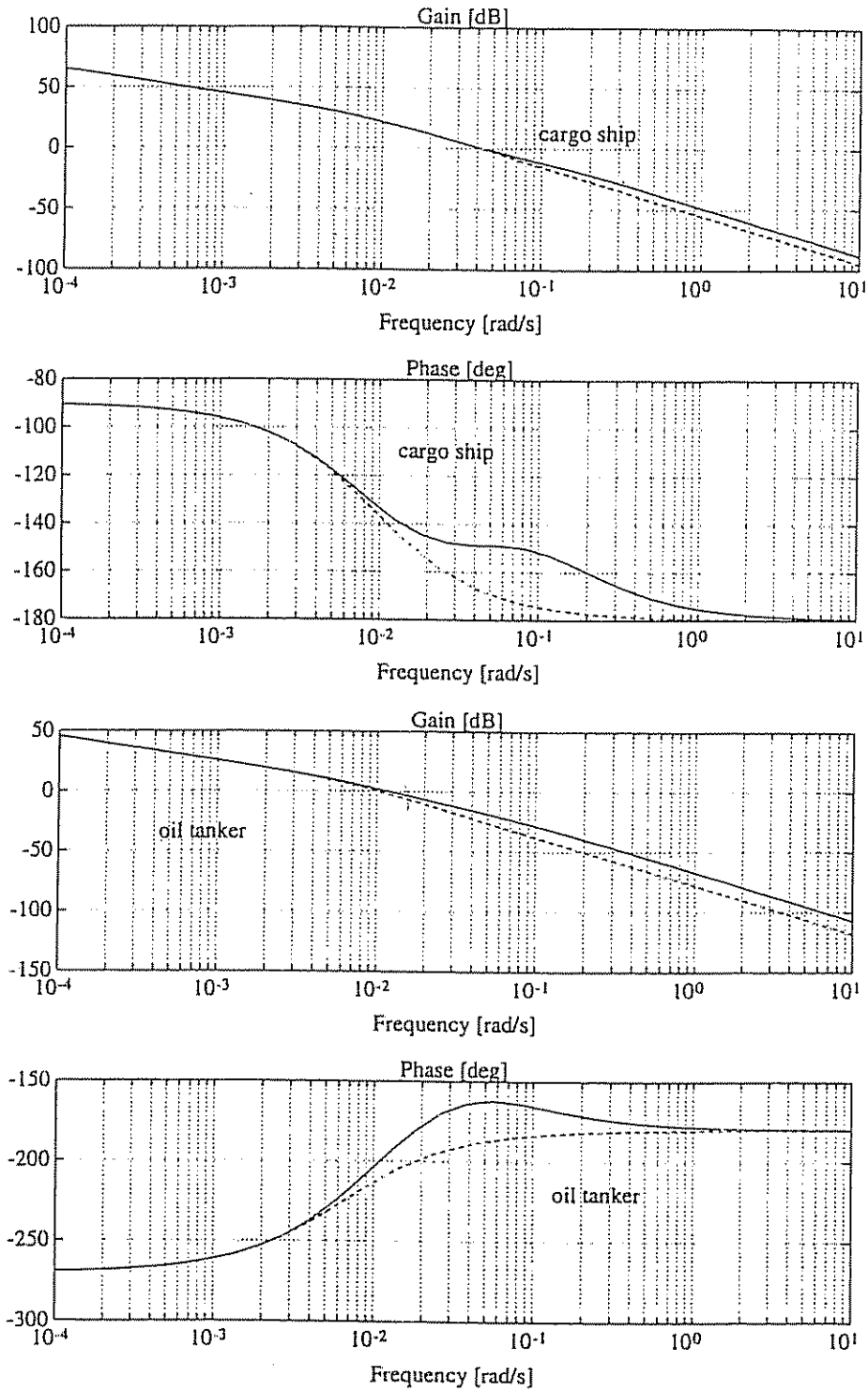

Figure 5.3: 1st-order (dotted) and 2nd-order (solid) Nomoto models for a stable cargo ship and an unstable oil tanker.

5.3.3 Non-Dimensional Ship Steering Equations of Motion

When designing the autopilot it is often convenient to normalize the ship steering equations of motion such that the model parameters can be treated as constants with respect to the instantaneous speed U. The velocity components in surge and sway have already been defined as $u = u_0 + \Delta u$ and $v = \Delta v$. Hence, the total speed is:

$$U = \sqrt{u^2 + v^2} = \sqrt{(u_0 + \Delta u)^2 + \Delta v^2} \tag{5.32}$$

For a ship moving at a constant speed on a constant course both Δu and Δv will be small. Hence,

$$U \approx u_0 \tag{5.33}$$

where u_0 is referred to as the *service speed*. However, during course changing maneuvers the instantaneous speed will decrease due to increased resistance during the turn.

Normalization Forms

The most commonly used normalization form for the ship steering equations of motion is the *Prime-system* of SNAME (1950). This system uses the ship's instantaneous speed U, the length $L = L_{pp}$ (the length between the fore and aft perpendiculars), the time unit L/U and the mass unit $\frac{1}{2}\rho L^3$ or $\frac{1}{2}\rho L^2 T$ as normalization variables. The latter is inspired by wing theory where the reference area LT is used instead of L^2. An alternative system, the so-called *Bis-system* was proposed by Norrbin (1970). This system is based on the use of the time unit $\sqrt{L/g}$, the mass unit m and the body mass density ratio $\mu = m/\rho\nabla$ where ∇ is the hull contour displacement. For positive buoyant underwater vehicles $\mu < 1$, ships and neutrally buoyant underwater vehicles use $\mu = 1$, while for a heavy torpedo μ will typically be in the range 1.3–1.5. The normalization variables for the *Prime-* and *Bis-systems* are given in Table 5.1. The non-dimensional quantities in the *Prime-* and *Bis-systems* will be distinguished from those with dimension by applying the notation $(\cdot)'$ for the *Prime-system* and $(\cdot)''$ for the *Bis-system*.

Example 5.2 (Normalization of the Model of Davidson and Schiff 1946)
Normalization of the model of (5.18) according to the Prime-system suggests:

$$M'\dot{\nu}' + N'(u_0')\nu' = b'\delta_R' \tag{5.34}$$

where $\nu' = [v', r']^T$ *and*

$$M' = \begin{bmatrix} m' - Y_{\dot{v}}' & m'x_G' - Y_{\dot{r}}' \\ m'x_G' - N_{\dot{v}}' & I_z' - N_{\dot{r}}' \end{bmatrix} \quad N'(u_0') = \begin{bmatrix} -Y_v' & m'u_0' - Y_r' \\ -N_v' & m'x_G'u_0' - N_r' \end{bmatrix} \quad b' = \begin{bmatrix} Y_\delta' \\ N_\delta' \end{bmatrix}$$

Table 5.1: Normalization variables used for the Prime-system and Bis-system

Unit	Prime-system I	Prime-system II	Bis-system
Length	L	L	L
Mass	$\frac{\varrho}{2}L^3$	$\frac{\varrho}{2}L^2T$	$\mu\rho\nabla$
Inertia moment	$\frac{\varrho}{2}L^5$	$\frac{\varrho}{2}L^4T$	$\mu\rho\nabla L^2$
Time	$\frac{L}{U}$	$\frac{L}{U}$	$\sqrt{L/g}$
Reference area	L^2	LT	$\mu\frac{2\nabla}{L}$
Position	L	L	L
Angle	1	1	1
Linear velocity	U	U	$\sqrt{Lg}$
Angular velocity	$\frac{U}{L}$	$\frac{U}{L}$	$\sqrt{\frac{g}{L}}$
Linear acceleration	$\frac{U^2}{L}$	$\frac{U^2}{L}$	g
Angular acceleration	$\frac{U^2}{L^2}$	$\frac{U^2}{L^2}$	$\frac{g}{L}$
Force	$\frac{\varrho}{2}U^2L^2$	$\frac{\varrho}{2}U^2LT$	$\mu\rho g\nabla$
Moment	$\frac{\varrho}{2}U^2L^3$	$\frac{\varrho}{2}U^2L^2T$	$\mu\rho g\nabla L$

where

$$u_0' = \frac{u_0}{U} = \frac{u_0}{\sqrt{(u_0+\Delta u)^2+\Delta v^2}} \approx 1 \tag{5.35}$$

for small values of Δu and Δv. The non-dimensional system (5.34) can be related to the original system (5.18) by simply applying the transformations:

$$v = U\,v'\,; \qquad r = \frac{U}{L}r'\,; \qquad \delta_R = \delta_R' \tag{5.36}$$

□

Example 5.3 (Models Combining Actual States Variables and Non-Dimensional Model Parameters)
An alternative representation to the previous example is obtained by using a model structure where the actual state variables are combined with the non-dimensional model parameters. This suggests that the model of Davidson and Schiff (1946) can be written:

$$\begin{bmatrix} \frac{L}{U^2}m_{11}' & \frac{L^2}{U^2}m_{12}' \\ \frac{L}{U^2}m_{21}' & \frac{L^2}{U^2}m_{22}' \end{bmatrix}\begin{bmatrix} \dot v \\ \dot r \end{bmatrix} + \begin{bmatrix} \frac{1}{U}n_{11}' & \frac{L}{U}n_{12}' \\ \frac{1}{U}n_{21}' & \frac{L}{U}n_{22}' \end{bmatrix}\begin{bmatrix} v \\ r \end{bmatrix} = \begin{bmatrix} b_1' \\ b_2' \end{bmatrix}\delta_R \tag{5.37}$$

where m_{ij}', d_{ij}' and b_i' are defined according to Prime systems I or II in Table 5.1. Similarly the gain and time constants in Nomoto's 1st-order model can be made invariant with respect to L and U by defining:

$$K' = (L/U)\, K; \qquad T' = (U/L)\, T \tag{5.38}$$

This suggests that the 1st-order ship dynamics can be expressed as:

$$(L/U)\, T'\, \dot{r} + r = (U/L)\, K'\, \delta \tag{5.39}$$

This representation is advantageous since the non-dimensional gain and time constants will typically be in the range: $0.5 < K' < 2$ *and* $0.5 < T' < 2$ *for most ships. An extension to Nomoto's 2nd-order model is obtained by writing:*

$$(L/U)^2\, T_1'\, T_2'\, \psi^{(3)} + (L/U)\, (T_1' + T_2')\, \ddot{\psi} + \dot{\psi} = (U/L)\, K'\, \delta + K'\, T_3'\, \dot{\delta} \tag{5.40}$$

where the non-dimensional time constants T_i' *are defined as:* $T_i' = T_i\, (U/L)$ *for* $(i = 1, 2, 3)$ *and the non-dimensional gain constant is* $K' = (L/U)\, K$.
□

Both model representations (5.34) and (5.37) are based on speed-independent non-dimensional hydrodynamic derivatives. Notice that time integration of (5.34) implies use of non-dimensional time t' and state variables v' and r'. The model (5.37), however, can be integrated directly with respect to dimensional time t (s) to yield dimensional state variables v (m/s) and r (rad/s).

5.3.4 Determination of Hydrodynamic Derivatives

A large number of experimental methods can be used to determine forces and moments associated with variations in linear and angular velocity and acceleration. Typical facilities are the rotating arm, the free oscillator, the forced oscillator, the curved-flow tunnel, the curved models in a straight flow facility and the Planar Motion Mechanism (PMM) technique. Nevertheless, it is difficult to determine all hydrodynamic coefficients for an ocean vehicle. It is necessary to know these coefficients with reasonable accuracy to obtain a good model of the vehicle. Besides this some hydrodynamic coefficients can be determined by theoretical and semi-empirical methods. Strip theory has been successfully applied for ships, for instance. Finally, system identification (SI) and recursive parameter estimation techniques have been applied to determine the hydrodynamic derivatives. SI techniques are economical in tank time and provide a more direct answer free from the cumulative error of measuring many coefficients individually. The disadvantage is the quite harsh requirement of persistent excitation of the control input sequence.

SI techniques are described more closely in Section 6.8, while Chapter VIII, Sections 9 and 10 in Comstock (1967) give a survey of experimental and theoretical methods for determination of the hydrodynamic derivatives. Some of these methods are briefly described below.

Straight-Line Test and Rotating-Arm Technique in a Towing Tank

The velocity dependent derivatives Y_v and N_v of a ship can be determined by using a model of the ship which is towed in a conventional towing tank. The force and moment coefficients are usually measured by a dynamometer. Furthermore, the rotary derivatives Y_r and N_r can be measured on a model by using a towing tank apparatus denoted as a rotating-arm facility. The model is rotated about an axis fixed in the tank with constant speed while a dynamometer is used to measure the force and moment. Straight-line tests in a towing tank can also be used to determine the control derivatives Y_δ and N_δ by simply towing the model with various values of rudder angle to obtain a plot of these derivatives versus rudder angle.

Planar Motion Mechanism (PMM) Technique

Another promising technique was developed by a research team at the David Taylor Model Basin in 1957. They applied a device called the Planar Motion Mechanism (PMM) System (Gertler 1959). The PMM system can be used to experimentally determine all of the hydrodynamic stability coefficients in 6 DOF. These include static stability coefficients, rotary stability coefficients and acceleration derivatives.

The PMM consists of two oscillators mounted at the bow and stern of the model. These oscillators are used to produce a transverse oscillation of the moving model. The forces induced by the oscillators can then be measured by two transducers.

Strip Theory

An estimate of the hydrodynamic derivatives can be obtained by applying *strip theory*. The principle of strip theory involves dividing the underwater part of the ship into a number of strips. Hence, two-dimensional hydrodynamic coefficients for added mass and damping can be computed for each strip and summarized to yield the three-dimensional coefficients (see Section 2.4.1). Consider the linear ship model:

$$\begin{bmatrix} m - Y_{\dot v} & mx_G - Y_{\dot r} \\ mx_G - N_{\dot v} & I_z - N_{\dot r} \end{bmatrix} \begin{bmatrix} \dot v \\ \dot r \end{bmatrix} + \begin{bmatrix} -Y_v & mu_0 - Y_r \\ -N_v & mx_G u_0 - N_r \end{bmatrix} \begin{bmatrix} v \\ r \end{bmatrix} = \begin{bmatrix} Y_\delta \\ N_\delta \end{bmatrix} \delta \quad (5.41)$$

Using the results of Chapter VIII, Section 10 in Comstock (1967) and Newman (1977), together with some engineering judgment, we can approximate the hydrodynamic derivatives for a symmetrical ship by:

$$Y'_v = \frac{Y_v}{\frac{1}{2}\rho LT U} = -(\frac{\pi T}{L} - C_{D0}) \quad (5.42)$$

$$Y'_r = \frac{Y_r}{\frac{1}{2}\rho L^2 T U} = X'_{\dot{u}} + \frac{x_P}{L} Y'_v \tag{5.43}$$

$$N'_v = \frac{N_v}{\frac{1}{2}\rho L^2 T U} = -(X'_{\dot{u}} - Y'_{\dot{v}}) + \frac{x_P}{L} Y'_v \tag{5.44}$$

$$N'_r = \frac{N_r}{\frac{1}{2}\rho L^3 T U} = \frac{1}{4} Y'_v \tag{5.45}$$

$$Y'_\delta = \frac{Y_\delta}{\frac{1}{2}\rho L T U^2} = \rho \frac{\pi}{4} \frac{A_\delta}{LT} \tag{5.46}$$

$$N'_\delta = \frac{N_\delta}{\frac{1}{2}\rho L^2 T U^2} = -\frac{1}{2} Y'_\delta \tag{5.47}$$

where C_{D0} is the drag coefficient of the ship at zero angle of attack (small for slender bodies), L (m) is the hull length, ρ (kg/m^3) is the sea water density, T (m) is the draft depth, U (m/s) is the speed of the ship, A_δ (m^2) is the rudder area, I_z (kgm^2) is the moment of inertia and x_P (m) is the distance between the center of gravity and the center of pressure. Moreover,

$$I_z = m\, x_G^2 + I_r \tag{5.48}$$

where m (kg) is the mass of the ship, r denotes the *radius of gyration* and:

$$I_r = m\, r^2 \quad \text{where} \quad 0.15L < r < 0.3L \tag{5.49}$$

$$x_P = x_G \pm 0.1L \tag{5.50}$$

The added mass derivatives can be approximated by:

$$X_{\dot{u}} = -(0.05m \text{ to } 0.10m) \tag{5.51}$$

$$Y_{\dot{v}} = -(0.70m \text{ to } 1.00m) \tag{5.52}$$

$$Y_{\dot{r}} = 0 \tag{5.53}$$

$$N_{\dot{v}} = 0 \tag{5.54}$$

$$N_{\dot{r}} = -(0.01I_z \text{ to } 0.1I_z) \tag{5.55}$$

Care should be taken when using these formulas for prediction since some rough approximations have been made. However, these values are highly useful as *a priori* information for a recursive parameter estimator.

5.4 The Steering Machine

The mathematical model of the steering machine in this section is based on the results of Van Amerongen (1982). The ship actuator or the steering machine is usually controlled by an on-off rudder control system. The on-off signals from

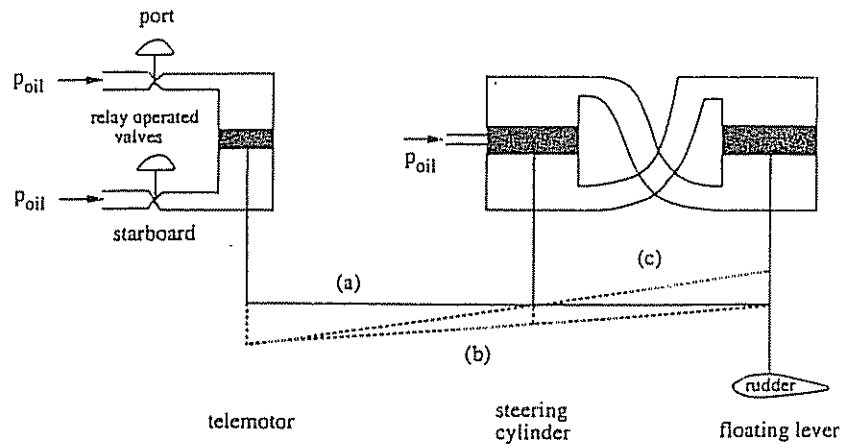

Figure 5.4: Simplified diagram of a two-stage hydraulic steering machine (Van Amerongen 1982).

the rudder controller are used to open and close the port and starboard valves of the telemotor system, see Figure 5.4.

Assume that both the telemotor and floating lever are initially at rest in position (a). The telemotor can be moved to position (b) by opening the port valve. Suppose that the rudder is still in its original position corresponding to position (b); this will cause the steering cylinder valve to open. Consequently, the floating lever will move to position (c) when the desired rudder angle has been reached. The maximum opening of the steering cylinder valve, together with the pump capacity, determines the maximum rudder speed. A block diagram of the steering machine with its dynamics is shown in Figure 5.5.

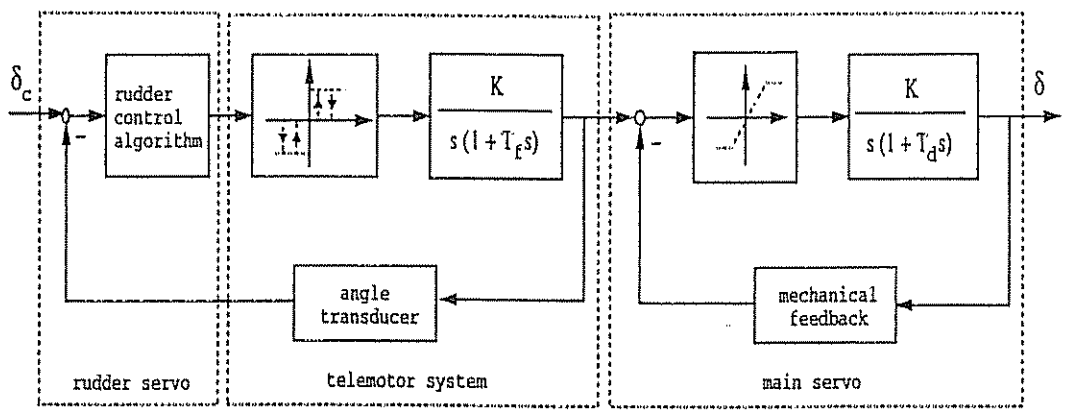

Figure 5.5: Block diagram of the rudder control loop relating the commanded rudder angle δ_c set by the helmsman to the actual rudder angle δ (Van Amerongen 1982).

In computer simulations and when designing autopilots, Van Amerongen (1982) suggests using a simplified representation of the steering machine, see Figure 5.6. This representation is based on the telemotor being much faster than the main

servo and that the time constant T_d is of minor importance compared with the influence of the rudder speed. Generally, the rudder angle and rudder rate limiters in Figure 5.5 will typically be in the ranges:

$$\delta_{\max} = 35 \ \text{(deg)}; \qquad 2\frac{1}{3} \ \text{(deg/s)} \leq \dot{\delta}_{\max} < 7 \ \text{(deg/s)}$$

for most commercial ships. The requirement for minimum average rudder rate is specified by the classification societies[2]. It is required that the rudder can be moved from 35 degrees port to 35 degrees starboard within 30 seconds. According to Eda and Crane (1965), the minimum design rudder rate in dimensional terms should satisfy:

$$\dot{\delta}_{\min} = 132.9\,(U/L) \ \text{(deg/s)}$$

where U is the ship speed in m/s and L is the ship length in m. Recently, much faster steering machines have been designed with rudder speeds up to 15–20 (deg/s). A rudder speed of 5–20 (deg/s) is usually required for a rudder-roll stabilization (RRS) system to work properly.

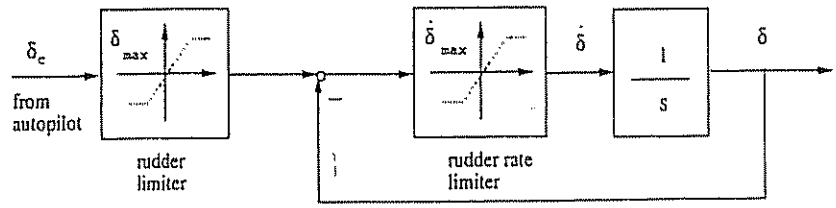

Figure 5.6: Simplified diagram of the rudder control loop (Van Amerongen 1982).

Another model of the rudder could be (Rios–Neto and Da Cruz 1985):

$$\dot{\delta} = \begin{cases} \dot{\delta}_{\max}\,(1 - \exp(-(\delta_c - \delta)/\Delta)) & \text{if } \delta_c - \delta \geq 0 \\ -\dot{\delta}_{\max}\,(1 - \exp((\delta_c - \delta)/\Delta)) & \text{if } \delta_c - \delta < 0 \end{cases} \tag{5.56}$$

The parameter Δ will depend on the moment of inertia of the rudder. Typical values will be in the range $3 \leq \Delta \leq 10$.

The limitations of the rudder angle and the rudder speed can be illustrated with the following two simple examples adopted from Van der Klugt (1987).

Example 5.4 (Limitation of the Rudder Angle)
Consider the rudder angle limiter in Figure 5.7 where δ_c is the commanded rudder angle and δ is the actual rudder angle. Let the controller output be given by:

$$\delta_c = A \sin(\omega_0 t) \tag{5.57}$$

[2]American Bureau of Shipping (ABS), Det norske Veritas (DnV), Lloyds etc.

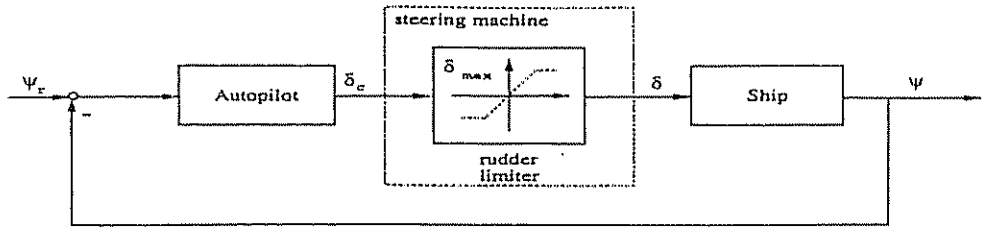

Figure 5.7: Simplified system with rudder limiter (Van der Klugt 1987).

Figure 5.8 shows the actual rudder angle for three different cases $A = 3/4\ \delta_{\max}$, $A = \delta_{\max}$ *and* $A = 4/3\ \delta_{\max}$ *where* $\delta_{\max} = 30$ *(deg) and* $\omega_0 = \pi/10$ *(rad/s). It is seen from the figure that no extra phase lag is introduced for any of the cases. However, an obvious reduction in amplitude is observed for the saturated case. This amplitude reduction may lead to instability for autopilots based on adaptive control theory. A simple controller of PID-type will usually suffer from reduced performance but it will be stable.*

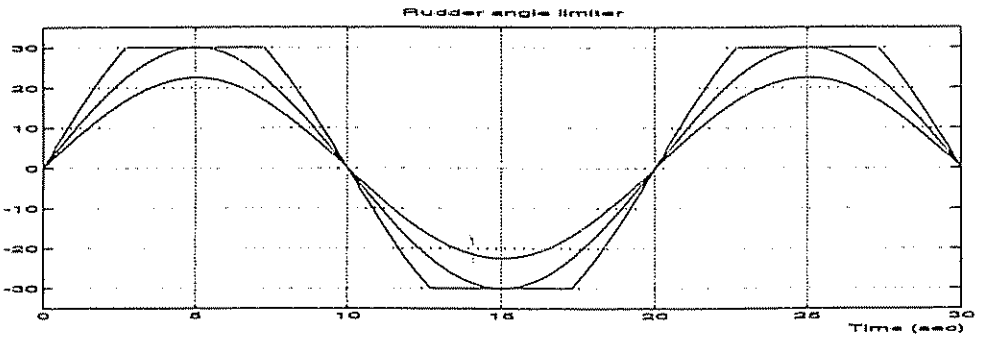

Figure 5.8: Influence of the rudder limiter (Van der Klugt 1987).

□

Example 5.5 (Limitation of the Rudder Rate)

Consider the rudder rate limiter in Figure 5.9 where δ_c *is the commanded rudder angle and* δ *is the actual rudder angle. Let the controller output be given by:*

$$\delta_c = A\ \sin(\omega_0 t) \tag{5.58}$$

Figure 5.10 shows the actual and commanded rudder angle for $\dot{\delta}_{\max} = 4$ *(deg/s),* $A = 30$ *(deg) and* $\omega_0 = \pi/10$ *(rad/s).*

Besides saturation we now observe that an additional phase lag has been introduced. In fact reduced phase margins can lead to severe stability problems for the control system. In practice, rudder rate limitations are typical in extreme weather conditions since compensation of high frequency disturbances require a faster rudder. Therefore, solving this problem is crucial for a good autopilot design.

□

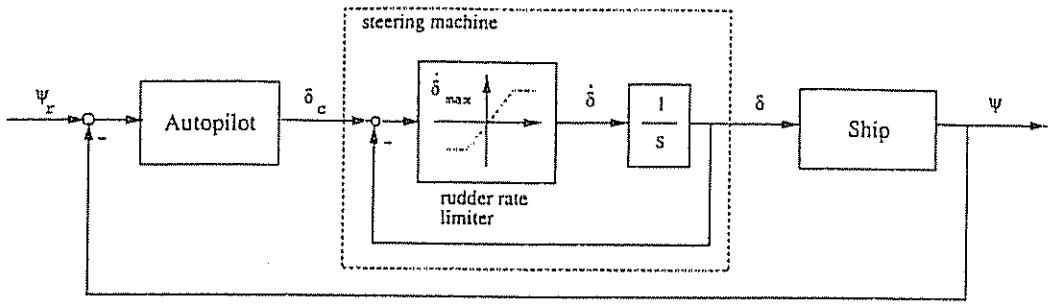

Figure 5.9: Simplified system with rudder rate limiter (Van der Klugt 1987).

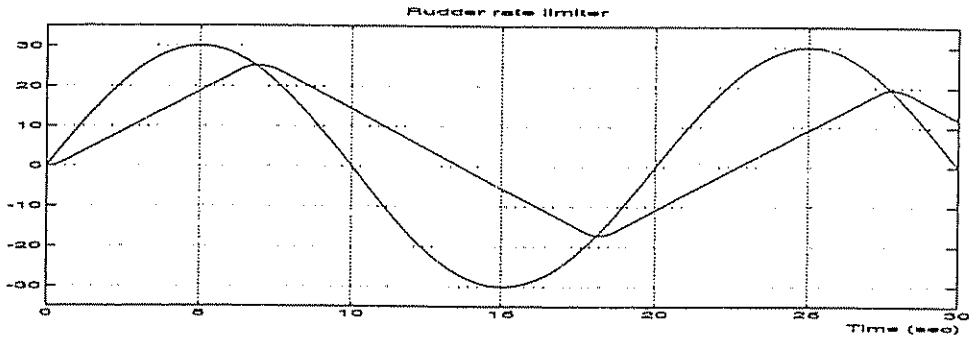

Figure 5.10: Influence of the rudder rate limiter (Van der Klugt 1987).

5.5 Stability of Ships

Stability of the uncontrolled ship can be defined as the ability of returning to an equilibrium point after a disturbance without any corrective action of the rudder. Hence, *maneuverability* can be defined as the capability of the ship to carry out specific maneuvers. Excessive stability implies that the control effort will be excessive whereas a marginally stable ship is easy to control. Thus, a compromise between stability and maneuverability must be made. Furthermore *ship maneuvering* can be defined as the ability of the controlled ship to change or retain the direction of motion and its speed in that direction.

5.5.1 Basic Stability Definitions

This section will give a brief introduction to *controls-fixed* and *controls-free* stability for rudder controlled ships. Controls-fixed stability implies investigating the vehicle's stability when the rudder is fixed, whereas working (free) controls refers to the case when the rudder is moving. This implies that the dynamics of the control system also must be considered in the stability analysis.

For ships it is common to distinguish between three types of stability, namely *straight-line, directional* and *positional motion stability*. For simplicity we will use Nomoto's 1st-order model to illustrate these basic concepts. Consider the model:

$$T\,\dot{r}(t) + r(t) = K\,\delta(t) + w(t) \tag{5.59}$$

where $w(t)$ is the external disturbances. Let the rudder control system be of proportional and derivative (PD) type, that is:

$$\delta(t) = K_p\,[\psi_d - \psi(t)] - K_d\,r(t) \tag{5.60}$$

where ψ_d = constant is used to denote the desired heading angle and K_p and K_d are two positive regulator gains. Substituting the control law (5.60) into Nomoto's 1st-order model yields the closed loop system:

$$T\ddot{\psi}(t) + (1 + KK_d)\,\dot{\psi}(t) + KK_p\,\psi(t) = KK_p\,\psi_d + w(t) \tag{5.61}$$

This system can be transformed to a 2nd-order "mass–damper–spring" system:

$$m\,\ddot{\psi}(t) + d\,\dot{\psi}(t) + k\,\psi(t) = f(t) \tag{5.62}$$

by defining $d = m\,(1 + KK_d)/T$, $k = m\,(KK_p)/T$ and $f(t) = k\psi_d + mw(t)/T$. The eigenvalues $\lambda_{1,2}$, the natural frequency ω_n and the relative damping ratio ζ for the mass–damper–spring system are:

$$\lambda_{1,2} = \frac{-d \mp \sqrt{d^2 - 4mk}}{2m}; \qquad \omega_n = \sqrt{\frac{k}{m}}; \qquad \zeta = \frac{d}{2\sqrt{k\,m}} \tag{5.63}$$

Example 5.6 (Simulation of a 2nd-Order System)
The following MATLAB program is used to generate the following step responses for the 2nd-order system (5.62). The plots are shown in Figure 5.11.

```
% MATLAB program
%   ..
%   x  + 2 zeta w x + w^2 x = w^2 x_d
%     ..     .
%   m x  + d x + k x = k x_d

w  = 1;                 % natural frequency
xd = 1*ones(160,1);     % commanded heading
t  = 0:0.1:16;          % time vector

clg
[A,B,C,D] = ord2(w,0.2); [y,x]=lsim(A,B,C,D,psid,t); plot(t,y);hold on;
[A,B,C,D] = ord2(w,0.8); [y,x]=lsim(A,B,C,D,psid,t); plot(t,y);hold on;
[A,B,C,D] = ord2(w,1);   [y,x]=lsim(A,B,C,D,psid,t); plot(t,y);hold on;
[A,B,C,D] = ord2(w,2);   [y,x]=lsim(A,B,C,D,psid,t); plot(t,y);grid
hold off
```

□

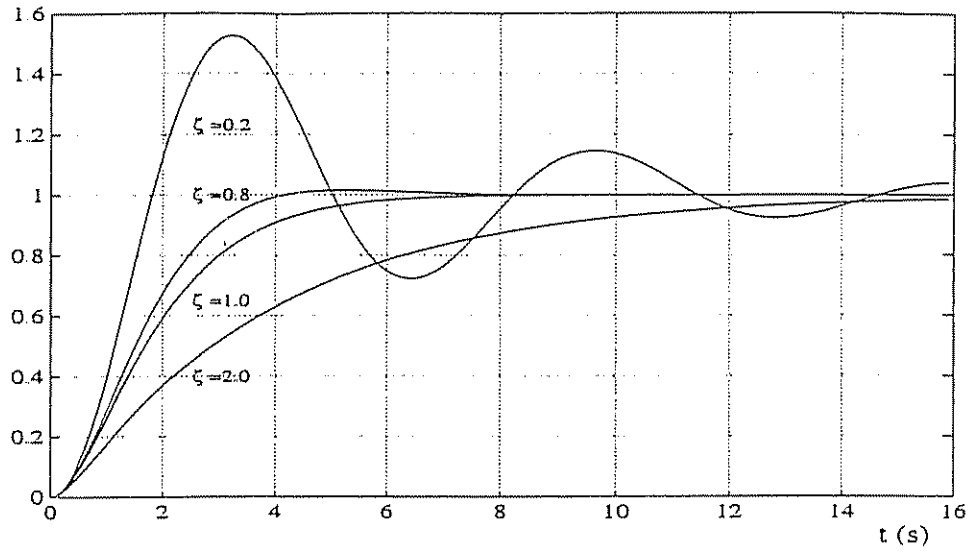

Figure 5.11: Step responses for the 2nd-order mass–damper–spring system (5.62) with $\psi_d = 1.0$, $\omega = 1.0$ and $\zeta \in \{0.2, 0.8, 1.0, 2.0\}$

Stability Considerations for Ship Steering and Positioning

The global x- and y-positions for a ship moving with constant forward speed u_o under the assumption that Δu and Δv are small, are found by integrating the following set of differential equations:

$$\ddot{\psi}(t) = -\frac{1}{T}\,\dot{\psi}(t) + \frac{K}{T}\,\delta(t) + \frac{1}{T}\,w(t) \tag{5.64}$$

$$\dot{x}(t) = u_o \cos\psi(t) \tag{5.65}$$

$$\dot{y}(t) = u_o \sin\psi(t) \tag{5.66}$$

For this system, the following considerations can be made:

- **Instability:**

  Instability can occur both for controlled and uncontrolled ships. For instance, large tankers can be unstable even around $\delta = 0$. This occurs when:

  $$\lambda_1 = -\frac{d}{m} = -\frac{1}{T} > 0 \qquad \text{and} \qquad \lambda_2 = 0$$

  which simply states that $T < 0$. For the controlled ship to be unstable K_p and K_d must be chosen such that at least one of the eigenvalues are positive. This will not happen if the controller is properly designed.

- **Straight-Line Stability:**

  Consider an uncontrolled ship moving in a straight path. If the new path is straight after a disturbance in yaw the ship is said to have straight-line stability. The direction of the new path will usually differ from the initial path because no restoring forces are present ($k = 0$). This corresponds to:

  $$\lambda_1 = -\frac{d}{m} = -\frac{1}{T} < 0 \qquad \text{and} \qquad \lambda_2 = 0$$

  Consequently the requirement $T > 0$ implies straight-line stability for the uncontrolled ship ($\delta = 0$).

- **Directional Stability (Stability on Course):**

  Directional stability is a much stronger requirement than straight-line stability. Directional stability requires the final path to be parallel to the initial path. The ship is said to be directionally stable if both eigenvalues have negative real parts that is:

  $$Re\{\lambda_{1,2}\} < 0$$

  The following two types of directional stability are observed:

  1. **Non-oscillatoric** ($d^2 - 4mk \geq 0$):
     This implies that both eigenvalues are negative and real.
  2. **Oscillatoric** ($d^2 - 4mk < 0$):
     This corresponds to two imaginary eigenvalues with negative real parts.

  Directional stability is observed for the uncontrolled ship in roll and pitch where metacentric restoring forces are present. Directional stability in yaw cannot be obtained without corrective action from the rudder control system.

- **Positional Motion Stability:**

  Positional motion stability implies that the ship should return to its original path after a disturbance. This is generally impossible in surge, sway and yaw for an uncontrolled vehicle without using thrust or control surfaces.

It should be noted that linear theory like the models of Davidson and Schiff (1946) and Nomoto et al. (1957) are based on the assumption that the ship can be made course-stable by applying small rudder deflections. However, a nonlinear behavior may be observed for certain ships like large tankers even for small rudder angles. Mathematical models incorporating these effects will be discussed in later sections.

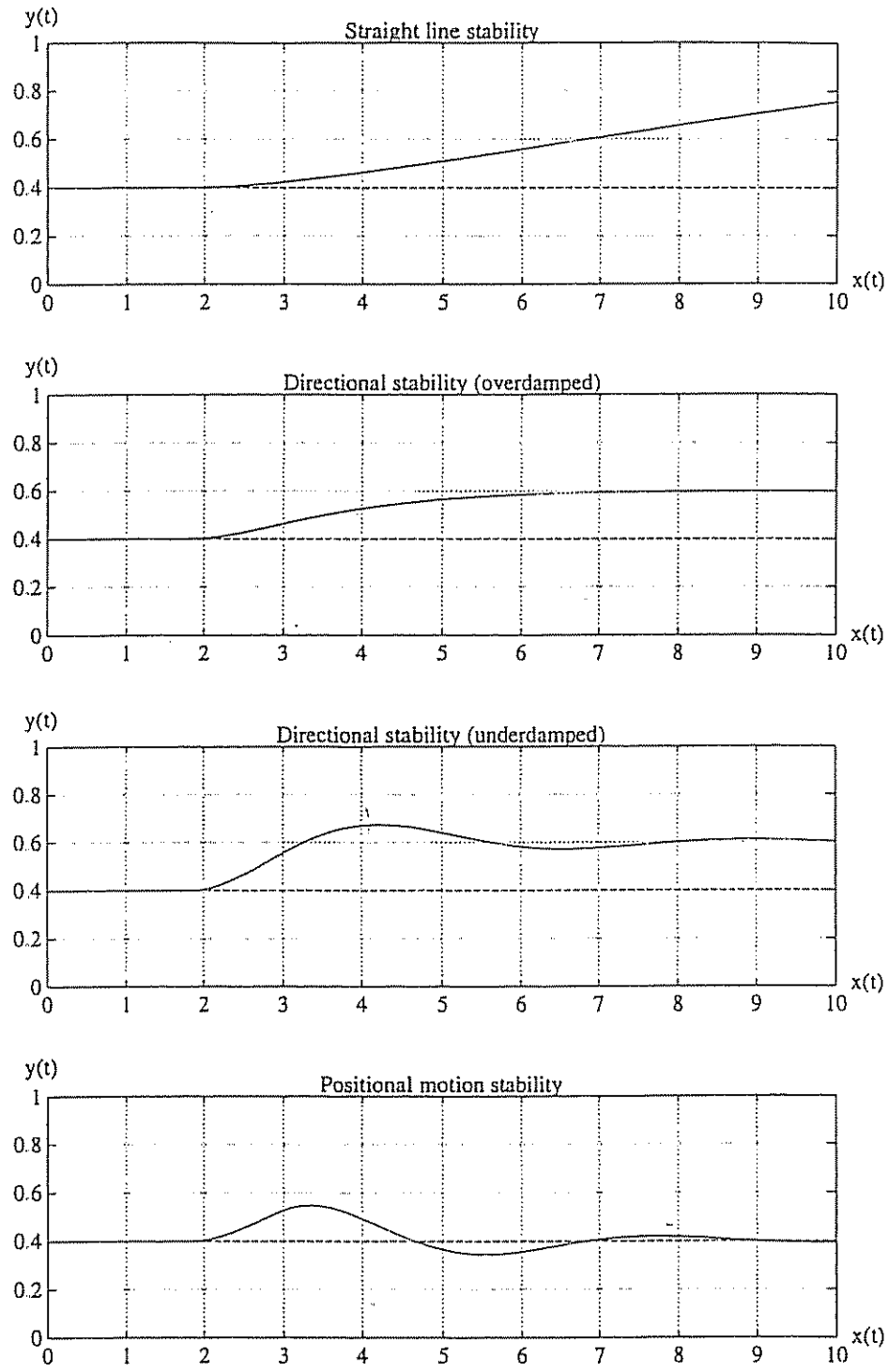

Figure 5.12: xy-plots showing straight-line, directional and position motion stability for a typical ship when an impulse $w(t)$ is injected at $x = 2$ m.

Example 5.7 (Straight-Line Stability)
Consider the cargo ship and oil tanker of Example 5.1. Recall that the equivalent time constant in Nomoto's 1st-order model was defined as:

$$T = T_1 + T_2 - T_3$$

Hence, the uncontrolled cargo ship has an equivalent time constant $T = 107.3\ s > 0$ *while the oil tanker has an equivalent time constant* $T = -153.6\ s < 0$. *This implies that the cargo ship is straight-line stable while the oil tanker is unstable.* □

5.5.2 Metacentric Stability

Besides the mass and damping forces, a surface ship will also be affected by the restoring forces caused by the weight and buoyancy. The restoring forces are equivalent to the spring forces in a mass–damper–spring system. Static stability considerations due to restoring forces are usually referred to as *metacentric stability* in the hydrostatic literature. Hence, a metacentric stable vehicle will resist inclinations away from its static equilibrium point in the horizontal plane. This can easily be understood by considering the linearized equations of motion:

$$\boldsymbol{M}\,\ddot{\boldsymbol{\eta}} + \boldsymbol{N}\,\dot{\boldsymbol{\eta}} + \boldsymbol{G}\,\boldsymbol{\eta} = \boldsymbol{\tau} \tag{5.67}$$

where $\boldsymbol{\eta} = [x, y, z, \phi, \theta, \psi]^T$ and $\boldsymbol{M}$, $\boldsymbol{N}$ and $\boldsymbol{G}$ are constant matrices. For a body with xz-plane symmetry the $\boldsymbol{G}$ matrix takes the following form:

$$\boldsymbol{G} = -\begin{bmatrix} 0 & 0 & 0 & 0 & 0 & 0 \\ 0 & 0 & 0 & 0 & 0 & 0 \\ 0 & 0 & Z_z & 0 & Z_\theta & 0 \\ 0 & 0 & 0 & K_\phi & 0 & 0 \\ 0 & 0 & M_z & 0 & M_\theta & 0 \\ 0 & 0 & 0 & 0 & 0 & 0 \end{bmatrix}$$

This implies that the restoring forces only affect the heave, pitch and roll modes. If we also have yz-plane symmetry, $Z_\theta = M_z = 0$, the force and moment components are:

$$Z_z = -\rho g\, A_{wp} \tag{5.68}$$

$$Z_\theta = +\rho g \iint_{A_{wp}} x\, dA \tag{5.69}$$

$$M_z = Z_\theta \tag{5.70}$$

$$K_\phi = -\rho g \nabla (z_B - z_G) + \rho g \iint_{A_{wp}} y^2\, dA \triangleq -\rho g \nabla\, \overline{GM}_T \tag{5.71}$$

$$M_\theta = -\rho g \nabla (z_B - z_G) + \rho g \iint_{A_{wp}} x^2\, dA \triangleq -\rho g \nabla\, \overline{GM}_L \tag{5.72}$$

where

ρ = water density (kg/m^3)
z_G = z-coordinate center of gravity (m)
z_B = z-coordinate center of buoyancy (m)
∇ = displaced volume of water (m^3)
A_{wp} = water plane area (m^2)
$\overline{GM}_T$ = transverse metacentric height (m)
$\overline{GM}_L$ = longitudinal metacentric height (m)

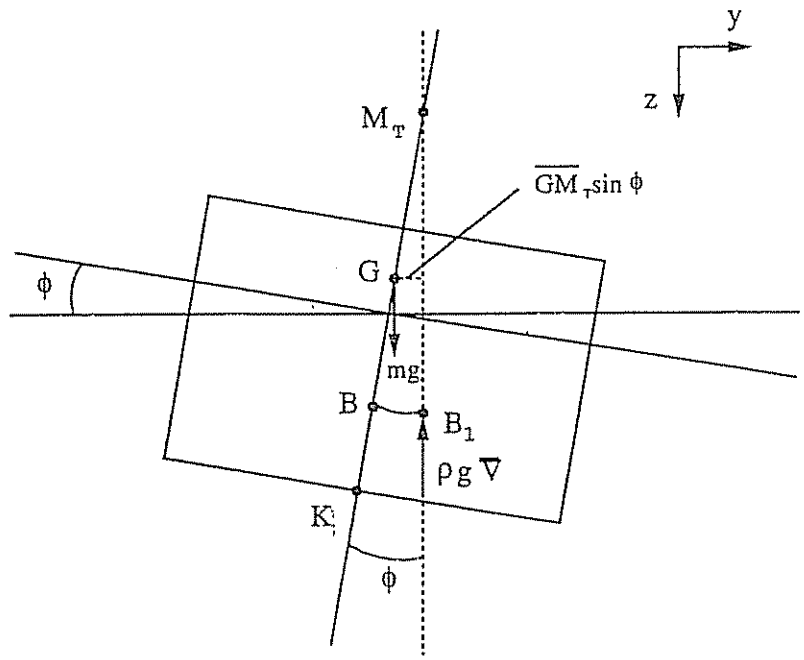

Figure 5.13: Transverse metacentric stability. Notice that $mg = \rho g \nabla$. A similar figure can be drawn to illustrate lateral metacentric stability by simply replacing M_T and ϕ with M_L and θ, respectively.

This implies that the restoring force in heave and the restoring moments in roll and pitch (neglecting cross-couplings) can be written as:

$$\begin{aligned} Z_{\text{restoring}} &= -\rho\, g\, A_{wp}\, z \\ K_{\text{restoring}} &= -\rho\, g\, \nabla\, \overline{GM}_T\, \sin\phi \\ M_{\text{restoring}} &= -\rho\, g\, \nabla\, \overline{GM}_L\, \sin\theta \end{aligned}$$

where z is the vertical displacement (positive downward) and $(\overline{GM}_T \sin\phi)$ and $(\overline{GM}_L \sin\theta)$ can be interpreted as the moment arms in roll and pitch. A commonly used formula for the metacentric height is obtained by defining the vertical distance between the center of gravity (G) and the center of buoyancy (B) as:

$$\overline{BG} \triangleq z_B - z_G \tag{5.73}$$

From basic hydrostatics, we have:

$$\overline{GM}_T = \overline{BM}_T - \overline{BG}; \qquad \overline{GM}_L = \overline{BM}_L - \overline{BG} \tag{5.74}$$

This relationship is seen directly from Figure 5.13 where M_T denotes the transverse metacenter (the intersection between the vertical line through B and B_1 when ϕ and θ approaches zero) and K is the keel line. For small inclinations (ϕ and θ are small) the longitudinal and transverse radius of curvature can be approximated by:

$$\overline{BM}_L = \frac{I_L}{\nabla}; \qquad \overline{BM}_T = \frac{I_T}{\nabla} \tag{5.75}$$

Here the moments of area about the water plane are defined as:

$$I_L \triangleq \iint_{A_{wp}} x^2 \, dA; \qquad I_T \triangleq \iint_{A_{wp}} y^2 \, dA \tag{5.76}$$

For conventional ships these integrals will satisfy the bounds:

$$I_T < \frac{1}{12} B^3 L; \qquad I_L < \frac{1}{12} B L^3 \tag{5.77}$$

A ship is said to be metacentric stable if $\overline{GM}_T > 0$ and $\overline{GM}_L > 0$. The longitudinal stability requirement is easy to satisfy since the pitching motion is limited for most ships. The rolling motion, however, must satisfy $\overline{GM}_T > 0.15\ m$ to guarantee a proper stability margin in roll.

Natural Frequency, Relative Damping Ratio and Natural Period

Neglecting the cross-coupling effects, the natural frequency and relative damping ratios for heave, roll and pitch are (see Equation (5.63)):

$$\omega_z = \sqrt{\frac{\rho g \, A_{wp}}{m - Z_{\dot{w}}}} \qquad \zeta_z = \frac{-Z_w}{2\sqrt{\rho g \, A_{wp}(m - Z_{\dot{w}})}} \tag{5.78}$$

$$\omega_\phi = \sqrt{\frac{\rho g \nabla \, \overline{GM}_T}{I_x - K_{\dot{p}}}} \qquad \zeta_\phi = \frac{-K_p}{2\sqrt{\rho g \nabla \, \overline{GM}_T (I_x - K_{\dot{p}})}} \tag{5.79}$$

$$\omega_\theta = \sqrt{\frac{\rho g \nabla \, \overline{GM}_L}{I_y - M_{\dot{q}}}} \qquad \zeta_\theta = \frac{-M_q}{2\sqrt{\rho g \nabla \, \overline{GM}_L (I_y - M_{\dot{q}})}} \tag{5.80}$$

This in turn implies that the natural periods ($T_i = 2\pi/\omega_i$) in heave, roll and pitch can be written as:

$$T_z = 2\pi\sqrt{\frac{m - Z_{\dot{w}}}{\rho g \, A_{wp}}} \quad T_\phi = 2\pi\sqrt{\frac{I_x - K_{\dot{p}}}{\rho g \nabla \, \overline{GM}_T}} \quad T_\theta = 2\pi\sqrt{\frac{I_y - M_{\dot{q}}}{\rho g \nabla \, \overline{GM}_L}} \tag{5.81}$$

5.5.3 Criteria for Dynamic Stability in Straight-Line Motion

Recall from Section 5.5.1 that a ship is said to be dynamic straight-line stable if it returns to a straight-line motion after a disturbance in yaw without any corrective action from the rudder. Consequently, instability refers to the case when the ship goes into a starboard or port turn without any rudder deflections. In the same section Nomoto's 1st-order model was used to find a simple criterion for straight-line motion. This leads to the requirement that the time constant T must be positive. Similarly, it is possible to derive a criterion for straight-line stability for the more general model:

$$M\,\dot{\nu} + N(u_0)\,\nu = b\,\delta_R \tag{5.82}$$

where both the sway and yaw modes are included, that is $\nu = [v, r]^T$. Applications of Laplace's transformation to the linear model (5.82), yield:

$$(Ms + N(u_0))\,\nu(s) - M\,\nu(t{=}0) = b\,\delta_R(s) \tag{5.83}$$

Hence,

$$\nu(s) = \frac{\mathrm{adj}(Ms + N(u_0))}{\det(Ms + N)}\;[b\,\delta_R(s) + M\,\nu(t{=}0)] \tag{5.84}$$

Assuming that the rudder is fixed in its initial position, that is $\delta_R(s) = 0$, we obtain the following characteristic equation from (5.84):

$$\det(M\,\sigma + N(u_0)) = A\,\sigma^2 + B\,\sigma + C = 0 \tag{5.85}$$

where

$$\begin{aligned} A &= \det(M) \\ B &= n_{11}m_{22} + n_{22}m_{11} - n_{12}m_{21} - n_{21}m_{12} \\ C &= \det(N) \end{aligned} \tag{5.86}$$

The two roots of (5.85), both of which must have negative real parts for controls-fixed stability are:

$$\sigma_{1,2} = \frac{-B/A \pm \sqrt{(B/A)^2 - 4(C/A)}}{2} \tag{5.87}$$

$\sigma_{1,2}$ are often referred to as the controls-fixed stability indexes for straight-line stability. Alternatively, a straight-line stability criterion can be derived by applying Routh's stability criterion.

Theorem 5.1 (The Routh Stability Criterion)
The Routh stability criterion was developed in the 1860s by the British scientist E. J. Routh. Consider the characteristic equation:

$$a_n\lambda^n + a_{n-1}\lambda^{n-1} + a_{n-2}\lambda^{n-2} + \ldots + a_0 = 0 \tag{5.88}$$

To apply the Routh criterion we must form the so-called Routh array:

	Routh array			
λ^n	a_n	a_{n-2}	a_{n-4}	...
λ^{n-1}	a_{n-1}	a_{n-3}	a_{n-5}	...
λ^{n-2}	b_1	b_2	b_3	...
λ^{n-3}	c_1	c_2	c_3	...
λ^{n-4}	d_1	d_2	d_3	...
$\vdots$	...			

where the coefficients a_i are the coefficients of the characteristic equation (5.88) and b_i, c_i, d_i etc. are defined as:

$$b_1 = \frac{a_{n-1}a_{n-2} - a_n a_{n-3}}{a_{n-1}} \qquad b_2 = \frac{a_{n-1}a_{n-4} - a_n a_{n-5}}{a_{n-1}} \qquad \ldots$$

$$c_1 = \frac{b_1 a_{n-3} - a_{n-1}b_2}{b_1} \qquad c_2 = \frac{b_1 a_{n-5} - a_{n-1}b_3}{b_1} \qquad \ldots$$

$$d_1 = \frac{c_1 b_2 - c_2 b_1}{c_1} \qquad \ldots$$

Necessary and sufficient conditions for the system to be stable are:

1. *All the coefficients of the characteristic equation must exist and have the same sign.*
2. *All the coefficients of the first column of the Routh array must have the same sign.*

If condition 2 is violated, the number of sign changes will indicate how many roots of the characteristic equation which will have positive real parts. Hence, the system will be unstable.

Proof: *Routh (1877).*
□

Forming the Routh array for (5.85) yields:

$$\begin{matrix} A & C \\ B & 0 \\ C & \end{matrix} \tag{5.89}$$

Hence, necessary and sufficient conditions for the ship to be stable are:

$$A,\ B,\ C\ >\ 0 \tag{5.90}$$

The first condition $A > 0$ is automatically satisfied since the vehicle's inertia matrix M always is positive definite. Condition $B > 0$ is also trivial because:

$$n_{11}m_{22} + n_{22}m_{11} > n_{12}m_{21} + n_{21}m_{12} \tag{5.91}$$

for most ships. This relation simply states that the products of the diagonal elements of M and $N(u_0)$ must be larger than the products of the off-diagonal elements. Consequently, condition (5.90) reduces to $C > 0$. This condition can be related to the hydrodynamic derivatives by the following theorem.

Theorem 5.2 (Dynamic Straight-Line Stability (Abkowitz 1964))
A ship is dynamic stable in straight-line motion if the hydrodynamic derivatives satisfy:

$$Y_v(N_r - mx_G u_0) - N_v(Y_r - mu_0) > 0 \tag{5.92}$$

This is based on the assumption that the ship dynamics can be described by the linear model (5.18).
□

From this expression it is seen that making C more positive will improve stability and thus reduce the ship's maneuverability, and the other way around. Straight-line stability implies that the new path of the ship will be a straight line after a disturbance in yaw. The direction of the new path will usually differ from the initial path. As opposed to this, unstable ships will go into a starboard or port turn without any rudder deflection. It should be noted that most modern large tankers are slightly unstable. For such ships, the criterion (5.92) corresponds to one of the poles being in the right half-plane. The stability criterion (5.92) can also be expressed in moment–force ratios. This suggests the equivalent criterion:

$$\frac{N_r - mx_G u_0}{Y_r - mu_0} > \frac{N_v}{Y_v} \tag{5.93}$$

where each side corresponds to the *moment arms* for the yaw force $(Y_r - mu_0)\, r$ and the sway force $Y_v\, v$, respectively. Consequently, straight-line stability implies that the sway force must attack behind the yaw force. If the sway and yaw forces are attacking in the same point the ship is said to be marginally stable.

Straight-Line Stability in Terms of Time Constants

The criterion (5.90) can be related to Nomoto's 2nd-order model by combining (5.86) with (5.25), resulting in:

$$\frac{A}{C} = T_1 T_2 > 0; \qquad \frac{B}{C} = T_1 + T_2 > 0 \tag{5.94}$$

Consequently, straight-line stability is guaranteed if $T_1 > 0$ and $T_2 > 0$. This can also be seen from:

$$\sigma_{1,2} = -\frac{1}{T_{1,2}} = \mathrm{Re}\left\{ \frac{-(B/A) \pm \sqrt{(B/A)^2 - 4(C/A)}}{2} \right\} < 0 \tag{5.95}$$

Semi-Empirical Criterion for Straight-Line Stability

If the hydrodynamic derivatives of the ship are unknown, semi-empirical methods based on the ship hull main dimensions, that is length of hull (L), beam of hull (B) and hull draft (T), can be used to check straight-line stability. For instance, straight-line stability is guaranteed for:

$$\left(\frac{T}{L}\right)^4 \left(5.23 - 3.88\, C_B \left(\frac{B}{T}\right) + 0.0050 \left(\frac{L}{T}\right)^2\right) > 0 \tag{5.96}$$

Here the block coefficient is defined as:

$$C_B \triangleq \frac{\nabla}{LBT} \tag{5.97}$$

where ∇ is the displaced volume of the ship. For large tankers $C_B \approx 0.80$–0.84, for line carriers $C_B \approx 0.60$–0.70 whereas a fast container ship satisfies $C_B \approx 0.55$–0.60. The criterion (5.96) is illustrated graphically in Figure 5.14 where B/T is plotted versus L/T according to the lines:

$$5.23 - 3.88\, C_B \left(\frac{B}{T}\right) + 0.0050 \left(\frac{L}{T}\right)^2 = 0 \tag{5.98}$$

The hull length is usually chosen as $L = L_{pp}$ where L_{pp} is the length between the fore and aft perpendiculars. The fore perpendicular (FP) is usually taken as the intersection of the stem with the water line at the design load, and the aft perpendicular (AP) is often referred to as the line through the rudder stock.

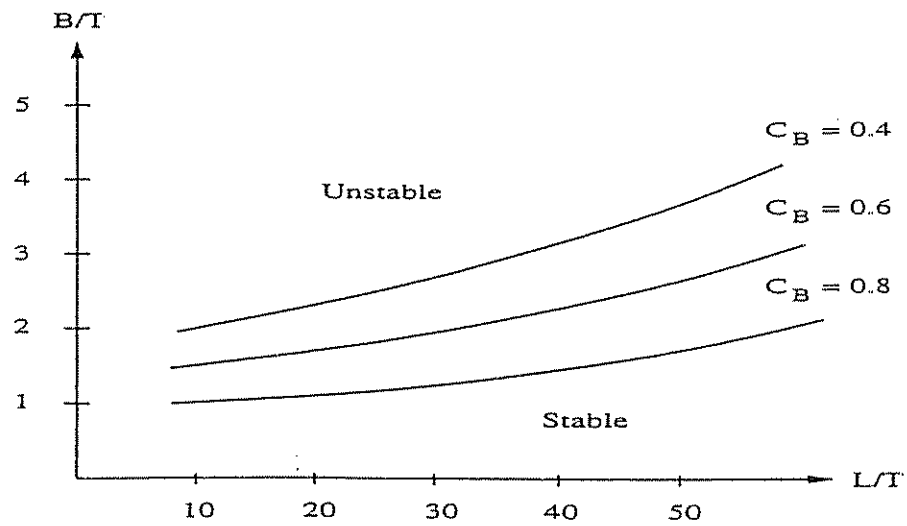

Figure 5.14: Semi-empirical criterion for straight-line stability.

5.5.4 Dynamic Stability on Course

Dynamic stability on course or directional stability cannot be obtained without activating the rudder. Usually an automatic control system is used to generate the necessary rudder action to stabilize the ship. This is often referred to as controls-free stability analysis.

For simplicity, we will consider the automatic control system of proportional and derivative (PD) type described by:

$$\delta = K_p\,(\psi_d - \psi) - K_d\,r \tag{5.99}$$

Here the constant ψ_d is the desired heading angle. The PD-control law requires that both the heading angle and the heading rate are measured or at least estimated. This can be done by applying a compass and a rate sensor, for instance. Substituting the PD-control law into Nomoto's 2nd-order model, yields the closed-loop dynamics:

$$T_1T_2\,\psi^{(3)} + (T_1 + T_2 + T_3KK_d)\,\ddot{\psi} + (1 + KK_d + T_3KK_p)\,\dot{\psi} + KK_p\,\psi = KK_p\,\psi_d \tag{5.100}$$

From this expression, we can form the cubic characteristic equation:

$$A\,\sigma^3 + B\,\sigma^2 + C\,\sigma + D = 0 \tag{5.101}$$

where

$$\begin{aligned} A &= T_1T_2 && (5.102)\\ B &= T_1 + T_2 + T_3KK_d && (5.103)\\ C &= 1 + KK_d + T_3KK_p && (5.104)\\ D &= KK_p && (5.105) \end{aligned}$$

Forming the so-called Routh array yields:

$$\begin{array}{ll} A & C \\ B & D \\ \frac{BC-AD}{B} & 0 \\ D & \end{array} \tag{5.106}$$

Hence, sufficient and necessary conditions for the ship to be dynamic stable on course are:

$$\begin{aligned} &\text{(i)} && A, B, C, D > 0 && (5.107)\\ &\text{(ii)} && BC - AD > 0 && (5.108) \end{aligned}$$

Hence, K_p and K_d must be chosen such that the conditions (5.107) and (5.108) are satisfied.

5.6 Nonlinear Ship Steering Equations

Obvious limitations of the linear ship steering equations of motion like the assumption of small rudder angles can be avoided by considering nonlinear modeling techniques. Some frequently used nonlinear ship steering equations of motion are described in this section.

5.6.1 The Nonlinear Model of Abkowitz (1964)

Recall from (5.1) that the rigid-body equations of motion can be written as:

$$\begin{aligned} m(\dot{u} - vr - x_G r^2) &= X \\ m(\dot{v} + ur + x_G \dot{r}) &= Y \\ I_z \dot{r} + m x_G (\dot{v} + ur) &= N \end{aligned} \tag{5.109}$$

Based on these equations, Abkowitz (1964) has proposed using a 3rd-order truncated *Taylor series* expansion of the functions X, Y and N at $u = u_0$, $v = 0$ and $r = 0$. Moreover,

$$\begin{aligned} X &= X(\Delta u, v, r, \dot{u}, \dot{v}, \dot{r}, \delta) \\ Y &= Y(\Delta u, v, r, \dot{u}, \dot{v}, \dot{r}, \delta) \\ N &= N(\Delta u, v, r, \dot{u}, \dot{v}, \dot{r}, \delta) \end{aligned} \tag{5.110}$$

where $\Delta u = u - u_0$. Notice that $\Delta v = v$ and $\Delta r = r$. A Taylor series expansion of these functions can be obtained by applying the following definition:

Definition 5.1 (n-th Order Taylor Series Expansion)
Consider the nonlinear function $f(\boldsymbol{x})$ with argument $\boldsymbol{x} = [x_1, ..., x_k]^T$. Let the nominal values be defined by the vector $\boldsymbol{x}_0$. Hence, the Taylor series expansion of the function $f(\boldsymbol{x})$ at $\boldsymbol{x}_0$ is defined as:

$$f(\boldsymbol{x}) = f(\boldsymbol{x}_0) + Df(\boldsymbol{x})|_{\boldsymbol{x}_0} + \frac{1}{2} D^2 f(\boldsymbol{x})\Big|_{\boldsymbol{x}_0} + \frac{1}{6} D^3 f(\boldsymbol{x})\Big|_{\boldsymbol{x}_0} + ... + \frac{1}{n!} D^n f(\boldsymbol{x})|_{\boldsymbol{x}_0} \tag{5.111}$$

where $\Delta \boldsymbol{x} = \boldsymbol{x} - \boldsymbol{x}_0$ and:

$$D = \left(\Delta x_1 \frac{\partial}{\partial x_1} + \Delta x_2 \frac{\partial}{\partial x_2} + \Delta x_3 \frac{\partial}{\partial x_3} + ... + \Delta x_k \frac{\partial}{\partial x_k} \right) \tag{5.112}$$

□

A 3rd-order Taylor series expansion of the functions (5.110) will consist of a large number of terms. By applying some physical insight, the complexity of these expressions can be reduced. Abkowitz (1964) makes the following assumptions:

Assumptions:

1. *Most ship maneuvers can be described with a 3rd-order truncated Taylor expansion about the steady state condition $u = u_0$.*
2. *Only 1st-order acceleration terms are considered.*
3. *Standard port/starboard symmetry simplifications except terms describing the constant force and moment arising from single-screw propellers.*
4. *The coupling between the acceleration and velocity terms is negligible.*

Simulations of standard ship maneuvers show that these assumptions are quite good. Applying these assumptions to the functions (5.110) yields:

$$\begin{aligned}
X &= X^* + X_{\dot{u}}\dot{u} + X_u\Delta u + X_{uu}\Delta u^2 + X_{uuu}\Delta u^3 + X_{vv}v^2 + X_{rr}r^2 + X_{\delta\delta}\delta^2 \\
&+ X_{rv}rv\delta + X_{r\delta}r + X_{v\delta}v\delta + X_{vvu}v^2\Delta u + X_{rru}r^2\Delta u + X_{\delta\delta u}\delta^2\Delta u \\
&+ X_{rvu}rvu + X_{r\delta u}r\delta\Delta u + X_{v\delta u}v\delta\Delta u \\
Y &= Y^* + Y_u\Delta u + Y_{uu}\Delta u^2 + Y_{\dot{r}}\dot{r} + Y_{\dot{v}}\dot{v} + Y_\delta\delta + Y_{rrr}r^3 + Y_{vvv}v^3 \\
&+ Y_{\delta\delta\delta}\delta^3 + Y_{rr\delta}r^2\delta + Y_{\delta\delta r}\delta^2 r + Y_{rrv}r^2v + Y_{vvr}v^2r + Y_{\delta\delta v}\delta^2 v + Y_{vv\delta}v^2\delta + Y_{\delta vr}\delta vr \\
&+ Y_{vu}v\Delta u + Y_{vuu}v\Delta u^2 + Y_{ru}r\Delta u + Y_{ruu}r\Delta u^2 + Y_{\delta u}\delta\Delta u + Y_{\delta uu}\delta\Delta u^2 \\
N &= N^* + N_u\Delta u + N_{uu}\Delta u^2 + N_{\dot{r}}\dot{r} + N_{\dot{v}}\dot{v} + N_\delta\delta + N_{rrr}r^3 + N_{vvv}v^3 \\
&+ N_{\delta\delta\delta}\delta^3 + N_{rr\delta}r^2\delta + N_{\delta\delta r}\delta^2 r + N_{rrv}r^2v + N_{vvr}v^2r + N_{\delta\delta v}\delta^2 v + N_{vv\delta}v^2\delta \\
&+ N_{\delta vr}\delta vr + N_{vu}v\Delta u + N_{vuu}v\Delta u^2 + N_{ru}r\Delta u + N_{ruu}r\Delta u^2 + N_{\delta u}\delta\Delta u \\
&+ N_{\delta uu}\delta\Delta u^2
\end{aligned} \tag{5.113}$$

Here the partial derivatives are defined as:

$$A_\nu \triangleq \alpha\frac{\partial A}{\partial \nu}; \qquad \alpha \in \left\{1, \frac{1}{2}, \frac{1}{6}, \ldots, \frac{1}{n!}\right\} \tag{5.114}$$

with obvious choices of A and ν. Notice that for simplicity, the factor α is incorporated in the definition of the hydrodynamic derivatives. A large number of mathematical models are based on simplifications and modifications of Abkowitz's model.

5.6.2 The Nonlinear Model of Norrbin (1970)

Norrbin (1970) has proposed using a nonlinear mathematical model for ship maneuvering in deep and confined waters. This model is based on both experimental and analytical methods.

Norrbin's model consists essentially of three principal equations describing the axial and transverse forces (X and Y) and yaw moment (N). Coefficients and parameters are made non-dimensional by applying the *Bis-system* (see Section 5.3.3). For *deep* water Norrbin's model takes the following form:

Speed Equation:

$$(1 - X''_{\dot{u}})\,\dot{u} = L^{-1}\,\frac{1}{2}X''_{uu}u^2 + L^{-2}g^{-1}\,\frac{1}{24}X''_{uuuu}u^4 + g\,(1-t)\,T'' + (1 + X''_{vr})vr$$
$$+L(x''_G + \frac{1}{2}X''_{rr})r^2 + L^{-2}g^{-1}\,\frac{1}{6}X''_{uvvv}u|v|v^2 + L^{-1}\frac{1}{4}X_{c|c|\delta\delta}\,|c|c\delta_e^2 \quad (5.115)$$

Steering Equations:

$$(1 - Y''_{\dot{v}})\,\dot{v} = L(Y''_{\dot{r}} - x''_G)\dot{r} + (Y''_{ur} - 1)ur + (Lg)^{-1/2}\,\frac{1}{2}Y''_{uur}u^2r + L^{-1}Y''_{uv}uv$$
$$+L^{-3/2}g^{-1/2}\,\frac{1}{2}Y''_{uuv}u^2v + L^{-1}\,\frac{1}{2}Y''_{|v|v}\,|v|v + L\,\frac{1}{2}Y''_{|r|r}\,|r|r + Y''_{|v|r}\,|v|r + Y''_{v|r|}\,v|r|$$
$$+L^{-1}\,\frac{1}{2}Y''_{|c|c\delta}\,|c|c\delta_e + k_\gamma g\,T'' \quad (5.116)$$

$$((k''_z)^2 - N''_{\dot{r}})\,\dot{r} = L^{-1}(N''_{\dot{v}} - x''_G)\dot{v} + L^{-1}(N''_{ur} - x''_G)ur + L^{-3/2}g^{-1/2}\,\frac{1}{2}N''_{uur}u^2r$$
$$+L^{-2}\,N''_{uv}uv + L^{-5/2}g^{-1/2}\,\frac{1}{2}N''_{uuv}u^2v + L^{-2}\,\frac{1}{2}N''_{|v|v}\,|v|v + \frac{1}{2}N''_{|r|r}\,|r|r$$
$$+L^{-1}\,N''_{|v|r}\,|v|r + L^{-1}\,N''_{v|r|}\,v|r| + L^{-2}\,\frac{1}{2}N''_{|c|c\delta}\,|c|c\delta_e + L^{-1}g\,k_N T'' \quad (5.117)$$

where

δ_e	=	effective rudder angle ($\delta_e = \delta$ for $v = r = 0$)
c	=	flow velocity past rudder
T''	=	non-dimensional propeller thrust
t	=	thrust deduction factor
$(k''_z)^2 = I''_z$	=	non-dimensional squared radius of gyration
g	=	acceleration of gravity
L	=	length of hull

The *radius of gyration* with respect to the z-axis is defined as:

$$k_z \triangleq \sqrt{\frac{I_z}{m}} \quad (5.118)$$

This number simply tells how far from the z-axis the entire mass m might be concentrated and still give the same I_z. Semi-empirical methods for estimation of the force and moment derivatives are found in Norrbin (1970).

A quasi-stationary approach can be used to model the effective rudder angle. Norrbin (1970) gives the following expression for δ_e:

$$\delta_e = \delta + (k_v\frac{v}{c} + k_r\frac{Lr}{2c})\,|\delta| \quad (5.119)$$

Here δ is the rudder angle and typical values for k_v and k_r are $k_v = -0.5$ and $k_r = 0.5$. Norrbin (1970) suggests approximating the flow velocity past the rudder for positive thrust from the open water propeller diagram as:

$$c^2 = \frac{1}{2}c_{uu}^2 u^2 + c_{un}^2 un + \frac{1}{2}c_{|n|n}^2 |n|n + \frac{1}{2}c_{nn}^2 n^2 \tag{5.120}$$

Here n is the propeller revolution. The four constants in this equation depend on the screw characteristics as well as the wake factors. Besides, the equation for the flow velocity c at the rudder an auxiliary equation for the propeller thrust T is needed. This equation is written:

$$g\,T'' = L^{-1}\,\frac{1}{2}\,T''_{uu}u^2 + T''_{un}un + L\,\frac{1}{2}\,T_{|n|n}|n|n + L\,\frac{1}{2}\,T_{nn}n^2 \tag{5.121}$$

In Appendix E.1.2 a more general version of this model describing large tankers in deep and confine waters is presented.

5.6.3 The Nonlinear Model of Blanke (1981)

A simplified form of Norrbin's nonlinear model which retains the most important terms for steering and propulsion loss assignment has been proposed by Blanke (1981). For convenience, we will write this model in dimensional form according to (see Section 5.2):

Speed Equation:

$$(m - X_{\dot{u}})\,\dot{u} = X_{|u|u}\,|u|u + (1-t)\,T + T_{\text{loss}} \tag{5.122}$$

where the loss term is:

$$T_{\text{loss}} = (m + X_{vr})\,vr + (mx_G + X_{rr})\,r^2 + X_{\delta\delta}\,\delta^2 + X_{\text{ext}} \tag{5.123}$$

In addition to this simplification, Blanke suggests that the terms $X_{\dot{u}}$ and $(mx_G + X_{rr})$ can be taken to be zero since these terms will be quite small for most ships. In fact, $X_{\dot{u}}$ will typically be less than 5 % of the ship mass. The last term is multiplied with the square angular rate r^2, which will be less than 0.0003 $(\text{rad/s})^2$ for a ship limited by a turning rate of $r_{\max} = 1$ (deg/s) $= 0.0175$ (rad/s).

Steering Equations:

$$\begin{aligned}&(m - Y_{\dot{v}})\,\dot{v} + (mx_G - Y_{\dot{r}})\,\dot{r} = \\ &\quad -(m - Y_{ur})\,ur + Y_{uv}\,uv + Y_{|v|v}\,|v|v + Y_{|v|r}\,|v|r + Y_{\delta}\,\delta + Y_{\text{ext}}\end{aligned} \tag{5.124}$$

$$\begin{aligned}&(mx_G - N_{\dot{v}})\,\dot{v} + (I_z - N_{\dot{r}})\,\dot{r} = \\ &\quad -(mx_G - N_{ur})\,ur + N_{uv}\,uv + N_{|v|v}\,|v|v + N_{|v|r}\,|v|r + N_{\delta}\,\delta + N_{\text{ext}}\end{aligned} \tag{5.125}$$

It should be noted that all models discussed so far in this chapter are based on the assumption that the ship motion is restricted to the horizontal plane. In the next section, we will show how the roll motion can be included as well to describe the coupled ship motion in 4 DOF; that is surge, sway, roll and yaw.

5.7 Coupled Equations for Steering and Rolling

Consider a ship with homogeneous mass distribution and xz-plane symmetry, that is $I_{xy} = I_{yz} = 0$ and $y_G = 0$. In addition to this, we will choose the origin of the body-fixed coordinate system such that $I_{xz} = 0$ by defining $\boldsymbol{r}_G = [x_G, 0, z_G]^T$. The assumption that the motion in heave and pitch can be neglected, that is $\dot{w} = \dot{q} = w = q = 0$, implies that the general expression (2.89) for the rigid-body dynamics reduces to:

$$\begin{array}{lrcl} \text{Surge:} & m(\dot{u} - vr - x_G r^2 + z_G pr) & = & X \\ \text{Sway:} & m(\dot{v} + ur + x_G \dot{r} - z_G \dot{p}) & = & Y \\ \text{Roll:} & I_x \dot{p} - m z_G(\dot{v} + ur) & = & K - W\,\overline{GM}_T\,\phi \\ \text{Yaw:} & I_z \dot{r} + m x_G(\dot{v} + ur) & = & N \end{array} \tag{5.126}$$

where we have added the metacentric restoring moment in roll to the right-hand side of the third equation. We recall from Section 5.5.2, Equation (5.71), that this moment can be written:

$$K_\phi = W\,\overline{GM}_T\,\sin\phi \approx W\,\overline{GM}_T\,\phi \tag{5.127}$$

where $W = mg$ is the weight of water in kg m/s^2 displaced by the ship hull. In the forthcoming sections we will discuss different choices for the hydrodynamic forces and moments X, Y, K and N.

5.7.1 The Model of Van Amerongen and Van Cappelle (1981)

Modern roll stabilization systems like fins, anti-roll tanks and high-frequency rudder action are used alone or in combination on most passenger and naval ships. In such systems the low-frequency rudder motion is used exclusively to control the heading. Since anti-roll tanks are expensive and also require considerably space, the combination of fins and rudder seems to be an attractive alternative for roll damping. However, fin motions as well as high-frequency rudder motions disturb the heading control system. In order to reduce this interaction, Van Amerongen and Van Cappelle (1981) have proposed an explicit linear model describing these couplings in terms of the transfer between the fin and rudder angles to the linear and angular velocity in sway and yaw, respectively.

Linear Ship Model for Combined Fin and Rudder Control

Consider a ship with port and starboard fins where α is used to denote the fin angle deflections. For simplicity, we will assume that neither of the fins can be

controlled independently. Let δ be the rudder deflection. Hence, the combined model can be written:

$$M\,\dot{\nu} + N\,\nu + G\,\eta = B\,u \tag{5.128}$$

where $\nu = [v, p, r]^T$ and $\eta = [y, \phi, \psi]^T$ are the states and $u = [\alpha, \delta]^T$ is the control vector. The corresponding matrices are:

$$M = \begin{bmatrix} m - Y_{\dot{v}} & -mz_G - Y_{\dot{p}} & mx_G - Y_{\dot{r}} \\ -mz_G - K_{\dot{v}} & I_x - K_{\dot{p}} & mx_G - K_{\dot{r}} \\ mx_G - N_{\dot{v}} & mx_G - N_{\dot{p}} & I_z - N_{\dot{r}} \end{bmatrix} \quad N = \begin{bmatrix} -Y_v & -Y_p & mu_0 - Y_r \\ -K_v & -K_p & -mz_G u_0 - K_r \\ -N_v & -N_p & mx_G u_0 - N_r \end{bmatrix}$$

$$G = \begin{bmatrix} 0 & 0 & 0 \\ 0 & W\overline{GM}_T & 0 \\ 0 & 0 & \end{bmatrix} \quad B = \begin{bmatrix} Y_\alpha & Y_\delta \\ K_\alpha & K_\delta \\ N_\alpha & N_\delta \end{bmatrix}$$

In addition to these equations, the kinematic equations (assuming $q = \theta = 0$):

$$\dot{\phi} = p \qquad \dot{\psi} = \cos\phi\, r \approx r \tag{5.129}$$

are used to describe the roll and yaw angle. Applying the *Laplace transformation* to this system, the following equivalent representation is obtained:

$$\phi(s) = \omega_n^2\, \frac{K_\delta\,\delta(s) + K_\alpha\,\alpha(s) - K_r\,r(s)}{s^2 + 2\,\zeta\,\omega_n\,s + \omega_n^2} \tag{5.130}$$

$$r(s) = s\,\psi(s) = \frac{N_\delta\,\delta(s) + N_\alpha\,\alpha(s) - N_\phi\,\phi(s)}{1 + T_r\,s} \tag{5.131}$$

where ζ and ω_n are the relative damping ratio and natural frequency in roll, respectively and T_r is dominant time constant in sway. This model suggests that a multivariable control system can be designed for heading control and roll damping.

5.7.2 The Model of Son and Nomoto (1981)

A nonlinear rolling coupled steering model for high speed container ships has been proposed by Son and Nomoto (1981, 1982). In this work, the rigid-body dynamics including the contribution from the hydrodynamic added mass derivatives, is written:

$$(m + m_x)\,\dot{u} - (m + m_y)\,vr = X \tag{5.132}$$

$$(m + m_y)\,\dot{v} + (m + m_x)\,ur + m_y\,\alpha_y\,\dot{r} - m_y l_y\,\dot{p} = Y \tag{5.133}$$

$$(I_x + J_x)\,\dot{p} - m_y l_y\,\dot{v} - m_x l_x\,ur = K - W\,\overline{GM}_T\,\phi \tag{5.134}$$

$$(I_z + J_z)\,\dot{r} + m_y \alpha_y\,\dot{v} = N - x_G Y \tag{5.135}$$

where m_x, m_y, J_x and J_y denote the added mass and added moment of inertia in the x- and y-directions about the z- and x-axes, respectively. The center of added mass for m_y is denoted by α_y (x-coordinate) while l_x and l_y are the added mass z-coordinates of m_x and m_y, respectively. The terms on the right-hand side of these four equations are defined as:

$$X = X(u) + (1-t)\,T + X_{vr}\,vr + X_{vv}\,v^2 + X_{rr}\,r^2 + X_{\phi\phi}\,\phi^2 + X_{\delta}\,\sin\delta + X_{\text{ext}} \tag{5.136}$$

$$Y = Y_v\,v + Y_r\,r + Y_\phi\,\phi + Y_p\,p + Y_{vvv}\,v^3 + Y_{rrr}\,r^3 + Y_{vvr}\,v^2 r + Y_{vrr}\,vr^2 + Y_{vv\phi}\,v^2\phi + Y_{v\phi\phi}\,v\phi^2 + Y_{rr\phi}\,r^2\phi + Y_{r\phi\phi}\,r\phi^2 + Y_\delta\,\cos\delta + Y_{\text{ext}} \tag{5.137}$$

$$K = K_v\,v + K_r\,r + K_\phi\,\phi + K_p\,p + K_{vvv}\,v^3 + K_{rrr}\,r^3 + K_{vvr}\,v^2 r + K_{vrr}\,vr^2 + K_{vv\phi}\,v^2\phi + K_{v\phi\phi}\,v\phi^2 + K_{rr\phi}\,r^2\phi + K_{r\phi\phi}\,r\phi^2 + K_\delta\,\cos\delta + K_{\text{ext}} \tag{5.138}$$

$$N = N_v\,v + N_r\,r + N_\phi\,\phi + N_p\,p + N_{vvv}\,v^3 + N_{rrr}\,r^3 + N_{vvr}\,v^2 r + N_{vrr}\,vr^2 + N_{vv\phi}\,v^2\phi + N_{v\phi\phi}\,v\phi^2 + N_{rr\phi}\,r^2\phi + N_{r\phi\phi}\,r\phi^2 + N_\delta\,\cos\delta + N_{\text{ext}} \tag{5.139}$$

where $X(u)$ is a velocity-dependent damping function, for instance $X(u) = X_{|u|u}\,|u|u$. A more general model description together with numerical values for the hydrodynamic derivatives of a container ship is found in Appendix E.1.3.

5.7.3 The Model of Christensen and Blanke (1986)

An alternative model formulation describing the steering and roll motion of ships has been proposed by Christensen and Blanke (1986). We will first discuss a nonlinear representation of the coupled steering and roll dynamics and then show how a linearized state-space model can be obtained.

Nonlinear Model in Steering and Roll

Christensen and Blanke suggested that the nonlinear steering and roll dynamics can be approximated by the following set of equations:

$$\begin{bmatrix} m-Y_{\dot v} & -mz_G-Y_{\dot p} & mx_G-Y_{\dot r} & 0 & 0 \\ -mz_G-K_{\dot v} & I_x-K_{\dot p} & 0 & 0 & 0 \\ mx_G-N_{\dot v} & 0 & I_z-N_{\dot r} & 0 & 0 \\ 0 & 0 & 0 & 1 & 0 \\ 0 & 0 & 0 & 0 & 1 \end{bmatrix} \begin{bmatrix} \dot v \\ \dot p \\ \dot r \\ \dot\phi \\ \dot\psi \end{bmatrix} =$$

$$\begin{bmatrix} Y_{uv}|u| & Y_{|u|p}|u| & -mu+Y_{ur}u & Y_{uu\phi}u^2 & 0 \\ K_{|u|v}|u| & K_{up}u+K_p & K_{ur}u & \overline{WGM}_T+K_{uu\phi}u^2 & 0 \\ N_{uv}u & 0 & N_{|u|r}|u|-mx_Gu & N_{|u|u\phi}|u|u & 0 \\ 0 & 1 & 0 & 0 & 0 \\ 0 & 0 & 1 & 0 & 0 \end{bmatrix} \begin{bmatrix} v \\ p \\ r \\ \phi \\ \psi \end{bmatrix} + \begin{bmatrix} Y_{\text{ext}} \\ K_{\text{ext}} \\ N_{\text{ext}} \\ 0 \\ 0 \end{bmatrix}$$

where the forces and moments associated with the roll motion are assumed to involve the square term of the surge speed u^2 and $|u|u$. The terms Y_{ext}, K_{ext} and N_{ext} consist of possible contributions from external disturbances, rudders, propellers, bow thrusters and other devices.

Linearized State-Space Model in Steering and Roll

For simplicity we will assume that the only external forces and moments are caused by a single rudder whereas the rudder angle is denoted by δ. Linear theory suggests that the rudder forces and moments can be represented by the vector:

$$[Y_{\text{ext}},\ K_{\text{ext}},\ N_{\text{ext}},\ 0,\ 0]^T = [Y_\delta,\ K_\delta,\ N_\delta,\ 0,\ 0]^T\ \delta \tag{5.140}$$

Linearization of the above nonlinear model about $u = u_0$ (service speed) implies that we can write the linearized model in standard state-space form:

$$\dot{\boldsymbol{x}} = \boldsymbol{A}\,\boldsymbol{x} + \boldsymbol{b}\,\delta \tag{5.141}$$

For notational convenience, we will define the state vector as $\boldsymbol{x} = [v, r, p, \phi, \psi]^T$ and the elements associated with $\boldsymbol{A}$ and $\boldsymbol{b}$ according to:

$$\begin{bmatrix} \dot{v} \\ \dot{r} \\ \dot{p} \\ \dot{\phi} \\ \dot{\psi} \end{bmatrix} = \begin{bmatrix} a_{11} & a_{12} & a_{13} & a_{14} & 0 \\ a_{21} & a_{22} & a_{23} & a_{24} & 0 \\ a_{31} & a_{32} & a_{33} & a_{34} & 0 \\ 0 & 0 & 1 & 0 & 0 \\ 0 & 1 & 0 & 0 & 0 \end{bmatrix} \begin{bmatrix} v \\ r \\ p \\ \phi \\ \psi \end{bmatrix} + \begin{bmatrix} b_1 \\ b_2 \\ b_3 \\ 0 \\ 0 \end{bmatrix} \delta \tag{5.142}$$

with obvious definitions of a_{ij} and b_i; see Christensen and Blanke (1986) for details.

Decompositions in Roll and Sway-Yaw Subsystems

To simplify the system for further analysis, we can reorganize the state vector again such that state variables associated with the steering and roll dynamics are separated. Moreover, (5.142) can be rewritten as:

$$\left[\begin{array}{c} \dot{v} \\ \dot{r} \\ \dot{\psi} \\ \hline \dot{p} \\ \dot{\phi} \end{array}\right] = \left[\begin{array}{ccc|cc} a_{11} & a_{12} & 0 & a_{13} & a_{14} \\ a_{21} & a_{22} & 0 & a_{23} & a_{24} \\ 0 & 1 & 0 & 0 & 0 \\ \hline a_{31} & a_{32} & 0 & a_{33} & a_{34} \\ 0 & 0 & 0 & 1 & 0 \end{array}\right] \left[\begin{array}{c} v \\ r \\ \psi \\ \hline p \\ \phi \end{array}\right] + \left[\begin{array}{c} b_1 \\ b_2 \\ 0 \\ \hline b_3 \\ 0 \end{array}\right] \delta \tag{5.143}$$

Introducing the notation:

$$\begin{bmatrix} \dot{x}_\psi \\ \dot{x}_\phi \end{bmatrix} = \begin{bmatrix} A_{\psi\psi} & A_{\psi\phi} \\ A_{\phi\psi} & A_{\phi\phi} \end{bmatrix} \begin{bmatrix} x_\psi \\ x_\phi \end{bmatrix} + \begin{bmatrix} b_\psi \\ b_\phi \end{bmatrix} \delta \tag{5.144}$$

where $x_\psi = [v, r, \psi]^T$ and $x_\phi = [p, \phi]^T$ implies that the total system can be described by the partitions:

$$\begin{aligned} &\text{(sway-yaw dynamics)} && \dot{x}_\psi = A_{\psi\psi}x_\psi + A_{\psi\phi}x_\phi + b_\psi\delta \\ &\text{(roll dynamics)} && \dot{x}_\phi = A_{\phi\phi}x_\phi + A_{\phi\psi}x_\psi + b_\phi\delta \end{aligned}$$

corresponding to Figure 5.15.

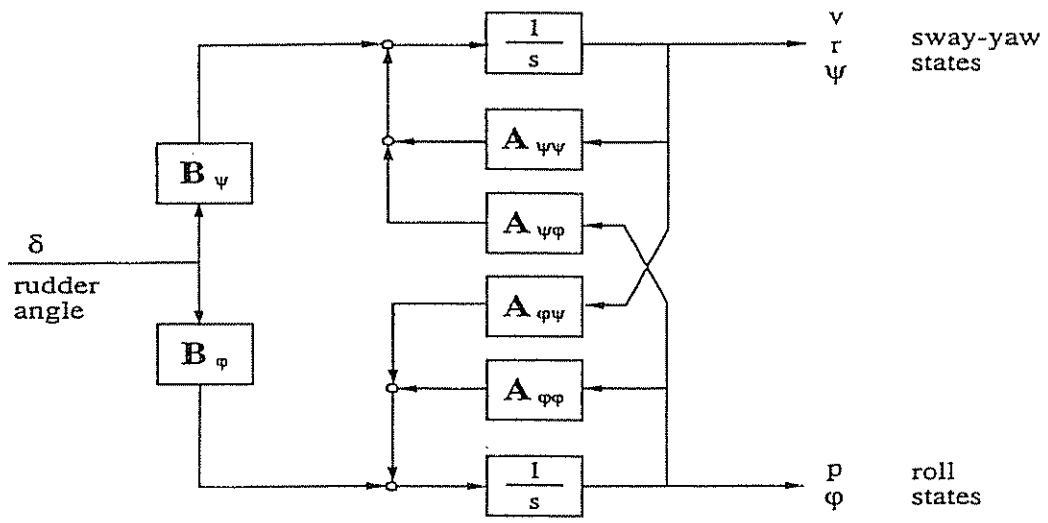

Figure 5.15: Diagram showing the sway-yaw and roll subsystems (Christensen and Blanke 1986).

Neglecting the coupling matrices ($A_{\psi\phi} = A_{\phi\psi} = 0$) implies that:

$$\begin{bmatrix} \dot{p} \\ \dot{\phi} \end{bmatrix} = \begin{bmatrix} a_{33} & a_{34} \\ 1 & 0 \end{bmatrix} \begin{bmatrix} p \\ \phi \end{bmatrix} + \begin{bmatrix} b_3 \\ 0 \end{bmatrix} \delta \tag{5.145}$$

and

$$\begin{bmatrix} \dot{v} \\ \dot{r} \\ \dot{\psi} \end{bmatrix} = \begin{bmatrix} a_{11} & a_{12} & 0 \\ a_{21} & a_{22} & 0 \\ 0 & 1 & 0 \end{bmatrix} \begin{bmatrix} v \\ r \\ \psi \end{bmatrix} + \begin{bmatrix} b_1 \\ b_2 \\ 0 \end{bmatrix} \delta \tag{5.146}$$

where the last expression is recognized as the Nomoto model.

5.8 Steering Maneuvering Characteristics

Standard ship maneuvers can be used to evaluate the robustness, performance and limitations of the ship control system. This is usually done by defining a criterion in terms of a maneuvering index or by simply using a maneuvering characteristic to compare the maneuverability of the test ship with previously obtained results from other ships.

A maneuvering characteristic can be obtained by changing or keeping a predefined course and speed of the ship in a systematic manner by means of working controls. For most surface vessels these controls are rudders, fins, propellers and thrusters. However, since ship maneuverability depends on the water depth, environmental disturbances, ship speed and hydrodynamic derivatives etc. care must be taken when performing a full-scale maneuvering test. We will now discuss different standard tests that are well suited for this purpose. A guide for sea trials describing how these maneuvers should be performed is found in SNAME (1989).

5.8.1 Full-Scale Maneuvering Trials

As mentioned above the different maneuvering characteristics of the ship can be determined by full-scale maneuvering trials. The data from these tests can be used to evaluate dynamic stability, turning diameter, model parameters of the ship etc. For sea trials, the following standard ship maneuvers have been proposed by the International Towing Tank Conference (ITTC):

- **Turning Circle.** This trial is mainly used to calculate the ship's steady turning radius and to check how well the steering machine performs under course-changing maneuvers.

- **Kempf's Zig-Zag Maneuver.** The zig-zag test is a standard maneuver used to compare the maneuvering properties and control characteristic of a ship with those of other ships. Another feature is that the experimental results of the test can be used to calculate the K and T values of Nomoto's 1st-order model.

- **Pull-Out Maneuver.** The pull-out maneuver can be used to check whether the ship is straight-line stable or not. The maneuver can also be used to indicate the degree of stability.

- **Dieudonné's Spiral Maneuver.** The spiral maneuver is also used to check straight-line stability. The maneuver gives an indication of the range of validity of the linear theory.

- **Bech's Reverse Spiral Maneuver.** The reverse spiral maneuver can be used for unstable ships to produce a nonlinear maneuvering characteristic. The results from the test indicate which rudder corrections that are required to stabilize an unstable ship.

- **Stopping Trials.** Crash-stops and low-speed stopping trials can be used to determine the ship's head reach and maneuverability during emergency situations.

Turning Circle

This is probably the oldest maneuvering test. The test can be used as an indication on how well the steering machine and rudder control performs during course-changing maneuvers. It is also used to calculate standard measures of maneuverability like *tactical diameter*, *advance* and *transfer* (Figure 5.16); see Gertler and Hagen (1960) for a detailed description.

The *steady turning radius* R is perhaps the most interesting quantity obtained from the turning trials. In the maneuvering trial code of the 14th ITTC (1975) it is proposed to turn the ship over at maximum speed and with a rudder angle of minimum 15 degrees to obtain the turning circle. The rudder angle δ should be held constant such that a constant rate of turn is reached (in practice a turning circle of 540 degrees may be necessary).

The output from a positioning system is used to calculate the tactical diameter, steady turning radius, maximum advance and maximum transfer. A typically turning circle corresponding to a negative rudder angle is shown in Figure 5.16.

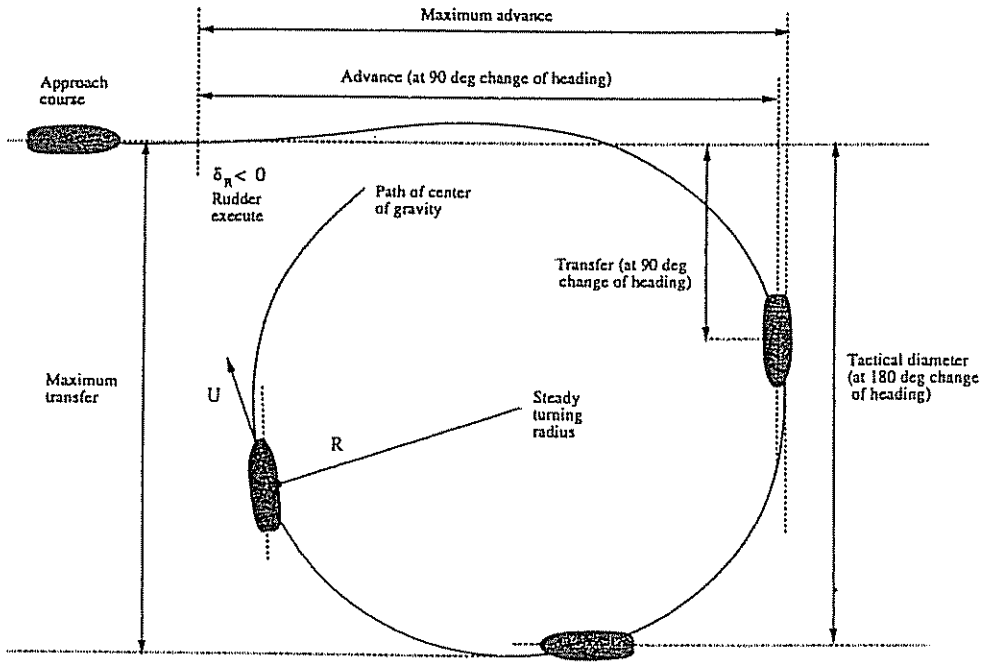

Figure 5.16: Turning circle for a constant rudder angle $\delta_R < 0$ ($\delta > 0$).

Since the ship will move in a circle with constant radius in steady state, both r and v will be constant and thus $\dot{v} = \dot{r} = 0$. Solving (5.18) for the steady-state solution of v and r, yields:

$$\begin{bmatrix} -Y_v & mu_0 - Y_r \\ -N_v & mx_G u_0 - N_r \end{bmatrix} \begin{bmatrix} v \\ r \end{bmatrix} = \begin{bmatrix} Y_\delta \\ N_\delta \end{bmatrix} \delta_R \tag{5.147}$$

Eliminating v from this expression yields:

$$r = -\frac{(Y_v N_\delta - N_v Y_\delta)}{Y_v(N_r - m x_G u_0) - N_v(Y_r - m u_0)}\,\delta_R \tag{5.148}$$

Consequently, the ship's turning radius R can be defined as:

$$R \triangleq \frac{U}{r} \qquad \text{where} \qquad U = \sqrt{u^2 + v^2} \tag{5.149}$$

Introducing the length $L = L_{pp}$ of the ship and the definition $\delta = -\delta_R$, the following expression for the ratio (R/L) is obtained:

$$\left(\frac{R}{L}\right) = \left(\frac{U}{L}\right)\frac{C}{(Y_v N_\delta - N_v Y_\delta)}\,\frac{1}{\delta} \tag{5.150}$$

where C is recognized as one of the stability derivatives in the straight-line stability criterion discussed in Section 5.5.3, that is:

$$C = Y_v(N_r - m x_G u_0) - N_v(Y_r - m u_0) > 0 \qquad \text{(stable ship)} \tag{5.151}$$

In fact, C will be positive for most ships with aft rudder. This is due to the fact that:

$$\begin{array}{lcll} Y_v & < & 0 & \text{always} \\ N_\delta & < & 0 & \text{for aft rudder} \\ Y_\delta & > & 0 & \text{always} \\ N_v & < & 0 & \text{for most ships} \end{array}$$

In the few cases where $N_v > 0$, N_v will usually be so small that $Y_v N_\delta > N_v Y_\delta$ still holds. From (5.150) it is seen that increased stability (large C) implies that the turning radius will increase. Consequently, a highly stable ship requires more maneuvering effort than a marginally stable one. The ratio (R/L) can be written in terms of non-dimensional quantities by:

$$\left(\frac{R}{L}\right) = \frac{Y'_v(N'_r - m' x'_G) - N'_v(Y'_r - m')}{(Y'_v N'_\delta - N'_v Y'_\delta)}\,\frac{1}{\delta} \tag{5.152}$$

This formula is independent of the ship speed. It should be noted that the formulas for the turning radius are based on linear theory which assumes that δ is small and accordingly that R is large. Another feature of the turning test is that the Nomoto gain and time constant can be determined. This is illustrated in the following example.

Example 5.8 (Determination of the Nomoto Gain and Time Constants)

Recall that the dimensionless (with respect to speed U and hull length L) Nomoto gain and time constants were defined as:

$$K' = (L/U)\,K; \qquad T' = (U/L)\,T \tag{5.153}$$

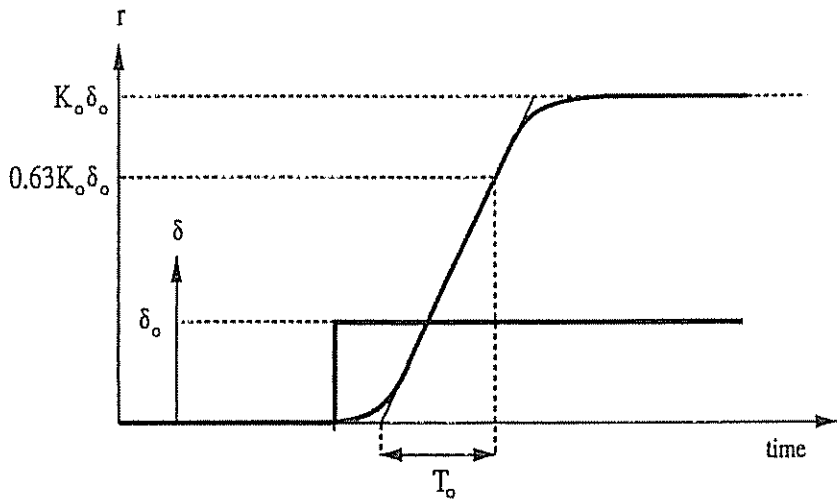

Figure 5.17: Yaw rate r versus time for a constant rudder angle δ_0.

Let the nominal speed U_0 correspond to the nominal values K_0 and T_0 of Nomoto's 1st-order model. Hence,

$$K' = (L/U_0)\, K_0; \qquad T' = (U_0/L)\, T_0 \tag{5.154}$$

Applying the results above, the Nomoto gain and time constant can be expressed as:

$$\boxed{K = (U/U_0)\, K_0} \qquad \boxed{T = (U_0/U)\, T_0} \tag{5.155}$$

where K_0 and T_0 are found from Figure 5.17, showing a step response $\delta = \delta_0 =$ constant applied to a ship at nominal speed $U = U_0$. Hence, K and T can be computed from (5.155) if U is measured.

□

Kempf's Zig-Zag Maneuver

The zig-zag test was first proposed by the German scientist Günther Kempf (1932). 12 years later, Kempf (1944) published the comprehensive test results of 75 freighters.

The zig-zag time-response (see Figure 5.18) is obtained by moving the rudder to 20 degrees starboard from an initially straight course. The rudder setting is kept constant until the heading is changed 20 degrees, then the rudder is reversed 20 degrees to port. Again, this rudder setting is maintained until the ship's heading has reached 20 degrees in the opposite direction. This process continues until a total of 5 rudder step responses have been completed. This test is usually referred to as a 20°–20° maneuver (the first angle refers to the actual rudder settings while the second angle denotes how much the heading angle should change before the rudder is reversed) and was standardized by the

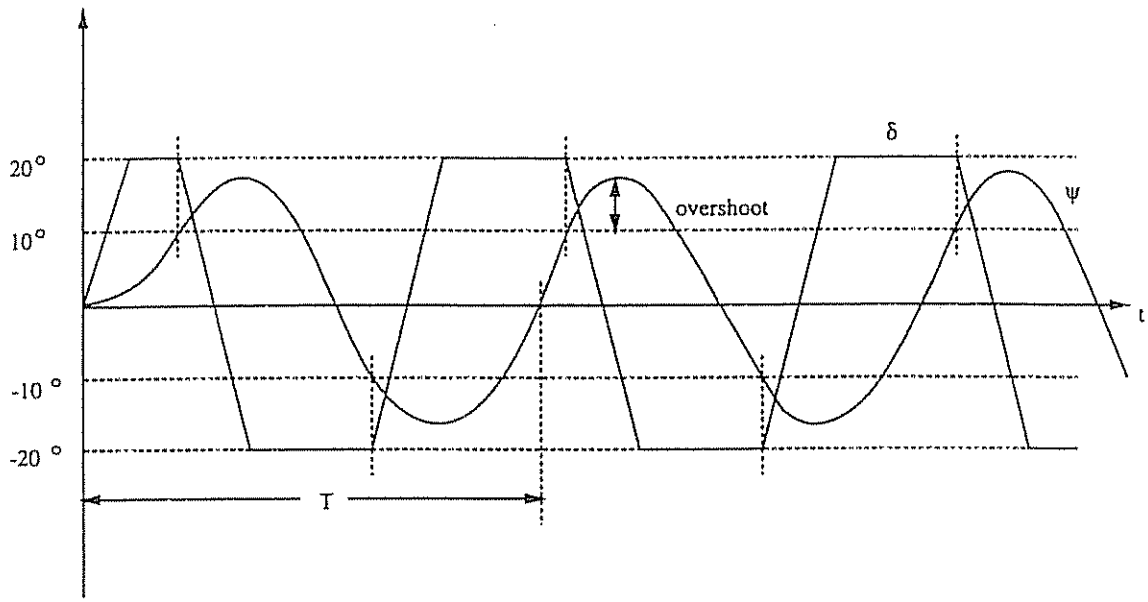

Figure 5.18: 20°–10° zig-zag maneuver.

International Towing Tank Conference (ITTC) in 1963. For larger ships, ITTC has recommended the use of a 10°–10° or a 20°–10° maneuver to reduce the time and waterspace required. The only apparatus required to perform the test is a compass and a stopwatch. The results from the zig-zag maneuver can be used to compare the maneuvering properties of different ships. The maneuver can also be used to compute estimates of K' and T' by solving:

$$T' \dot{r}' + r' = K' \delta' \tag{5.156}$$

with different boundary conditions. This approach is described in detail by Norrbin (1963). An alternative approach to solving the system equations could be to use a system identification algorithm.

Pull-Out Maneuver

In 1969 Roy Burcher proposed a new simple test procedure to determine whether a ship is straight-line stable or not. This test is referred to as the pull-out maneuver (12th ITTC 1969a). The pull-out maneuver involves a pair of maneuvers in which a rudder angle of approximately 20 degrees is applied and returned to midships after steady turning has been attained. Both a port and starboard turn should be performed (see Figure 5.19).

During the test the ship's rate of turn must be measured or at least calculated by numerical derivation of the measured compass heading. If the ship is straight-line stable the rate of turn will decay to the same value for both the starboard and port turn. The ship is unstable if the steady rate of turn from the port

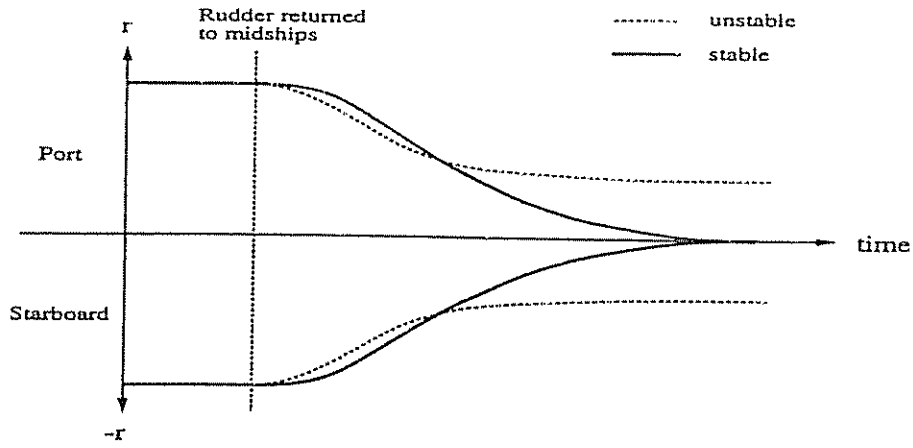

Figure 5.19: Pull-out maneuver.

and starboard turn differ. The difference between these two steady rates of turn corresponds exactly to the height of Dieudonné's spiral loop.

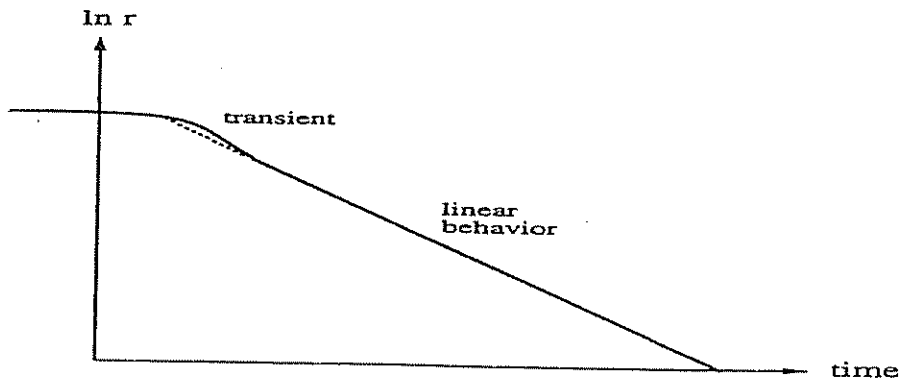

Figure 5.20: Logarithmic presentation of the pull-out maneuver.

The pull-out maneuver can also be used to give information to the degree of stability. In Figure 5.20 the natural logarithm of the rate turn is plotted versus time. Besides a small initial transient the logarithmic curve shows a linear behavior for a stable ship. In the linear range the slope of the logarithmic curve can be used as an indication of the degree of the stability. For instance, increased steepness of the logarithmic curve indicates a more stable (less maneuverable) ship, and the opposite.

Dieudonné's Spiral Maneuver

The direct spiral test was published first in 1949–1950 by the French scientist Jean Dieudonné. An English translation of these French papers is found in Dieudonné (1953). The direct spiral maneuver is used to check straight-line stability. As seen

from the figure, the maneuver also gives an indication of the degree of stability and the range of validity of the linear theory.

To perform the test the ship should initially be held on a straight course. The rudder angle is then put to 25 degrees starboard and held until steady yawing rate is obtained. After this the rudder angle is decreased in steps of 5 degrees and again held until constant yawing rates are obtained for all the rudder angles. The procedure is performed for all rudder angles between 25 degrees starboard and 25 degrees port. In the range around zero rudder angle the step of 5 degrees rudder should be reduced to obtain more precise values. The results are plotted in an r–δ diagram as shown in Figure 5.21. It should be noted that the spiral maneuver should be performed in still air and calm water to obtain the best results. For straight-line unstable ships it is recommended to use Bech's reverse spiral maneuver.

Bech's Reverse Spiral Maneuver

For stable ships both Dieudonné's direct and Bech's reverse spiral tests can be used. For unstable ships within the limits indicated by the pull-out maneuver Bech's reverse spiral should be applied. The reverse spiral test was first published by Mogens Bech in 1966 at the Nordic ship technical meeting in Malmö, Sweden and later by Bech (1968). Since then the reverse spiral test has been quite popular, because of the simplicity and reliability of the method. The reverse spiral is particular attractive since it is less time-consuming than Dieudonné's spiral test.

By observing that the ship steering characteristic is nonlinear outside a limited area, Bech (1968) suggested that one describe the *mean* value of the required rudder deflection $\overline{\delta}$ to steer the ship at a constant rate of turn as a nonlinear function:

$$\overline{\delta} = H(r) \tag{5.157}$$

where $H(r)$ is a nonlinear function describing the maneuvering characteristic. This can be understood by considering Nomoto's 2nd-order model:

$$T_1 T_2 \ddot{r} + (T_1 + T_2)\dot{r} + KH(r) = K(\delta + T_3 \dot{\delta}) \tag{5.158}$$

where the linear term r has been replaced with a function $H(r)$. Assuming that r is constant, that is $\ddot{r} = \dot{r} = 0$, yields:

$$\delta + T_3 \dot{\delta} = H(r) \tag{5.159}$$

Indeed, this shows that the rudder deflection as time reaches infinity can be described by the *mean* rudder deflection defined in (5.157). This definition implies that the r–δ curve will be a single-valued (one-to-one) function of r for both the stable and unstable ship, see Figure 5.21. If the conventional spiral test is applied to an unstable ship a hysteresis loop will be observed.

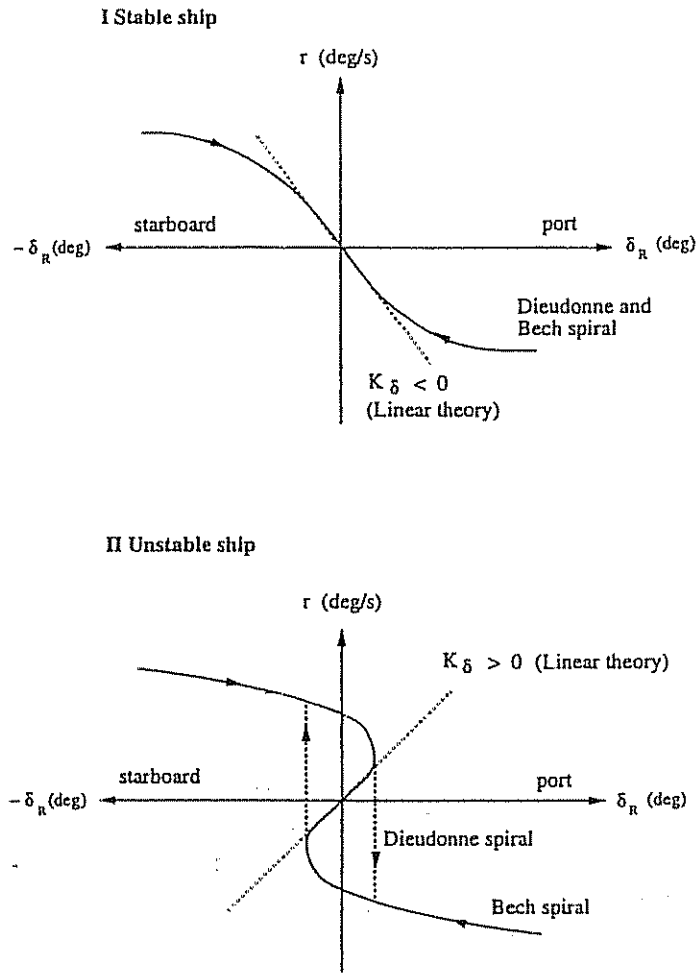

Figure 5.21: r–δ diagram showing the Dieudonné and Bech spirals for both a stable and unstable ship. Notice the hysteresis loop in the Dieudonné spiral for the unstable ship.

The full-scale test is performed by measuring the necessary rudder action required to bring the ship into a desired rate of turn. For an unstable ship this implies that the rudder angle will oscillate about a mean rudder angle. The amplitude of the rudder oscillations should be kept to a minimum. After some time a "balance condition" is reached and both the mean rudder angle and rate of turn can be calculated. Care should be taken for large ships since they will require some more time to converge to their "balance condition".

Linear Models With Added Nonlinearity

Norrbin (1963) and Bech and Wagner Smith (1969) proposed replacing the linear term $\dot{\psi}$ with a nonlinear maneuvering characteristic $H_N(\dot{\psi})$ and $H_B(\dot{\psi})$ in Nomoto's 1st- and 2nd-order models, respectively. These models are written:

$$T\ddot{\psi} + H_N(\dot{\psi}) = K\,\delta \tag{5.160}$$

$$T_1T_2\psi^{(3)} + (T_1 + T_2)\ddot{\psi} + KH_B(\dot{\psi}) = K(\delta + T_3\dot{\delta}) \tag{5.161}$$

The functions $H_N(\dot{\psi})$ and $H_B(\dot{\psi})$ will describe the nonlinear maneuvering characteristic produced by Bech's reverse spiral maneuver. The maneuvering characteristic is usually taken to be a 3rd-order polynomial, see Figure 5.21:

$$H_N(\dot{\psi}) = n_3\,\dot{\psi}^3 + n_2\,\dot{\psi}^2 + n_1\,\dot{\psi} + n_0 \tag{5.162}$$

$$H_B(\dot{\psi}) = b_3\,\dot{\psi}^3 + b_2\,\dot{\psi}^2 + b_1\,\dot{\psi} + b_0 \tag{5.163}$$

For a course-unstable ship we will have that $b_1 < 0$ whereas a course-stable ship satisfies $b_1 > 0$. A single-screw propeller or asymmetry in the hull will cause a non-zero value of b_0. Similarly, symmetry in the hull implies that $b_2 = 0$. Since a constant rudder angle is required to compensate for constant steady state wind and current disturbances, the bias term b_0 could conveniently be treated as an additional rudder off-set. This in turn implies that a large number of ships can be described with the simple polynomial:

$$H_B(\dot{\psi}) = b_3\,\dot{\psi}^3 + b_1\,\dot{\psi} \tag{5.164}$$

The coefficients b_i $(i = 0...3)$ are related to those of Norrbin's model n_i $(i = 0...3)$ as:

$$n_i = \frac{b_i}{|b_1|} \tag{5.165}$$

Hence, $n_1 = 1$ for a course-stable ship and $n_1 = -1$ for a course-unstable ship.

Nonlinear Theory

Let the nonlinear ship steering equations of motion be described by two functions $f_1(\cdot)$ and $f_2(\cdot)$, that is:

$$\begin{aligned} \dot{v} &= f_1(u_0, v, r, \delta) \\ \dot{r} &= f_2(u_0, v, r, \delta) \end{aligned} \tag{5.166}$$

Hence, a theoretical r–δ curve describing the function $H(r)$ can be obtained by eliminating v from the expressions:

$$\begin{aligned} f_1(u_0, v, r, \delta) &= 0 \\ f_2(u_0, v, r, \delta) &= 0 \end{aligned} \tag{5.167}$$

For a stable ship this curve will be one-to-one whereas the unstable ship will have three solutions corresponding to $\delta = 0$, see Figure 5.21.

Linear Theory

Linear theory implies that r will be proportional to δ_R, that is:

$$r = K_\delta \, \dot{\delta}_R \tag{5.168}$$

The proportional coefficient is found from (5.148) as:

$$K_\delta = -\frac{Y_v N_\delta - N_v Y_\delta}{C} \tag{5.169}$$

This corresponds to a straight line in the r–δ_R diagram. Since,

$$Y_v N_\delta - N_v Y_\delta \; > \; 0 \tag{5.170}$$

for ships with aft rudder, see (5.150), the following considerations can be obtained:

$$\begin{array}{llcl} \text{stable ship} & (C > 0) & \Longrightarrow & K_\delta < 0 \\ \text{unstable ship} & (C < 0) & \Longrightarrow & K_\delta > 0 \end{array}$$

Stopping Trials

The most common stopping trials are probably the *crash-stop* and the *low-speed stopping trial*. Crash-stops are usually performed from full ahead speed by simply reversing the engine at full astern. The path of the ship is measured by a tracking system. Most ships are uncontrollable during crash-stops. Consequently, this maneuver will be strongly affected by both the wind and the ambient water conditions.

In the maneuvering trial code of the 14th ITTC (1975) the low-speed stopping trial is recommended for navigation purposes. Like the crash-stop maneuver, the low-speed stopping trial is performed by reversing the engine at full astern while the path of the ship is measured by a tracking system. A typical path is shown in Figure 5.22.

5.8.2 The Norrbin Measure of Maneuverability

Norrbin (1965) has proposed a course change quality number P as a measure of turning ability or maneuverability. The *turning index* is defined as:

$$P \triangleq \frac{\psi'(t'=1)}{\delta'(t'=1)} \qquad \text{where} \qquad t' = t\,(U/L) \tag{5.171}$$

P can simply be interpreted as the heading change per unit rudder angle in one ship length traveled with $U = 1$. By solving the equation:

$$T' \, \ddot{\psi}' + \dot{\psi}' = K' \, \delta' \tag{5.172}$$

with $\delta' =$ constant we obtain:

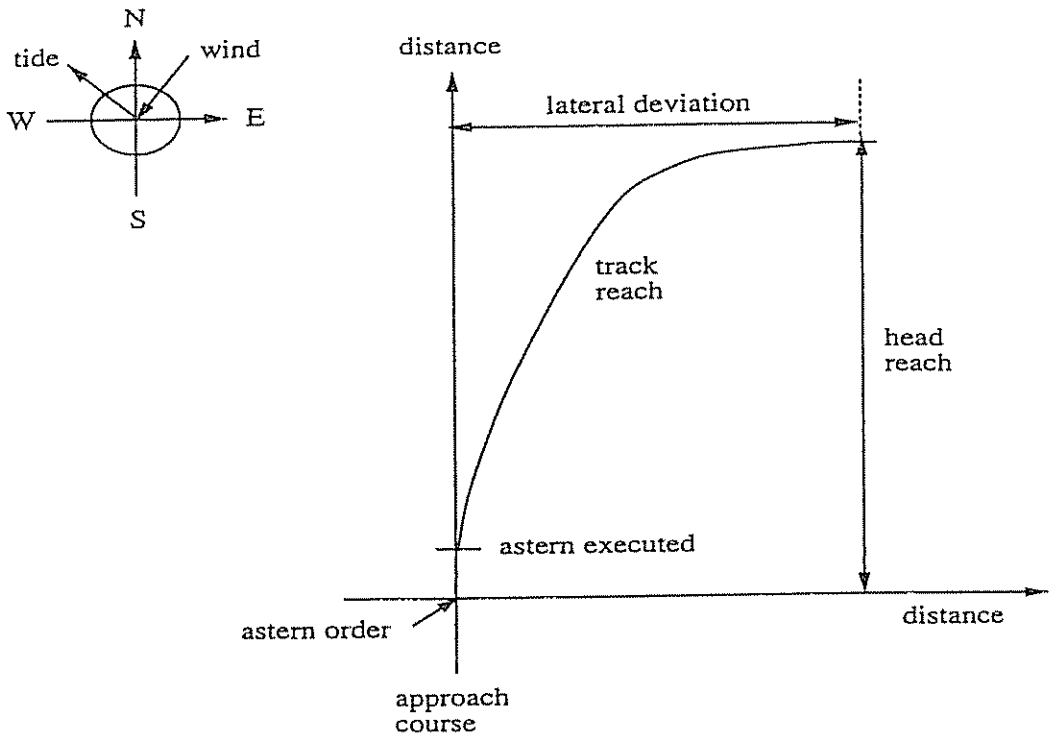

Figure 5.22: Stopping trial.

$$\psi'(t') = K' \left[t' - T' + T' \exp(-(t'/T'))\right] \delta'(t') \tag{5.173}$$

Hence,

$$P = K' \left[1 - T' + T' \exp(-(1/T'))\right] \tag{5.174}$$

A frequently used approximation to (5.174) is obtained by Taylor expansion of $\exp(-1/T')$, that is:

$$\exp(-1/T') \approx 1 - \frac{1}{T'} + \frac{1}{2(T')^2} \tag{5.175}$$

which yields:

$$P \approx \frac{1}{2} \frac{K'}{T'} \tag{5.176}$$

This formula can be used for both stable and marginally stable ships. Norrbin concludes that $P > 0.3$ guarantees a reasonable standard of course change quality for most ships while $P > 0.2$ seems to be sufficient for large oil-tankers. The P-number is a good measure of maneuverability for course-stable ships.

For poorly stable ships it is recommended to use P together with another maneuverability index, for instance the slope $dr'/d\delta'$ or the width of the r'–δ' loop.

5.9 Conclusions

In this chapter we have discussed mathematical models for ship control systems design and stability analyses. This includes system models for forward speed (surge), steering (sway and yaw) and roll. In addition to this, we have discussed mathematical models for the steering machine.

Ship stability is mainly discussed in the context of Routh's stability criterion, eigenvalue considerations and empirical formulas. Besides this, a brief introduction to ship maneuverability is made. This includes the description of standard sea trials like the turning circle, Kempf's zig-zag maneuver, the pull-out maneuver, Dieudonné's spiral maneuver, Bech's reverse spiral maneuver and stopping trials.

The interested reader is advised to consult the proceedings of the *Ship Control Systems Symposium (SCSS)* and the International Federation of Automatic Control (IFAC) workshop on *Control Applications in Marine Systems (CAMS)* for contributions on ship control modeling, while Comstock (1967) is an excellent reference on ship hydrodynamics and maneuverability. A detailed description on maneuvering tests is also found in the 14th ITTC (1975), while a detailed guide on how to perform full-scale sea trials is given by SNAME (1989).

Finally, an extensive list of references on ship simulation, maneuvering and modeling can be found in Webster (1992). In this work, the different publications are classified according to topic and subject area.

5.10 Exercises

5.1 Let Nomoto's 2nd-order model be written in the form:

$$r(s) = \frac{K(1+T_3 s)}{(1+T_1 s)(1+T_2 s)}\,\delta(s) \tag{5.177}$$

Show that the resulting transfer function between $\delta(s)$ and $v(s)$ can be expressed in a similar manner as:

$$v(s) = \frac{K_v(1+T_v s)}{(1+T_1 s)(1+T_2 s)}\,\delta(s) \tag{5.178}$$

by using the model of Davidson and Schiff. Find the expressions for K_v and T_v as a function of the hydrodynamic derivatives. Finally, show that:

$$v(s) = \frac{K_v(1+T_v s)}{K(1+T_3 s)}\,r(s) \tag{5.179}$$

Find the transfer functions $v(s)/\delta(s)$ and $v(s)/r(s)$ by applying Nomoto's 1st-order model for $r(s)/\delta(s)$.

5.2 Prove Abkowitz's straight-line stability criterion by applying Routh's criterion.

5.3 Consider the linear course-keeping equations of motion in Appendix E.1.3 corresponding to a container ship.

(a) Neglect roll and find a non-dimensional state-space model in sway and yaw for the container ship.

(b) Compute the Nomoto time and gain constants for both the 1st-order and 2nd-order models.

(c) What are the non-dimensional eigenvalues of the model ? Plot both eigenvalues with dimension and as a function of speed U. Is the ship straight-line stable ?

(d) Is the container ship straight-line stable if Abkowitz's criterion for straight-line stability is used ?

(e) Compute the Norrbin measure of maneuverability. Is this ship easy to maneuver ?

5.4 Consider the linear course-keeping equations of motion in Appendix E.1.3 corresponding to a container ship.

(a) Find a a non-dimensional state-space model in sway, roll and yaw for the container ship.

(b) What are the non-dimensional eigenvalues of the model ? Plot all three eigenvalues with dimension and as a function of speed U. Is the ship straight-line stable ? Compare the results with those from Exercise 5.3 (c). Does the ship exhibit non-minimum phase behavior in response to a rudder input ?

(c) Simulate a turning test for the container ship. Compute the turning radius and comment on the simulation results.

(d) Simulate the same turning test for the nonlinear course-keeping equations of motion (see the Matlab m-file at the end of Appendix E.1.3). Compare the simulation results with those under (c) and explain what you see.

(e) Perform a 10^o–10^o zig-zag maneuver and plot the Bech spiral. Explain the results.

5.5 Simulate a turning test, a 10^o–10^o zig-zag maneuver and a pull-out maneuver for the Mariner Class vessel given in Appendix E.1.1.

(a) Use these tests to estimate the Nomoto time and gain constant (1st-order model).

(b) Compare the performance of the estimated linear model with the nonlinear model.

(c) Include a model of the rudder servo in the simulator. Use $\delta_{\max} = 10$ (deg) and $\dot{\delta}_{\max} = 2.3$ (deg/s). Estimate the Nomoto time and gain constant for the Mariner Class vessel with rudder servo loop. Are the results from (a) still valid ?

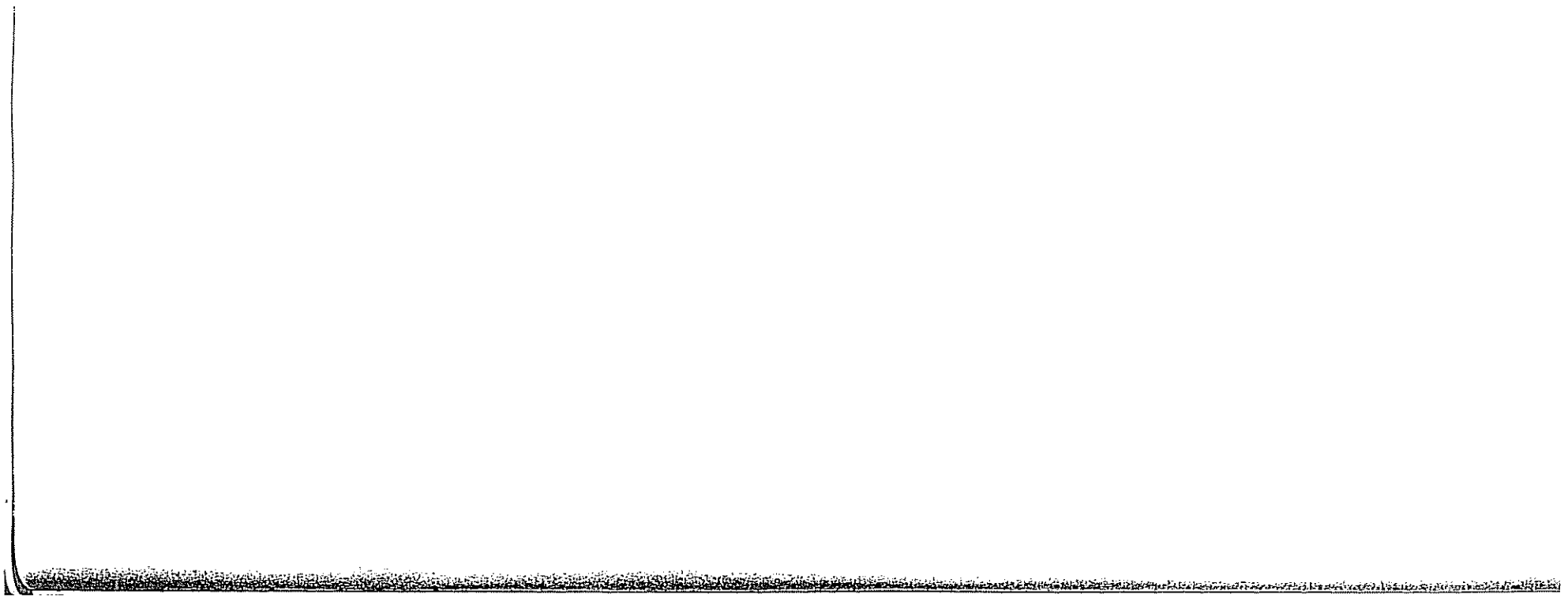

Chapter 6

Automatic Control of Ships

Automatic ship control systems design involves the design of systems for forward speed control, motion (vibration) damping, steering, tracking and positioning. The development of modern control theory together with faster digital computer systems allows more sophisticated control systems to be designed. The most important features of modern ship control systems are improved performance, robustness and the fuel saving potential. In the last two decades fuel saving autopilots have been designed by applying optimal control theory. This chapter will discuss:

- Systems for forward speed control
- Autopilots for course-keeping
- Turning controllers
- Track-keeping systems
- Positioning systems
- Rudder-roll stabilization (RRS) systems
- Self-tuning and adaptive systems
- Identification of ship dynamics

The complexity, number of DOF and type of mathematical models required for each of these tasks will vary. For instance, standard autopilots for automatic course control require the yawing and often also the swaying motion to be modelled. If rudder-roll stabilization is of interest an additional mode describing the rolling motion is required. A dynamic positioned ship is usually fairly well described by a model of the horizontal motion, that is the motion variables in surge, sway and yaw. Hence, we will restrict our discussion to 4 DOF ship models, neglecting the motion in heave and pitch.

In most ship applications, it is important that the contribution from the high-frequency wave motion is suppressed. If not, wave disturbances can cause wear on the rudder, propeller and the thruster actuators.

Before discussing conventional and adaptive autopilots, we will discuss three methods for suppression of high-frequency wave disturbances:

- Dead-band techniques
- Conventional filter design
- State estimation

6.1 Filtering of First-Order Wave Disturbances

In general, the resulting pattern of the waves will consist of a large number of wave components with various directions of propagation, different amplitudes and phases. In order to describe the wave induced motion, we will assume that the waves can be described as long crested waves generated by the wind. For wave periods in the interval 5 s $< T_0 <$ 20 s the dominating wave frequency (modal frequency) f_0 of the Pierson–Moskowitz wave spectrum will be in the range:

$$0.05 < f_0 < 0.2 \qquad \text{(Hz)} \tag{6.1}$$

Waves in this frequency range produce large *oscillatoric* forces and moments. These are called 1st-order wave forces and moments. In addition to the oscillatoric motion a *mean* wave force caused by 2nd-order wave disturbances is observed. 2nd-order wave drift forces can be counteracted by the autopilot, whereas 1st-order wave disturbances, usually around 0.1 (Hz), are close to or outside the control bandwidth of the vessel. However, the disturbances will be inside the bandwidth of the servos and actuators of the vehicle. This suggests that proper filtering of all feedback state variables must be performed to avoid 1st-order wave noise causing too much control action. In other words, we do not want the rudder and thruster actuator of the ship compensating for the oscillatory high-frequency wave-induced motion. This is usually referred to as *wave filtering*. To accomplish this task, it is common to assume that the total motion of the ship-wave system can be described in terms of a low-frequency (LF) model representing the motion of the vessel and a high-frequency (HF) 1st-order wave induced motion. For a ship autopilot, this assumption suggests that we can write the yaw dynamics as:

$$\psi(s) = \psi_L(s) + \psi_H(s) = h_{\text{ship}}(s)\,\delta(s) + h_{\text{wave}}(s)\,w(s) \tag{6.2}$$

where $w(s)$ is a zero-mean Gaussian white noise process and

$$h_{\text{ship}}(s) = \frac{K\,(1+T_3 s)}{s(1+T_1 s)(1+T_2 s)} \tag{6.3}$$

$$h_{\text{wave}}(s) = \frac{K_w\,s}{s^2 + 2\,\zeta\,\omega_0\,s + \omega_0^2} \tag{6.4}$$

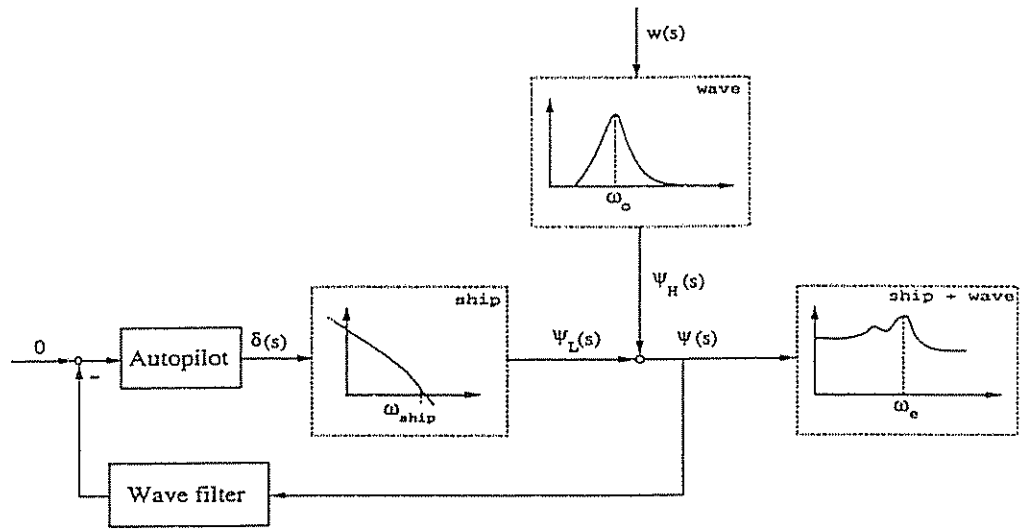

Figure 6.1: Linear superposition of wave disturbances and steering dynamics.

By exclusively using the LF components of the measured state variables in the control system, HF rudder motions and excessive thruster modulation are avoided. The frequency spectrum of the measured yaw angle for a well controlled ship is illustrated to the right in Figure 6.1 where the first peak in the resulting frequency spectrum corresponds to the LF rudder motion and the second peak is recognized as the wave encounter frequency. The non-zero LF component is due to the rudder off-set required to compensate for slowly-varying environmental disturbances.

We recall that for a ship moving at speed U the waves cause a shift in the frequencies of the encountered waves which implies that the modal frequency ω_0 will be modified according to (see Equation (3.63)):

$$\omega_e(U, \omega_0, \beta) = \omega_0 - \frac{\omega_0^2}{g} U \cos\beta \quad \text{(rad/s)} \tag{6.5}$$

Here β is the wave direction (encounter angle). According to (6.1) the wave circular frequency $\omega_0 = 2\,\pi\,f_0$ will be in the range of:

$$0.3 < \omega_0 < 1.3 \qquad \text{(rad/s)} \tag{6.6}$$

6.1.1 Dead-Band Techniques

The application of a dead-band in the control-loop is widely used to suppress the HF rudder motion (see Figure 6.2). A disadvantage with the dead-band technique is that LF motions of small amplitudes are also suppressed. Hence, the course-keeping accuracy of the autopilot will be affected.

A dead-band in combination with integral action in the controller will lead to an undesired oscillation around the desired heading. This increases the ship resis-

tance and thus the fuel consumption. Consequently, more sophisticated filtering techniques are recommended for modern ship feedback control systems.

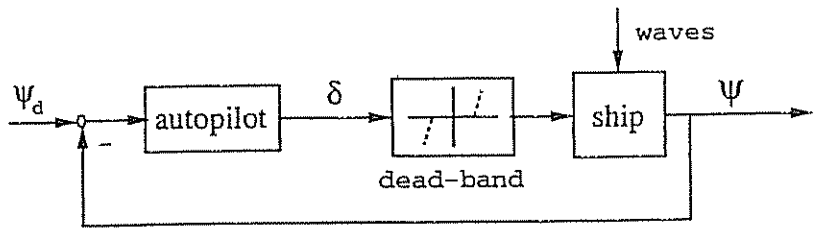

Figure 6.2: Dead-band for suppression of 1st-order wave disturbances.

6.1.2 Conventional Filter Design

Low-Pass Filter

If the control bandwidth is much smaller than the encounter frequency, that is:

$$\omega_{\text{ship}} \ll \omega_e \tag{6.7}$$

HF rudder motions can be suppressed by low-pass filtering. For instance, a first order low-pass filter with time constant T_f:

$$h_{LP}(s) = \frac{1}{1+T_f s} \qquad \omega_{\text{ship}} < \frac{1}{T_f} < \omega_e \qquad \text{(rad/s)} \tag{6.8}$$

will suppress disturbances over the frequency $1/T_f$. This criterion is hard to satisfy for small vessels, but for large tankers we have typically that the control bandwidth satisfies $\omega_{ship} < 0.1$ (rad/s). An alternative to the simple filter structure of Equation (6.8) could be to use an n-th order *Butterworth filter* to attenuate the HF wave motion. The *Butterworth filter* is obtained by solving the Butterworth polynomial:

$$p(s)\,p(-s) = 1 + (s/j\omega_f)^{2n} \tag{6.9}$$

for $p(s)$. Here ω_f is the desired cut-off frequency. Finally, we define the low-pass filter polynomial as:

$$h_{LP}(s) = 1/p(s) \tag{6.10}$$

Example 6.1 (Design of Butterworth Low-Pass Filter)
The $2n$ roots of the filter polynomial $p(s)p(-s)$ are shown in Figure 6.3 for $(n = 1...4)$. The left-half plane poles correspond to $p(s)$ while the right-half plane contains the poles of $p(-s)$. We also notice that for even numbers of n there are only complex conjugate poles, but for odd numbers of n there will be one real pole in both the left and right half-planes. In addition to this all poles will be equally spaced on a circle with radius ω_f.

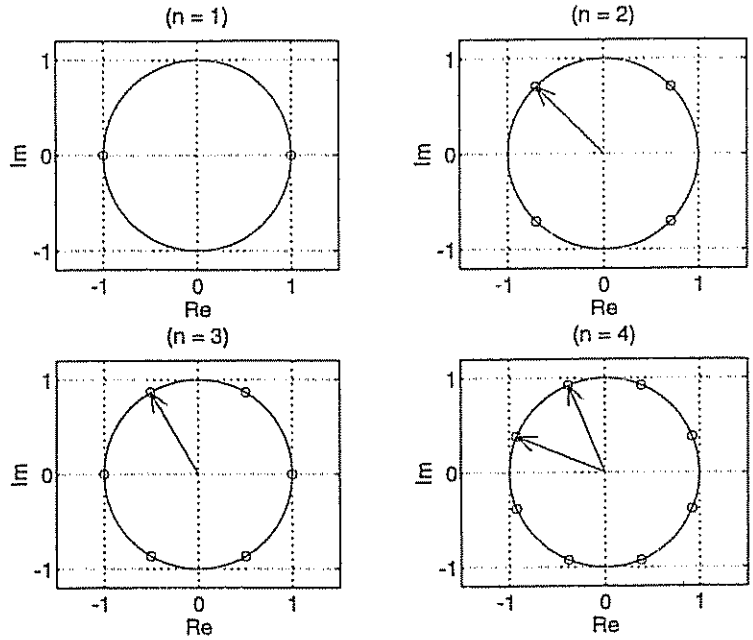

Figure 6.3: Pole configuration for Butterworth low-pass filter ($n = 1...4$) and radius (cut-off frequency) $\omega_f = 1.0$ (rad/s). For the complex conjugate pairs, the relative damping ratio ζ is given by the angle ϕ between the positive y-axis and the arrows in the figure, according to the formula $\zeta = \sin\phi$.

The pole configuration (only left-half plane) shown in Figure 6.3 can be represented by the following simple transfer functions:

$$(n=1) \qquad h_{LP}(s) = \frac{1}{1 + s/\omega_f}$$

$$(n=2) \qquad h_{LP}(s) = \frac{\omega_f^2}{s^2 + 2\,\zeta\,\omega_f\,s + \omega_f^2}; \quad \zeta = \sin(45^o)$$

$$(n=3) \qquad h_{LP}(s) = \frac{\omega_f^2}{s^2 + 2\,\zeta\,\omega_f\,s + \omega_f^2} \cdot \frac{1}{1 + s/\omega_f}; \quad \zeta = \sin(30^o)$$

$$(n=4) \qquad h_{LP}(s) = \prod_{i=1}^{2} \frac{\omega_f^2}{s^2 + 2\,\zeta_i\,\omega_f\,s + \omega_f^2}; \quad \zeta_1 = \sin(22.5^o), \quad \zeta_2 = \sin(67.5^o)$$

□

The main disadvantage with the low-pass filter is that additional phase lag is introduced, see Figure 6.4. It is seen from the Bode plot that this problem increases with the order of the filter polynomial. Another problem is that the encounter frequency will vary with different sea states as well as the speed of the ship. This suggests that $\omega_f = 1/T_f$ (rad/s) should be adjusted according to the

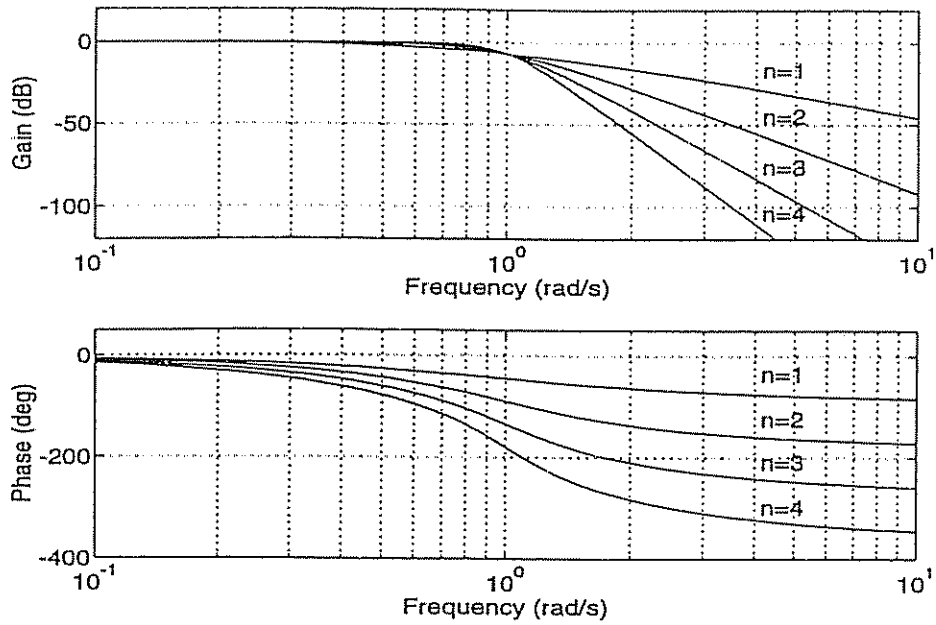

Figure 6.4: Bode plot showing the Butterworth low-pass filter for $\omega_f = 1.0$ (rad/s) and $(n = 1...4)$.

encounter frequency. For ships where the control bandwidth is approximately of the same magnitude as the encounter frequency, a low-pass filter will yield poor filtering. This problem can be handled by applying a band-stop filter or by estimation of the HF wave-induced motion in a Kalman filter.

Bandstop Filter

Since most of the energy in the wave spectrum is located around the modal frequency of the wave spectrum, a bandstop filter can be used to attenuate HF wave motions. In fact, this method is highly attractive due to its simplicity. Consider the following 2nd-order bandstop filter:

$$h_{BS}(s) = \frac{(s/\omega_n)^2 + 2\,\zeta\,(s/\omega_n) + 1}{(1 + T_1 s)(1 + T_2 s)} \qquad 1/T_1 < \omega_n < 1/T_2 \qquad (6.11)$$

where ζ is the relative damping factor and ω_n is the natural frequency of the filter. This filter structure will attenuate wave disturbances in the frequency range of $1/T_1$ to $1/T_2$. The price of course is that additional phase lag is introduced.

Notch Filter

An attractive simplification of the bandstop filter could be to choose the natural frequency $\omega_n = 1/T_1 = 1/T_2$. This filter structure is usually referred to as a notch. Consequently, the notch filter will take the form (see Figure 6.5):

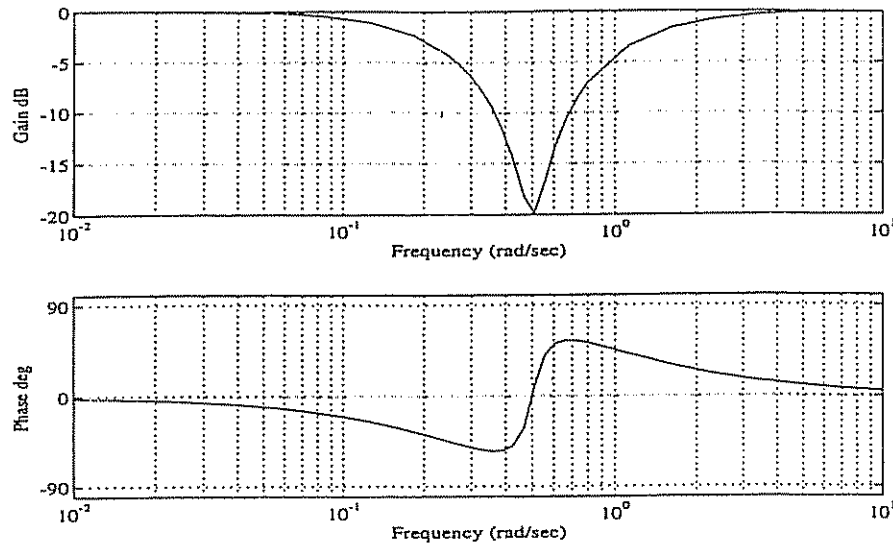

Figure 6.5: Bode plot showing the 2nd-order notch filter for $\omega_n = 0.5$ (rad/s) and $\zeta = 0.1$.

$$h_{NO}(s) = \frac{s^2 + 2\,\zeta\,\omega_n\,s + \omega_n^2}{(s + \omega_n)^2} \tag{6.12}$$

This filter is effective over a much smaller frequency range than the bandstop filter. Application of the bandstop or notch filter structure suggests that ω_n should be chosen equal to the encounter frequency ω_e, that is:

$$\omega_n \triangleq \omega_e \tag{6.13}$$

An estimate of the encounter frequency can be computed by the help of (3.63) if β and ω_0 are known. We recall from (3.26) that the modal frequency ω_0 of the Pierson–Moskovitz spectrum is:

$$\omega_0 = \sqrt[4]{\frac{4B}{5}} \tag{6.14}$$

Alternatively, we can write:

$$\omega_0 = 0.88\,\frac{g}{V} = 0.40\,\sqrt{\frac{g}{H_s}} \tag{6.15}$$

where V is the speed of the wind at an elevation of 19.4 m, H_s is the significant wave height and g is the acceleration of gravity. This suggests that the natural filter frequency ω_n should be varied according to V or H_s to obtain best filtering.

Cascaded Notch Filter

Since the estimate of ω_n can be poor and one single-notch filter only covers a small part of the actual frequency range of the wave spectrum, an alternative filter structure consisting of three cascaded notch filters with fixed center frequencies is suggested; see page 921 of Grimble and Johnson (1989). The center frequencies of the notch filters are typically chosen as $\omega_1 = 0.4$ (rad/s), $\omega_2 = 0.63$ (rad/s) and $\omega_3 = 1.0$ (rad/s). The cascaded filter structure is written as:

$$h_C(s) = \prod_{i=1}^{3} \frac{s^2 + 2\,\zeta\,\omega_i\,s + \omega_i^2}{(s+\omega_i)^2} \tag{6.16}$$

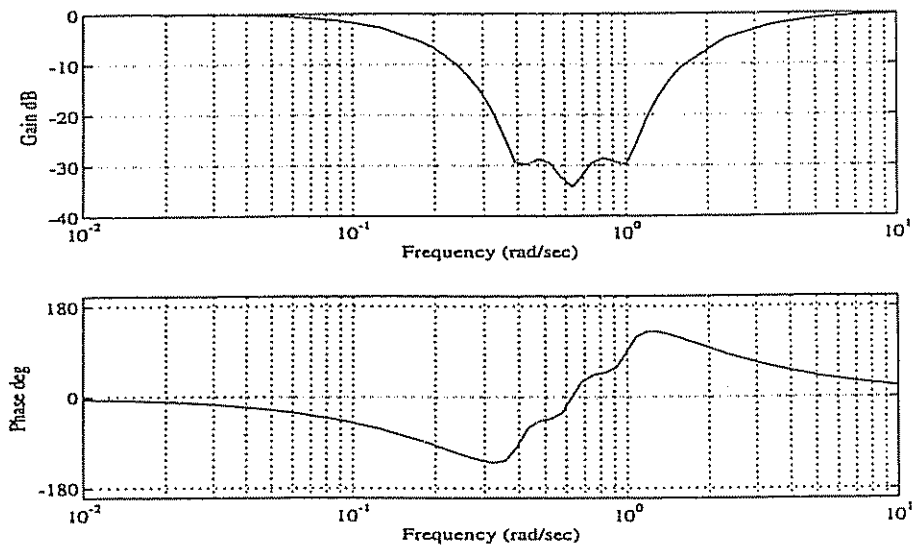

Figure 6.6: Bode plot showing three cascaded 2nd-order notch filters with frequencies $\omega_1 = 0.4$ (rad/s), $\omega_2 = 0.63$ (rad/s) and $\omega_3 = 1.0$ (rad/s) and $\zeta = 0.1$.

6.1.3 Observer-Based Wave Filter Design

An alternative to conventional filtering of wave disturbances is to apply a state estimator (observer). Moreover, a state estimator can be designed to separate the LF components of the motion from the noisy measurements by using a model of the ship and the wave disturbances. In fact, a model-based wave filter is well suited to separate the LF and HF motions from each other even for vessels where the control bandwidth is close to or higher than the encounter frequency. We will restrict our treatment to wave filters based on linear theory.

LF Ship Model (Nomoto)

Let a 1st-order Nomoto model (without loss of generality) be used to describe the LF motion of the ship. Moreover:

$$\dot{\delta}_0 = w_0 \tag{6.17}$$
$$\dot{\psi}_L = r_L \tag{6.18}$$
$$\dot{r}_L = -\frac{1}{T} r_L + \frac{K}{T} (\delta - \delta_0) + w_L \tag{6.19}$$

Here the rudder off-set δ_0 is included to counteract slowly-varying moments on the ship due to wave drift forces, LF wind and current components. In this model, ω_0 and ω_L are modelled as zero-mean Gaussian white noise processes.

HF Wave Model (1st-Order Wave Disturbances)

The oscillatoric motion of the waves is usually described by the following transfer function:

$$\psi_H(s) = \frac{K_w\, s}{s^2 + 2\,\zeta\,\omega_n\, s + \omega_n^2}\, w_H(s) \tag{6.20}$$

where w_H is a zero-mean Gaussian white noise process and the filter frequency ω_n is an estimate of the frequency of encounter ω_e. This model is inspired by the early work of Balchen et al. (1976) and Balchen, Jenssen, Mathisen and Sælid (1980b). They first applied an undamped oscillator ($\zeta = 0$) to describe the wave interactions on a dynamically positioned ship. Later Balchen and Norwegian co-workers showed that better performance was obtained by introducing a small positive value for ζ (see Sælid et al. 1983). Extensions of this work to ship steering have been made by Sælid and Jenssen (1983), and Holzhüter and Strauch (1987).

The transfer function (6.20) is usually represented by one of the following two equivalent state-space representations:

$$\dot{\xi}_H = \psi_H \tag{6.21}$$
$$\dot{\psi}_H = -2\,\zeta\,\omega_n\,\psi_H - \omega_n^2\,\xi_H + K_w\,w_H \tag{6.22}$$

or alternatively:

$$\dot{\psi}_H = \xi_H + K_w\,w_H \tag{6.23}$$
$$\dot{\xi}_H = -2\,\zeta\,\omega_n\,\xi_H - \omega_n^2\,\psi_H - 2\,\zeta\omega_n\,K_w\,w_H \tag{6.24}$$

Compass Measurement Model

By combining the ship and wave model the heading angle can be expressed as a sum:

$$\psi = \psi_L + \psi_H + v_H \tag{6.25}$$

where v_H represents zero-mean Gaussian measurement noise. The resulting model is shown in Figure 6.7.

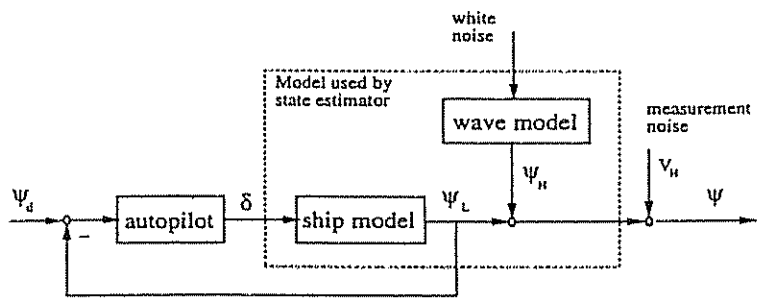

Figure 6.7: Low-frequency (LF) and high-frequency (HF) submodels. Notice that the autopilot uses feedback from the LF yaw angle.

State Estimator

We will now illustrate how pole-placement techniques can be used to design the LF and HF state estimator. Let the ship state estimator be written:

$$\dot{\hat{\delta}}_0 = K_0 \left(\psi - \hat{\psi}_L - \hat{\psi}_H\right) \tag{6.26}$$

$$\dot{\hat{\psi}}_L = \hat{r}_L + K_1 \left(\psi - \hat{\psi}_L - \hat{\psi}_H\right) \tag{6.27}$$

$$\dot{\hat{r}}_L = -\frac{1}{T}\hat{r}_L + \frac{K}{T}\left(\delta - \hat{\delta}_0\right) + K_2 \left(\psi - \hat{\psi}_L - \hat{\psi}_H\right) \tag{6.28}$$

1st-order wave disturbances are estimated according to:

$$\dot{\hat{\xi}}_H = \hat{\psi}_H + K_3 \left(\psi - \hat{\psi}_L - \hat{\psi}_H\right) \tag{6.29}$$

$$\dot{\hat{\psi}}_H = -2\,\zeta\,\omega_n\,\hat{\psi}_H - \omega_n^2\,\hat{\xi}_H + K_4 \left(\psi - \hat{\psi}_L - \hat{\psi}_H\right) \tag{6.30}$$

where the *hat* is used to denote the state estimates and K_i $(i = 0...4)$ are five unknown estimator gains to be determined.

Simplified State Estimator (No Wave Model)

We will first illustrate the observer design by showing how a simple state estimator can be designed by neglecting the model of the wave disturbances ($\dot{\psi}_H = \dot{\psi}_H = 0$). In the next section we will improve the design by including a 2nd-order wave model.

Let us first design an LF state estimator under the assumption that the HF motion is measurement noise. Moreover, we write the estimation error dynamics as:

$$\begin{bmatrix} \Delta\dot{\delta}_0 \\ \Delta\dot{\psi}_L \\ \Delta\dot{r}_L \end{bmatrix} = \begin{bmatrix} 0 & -K_0 & 0 \\ 0 & -K_1 & 1 \\ -\frac{K}{T} & -K_2 & -\frac{1}{T} \end{bmatrix} \begin{bmatrix} \Delta\delta_0 \\ \Delta\psi_L \\ \Delta r_L \end{bmatrix} - \begin{bmatrix} K_0 \\ K_1 \\ K_2 \end{bmatrix} (\psi_H + v_H) \tag{6.31}$$

where $\Delta r_L = r_L - \hat{r}_L$, $\Delta\psi_L = \psi_L - \hat{\psi}_L$ and $\Delta\delta_0 = \delta_0 - \hat{\delta}_0$. A block diagram of the state estimator is shown in Figure 6.8.

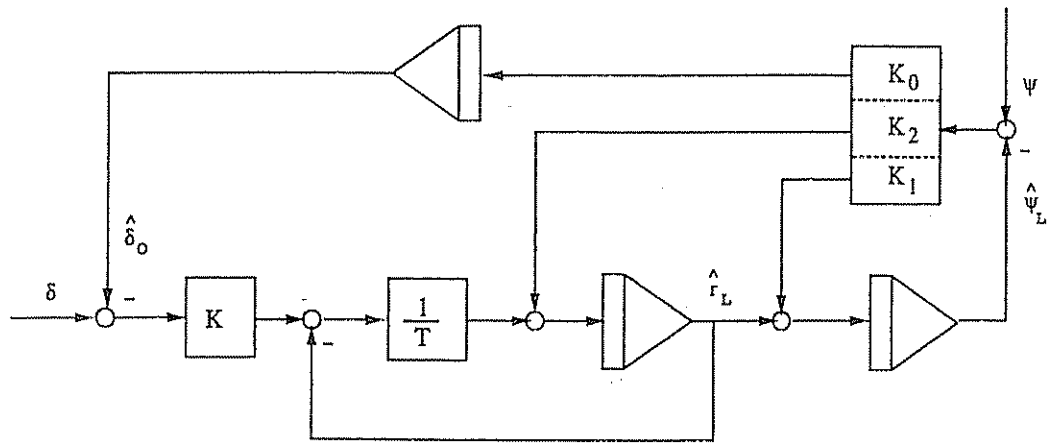

Figure 6.8: Model-based wave filter.

One way to calculate the estimator gains K_0, K_1 and K_2 is by applying a pole-placement technique. The eigenvalue assignment of the error dynamics can be simplified by assuming that δ_0 is slow compared to the yaw mode (ψ_L and r_L) which suggests a small value for K_0. Indeed, this is a reasonable assumption since the rudder off-set is slowly-varying compared to the yaw dynamics. Hence, the LF estimator gains K_1 and K_2 can be chosen independently of K_0 by considering a *quadratic* characteristic polynomial corresponding to $\Delta\psi_L$ and Δr_L in (6.31):

$$\pi(s) = s^2 + (K_1 + 1/T)\ s + (K_2 + K_1/T) \tag{6.32}$$

Since this a 2nd-order system, we can specify the relative damping factor ζ and natural frequency ω_n by requiring that (6.32) should be equal to the polynomial:

$$\pi(s) = s^2 + 2\,\zeta\,\omega_n\,s + \omega_n^2 \tag{6.33}$$

Hence the following expressions for K_1 and K_2 are obtained:

$$K_1 = 2\,\zeta\,\omega_n - 1/T \tag{6.34}$$
$$K_2 = \omega_n^2 - (2\,\zeta\,\omega_n)/T + 1/T^2 \tag{6.35}$$

Adaptive Observer Based on Pole-Placement (No Wave Model)

Van Amerongen (1982, 1984) suggests using an adaptive gain update for K_1 and K_2. The motivation for this approach is that the estimator gains should be modified according to the standard deviation of the HF wave motion. Let the innovation process be described by:

$$\varepsilon = \psi - \hat{\psi}_L \tag{6.36}$$

Furthermore, the innovation process can be low-pass filtered according to:

$$\varepsilon_L = \frac{1}{1+T_f\,s}\varepsilon; \qquad \varepsilon_H = \varepsilon - \varepsilon_L \tag{6.37}$$

which enables the computation of the variances:

$$\sigma_L^2 = E\,\{\varepsilon_L^2\}; \qquad \sigma_H^2 = E\,\{\varepsilon_H^2\} \tag{6.38}$$

Motivated by this, we can update the estimator gains according to:

$$K_1 = \gamma\,K_{10}; \qquad K_2 = \frac{1}{T}\,\gamma\,K_{20} \tag{6.39}$$

where K_{10} and K_{20} are two constant design parameters given by some pole-placement technique and $0 \leq \gamma \leq 1$ is an adjustable ratio defined as:

$$\gamma = \frac{\sigma_L^2}{\sigma_L^2 + \sigma_H^2} \tag{6.40}$$

Notice that in calm sea ($\sigma_H = 0$) we have $\gamma = 1$ but rough sea ($\sigma_H \gg 0$) implies that $\gamma = 0$. During practical operations of ships, rough sea can cause large heading errors, which will be filtered to strong because of the relatively low value of γ. This suggests that a lower bound on γ should be defined to ensure that the state estimator is updated in rough sea as well. Van Amerongen (1982) proposes:

$$\text{(rough sea)} \qquad 0.1 \leq \gamma \leq 1.0 \qquad \text{(calm sea)} \tag{6.41}$$

Full State Observer Design (Ship and Wave Model)

We will in this section show how a full state observer can be designed by using the approach of Fossen (1993b). Again, we will assume that the rudder off-set is slowly-varying compared to the yaw dynamics, that is $\dot{\delta}_0 \approx 0$ and $K_0 \ll 1$. Consider the error dynamics in the form:

$$\begin{bmatrix} \Delta\dot{\psi}_L \\ \Delta\dot{r}_L \\ \Delta\dot{\xi}_H \\ \Delta\dot{\psi}_H \end{bmatrix} = \begin{bmatrix} -K_1 & 1 & 0 & -K_1 \\ -K_2 & -\frac{1}{T} & 0 & -K_2 \\ -K_3 & 0 & 0 & 1-K_3 \\ -K_4 & 0 & -\omega_n^2 & -2\,\zeta\omega_n - K_4 \end{bmatrix} \begin{bmatrix} \Delta\psi_L \\ \Delta r_L \\ \Delta\xi_H \\ \Delta\psi_H \end{bmatrix} \tag{6.42}$$

Hence, the characteristic equation can be shown to satisfy:

$$\pi(s) = s^4 + a_3\, s^3 + a_2\, s^2 + a_1\, s + a_0 \tag{6.43}$$

where

$$a_3 = K_1 + K_4 + 2\zeta\omega_n + 1/T \tag{6.44}$$
$$a_2 = (1/T + 2\zeta\omega_n)\, K_1 + K_2 - \omega_n^2\, K_3 + 1/T\, K_4 + (\omega_n^2 + 2\zeta\omega_n/T) \tag{6.45}$$
$$a_1 = (2\zeta\omega_n/T + \omega_n^2)\, K_1 + 2\zeta\omega_n\, K_2 - \omega_n^2/T\, K_3 + \omega_n^2/T \tag{6.46}$$
$$a_0 = \omega_n^2/T\, K_1 + \omega_n^2\, K_2 \tag{6.47}$$

Furthermore, the eigenvalue assignment can be done by requiring that the error dynamics must satisfy:

$$\prod_{i=1}^{4}(s - p_i) \triangleq \pi(s) \tag{6.48}$$

where p_i $(i = 1...4)$ are *real values* specifying the desired poles of the error dynamics. The solution can be written in abbreviated form as:

$$\Sigma\, \overline{k} = \mu \tag{6.49}$$

where $\overline{k} = [K_1, K_2, K_3, K_4]^T$ is the estimator gain vector and:

$$\Sigma = \begin{bmatrix} \omega_n^2/T & \omega_n^2 & 0 & 0 \\ 2\zeta\omega_n/T + \omega_n^2 & 2\zeta\omega_n & -\omega_n^2/T & 0 \\ (1/T + 2\zeta\omega_n) & 1 & -\omega_n^2 & 1/T \\ 1 & 0 & 0 & 1 \end{bmatrix} \tag{6.50}$$

$$\mu = \begin{bmatrix} p_1p_2p_3p_4 \\ -p_1p_2p_4 - p_1p_2p_3 - p_2p_3p_4 - p_1p_3p_4 - \omega_n^2/T \\ p_1p_2 + p_2p_4 + p_2p_3 + p_1p_4 + p_1p_3 + p_3p_4 - (\omega_n^2 + 2\zeta\omega_n/T) \\ -p_1 - p_2 - p_3 - p_4 - (2\zeta\omega_n + 1/T) \end{bmatrix} \tag{6.51}$$

Consequently, $\overline{k}$ can be computed as:

$$\overline{k} = \Sigma^{-1}\, \mu \tag{6.52}$$

Notice that $\overline{k}$ depends on the ship time constant (T) and the wave model parameters (ζ, ω_n) while p_i $(i = 1...4)$ are four design parameters specifying the poles of the error dynamics. Typical Bode plots for $\hat{\psi}_L/\psi$, $\hat{\psi}_H/\psi$ and $\hat{r}_L/\psi$ are shown in Figures 6.9–6.11, respectively.

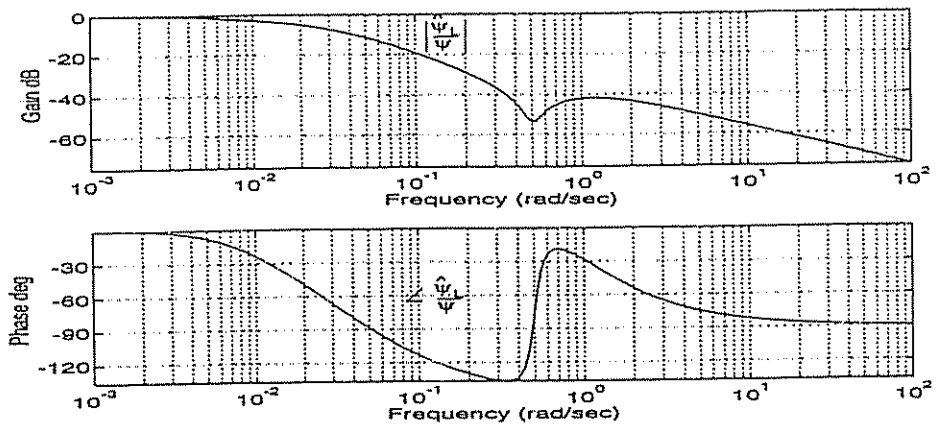

Figure 6.9: Bode plot showing $\hat{\psi}_L(s)/\psi(s)$. Notice that wave disturbances are suppressed around the modal frequency $\omega_n = 0.5$ (rad/s).

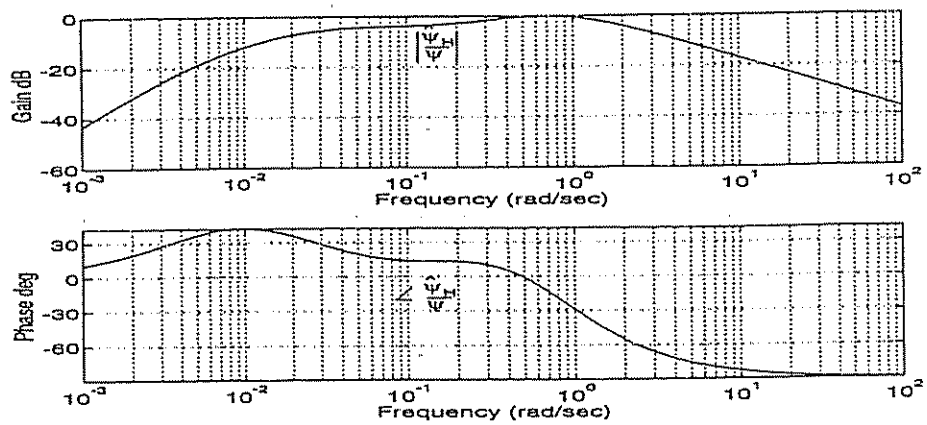

Figure 6.10: Bode plot showing $\hat{\psi}_H(s)/\psi(s)$. Notice that $\psi_H(s) \approx \psi(s)$ in the frequency band around the wave frequency $\omega_n = 0.5$ (rad/s) while LF components of the ship dynamics and HF noise are attenuated.

Computer simulations show that the observer is highly robust for parameter uncertainties if the pole locations are chosen carefully. A guideline could be to choose the real p_i-values according to:

$$p_1 < -1/T \tag{6.53}$$

$$p_2 < 0 \tag{6.54}$$

$$p_3 = p_4 < -\zeta\omega_n \tag{6.55}$$

Typical values are $p_1 = -1.1/T$, $p_2 = -10^{-4}$ and $p_3 = p_4 = -15\,\zeta\omega_n$ where $\zeta = 0.01$–0.1 . The real part of the first two poles p_1 and p_2 are chosen slightly to

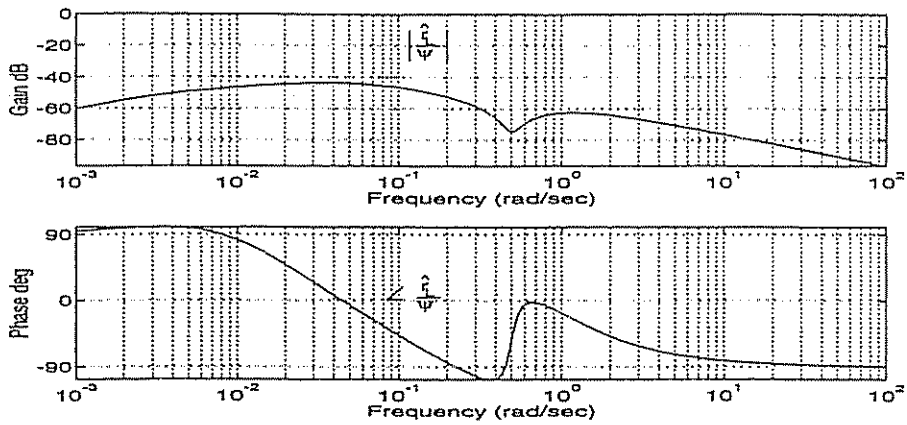

Figure 6.11: Bode plot showing $\hat{r}_L(s)/\psi(s)$. Notice that the LF yaw rate signal $\hat{r}_L(s)$ is equal to $s\hat{\psi}_L(s)$ for frequencies less than ω_n, but the same signal is notch and low-pass filtered for frequencies higher than ω_n.

the left of the open-loop poles $-1/T$ and 0 of the LF model, respectively. This ensures that the error dynamics corresponding to the LF states are faster than the ship dynamics. To obtain proper filtering, the HF estimation error corresponding to the 1st-order wave disturbances should converge to zero much faster than the LF states. This is done by choosing $p_3 = p_4$ to the left of p_1 and p_2. Both HF poles are real in order to avoid an oscillatoric convergence of the HF state estimation error to zero. Notice that the convergence of the HF state estimation error is not affected by the complex conjugate poles of the wave model.

The state estimator (6.26)–(6.30) with gain update (6.52) can be written in state-space form according to:

$$\dot{\hat{\boldsymbol{x}}} = \boldsymbol{A}\,\hat{\boldsymbol{x}} + \boldsymbol{b}\,u + \boldsymbol{k}\,(y - \boldsymbol{c}^T\hat{\boldsymbol{x}}) \tag{6.56}$$

where $\hat{\boldsymbol{x}} = [\hat{\delta}_0, \hat{\psi}_L, \hat{r}_L, \hat{\xi}_H, \hat{\psi}_H]^T$, $u = \delta$, $\boldsymbol{k} = [K_0, K_1, K_2, K_3, K_4]^T$ and:

$$\boldsymbol{A} = \left[\begin{array}{ccc|cc} 0 & 0 & 0 & 0 & 0 \\ 0 & 0 & 1 & 0 & 0 \\ -\frac{K}{T} & 0 & -\frac{1}{T} & 0 & 0 \\ \hline 0 & 0 & 0 & 0 & 1 \\ 0 & 0 & 0 & -\omega_n^2 & -2\,\zeta\,\omega_n \end{array}\right]; \qquad \boldsymbol{b} = \left[\begin{array}{c} 0 \\ 0 \\ \frac{K}{T} \\ \hline 0 \\ 0 \end{array}\right] \tag{6.57}$$

It is then straightforward to show that:

$$\hat{\boldsymbol{x}}(s) = (sI - \boldsymbol{A} + \boldsymbol{k}\boldsymbol{c}^T)^{-1}\,(\boldsymbol{k}\,y(s) + \boldsymbol{b}\,u(s)) \tag{6.58}$$

Assume that $u(s) = 0$ (no feedback). Hence, we can define:

$$\boldsymbol{h}(s) = [h_1, h_2, h_3, h_4, h_5]^T = (sI - \boldsymbol{A} + \boldsymbol{k}\boldsymbol{c}^T)^{-1}\,\boldsymbol{k} \tag{6.59}$$

which implies that $\hat{\psi}_L(s)$ can be written:

$$\hat{\psi}_L(s) = h_2(s)\,\psi(s) \tag{6.60}$$

Moreover, it can be seen from the Bode plot that the low-frequency yaw angle state estimate can be generated by using two filters:

$$h_2(s) = h_{\text{notch}}(s)\,h_{\text{low pass}}(s) \tag{6.61}$$

which simply states that $\hat{\psi}_L(s)$ is obtained by cascading a notch filter with a low-pass filter. This result has been theoretically verified by Grimble (1978). In this work Grimble showed that the stationary Kalman filter for the ship positioning problem will be approximately equivalent to a notch filter in cascade with a second filter, typically a low-pass filter.

However, if feedback is present it is well known that application of a Kalman filter is superior to notch filtering since the Kalman filter algorithm includes feedforward from the input $\boldsymbol{u}$ in addition to filtering of the measured output $\boldsymbol{y}$. In fact, this feedforward term removes the problems associated with additional phase lag in the filtered signal which is the main problem of most standard filters (low-pass, high-pass, notch etc.). Simulation results verifying these observations have been documented in Grimble et al. (1980a).

Example 6.2 (Design of State Estimator for Course Control)
The performance of the state estimator is best illustrated by considering an example (Fossen 1993b). Consider a cargo ship described by $K = 0.35$ (s^{-1}) and $T = 29.0$ (s). Furthermore let the wave disturbances be described by $\omega_n = 0.5$ (rad/s), $\zeta = 0.1$ and:

$$K_w = \begin{cases} 0.03 & \text{for } t \leq 100\ (s) \\ 0.10 & \text{for } t > 100\ (s) \end{cases}$$

Let the yaw angle of the ship be controlled by a PD-control law:

$$\delta = 0.83\,(\psi_d - \hat{\psi}_L) - 13.71\,\hat{r}_L \tag{6.62}$$

which yields a closed-loop system with natural frequency $\omega_n = 0.1$ (rad/s). In the simulation study, the desired yaw angle was chosen as $\psi_d = 10^\circ$ for $t \leq 100$ (s) and $\psi_d = 0^\circ$ for $t > 100$ (s). Furthermore, the state estimates were computed by choosing the error dynamics poles according to $p_1 = -1.1/T$, $p_2 = -10^{-4}$ and $p_3 = p_4 = -15\,\zeta\omega_n$, which yields the estimator gain vector:

$$\overline{k} = [7.3528 \cdot 10^{-3},\ -2.4501 \cdot 10^{-4},\ -1.2689,\ 1.3962]^T \tag{6.63}$$

A typical time-series for this set of parameters is shown in Figure 6.12. We see that the state estimation errors are small and that excellent performance is obtained even for wave disturbances up to $\pm 10^\circ$ in amplitude.

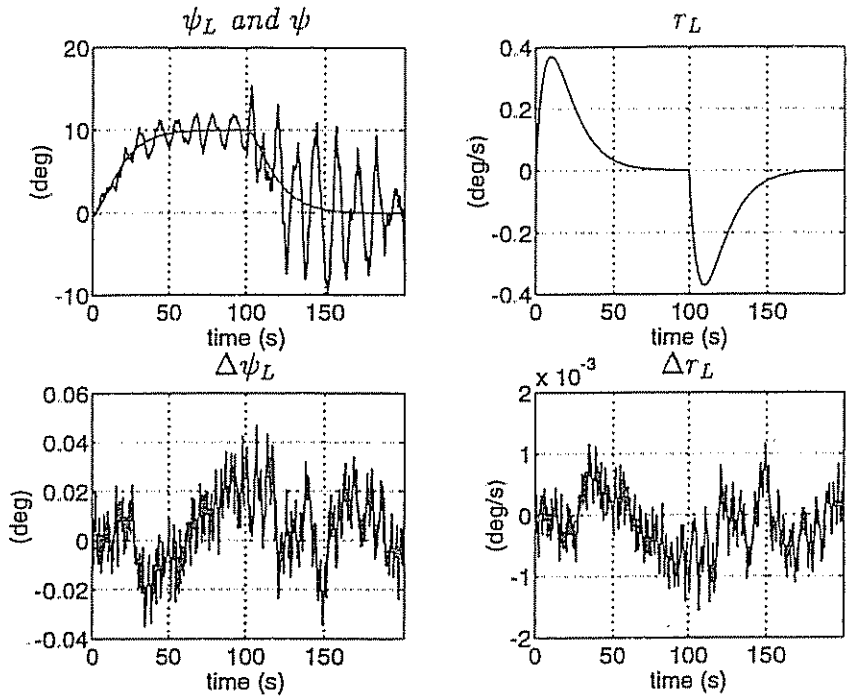

Figure 6.12: LF yaw angle ψ_L and measured yaw angle $\psi = \psi_L + \psi_H$ (upper left), LF yaw rate r_L (upper right), LF yaw angle estimation error $\Delta\psi_L$ (lower left) and LF yaw rate estimation error Δr_L (lower right) versus time. The simulation study was performed with a sampling time of 0.3 (s) while the yaw angle measurement noise was limited to ± 0.1 (deg).

6.1.4 Kalman Filter Based Wave Filter Design

An alternative solution to the pole-placement technique is to apply a Kalman filter (KF) to compute the gain vector $\boldsymbol{k}$. Kalman filtering (or *optimal state estimation* in sense of minimum variance) allows the user to estimate the state $\boldsymbol{x}$ of a dynamic system recursively from a noise-contaminated measurement $\boldsymbol{y}$. The interested reader is advised to consult Gelb et al. (1988) for details on Kalman filter design, whereas applications in the field of guidance and control can be found in Lin (1992).

Linear Problem Statement

Consider the linear continuous-time system:

$$\dot{\boldsymbol{x}}(t) = \boldsymbol{A}(t)\,\boldsymbol{x}(t) + \boldsymbol{B}(t)\,\boldsymbol{u}(t) + \boldsymbol{E}(t)\,\boldsymbol{w}(t) \tag{6.64}$$

where the process noise is described by $\boldsymbol{w}(t) \sim N(0, \boldsymbol{Q}(t))$. The notation:

$$x(t) \sim N(m, X(t)) \tag{6.65}$$

is adopted from Gelb et al. (1988) and indicates that $x(t)$ is a Gaussian (normal) random vector with mean m and covariance matrix $X(t)$. In the one-dimensional case $X(t)$ corresponds to the squared *standard deviation* σ^2, such that:

$$x(t) \sim N(m, \sigma^2) \tag{6.66}$$

Furthermore, let the measurement equation (sensor system) be represented by:

$$z(t) = H(t)\, x(t) + v(t) \tag{6.67}$$

where $v(t) \sim N(0, R)$ is the measurement noise.

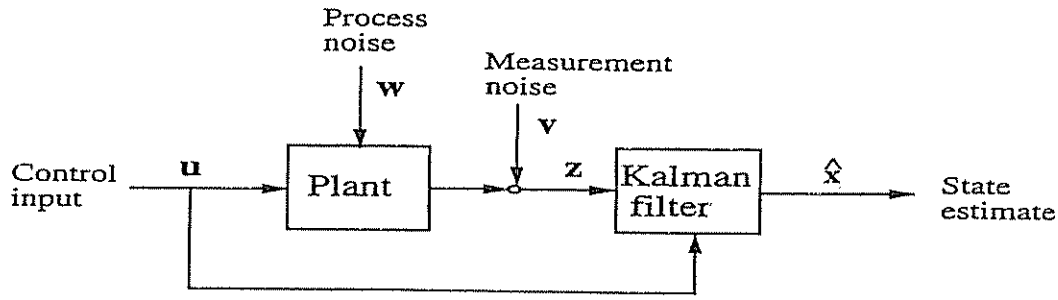

Figure 6.13: Optimal state estimation.

If the system (6.64) and (6.67) is *observable*, the state vector $x(t) \in \mathbb{R}^n$ can be reconstructed recursively through the measurement vector $z(t) \in \mathbb{R}^m$ and the control input vector $u(t) \in \mathbb{R}^p$, see Figure 6.13. Moreover, observability simply defines the ability to determine the state $x(t)$ from the measurement $z(t)$.

The conditions for observability are given below while the optimal state estimator for the system (6.64) and (6.67) is given in Table 6.1.

Definition 6.1 (Observability: Time-Invariant System)
A linear time-invariant system with state and measurement matrices (A, H) is observable if the $n \times n$ observability matrix *(Gelb et al. 1988):*

$$\mathcal{O} = [H^T \mid A^T H^T \mid \ldots \mid (A^T)^{n-1} H^T] \tag{6.68}$$

has full rank.

Definition 6.2 (Observability: Time-Varying System)
A linear time-varying system with state and measurement matrices $(A(t), H(t))$ is observable if $\exists\, T > 0$ and $\beta \geq \alpha > 0$ such that:

$$\alpha\, I \leq \frac{1}{T} \int_{t_0}^{t_0+T} \exp(A^T(\tau)\tau)) H^T(\tau) H(\tau) \exp(A(\tau)\ )\ d\tau \leq \beta\, I \tag{6.69}$$

$\forall\, t_0 \in \mathbb{R}_+$. *This simply states that the integral of the matrix* $\exp(A^T\tau) H^T H \exp(A\tau)$ *is uniformly positive definite over any interval of length T.*

Table 6.1: Summary of continuous-time Kalman filter (Gelb et al. 1988).

Initial conditions	$\hat{x}(0) = x_0$ $X(0) = E[(x(0) - \hat{x}(0))(x(0) - \hat{x}(0))^T] = X_0$
Kalman gain matrix	$K(t) = X(t)H^T(t)\,R^{-1}(t)$
State estimate propagation	$\dot{\hat{x}}(t) = A(t)\,\hat{x}(t) + B(t)\,u(t) + K(t)\,[z(t) - H(t)\,\hat{x}(t)]$
Error covariance propagation	$\dot{X}(t) = A(t)\,X(t) + X(t)\,A^T(t) + E(t)\,Q(t)\,E^T(t)$ $-X(t)H^T(t)R^{-1}(t)H(t)X(t)$

Continuous-Time Steady-State Kalman Filter

An attractive simplification of the continuous-time Kalman filter is the steady-state solution obtained for the time-invariant system:

$$\dot{x}(t) = A\,x(t) + B\,u(t) + E\,w(t); \qquad w(t) \sim N(0, Q) \tag{6.70}$$

$$z(t) = H\,x(t) + v(t); \qquad v(t) \sim N(0, R) \tag{6.71}$$

The steady-state Kalman filter gain is given by:

$$K_\infty = X_\infty\,H^T\,R^{-1} \tag{6.72}$$

where X_∞ is the steady-state solution of the matrix Ricatti equation:

$$A\,X_\infty + X_\infty\,A^T + E\,Q\,E^T - X_\infty H^T R^{-1} H X_\infty = 0 \tag{6.73}$$

Hence, we can compute the state estimates according to:

$$\dot{\hat{x}}(t) = A\,\hat{x}(t) + B\,u(t) + K_\infty\,[z(t) - H\,\hat{x}(t)] \tag{6.74}$$

Applications to the Ship-Wave System

The ship-wave system is described by the state $x = [\delta_0, \psi_L, r_L, \xi_H, \psi_H]^T$, input $u = \delta$ and process noise $w = [w_0, w_L, w_H]^T$. Furthermore, we assume that $w \sim N(0, Q)$ and $v \sim N(0, r)$. The model is given by:

$$A = \left[\begin{array}{ccc|cc} 0 & 0 & 0 & 0 & 0 \\ 0 & 0 & 1 & 0 & 0 \\ -\frac{K}{T} & 0 & -\frac{1}{T} & 0 & 0 \\ \hline 0 & 0 & 0 & 0 & 1 \\ 0 & 0 & 0 & -\omega_n^2 & -2\,\zeta\,\omega_n \end{array}\right] \quad b = \left[\begin{array}{c} 0 \\ 0 \\ \frac{K}{T} \\ \hline 0 \\ 0 \end{array}\right] \quad E = \left[\begin{array}{ccc} 1 & 0 & 0 \\ 0 & 0 & 0 \\ 0 & 1 & 0 \\ \hline 0 & 0 & 0 \\ 0 & 0 & 1 \end{array}\right] \quad h = \left[\begin{array}{c} 0 \\ 1 \\ 0 \\ \hline 0 \\ 1 \end{array}\right]$$

Continuous-Time Wave Filter Design

According to Table 6.1, the SISO continuous-time state estimator takes the form:

$$\dot{\hat{x}}(t) = A(t)\,\hat{x}(t) + b(t)\,u(t) + k(t)\,[z(t) - h^T\,x(t)] \tag{6.75}$$

where the Kalman filter gain is computed as:

$$k(t) = \frac{1}{r}\,X(t)\,h \tag{6.76}$$

Furthermore, the covariance matrix $X(t) = E[\tilde{x}(t)\tilde{x}^T(t)]$ where $\tilde{x}(t) = x(t) - \hat{x}(t)$ is computed by numerical integration of:

$$\dot{X}(t) = A(t)\,X(t) + X(t)\,A^T(t) + E\,Q\,E^T - \frac{1}{r}X(t)hh^TX(t) \tag{6.77}$$

The disadvantage with the Kalman filter approach is that information about the process and measurement noise is required. In fact, the variance of the process and measurement noise will vary with each sea state, which means that a large number of Kalman gains must be computed. Since the gain and time constants are speed- and thus time-dependent a steady-state solution of $X(t)$ and $k(t)$ cannot be computed directly. However, by properly scaling the system matrices with respect to $U(t)$ and L a steady-state solution can be found.

Continuous-Time Steady-State Wave Filter Design

The model parameters can be made non-dimensional by defining the time and gain constants as $T' = T\,(U/L)$ and $K' = K\,(L/U)$, respectively; the wave frequency is scaled according to $\omega_n' = \omega_n\,(L/U)$. Furthermore, we introduce the time scaling $t' = t\,(U/L)$ and:

$$\begin{array}{lllllllll}
\dot{r}_L' & = & \dot{r}_L\,(L/U)^2 & r_L' & = & r_L\,(L/U) & w_L' & = & w_L\,(L/U)^2 \\
\dot{\psi}_L' & = & \dot{\psi}_L\,(L/U) & \psi_L' & = & \psi_L & w_0' & = & w_0\,(L/U) \\
\dot{\delta}_0' & = & \dot{\delta}_0\,(L/U) & \delta_0' & = & \delta_0 & w_H' & = & w_H\,(L/U) \\
\dot{\psi}_H' & = & \dot{\psi}_H\,(L/U) & \psi_H' & = & \psi_H & \delta' & = & \delta \\
\dot{\xi}_H' & = & \dot{\xi}_H & \xi_H' & = & \xi_H\,(U/L) & v' & = & v
\end{array} \tag{6.78}$$

Hence, the scaled ship-wave model can be written in vector form as:

$$\dot{x}'(t) = A'x'(t) + b'u'(t) + E'w'(t) \tag{6.79}$$

with time-invariant quantities:

$$A' = \left[\begin{array}{ccc|cc} 0 & 0 & 0 & 0 & 0 \\ 0 & 0 & 1 & 0 & 0 \\ -\frac{K'}{T'} & 0 & -\frac{1}{T'} & 0 & 0 \\ \hline 0 & 0 & 0 & 0 & 1 \\ 0 & 0 & 0 & -(\omega_n')^2 & -2\,\zeta\,\omega_n' \end{array}\right] \quad b' = \left[\begin{array}{c} 0 \\ 0 \\ \frac{K'}{T'} \\ \hline 0 \\ 0 \end{array}\right] \quad E' = E \quad h' = h$$

Notice that all these matrices and vectors are independent of $U(t)$ and L. We now compute a non-dimensional *constant* Kalman gain as:

$$k'_\infty = \frac{1}{\tau'} X'_\infty h' \tag{6.80}$$

where X'_∞ is the steady-state solution found by solving:

$$A' X'_\infty + X'_\infty (A')^T + E' Q' (E')^T - \frac{1}{\tau'} X'_\infty h' (h')^T X'_\infty = 0 \tag{6.81}$$

The last step in the design involves transforming the constant gain k'_∞ to:

$$k_\infty(t) = S(t) k'_\infty \tag{6.82}$$

where $S(t)$ is a scaling matrix defined as:

$$S(t) = \begin{bmatrix} U(t)/L & 0 & 0 & 0 & 0 \\ 0 & U(t)/L & 0 & 0 & 0 \\ 0 & 0 & [U(t)/L]^2 & 0 & 0 \\ 0 & 0 & 0 & 1 & 0 \\ 0 & 0 & 0 & 0 & U(t)/L \end{bmatrix} \tag{6.83}$$

By doing this, we can precompute k'_∞ and then use $U(t)$ to compute k_∞ in (6.74). We will now show how a discrete-time version of the wave filter can be designed.

Discrete-Time Wave Filter Design

The steady-state Kalman filter (6.74) can be written as:

$$\dot{\hat{x}}(t) = A_f \hat{x}(t) + B u(t) + K_\infty z(t) \tag{6.84}$$

where u and z are the measured signals and:

$$A_f = A - K_\infty H \tag{6.85}$$

A discrete-time representation of this model is (see Appendix B.1):

$$\hat{x}(k+1) = \Phi \hat{x}(k) + \Delta u(k) + \Omega z(k) \tag{6.86}$$

where

$$\Phi = \exp(A_f h) \approx I + A_f h + \frac{1}{2}(A_f h)^2 + \ldots + \frac{1}{N!}(A_f h)^N \tag{6.87}$$

$$\Delta = A_f^{-1}(\Phi - I) B \tag{6.88}$$

$$\Omega = A_f^{-1}(\Phi - I) K_\infty \tag{6.89}$$

and h is the sampling time. Notice that Euler integration implies choosing $N = 1$, that is $\Phi(k) = I + A_f h$.

An alternative approach could be to use the discrete-time Kalman filter algorithm in Table 6.2. This algorithm, however, requires that the state estimation error covariance matrix $\hat{\boldsymbol{X}}(k)$ ($n(n+1)/2$ differential equations) is computed on-line together with the state estimation vector $\hat{\boldsymbol{x}}(k)$ (n differential equations).

Table 6.2: Summary of discrete-time Kalman filter (Gelb et al. 1988).

Initial conditions	$\overline{\boldsymbol{x}}(0) = \boldsymbol{x}_0$ $\overline{\boldsymbol{X}}(0) = E[(\boldsymbol{x}(0) - \hat{\boldsymbol{x}}(0))(\boldsymbol{x}(0) - \hat{\boldsymbol{x}}(0))^T] = \boldsymbol{X}_0$
Kalman gain matrix State estimate update Error covariance update	$\boldsymbol{K}(k) = \overline{\boldsymbol{X}}(k)\boldsymbol{H}^T(k)\,[\boldsymbol{H}(k)\overline{\boldsymbol{X}}(k)\boldsymbol{H}^T(k) + \boldsymbol{R}(k)]^{-1}$ $\hat{\boldsymbol{x}}(k) = \overline{\boldsymbol{x}}(k) + \boldsymbol{K}(k)\,[\boldsymbol{z}(k) - \boldsymbol{H}(k)\,\overline{\boldsymbol{x}}(k)]$ $\hat{\boldsymbol{X}}(k) = [\boldsymbol{I} - \boldsymbol{K}(k)\boldsymbol{H}(k)]\,\overline{\boldsymbol{X}}(k)\,[\boldsymbol{I} - \boldsymbol{K}(k)\boldsymbol{H}(k)]^T$ $+\boldsymbol{K}(k)\,\boldsymbol{R}(k)\,\boldsymbol{K}^T(k)$
State estimate propagation Error covariance propagation	$\overline{\boldsymbol{x}}(k+1) = \boldsymbol{\Phi}(k)\hat{\boldsymbol{x}}(k) + \boldsymbol{\Delta}(k)\boldsymbol{u}(k)$ $\overline{\boldsymbol{X}}(k+1) = \boldsymbol{\Phi}(k)\,\hat{\boldsymbol{X}}(k)\,\boldsymbol{\Phi}^T(k) + \boldsymbol{\Gamma}(k)\,\boldsymbol{Q}(k)\,\boldsymbol{\Gamma}^T(k)$

The main problem in the realization of the state estimator is that the parameters K, T, ω_n and ζ are unknown. Satisfactory values for the non-dimensional ship parameters (K', T') can usually be found from maneuvering trials or by parameter estimation (see Section 6.8). Holzhüter (1992) claims that the damping coefficient in the wave model can be chosen rather arbitrarily as long as it is low (typically $\zeta = 0.01$–0.1) whereas the wave frequency ω_n can be treated as a tunable parameter. In some cases it can be advantageous to estimate ω_n on-line by applying a frequency tracker (see below).

Kalman filter based wave filtering has been discussed by numerous authors. The interested reader is advised to consult the following references for details; Balchen et al. (1976), Balchen, Jenssen and Sælid (1980a, 1980b), Grimble et al. (1980a, 1980b), Fung and Grimble (1981, 1983), Fotakis, Grimble and Kouvaritakis (1982), Sagatun, Sørensen and Fossen (1994a), Sælid and Jenssen (1983), Sælid et al. (1983), Holzhüter and Strauch (1987), Holzhüter (1992), Reid, Tugcu and Mears (1984).

6.1.5 Wave Frequency Tracker

In this section we will show that the peak frequency of a wave spectrum can be estimated by fitting an ARMA-model (see Section 6.8.4) to the following wave transfer function approximation:

$$\psi_H(s) = \frac{K_w\, s}{s^2 + 2\zeta\omega\, s + \omega^2}\, w(s) \tag{6.90}$$

Unfortunately, we cannot measure $\psi_H(s)$ directly since a compass measurement will contain both the LF ship motion $\psi_L(s)$ and the 1st-order wave disturbances $\psi_H(s)$, that is:

$$\psi(s) = \psi_L(s) + \psi_H(s) \tag{6.91}$$

This problem can be circumvented by applying the approach proposed by Holzhüter and Strauch (1987) who suggest that $\psi_H(s)$ can be separated from the measurement by introducing a filtered signal $\hat{\psi}_H(s)$. Moreover, we can generate an approximation of $\psi_H(s)$ by:

$$\hat{\psi}_H(s) = h_{HP}(s)\, \psi(s) \tag{6.92}$$

where $h_{HP}(s)$ is a high-pass filter with cut-off frequency lower than the dominating wave frequency. This is based on the assumption that the high-pass filter will attenuate LF motion components generated by the control input $u(s)$, according to:

$$h_{HP}(s)\, \psi_L(s) = h_{HP}(s)\, h_{ship}(s)\, u(s) \ll 1 \tag{6.93}$$

If this holds, then $\psi_H(s) \approx \hat{\psi}_H(s)$ in the actual region of the wave disturbance (see Figure 6.14).

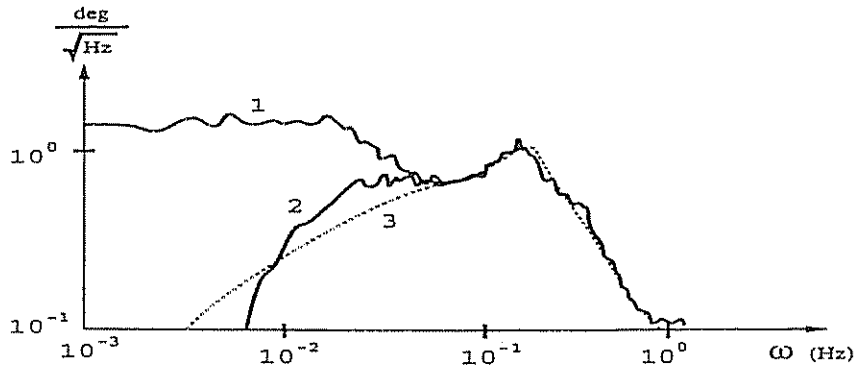

Figure 6.14: (1) original, (2) filtered and (3) estimated yaw angle spectrum (Holzhüter and Strauch 1987).

This suggests that we can design a frequency tracker based on the filtered signal $\hat{\psi}_H(s)$ instead. Let us define a new state variable $\xi_H(s)$ according to (see Figure 6.15):

$$\xi_H(s) = \frac{1}{s}\, \psi_H(s) = \frac{K_w}{s^2 + 2\zeta\omega\, s + \omega^2}\, w(s) \tag{6.94}$$

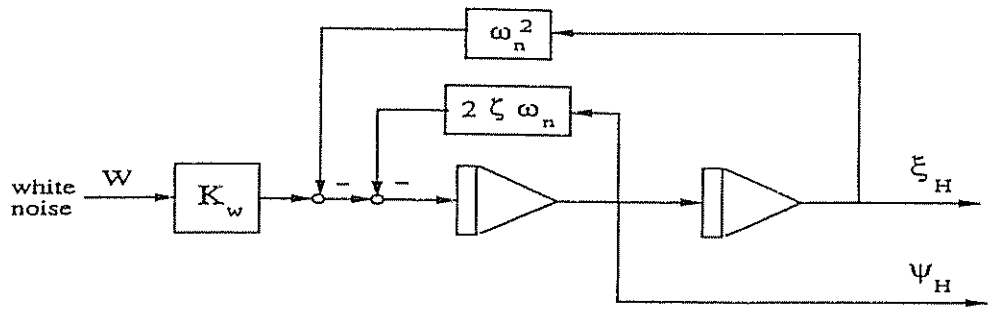

Figure 6.15: Block-diagram showing linear wave model in terms of ψ_H and ξ_H.

We can estimate $\psi_H(s)$ by using a 1st-order high-pass filter:

$$\hat{\psi}_H(s) = \frac{T_f s}{1 + T_f s}\,\psi(s) \qquad \text{(High-Pass)} \tag{6.95}$$

with filter time constant T_f. Hence an estimate of $\xi_H(s)$ can be computed according to:

$$\hat{\xi}_H(s) = \frac{T_f}{1 + T_f s}\,\psi(s) \qquad \text{(Low-Pass + Amplifier)} \tag{6.96}$$

This is advantageous since the filtered signal $\hat{\xi}_H(s)$ can be described by a simple AR-model corresponding to a 2nd-order wave disturbance model while pure derivation of $w(s)$ implies that $\hat{\psi}_H(s)$ must be modelled as an ARMA-model. This is the main motivation for using the signal $\hat{\xi}_H(s)$ instead of $\hat{\psi}_H(s)$ in the parameter estimation algorithm.

Holzhüter and Strauch (1987), however, claim that a third pole $-1/T$ should be included in the model (6.94) to account for LF parts that have passed the filter (6.96). Moreover:

$$\hat{\xi}_H(s) = \frac{1}{(s^2 + 2\zeta\omega\, s + \omega^2)(1 + Ts)}\,e(s) \tag{6.97}$$

where $e(s) = K_w w(s)$. This model can be represented by an AR-model:

$$A(z^{-1})\,\hat{\xi}_H(k) = e(k) \tag{6.98}$$

where

$$A(z^{-1}) = 1 + a_1\, z^{-1} + a_2\, z^{-2} + a_3\, z^{-3} \tag{6.99}$$

The parameters a_1, a_2 and a_3 in this model can be estimated by means of recursive least squares (RLS) estimation with constant forgetting (see Section 6.8.4):

$$\hat{\theta}(k) \;=\; \hat{\theta}(k-1) + \boldsymbol{K}(k)\,[y(k) - \boldsymbol{\phi}^T(k)\,\hat{\theta}(k-1)] \tag{6.100}$$

$$K(k) = \frac{P(k-1)\phi(k)}{\lambda + \phi^T(k)P(k-1)\phi(k)} \tag{6.101}$$

$$P(k) = \frac{1}{\lambda}[I - K(k)\phi^T(k)]\, P(k-1)] \tag{6.102}$$

Here $y(k) = \hat{\xi}_H(k)$ is the filtered signal, $\phi(k) = [-y(k-1), -y(k-2), -y(k-3)]^T$ and $\theta(k) = [a_1(k), a_2(k), a_3(k)]^T$. The wave frequency estimate can be computed from the a_i-values by transforming the roots z_i $(i = 1...3)$ of the discrete-time equation:

$$A(z^{-1}) = 1 + a_1\, z^{-1} + a_2\, z^{-2} + a_3\, z^{-3} = 0 \tag{6.103}$$

to the continuous-time domain by:

$$z_i = \exp(h\, s_i) \quad \Longrightarrow \quad s_i = \frac{1}{h}\ln(z_i) \tag{6.104}$$

where s_i $(i = 1...3)$ is the continuous-time pole locations and h is the sampling time. This yields one real solution s_3 corresponding to the estimated pole $1/T$ and a complex conjugate pair $s_{1,2}$ corresponding to the pole locations of the 2nd-order wave model, that is:

$$s_{1,2} = -\alpha \pm j\,\beta \tag{6.105}$$

Hence, the wave frequency estimate is:

$$\omega_n = |s_{1,2}| = \sqrt{\alpha^2 + \beta^2} \tag{6.106}$$

The performance of the wave frequency adaptation algorithm for a heading controlled ship is illustrated in Figure 6.16.

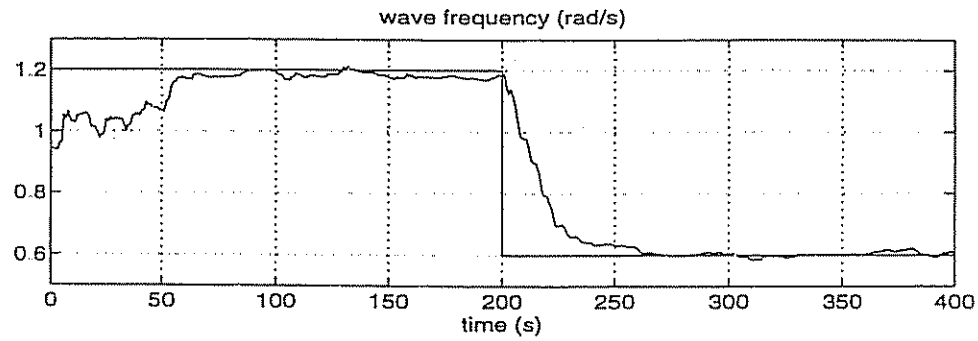

Figure 6.16: Estimated frequency as a function of time. Notice that ω_n is changed from 1.2 (rad/s) to 0.6 (rad/s) after 200 (s).

An alternative wave frequency adaptation algorithm is proposed by Sælid et al. (1983) who use a recursive prediction error method together with a Kalman filter to estimate the wave frequency.

6.2 Forward Speed Control

by Mogens Blanke[1] and Thor I. Fossen

This section describes the most important thrust devices and machinery in ship speed-propulsion systems. Emphasis is placed on propellers as thrust devices, prime mover control, ship speed control and speed control for cruising.

6.2.1 Propellers as Thrust Devices

The two main types of propellers available for ordinary merchant vessels are fixed blade propellers (FP) and controllable pitch (CP) propellers. These two types are widely used as prime mover thrust devices and are also the basis for most thrusters.

Fixed Pitch Propeller

A 1st-order approximation of the propeller thrust T and torque Q can be found from lift force calculations. This approach was taken by Blanke (1981) who used lift force calculations as the basis for approximation of the open water propeller diagram.

Ships usually operate with variable forward speed. Therefore the performance of the propeller will be a function of the speed of the water in the wake of the hull (advance speed) V_a (m/s), propeller revolutions per second n (rps) and propeller diameter D (m). The non-dimensional open water characteristics are defined in terms of the open water advance coefficient J_0:

$$J_0 = \frac{V_a}{nD} \tag{6.107}$$

The range of J_0 values relevant to normal operation is quite narrow. It is only during heavy accelerations and decelerations that the propeller gets exposed to larger parts of the diagram.

The non-dimensional propeller thrust and propeller torque coefficients K_T and K_Q and the thruster open water efficiency η_0, that is the efficiency in undisturbed water, are defined as:

$$K_T = \frac{T}{\rho |n| n\, D^4} \qquad K_Q = \frac{Q}{\rho |n| n\, D^5} \qquad \eta_0 = \frac{J_0}{2\pi} \cdot \frac{K_T}{K_Q} \tag{6.108}$$

Here ρ (kg/m^3) is the water density and T (N) and Q (Nm) are the propeller thrust and torque, respectively. The difference between the ship speed and the average flow velocity over the propeller disc is called the wake. It is common to define the relative speed reduction by introducing the advance speed at the propeller (speed of the water going into the propeller) as:

[1]Department of Control Engineering, Aalborg University, Aalborg, Denmark.

$$V_a = (1 - w)\, U \tag{6.109}$$

where w is the wake fraction number (typically: $0.1 - 0.4$) and U (m/s) is the forward speed of the ship. In practice, the wake fraction number can be determined directly from the open water test results.

Another effect to be considered is the so-called *thrust deduction*. An increase in the flow velocity in the boundary layer behind the ship as a result of the propeller will disturb the pressure balance between the bow and stern. This phenomenon causes extra resistance on the hull which can be described by the thrust deduction number t (typically: 0.05–0.2) by modifying the propeller thrust T to $(1-t)T$. The thrust deduction number will strongly depend on the shape of the stern. Hence, the influence of the hull will be described by the hull efficiency:

$$\eta_H = \frac{1 - t}{1 - w} \tag{6.110}$$

In practice, the ratio between the propeller thrust and torque in open water and behind the stern will differ. This effect can be described by the ratio:

$$\eta_B = \frac{J_0}{2\pi} \frac{K_T}{K_{QB}} = \frac{K_Q}{K_{QB}} \tag{6.111}$$

where K_{QB} is the torque coefficient measured for a propeller behind the stern. Let the relative rotative efficiency η_R be defined as the ratio: $\eta_R = \eta_B/\eta_0$. Hence the total propeller thrust efficiency can be defined as the product:

$$\eta_{TOT} = \eta_0 \cdot \eta_M \cdot \eta_H \cdot \eta_B \tag{6.112}$$

Here η_M is the mechanical efficiency (typically 0.8–0.9). The open water test is usually performed by using a towing carriage or a cavitation tunnel. Then force and torque sensors can be applied to measure the propeller force T and torque Q, respectively. Since the speed V_a of the towing carriage or the water stream in the cavitation tunnel also can be measured, K_T, K_Q and η_0 can be calculated from (6.108). This is usually done by applying a nominal (design) value for n.

Bilinear Thruster Model

Typical curves are shown in Figure 6.17, where K_T and $10 \cdot K_Q$ are plotted versus J_0. It can be shown that the positive propeller thrust and torque can be written (Blanke 1981):

$$T = \rho\, D^4 \underbrace{(\alpha_1 + \alpha_2\, J_0)}_{K_T} |n|n; \qquad Q = \rho\, D^5 \underbrace{(\beta_1 + \beta_2\, J_0)}_{K_Q} |n|n \tag{6.113}$$

where α_1, α_2, β_1 and β_2 are four constants. For convenience, Blanke introduces the notation:

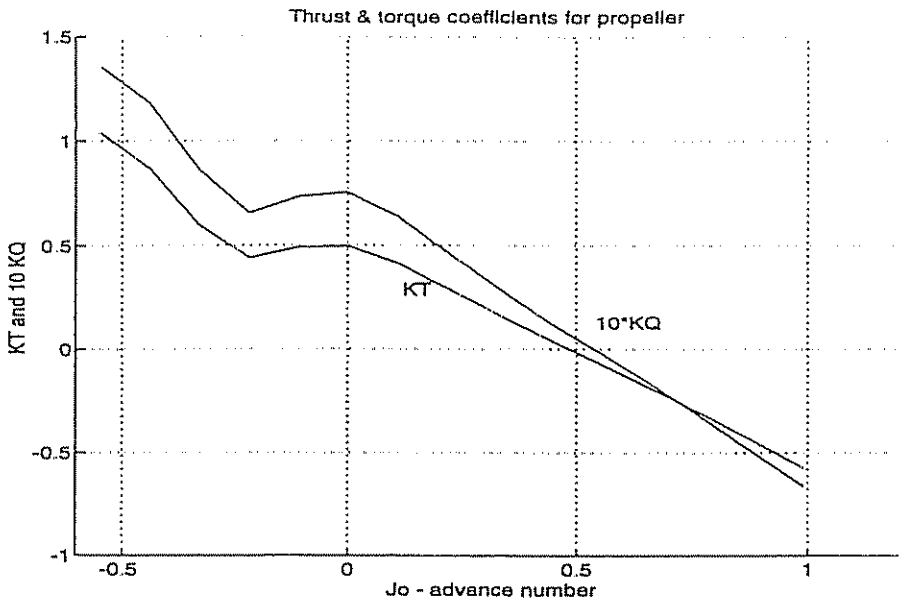

Figure 6.17: Thrust and torque curves for propeller in both ahead ($V_a > 0$) and astern ($V_a < 0$) conditions. n is positive in both cases (Blanke 1994).

$$\begin{aligned} T_{|n|n} &= \rho D^4 \alpha_1 > 0 & \qquad Q_{|n|n} &= \rho D^5 \beta_1 > 0 \\ T_{|n|V_a} &= \rho D^3 \alpha_2 < 0 & \qquad Q_{|n|V_a} &= \rho D^4 \beta_2 < 0 \end{aligned} \tag{6.114}$$

where $T_{|n|n}$, $T_{|n|V_a}$, $Q_{|n|n}$ and $Q_{|n|V_a}$ are design parameters found directly from the open water propeller diagram. Consequently,

$$T = T_{|n|n}\,|n|n + T_{|n|V_a}\,|n|V_a \tag{6.115}$$

$$Q = Q_{|n|n}\,|n|n + Q_{|n|V_a}\,|n|V_a \tag{6.116}$$

Controllable Pitch Propeller

Controllable pitch propellers are screw blade propellers where the blades can be turned under the control of a hydraulic servo system. CP propellers are used where maneuvering properties need to be improved, where a ship has equipment that requires constant shaft speed, or with most twin screw ships. Equipment that requires constant shaft speed includes axis generators coupled directly to the shaft via a gear, that is the generator runs with a multiple of the shaft's angular speed, and certain types of trawl drives used in the fisheries.

For the constant pitch propeller, developed thrust and propeller shaft torque were determined by the bilinear relation with propeller turn rate n and the water velocity V_a at the propeller disc. This is also the case for a variable pitch propeller. Let T and Q be written:

$$T = T_{|n|n}(\theta)\,|n|n + T_{|n|V_a}(\theta)\,|n|V_a \tag{6.117}$$
$$Q = Q_0\,|n|n + Q_{|n|n}(\theta)\,|n|n + Q_{|n|V_a}(\theta)\,|n|V_a \tag{6.118}$$

where the $Q_0\,|n|n$ term represents a torque term that exists even at zero pitch angle. For many propellers Q_0 will be about 5 % of Q at the nominal point of operation.

The coefficients $T_{|n|n}$ etc. are complex functions of the pitch angle θ. This is apparent from Figures 6.18 and 6.19 showing K_T and K_Q curves for a CP propeller with various values of relative pitch, between full ahead (100%) and full astern (−100%). On closer inspection, the curves are not too difficult to approximate, and in a simplified analysis we can assume the linear relations:

$$K_T = (\alpha_1\,\theta) + \alpha_2\,J_0 \tag{6.119}$$
$$K_Q = (\beta_1\,|\theta|) + (\beta_2\,\theta)\,J_0 \tag{6.120}$$

which implies that we can define:

$$\begin{array}{llll} T_{|n|n}(\theta) = T_{|n|n}\,\theta & & T_{|n|V_a}(\theta) = T_{|n|V_a} \\ Q_{|n|n}(\theta) = Q_{|n|n}\,|\theta| & & Q_{|n|V_a}(\theta) = Q_{|n|V_a}\,\theta \end{array} \tag{6.121}$$

Hence we obtain the following thrust and torque for the CP propeller:

$$T = T_{|n|n}\,\theta\,|n|n + T_{|n|V_a}\,|n|V_a \tag{6.122}$$
$$Q = Q_0\,|n|n + Q_{|n|n}\,|\theta|\,|n|n + Q_{|n|V_a}\,\theta\,|n|V_a \tag{6.123}$$

The bilinear approximation gives quite a good approximation in the following cases:

- positive shaft speed, ship speed ahead, positive pitch
- positive shaft speed, ship speed astern, negative pitch

These are the steady-state conditions. The bilinear approximation is up to 40 % erroneous in the transient cases:

- positive shaft speed, ship speed ahead, negative pitch
- positive shaft speed, ship speed astern, positive pitch

Furthermore, cavitation may occur during heavy transients. This, together with the model uncertainty, makes it necessary that controllers are designed with considerable robustness when intended to work during transient conditions.

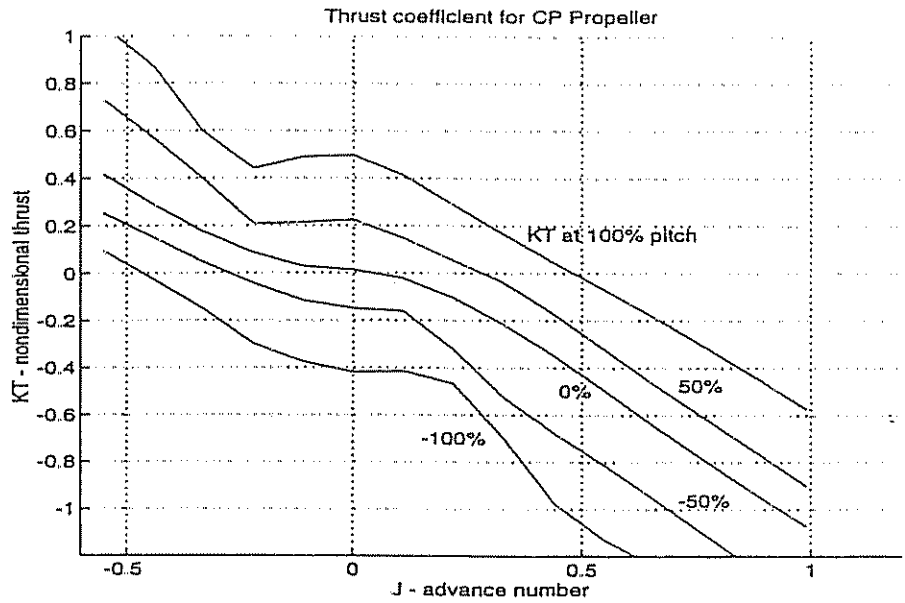

Figure 6.18: K_T characteristic for controllable pitch propeller for medium speed application. Bilinear theory is fairly accurate in steady ahead ($V_a > 0, n > 0$) and astern ($V_a < 0, n > 0$) cases, but not under transient conditions (Blanke 1994).

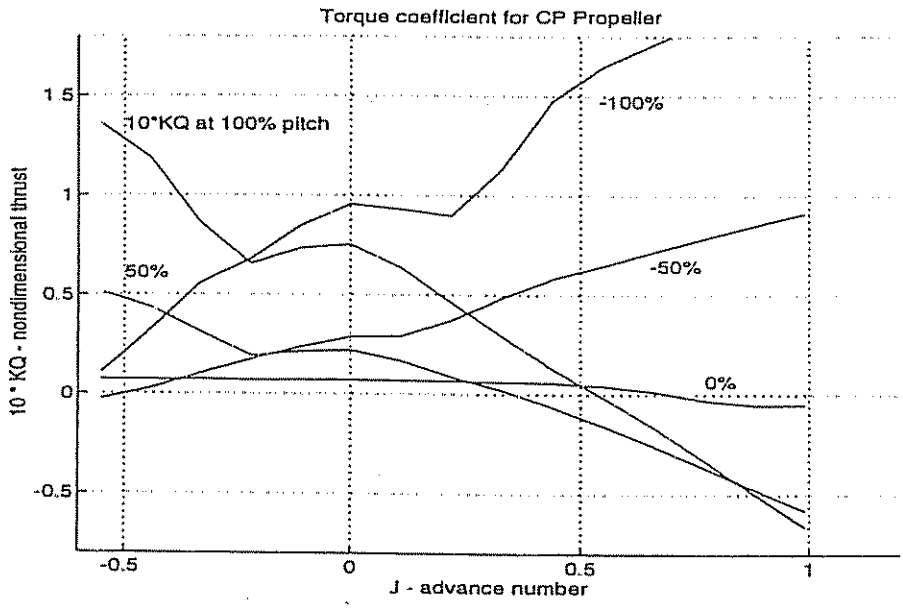

Figure 6.19: K_Q characteristic for controllable pitch propeller for medium speed application. Pitch values from -100 % to 100 % are shown for positive n. Bilinear theory is seen to be fairly accurate in steady ahead and astern cases but not otherwise (Blanke 1994).

Prime Mover Dynamics

The dynamics of the prime mover and its control system is tightly coupled to the speed dynamics of the ship. We will restrict our treatment to standard diesel engines which are used in most new ships. For the interested reader, a reference describing steam turbine systems is Åström and Eklund (1971) while large diesel engines are treated in Andersen (1974). In Blanke (1981) the dynamics of the diesel engine is written as:

$$\frac{d}{dt}\left(\frac{1}{2} I_m\, n^2\right) = (Q_m - Q - Q_f)\, n \tag{6.124}$$

where

n	=	shaft speed (rad/s)
I_m	=	inertia of the rotating parts including the propeller and added inertia of the water (kg m^2)
Q	=	propeller torque (Nm)
Q_m	=	produced torque developed by the diesel engine (Nm)
Q_f	=	friction torque (Nm)

This expression can also be written:

$$I_m \dot{n} = Q_m - Q - Q_f \tag{6.125}$$

Neglecting the friction torque, we obtain the following transfer function:

$$n(s) = \frac{1}{I_m\, s}\left[Q_m(s) - Q(s)\right] \tag{6.126}$$

The transfer function from the position of the fuel pump rack $Y(s)$ to the produced torque developed by the diesel engine $Q_m(s)$ (see Figure 6.20) is usually described by one of the following simple transfer functions:

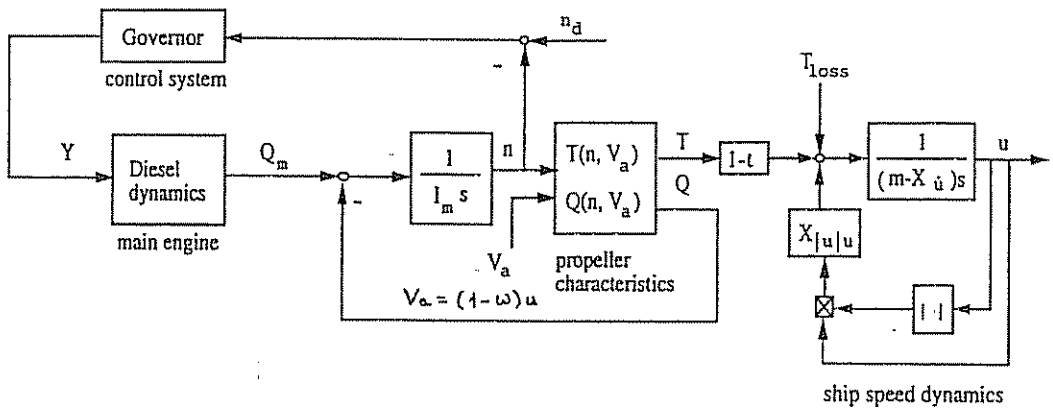

Figure 6.20: Simplified diagram showing the speed-propulsion system (Blanke 1981).

(1) Model of Blanke (1981)

Consider the nonlinear transfer function:

$$\frac{Q_m}{Y}(s) = \frac{K_y \exp(-\tau s)}{1 + T_y s} \tag{6.127}$$

where τ represents the time delay (half the period between consecutive cylinder firings), K_y is the gain constant and T_y is the time constant. On average the developed power $Q_m n$ is proportional to the product Yn of the fuel pump index and shaft speed. Hence, we can compute the torque constant K_y for one constant shaft speed n_0 according to:

$$K_y = \frac{Q_m(n_0)}{Y(n_0)} \tag{6.128}$$

The time delay, from the index setting to the fuel led into each cylinder, can be calculated as:

$$\tau = \frac{1}{2Nn} \tag{6.129}$$

Here N is the number of cylinders each rotating with n (rps). The value of the time constant is approximated as:

$$T_y \approx 0.9 \frac{2\pi}{n} \tag{6.130}$$

where n is in (rps). This model is valid for steady-state operation of two-stroke diesel engines. If a large increase in shaft speed is desired, scavenging air pressure needs to build up to enable acceleration. Large two-stroke engines run at 25–125 (rpm) and are connected directly to the propeller.

(2) Model of Horigome, Hara, Hotta and Ohtsu (1990)

In many applications where a medium speed engine is used it is reasonable to assume that the sampling rate and thus the bandwidth of the main engine governor is somewhat lower than the frequency $1/\tau$ corresponding to the time delay. The medium speed engine runs at 150–500 (rpm) and is connected to the main propellers in a gear box. This suggests that a medium speed diesel engine can be approximated as:

$$\frac{Q_m}{Y}(s) = \frac{K_y}{1 + T_y s} \tag{6.131}$$

for low frequencies.

(3) Model of Ohtsu and Ishizuka (1992)

Statistical identification of the governor–propeller system has shown that a 2nd-order model often yields a better fit to the low pass characteristics of the main engine, that is:

$$\frac{Q_m}{Y}(s) = \frac{K_y}{(1+T_{y_1}s)(1+T_{y_2}s)} \tag{6.132}$$

Here T_{y_1} and T_{y_2} are two time constants. The reason for this is probably the dynamics of the engine's fuel injection system.

Operational Limits for Diesel Engines

The mathematical models above do not assume any limits to developed torque from the diesel engine. There is, however, a maximum torque value that the engine cannot exceed. This value is a function of the shaft speed. On large slow-speed engines it is also a function of the scavenging air pressure.

A torque limit is necessary to avoid mechanical overload of the crankshaft and other mechanical parts. This torque limit is shaft-speed-dependent. At low speed, a certain torque can be allowed. The limit increases gradually and reaches a maximum value.

A scavenging air pressure limit is necessary to keep the oxygen to fuel ratio in the combustion process above a certain value. This is required since the engine will stop if too little oxygen is available for combustion. Before this happen a less severe but certainly undesired effect is caused by a low air to fuel ratio. This results in dramatic pollution from the combustion.

Scavenging air problems are only an issue for large slow-speed engines (25–125 rpm). These have large turbo chargers for the supply of scavenging air pressure, and very large exhaust gas systems to drive the turbo chargers. Time constants of up to 20–30 seconds in the air supply system will limit the increase of fuel during a desired acceleration. Decelerations in shaft speed are not hindered (Blanke and Andersen 1984).

Medium-speed diesel engines (150–500 rpm) have such fast air system response that rapid maneuvers will not be limited by available air supply.

Let p_s denote the scavenging air pressure and n the shaft speed. If the available torque is limited to $Q_{\text{shaft,max}}(n, p_s)$ then the obtainable shaft speed is limited by the torque limit and the ship's speed U as:

$$n = \frac{-Q_{|n|V_a}(1-w)U + \sqrt{[Q_{|n|V_a}(1-w)U]^2 + 4\,Q_{|n|n}Q_{\text{shaft,max}}(n,p_s)}}{2\,Q_{|n|n}} \tag{6.133}$$

Note that $Q_{|n|V_a}$ is a negative quantity and n is therefore positive. A diesel engine manufacturer will always specify the limits of safe operation of a particular engine. The engine controller needs to incorporate these limits in his control strategy; see Figure 6.21, where a slow speed diesel engine is used for illustration.

Prime Mover Control

Figure 6.20 shows the structure of the prime mover controller. The measured shaft speed is compared with a reference speed. A governor (speed controller) controls the fuel injection to the engine in order to obtain the desired speed. Limit curves are incorporated for shaft-speed-dependent torque and air pressure as explained above. The diesel engine control is usually shaft-speed-scaled (Blanke 1986 and Blanke and Nielsen 1990).

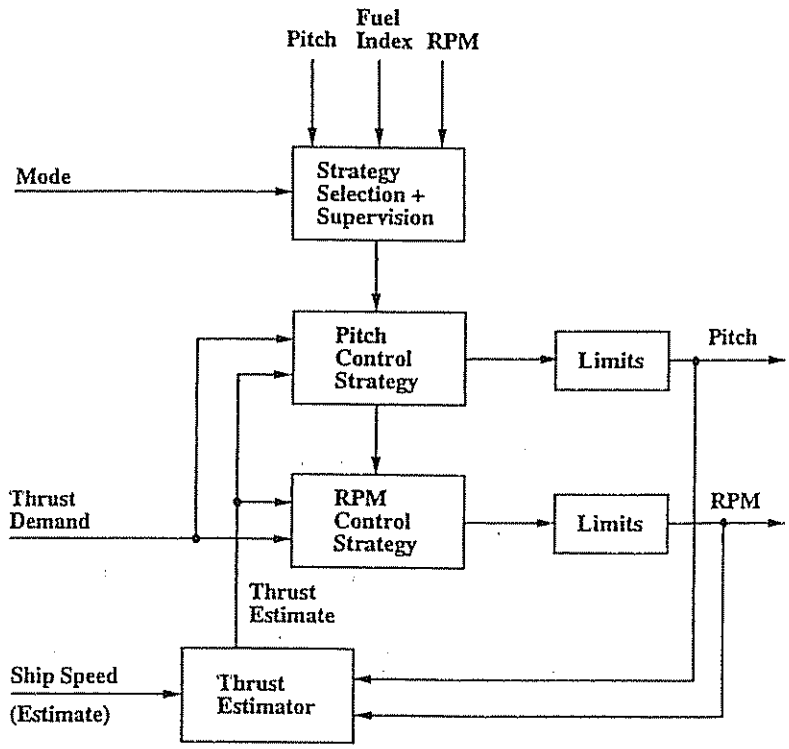

Figure 6.21: Block diagram showing engine controller and limiting functions (Blanke 1994).

6.2.2 Control of Ship Speed

In FP propeller ships, thrust is obtained by adjusting the set-point to the governor. The ship's speed will increase/decrease until an equilibrium speed is obtained that satisfies:

$$(m - X_{\dot{u}})\,\dot{u} = X_{|u|u}\,|u|u + (1-t)T + T_{\text{loss}} + T_{\text{ext}} \tag{6.134}$$

$$T = T_{|n|n}\,|n|n + T_{|n|V_a}\,|n|V_a \tag{6.135}$$

Braking of the ship is done by slowing the engine. When rapid deceleration is needed, the engine is reversed, that is n becomes negative. The steady-state solution for ship speed is straightforward. Moreover for positive u and n we have:

$$\begin{aligned} u &= n \frac{1}{-2X_{|u|u}} \Big[T_{|n|V_a}(1-w)(1-t) \\ &+ \sqrt{[T_{|n|V_a}(1-w)(1-t)]^2 - 4(1-t)T_{|n|n}X_{|u|u} - 4\frac{T_{\text{ext}}+T_{\text{loss}}}{n^2}X_{|u|u}} \Big] \end{aligned} \tag{6.136}$$

Notice that $X_{|u|u}$ and $T_{|n|V_a}$ are negative. Ship speed u is thus very close to be linearly related to the shaft speed n.

With CP propellers, the CP propeller relation between pitch, shaft speed, and ship speed is determined by:

$$(m - X_{\dot{u}})\,\dot{u} = X_{|u|u}\,|u|u + (1-t)\,T + T_{\text{loss}} + T_{\text{ext}} \tag{6.137}$$

$$T = T_{|n|n}\,\theta\,|n|n + T_{|n|V_a}\,|n|V_a \tag{6.138}$$

Again, assuming positive n and u together with $\theta > 0$ we get:

$$\begin{aligned} u &= n \frac{1}{-2X_{|u|u}} \Big[T_{|n|V_a}(1-w)(1-t) \\ &+ \sqrt{[T_{|n|V_a}(1-w)(1-t)]^2 - 4\theta(1-t)T_{|n|n}X_{|u|u} - 4\frac{T_{\text{ext}}+T_{\text{loss}}}{n^2}X_{|u|u}} \Big] \end{aligned} \tag{6.139}$$

CP propeller installations are, in many cases, required to operate at a certain shaft speed, or within a narrow range. A certain speed is then obtained by adjusting the propeller pitch to an appropriate value. This value is, again, very close to be linearly related to the desired ship speed.

Manual Speed Control

Using the above expressions, ship speed is normally controlled by setting a desired reference in shaft speed for FP or in combined shaft speed and pitch for CP.

The limits to this procedure are that ship resistance is not exactly a square function in u. At higher ship speeds, wave making plays an important role, and the resistance curve turns into a 3rd-order curve and higher. The external thrust from wind and waves is further an unknown and stochastic value that can easily amount to 20–40 % of hull resistance in a storm. Such variation will cause a speed change (decrease) of 10–20 % and an increase in power consumption. Blanke (1981) has shown that speed decrease and power consumption when exerted to external thrust depends very much on the governor parameters.

Automatic Speed Control

For ocean passage a tighter speed control than can be obtained with manual control is often desired. One reason is to keep a sailing schedule within tight limits. Another is the fuel costs imposed if a master sails too fast on part of the route and slows down when approaching harbor. Such a strategy can be

expensive in fuel consumption because power is related to speed as the 3rd-order expression:

$$P_{\text{shaft}} = Q\,n = Q_0\,|n^3| + Q_{|n|n}(\theta)\,|n^3| + Q_{|n|V_a}(\theta)\,|n|nV_a \tag{6.140}$$

An increase in speed is thus more expensive in power than the saving gained when decreasing speed such that the desired average cruising speed is obtained.

Optimal Efficiency Control

In CP propeller installations, the pitch is the main factor to control. When shaft speed is also allowed to be varied, it is possible to optimize on the propulsion efficiency η:

$$\eta = \frac{T\,u}{Q\,n} = \frac{T_{|n|n}\,\theta\,|n|nu + T_{|n|V_a}\,|n|(1-w)u^2}{Q_{|n|n}\,|\theta|\,|n^3| + Q_{|n|V_a}\,\theta\,|n|n(1-w)u} \tag{6.141}$$

With the ship speed being given by the more general expression:

$$(m - X_{\dot{u}})\,\dot{u} = X(u) + (1-t)\,T + T_{\text{loss}} + T_{\text{ext}} \tag{6.142}$$

where $X(u)$ is a velocity-dependent resistance function. This problem is clearly a nonlinear optimization problem. The overall efficiency is optimized in real time in a multivariable pitch and shaft speed controller. The solution can be written:

$$\begin{bmatrix} \theta_d \\ n_d \end{bmatrix} = f_1(u, \theta, n) \tag{6.143}$$

where θ_d and n_d are the desired values, and $f_1(u, \theta, n)$ is a nonlinear function depending on what type of optimization method which is used. Perturbation- and gradient-based optimization methods are commonly used for this purpose.

Overload Control

When optimizing the combined θ and n, the problem occurs that the optimum is often the largest possible θ and the n value that gives the desired thrust. This inevitably brings the prime mover diesel into the torque limit. It is therefore necessary to incorporate overload control. The fuel index is used to determine an approaching overload condition by comparing the fuel index demand Y_d with a value Y_{lim}, which is lower than the hard limit specified for the engine. The overload controller has the following function:

$$(Y_d - Y_{\text{lim}}) = \Delta Y > 0 \Rightarrow \begin{cases} \theta > 0 \Rightarrow \dot{\theta}_d = -k_1 \Delta Y \\ \theta < 0 \Rightarrow \dot{\theta}_d = +k_2 \Delta Y \\ \theta = 0 \Rightarrow \dot{n}_d = -k_3 \Delta Y \end{cases}$$

The concern for the sign of θ is seen from the torque equation above where it is apparent that the slope of the Q curve changes with the sign of θ.

6.2.3 Speed Control for Cruising

Speed control is implemented using the elements described above. The control of the ship's speed is conveniently broken up into a hierarchy of control loops because manual override and gradual activation of control loops is a practical advantage for the person in control. The control loops in the speed control hierarchy are:

(1) **speed control:** *inputs:* speed reference u_d and speed estimate $\hat{u}$; *output:* thrust demand T_d.

(2) **thrust control:** *inputs:* thrust demand T_d, thrust estimate $\hat{T}$, fuel index Y; *outputs:* pitch demand θ_d and shaft speed demand n_d.

(3) **shaft speed control (governor):** *inputs:* shaft speed demand n_d, measured shaft speed n, measured fuel index Y, measured scavenging air pressure p_s;*output:* fuel index demand Y_d to engine.

(4) **CP propeller control:** *inputs:* pitch demand θ_d, measured pitch θ; *output:* pitch control valve position.

This is illustrated in Figure 6.22.

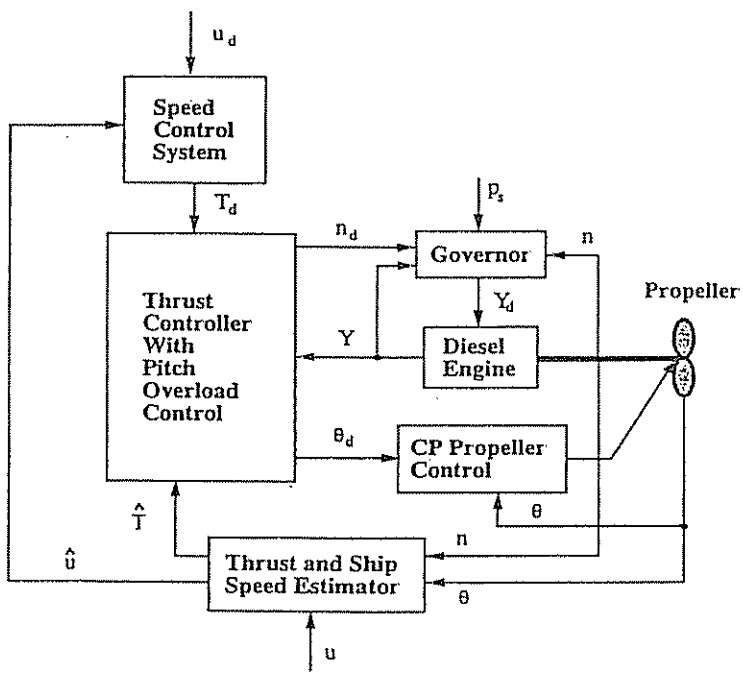

Figure 6.22: Control loops in the speed control hierarchy (Blanke 1994).

Ship Speed Controller

The desired speed accuracy for a ship speed controller is about 0.1 (knots) or 0.05 (m/s). The ship speed controller could be implemented as a simple PI controller

if appropriate gain scheduling was used to compensate the change in gain from thrust to ship speed as a function of ship speed. However, integral action must be used with care in the speed control case. The reason is power considerations that require that no overshoot whatsoever is accepted in ship speed. Furthermore, if the speed controller for some reason has used precious power to increase ship speed to above the set-point, it would not be wise to use additional power to decrease the ship speed to the set-point. Therefore a no-braking strategy has to be used. The detailed analysis of this problem is not within the scope of this text and details can be found in Blanke (1994).

Thrust Controller

Thrust control with a fixed pitch propeller is straightforward in the sense that there is no optimization involved. The only obstacle is robust estimation of propeller thrust.

For the CP propeller, the overload control and optimal pitch method make a somewhat coupled nonlinear control problem. Particularly, care needs to be taken in considering the sign relations involved since the sign in the control loop will change with the sign of pitch, sign of ship speed, and direction of shaft speed.

Estimation of Propeller Thrust

From the propeller equations, the obvious possibility for the estimation of propeller thrust is to use the thrust relation. Moreover:

$$\hat{T} = T_{|n|n}(\theta)\,|n|n + T_{|n|V_a}(\theta)\,|n|(1-w)\hat{u} \tag{6.144}$$

where ship speed is estimated through (see (6.123)):

$$\hat{u} = \frac{Q - (Q_0\,|n|n + Q_{|n|n}(\theta)\,|n|n)}{Q_{|n|V_a}(\theta)\,|n|(1-w)} \tag{6.145}$$

However, increased robustness is obtained if a nonlinear observer is designed using the thrust and torque relations above together with the forward speed equation:

$$(m - X_{\dot{u}})\,\dot{\hat{u}} = X(\hat{u}) + (1-t)\hat{T} + \hat{T}_{\text{loss}} + \hat{T}_{\text{ext}} \tag{6.146}$$

A recursive prediction error method to estimate this nonlinear continuous-time equation was developed in Zhou and Blanke (1989).

Shaft Speed and CP Controllers

In an overall speed control context, these controllers can be treated as fairly ideal devices where the limits need to be taken into context, whereas the detailed controller dynamics can be neglected.

6.3 Course-Keeping Autopilots

Autopilots for course-keeping are normally based on feedback from a gyrocompass measuring the heading. Heading rate measurements can be obtained by a rate sensor, gyro, numerical differentiation of the heading measurement or a state estimator. This is common practice in most control laws utilizing proportional, derivative and integral action. The control objective for a course-keeping autopilot can be expressed as:

$$\psi_d = \text{constant} \tag{6.147}$$

This is illustrated in Figure 6.23. On the contrary, course-changing maneuvers suggest that the dynamics of the desired heading should be considered in addition. This will be discussed in Section 6.4.

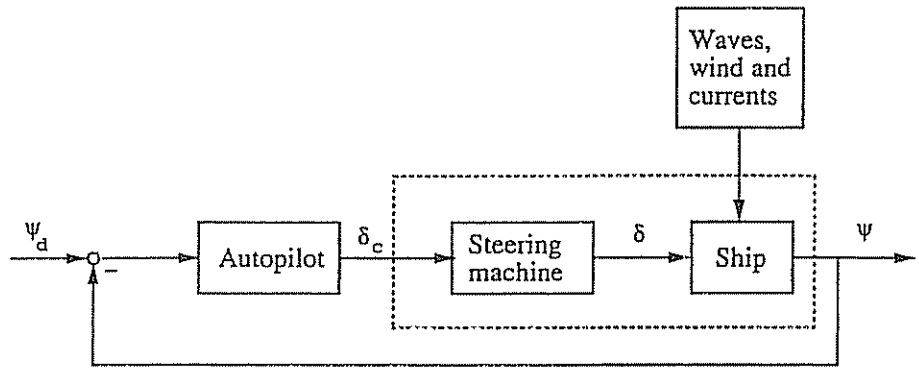

Figure 6.23: Autopilot for automatic heading.

6.3.1 Autopilots of PID-Type

Most autopilots for ship steering are based on simple PID-control laws with fixed parameters. To avoid that the performance of the autopilot deteriorating in bad weather and when the speed of the ship changes, HF rudder motions must be suppressed by proper wave filtering, while a gain scheduling technique can be applied to remove the influence of the ship speed on the hydrodynamic parameters. For simplicity, let the LF motion of a ship be described by Nomoto's 1st-order model:

$$T\,\ddot{\psi} + \dot{\psi} = K\,\delta \tag{6.148}$$

Based on this simple model we will discuss control laws of P-, PD- and PID-type utilizing feedback from the LF state estimates. The performance and robustness of the autopilot can be evaluated by using the simulation set-up showed in Figure 6.24. The proposed simulator models 1st-order wave disturbances as measurement noise while wave drift forces, wind and sea currents are treated as a constant disturbance.

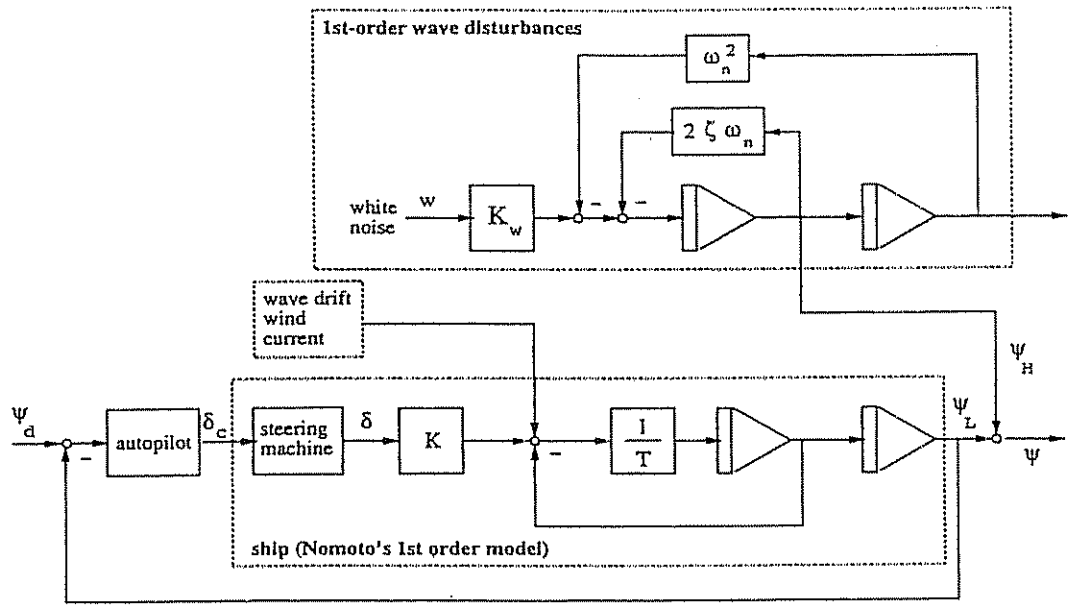

Figure 6.24: Simplified simulation set-up for course-keeping autopilot.

P-Control

Let us first consider a proportional control law:

$$\boxed{\delta = K_p\,(\psi_d - \psi)} \tag{6.149}$$

where $K_p > 0$ is a regulator design parameter. Substitution of (6.149) into (6.148), yields the closed-loop dynamics:

$$T\,\ddot{\psi} + \dot{\psi} + KK_p\psi = KK_p\psi_d \tag{6.150}$$

From this expression the eigenvalues are found to be:

$$\lambda_{1,2} = \frac{-1 \pm \sqrt{1 - 4TKK_p}}{2T} \tag{6.151}$$

Since, $1 - 4TKK_p < 0$ for most ships, it is seen that the real part of the eigenvalues are given as:

$$\mathrm{Re}\{\lambda_{1,2}\} = -\frac{1}{2T} \tag{6.152}$$

Consequently, the suggested P-controller will not stabilize an open-loop unstable ship ($T < 0$). For stable ships ($T > 0$) the imaginary part of the closed-loop eigenvalues and thus the oscillatoric motion can be modified by adjusting the regulator gain K_p. For instance, a critically damped system is obtained by choosing:

$$K_p = \frac{1}{4TK} \tag{6.153}$$

PD-Control

Since, the use of a P-controller is restricted to open-loop stable ships with a certain degree of stability, another approach has to be used for marginally stable and unstable ships. A stabilizing control law is obtained by simply including derivative action in the control law. Consider a control law of PD-type in the form:

$$\boxed{\delta = K_p\,(\psi_d - \psi) - K_d\,\dot{\psi}} \tag{6.154}$$

Here $K_p > 0$ and $K_d > 0$ are the controller design parameters. The closed-loop dynamics resulting from the ship dynamics and the PD-controller are:

$$T\,\ddot{\psi} + (1 + KK_d)\dot{\psi} + KK_p\psi = KK_p\psi_d \tag{6.155}$$

This expression simply corresponds to a 2nd-order system in the form:

$$\ddot{\psi} + 2\zeta\,\omega_n\,\dot{\psi} + \omega_n^2\,\psi = \omega_n^2\,\psi_d \tag{6.156}$$

with natural frequency ω_n (rad/s) and relative damping ratio ζ. Combining (6.155) and (6.156) yields:

$$\omega_n = \sqrt{\frac{KK_p}{T}}; \qquad \zeta = \frac{1 + KK_d}{2\sqrt{TKK_p}} \tag{6.157}$$

The relative damping ratio is typically chosen in the interval $0.8 \leq \zeta \leq 1.0$, whereas the choice of ω_n will be limited by the resulting bandwidth of the rudder ω_δ (rad/s) and the ship dynamics $1/T$ (rad/s) according to:

$$\underbrace{1/T}_{\text{ship dynamics}} < \underbrace{\omega_n\sqrt{1 - 2\,\zeta^2 + \sqrt{4\,\zeta^4 - 4\,\zeta^2 + 2}}}_{\text{closed-loop bandwidth}} < \underbrace{\omega_\delta}_{\text{rudder servo}} \tag{6.158}$$

For a critically damped ship ($\zeta = 1$) the closed-loop bandwidth ω_b is related to the natural frequency ω_n of the closed-loop system (6.156) by a factor of 0.64, that is $\omega_b = 0.64 \cdot \omega_n$ (see Exercise 6.6). Alternatively, we can solve (6.157) for K_p and K_d which yields:

$$K_p = \frac{T\,\omega_n^2}{K}; \qquad K_d = \frac{2T\,\zeta\,\omega_n - 1}{K} \tag{6.159}$$

Here ω_n and ζ can be treated as design parameters.

Example 6.3 (PD-Control)
Consider an unstable ship with time constant $T = -10$ (s) and gain constant $K = -0.1$ (s^{-1}). If we choose the natural frequency as:

$$\omega_n = 0.05 \; (rad/s) \tag{6.160}$$

and the desired damping ratio as:

$$\zeta = 0.8 \tag{6.161}$$

we obtain the following regulator gains:

$$K_p = 0.25; \qquad K_d = 18.0 \tag{6.162}$$

This corresponds to a bandwidth of $\omega_b = 0.87 \cdot \omega_n = 0.04 \; (rad/s)$. *The open-loop and closed-loop poles for this system are shown in Figure 6.25.*

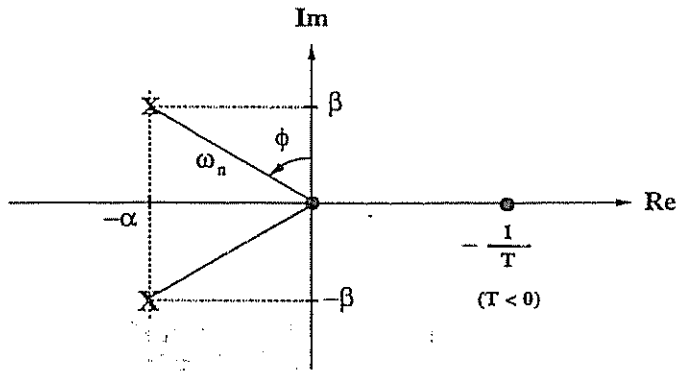

Figure 6.25: Plot showing the poles of the unstable ship (•) and the PD-controlled ship (X). The relative damping ratio and natural frequency of the closed-loop system is: $\zeta = \sin\phi$ and $\omega_n = \sqrt{\alpha^2 + \beta^2}$, respectively.

□

PID-Control

During autopilot control of a ship it is observed that a rudder off-set is required to maintain the ship on constant course. The reason for this is a yaw moment caused by the rotating propeller and the slowly-varying environmental disturbances. These are wave drift forces (2nd-order wave disturbances) and LF components of wind and sea currents. However, steady-state errors due to wind, current and wave drift can all be compensated for by adding integral action to the control law. Consider the PID-control law:

$$\boxed{\delta = K_p \, (\psi_d - \psi) - K_d \, \dot{\psi} + K_i \int_0^t (\psi_d - \psi(\tau)) \, d\tau} \tag{6.163}$$

where $K_p > 0$, $K_d > 0$ and $K_i > 0$ are the regulator design parameters. Applying this control law to Nomoto's 1st-order model

$$T \, \ddot{\psi} + \dot{\psi} = K \, (\delta - \delta_0) \tag{6.164}$$

where δ_0 is the steady-state rudder off-set, yields the following closed-loop characteristic equation:

$$T\,\sigma^3 + (1 + KK_d)\,\sigma^2 + KK_p\,\sigma + KK_i = 0 \tag{6.165}$$

Hence the triple (K_p, K_d, K_i) must be chosen such that all the roots of this 3rd-order polynomial become negative, that is:

$$\mathrm{Re}\{\sigma_i\} < 0 \quad \text{for} \quad (i = 1, 2, 3) \tag{6.166}$$

This can be done by applying Routh's stability criterion (see Theorem 5.1). Another simple intuitive way to do this is by noticing that δ can be written as:

$$\delta = K_p\,(1 + T_d\,s + \frac{1}{T_i\,s})\,(\psi_d - \psi) \tag{6.167}$$

where the derivative and integral time constants are $T_d = K_d/K_p$ and $T_i = K_p/K_i$, respectively. Hence, integral action can be obtained by first designing the PD-controller gains K_d and K_p according to the previous discussions. This ensures that sufficient stability is obtained. The next step is to include integral action by adjusting the integral gain K_i. A rule of thumb can be to choose:

$$\frac{1}{T_i} \approx \frac{\omega_n}{10} \tag{6.168}$$

which suggests that K_i should be chosen as:

$$K_i = \frac{\omega_n}{10}\,K_p = \frac{\omega_n^3}{10}\,\frac{T}{K} \tag{6.169}$$

Example 6.4 (PID-Control)
Again consider the unstable tanker in Example 6.3 with K_p and K_d chosen according to (6.162). The integral gain is calculated as (6.169) which yields:

$$K_i = 0.0013\ (s^{-1}) \tag{6.170}$$

The root-locus curves for increasing values of K_i are shown in Figure 6.26. Notice that the system is stable for $K_i = 0.0013\ (s^{-1})$ indicated by the three asterisks in Figure 6.26.
□

6.3.2 Compensation of Forward Speed Effects

Simple gain scheduling techniques can be applied to remove the influence of forward speed. We will discuss two different methods which can be used to compute a set of velocity scheduled regulator gains (K_p, K_d, K_i).

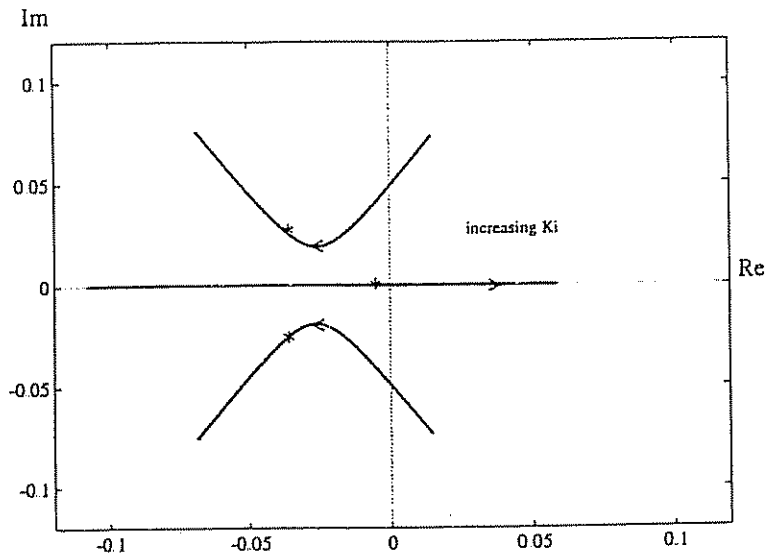

Figure 6.26: Root-locus curve for the unstable tanker with PID-control when K_i is allowed to vary, and K_p and K_d are fixed. The three asterisks denote the "rule of thumb" solution $K_i = (\omega_n^3/10)\,(T/K)$ which clearly is stable.

Velocity Gain Scheduling Using the Ratio (U/L)

The most common gain scheduling technique is probably to replace the (K, T) values in the PID control law with:

$$K = (U/L)\,K' \tag{6.171}$$
$$T = (L/U)\,T' \tag{6.172}$$

where L is the length of the ship and U is the forward speed. However, this technique requires that the non-dimensional gain K' and time T' constants are known.

Velocity Gain Scheduling Using the Ratio (U/U_0)

Assume that the gain constant K_0 and time constant T_0 corresponding to the service speed U_0 of the ship are known. The values for (K_0, T_0) can be found from a maneuvering test, see Example 5.8. From (6.171) and (6.172) we have that:

$$K_0 = (U_0/L)\,K'; \qquad T_0 = (L/U_0)\,T' \tag{6.173}$$

Eliminating K' and T' from these expressions by using (6.171) and (6.172) yields:

$$\boxed{K = (U/U_0)\,K_0} \qquad \boxed{T = (U_0/U)\,T_0} \tag{6.174}$$

Substituting these results into the expressions for K_p and K_d finally yields:

$$K_p(U) = \frac{T_0\,\omega_n^2}{K_0}\,(U_0/U)^2; \qquad K_d(U) = \frac{2\,T_0\,(U_0/U)\,\zeta\,\omega_n - 1}{K_0}\,(U_0/U) \quad (6.175)$$

Similarly, we obtain a rule of thumb for the integral gain K_i as:

$$K_i(U) = \frac{\omega_n^3}{10}\,\frac{T_0}{K_0}\,(U_0/U)^2 \quad (6.176)$$

Hence, the influence of the forward speed is compensated for directly by including speed measurements. Velocity scheduling should be applied to the regulator, state estimator and the parameter estimator. It should be noted that the response to velocity variations by gain scheduling is much quicker than what is obtained by parameter adaptation.

6.3.3 Linear Quadratic Optimal Autopilot

Linear quadratic optimal control theory can be applied to obtain increased performance and reduced fuel consumption. The trade-off between accurate steering and economical steering can be related to a quadratic criterion:

$$\min J = \frac{\alpha}{T}\int_0^T (\varepsilon^2 + \lambda\,\delta^2)\,d\tau \quad (6.177)$$

where α is a constant to be interpreted later, ε is the heading error, δ is the actual rudder angle and λ is a weighting factor weighting the cost of heading errors against the control effort.

Sailing in restricted waters usually requires accurate control, but minimization of the fuel consumption is more important in open sea. Minimum fuel consumption with respect to steering resistance has been addressed by several authors. We will discuss three of the criteria in the literature.

The Steering Criterion of Koyama (1967)

Koyama (1967) observed that the ship's yawing motion could be described by a sinusoid during autopilot control, that is:

$$y = \sin(\varepsilon\,t) \quad \Longrightarrow \quad \dot{y} = \varepsilon\cos(\varepsilon\,t) \quad (6.178)$$

Hence, the percentage loss of speed during course control can be calculated by using the elongation in distance due to a course error, see Figure 6.27. This approach uses the fact that the length of one arch L_a of the sinusoid can be calculated as:

$$L_a = \int_0^\pi \sqrt{(1+\dot{y}^2)}\,d\tau = \int_0^\pi \sqrt{[1+\varepsilon^2\,\cos^2(\varepsilon\,\tau)]}\,d\tau \approx \pi\,(1+\frac{\varepsilon^2}{4}) \quad (6.179)$$

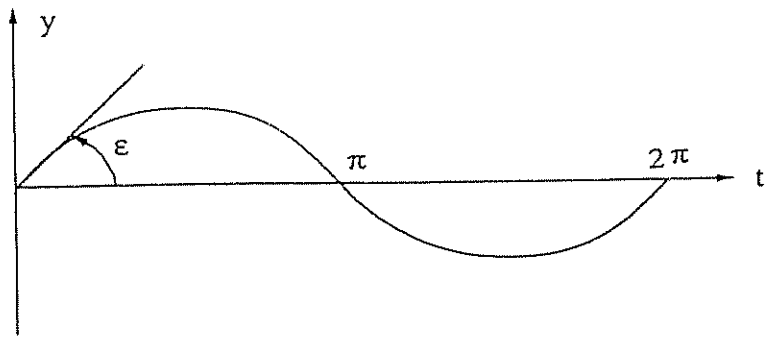

Figure 6.27: Sinusoidal course error during autopilot control.

Hence, the relative elongation due to a sinusoidal course error is:

$$\frac{\Delta L}{L} = \frac{L_a - L}{L} = \frac{\pi(1 + \varepsilon^2/4) - \pi}{\pi} = \frac{\varepsilon^2}{4} \tag{6.180}$$

In fact, this term can be interpreted as the percentage speed loss during a sinusoidal maneuver. Consequently, Koyama proposed minimizing the speed loss term $\varepsilon^2/4$ against the increased resistance due to steering given by the term δ^2. This leads to the following performance index:

$$\min J = 100 \left(\frac{\pi}{180}\right)^2 \frac{1}{4T} \int_0^T (\varepsilon^2 + \lambda\, \delta^2)\, d\tau \approx \frac{0.0076}{T} \int_0^T (\varepsilon^2 + \lambda\, \delta^2)\, d\tau \tag{6.181}$$

where

$$\begin{aligned} J &= \text{loss of speed (\%)} \\ \varepsilon &= \text{heading error (deg)} \\ \delta &= \text{rudder angle (deg)} \\ \lambda &= \text{weighting factor} \end{aligned}$$

The weighting factor λ is obtained by normalizing ε^2 such that $\varepsilon^2 \leq 1$. Koyama suggested a λ-factor of approximately 8–10. Experiments show that such high values for λ avoids large rudder angles and thus high turning rates. Therefore, $\lambda = 10$ will be a good choice in bad weather where it is important to suppress high frequency rudder motions.

The Steering Criterion of Norrbin (1972)

Norrbin (1972) has suggested minimizing the loss term:

$$T_{\text{loss}} = (m + X_{vr})\, vr + X_{cc\delta\delta}\, c^2\, \delta^2 + (X_{rr} + mx_G)\, r^2 + X_{\text{ext}} \tag{6.182}$$

arising from (5.9). Consequently, an optimal controller should minimize the centripetal term vr, the square rudder angle δ^2 and the square heading rate r^2.

The disturbance term X_{ext} is assumed to be negligible. For most ships the sway velocity v is approximately proportional to r (see Exercise 5.1), that is:

$$v(s) = \frac{K_v(1+T_v s)}{K\,(1+Ts)} r(s) \;\approx\; k\,r(s) \tag{6.183}$$

where $k = K_v/K$ is a constant. Hence, the centripetal term vr will be approximately proportional to the square of the heading rate, that is:

$$vr \approx k\,r^2 \tag{6.184}$$

The next step is to assume that the ship's yawing motion will be periodically (sinusoidaly) under autopilot control such that the following holds:

$$r_{\max} = \omega_r\,\varepsilon_{\max} \tag{6.185}$$

Here ω_r is the frequency of the sinusoidal yawing. Consequently, the criterion for increased resistance during turns can be expressed as a quadratic criterion similar to that of (6.181), see Exercise 6.7. The only difference between the criteria of Norrbin and Koyama is that the λ values arising from Norrbin's approach will be different. In fact, Norrbin suggests values around $\lambda = 0.1$. Experiments show that $\lambda = 0.1$ may be an optimum choice in calm sea.

The optimal choice of λ should be a trade-off between accurate steering (small λ-values) and economical steering (large λ-values). In rough sea Norrbin's criterion ($\lambda = 0.1$) might result in undesired HF motion of the rudder since higher controller gains are allowed. This suggests that a trade-off between the λ values proposed by Koyama and Norrbin could be made according to the weather conditions as:

$$\text{(calm sea)} \qquad 0.1 \;\le\; \lambda \;\le\; 10 \qquad \text{(rough sea)} \tag{6.186}$$

Norrbin expresses the losses due to steering in the term ε^2 while Koyama includes the same losses in the term δ^2. This is the main reason for the great difference in the values of λ.

The Steering Criterion of Van Amerongen and Van Nauta Lemke (1978)

Since the increased resistance due to steering is dominated by the component caused by the turning, Van Amerongen and Van Nauta Lemke (1978, 1980) suggest including an additional term r^2 in the criterion (6.181) to penalize the turning. Moreover, the following criterion is proposed:

$$\min J = \frac{0.0076}{T} \int_0^T (\varepsilon^2 + \lambda_1\,r^2 + \lambda_2\,\delta^2)\,d\tau \tag{6.187}$$

where

J = percentage loss of speed (%)
r = the LF component of the heading rate (deg/s)
ε = the LF component the heading error (deg)
δ = the rudder angle (deg)
$\lambda_{1,2}$ = weighting factors

For a tanker and a cargo ship, Van Amerongen and Van Nauta Lemke (1978, 1980) give the following values for the weighting factors λ_1 and λ_2 corresponding to the data set of Norrbin (1972).

tanker:	$L =$	$300\,m$	$\lambda_1 =$	15.000	$\lambda_2 =$	8.0
cargo ship:	$L =$	$200\,m$	$\lambda_1 =$	1.600	$\lambda_2 =$	6.0

Solution of the Optimal Steering Criteria

Consider Nomoto's 1st-order model in the form:

$$T' \dot{r} + (U/L)\, r = (U/L)^2\, K'\, \delta \tag{6.188}$$

Straightforward application of optimal control theory to the criterion of Van Amerongen and Van Nauta Lempke (1978), yields (see Appendix D):

$$\delta = K_p\, (\psi_d - \psi) - K_d\, r \tag{6.189}$$

where

$$K_p = \sqrt{\frac{1}{\lambda_2}} \tag{6.190}$$

$$K_d = \frac{L}{U} \frac{\sqrt{1 + 2K_p K' T' + K'^2 (U/L)^2\, (\lambda_1/\lambda_2)} - 1}{K'} \tag{6.191}$$

The proof is left as an exercise. The solution of the criteria of Koyama and Norrbin is obtained for $\lambda_1 = 0$ and $\lambda_2 = \lambda$ which yields:

$$K_p = \sqrt{\frac{1}{\lambda}} \tag{6.192}$$

$$K_d = \frac{L}{U} \frac{\sqrt{1 + 2K_p K' T'} - 1}{K'} \tag{6.193}$$

From these expressions it is seen that K_p depends on a weighting factor while K_d depends on K_p as well as the model parameters K' and T'. Hence, accurate steering requires that K' and T' are known with sufficient accuracy. This suggests that the optimal controller should be combined with a parameter estimator for

estimation of K' and T'. Van Amerongen (1982) claims that K_p and K_d will be in the range of:

$$0.5 < K_p < 5; \qquad K_p < K_d < (L/U)\, K_p \tag{6.194}$$

for most ships.

Extensions to Nomoto's 2nd-Order Model

Consider Nomoto's 2nd-order model in state-space form:

$$\dot{\boldsymbol{x}} = \boldsymbol{A}\,\boldsymbol{x} + \boldsymbol{B}\,\boldsymbol{u} \tag{6.195}$$

where $\boldsymbol{x} = [v, r, \psi]^T$, $u = \delta$ and

$$\boldsymbol{A} = \begin{bmatrix} a_{11} & a_{12} & 0 \\ a_{21} & a_{22} & 0 \\ 0 & 1 & 0 \end{bmatrix}; \qquad \boldsymbol{B} = \begin{bmatrix} b_1 \\ b_2 \\ 0 \end{bmatrix} \tag{6.196}$$

Let the control objective be described by:

$$\boldsymbol{e} = \boldsymbol{y} - \boldsymbol{y}_d = \boldsymbol{C}\,(\boldsymbol{x} - \boldsymbol{x}_d) \tag{6.197}$$

where $\boldsymbol{C}$ is a known matrix specifying the control objective and $\boldsymbol{y}_d = \boldsymbol{C}\,\boldsymbol{x}_d$ is the desired output. The steady-state optimal solution minimizing the quadratic performance index (assuming $\boldsymbol{y}_d = \text{constant}$):

$$\min\, J = \frac{1}{2}\int_0^T (\boldsymbol{e}^T \boldsymbol{Q} \boldsymbol{e} + \boldsymbol{u}^T\, \boldsymbol{P}\, \boldsymbol{u})\, d\tau \tag{6.198}$$

where $\boldsymbol{P} > 0$ and $\boldsymbol{Q} \geq 0$ are two weighting matrices, is (see Appendix D):

$$\boldsymbol{u} = \boldsymbol{G}_1\, \boldsymbol{x} + \boldsymbol{G}_2\, \boldsymbol{y}_d \tag{6.199}$$

Here

$$\boldsymbol{G}_1 = -\boldsymbol{P}^{-1}\boldsymbol{B}^T\boldsymbol{R}_\infty \tag{6.200}$$

$$\boldsymbol{G}_2 = -\boldsymbol{P}^{-1}\boldsymbol{B}^T(\boldsymbol{A} + \boldsymbol{B}\boldsymbol{G}_1)^{-T}\boldsymbol{C}^T\boldsymbol{Q} \tag{6.201}$$

and $\boldsymbol{R}_\infty$ is the solution of the matrix Riccati equation:

$$\boldsymbol{R}_\infty\boldsymbol{A} + \boldsymbol{A}^T\boldsymbol{R}_\infty - \boldsymbol{R}_\infty\boldsymbol{B}\boldsymbol{P}^{-1}\boldsymbol{B}^T\boldsymbol{R}_\infty + \boldsymbol{C}^T\boldsymbol{Q}\boldsymbol{C} = 0 \tag{6.202}$$

This approach requires that all states are measured or at least estimated. The robustness of optimal autopilots for course-keeping control with state estimator is analyzed in Holzhüter (1992).

Limitations of the Steering Machine

In Section 5.4 it was shown that the limitations in the rudder rate could introduce an additional phase lag. This effect can lead to instability of the optimal controller. One intuitive solution to this problem could be to apply a gain scheduling technique. For instance, the output of the controller could be automatically reduced as soon as the controller rate of change is so large that it will cause saturation.

Van der Klugt (1987) proposes to use the automatic gain controller (AGC) of Figure 6.28 to adjust the controller gain. In Figure 6.28 δ_c is the controller output, $\dot{\delta}_{\max}$ is the maximum allowed rudder rate, and the signal y is the maximum of three signals; (1) the maximum rudder rate, (2) the absolute value of the time derivative of the commanded input and (3) the output of a memory function. Moreover,

$$y(k) = \max \begin{cases} \dot{\delta}_{\max} \\ |\, \dot{\delta}_c(k) \,| \\ \lambda \cdot y(k-1) \end{cases} \tag{6.203}$$

where $0 < \lambda < 1$ is a forgetting factor. An estimate of the signal $\dot{\delta}_c(k)$ can be computed by numerical derivation, for instance (see Appendix B.3):

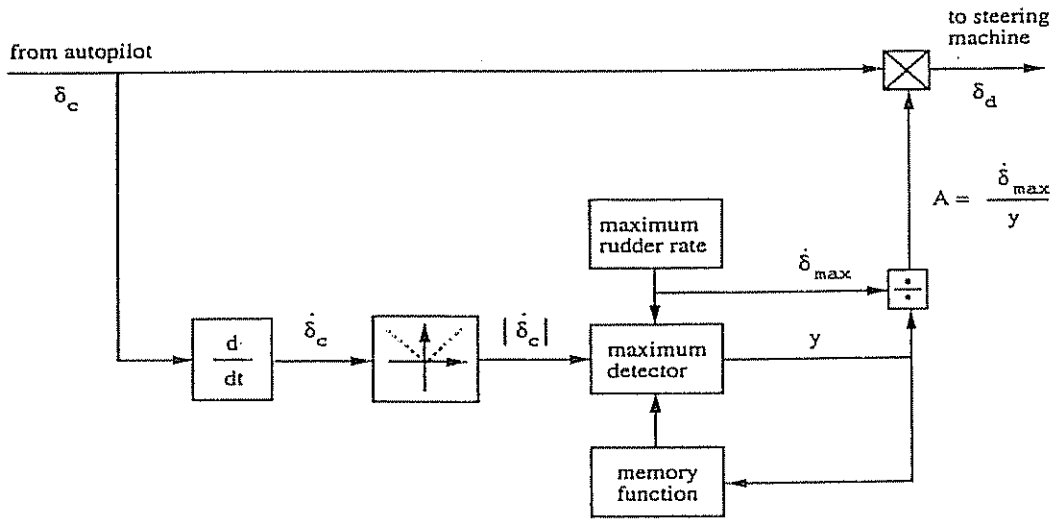

Figure 6.28: The automatic gain controller (AGC), Van der Klugt (1987) and Van Amerongen et al. (1990).

$$\dot{\delta}_c(s) = \frac{T_d\, s}{1 + T_d\, s}\, \delta_c(s) \tag{6.204}$$

where $1/T_d$ is the cut-off frequency. The gain needed to adjust the controller is computed as:

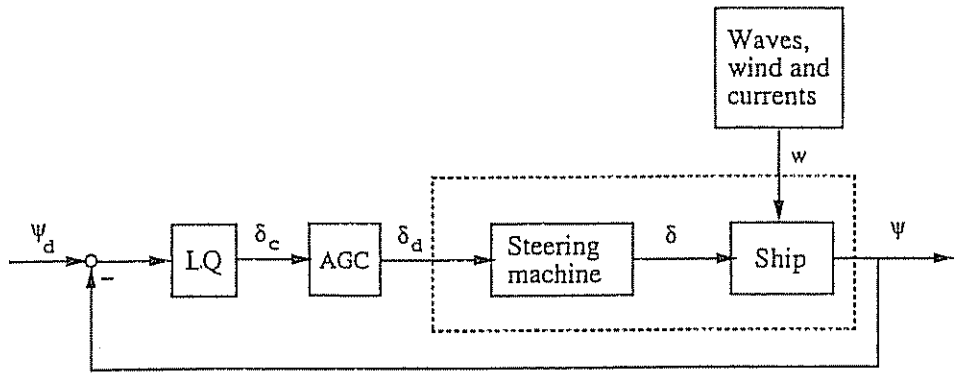

Figure 6.29: Diagram showing a linear quadratic optimal autopilot together with the automatic gain controller.

$$0 < A \leq 1 \quad \text{where} \quad A = \frac{\dot{\delta}_{\max}}{y} \tag{6.205}$$

Hence the output from the AGC will be:

$$\delta_d = A\,\delta_c \tag{6.206}$$

Notice that if $|\dot{\delta}_c|$ is larger than $\dot{\delta}_{\max}$ the gain A is instantaneously decreased and thus the desired rudder angle δ_d to the steering machine is decreased. When $|\dot{\delta}_c|$ is not too large any more, the memory function ensures that the gain A slowly increases. In fact, the memory function is the major mechanism which reduces the phase lag introduced by the steering machine.

The robustness of the AGC mechanism has been demonstrated by Van der Klugt and Dutch co-workers (Van der Klugt 1987). They conclude that the AGC mechanism is highly effective during rudder rate limitation.

6.3.4 Adaptive Linear Quadratic Optimal Control

An adaptive optimal course-keeping autopilot can be derived by means of Lyapunov stability theory (Fossen and Paulsen 1992). Consider the linear ship steering dynamics in the form:

$$m\,\ddot{\psi} + d\,\dot{\psi} = \delta \tag{6.207}$$

Let $\psi_d = \text{constant}$ denote the desired heading. Consider a 2nd-order system:

$$\boxed{\ddot{\psi} = a_\psi} \tag{6.208}$$

where a_ψ can be interpreted as the *commanded acceleration*. Hence, we can formulate the optimal control problem as:

$$\min J = \int_0^T \left[(\psi_d - \psi)^2 + \lambda_1\,\dot{\psi}^2 + \lambda_2\,a_\psi^2\right] d\tau \tag{6.209}$$

Here the tracking error $\psi_d - \psi$ is weighted against the yawing rate $\dot{\psi}$ and the commanded acceleration a_ψ with weighting factors λ_1 and λ_2, respectively. This yields the following steady-state solution for the optimal commanded acceleration:

$$\boxed{a_\psi = K_p\,(\psi_d - \psi) - K_d\,\dot{\psi}} \tag{6.210}$$

where

$$K_p = \sqrt{\frac{1}{\lambda_2}}; \qquad K_d = \sqrt{2\sqrt{\frac{1}{\lambda_2}} + \frac{\lambda_1}{\lambda_2}} \tag{6.211}$$

The proof is left as an exercise. Integral action may be obtained by modifying the commanded acceleration according to:

$$a_\psi = K_p\,(\psi_d - \psi) - K_d\,\dot{\psi} + K_i \int_0^t (\psi_d - \psi(\tau))\,d\tau \tag{6.212}$$

where a suitable choice of K_i is:

$$K_i \approx \frac{K_p}{5\,K_d} \tag{6.213}$$

This corresponds to $T_i = 5\,T_d$ in a PID-controller.

Computation of Optimal Rudder from Commanded Acceleration

The control input is simply computed by transforming the commanded acceleration according to:

$$\boxed{\delta = \hat{m}\,a_\psi + \hat{d}\,\dot{\psi}} \tag{6.214}$$

where the hat denotes the parameter estimates. Let us define the parameter estimation errors as $\tilde{m} = \hat{m} - m$ and $\tilde{d} = \hat{d} - \mathrm{d}$. Consequently, the closed-loop dynamics can be written:

$$m\,[\ddot{\psi} - a_\psi] = \tilde{m}\,a_\psi + \tilde{d}\,\dot{\psi} \tag{6.215}$$

Substituting the PD-controller (6.210) into this expression, yields:

$$m\,[\ddot{\psi} + K_d\,\dot{\psi} + K_p\,(\psi - \psi_d)] = \tilde{m}\,a_\psi + \tilde{d}\,\dot{\psi} \tag{6.216}$$

Optimality with respect to (6.209) requires that $\tilde{m} = 0$ and $\tilde{d} = 0$ (no parametric uncertainties). With these goals in mind a parameter estimator can be derived by applying Lyapunov stability theory. Let the closed-loop dynamics be written in abbreviated form as:

$$\dot{\boldsymbol{x}} = \boldsymbol{A}\boldsymbol{x} + \boldsymbol{b}\,\frac{1}{m}\boldsymbol{\phi}^T\,\tilde{\boldsymbol{\theta}} \tag{6.217}$$

where $\boldsymbol{x} = [\psi - \psi_d, \dot{\psi}]^T$ is the state vector and

$$A = \begin{bmatrix} 0 & 1 \\ -K_p & -K_d \end{bmatrix} \quad b = \begin{bmatrix} 0 \\ 1 \end{bmatrix} \quad \phi = [a_\psi,\ \dot{\psi}]^T \quad \tilde{\theta} = [\tilde{m},\ \tilde{d}]^T \tag{6.218}$$

Theorem 6.1 (Adaptive Linear Quadratic Optimal Control)
The control law (6.214) with the optimal commanded acceleration (6.210) and the parameter update law:

$$\dot{\hat{\theta}} = -\Gamma\,\phi\,e \qquad \Gamma = \Gamma^T > 0 \tag{6.219}$$

where $e = c^T x$ *and*

$$\begin{aligned} A^T P + P A &= -Q \\ P b &= c \end{aligned} \tag{6.220}$$

where $P = P^T > 0$ *and* $Q = Q^T > 0$, *yields a stable system.*

Proof: *Define a scalar function:*

$$V(x, \tilde{\theta}) = x^T P x + \frac{1}{m}\tilde{\theta}^T \Gamma^{-1} \tilde{\theta} \tag{6.221}$$

Differentiating V *with respect to time yields:*

$$\dot{V} = x^T (A^T P + P A) x + \frac{2}{m}\,\tilde{\theta}^T (\Gamma^{-1}\,\dot{\tilde{\theta}} + \phi\, b^T\, P\, x) \tag{6.222}$$

Finally, substituting (6.219) and (6.220) into (6.222) yields:

$$\dot{V} = -x^T Q x \leq 0 \tag{6.223}$$

which according to Lyapunov stability theory for autonomous systems ensures that $\psi(t) \to \psi_d$ *and* $\dot{\psi}(t) \to 0$ *as* $t \to \infty$, *and that* $\tilde{\theta}$ *is bounded. It should be noted that* θ *will converge to zero only if the system is persistently excited. This is, however, not necessary for perfect tracking.*
□

6.4 Turning Controllers

During course-changing maneuvers it is desirable to specify the dynamics of the desired heading instead of using a constant reference signal as in the course-keeping modus. One simple way to do this is by applying model reference techniques.

2nd-Order Reference Model

The reference model can be selected as a 2nd-order system by combining Nomoto's 1st-order model and a PD-control law, that is:

$$T\,\ddot{\psi}_d + \dot{\psi}_d = K\,\delta \tag{6.224}$$

$$\delta = K_p\,(\psi_r - \psi_d) - K_d\,\dot{\psi}_d \tag{6.225}$$

where ψ_d, $\dot{\psi}_d$ and $\ddot{\psi}_d$ are the desired outputs and ψ_r is the commanded (pilot) input. Defining two reference model design parameters T_m and K_m as:

$$T_m = \frac{T}{1 + KK_d} \tag{6.226}$$

$$K_m = \frac{KK_p}{1 + KK_d} \tag{6.227}$$

implies that the reference model (6.224) and (6.225) can be written as:

$$\boxed{T_m\ddot{\psi}_d + \dot{\psi}_d + K_m\psi_d = K_m\psi_r} \tag{6.228}$$

where T_m and K_m are two design parameters describing the closed-loop behavior of the system. This model is shown in Figure 6.30. Alternatively, we can express (6.228) by:

$$\boxed{\ddot{\psi}_d + 2\,\zeta\,\omega_n\,\dot{\psi}_d + \omega_n^2\,\psi_d = \omega_n^2\,\psi_r} \tag{6.229}$$

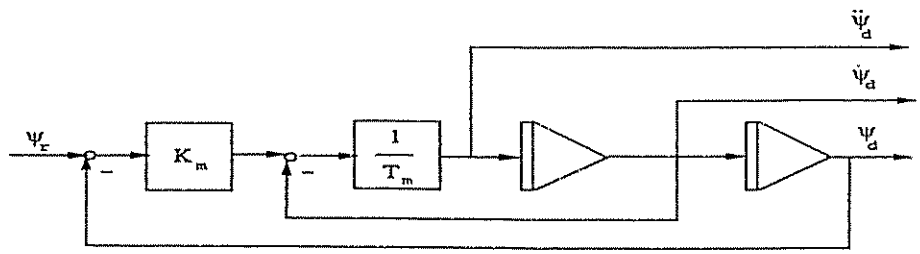

Figure 6.30: Reference model for course-changing maneuver.

by requiring that:

$$2\,\zeta\,\omega_n \triangleq \frac{1}{T_m} \qquad\qquad \omega_n^2 \triangleq \frac{K_m}{T_m} \tag{6.230}$$

Notice that in steady state:

$$\lim_{t\to\infty} \psi_d(t) = \psi_r \tag{6.231}$$

Since T and K not are perfectly known, T_m and K_m cannot be directly calculated from (6.226) and (6.227). For most practical implementations, however, it seems reasonable to choose:

$$T_m \leq \frac{1}{2}\frac{L}{U}T' \tag{6.232}$$

where $T' = (U/L)\,T$ is the non-dimensional ship time constant. This ensures sufficiently tight control at full speed and does not lead to unrealistic high gains at lower speeds. With T_m known, we can show that:

$$K_m = \frac{1}{4\zeta^2 T_m} \tag{6.233}$$

Here ζ can be interpreted as the desired damping ratio of the closed-loop system, typically chosen in the interval:

$$0.8 \leq \zeta \leq 1.0 \tag{6.234}$$

The different choices of the damping ratio are illustrated in Figure 6.31. The reference model (6.229) can be interpreted as a pre-filter for the commanded heading, that is:

$$\psi_d(s) = \frac{\omega_n^2}{s^2 + 2\,\zeta\,\omega_n\,s + \omega_n^2}\,\psi_r(s) \tag{6.235}$$

The pre-filter ensures that numerical difficulties associated with large step inputs are avoided.

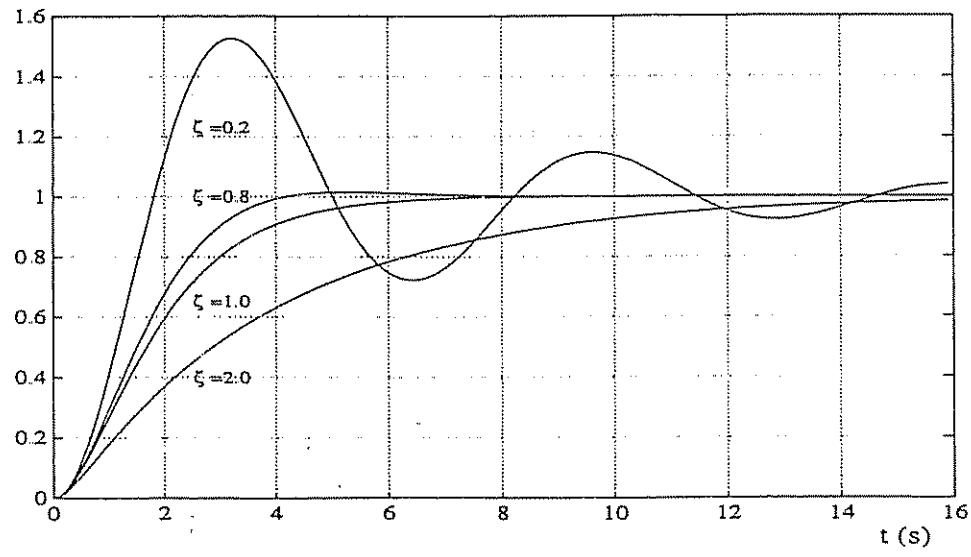

Figure 6.31: Desired state $\psi_d(t)$ for $\psi_r = 1.0$, $\omega_n = 1.0$ and $\zeta \in \{0.2, 0.8, 1.0, 2.0\}$.

Higher Order Reference Models

In some cases it can be desirable to use higher order reference models to generate smooth trajectories, for instance an n-th order reference model with n real poles at λ can be generated by:

$$\psi_d(s) = \frac{\lambda^n}{(s+\lambda)^n}\,\psi_r(s) \tag{6.236}$$

Notice that a 2nd-order reference model is not sufficient to generate smooth accelerations since:

$$\ddot{\psi}_d = -2\lambda\,\dot{\psi}_d - \lambda^2\,(\psi_d - \psi_r) \tag{6.237}$$

will not be smooth if the commanded input ψ_r is a step input. This suggests that a 3rd-order reference model should be used in cases where smooth accelerations are of importance.

6.4.1 PID-Control

The intuitive solution to the turning control problem is to define the tracking error in the PID-control according to:

$$\tilde{\psi}(t) = \psi_r - \psi(t) \tag{6.238}$$

where $\psi_r = \text{constant}$. However, this design is not a good design since large values for ψ_r may lead to rudder saturation and integral wind-up. One simple way to avoid this problem is to limit the tracking error $\tilde{\psi}(t)$ in the PID-control law according to:

$$|\,\tilde{\psi}(t)\,| \;\leq\; \tilde{\psi}_{\max} \tag{6.239}$$

where $\tilde{\psi}_{\max}$ is a small positive constant. An even more sophisticated approach is to apply the reference model of the previous section. Let the tracking error be defined as:

$$e(t) = \psi_d(t) - \psi(t) \tag{6.240}$$

where $\psi_d(t)$ is a smooth reference trajectory generated by the reference model (6.228). Hence, a robust PID-control law for tracking of a time-varying reference trajectory can be designed according to:

$$\delta(t) = K_p\,e(t) + K_d\,\dot{e}(t) + K_i\int_0^t e(\tau)\,d\tau \tag{6.241}$$

6.4.2 Combined Optimal and Feedforward Turning Controller

A linear quadratic optimal controller can also be used for course changing by introducing a feedforward model of the ship steering dynamics. Källström and Theorén (1992) have proposed to write the control law as:

$$\delta(t) = \delta_{FF}(t) + \delta_{LQ}(t) \tag{6.242}$$

where $\delta_{FF}(t)$ and $\delta_{LQ}(t)$ represent a feedforward and optimal feedback term, respectively. Let the desired tracking errors be described by (6.240). Hence, the optimal control law can be expressed in the form:

$$\delta_{LQ}(t) = K_p\, e(t) + K_d\, \dot{e}(t) + K_i \int_0^t e(\tau)\, d\tau \tag{6.243}$$

where K_p, K_d and K_i are the optimal controller gains. The feedforward term is computed from the Nomoto model, according to:

$$T\, \dot{r}_d(t) + r_d(t) = K\, \delta_{FF}(t) \tag{6.244}$$

where T and K are scaled according to Example 5.8 to compensate for speed variations. Hence,

$$\delta_{FF}(t) = \frac{T}{K}\, \dot{r}_d(t) + \frac{1}{K}\, r_d(t) = \frac{T_0}{K_0} \left(\frac{U_0}{U}\right)^2 \dot{r}_d(t) + \frac{1}{K_0} \left(\frac{U_0}{U}\right) r_d(t) \tag{6.245}$$

where U_0 is the nominal speed corresponding to the nominal values K_0 and T_0.

These values can be obtained from a turning circle test, see Example 5.8. Källström and Theorén (1992) define two modes of the feedforward model. One for steady-state turning and one for start and end of the turn. In the first mode only the yaw rate set-point value is used, while the second mode also includes the heading reference. This suggests that a 1st-order reference model should be applied in the first case and a 2nd-order reference model in the latter.

The first switching between the reference models is governed by a parameter T_{lim}. If the time left for turning is less than T_{lim} then the second model is used, and the opposite. This parameter can be tuned according to a design ship. Källström and Theorén (1992) use a design ship given by the following set of model parameters:

$$\begin{array}{ll} L_d = 33 \quad \text{(m)} & \zeta_d = 0.9 \\ T_{md} = 5 \quad \text{(s)} & \omega_{nd} = 0.15 \quad \text{(rad/s)} \end{array}$$

where L_d is the hull length, T_{md} is desired ship time constant, $\omega_{nd} = 0.15$ is the desired natural frequency and ζ_d is the desired relative damping ratio. The switching parameter is scaled according to:

$$T_{lim} = T_{limd} \sqrt{L/L_d}; \qquad T_{limd} = 12 \text{ (s)} \tag{6.246}$$

where L is the length of the actual ship. Based on this design ship we can define two reference models for turning.

Mode One Reference Model (Steady Turning Rate)

During steady turn the reference model is defined as:

$$T_m \dot{r}_d(t) + r_d(t) = r_c \tag{6.247}$$

Here r_c is the commanded yaw rate. The desired behavior of the ship is scaled in terms of the reference ship such that:

$$T_m = T_{md} \sqrt{L/L_d} \tag{6.248}$$

Mode Two Reference Model (Start and End of Turn)

Start and end of the turn are described by the 2nd-order model:

$$\ddot{\psi}_d(t) + 2\,\zeta_m\,\omega_m\,\dot{\psi}_d(t) + \omega_m^2\,\psi_d(t) = \omega_m^2\,\psi_c \tag{6.249}$$

where ψ_c is the commanded heading angle, ζ_m is the desired damping ratio and ω_m is the desired bandwidth. Scaling against a design ship yields:

$$\omega_m = \omega_{md} \sqrt{L_d/L}; \qquad \zeta_m = \zeta_{md} \tag{6.250}$$

6.4.3 Nonlinear Autopilot Design

This section shows how Lyapunov stability theory can be used to design a nonlinear autopilot for ship steering (Fossen 1993b). For notational simplicity, we will consider Norrbin's steering equations of motion in the following form:

$$m\,\dot{r} + d(r)\,r = \delta \tag{6.251}$$

where $m = T/K$ and:

$$d(r) = (n_3\,r^2 + n_2\,r + n_1)/K \tag{6.252}$$

The constant n_0 is omitted since this parameter can be treated as an additional rudder off-set to be compensated for by adding integral action in the controller. In addition to this, slowly-varying disturbances (wind, wave drift forces and currents) are assumed included in the parameter n_0. Let the *pseudo-kinetic energy* of the ship be written as:

$$V(s) = \frac{1}{2} m\,s^2 \tag{6.253}$$

where s is a measure of tracking defined according to Slotine and Li (1987):

$$s = \tilde{r} + 2\lambda\,\tilde{\psi} + \lambda^2 \int_0^t \tilde{\psi}(\tau)\,d\tau \tag{6.254}$$

Here $\tilde{\psi} = \psi - \psi_d$ and $\tilde{r} = r - r_d$ are the yaw angle and yaw rate tracking errors, respectively. $\lambda > 0$ can be interpreted as the control bandwidth. Let us define a *virtual yaw rate* v as:

$$v = r - s = r_d - 2\lambda\,\tilde{\psi} - \lambda^2 \int_0^t \tilde{\psi}(\tau)\,d\tau \tag{6.255}$$

Differentiating V with respect to time, yields:

$$\dot{V} = ms\dot{s} = s\,[m\,\dot{r} - m\dot{v}] \tag{6.256}$$

Substitution of (6.251) into this expression for $\dot{V}$, yields:

$$\dot{V} = s\,[\delta - d(r)\,r - m\,\dot{v}] = -d(r)\,s^2 + s\,[\delta - m\,\dot{v} - d(r)\,v] \tag{6.257}$$

This suggests that the nonlinear control law could be chosen according to:

$$\boxed{\delta = m\,\dot{v} + d(r)\,v - K_d\,s} \tag{6.258}$$

where $K_d > 0$ is a design parameter. This yields:

$$\dot{V} = -[d(r) + K_d]\,s^2 \tag{6.259}$$

K_d must be chosen such that $\dot{V} \leq 0 \;\; \forall \;\; r$. A guideline could be to choose:

$$K_d = -d(r) + \frac{\lambda}{2}\,m > 0 \tag{6.260}$$

which yields:

$$\dot{V} = -\frac{\lambda}{2} m\,s^2 \leq 0 \tag{6.261}$$

According to Barbălat's lemma convergence of $V(t)$ to zero and thus $s(t)$ to zero is guaranteed. In view of (6.254), $\psi(t) \to \psi_d(t)$ in finite time. The "bandwidth" of the controller can be specified in terms of λ. Substituting (6.253) into (6.261), yields:

$$\dot{V}(t) = -\lambda\,V(t) \qquad \Longrightarrow \qquad V(t) = e^{-\lambda t}\,V(0) \tag{6.262}$$

Hence, it is seen that an initial error $s(0) \neq 0$ implies that $V(0) = ms^2(0)/2 > 0$. Furthermore, $V(t)$ will converge exponentially to zero if $\lambda > 0$. Hence, fast convergence of the s-dynamics to zero can simply be obtained by specifying the design parameter λ large enough.

Example 6.5 (Experimental Results With the M/S Nornews Express)
An autopilot experiment with the M/S Nornews Express in cooperation with Robertson Tritech A.S. in Egersund was carried out on the west coast of Norway to investigate the performance of the control law. For M/S Nornews Express the hull contour displacement is 4600 (dwt) while the main dimensions are $L_{pp} = 110$

(m) and $B = 17.5$ (m). This ship can be fairly described by Nomoto's 1st-order model with gain $K = 0.35$ (s^{-1}) and time constant $T = 29.0$ (s). Hence, the commanded rudder can be computed according to:

$$\delta = m\,\dot{v} + d\,v - K_d\,s \tag{6.263}$$

with $d = 1/K = 2.86$ and $m = T/K = 82.86$. The performance of the autopilot with these parameters is shown in Figure 6.32.

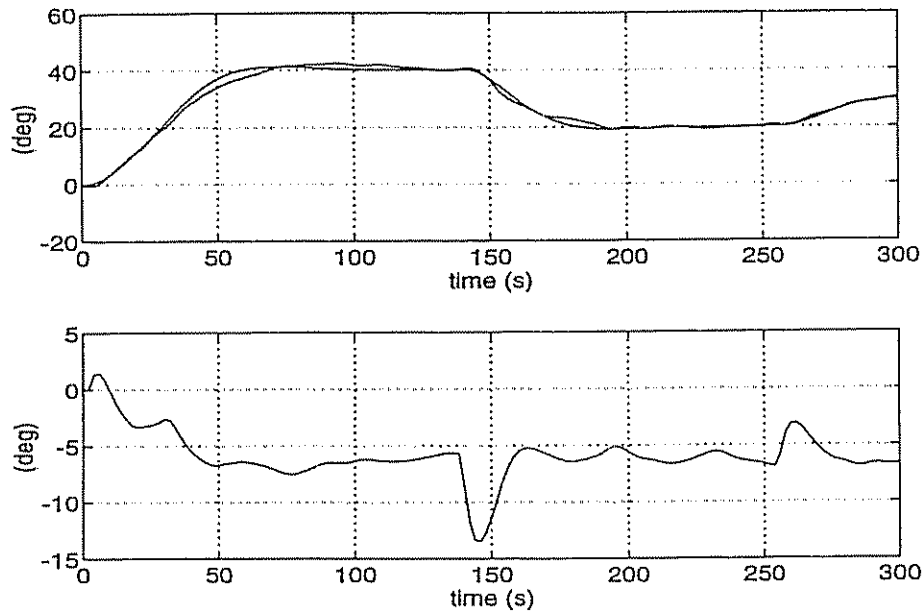

Figure 6.32: Course-changing maneuvers with the M/S Nornews Express. Desired and measured yaw angle versus time (upper plot) and rudder angle (lower plot) versus time.

□

Analogy to Feedback Linearization

The control law (6.258) with K_d defined in (6.260) can be rewritten according to:

$$\delta = m\,a_\psi + d(r)\,r \tag{6.264}$$

by defining a_ψ as:

$$a_\psi = \dot{r}_d - \frac{5}{2}\lambda\,\tilde{r} - 2\lambda^2\,\tilde{\psi} - \frac{1}{2}\lambda^3 \int_0^t \tilde{\psi}(\tau)\,d\tau \tag{6.265}$$

From the theory of feedback linearization a_ψ can be interpreted as the *commanded angular acceleration*. The nonlinear term $d(r)r$ is included to cancel out the model

nonlinearities. Moreover, combining (6.264) with (6.251) yields the following linear system:

$$\ddot{\psi} = a_\psi \tag{6.266}$$

This is a linear control problem which can be solved in terms of the new control variable a_ψ. More generally, we could choose:

$$a_\psi = \dot{r}_d - K_d\,\tilde{r} - K_p\,\tilde{\psi} - K_i \int_0^t \tilde{\psi}(\tau)\,d\tau \tag{6.267}$$

where K_p, K_d and K_i can be interpreted as the proportional, derivative and integral gains, respectively. The first term in the commanded acceleration is simply an acceleration feedforward term. Finally, the nonlinear control law for δ is obtained by substituting a_ψ into (6.264).

6.4.4 Adaptive Feedback Linearization

We will now show how adaptive feedback linearization can be applied to nonlinear ship steering in the presence of parametric uncertainties (Fossen and Paulsen 1992). Consider the nonlinear model of Norrbin, Equation (5.160), which can be written:

$$m\,\ddot{\psi} + d_1\,\dot{\psi} + d_3\,\dot{\psi}^3 = \delta; \qquad m > 0 \tag{6.268}$$

Here $m = T/K$, $d_1 = n_1/K$ and $d_3 = n_3/K$. For simplicity, the coefficients n_0 and n_2 in Norrbin's model are assumed to be zero. Taking the control law to be:

$$\boxed{\delta = \hat{m}\,a_\psi + \hat{d}_1\,\dot{\psi} + \hat{d}_3\,\dot{\psi}^3} \tag{6.269}$$

where the hat denotes the estimates of the parameters and a_ψ can be interpreted as the commanded acceleration, yields:

$$m\,(\ddot{\psi} - a_\psi) = \tilde{m}\,a_\psi + \tilde{d}_1\,\dot{\psi} + \tilde{d}_3\,\dot{\psi}^3 \tag{6.270}$$

Here $\tilde{m} = \hat{m} - m$, $\tilde{d}_1 = \hat{d}_1 - d_1$ and $\tilde{d}_3 = \hat{d}_3 - d_3$ are the parameter errors. The control law (6.269) can be made adaptive by including a parameter estimator to update $\hat{m}$, $\hat{d}_1$ and $\hat{d}_3$. We will now show how a pole-placement algorithm can be used to design the turning controller.

Pole-Placement Algorithm

In the case of no parametric uncertainties, Equation (6.270) reduces to:

$$\boxed{\ddot{\psi} = a_\psi} \tag{6.271}$$

which suggests that the commanded acceleration should be chosen as:

$$\boxed{a_\psi = \ddot{\psi}_d - K_d\,\dot{\tilde{\psi}} - K_p\,\tilde{\psi}} \tag{6.272}$$

where ψ_d is the desired heading and $\tilde{\psi} = \psi - \psi_d$ is the heading error. This in turn yields the error dynamics:

$$\ddot{\tilde{\psi}} + K_d\,\dot{\tilde{\psi}} + K_p\,\tilde{\psi} = 0 \tag{6.273}$$

The desired states ψ_d, $\dot{\psi}_d$ and $\ddot{\psi}_d$ can be generated by a reference model similar to (6.228). A simple pole-placement algorithm could be to choose:

$$K_p = \lambda^2; \qquad K_d = 2\,\lambda; \qquad \lambda > 0 \tag{6.274}$$

which yields the critically damped error dynamics:

$$\ddot{\tilde{\psi}} + 2\,\lambda\,\dot{\tilde{\psi}} + \lambda^2\,\tilde{\psi} = 0 \tag{6.275}$$

or equivalently,

$$\dot{s} + \lambda\,s = 0 \quad \text{with} \quad s = \dot{\tilde{\psi}} + \lambda\,\tilde{\psi} \tag{6.276}$$

Here s can be interpreted as a measure of tracking. An adaptive version of the pole-placement algorithm is given in Theorem 6.2.

Theorem 6.2 (Adaptive Pole-Placement)
The parameter update laws:

$$\begin{aligned} \dot{\hat{m}} &= -\gamma_1\,a_\psi\,s \\ \dot{\hat{d}}_1 &= -\gamma_2\,\dot{\psi}\,s \\ \dot{\hat{d}}_3 &= -\gamma_3\,\dot{\psi}^3\,s \end{aligned} \tag{6.277}$$

with $\gamma_i > 0$ for $(i = 1,2,3)$ yields a stable system.

Proof: *Substituting (6.272) and (6.274) into the error dynamics (6.270), yields:*

$$m\,(\dot{s} + \lambda\,s) = \tilde{m}\,a_\psi + \tilde{d}_1\,\dot{\psi} + \tilde{d}_3\,\dot{\psi}^3 \tag{6.278}$$

Choosing a Lyapunov function candidate:

$$V(s, \tilde{m}, \tilde{d}_1, \tilde{d}_3, t) = \frac{1}{2}\left[m\,s^2 + \frac{1}{\gamma_1}\,\tilde{m}^2 + \frac{1}{\gamma_2}\,\tilde{d}_1^2 + \frac{1}{\gamma_3}\,\tilde{d}_3^2\right] \tag{6.279}$$

Consequently, differentiation of V with respect to time yields:

$$\dot{V} = -\lambda\,m\,s^2 + \tilde{m}\,[\frac{1}{\gamma_1}\,\dot{\tilde{m}} + a_\psi\,s] + \tilde{d}_1\,[\frac{1}{\gamma_2}\,\dot{\tilde{d}}_1 + \dot{\psi}\,s] + \tilde{d}_3\,[\frac{1}{\gamma_3}\,\dot{\tilde{d}}_3 + \dot{\psi}^3\,s] \tag{6.280}$$

Assuming that $\dot{m} = \dot{d}_1 = \dot{d}_3 = 0$, the particular choice (6.277) of the parameter update laws implies that (6.280) reduces to:

$$\dot{V} = -\lambda\, m\, s^2 \leq 0 \tag{6.281}$$

This implies that $V(t) \leq V(0)$, and therefore that s, $\bar{m}$, $\bar{d}_1$ and $\bar{d}_3$ remains bounded in all time. Differentiating $\dot{V}$ with respect to time, yields:

$$\ddot{V} = -2\,\lambda\, m\, s\, \dot{s} \tag{6.282}$$

Assuming that a_ψ is bounded implies that $\dot{s}$ is bounded and consequently that $\ddot{V}$ is bounded. Hence, $\dot{V}$ must be uniformly continuous. Convergence is guaranteed by application of Barbălat's lemma, see Appendix C.1.2. This in turn implies that $s \to 0$ as $t \to \infty$ and thus that the tracking error $\tilde{\psi}$ converges asymptotically to zero. Convergence of the parameter errors $\bar{m}$, $\bar{d}_1$ and $\bar{d}_3$ to zero, however, requires that the system is persistently excited.
□

In the implementation of the control law it is desirable to include integral action to ensure that the tracking error converges to zero in the presence of constant wind and current disturbances. This can be done by simply modifying the measure of tracking according to:

$$s = \dot{\tilde{\psi}} + 2\,\lambda\,\tilde{\psi} + \lambda^2 \int_0^t \tilde{\psi}(\tau)\, d\tau \tag{6.283}$$

Hence, the error dynamics:

$$\dot{s} + \lambda s = 0 \tag{6.284}$$

is equivalent with:

$$\ddot{\tilde{\psi}} + 3\,\lambda\,\dot{\tilde{\psi}} + 3\,\lambda^2\,\tilde{\psi} + \lambda^3 \int_0^t \tilde{\psi}(\tau)\, d\tau = 0 \tag{6.285}$$

This in turn suggests that the commanded acceleration should be chosen as:

$$\boxed{a_\psi = \ddot{\psi}_d - K_d\,\dot{\tilde{\psi}} - K_p\,\tilde{\psi} - K_i \int_0^t \tilde{\psi}(\tau)\, d\tau} \tag{6.286}$$

where $K_d = 3\,\lambda$, $K_p = 3\,\lambda^2$ and $K_i = \lambda^3$, to obtain: $\ddot{\tilde{\psi}} = a_\psi$.

6.4.5 Model Reference Adaptive Control

Model reference adaptive control (MRAC) utilizing Lyapunov stability theory was first applied to course-changing autopilots by Van Amerongen and ten Cate (1975). This section reviews the MRAC design of Van Amerongen (1982, 1984).

The MRAC design is based on the *parallel configuration* shown in Figure 6.33 where the desired closed-loop dynamics is specified by a linear 2nd-order reference model.

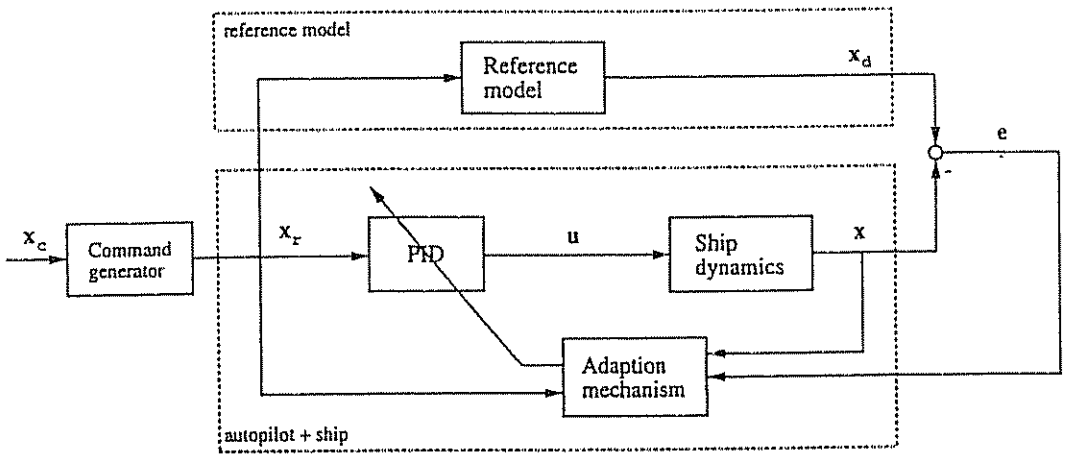

Figure 6.33: Model reference adaptive controller.

The main idea is to match the reference model dynamics by the resulting dynamics of the ship and the autopilot such that:

$$\textbf{Reference model} = \textbf{Autopilot} + \textbf{Ship steering dynamics}$$

We will now show how this can be done. Consider Nomoto's 1st-order model in the form:

$$T\ddot{\psi} + \dot{\psi} = K\delta + K_w \tag{6.287}$$

where the wind and current disturbances are modelled as an unknown slowly-varying gain denoted as K_w. The unknown process gain and time constants are denoted as K and T, respectively. Let the adaptive control law be chosen as:

$$\boxed{\delta = \hat{K}_p(\psi_r - \psi) - \hat{K}_d\dot{\psi} - \hat{K}_i} \tag{6.288}$$

where $\hat{K}_p$, $\hat{K}_d$ and $\hat{K}_i$ are adaptive estimates of the PID-regulator gains to be determined later, see Figure 6.34. Substituting (6.288) into (6.287) yields:

$$\boxed{T\,\ddot{\psi} + (1 + K\hat{K}_d)\,\dot{\psi} + K\hat{K}_p\,\psi = K\hat{K}_p\,\psi_r + (K_w - K\hat{K}_i)} \tag{6.289}$$

We now want this dynamics to be equal the dynamics (6.228) of the reference model, that is:

$$\boxed{T_m\ddot{\psi}_d + \dot{\psi}_d + K_m\psi_d = K_m\psi_r} \tag{6.290}$$

Solving (6.289) and (6.290) for K_p, K_d and K_i, yields:

$$K_p = \frac{K_m}{T_m}\frac{T}{K} \tag{6.291}$$

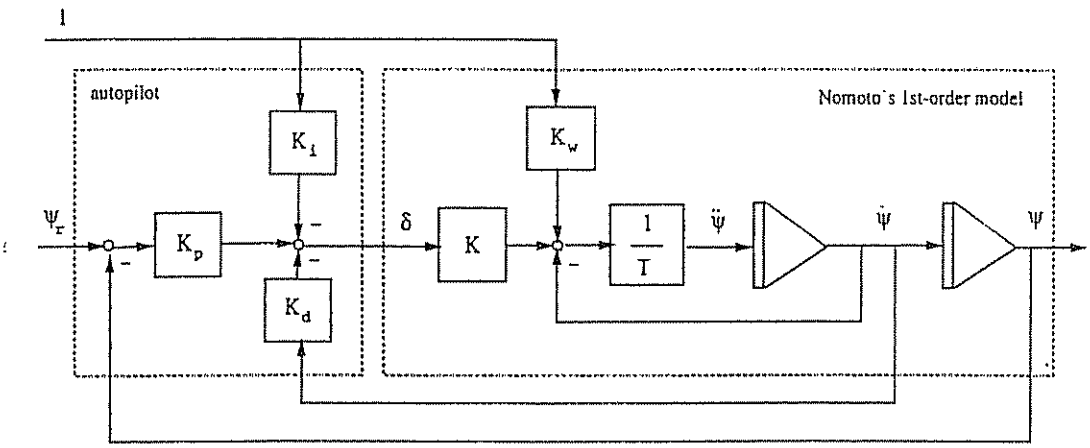

Figure 6.34: Diagram showing the autopilot of Van Amerongen (1982).

$$K_d = \frac{1}{K}(\frac{T}{T_m} - 1) \tag{6.292}$$

$$K_i = \frac{K_w}{K} \tag{6.293}$$

These values for K_p, K_d and K_i are referred to as the *perfect model matching conditions*. Notice that these expressions assume that the plant parameters are known. We will now show how estimates of $\hat{K}_p, \hat{K}_d$ and $\hat{K}_i$ can be computed. Defining the tracking error as: $\tilde{\psi} = \psi_d - \psi$ and using the reference model (6.290) yield the error dynamics:

$$\frac{T}{K}(\dddot{\tilde{\psi}} + \frac{1}{T_m}\ddot{\tilde{\psi}} + \frac{K_m}{T_m}\dot{\tilde{\psi}}) = \frac{T}{K}(\frac{K_m}{T_m}\dot{\psi}_r - \ddot{\psi} - \frac{1}{T_m}\dot{\psi} - \frac{K_m}{T_m}\psi) \tag{6.294}$$

Applying the *perfect model matching condition* (6.291) and (6.292) to this expression yields:

$$\frac{T}{K}(\dddot{\tilde{\psi}} + \frac{1}{T_m}\ddot{\tilde{\psi}} + \frac{K_m}{T_m}\dot{\tilde{\psi}}) = -K_p(\psi - \psi_r) - (\frac{1}{K} + K_d)\dot{\psi} - \frac{T}{K}\ddot{\psi} \tag{6.295}$$

The last term on the right-hand side of this expression can be rewritten by applying the closed-loop dynamics (6.289), that is

$$\frac{T}{K}\ddot{\psi} = -\hat{K}_p(\psi - \psi_r) - (\hat{K}_i - \frac{K_w}{K}) - (\frac{1}{K} + \hat{K}_d)\dot{\psi} \tag{6.296}$$

Applying the *perfect model matching condition* (6.293), yields:

$$\frac{T}{K}\ddot{\psi} = -\hat{K}_p\,(\psi - \psi_r) - (\hat{K}_i - K_i) - (\frac{1}{K} + \hat{K}_d)\,\dot{\psi} \tag{6.297}$$

Finally, combining (6.295) and (6.297), yields the error dynamics:

$$\frac{T}{K}(\dddot{\tilde{\psi}} + \frac{1}{T_m}\ddot{\tilde{\psi}} + \frac{K_m}{T_m}\dot{\tilde{\psi}}) = (\hat{K}_p - K_p)\,(\psi - \psi_r) + (\hat{K}_d - K_d)\,\dot{\psi} + (\hat{K}_i - K_i) \tag{6.298}$$

This system can be expressed in a more compact form as:

$$\dot{x} = Ax + b\,\phi^T\,\tilde{\theta} \tag{6.299}$$

where $x = [\psi_d - \psi, \dot{\psi}_d - \dot{\psi}]^T$ and

$$A = \begin{bmatrix} 0 & 1 \\ -\frac{K_m}{T_m} & -\frac{1}{T_m} \end{bmatrix}; \quad b = \begin{bmatrix} 0 \\ b_0 \end{bmatrix}; \quad \phi = [\psi - \psi_r, \dot{\psi}, 1]^T; \quad \tilde{\theta} = [\tilde{K}_p, \tilde{K}_d, \tilde{K}_i]^T \tag{6.300}$$

Here $b_0 = K/T$ and $\tilde{K}_p = \hat{K}_p - K_p$, $\tilde{K}_d = \hat{K}_d - K_d$ and $\tilde{K}_i = \hat{K}_i - K_i$ are the parameter estimation errors. Hence, the control objective can be expressed as:

$$\lim_{t\to\infty} x(t) = 0 \tag{6.301}$$

which simply states that both the heading angle error and heading rate error should converge to zero. This is guaranteed by applying the following theorem.

Theorem 6.3 (Model Reference Adaptive Control)
The adaptive control law:

$$\dot{\hat{\theta}} = -\Gamma\,\frac{1}{|b_0|}\,\phi\,b^T P x; \qquad \Gamma = \Gamma^T > 0 \tag{6.302}$$

where $P = P^T > 0$ satisfies the Lyapunov equation:

$$A^T P + PA = -Q; \qquad Q = Q^T > 0 \tag{6.303}$$

guarantees that the tracking error $x \to 0$ as $t \to \infty$ and that the parameter estimation error $\tilde{\theta}$ is bounded.

Proof: *Consider the Lyapunov function candidate:*

$$V(x, \tilde{\theta}, t) = x^T P x + |b_0|\,\tilde{\theta}^T \Gamma^{-1} \tilde{\theta} \tag{6.304}$$

Differentiating V with respect to time yields:

$$\dot{V} = x^T(A^T P + PA)x + 2\,|b_0|\,\tilde{\theta}^T(\Gamma^{-1}\,\dot{\tilde{\theta}} + \frac{1}{|b_0|}\,\phi\,b^T\,P\,x) \tag{6.305}$$

Substituting (6.302) and (6.303) into the expression for $\dot{V}$ yields:

$$\dot{V} = -x^T Q x \leq 0 \tag{6.306}$$

This implies that $V(t) \leq V(0)$, and therefore that x and $\tilde{\theta}$ are bounded. Differentiating $\dot{V}$ with respect to time, yields:

$$\ddot{V} = -2\,x^T Q \dot{x} \tag{6.307}$$

Assuming that ϕ is bounded implies that $\dot{x}$ is bounded, see (6.299). This in turn implies that $\ddot{V}$ is bounded. Hence, $\dot{V}$ must be uniformly continuous. Application of Barbălat's lemma (see Appendix C.1) then indicates that $x \to 0$ as $t \to \infty$.
□

To implement the parameter adaptation law (6.302) we have to rewrite the *unknown* term:

$$\frac{b^T}{|b_0|} = \left[0, \quad \frac{b_0}{|b_0|} \right] = [\, 0, \quad \mathrm{sgn}(b_0) \,] \tag{6.308}$$

This implies that only the sign of the ratio $b_0 = K/T$ must be known while the magnitude of b_0 not is used. Let $\boldsymbol{\Gamma} = \mathrm{diag}(\gamma_1, \gamma_2, \gamma_3)$. Hence, (6.302) can be written in component form as:

$$\dot{\hat{K}}_p = -\gamma_1 \,\mathrm{sgn}(b_0)\, (\psi - \psi_r) e \tag{6.309}$$

$$\dot{\hat{K}}_d = -\gamma_2 \,\mathrm{sgn}(b_0)\, \dot{\psi} e \tag{6.310}$$

$$\dot{\hat{K}}_i = -\gamma_3 \,\mathrm{sgn}(b_0)\, e \tag{6.311}$$

where $\gamma_i > 0$ for $(i = 1, 2, 3)$. The error signal is computed as:

$$e = p_{21}\, (\psi_d - \psi) + p_{22}\, (\dot{\psi}_d - \dot{\psi}) \tag{6.312}$$

where the elements $p_{21} = p_{12}$ and p_{22} of:

$$\boldsymbol{P} = \begin{bmatrix} p_{11} & p_{12} \\ p_{21} & p_{22} \end{bmatrix} \tag{6.313}$$

are given from (6.303).

Limitations of the Steering Machine

The direct MRAC is based on the assumption that perfect model matching can be achieved. Hard nonlinearities like saturation in the rudder angle and the rudder rate implies that the linear reference model specifying the desired closed-loop dynamics cannot be matched by the system resulting from the ship dynamics and the adaptive controller. Instead of introducing nonlinearities in the reference model, Van Amerongen (1982, 1984) suggests modifying the commanded input ψ_r to the reference model such that the reference model remain linear. This can be done by introducing a *command generator* according to Figure 6.35.

The command generator should be designed such that the reference model remains linear and thus that the parameter estimates remains bounded. This can be done by introducing a new mechanism for compensation of rudder angle and rudder rate saturation, see Figure 6.36.

The SAT function in Figure 6.36 is defined as:

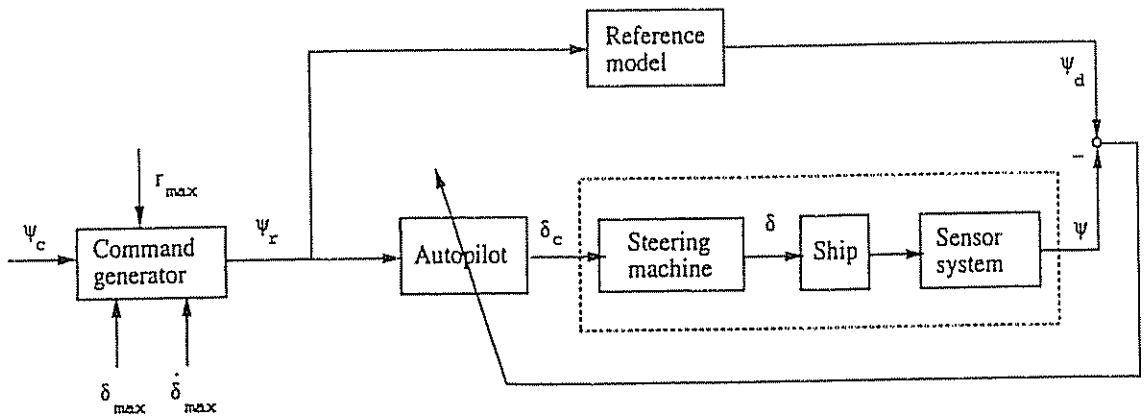

Figure 6.35: MRAC structure with reference model and command generator in series.

$$SAT = \begin{cases} \frac{\delta_{max}}{|\delta_c|} \cdot \frac{1}{1+T_A s} & \text{if} \quad |\delta_c| > \delta_{max} \\ \frac{1}{1+T_A s} & \text{if} \quad |\delta_c| \leq \delta_{max} \end{cases} \tag{6.314}$$

where δ_c is the commanded rudder angle from the autopilot and δ_{max} is the maximum allowed rudder angle. Rudder rate limitations are avoided by selecting the time constant T_A in the low-pass filter large enough, for instance by manually increasing the value of T_A until $\delta(t)$ tracks $\delta_c(t)$. In fact, this simple modification implies that the MRAC scheme remains stable since nonlinearities in the steering machine will not affect the perfect model matching conditions.

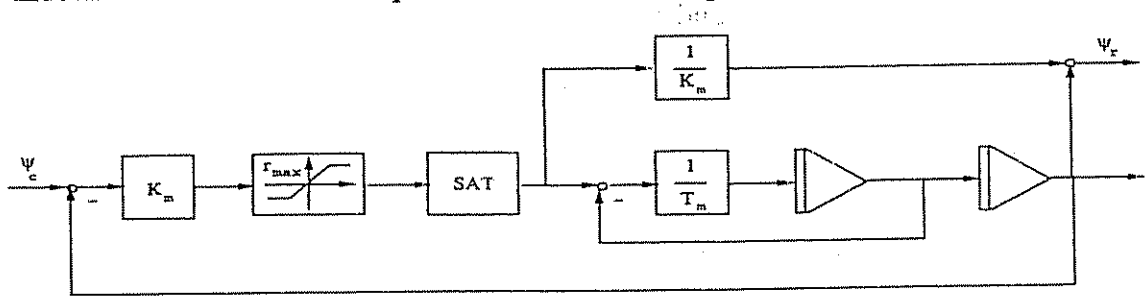

Figure 6.36: Command generator

The last element in the command generator, the yaw rate limiter, is motivated by the desire to describe a course-changing maneuver by three phases:

1) Start of turn

2) Stationary turn ($r = r_{max}$ and $\dot{r} = 0$)

3) End of turn

Hence, the user can specify the maximum allowed turning rate during the second phase of the turn. The location of the yawing rate limiter is shown in Figure 6.36.

6.5 Track-Keeping Systems

Classical autopilot control of ships involves controlling the course angle ψ. However, by including an additional control-loop in the control system with position feedback a ship guidance system can be designed. This system is usually designed such that the ship can move forward with constant speed U at the same time as the sway position y is controlled. Hence, the ship can be made to track a predefined reference path which again can be generated by some route management system. The desired route is most easily specified by way points. If weather data are available, the optimal route can be generated such that the ship's wind and water resistance is minimized. Hence, fuel can be saved.

Many track controllers are based on low-accuracy positioning systems like *Decca*, *Omega* and *Loran-C* (Forssell 1991). These systems are usually combined with a low-gain PI-controller in cascade with the autopilot. The output from the autopilot will then represent the desired course angle. Unfortunately such systems result in tracking errors up to 300 m, which are only satisfactory in open seas.

Recently, more sophisticated high-precision track controllers have been designed. These systems are based on optimal control theory utilizing *Navstar GPS* (Global Positioning System). *Navstar GPS* consists of 21 satellites in six orbital planes, with three or four satellites in each plane, together with three active spares. By measuring the distance to the satellite, the global position (x, y, z) of the vessel can be computed by application of the Kalman filter algorithm. A more detailed description of the GPS receiver and the Kalman filter implementation is given by Bardal and Ørpen (1983).

Kinematics

For the design of the track controller it is convenient to describe the kinematics of the ship according to Figure 6.37. From the figure it is seen that (assuming that $\theta = \phi = 0$):

$$\dot{x} = u\cos\psi - v\sin\psi \tag{6.315}$$

$$\dot{y} = u\sin\psi + v\cos\psi \tag{6.316}$$

$$\dot{\psi} = r \tag{6.317}$$

Unfortunately, these equations are nonlinear in the states u, v and ψ. However a linear approximation can be derived under the assumption that the earth-fixed coordinate system can be rotated such that the desired heading is $\psi_d = 0$. We can also move the origin of the coordinate system such that it coincides with the starting point $[x_d(t_0), y_d(t_0)]$. Hence, the heading angle ψ will be small during track control such that:

$$\sin\psi \approx \psi; \qquad \cos\psi \approx 1 \tag{6.318}$$

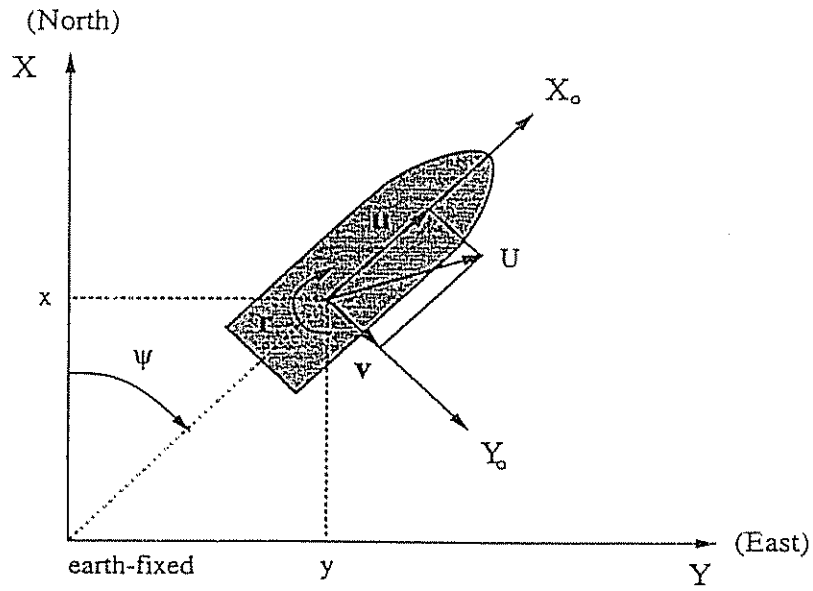

Figure 6.37: Coordinate systems for global tracking.

We also have that $u \approx U$. Hence, the kinematic equations of motion reduce to a set of linear equations:

$$\boxed{\dot{x} = U + d_x} \qquad \boxed{\dot{y} = U\,\psi + v + d_y} \tag{6.319}$$

We have here included two additional terms (d_x, d_y) describing errors due to linearization and drift caused by environmental disturbances. It turns out that these terms are important for the performance of the state estimator. Moreover, permanent estimation of these terms leads to fewer track deviations.

Way Point Guidance Based on the Straight Line Between Two Points

Let us assume that we want to design a guidance system based on two way points A and B with coordinates $[x_d(t_0), y_d(t_0)]$ and $[x_d(t_f), y_d(t_f)]$, respectively. Furthermore, assume that the ship is moving with forward speed U and that the approach time t_f is unknown. Hence, we can eliminate the time variable from (6.315) and (6.316) to obtain the desired heading angle:

$$\psi_d = \tan^{-1}\left(\frac{y_d(t_f) - y_d(t_0)}{x_d(t_f) - x_d(t_0)}\right) \tag{6.320}$$

This formula requires that a sign test is included to ensure that ψ_d is in the proper quadrant. We also notice that the desired heading angle is only changed at each way point. Hence some overshoot is observed when changing way point. An alternative algorithm to generate a smooth reference trajectory is given below.

Way Point Guidance by Line of Sight (LOS)

Let the vehicle mission be given by a set of way points $[x_d(k), y_d(k)]$ for $(k = 1...N)$. Hence, we can define the LOS in terms of a desired heading angle (Healey and Lienard 1993):

$$\psi_d(t) = \tan^{-1}\left(\frac{y_d(k) - y(t)}{x_d(k) - x(t)}\right) \tag{6.321}$$

Care must be taken to select the proper quadrant for ψ_d. After the quadrant check is performed, the next way point can be selected on a basis of whether the vessel lies within a *circle of acceptance* with radius ρ_0 around the way point $[x_d(k), y_d(k)]$. Moreover if the vehicle location $[x(t), y(t)]$ at the time t satisfies:

$$[x_d(k) - x(t)]^2 + [y_d(k) - y(t)]^2 \leq \rho_0^2 \tag{6.322}$$

the next way point $[x_d(k+1), y_d(k+1)]$ should be selected. A guideline could be to choose ρ_0 equal to two ship lengths, that is $\rho_0 = 2\,L$ (see Figure 6.38).

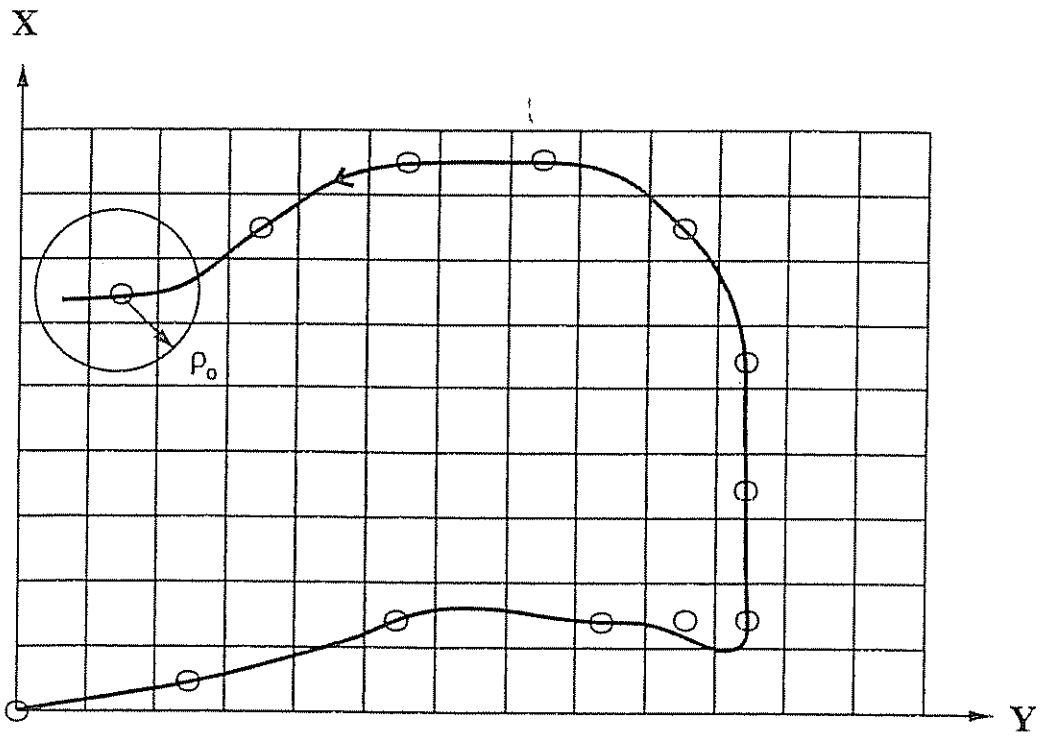

Figure 6.38: Path planning by means of LOS. Way points are indicated as small circles and the large circle represents the circle of acceptance (radius ρ_0).

6.5.1 Conventional Guidance System

A conventional guidance system is usually designed by neglecting the sway mode such that the following holds (see (6.319)):

$$y(s) = \frac{U}{s}\,\psi(s) + \frac{1}{s}\,d_y(s) \tag{6.323}$$

Let the ship dynamics be described by the Nomoto model:

$$T\,\dot{r} + r = K\,\delta + r_b; \qquad \dot{\psi} = r \tag{6.324}$$

where r_b is a slowly-varying parameter due to environmental disturbances. Next, we define:

$$h_\delta(s) = \frac{y}{\delta}(s) = \frac{K\,U}{s^2\,(1+T\,s)} \tag{6.325}$$

$$h_b(s) = \frac{y}{r_b}(s) = \frac{U}{s^2\,(1+Ts)} \tag{6.326}$$

$$h_d(s) = \frac{y}{d_y}(s) = \frac{1}{s} \tag{6.327}$$

such that $y(s)$ can be written:

$$y(s) = h_\delta(s)\,\delta(s) + h_b(s)\,r_b(s) + h_d(s)\,d_y(s) \tag{6.328}$$

We can now write the control law as:

$$\delta(s) = h_r(s)\,[y_d(s) - y(s)] \tag{6.329}$$

where $y_d(s)$ is the desired sway position and $h_r(s)$ is the regulator transfer function. This implies that:

$$y(s) = \frac{l(s)}{1+l(s)}\,y_d(s) + \frac{h_b(s)}{1+l(s)}\,r_b(s) + \frac{h_d(s)}{1+l(s)}\,d_y(s) \tag{6.330}$$

Here $l(s) = h_\delta(s)\,h_r(s)$ is the loop transfer function. By choosing $h_r(s)$ of PID-type it is straightforward to show that:

$$\lim_{t\to\infty} y(t) = y_d \quad \text{(constant)} \tag{6.331}$$

under the assumption of r_b = constant and y_d = constant. In cases where an existing autopilot system (course controller) is used, a track-keeping system can be designed by simply adding feedback from the sway position in an outer loop. This illustrated in Figure 6.39 where an outer loop PI-controller is used. Since a course-keeping controller is assumed to stabilize the steering dynamics, derivative action is not necessary in the outer-loop. Integral action should still be used in order to avoid steady-state errors due to environmental disturbances.

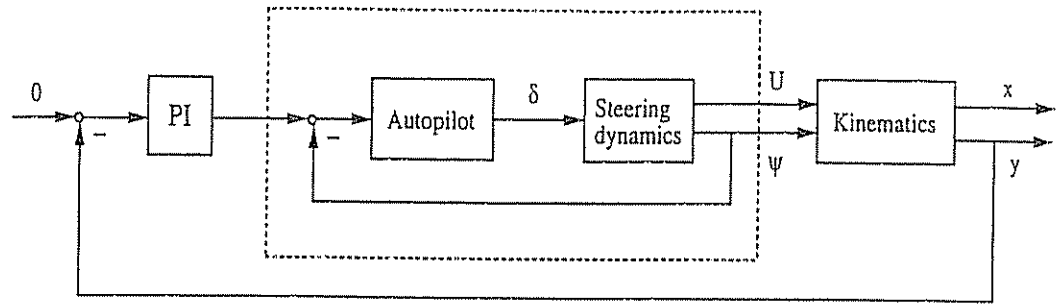

Figure 6.39: Conventional track-keeping system based on an existing autopilot system.

6.5.2 Optimal Guidance System

Extensions to optimal tracking have been discussed by Holzhüter (1990). This design is mainly an LQG design utilizing optimal control and filtering theory. Combining the kinematic relation (6.319) with the ship steering dynamics (5.21), we obtain the following state-space model:

$$\begin{bmatrix} \dot{v} \\ \dot{r} \\ \dot{\psi} \\ \dot{y} \\ \dot{v}_b \\ \dot{r}_b \\ \dot{d}_y \end{bmatrix} = \begin{bmatrix} a_{11} & a_{12} & 0 & 0 & -a_{11} & -a_{12} & 0 \\ a_{21} & a_{22} & 0 & 0 & -a_{21} & -a_{22} & 0 \\ 0 & 1 & 0 & 0 & 0 & 0 & 0 \\ 1 & 0 & U & 0 & 0 & 0 & 1 \\ 0 & 0 & 0 & 0 & 0 & 0 & 0 \\ 0 & 0 & 0 & 0 & 0 & 0 & 0 \\ 0 & 0 & 0 & 0 & 0 & 0 & 0 \end{bmatrix} \begin{bmatrix} v \\ r \\ \psi \\ y \\ v_b \\ r_b \\ d_y \end{bmatrix} + \begin{bmatrix} b_1 \\ b_2 \\ 0 \\ 0 \\ 0 \\ 0 \\ 0 \end{bmatrix} \delta + \begin{bmatrix} 0 & 0 & 0 \\ 0 & 0 & 0 \\ 0 & 0 & 0 \\ 0 & 0 & 0 \\ 1 & 0 & 0 \\ 0 & 1 & 0 \\ 0 & 0 & 1 \end{bmatrix} \begin{bmatrix} w_1 \\ w_2 \\ w_3 \end{bmatrix}$$

Here a_{ij} and b_i are defined in (5.21) and v_b and r_b are two slowly-varying parameters describing modeling errors and environmental disturbances. The control variables ψ and y are obtained by defining:

$$y = C\,x \tag{6.332}$$

with

$$C = \begin{bmatrix} 0 & 0 & 1 & 0 & 0 & 0 & 0 \\ 0 & 0 & 0 & 1 & 0 & 0 & 0 \end{bmatrix} \tag{6.333}$$

In many applications only forward speed U, heading angle ψ and position (x, y) are measured. Often estimation of the sway velocity v is ill-conditioned. In such cases it is suggested to use a simpler model structure, neglecting the sway dynamics, for instance (6.323) and (6.324). We can then write:

$$\begin{bmatrix} \dot{r} \\ \dot{\psi} \\ \dot{y} \\ \dot{r}_b \\ \dot{d}_y \end{bmatrix} = \begin{bmatrix} -1/T & 0 & 0 & 1/T & 0 \\ 1 & 0 & 0 & 0 & 0 \\ 0 & U & 0 & 0 & 1 \\ 0 & 0 & 0 & 0 & 0 \\ 0 & 0 & 0 & 0 & 0 \end{bmatrix} \begin{bmatrix} r \\ \psi \\ y \\ r_b \\ d_y \end{bmatrix} + \begin{bmatrix} K/T \\ 0 \\ 0 \\ 0 \\ 0 \end{bmatrix} \delta + \begin{bmatrix} 0 & 0 \\ 0 & 0 \\ 0 & 0 \\ 1 & 0 \\ 0 & 1 \end{bmatrix} \begin{bmatrix} w_1 \\ w_2 \end{bmatrix} \tag{6.334}$$

For this system C reduces to:

$$C = \begin{bmatrix} 0 & 1 & 0 & 0 & 0 \\ 0 & 0 & 1 & 0 & 0 \end{bmatrix} \tag{6.335}$$

Hence, the tracking problem can be formulated as:

$$\min J = \frac{1}{2}\int_0^T \left(y^T Q y + u^T P u\right)\, dt = \frac{1}{2}\int_0^T \left(\lambda_1\, y^2 + \lambda_2\, \psi^2 + \delta^2\right)\, dt \tag{6.336}$$

where λ_1 and λ_2 are two scalar weights. Since the closed-loop dynamics is highly affected by change of forward speed, the following normalization procedure can be used:

$$\begin{aligned} t^* &= t/T & \qquad \psi^* &= \psi \\ \delta^* &= \delta\, KT & \qquad y^* &= y/(UT) \\ r^* &= r\, T \end{aligned}$$

Consequently, we can rewrite the performance index according to:

$$\min J^* = \frac{1}{2}\int_0^T \left[\lambda_1^*\,(y^*)^2 + \lambda_2^*\,(\psi^*)^2 + (\delta^*)^2\right]\, dt^* \tag{6.337}$$

where

$$\lambda_1^* = \lambda_1\,(UT)^2(KT)^3; \qquad \lambda_2^* = \lambda_2\,(KT)^2 \tag{6.338}$$

Here λ_1^* and λ_2^* are constant with respect to U. The solution of the optimal tracking problem with $y_d^* = [0,\ 0]^T$ is found in Appendix D and can be written:

$$\delta^* = g^T\, x^* \tag{6.339}$$

where g is the optimal feedback gain vector. Hence, the optimal rudder angle is given by the transformation $\delta = \delta^*/(KT)$.

State Estimator

Since not all states in the control model are measurable and the measurements are corrupted with noise, we must design a state estimator to estimate the LF motion components of the ship. A Kalman filter can be designed for this purpose. The state vector used in the Kalman filter may be taken to be:

$$x = [r,\ \psi,\ r_b,\ x,\ y,\ d_x,\ d_y,\ \xi_H,\ \psi_H]^T \tag{6.340}$$

We have here included two new states ξ_H and ψ_H to describe 1st-order wave disturbances in terms of a high-frequency model. This model is written:

$$\dot{\xi}_H = \psi_H \tag{6.341}$$
$$\dot{\psi}_H = -2\zeta\omega_n\,\psi_H - \omega_n^2\,\xi_H + K_w\,w \tag{6.342}$$

Also notice that we have included the surge position x and the drift term d_x in the state vector. These states are not used in the control design. However, permanent estimation of x and d_x leads to fewer track deviations during track changes. The drift terms d_x and d_y and the yaw angle rate bias r_b are modelled as random walk processes, that is:

$$\dot{d}_x = w_1; \qquad \dot{d}_y = w_2; \qquad \dot{r}_b = w_3 \tag{6.343}$$

where w_i $(i = 1...3)$ are zero-mean Gaussian white noise processes. Finally, the Kalman filter measurement equation corresponding to a GPS system and a gyro compass can be written as:

$$z = H\,x + v \tag{6.344}$$

where

$$H = \begin{bmatrix} 0 & 1 & 0 & 0 & 0 & 0 & 0 & 0 & 1 \\ 0 & 0 & 0 & 1 & 0 & 0 & 0 & 0 & 0 \\ 0 & 0 & 0 & 0 & 1 & 0 & 0 & 0 & 0 \end{bmatrix} \tag{6.345}$$

Hence, $z = [\psi + \psi_H + v_1, x + v_2, y + v_3]^T$. The Kalman filter algorithm for this problem is given in Table 6.1.

6.6 Rudder-Roll Stabilization

The main reasons for using roll stabilizing systems on merchant ships are to prevent cargo damage and to increase the effectiveness of the crew. From a safety point of view it is well known that large roll motions cause people to make more mistakes during operation due to sea sickness and tiredness. For naval ships certain operations such as landing a helicopter or the effectiveness of the crew during combat are of major importance. Therefore, roll reduction is an important area of research.

Several solutions have been proposed to accomplish roll reduction; see Burger and Corbet (1960), Lewis (1967) or Bhattacharyya (1978) for a more detailed discussion. The most widely used systems are (Van der Klugt 1987):

Bilge keels: Bilge keels are fins in planes approximately perpendicular to the hull or near the turn of the bilge. The longitudinal extent varies from about 25 to 50 percent of the length of the ship. Bilge keels are widely used, are inexpensive but increase the hull resistance. In addition to this they are effective mainly around the natural roll frequency of the ship. This effect

significantly decreases with the speed of the ship. Bilge keels were first demonstrated in about 1870.

Anti-Rolling Tanks: The most common anti-rolling tanks in use are free-surface tanks, U-tube tanks and diversified tanks. These systems provide damping of the roll motion even at small speeds. The disadvantages of course are the reduction in metacenter height due to free water surface effects and that a large amount of space is required. The earliest versions were installed about 1874.

Fin Stabilizers: Fin stabilizers are a highly attractive device for roll damping. They provide considerable damping if the speed of the ship is not too low. The disadvantage with additional fins are increased hull resistance (except for some systems that are retractable) and high costs associated with the installation. They also require that at least two new hydraulic systems are installed. It should be noted that fins are not effective at low speed and that they cause drag and underwater noise. They were first granted a patent by John I. Thornycroft in 1889.

Rudder-Roll Stabilization (RRS): Roll stabilization by means of the rudder is relatively inexpensive compared to fin stabilizers, has approximately the same effectiveness, and causes no drag or underwater noise if the system is turned off. However, RRS requires a relatively fast rudder to be effective, typically $\dot{\delta}_{\max} = 5$–20 (deg/s). Another disadvantage is that the RRS will not be effective if the ship's speed is low. Early versions discussing the possible use of RRS are reported in Cowley and Lambert (1972, 1975), Carley (1975), Lloyd (1975) and Baitis (1980).

For ship stabilization history, the interested reader is advised to consult Bennett (1991) and a detailed evaluation of different ship roll stabilization systems is found in Sellars and Martin (1992).

RRCS design for naval vessels can be found in Baitis, Woolaver and Beck (1983, 1989), Källström, Wessel and Sjölander (1988) and Van Amerongen, Van der Klugt and Pieffers (1987). Other useful references discussing RRCS design are Blanke, Haals and Andreasen (1989), Blanke and Christensen (1993), Källström (1987), Källström et al. (1988), Källström and Schultz (1990), Katebi, Wong and Grimble (1987), Van Amerongen and Van Nauta Lempke (1987), Van der Klugt (1987) and Zhou (1990).

In the following we will discuss two methods for rudder-roll control system (RRCS) design. The first method uses pole-placement and the second is an optimal controller.

6.6.1 A Mathematical Model for RRCS Design

We will now demonstrate how an RRCS can be designed by applying an approximative model to describe cross-couplings between sway, roll and yaw. More

Table 6.3: Overall comparison of ship roll stabilizer systems (Sellars and Martin 1992)

Stabilizer Type	General Application	% Roll Reduction	Price ($ × 1000)	Installation	Remarks
FINS (small fixed)	mega yachts; naval auxiliaries	90	100-200	hull attachment; supply and install power and control cables	speed loss; largest size about 2 m^2
FINS (retractable)	passenger, cruise, ferries, large RO/RO, naval combatants	90	400-1500	hull attachment; supply and install power and control cables	sizes range from 2 m^2 to about 15 m^2
FINS (large fixed)	naval combatants	90	300-1300	hull attachment; supply and install power and control cables	speed loss
TANKS (free surface)	work vessels, ferries, small passenger and cargo ships	75	30-50	install steelwork supply and install power and control cables	includes liquid level monitor
TANKS (U-tube)	work vessels, RO/RO vessels	75	200-300	install steelwork and piping and valves; install instrument cables	includes heel control system capability
RRS	small, high speed vessels	50-75	50-250	install power and control cables	new development; more robust steering gear may be required
Bilge keels	universal	25-50	...	hull attachment	speed loss

general models are found in Section 5.7.

Approximative Model of Roll and Sway-Yaw Cross-Couplings

A linear model describing the sway, roll and yaw interactions is (Christensen and Blanke 1986):

$$\begin{bmatrix} \dot{v} \\ \dot{r} \\ \dot{p} \\ \dot{\phi} \\ \dot{\psi} \end{bmatrix} = \begin{bmatrix} a_{11} & a_{12} & a_{13} & a_{14} & 0 \\ a_{21} & a_{22} & a_{23} & a_{24} & 0 \\ a_{31} & a_{32} & a_{33} & a_{34} & 0 \\ 0 & 0 & 1 & 0 & 0 \\ 0 & 1 & 0 & 0 & 0 \end{bmatrix} \begin{bmatrix} v \\ r \\ p \\ \phi \\ \psi \end{bmatrix} + \begin{bmatrix} b_1 \\ b_2 \\ b_3 \\ 0 \\ 0 \end{bmatrix} \delta \tag{6.346}$$

This model can be rewritten in terms of two subsystems for sway-yaw and roll, that is:

$$\left[\begin{array}{c} \dot{v} \\ \dot{r} \\ \dot{\psi} \\ \hline \dot{p} \\ \dot{\phi} \end{array}\right] = \left[\begin{array}{ccc|cc} a_{11} & a_{12} & 0 & a_{13} & a_{14} \\ a_{21} & a_{22} & 0 & a_{23} & a_{24} \\ 0 & 1 & 0 & 0 & 0 \\ \hline a_{31} & a_{32} & 0 & a_{33} & a_{34} \\ 0 & 0 & 0 & 1 & 0 \end{array}\right] \left[\begin{array}{c} v \\ r \\ \psi \\ \hline p \\ \phi \end{array}\right] + \left[\begin{array}{c} b_1 \\ b_2 \\ 0 \\ \hline b_3 \\ 0 \end{array}\right] \delta \tag{6.347}$$

Van der Klugt (1987) has proposed a simplified mathematical model of the sway-yaw and roll subsystems which only includes the most important cross-couplings. This model has shown to be practical for rudder roll and autopilot control system design (Van Amerongen et al. 1987, 1990). The transfer functions for the simplified model are:

$$v'(s) = \frac{K_{dv}}{1+T_v s}\delta(s) \tag{6.348}$$

$$\phi(s) = \frac{\omega_n^2}{s^2+2\zeta\omega_n\, s+\omega_n^2}\left[K_{dp}\,\delta(s)+K_{vp}\,v'(s)+w_\phi(s)\right] \tag{6.349}$$

$$\psi(s) = \frac{1}{(1+T_r s)s}\left[K_{dr}\,\delta(s)+K_{vr}\,v'(s)+w_\psi(s)\right] \tag{6.350}$$

where v' is a *new* state new variable representing the *sway velocity caused by the rudder motion alone*. This state variable cannot be measured but a Kalman filter can be used to estimate v'. The main reason for including v' in the model is that this transfer function describes the system zeros in roll and yaw.

The signals w_ϕ and w_ψ are included in the above model to describe wave-induced disturbances. A block diagram of the model of Van der Klugt (1987) is shown in Figure 6.40.

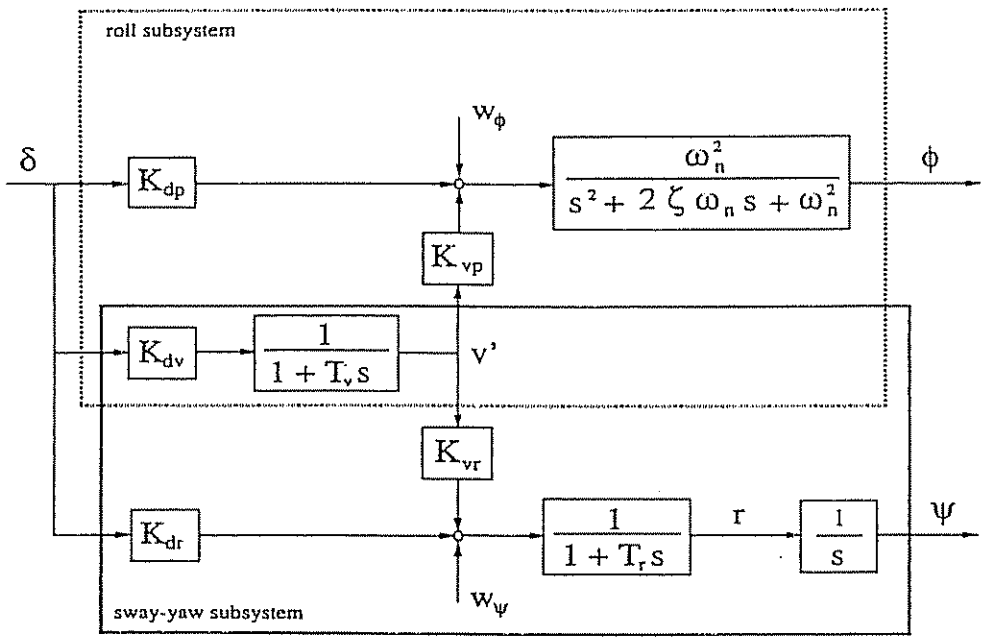

Figure 6.40: Diagram showing the cross-couplings between the sway-yaw and roll subsystems (Van der Klugt 1987).

The corresponding state-space model is:

$$\begin{bmatrix} \dot{v}' \\ \dot{r} \\ \dot{\psi} \\ \hline \dot{p} \\ \dot{\phi} \end{bmatrix} = \left[\begin{array}{ccc|cc} -\frac{1}{T_v} & 0 & 0 & 0 & 0 \\ \frac{K_{vr}}{T_r} & -\frac{1}{T_r} & 0 & 0 & 0 \\ 0 & 1 & 0 & 0 & 0 \\ \hline \omega_n^2 K_{vp} & 0 & 0 & -2\zeta\omega_n & -\omega_n^2 \\ 0 & 0 & 0 & 1 & 0 \end{array}\right] \begin{bmatrix} v' \\ r \\ \psi \\ \hline p \\ \phi \end{bmatrix} + \begin{bmatrix} \frac{K_{dv}}{T_v} \\ \frac{K_{dr}}{T_r} \\ 0 \\ \hline \omega_n^2 K_{dp} \\ 0 \end{bmatrix} \delta + \left[\begin{array}{cc} 0 & 0 \\ 1/T_r & 0 \\ 0 & 0 \\ \hline 0 & \omega_n^2 \\ 0 & 0 \end{array}\right] \begin{bmatrix} w_\psi \\ w_\phi \end{bmatrix} \quad (6.351)$$

In addition to the ship dynamics it is important to model the dynamics of the steering machine such that limitations of rudder angle $\delta_{\max}$ and rudder rate $\dot{\delta}_{\max}$ can be incorporated in the design. Models for this purpose are discussed in Section 5.4.

Control Objective

Although the most effective roll damping systems are those which combine stabilizing fins and rudders (see Källström 1981, Roberts and Braham 1990 and Roberts 1992) we will restrict our discussion to RRCS design. The control objectives of an RRCS are:

(1) Increase the natural frequency and damping ratio in roll.

(2) Control the heading angle of the ship with satisfactory accuracy.

These control objectives can be achieved by separation in the frequency domain. Moreover LF rudder motions are used to maintain the heading while HF rudder motions are used to reduce the roll motions. According to Figure 6.40, we obtain the following transfer functions (assuming $w_\phi = w_\psi = 0$):

$$\begin{aligned} \frac{\psi}{\delta}(s) &= \frac{1}{(1+T_r s)s}\left[K_{dr} + K_{dv}\frac{K_{vr}}{1+T_v s}\right] \triangleq \frac{K_1\,(1+T_3 s)}{(1+T_1 s)(1+T_2 s)s} \\ \frac{\phi}{\delta}(s) &= \frac{\omega_n^2}{s^2+2\zeta\omega_n\, s+\omega_n^2}\left[K_{dp} + K_{dv}\frac{K_{vp}}{1+T_v s}\right] \triangleq \frac{\omega_n^2\, K_2\,(1+T_4 s)}{(s^2+2\zeta\omega_n\, s+\omega_n^2)(1+T_2 s)} \end{aligned}$$

where

$$\begin{aligned} K_1 &= K_{dv}K_{vr} + K_{dr}; \qquad T_1 = T_r; \qquad T_3 = K_{dr}T_v/K_1 \\ K_2 &= K_{dv}K_{vp} + K_{dp}; \qquad T_2 = T_v; \qquad T_4 = K_{dp}T_v/K_2 \end{aligned}$$

The frequency separation between the roll and the yaw modes is shown in Figure 6.41 where the open-loop frequency response of the rudder to roll and rudder to

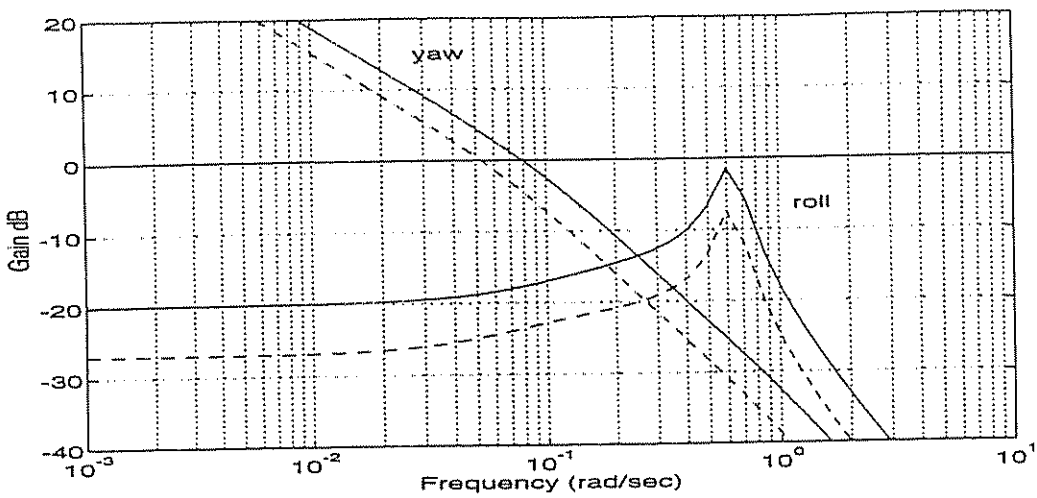

Figure 6.41: Typical frequency separation between roll transfer: ϕ/δ (fast) and yaw transfer: ψ/δ (slow) for the model in Example 6.6. The dotted line is used to denote forward speed $U = 8$ (m/s) while the solid line corresponds to $U = 12$ (m/s).

yaw dynamics is plotted for the ship in Example 6.6. For this particular ship, the figure shows the slowness of the yaw dynamics compared to the roll dynamics. Hence, one input (the rudder) can be used to control two outputs (the heading and roll angle) by designing two servo systems, see Figure 6.42.

It is important to notice that an RRCS as opposed to stabilizing fins cannot be designed to compensate for LF roll motions or a stationary roll angle since this will introduce an off-set in the course controller (due to steady-state couplings between roll and yaw). This suggests that the measured roll angle ϕ_m should be high-pass filtered to reduce the influence of LF roll motions in yaw. Moreover,

$$\phi(s) = \frac{T_c\, s}{1 + T_c\, s}\, \phi_m(s) \tag{6.352}$$

where the cut-off frequency $1/T_c$ should be higher than the bandwidth of the yaw angle controller. In addition to this ψ should be generated by proper wave filtering (low-pass and notch) to avoid the HF yaw motions influencing the roll channel.

6.6.2 Decoupled RRCS Design in Terms of Pole-Placement

We will first show that a decoupled control system design can be used to obtain roll damping. Let the rudder controller be written:

$$\boxed{\delta = \delta_{\text{roll}} + \delta_{\text{yaw}}} \tag{6.353}$$

where δ_{roll} is used to obtain roll damping and δ_{yaw} should maintain the course of the ship. Furthermore we choose:

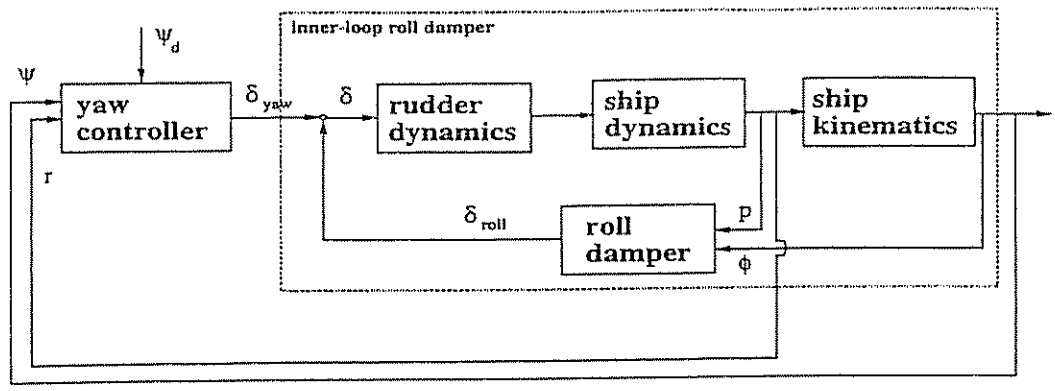

Figure 6.42: Figure showing inner-loop roll controller (fast) and outer-loop yaw controller (slow).

$$\delta_{\text{roll}} = -G_1\, p - G_2\, \phi \tag{6.354}$$

$$\delta_{\text{yaw}} = -G_3\, r - G_4\, (\psi - \psi_d) \tag{6.355}$$

where G_i $(i = 1...4)$ are the regulator gains. Decoupled pole-placement suggests that we should use the decoupled models (assuming $\dot{v}' = v' = 0$):

$$s^2 + 2\zeta_n\, \omega_n\, s + \omega_n^2 = \omega_n^2\, K_{dp}\, \delta_{\text{roll}} \tag{6.356}$$

$$(1 + T_r s)\, s\psi(s) = K_{dr}\, \delta_{\text{yaw}}(s) \tag{6.357}$$

Moreover, to compute the controller gains, let ω_ϕ and ζ_ϕ be the desired natural frequency and damping ratio in roll and ω_ψ and ζ_ψ be the desired natural frequency and damping ratio in yaw. Hence, we can compute G_i $(i = 1...4)$ by requiring that:

$$2\zeta_n\, \omega_n + \omega_n^2\, K_{dp}\, G_1 \triangleq 2\zeta_\phi\, \omega_\phi \tag{6.358}$$

$$(1 + K_{dp} G_2)\omega_n^2 \triangleq \omega_\phi^2 \tag{6.359}$$

$$\frac{1 + K_{dr}\, G_3}{T_r} \triangleq 2\zeta_\psi\, \omega_\psi \tag{6.360}$$

$$\frac{K_{dr}\, G_4}{T_r} \triangleq \omega_\psi^2 \tag{6.361}$$

Frequency separation suggests that the RRCS should be designed such that (see Exercise 6.6):

$$\underbrace{\omega_\psi \sqrt{1 - 2\,\zeta_\psi^2 + \sqrt{4\,\zeta_\psi^4 - 4\,\zeta_\psi^2 + 2}}}_{\text{bandwidth yaw}} < \frac{1}{T_c} < \underbrace{\omega_\phi \sqrt{1 - 2\,\zeta_\phi^2 + \sqrt{4\,\zeta_\phi^4 - 4\,\zeta_\phi^2 + 2}}}_{\text{bandwidth roll}}$$

For ships having zeros in the right half-plane the bandwidth in roll must be chosen lower than the smallest right half-plane zero. Hence the bandwidth in roll may be quite close to the bandwidth in yaw. This can result in bad performance since frequency separation is necessary. These effects cannot be properly analyzed by applying the simplified model of Van der Klugt (1987) since important coupling terms are neglected in the model. However, the models in Section 5.7 are well suited for this purpose. For instance, the effect of right half-plane zeros (unstable zero dynamics in nonlinear systems) has been analyzed for these models by Fossen and Lauvdal (1994).

Destabilizing effects due to parametric uncertainties and rudder-roll damping autopilot robustness due to sway-yaw-roll couplings are discussed by Christensen (1992), and Blanke and Christensen (1993).

Example 6.6 (Rudder-Roll Control System Design for Naval Vessel)
Consider a naval vessel given by the following set of parameters (page 37 of Van der Klugt 1987):

$$\begin{array}{llllll} T_v = 78/U & K_{dr} = -0.0027\,U & K_{vp} = 0.21\,U \\ T_r = 13/U & K_{dp} = -0.0014\,U^2 & \omega_n = 0.63 \\ K_{vr} = -0.46 & K_{dv} = 0.01\,U & \zeta_n = 0.064 + 0.0038\,U \end{array}$$

where U (m/s) is the forward speed. For this ship we computed the decoupled control law with $\omega_\psi = 0.35$ (rad/s), $\zeta_\psi = 1.0$, $\omega_\phi = 0.7$ (rad/s) and $\zeta_\phi = 0.5$, which resulted in:

$$\delta = -7.91\,r - 9.69\,(\psi - \psi_d) - 17.22\,p - 2.75\,\phi \tag{6.362}$$

The simulation results are shown in Figures 6.43 and 6.44 for $U = 7.8$ (m/s). Oda et al. (1992) define percentage roll reduction as:

$$\textit{Roll reduction}\ (\%) = \frac{AP - RRCS}{AP} \times 100 \tag{6.363}$$

where

$$\begin{array}{ll} AP & = \textit{standard deviation of roll rate, autopilot on, RRCS off} \\ RRCS & = \textit{standard deviation of roll rate, autopilot on, RRCS on} \end{array}$$

The roll reduction was computed to be 66 % and 49 % for $\dot{\delta}_{\max} = 15$ (deg/s) and $\dot{\delta}_{\max} = 5$ (deg/s), respectively. According to Table 6.6, it is reasonable to obtain a roll reduction of 50–75 *% for small high-speed vessels.*
□

6.6.3 Optimal Rudder-Roll Control System Design

A linear optimal controller can be designed by writing the mathematical model shown in Figure 6.40 in state-space form according to:

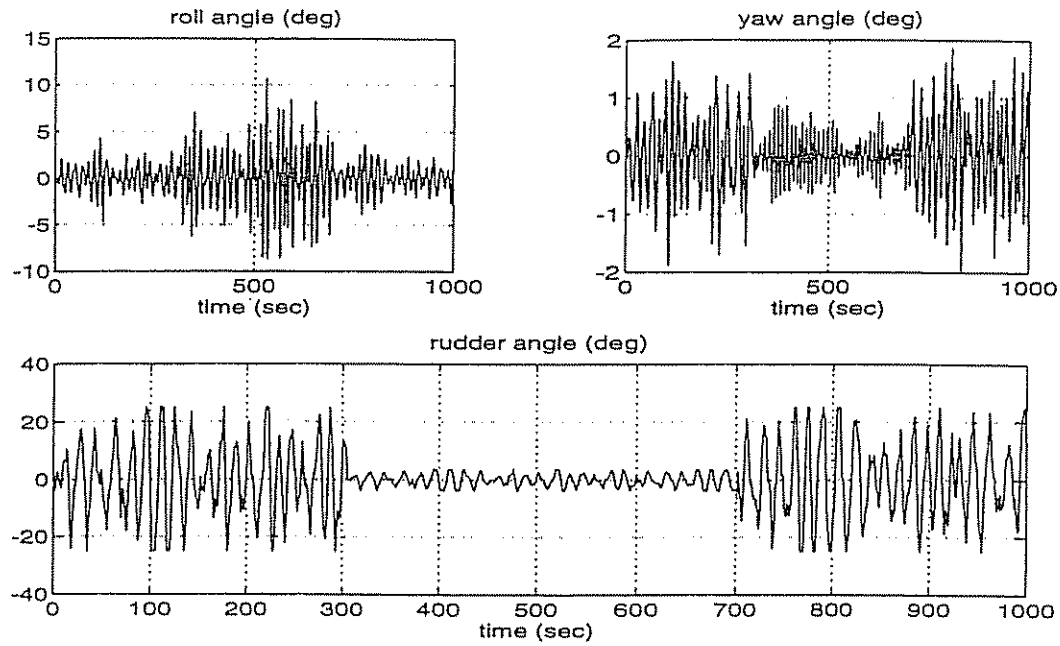

Figure 6.43: Performance of RRCS based on pole placement with $\dot{\delta}_{\max} = 15$ (deg/s). The RRCS is turned off after 300 (sec) and turned on again after 700 (sec).

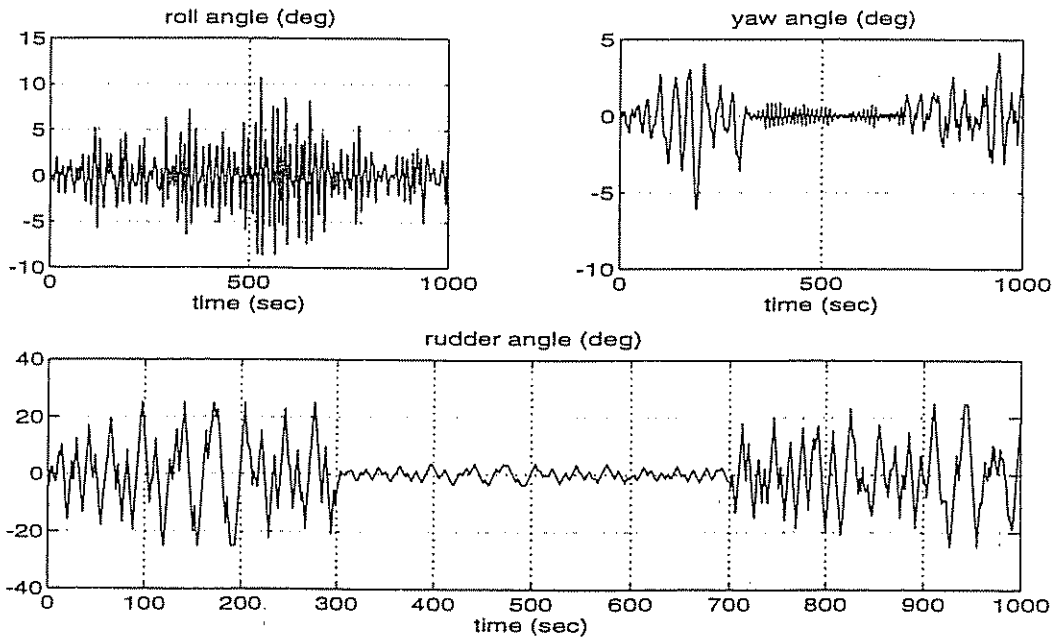

Figure 6.44: Performance of RRCS based on pole placement with $\dot{\delta}_{\max} = 5$ (deg/s). The RRCS is turned off after 300 (sec) and turned on again after 700 (sec).

$$\dot{x} = A\,x + b\,u + E\,w \tag{6.364}$$

where $x = [v', r, \psi, p, \phi]^T$, $u = \delta$ and $w = [w_\phi, w_\psi]^T$ whereas A, b and E are given in (6.351).

The roll angle ϕ and heading angle ψ can be measured by gyros and their derivatives p and r can be measured by rate gyros or be obtained from a state estimator. The sway velocity v' due to the rudder cannot be measured directly. Hence, a state estimator is required to obtain full state feedback in terms of optimal control theory.

Performance Index

Application of optimal control theory implies that we want to formulate the control problem as an optimization problem for maximum performance and reduced fuel consumption. Moreover, the trade-off between accurate steering, roll damping and economical operation can be expressed as:

$$\min\ J = \frac{\lambda}{T}\int_0^T (\tilde{y}^T\,Q\,\tilde{y} + u^2)\,d\tau \tag{6.365}$$

where $Q \geq 0$ is a weighting matrix weighting $\tilde{y} = y - y_d$ against the scalar input u and $\lambda > 0$ is a constant. Moreover, roll damping ($p_d = \phi_d = 0$) and automatic course control ($\psi = \psi_d$) suggest that:

$$y = [\psi, p, \phi]^T; \qquad y_d = [\psi_d, 0, 0]^T \tag{6.366}$$

Defining $y = C\,x$ implies that:

$$C = \begin{bmatrix} 0 & 0 & 1 & 0 & 0 \\ 0 & 0 & 0 & 1 & 0 \\ 0 & 0 & 0 & 0 & 1 \end{bmatrix} \tag{6.367}$$

The solution to (6.365) is (see Appendix D):

$$\boxed{u = g_1^T\,x + g_2^T\,y_d} \tag{6.368}$$

where

$$g_1^T = -\frac{1}{\lambda}b^T R_\infty \tag{6.369}$$

$$g_2^T = -\frac{1}{\lambda}b^T(A + bg_1^T)^{-T}C^T\,Q \tag{6.370}$$

Here R_∞ is the solution of the algebraic Riccati equation:

$$R_\infty A + A^T R_\infty - \frac{1}{\lambda}R_\infty b b^T R_\infty + C^T Q C = 0 \tag{6.371}$$

The Steering Criterion of Van Amerongen et al. (1987)

In the work of Van Amerongen et al. (1987) the optimal criterion to be minimized is written as a sum of two criteria representing the roll and yaw modes, respectively. The proposed criteria are:

$$J_\phi = \frac{1}{T}\int_0^T \left[\phi^2 + (p/\omega_n)^2\right]\, d\tau; \qquad J_\psi = \frac{1}{T}\int_0^T \left[\tilde{\psi}^2/\lambda + \delta^2\right]\, d\tau \tag{6.372}$$

where λ is a positive weighting factor. By using J_ϕ and J_ψ we can formulate a combined performance index according to:

$$\boxed{J = \lambda\,(q_\phi\, J_\phi + J_\psi)} \tag{6.373}$$

where $q_\phi \geq 0$. Alternatively, we can write:

$$J = \frac{\lambda}{T}\int_0^T \left[q_\phi\, \left(\phi^2 + (p/\omega_n)^2\right) + \tilde{\psi}^2/\lambda + \delta^2\right]\, d\tau \tag{6.374}$$

This corresponds to choosing:

$$Q = \mathrm{diag}\left\{1/\lambda,\ q_\phi/\omega_n^2,\ q_\phi\right\} \tag{6.375}$$

in the criterion (6.365).

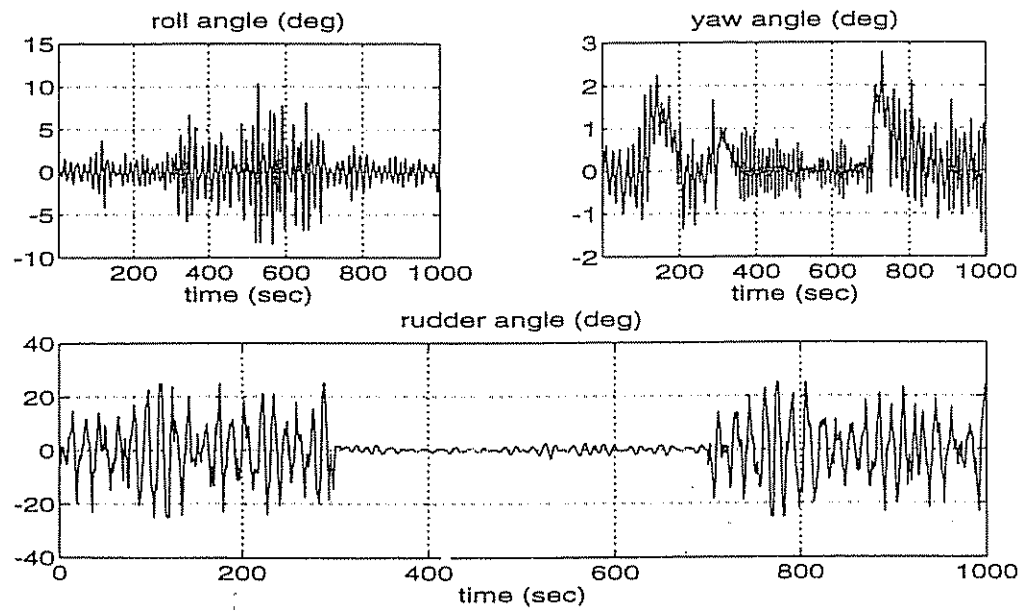

Figure 6.45: Performance of RRCS based on optimal control theory with $\dot{\delta}_{\max} = 15$ (deg/s). The weight q_ϕ is reduced from 500 to 1 in the time interval 300–700 (s).

Example 6.7 (Optimal Rudder-Roll Control System Design)
Again consider the naval vessel of Example 6.6. The optimal control law corresponding to fixed weighting parameters: $\lambda = 1.0$, $\omega_n = 0.63$, $q_\phi = 500$ and $\psi_d = 0$ was computed to be:

$$\delta = [2.80, -0.86, -0.52, -21.52, -4.38]\, x \tag{6.376}$$

For this control law the percentage roll reduction was found to be 68 % with a rudder rate limitation of 15 (deg/s). The performance of the optimal RRCS is shown in Figure 6.45.
□

Adaptation of the Criterion

Adaptation of the above criterion can be obtained by specifying the desired performance of the RRS system as a series of demands. The proposed method is related to the theory of *fuzzy sets*; see Van Nauta Lemke and De-Zhao (1985) where the demands are translated into a rate of change of the weighting parameter q_ϕ according to:

$$\dot{q}_\phi(t) = a \sum_{i=1}^{n} \Delta \dot{q}_i \tag{6.377}$$

Here $a > 0$ is the adaptation gain and Δq_i $(i = 1...n)$ is a rate of change parameter corresponding to demand i.

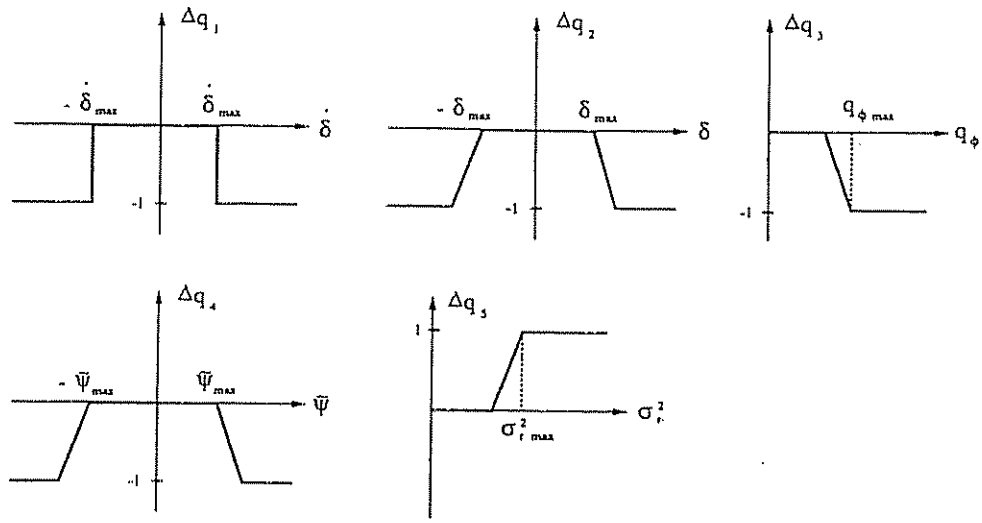

Figure 6.46: Typical controller demands in terms of rate of change of the weighting parameters (Van Amerongen et al. 1987).

Some typical demands are shown in Figure 6.46 where limitations on the rudder are described by $\delta_{\max}$ and $\dot{\delta}_{\max}$, $q_{\phi\ \max}$ represents the maximum allowed value of

q_ϕ, $\bar{\psi}_{\max}$ is the maximum allowed heading angle error and $\sigma^2_{r\ \max}$ is the maximum allowed variance in roll rate. These demands ensure that the controller gains will be adjusted automatically during operation. Hence, two of the elements in Q will be time-varying, that is:

$$Q(t) = \text{diag}\left\{ 1/\lambda,\ q_\phi(t)/\omega_n^2,\ q_\phi(t) \right\} \tag{6.378}$$

LQ optimal control of time-varying systems is discussed in Appendix D.1.1.

Operability Limiting Criteria in Roll

Operability for ships can be defined in terms of roll RMS values. For merchant and naval ships the RMS roll angle limits are 6 and 4 degrees, respectively.

Operability limiting criteria with regard to accelerations and roll angle for the effectiveness of the crew are given in Table 6.4.

Table 6.4: Criteria with regard to vertical and lateral accelerations, and roll angle (Faltinsen 1990).

Root Mean Square (RMS) Criterion			
Vertical acceleration	Lateral acceleration	Roll	Description
0.20 g	0.10 g	6.0 deg	Light manual work
0.15 g	0.07 g	4.0 deg	Heavy manual work
0.10 g	0.05 g	3.0 deg	Intellectual work
0.05 g	0.04 g	2.5 deg	Transit passengers
0.02 g	0.03 g	2.0 deg	Cruise liner

6.7 Dynamic Ship Positioning Systems

Dynamic positioning (DP) systems have been commercially available for drilling vessels, platforms and support vessels since the 1960s. The Norwegian classification society, DnV (1990), uses the following definition for a dynamically positioned vessel:

Definition 6.3 (Dynamically Positioned Vessel)
A dynamically positioned vessel is a vessel which maintains its position (fixed location or predetermined track) exclusively by means of active thrusters.
□

Early DP systems had designs that used conventional controllers in cascade with low-pass and/or notch filters where the control problem was solved by using

PID-controllers for motion in surge, sway and yaw under the assumption that the interactions were negligible (Sargent and Cowgill 1976 and Morgan 1978). The disadvantage of this approach is that the integral action of the controller must be quite slow due to the couplings. Besides this, it is important that high-frequency (HF) wave components in the position and heading measurements are suppressed, otherwise, excessive thruster modulation is required to compensate for the HF components of the motion. This will increase wear and tear on the thrusters and damage the thruster actuator over time. One way to solve this problem is to apply notch filtering to the motion measurements. Unfortunately, this method introduces additional phase lag into the control loops.

In 1975–1977, more advanced control techniques were applied to overcome these problems. A new model-based control concept utilizing stochastic optimal control theory and Kalman filtering techniques was employed with the DP problem by Balchen et al. (1976). The Kalman filter is used to separate the LF and HF motion components such that only feedback from the LF motion components is used. Later extensions and modifications of this work have been proposed by Balchen et al. (1980a, 1980b), Grimble et al. (1980a, 1980b), Fung and Grimble (1983), Sælid et al. (1983), Sagatun et al. (1994a), Fossen, Sagatun and Sørensen (1995) and Sørensen, Sagatun and Fossen (1995).

Today several DP systems are commercially available. The world-wide Norwegian company SIMRAD ALBATROSS has marketed a DP system under the name ALBATROSS since 1976. This system is based on the work of Balchen and co-authors and has been designed in cooperation with SINTEF (the Foundation for Scientific and Industrial Research at the Norwegian Institute of Technology). An overall description of the ALBATROSS system and the ship positioning problem is found in Balchen (1991), where the behavior of the vessel is modelled as a combination of LF ship motions and HF oscillation due to 1st-order wave disturbances, see Figure 6.47.

The LF model in Figure 6.47 is designed to represent the slow motion caused by wind, thrust, currents and 2nd-order wave disturbances. Oscillatoric movements due to waves are included in the HF model. The multivariable control system consists of the Kalman filter gains $\boldsymbol{K}_c$ (current model), $\boldsymbol{K}_L$ (low-frequency model) and $\boldsymbol{K}_H$ (high-frequency model). Feedback is obtained through the gain matrices $\boldsymbol{G}_c$ (current model) and $\boldsymbol{G}_L$ (low-frequency model) representing proportional and derivative action of the controller. Since the wind speed and direction can be measured fairly precisely, a feedforward gain matrix $\boldsymbol{G}_w$ can be included for wind compensation. Hence, the resulting control law is written as:

$$\boldsymbol{\tau} = \boldsymbol{G}_L \left(\boldsymbol{x}_d - \hat{\boldsymbol{x}}_L \right) - \boldsymbol{G}_c \, \hat{\boldsymbol{x}}_c - \boldsymbol{G}_w \, \boldsymbol{y}_w \tag{6.379}$$

The different matrices in this approach are computed by applying stochastic optimal control theory. Notice that feedback from the HF motions is omitted since we do not want to use HF signals in the feedback loop to counteract the 1st-order wave disturbances. In fact this is not possible for a ship equipped with

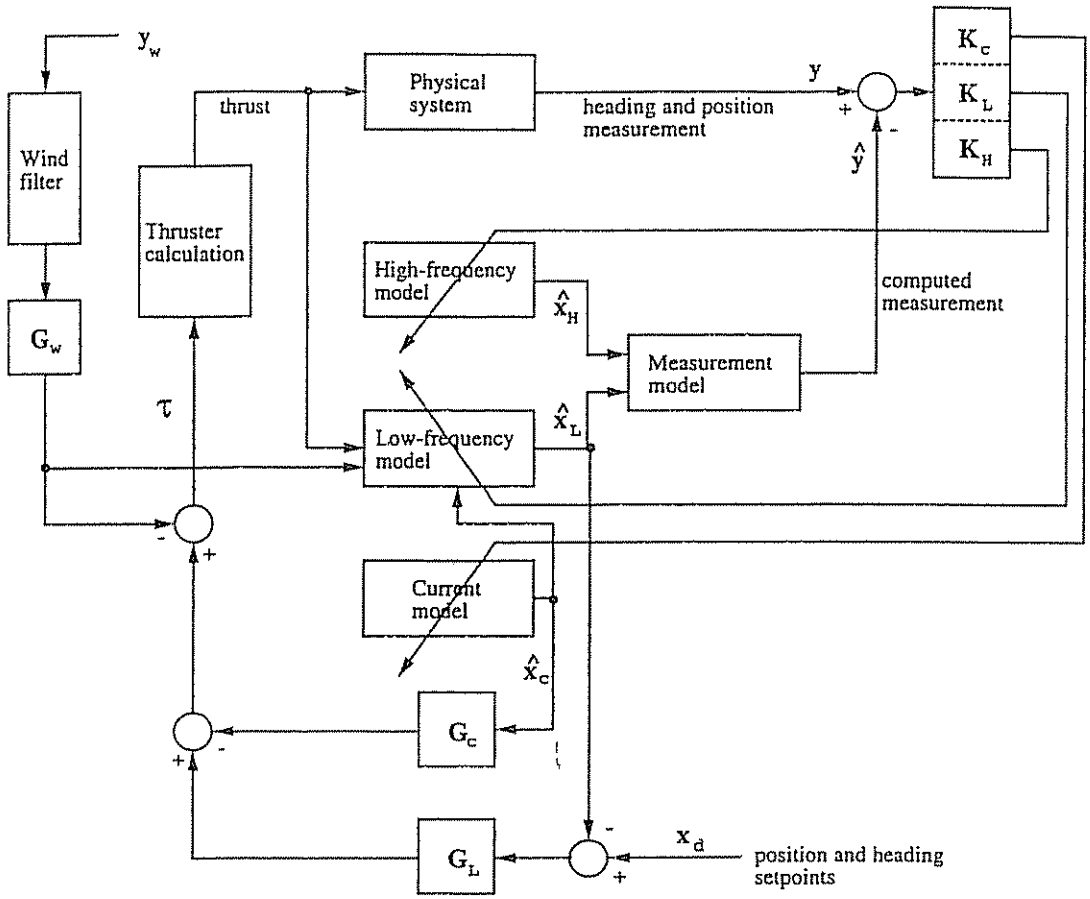

Figure 6.47: DP control system structure (Balchen 1991).

standard thruster devices (the mass of the ship is relatively large implying that the time constants in surge, sway and yaw are large).

Recently, a model-based DP system has been developed by ABB Industry in Oslo (Sagatun, Sørensen and Fossen 1994b). The theory presented in the next sections on vessel modeling, wave filtering and optimal control is based on experience with the ABB DP system. Experimental and theoretical results from this work are reported in Sagatun et al. (1994a), Fossen et al. (1995) and Sørensen et al. (1995).

6.7.1 Mathematical Modeling

In this section we will describe a mathematical model intended for DP control system design and state estimation.

DP Thruster Model

Most DP ships use thrusters to maintain their position and heading. The thruster force of a pitch-controlled propeller can be approximated by:

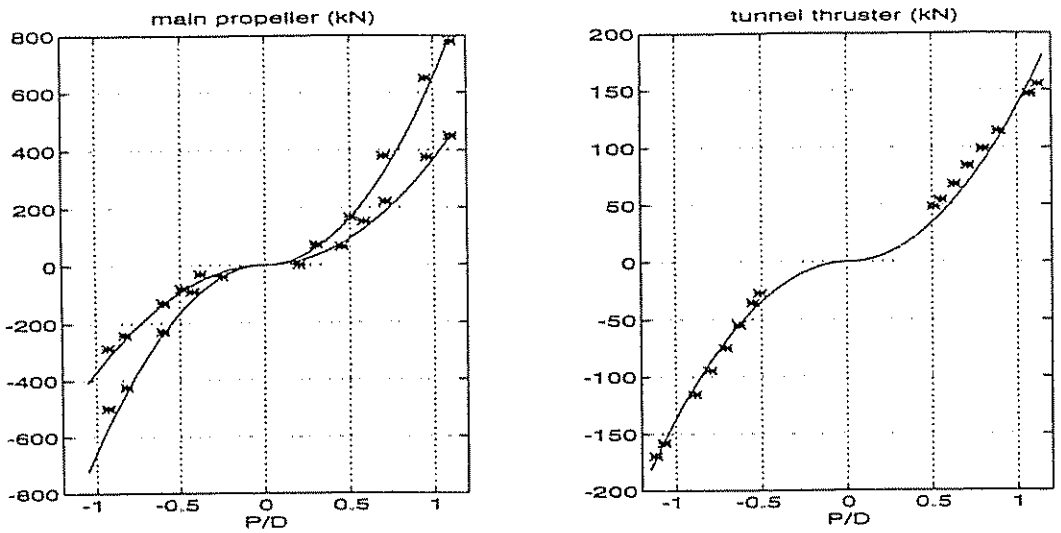

Figure 6.48: Experimentally measured thrust (asterisks) and thruster model approximation (6.380) versus $p = P/D$. Left plot: $F(122, p) = 370p|p|$ and $F(160, p) = 655p|p|$. Right plot: $F(236, p) = 137p|p|$. Propeller revolution is in rpm; reproduced by permission of ABB Industry, Oslo.

$$F(n, p) = K(n)\,|p - p_0|\,(p - p_0) \tag{6.380}$$

where the force coefficient $K(n)$ is assumed to be constant for constant propeller revolution n, P is the "traveled distance per revolution", D is the propeller diameter and $p = P/D$ is the pitch ratio. p_0 is pitch ratio off-set defined such that $p = p_0$ yields zero thrust, that is $F(n, p_0) = 0$.

The commanded thruster forces and moment $\tau \in \mathbb{R}^3$ (surge, sway and yaw) for the supply vessel in Figure 6.49 can be written:

$$\tau = \boldsymbol{T}\,\boldsymbol{K}\,\boldsymbol{u} \tag{6.381}$$

where $\boldsymbol{u} \in \mathbb{R}^r$ is a control variable defined as:

$$\boldsymbol{u} = [|p_1 - p_{10}|(p_1 - p_{10}),\ |p_2 - p_{20}|(p_2 - p_{20}),\ ...,\ |p_r - p_{r0}|(p_r - p_{r0})]^T \tag{6.382}$$

where p_{i0} $(i = 1...r)$ are the pitch ratio off-sets. $\boldsymbol{K}$ is a diagonal matrix of thruster force coefficients defined as:

$$\boldsymbol{K} = \text{diag}\{K_1(n_1),\ K_2(n_2),\ ...,\ K_r(n_r)\} \tag{6.383}$$

where n_i $(i = 1....r)$ is the propeller revolution of propeller number i. The thruster forces $K_i(n_i)u_i$ are distributed to the surge, sway and yaw modes by a $3 \times r$ thruster configuration matrix $\boldsymbol{T}$.

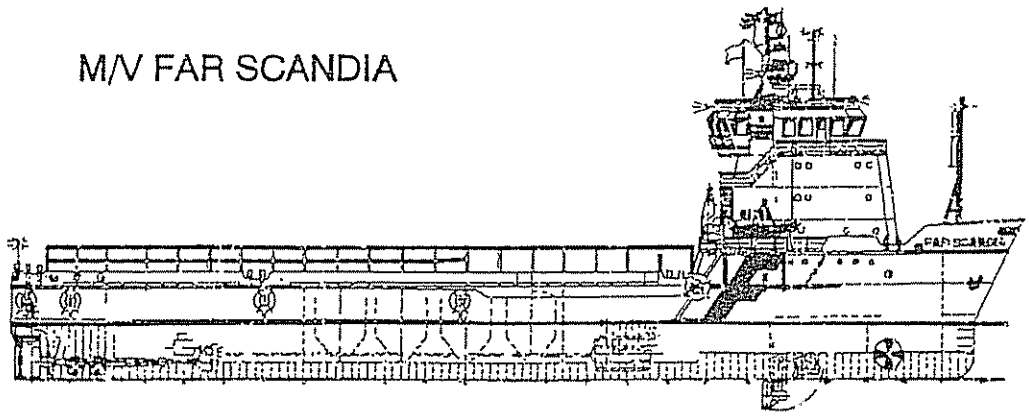

Figure 6.49: Supply vessel, reproduced by permission of ABB Industry, Oslo.

Thruster Configuration Matrix

The ship in Figure 6.49 is equipped with two main propellers, three tunnel thrusters and one azimuth thruster which can be rotated to an arbitrary angle α. If we assign the control variables according to (assuming that $\alpha = \text{constant}$):

$u_1 =$	port main propeller	$u_4 =$	aft tunnel thruster II
$u_2 =$	starboard main propeller	$u_5 =$	fore tunnel thruster
$u_3 =$	aft tunnel thruster I	$u_6 =$	azimuth thruster

we obtain the following thruster configuration matrix:

$$\boldsymbol{T} = \begin{bmatrix} 1 & 1 & 0 & 0 & 0 & \cos\alpha \\ 0 & 0 & 1 & 1 & 1 & \sin\alpha \\ l_1 & -l_2 & -l_3 & -l_4 & l_5 & l_6 \sin\alpha \end{bmatrix} \tag{6.384}$$

Here l_i $(i = 1...r)$ are the moment arms in yaw. It is also seen that $l_2 = l_1$ (symmetrical location of main propellers). The thrust demands are defined such that positive thruster force/moment results in positive motion according to the vessel parallel axis system.

Notice that uncertainties in the proposed model structure (6.381) only appear in the force coefficient matrix $\boldsymbol{K}$, since $\boldsymbol{T}$ is assumed to be known. This decomposition is highly advantageous since it can be exploited when designing the feedback control system.

Thruster Dynamics

The thruster dynamics can be modelled as:

$$\dot{\tau} = \boldsymbol{A}_{\text{thr}} \left(\tau - \tau_{\text{com}} \right) \tag{6.385}$$

where τ_{com} is the commanded thrust and $\boldsymbol{A}_{\text{thr}} = \text{diag}\{-1/T_1, -1/T_2, -1/T_3\}$ is a diagonal matrix containing the time constants T_i $(i = 1...3)$ in surge, sway and yaw.

Low-Frequency Ship Model

The LF velocities of a dynamically positioned ship can be described by a linear model in surge, sway and yaw. Simulation studies and full-scale experiments show that nonlinear Coriolis and damping can be neglected. This suggests the model:

$$M\,\dot{\nu}_L + D\,(\nu_L - \nu_c) = \tau_L + w_L \tag{6.386}$$

where $\nu_L = [u_L, v_L, r_L]^T$ denotes the LF velocity vector, $\nu_c = [u_c, v_c, r_c]^T$ is a vector of current velocities, τ_L is a vector of control forces and moments and $w_L = [w_u, w_v, w_r]^T$ is a vector of zero-mean Gaussian white noise processes describing unmodelled dynamics and disturbances. Notice that r_c does not represent a physical current velocity, but may be interpreted as the effect of currents in yaw. The current states are useful in the KF since they represent integral effect in the state estimator.

The inertia matrix (including hydrodynamic added mass) is assumed to be positive definite $M = M^T > 0$ for a dynamically positioned ship ($U \approx 0$), whereas $D > 0$ is a strictly positive matrix representing linear hydrodynamic damping. The structure of the matrices is (assuming slender body theory):

$$M = \begin{bmatrix} m - X_{\dot{u}} & 0 & 0 \\ 0 & m - Y_{\dot{v}} & mx_G - Y_{\dot{r}} \\ 0 & mx_G - Y_{\dot{r}} & I_z - N_{\dot{r}} \end{bmatrix} \qquad D = \begin{bmatrix} -X_u & 0 & 0 \\ 0 & -Y_v & -Y_r \\ 0 & -N_v & -N_r \end{bmatrix} \tag{6.387}$$

The nonlinearities in the kinematic equations of motion are usually removed by choosing the earth-fixed coordinate system such that the desired heading $\psi_d = 0$. Hence, we can approximate:

$$\dot{\eta}_L = \nu_L \tag{6.388}$$

where $\eta_L = [x_L, y_L, \psi_L]^T$. This is a good approximation for the DP control model since $\psi_L - \psi_d$ will be small for a dynamically positioned ship. Hence we can write:

$$\dot{x}_L = A_L\,x_L + B_L\,\tau_L + E_L\,w_L \tag{6.389}$$

where $x_L = [x_L, y_L, \psi_L, u_L, v_L, r_L]^T$ and:

$$A_L = \begin{bmatrix} 0 & I \\ 0 & -M^{-1}D \end{bmatrix}; \quad B_L = \begin{bmatrix} 0 \\ M^{-1} \end{bmatrix}; \quad E_L = \begin{bmatrix} 0 \\ M^{-1} \end{bmatrix} \tag{6.390}$$

High-Frequency Wave Model

The HF motion of the vessel is mainly due to 1st-order wave disturbances. The HF model is described by three harmonic oscillators with some damping to improve robustness. Consider the following linear approximation to the HF motion spectrum, see Section 3.2.2:

$$h(s) = \frac{K_w s}{s^2 + 2\,\zeta\,\omega_0\,s + \omega_0^2} \tag{6.391}$$

where the parameter K_w, depends on the sea state, ζ is the relative damping ratio and ω_0 is a design parameter. A high value for ω_0 implies that HF motion components are allowed in the feedback loop and a small value for ω_0 will give the vessel a smooth motion characteristic. The relative damping factor ζ can be chosen rather arbitrarily but is less than 1.0.

The HF model of the vessel in surge, sway and yaw can be described by the following set of differential equations:

$$\begin{aligned}
\dot{\xi}_x &= x_H && (6.392)\\
\dot{x}_H &= -2\,\zeta\,\omega_0\,x_H - \omega_0^2\,\xi_x + w_x && (6.393)\\
\dot{\xi}_y &= y_H && (6.394)\\
\dot{y}_H &= -2\,\zeta\,\omega_0\,y_H - \omega_0^2\,\xi_y + w_y && (6.395)\\
\dot{\xi}_\psi &= \psi_H && (6.396)\\
\dot{\psi}_H &= -2\,\zeta\,\omega_0\,\psi_H - \omega_0^2\,\xi_\psi + w_\psi && (6.397)
\end{aligned}$$

where w_x, w_y and w_ψ are zero-mean Gaussian white noise processes. Notice that the relative damping factor and wave frequency are chosen to be equal in surge, sway and yaw. This is a good approximation for practical operations, see Figure 3.5. The resulting HF wave model is written:

$$\dot{\boldsymbol{x}}_H = \boldsymbol{A}_H\,\boldsymbol{x}_H + \boldsymbol{E}_H\,\boldsymbol{w}_H \tag{6.398}$$

where $\boldsymbol{x}_H = [\xi_x, \xi_y, \xi_\psi, x_H, y_H, \psi_H]^T$, $\boldsymbol{w}_H = [w_x, w_y, w_\psi]^T$, and with obvious choices of $\boldsymbol{A}_H$ and $\boldsymbol{E}_H$.

Low-Frequency Current Model

It is assumed that the current is relatively constant both in direction and magnitude such that the current velocity V_c and direction β_c can be modelled as slowly-varying parameters in the earth-fixed reference. Moreover:

$$\begin{aligned}
\dot{V}_c &= w_{V_c} && (6.399)\\
\dot{\beta}_c &= w_{\beta_c} && (6.400)
\end{aligned}$$

where w_{V_c} and w_{β_c} are zero-mean Gaussian white noise processes. The current velocities in the body-fixed reference frame are obtained through the transformation (see Section 3.4.2):

$$\begin{aligned}
u_c &= V_c\,\cos(\beta_c - \psi_L - \psi_H) && (6.401)\\
v_c &= V_c\,\sin(\beta_c - \psi_L - \psi_H) && (6.402)
\end{aligned}$$

where ψ_L and ψ_H are the LF and HF components of the yaw angle, respectively. In addition to u_c and v_c a rotational current component r_c can be included to describe the motion in yaw. In fact this will improve the performance of the state estimator. The yaw model is written:

$$\dot{r}_c = w_r \tag{6.403}$$

where w_r is a zero-mean Gaussian white noise process. Notice that r_c does not represent any physical current model, but is included to improve the performance of the KF. The resulting model can be written in state-space form according to:

$$\dot{\boldsymbol{x}}_c = \boldsymbol{E}_c \, \boldsymbol{w}_c \tag{6.404}$$

where $\boldsymbol{x}_c = [V_c, \beta_c, r_c]^T$, $\boldsymbol{w}_c = [w_{V_c}, w_{\beta_c}, w_r]^T$ and $\boldsymbol{E}_c = \boldsymbol{I}$.

Low-Frequency Wind Model

LF wind speed V_w and direction β_w are modelled as slowly-varying parameters:

$$\dot{V}_w = w_{V_w} \tag{6.405}$$
$$\dot{\beta}_w = w_{\beta_w} \tag{6.406}$$

where w_{V_w} and w_{β_w} are zero-mean Gaussian white noise processes. We can express this model in state-space form according to:

$$\dot{\boldsymbol{x}}_w = \boldsymbol{E}_w \, \boldsymbol{w}_w \tag{6.407}$$

where $\boldsymbol{x}_w = [V_w, \beta_w]^T$, $\boldsymbol{w}_w = [w_{V_w}, w_{\beta_w}]^T$ and $\boldsymbol{E}_w = \boldsymbol{I}$. The wind forces and moments are given by Equations (3.89) to (3.91):

$$\boldsymbol{\tau}_w = \begin{bmatrix} 0.5 \, \rho_w \, C_X(\gamma_R) \, V_R^2 \, A_T \\ 0.5 \, \rho_w \, C_Y(\gamma_R) \, V_R^2 \, A_L \\ 0.5 \, \rho_w \, C_N(\gamma_R) \, V_R^2 \, A_L \, L \end{bmatrix} \tag{6.408}$$

where C_X, C_Y and C_N are wind drag and moment coefficients, ρ_w is the density of air, A_T and A_L are the transverse and lateral projected area and L is the length of the ship. The wind speed V_R and direction γ_R are computed as (assuming that the wind speed is much larger than the vessel speed U):

$$V_R = V_w; \qquad \gamma_R = \beta_w - \psi_L - \psi_H \tag{6.409}$$

6.7.2 Optimal State Estimation (Kalman Filtering)

Before designing the DP control system we need to compute noise free estimates of the states. This is usually done by applying a Kalman filter. The estimated states are denoted $\hat{\boldsymbol{x}}_L$, $\hat{\boldsymbol{x}}_H$, $\hat{\boldsymbol{x}}_c$, $\hat{\boldsymbol{x}}_w$ and $\hat{\boldsymbol{\tau}}$.

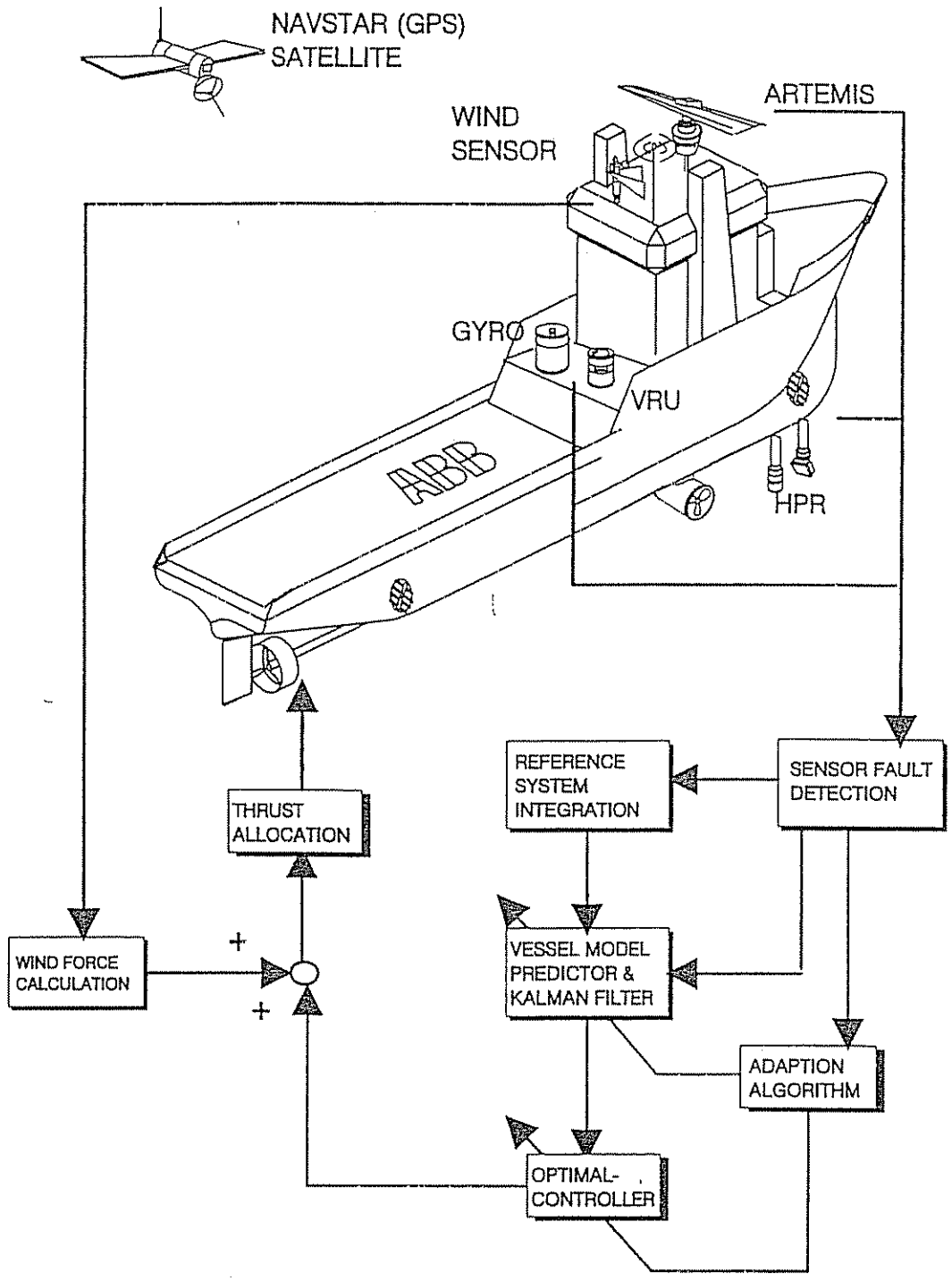

Figure 6.50: Block diagram of DP system, reproduced by permission of ABB Industry, Oslo.

Measurement Model

Position measurements are usually obtained from a satellite system, a hydro-acoustic reference system, a taut wire system or a radio navigation system. Heading is usually measured by a gyro compass. In addition to this, wind speed and direction measurements are necessary. For simplicity we will assume that only one position measurement system is active. Hence, the following set of measurement equations is obtained:

$$\begin{aligned} z_1 &= x_L + x_H + v_1 && \text{(surge position)} \\ z_2 &= y_L + y_H + v_2 && \text{(sway position)} \\ z_3 &= \psi_L + \psi_H + v_3 && \text{(yaw angle)} \\ z_4 &= V_w + v_4 && \text{(wind speed)} \\ z_5 &= \beta_w - \psi_L - \psi_H + v_5 && \text{(wind direction)} \end{aligned} \tag{6.410}$$

where the measurement noise v_i $(i = 1...5)$ is modelled as zero-mean Gaussian white noise processes. Consequently, the mathematical model of the ship and the environmental disturbances can be described by the following state-space model:

$$\dot{\boldsymbol{x}} = \boldsymbol{A}\,\boldsymbol{x} + \boldsymbol{B}\,\boldsymbol{u} + \boldsymbol{E}\,\boldsymbol{w} \tag{6.411}$$

$$\boldsymbol{z} = \boldsymbol{H}\,\boldsymbol{x} + \boldsymbol{v} \tag{6.412}$$

where $\boldsymbol{x} = [\boldsymbol{x}_L^T, \boldsymbol{x}_H^T, \boldsymbol{x}_c^T, \boldsymbol{x}_w^T, \boldsymbol{\tau}^T]^T$ is the state vector, $\boldsymbol{u} = \boldsymbol{\tau}_L + \boldsymbol{\tau}_w$ is the input vector, $\boldsymbol{z} = [z_1, z_2, z_3, z_4, z_5]^T$, $\boldsymbol{v} = [v_1, v_2, v_3, v_4, v_5]^T$ and $\boldsymbol{A}$, $\boldsymbol{B}$ and $\boldsymbol{E}$ are given by the mathematical model above. For this particular sensor configuration $\boldsymbol{H}$ will be a constant matrix of 0 and 1 elements.

The sensor and navigation system and thus the matrix $\boldsymbol{H}$ must satisfy the *Observability Condition*, see Definition 6.1, Section 6.1.4. Since this condition is satisfied for the DP model we can use a Kalman filter to compute noise-free estimates of $\boldsymbol{x}$.

Kalman Filter Algorithm

The ship, wave, current and wind subsystems can be written as a discrete-time state-space model:

$$\boldsymbol{x}(k+1) = \boldsymbol{\Phi}(k)\,\boldsymbol{x}(k) + \boldsymbol{\Delta}\,\boldsymbol{u}(k) + \boldsymbol{\Gamma}\,\boldsymbol{w}(k) \tag{6.413}$$

where $\boldsymbol{w}(k) \sim N(0, \boldsymbol{Q}(k))$, and $\boldsymbol{\Phi} = \boldsymbol{I} + h\,\boldsymbol{A}$, $\boldsymbol{\Delta} = h\boldsymbol{B}$ and $\boldsymbol{\Gamma} = h\boldsymbol{E}$ are obtained by using Euler integration with sampling time h. The discrete-time measurement equation is given by:

$$\boldsymbol{z}(k) = \boldsymbol{H}(k)\,\boldsymbol{x}(k) + \boldsymbol{v}(k) \tag{6.414}$$

where $\boldsymbol{v}(k) \sim N(0, \boldsymbol{R}(k))$. Hence, we can compute $\hat{\boldsymbol{x}}(k)$ by applying the discrete-time optimal state estimator in Table 6.2, Section 6.1.4. The algorithm is:

(1) $\overline{x}(0) = x_0,\ \overline{X}(0) = E[(x(0) - \hat{x}(0))(x(0) - \hat{x}(0))^T] = X_0$

(2) $K(k) = \overline{X}(k)H^T(k)\ [H(k)\overline{X}(k)H^T(k) + R(k)]^{-1}$

(3) $\hat{x}(k) = \overline{x}(k) + K(k)\ [z(k) - H(k)\,\overline{x}(k)]$

(4) $\hat{X}(k) = [I - K(k)H(k)]\ \overline{X}(k)\ [I - K(k)H(k)]^T + K(k)\ R(k)\ K^T(k)$

(5) $\overline{x}(k+1) = \Phi(k)\,\hat{x}(k) + \Delta(k)u(k)$

(6) $\overline{X}(k+1) = \Phi(k)\ \hat{X}(k)\,\Phi^T(k) + \Gamma(k)\,Q(k)\,\Gamma^T(k)$

(7) $k = k+1$, go to (2)

Typical performance of the Kalman filter algorithm is shown in Figure 6.51.

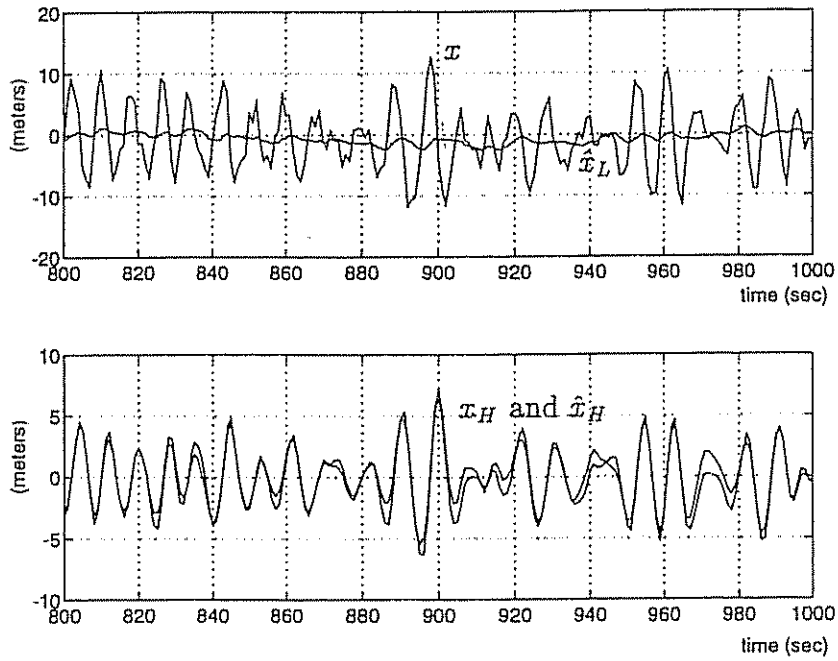

Figure 6.51: Simulated performance of the Kalman filter algorithm. Upper plot shows measured x-position and LF estimate $\hat{x}_L$. Lower plot shows actual x_H and estimated $\hat{x}_H$ (HF positions).

6.7.3 Control System Design

Optimal filtering of all state variables in terms of an LF and HF model implies that noise-free estimates of the LF ship motion are available for control design.

The HF estimates (1st-order wave induced motion) are not used for feedback since this will cause wear and tear on the thruster actuators. This is usually referred to as *wave filtering* in the ship control literature. However, wave drift (2nd-order wave-induced motion) and LF current disturbances should be compensated for by including integral action in the control law. In addition wind measurements will be used for feedforward control.

Linear Quadratic Optimal Feedback Control with Wind Feedforward

We will design an optimal control law with LF wind feedforward. Other LF disturbances are not included in the control model since they can be compensated for by including integral action. Consider the LQ control model:

$$\dot{x}_L = A_L x_L + B_L (\tau - \tau_w) \tag{6.415}$$
$$\dot{\tau} = A_{\text{thr}}(\tau - \tau_{\text{com}}) \tag{6.416}$$

where we have assumed that the commanded input τ_{com} can be divided into two parts; (1) optimal feedback τ_{LQ} and (2) LF wind feedforward, that is:

$$\boxed{\tau_{\text{com}} = \tau_{LQ} + \tau_w} \tag{6.417}$$

This representation assumes that $\dot{\tau}_w = 0$ (slowly-varying wind forces and moment) and that wind disturbances can be perfectly compensated for by applying Formula (6.408) for wind feedforward τ_w. Hence we can rewrite (6.415) and (6.416) according to:

$$\dot{x}_L = A_L x_L + B_L \tau_L \tag{6.418}$$
$$\dot{\tau}_L = A_{\text{thr}} (\tau_L - \tau_{LQ}) \tag{6.419}$$

where $\tau_L = \tau - \tau_w$, or equivalently:

$$\dot{x} = A x + B \tau_{LQ} \tag{6.420}$$

where $x = [x_L^T, \tau_L^T]^T$ and:

$$A = \begin{bmatrix} A_L & B_L \\ 0 & A_{\text{thr}} \end{bmatrix}; \qquad B = \begin{bmatrix} 0 \\ -A_{\text{thr}} \end{bmatrix} \tag{6.421}$$

The LQ control objective is to obtain $x = 0$. Hence, we can compute τ_{LQ} by minimizing the performance index:

$$\min J = \frac{1}{2} \int_0^T (x^T Q x + \tau_{LQ}^T P \tau_{LQ})\, d\tau \tag{6.422}$$

where $P > 0$ and $Q \geq 0$ are two weighting matrices. The optimal control law minimizing (6.422) is given by (see Appendix D):

$$\tau_{LQ} = G\,x \tag{6.423}$$

where the optimal feedback gain matrix is computed as:

$$G = -P^{-1}B^T R_\infty \tag{6.424}$$

Here R_∞ is the solution of the algebraic Riccati equation (ARE):

$$R_\infty A + A^T R_\infty - R_\infty B P^{-1} B^T R_\infty + Q = 0 \tag{6.425}$$

Integral Action

In order to obtain zero steady-state errors in surge, sway and yaw we must include integral action in the control law. Integral action can be included by using state augmentation. Let us define a new state variable $z = \int_0^t y(\tau)\,d\tau$, that is:

$$\dot{z} = y \tag{6.426}$$

where y is a subspace of x defined according to:

$$y = C\,x \tag{6.427}$$

Integral action for the state variables x_L, y_L and ψ_L are obtained by defining:

$$C = \begin{bmatrix} 1 & 0 & 0 & 0 & 0 & 0 & 0 & 0 & 0 \\ 0 & 1 & 0 & 0 & 0 & 0 & 0 & 0 & 0 \\ 0 & 0 & 1 & 0 & 0 & 0 & 0 & 0 & 0 \end{bmatrix} \tag{6.428}$$

Hence we can define an augmented model with state $\bar{x} = [x^T, z^T]^T$. The augmented state-space model is written:

$$\dot{\bar{x}} = \bar{A}\,\bar{x} + \bar{B}\,\tau_{LQ} \tag{6.429}$$

where

$$\bar{A} = \begin{bmatrix} A & 0 \\ C & 0 \end{bmatrix}; \qquad \bar{B} = \begin{bmatrix} B \\ 0 \end{bmatrix} \tag{6.430}$$

The performance index for the augmented model is chosen as:

$$\begin{aligned} \min J &= \frac{1}{2}\int_0^T (x^T Q x + z^T Q_I z + \tau_{LQ}^T P \tau_{LQ})\,d\tau \\ &= \frac{1}{2}\int_0^T (\bar{x}^T \bar{Q} \bar{x} + \tau_{LQ}^T P \tau_{LQ})\,d\tau \end{aligned} \tag{6.431}$$

where $P > 0$ and:

$$\bar{Q} = \begin{bmatrix} Q & 0 \\ 0 & Q_I \end{bmatrix} \geq 0 \tag{6.432}$$

The matrix Q_I can be used to specify the integral times for surge, sway and yaw. The optimal control law minimizing this performance index is:

$$\tau_{LQ} = \tilde{G}\,\tilde{x} = \tilde{G}_1\,x + \tilde{G}_2 \int_0^t y(\tau)\,d\tau \tag{6.433}$$

where $\tilde{G} = [\tilde{G}_1,\ \tilde{G}_2]$ and:

$$\tilde{G} = -P^{-1}\tilde{B}^T\tilde{R}_\infty \tag{6.434}$$

Here $\tilde{R}_\infty$ is the solution of the algebraic Riccati equation (ARE):

$$\tilde{R}_\infty\tilde{A} + \tilde{A}^T\tilde{R}_\infty - \tilde{R}_\infty\tilde{B}P^{-1}\tilde{B}^T\tilde{R}_\infty + \tilde{Q} = 0 \tag{6.435}$$

Typical performance of the optimal DP control system is shown in Figure 6.52.

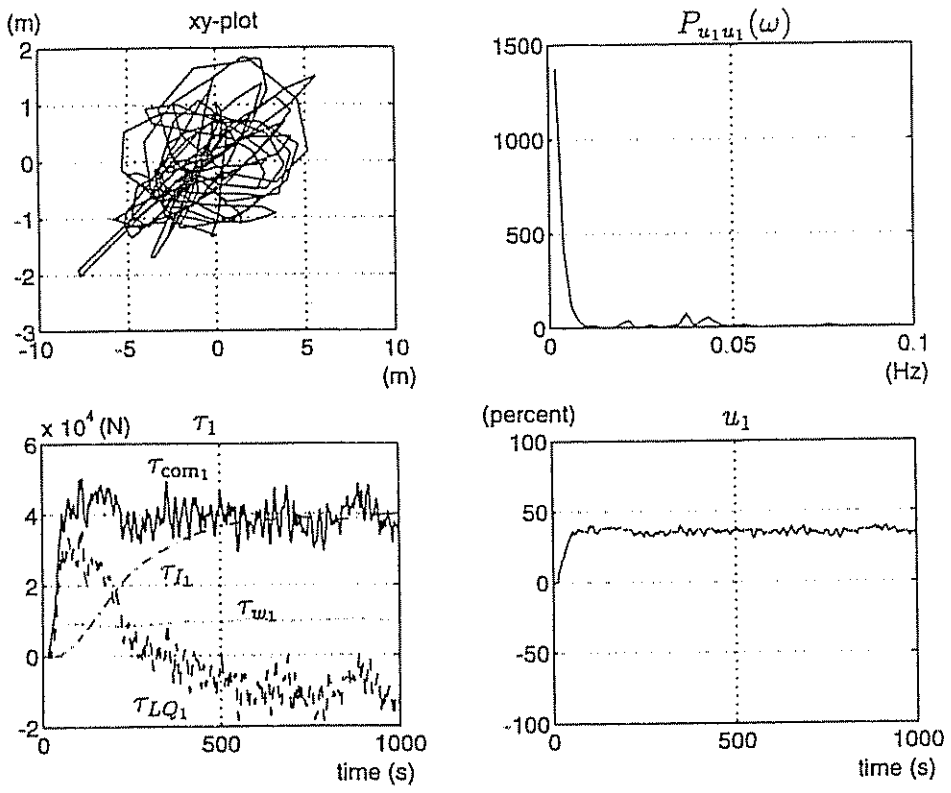

Figure 6.52: Simulated performance of the optimal control system. *Upper left:* xy-plot, *upper right:* power spectrum of main propeller u_1, *lower left:* commanded thrust $\tau_{com_1} = \tau_{LQ_1} + \tau_{I_1} + \tau_{w_1}$ in surge where τ_{LQ_1} is the optimal feedback component, τ_{I_1} represents integral effect and τ_{w_1} is the wind feedforward component, and *lower right:* time-series of pitch controlled propeller u_1 ($\pm 100\%$).

Thrust Allocation in Dynamic Positioning

Thrust allocation involves computing the thruster inputs $u_i = |p_i - p_{i0}|(p_i - p_{i0})$ $(i = 1...r)$ in an optimal manner such that (6.381) is satisfied. Moreover, we must solve:

$$\tau_{\text{com}} = T\,K\,u \tag{6.436}$$

for the optimal control input u. This can be done by minimizing the thruster force vector Ku according to a performance index:

$$\min J = \frac{1}{2}(Ku)^T W(Ku) \tag{6.437}$$

where $W = W^T > 0$ is a positive definite weighting matrix usually chosen as a diagonal matrix. W should be selected so that using the tunnel and azimuth thrusters is less expensive (small K_i-value) than using the main propellers (large K_i-value). The solution is (see Section 4.1.1):

$$K\,u = T^{\dagger}\,\tau_{\text{com}}; \qquad T^{\dagger} = W^{-1}T^T(TW^{-1}T^T)^{-1} \tag{6.438}$$

which implies that:

$$u = K^{-1}\,T^{\dagger}\,(\tau_{LQ} + \tau_w) \tag{6.439}$$

This solution can be improved by defining a set of constraints:

$$-\,a_i \leq K_i\,u_i \leq b_i \qquad (i = 1...r) \tag{6.440}$$

where $a_i > 0$ and $b_i > 0$. This constraint constitutes the lower and upper limits of thruster number i. Hence minimization of (6.437) subject to (6.436) and (6.440) yields a solution that handles thruster saturation. The disadvantage of course, is that a quadratic programming problem must be solved on-line; see Lindfors (1993) for details. Another useful reference discussing optimal thrust allocation in DP is Jenssen (1980).

6.8 Identification of Ship Dynamics

Prediction of ship motion, navigation, maneuverability and model-based control system design require that the hydrodynamic derivatives or the parameters of the model are known with satisfactory accuracy. This section discusses the problem of determining the ship parameters by means of system identification (SI) techniques.

As the subject of SI techniques applied to ship control is an extensive field of research, we will restrict our discussion to the following standard methods for parameter estimation:

- Indirect Model Reference Adaptive System
- Continuous Least-Squares Estimation
- Recursive Least-Squares Estimation
- Recursive Maximum Likelihood Estimation
- State Augmented Kalman Filter for Parameter Estimation

Before we discuss the different methods, there is a brief discussion about parameter identifiability. The interested reader it is recommended to consult Söderström and Stoica (1989) for a more detailed theoretical discussion on SI.

6.8.1 Parameter Identifiability

The problem of identifiability in linear systems can most easily be investigated by considering an *input–output* model. Roughly speaking, the number of identifiable parameters in a parametric model (equations of motion, state-space, transfer function etc.) is given by the number of parameters which can be determined *uniquely* for the system input–output model. We will consider the following three ship model representations proposed by Åström and Källström (1976) to illustrate the concept of *parameter identifiability*:

Equations of Motion (13 Parameters)

We recall from Section 5.3.1 that the ship steering equations of motion can be written:

$$M\dot{\nu} + N(u_0)\,\nu = b\,\delta_R \tag{6.441}$$

This model can be written in component form as:

$$\begin{bmatrix} m - Y_{\dot{v}} & mx_G - Y_{\dot{r}} & 0 \\ mx_G - N_{\dot{v}} & I_z - N_{\dot{r}} & 0 \\ 0 & 0 & 1 \end{bmatrix} \begin{bmatrix} \dot{v} \\ \dot{r} \\ \dot{\psi} \end{bmatrix} + \begin{bmatrix} -Y_v & mu_0 - Y_r & 0 \\ -N_v & mx_G u_0 - N_r & 0 \\ 0 & 1 & 0 \end{bmatrix} \begin{bmatrix} v \\ r \\ \psi \end{bmatrix} = \begin{bmatrix} Y_\delta \\ N_\delta \\ 0 \end{bmatrix} \delta_{\mathrm{R}} \tag{6.442}$$

This model representation has three unknown parameters m, x_G and I_z, and 10 unknown hydrodynamic derivatives $Y_{\dot{v}}, Y_{\dot{r}}, Y_v, Y_r, Y_\delta, N_{\dot{v}}, N_{\dot{r}}, N_v, N_r$ and N_δ. An alternative representation could be to use the matrix elements $\bar{m}_{ij}$, $\bar{n}_{ij}$ and b_i, which reduces the number of parameters to $4 + 4 + 2 = 10$.

State-Space Model (6 Parameters)

The equations of motion can be transformed to state-space form by:

$$\dot{x} = A\,x + b_1\,u \tag{6.443}$$

where $A = -M^{-1}N$ and $b_1 = M^{-1}b$. Hence the number of parameters is reduced to 6, that is:

$$\begin{bmatrix} \dot{v} \\ \dot{r} \\ \dot{\psi} \end{bmatrix} = \begin{bmatrix} a_{11} & a_{12} & 0 \\ a_{21} & a_{22} & 0 \\ 0 & 1 & 0 \end{bmatrix} \begin{bmatrix} v \\ r \\ \psi \end{bmatrix} + \begin{bmatrix} b_{11} \\ b_{21} \\ 0 \end{bmatrix} \delta \tag{6.444}$$

Transfer Function Models (4 Parameters Each Transfer Function)

The minimum parameterization is obtained by writing the state model in input–output form. Moreover,

$$\frac{\psi}{\delta}(s) = \frac{K(1+T_3 s)}{s(1+T_1 s)(1+T_2 s)} = \frac{b_1 s + b_2}{s(s^2 + a_1 s + a_2)} \tag{6.445}$$

$$\frac{v}{\delta}(s) = \frac{K_v(1+T_v s)}{(1+T_1 s)(1+T_2 s)} = \frac{c_1 s + c_2}{s^2 + a_1 s + a_2} \tag{6.446}$$

with cross-coupling:

$$v(s) = \frac{K_v\,(1+T_v s)}{K\,(1+T_3 s)}\,r(s) = \frac{c_1 s + c_2}{b_1 s + b_2}\,r(s) \tag{6.447}$$

Discussion on Parameter Identifiability (No Disturbances)

The 4 parameters in the transfer function (6.445) are identifiable if the pair (ψ, δ) is available from measurements. Similarly, the 4 parameters in the transfer function (6.446) are identifiable if the pair (v, δ) is available. However, if we want to determine all 6 parameters uniquely in these two input–output models by measuring v, ψ and δ, we must require that there is no pole-zero cancellation in (6.447). Moreover, we must require that the time constants in sway and yaw are different ($T_v \neq T_3$) or equivalently:

$$c_2 b_1 \neq c_1 b_2 \tag{6.448}$$

From this discussion it follows that the state-space model (6.444) is not identifiable if only ψ and δ are measured since only 4 parameters can be estimated for this configuration. However, if v is measured in addition and (6.444) is controllable, that is $c_2 b_1 \neq c_1 b_2$, all 6 parameters can be uniquely determined.

In many practical implementations, however, v cannot be measured. For this case, overparametrization can be avoided by using the 4 parameter model

proposed by Sælid and Jenssen (1983). This model redefines the sway velocity according to:

$$\dot{v}' = b_{11}\,\delta \tag{6.449}$$
$$\dot{r} = a_{21}\,v' + a_{22}\,r + b_{21}\,\delta \tag{6.450}$$

Here v' can be interpreted as the sway velocity caused by the rudder motion alone. The transfer function now takes the form:

$$\frac{\psi}{\delta}(s) = \frac{b_1 s + b_2}{s(a_1 s + a_2)} \tag{6.451}$$

where all 4 parameters can be uniquely determined from the measurements ψ and δ. From a control point of view, the performance of this model is often found to be superior to that obtained by applying the Nomoto model:

$$\frac{\psi}{\delta}(s) = \frac{b_2}{s(a_1 s + a_2)} \tag{6.452}$$

This is due to the fact that the zero in the transfer function can be shown to be quite important in the control design.

Discussion on Parameter Identifiability in Presence of Disturbances

We will now show that identifiability in the presence of external disturbances implies that the input–output characteristic is modified. Consider the linear state-space model:

$$\begin{bmatrix} \dot{v} \\ \dot{r} \\ \dot{\psi} \end{bmatrix} = \begin{bmatrix} a_{11} & a_{12} & a_{13} \\ a_{21} & a_{22} & a_{23} \\ 0 & 1 & 0 \end{bmatrix} \begin{bmatrix} v \\ r \\ \psi \end{bmatrix} + \begin{bmatrix} b_{11} \\ b_{21} \\ 0 \end{bmatrix} \delta + \begin{bmatrix} e_{11} \\ e_{21} \\ 0 \end{bmatrix} 1 \tag{6.453}$$

where we have included two additional terms e_{11} and e_{21} describing the constant component of the disturbances, and two elements a_{13} and a_{23} which are proportional to ψ. In fact the linearized wind force and moment in sway and yaw will depend on the heading of the ship. The transfer function for this system is:

$$\psi(s) = \frac{b_2 s + b_3}{s^3 + a_1 s^2 + a_2 s + a_3}\,\delta(s) + \frac{e_2 s + e_3}{s^3 + a_1 s^2 + a_2 s + a_3}\,1 \tag{6.454}$$

Notice that in presence of wind, current and wave drift disturbances the denominator will not necessarily contain an integrator, which is the case for (6.445). Note that if ψ and δ are measured (the constant 1 is known) all 8 parameters in this model can be uniquely determined.

Parameter Identifiability in Closed-Loop Systems

Parameter identifiability in a closed loop should be performed with care. This is illustrated by considering the system in Figure 6.53 where $H(s)$ is the process transfer function, $C(s)$ is the transfer function of the controller and:

r = reference	w = (non-measurable) process noise
n = (measurable) secondary input	v' = measurement noise

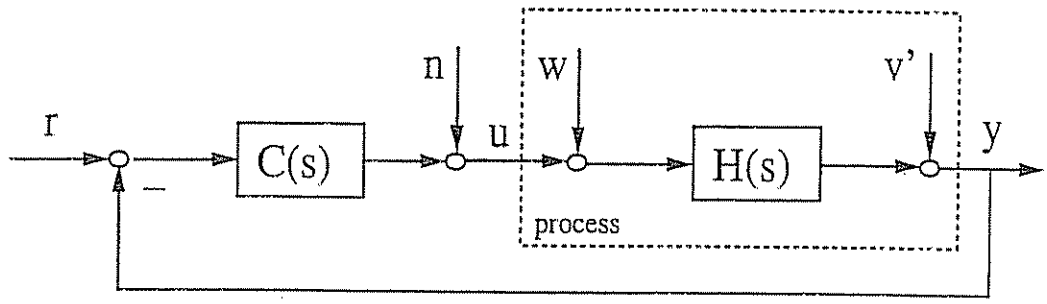

Figure 6.53: Estimation in closed-loop systems (Eykhoff 1988)

For linear systems we can include the process noise in the output noise by defining:

$$v(s) = v'(s) + H(s)\, w(s) \tag{6.455}$$

Consequently:

$$\frac{y}{u}(s) = \frac{H(s)C(s)\, r(s) + H(s)\, n(s) + v(s)}{C(s)\, r(s) + n(s) - C(s)\, v(s)} \tag{6.456}$$

Based on this expression, we can make the following considerations for closed-loop identifiability:

Table 6.5: Closed-Loop Identifiability adopted from Eykhoff (1988)

r	n	v	$y/u =$	comments
0	0	0	0	no identification possible
r	0	0	H	true transfer function
0	n	0	H	true transfer function
r	n	0	H	true transfer function
0	0	v	$-\frac{1}{C}$	inverse of controller
r	n	v	$H + \frac{1+CH}{\frac{Cr+n}{v} - C}$	true transfer function for high *signal-to-noise ratios*[2]

[2]The term $(Cr + n)/v$ can be interpreted as the *signal-to-noise ratio*. Moreover, it is seen that for acceptable identification this ratio should be quite high to ensure that $y/u \approx H$.

Notice that we identify the inverse of the controller $H = -1/C$ when we have much measurement noise v. Also notice that a good signal-to-noise ratio $(Cr + n)/v$ is important for the case $r \neq 0$, $n \neq 0$ and $v \neq 0$ in order to estimate H.

6.8.2 Indirect Model Reference Adaptive Systems

Indirect model reference adaptive systems (MRAS) can be applied to estimate the parameters in the ship plant; see Van Amerongen (1982). The estimated parameters can then be used in a linear quadratic optimal control law, for instance, to calculate the desired rudder action. The most popular MRAS structure is probably the parallel configuration shown in Figure 6.54 (Landau 1979).

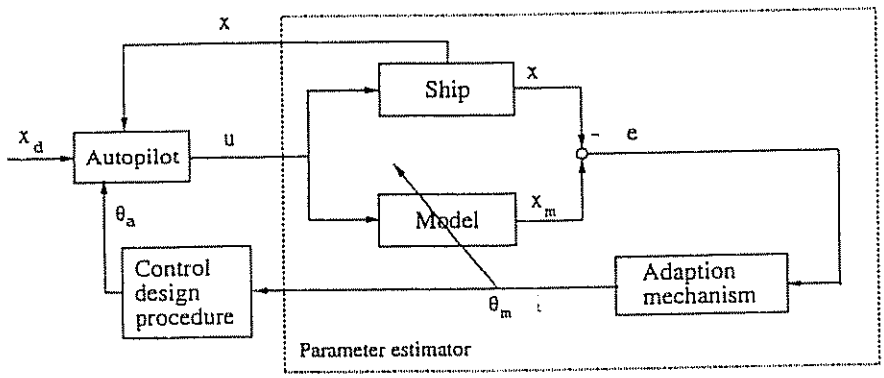

Figure 6.54: MRAS structure used for parameter estimation. In the figure θ_m is the estimated model parameter vector, θ_a denotes the parameters used in the autopilot and x, x_m and x_d are the process, model and desired state vectors, respectively.

Consider a system:

$$\dot{x} = A\,x + B\,u \tag{6.457}$$

where A and B are *unknown* constant matrices, and A is Hurwitz[3]. Let us define an adjustable model:

$$\dot{x}_m = A_m\,x_m + B_m\,u \tag{6.458}$$

where A_m and B_m are two adjustable matrices. Furthermore the output error vector is defined as:

$$e = x_m - x \tag{6.459}$$

which yields the error dynamics:

$$\dot{e} = A\,e + \tilde{A}\,x_m + \tilde{B}\,u \tag{6.460}$$

[3]A Hurwitz matrix has all eigenvalues with negative real parts and therefore verifies the Hurwitz stability criterion.

Here $\tilde{A} = A_m - A$, and $\tilde{B} = B_m - B$. A stable parameter adaptation law can be derived by applying Lyapunov stability theory, see Appendix C.1. Let V be a Lyapunov function candidate defined as:

$$V(e) = e^T P e + \text{tr}\,(\tilde{A}^T \Gamma_1^{-1} \tilde{A}) + \text{tr}\,(\tilde{B}^T \Gamma_2^{-1} \tilde{B}) \tag{6.461}$$

where $P = P^T > 0$, $\Gamma_1 = \Gamma_1^T > 0$ and $\Gamma_2 = \Gamma_2^T > 0$ are positive definite weighting matrices. tr(·) simply denotes the trace of the matrix, that is the sum of the diagonal elements. Differentiating V with respect to time yields:

$$\begin{aligned} \dot{V} &= e^T(A^T P + PA)e \\ &\quad +2e^T P(\tilde{A}x_m + \tilde{B}u) + 2\text{tr}\,(\tilde{A}^T \Gamma_1^{-1} \dot{\tilde{A}}) + 2\text{tr}\,(\tilde{B}^T \Gamma_2^{-1} \dot{\tilde{B}}) \end{aligned} \tag{6.462}$$

Here P must satisfy the Lyapunov equation:

$$A^T P + PA = -Q \qquad Q = Q^T > 0 \tag{6.463}$$

We can easily verify that the trace operator satisfies:

$$x^T A y = \text{tr}\,(A^T x y^T) \tag{6.464}$$

$$\text{tr}\,(A + B) = \text{tr}\,(A) + \text{tr}\,(B) \tag{6.465}$$

Formula (6.464) with $x = Pe$, y equal to x_m and u, and A equal to $\tilde{A}$ and $\tilde{B}$ respectively, yields:

$$\begin{aligned} \dot{V} &= -e^T Q e + 2\text{tr}\,(\tilde{A}^T P e x_m^T) \\ &\quad +2\text{tr}\,(\tilde{B}^T P e u^T) + 2\text{tr}\,(\tilde{A}^T \Gamma_1^{-1} \dot{\tilde{A}}) + 2\text{tr}\,(\tilde{B}^T \Gamma_2^{-1} \dot{\tilde{B}}) \end{aligned} \tag{6.466}$$

Finally, Formula (6.465) yields,

$$\dot{V} = -e^T Q e + 2\text{tr}\,(\tilde{A}^T [P e x_m^T + \Gamma_1^{-1} \dot{\tilde{A}}]) + 2\text{tr}\,(\tilde{B}^T [P e u^T + \Gamma_2^{-1} \dot{\tilde{B}}]) \tag{6.467}$$

The parameter adaptation laws are found by setting the arguments of the two last terms equal to zero, and using the fact: $\dot{\tilde{A}} = \dot{A}_m$ and $\dot{\tilde{B}} = \dot{B}_m$, which yields:

$$\dot{A}_m = -\Gamma_1 P e x_m^T \tag{6.468}$$

$$\dot{B}_m = -\Gamma_2 P e u^T \tag{6.469}$$

Hence, the expression for $\dot{V}$ reduces to:

$$\dot{V} = -e^T Q e < 0 \tag{6.470}$$

which guarantees that e converges to zero in finite time. However, convergence of $A_m \to A$ and $B_m \to B$ requires that the input signal u is persistently excited.

Example 6.8 (Identification of the Ship Steering Dynamics)
Consider Nomoto's 1st-order model in the form:

$$\dot{r} = a\,(U/L)\,r + b\,(U/L)^2\,\delta \tag{6.471}$$

where $a = -1/T' < 0$ and $b = K'/T' > 0$ are unknown constants. Application of (6.468) and (6.469) with $\mathbf{P} = 1$, yields the following parameter adaptation laws:

$$\dot{a}_m = -\gamma_1\,(U/L)\,r_m\,e \tag{6.472}$$
$$\dot{b}_m = -\gamma_2\,(U/L)^2\,\delta\,e \tag{6.473}$$

where $e = r_m - r$ and where r_m is calculated from the adjustable model:

$$\dot{r}_m = a_m\,(U/L)\,r_m + b_m\,(U/L)^2\,\delta \tag{6.474}$$

The convergence of the parameter estimates is shown in Figure 6.55. The following MATLAB program was used in the simulation study:

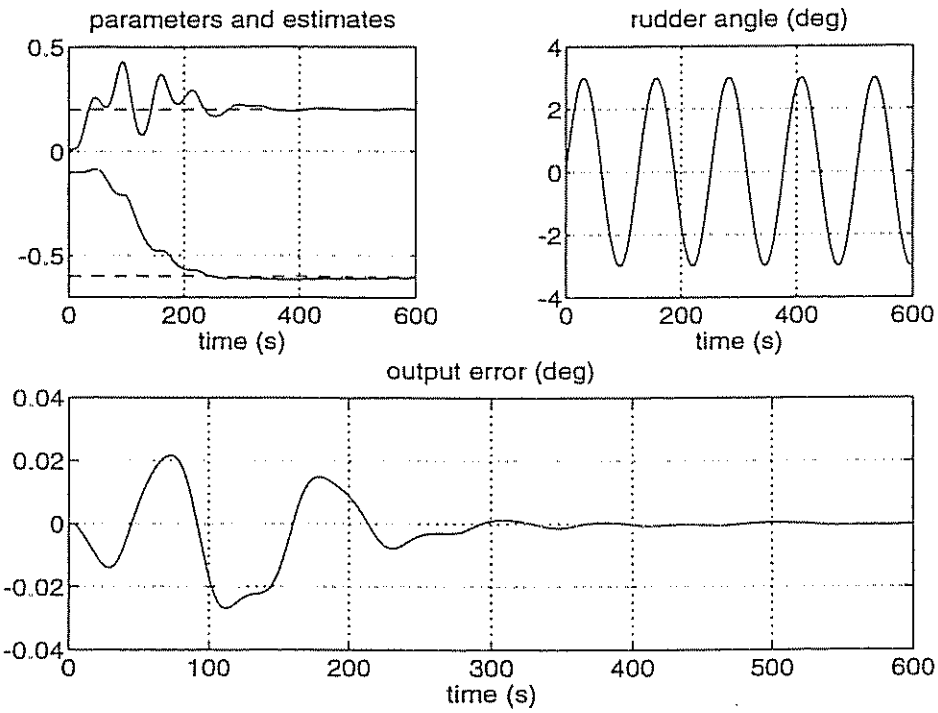

Figure 6.55: Convergence of parameter estimates for indirect MRAS.

```
% MATLAB program
h  = 1;                          % sampling time (s)
Tf = 600;                        % final simulation time (s)
U  = 8;                          % forward speed (m/s)
```

```
L  = 150;                                % length of hull (m)
a  = -0.6; b  = 0.2;                     % unknown model parameters
am = -0.1; bm = 0.01;                    % start estimates
g  = 100*[1 1];                          % adaptation gains
r  = 0; psi = 0; rm = 0; psim = 0;       % initial values
rm_old = rm;

tout = 0; est = [0 0]; out = [0,0];      % data storage

for t=h:h:Tf,
   delta = 3*sin(0.05*t);                    % control input

   e     = rm - r;                           % output error

   r     = r    + h*(a*(U/L)*r + b*(U/L)^2*delta);
   psi   = psi  + h*r;
   rm    = rm   + h*(am*(U/L)*rm + bm*(U/L)^2*delta);
   psim  = psim + h*rm;

   out   = [out; e delta];                   % data storage
   est   = [est; am bm];
   tout  = [tout; t];

   am    = am - h*g(1)*(U/L)*rm*e;           % parameter update laws
   bm    = bm - h*g(2)*(U/L)^2*delta*e;

   rm_old= rm;
end;

clg,subplot(221);                          % graphics
plot(tout,[est(:,1),est(:,2)],[0,Tf],[a,a],'--',[0,Tf],[b,b],'--');grid;
title('parameters and estimates');xlabel('time (s)');
subplot(222);
plot(tout,out(:,2));title('rudder angle (deg)');xlabel('time (s)');grid
subplot(212);
plot(tout,out(:,1));title('output error (deg)');xlabel('time (s)');grid
```

□

Self-Tuning Autopilots

Since the rapid increase in oil prices in 1973, self-tuning autopilots have been designed to reduce the fuel consumption. The motivation of using a parameter estimator is that the hydrodynamic parameters are known to change under different weather and load conditions. For self-tuning autopilots the regulator parameters are updated indirectly by means of parameter estimation and then used in a control design procedure. For instance, an optimal self-tuning autopilot minimizing the fuel consumption based on the criterion of Van Amerongen and van Nauta Lempke can be designed by (see Section 6.3.3):

$$\delta(t) = K_p[\psi_d - \psi(t)] - \hat{K}_d(t)\, r(t) \tag{6.475}$$

where

$$K_p = \sqrt{\frac{1}{\lambda_2}} \quad \text{(constant)} \tag{6.476}$$

$$\hat{K}_d(t) = \frac{L}{U(t)} \frac{\sqrt{1 + 2\hat{K}_p \hat{K}'(t)\hat{T}'(t) + (\hat{K}'(t)U(t)/L)^2 \ (\lambda_1/\lambda_2)} - 1}{\hat{K}'(t)} \tag{6.477}$$

Here $\hat{T}'(t)$ and $\hat{K}'(t)$ are the adaptive estimates of the time and gain constant, respectively. Let us define a model parameter vector:

$$\hat{\theta}_m(t) = \begin{bmatrix} \hat{K}'(t) \\ \hat{T}'(t) \end{bmatrix} \tag{6.478}$$

For the optimal controller (6.476) and (6.477), we have only one unknown gain, that is:

$$\hat{\theta}_a(t) = \hat{K}'_d(t) \tag{6.479}$$

which is computed through (6.477). This computation is the reason that this is an *indirect* algorithm as opposed to a *direct* algorithm where the controller parameters are updated directly. The indirect approach is illustrated in Figure 6.56 where an MRAS structure is used for parameter estimation.

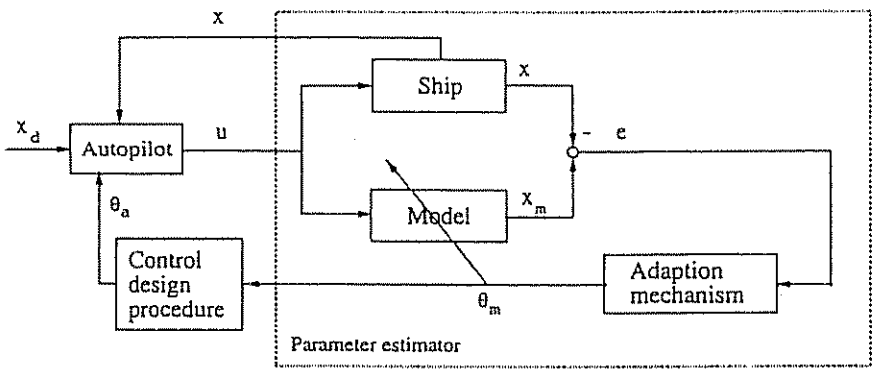

Figure 6.56: MRAS structure used for parameter estimation. In the figure x, x_m and x_d are the process, model and desired state vector, respectively.

More generally, we can define a self-tuning autopilot by:

$$u = f(\hat{\theta}_a, x, x_d) \qquad \text{where} \qquad \hat{\theta}_a = h(\hat{\theta}_m) \tag{6.480}$$

Here $f(\cdot)$ and $h(\cdot)$ are two functions depending on what control law and parameterization are used. In the literature indirect methods have also been called explicit self-tuning control, whereas direct methods have been referred to as implicit self-tuning control. To avoid confusion we will exclusively use the terms *direct* and *indirect* schemes.

SI applied to ship control is treated in Chapters 13 and 14 in Harris and Billings (1981). Chapter 13 of this reference discusses self-tuning controllers and course-keeping autopilots, and Chapter 14 is concerned with self-tuning control of ship positioning systems. Other useful references on self-tuning autopilots and ship parameter estimation techniques are: Abkowitz (1975, 1980), Åström and Källström (1976), Flobakk (1983), Holzhüter (1989), Kaasen (1986), Källström (1979, 1979), Källström and Åström (1981), Ohtsu, Horigome and Kitagawa (1979), Tiano and Volta (1978), Van Amerongen (1982) and Zhou (1987).

6.8.3 Continuous Least-Squares (CLS) Estimation

The least-squares algorithm is probably the most widely used parameter estimation technique and it can be dated back to the time of the German mathematician Karl Friedrich Gauss (1777–1855). We will consider both MIMO and SISO continuous-time systems.

MIMO Systems

Assume that the system description is given in the form:

$$y(t) = \Phi^T(t)\,\theta; \qquad \dot{\theta} = 0 \tag{6.481}$$

where $\Phi(t)$ is a matrix of known signals (regressor), y is a vector of known outputs and θ denotes the unknown parameter vector. Least-squares estimates are obtained by minimizing the integral square error with respect to the parameter estimate $\hat{\theta}(t)$, that is:

$$\min\ J = \int_0^t \| \, y(\tau) - \Phi^T(\tau)\,\hat{\theta}(\tau) \, \|^2 \, d\tau \tag{6.482}$$

Differentiating J with with respect to $\hat{\theta}(\tau)$ yields:

$$\frac{\partial J}{\partial \hat{\theta}(\tau)} = -2 \int_0^t \Phi(\tau) \left[y(\tau) - \Phi^T(\tau)\,\hat{\theta}(\tau) \right] d\tau = 0 \tag{6.483}$$

For $\hat{\theta}(\tau) = \hat{\theta}(t)$ the expression for $\partial J / \partial \hat{\theta}(\tau)$ simplifies to:

$$\left[\int_0^t \Phi(\tau)\Phi^T(\tau)\, d\tau \right] \hat{\theta}(t) = \int_0^t \Phi(\tau)\, y(\tau)\, d\tau \tag{6.484}$$

Defining the estimator gain matrix as:

$$P(t) = \left[\int_0^t \Phi(\tau)\Phi^T(\tau)\, d\tau \right]^{-1} \tag{6.485}$$

we obtain the following expression after differentiation:

$$\frac{d}{dt}[P^{-1}(t)] = \Phi(t)\,\Phi^T(t) \tag{6.486}$$

Since, $P(t)\,P^{-1}(t) = I$ it follows that:

$$\frac{d}{dt}[P(t)\,P^{-1}(t)] = \frac{d}{dt}[P(t)]\,P^{-1}(t) + P(t)\,\frac{d}{dt}[P^{-1}(t)] = 0 \tag{6.487}$$

and consequently,

$$\boxed{\dot{P}(t) = -P(t)\,\Phi(t)\,\Phi^T(t)\,P(t)} \tag{6.488}$$

where $P(0) > 0$. Differentiating (6.484) with respect to time, together with (6.485), yields:

$$\frac{d}{dt}[P^{-1}(t)]\,\hat{\theta}(t) + P^{-1}(t)\,\dot{\hat{\theta}}(t) = \Phi(t)\,y(t) \tag{6.489}$$

By using (6.486) we obtain

$$\Phi(t)\,[\Phi^T(t)\,\hat{\theta}(t) - y(t)] + P^{-1}(t)\,\dot{\hat{\theta}}(t) = 0 \tag{6.490}$$

Introducing:

$$e(t) = \Phi^T(t)\,\hat{\theta}(t) - y(t) \tag{6.491}$$

for the prediction error, finally yields the parameter update law:

$$\boxed{\dot{\hat{\theta}}(t) = -P(t)\,\Phi(t)\,e(t)} \tag{6.492}$$

SISO Systems

Consider the single-input single-output system in the form:

$$y(t) = \phi^T(t)\,\theta; \qquad \dot{\theta} = 0 \tag{6.493}$$

where $\phi(t)$ can be interpreted as the regression vector. The LS parameter estimates are computed from:

$$\boxed{\dot{\hat{\theta}}(t) = -P(t)\,\phi(t)\,e(t)} \qquad \boxed{e(t) = \phi^T(t)\,\hat{\theta}(t) - y(t)} \tag{6.494}$$

$$\boxed{\dot{P}(t) = -P(t)\,\phi(t)\,\phi^T(t)\,P(t)} \tag{6.495}$$

Normalized Least-Squares

The least-squares algorithm can be modified so that the adjustment rate does not depend on the magnitude of the signal values. For the SISO case Albert and Gardner (1967) and Nagumo and Noda (1967) propose using the following normalization procedure:

$$\dot{\hat{\theta}}(t) = -\alpha \frac{P(t)\,\phi(t)\,e(t)}{1+\gamma\,\phi^T(t)P(t)\phi(t)} \tag{6.496}$$

$$\dot{P}(t) = -\alpha \frac{P(t)\,\phi(t)\,\phi^T(t)\,P(t)}{1+\gamma\,\phi^T(t)P(t)\phi(t)} \tag{6.497}$$

where $\alpha > 0$ and $\gamma > 0$. For MIMO systems:

$$y(t) = \Phi^T(t)\,\theta \tag{6.498}$$

where each output y_i and input u_i can be described by one *unique* parameter vector θ_i, we can partition the MIMO system into m SISO systems:

$$\begin{bmatrix} y_1(t) \\ \vdots \\ y_m(t) \end{bmatrix} = \begin{bmatrix} \phi_1^T(t)\,\theta_1 \\ \vdots \\ \phi_m^T(t)\,\theta_m \end{bmatrix} \tag{6.499}$$

Hence, the SISO normalization algorithm should be applied to each of these m scalar equations. The normalized least-squares algorithm is more complicated to implement but is found in practice to be much more robust.

Continuous Least-Squares With Exponential Forgetting

The CLS parameter estimator may be modified to deal with time-varying parameters by modifying the gain update such that P will approach a non-zero value after some time. The intuitive solution to this problem is to modify the criterion (6.482) such that past data are given less influence than current data in estimation of the current parameters. This suggests that we minimize the exponential weighted criterion:

$$\min\ J = \int_0^t \exp(-\lambda\,(t-\tau))\,\|\,y(\tau) - \Phi^T(\tau)\,\hat{\theta}(\tau)\,\|^2\,d\tau \tag{6.500}$$

Here $\lambda > 0$ is a constant forgetting factor, typically chosen in the interval:

$$0.005 < \lambda < 0.02 \tag{6.501}$$

Minimizing, the exponential weighted criterion yields:

$$\boxed{\dot{\hat{\theta}}(t) = -P(t)\,\Phi(t)\,e(t)} \tag{6.502}$$

with the gain update:

$$\frac{d}{dt}[P^{-1}(t)] = -\lambda\,P^{-1}(t) + \Phi(t)\,\Phi^T(t) \tag{6.503}$$

which after matrix inversion, yields:

$$\boxed{\dot{P}(t) = \lambda\,P(t) - P(t)\,\Phi(t)\,\Phi^T(t)\,P(t)} \tag{6.504}$$

It should be noted that a constant forgetting factor should usually be applied to a system that changes gradually in a "stationary manner" or parameters that change abruptly but seldom. Rapid changing system parameters will require a time-varying forgetting profile.

Continuous Least-Squares With Covariance Resetting

Another possible method to avoid covariance wind-up, that is the problem that $\boldsymbol{P}^{-1}$ becomes large in some directions with resulting slow adaptation, can be using a covariance resetting technique. For instance, resetting $\boldsymbol{P}$ to a predefined positive definite value whenever the eigenvalues $\lambda_{\min}(\boldsymbol{P})$ fall under some specified minimum value will improve the tracking of slowly-varying parameters.

Persistency of Excitation

Convergence of the estimated parameter vector $\hat{\boldsymbol{\theta}}$ to the correct parameter vector $\boldsymbol{\theta}$ requires that the system is persistently excited (PE), that is parameter convergence occurs if $\exists\ T > 0$ and $\beta \geq \alpha > 0$ such that:

$$\alpha \boldsymbol{I} \leq \frac{1}{T} \int_s^{s+T} \boldsymbol{\Phi}(\tau)\boldsymbol{\Phi}^T(\tau)\, d\tau \leq \beta \boldsymbol{I} \quad , \quad \forall\ s \in \mathbb{R}_+ \tag{6.505}$$

This simply states that the integral of the matrix $\boldsymbol{\Phi}(\tau)\boldsymbol{\Phi}^T(\tau)$ is uniformly positive definite over any interval of length T.

Example 6.9 (CLS Estimation Applied to Nomoto's 1st-Order Model)
The unknown gain and time constants in Nomoto's 1st-order model can be estimated by applying the LS algorithm. For simplicity, we will assume that r and δ are available from measurements. Consider the ship dynamics in the form:

$$\dot{r} = -\frac{1}{T} r + \frac{K}{T} \delta \tag{6.506}$$

where T and K are unknown. Defining two filtered signals:

$$r_f = \frac{1}{1 + T_f s} r \tag{6.507}$$

$$\delta_f = \frac{1}{1 + T_f s} \delta \tag{6.508}$$

where $T_f > 0$ is a known filter time constant, yields:

$$r(t) = (1 - \frac{T_f}{T})\, r_f(t) + K \frac{T_f}{T}\, \delta_f(t) \tag{6.509}$$

This in turn suggests the regressor model:

$$r(t) = \boldsymbol{\phi}^T(t)\, \boldsymbol{\theta} \tag{6.510}$$

ARX Model

Many systems are described by a single white noise disturbance. This simply corresponds to $C(z^{-1}) = 1$. Hence, the ARMAX model reduces to:

$$A(z^{-1})y(k) = B(z^{-1})u(k) + e(k) \tag{6.517}$$

which usually is referred to as an ARX model.

AR Model

Finally, an AR model is defined as:

$$A(z^{-1})y(k) = e(k) \tag{6.518}$$

We recall that this model structure has already been applied to wave frequency tracking in Section 6.1.5.

Regression Form

The ARX model can be written in regression form as:

$$y(k) = \phi^T(k)\,\theta + e(k) \tag{6.519}$$

where ϕ is the *regression vector* or regressor and θ is the *parameter vector*, defined by:

$$\phi(k) = [-y(k-1), ..., -y(k-n), u(k-1), ..., u(k-m)]^T \tag{6.520}$$

$$\theta = [a_1, ..., a_n, b_1, ..., b_m] \tag{6.521}$$

This is also possible for nonlinear models which are linear in their parameters, for instance the nonlinear model:

$$y(k) = a\,y^2(k-1) + b\,\sin(u(k-1)) \tag{6.522}$$

can be written in linear regression form:

$$y(k) = \begin{bmatrix} y^2(k-1) & \sin(u(k-1)) \end{bmatrix} \begin{bmatrix} a \\ b \end{bmatrix} \tag{6.523}$$

Extensions to MIMO systems are done by defining the regression model according to:

$$y(k) = \Phi^T(k)\,\theta + e(k) \tag{6.524}$$

where Φ is a *regression matrix* of appropriate dimensions.

Algorithm 6.1 (MIMO RLS With Exponential Forgetting)
The RLS algorithm for the MIMO regression model (6.524) is obtained by minimizing the criterion function:

$$V_N(\theta) = \frac{1}{2N}\sum_{k=1}^{N} \lambda^{N-k}\,[y(k) - \Phi^T(k)\theta]^T[y(k) - \Phi^T(k)\theta] \tag{6.525}$$

with respect to θ (Åström and Wittenmark 1989):

$$\hat{\theta}(k) = \hat{\theta}(k-1) + K(k)\,[y(k) - \Phi^T(k)\,\hat{\theta}(k-1)] \tag{6.526}$$

$$K(k) = P(k-1)\Phi(k)\,[\lambda I + \Phi^T(k)P(k-1)\Phi(k)]^{-1} \tag{6.527}$$

$$P(k) = \frac{1}{\lambda}[I - K(k)\Phi^T(k)]\,P(k-1) \tag{6.528}$$

where a typical λ-value is $0.98 < \lambda < 0.995$.
□

An alternative formulation of the RLS algorithm is obtained by noticing that:

$$K(k) = P(k-1)\Phi(k)[\lambda I + \Phi^T(k)P(k-1)\Phi(k)]^{-1} = P(k)\Phi(k) \tag{6.529}$$

Hence, the RLS algorithm takes the form:

$$\hat{\theta}(k) = \hat{\theta}(k-1) + P(k)\Phi(k)\,[y(k) - \Phi^T(k)\,\hat{\theta}(k-1)] \tag{6.530}$$

$$P(k) = \frac{1}{\lambda}\Big[P(k-1) - P(k-1)\Phi(k)\,[\lambda I + \Phi^T(k)P(k-1)\Phi(k)]^{-1} \Phi^T(k)P(k-1)\Big] \tag{6.531}$$

For systems with colored noise, for instance the ARMAX model with $C(z^{-1}) \neq 1$, this method will give biased estimates. This problem can be circumvented by applying the *extended least-squares* (ELS), *recursive instrumental variables* (RIV) or the *recursive maximum likelihood* (RML) method, for instance. The interested reader can find a survey of recursive identification algorithms in Hunt (1986) while a more extensive discussion on recursive identification is given by Ljung and Söderström (1986).

Example 6.10 (ARX Model for Ship Parameter Estimation)
Assume that the LF heading estimates are available. The RLS estimation algorithm can then be applied to the Nomoto model:

$$T\dot{r}(t) + r(t) = K\,\delta(t) \tag{6.532}$$

by noticing that (see Appendix B.1.1):

$$r(k) = \exp(-h/T)\, r(k-1) + K(1-\exp(-h/T))\, \delta(k-1) \tag{6.533}$$

is an ARX model. Here h is the sampling time. This model can be written in linear regression form as:

$$r(k) = \phi^T(k)\, \theta \tag{6.534}$$

with

$$\phi(k) = [r(k-1)\ \ \delta(k-1)]^T \qquad \theta = [\exp(-h/T)\ \ K(1-\exp(-h/T)]^T \tag{6.535}$$

If $r(k)$ is not available we can modify the above regression model to use the LF estimate of the heading angle $\psi(k)$ instead. This can be done by introducing the following approximation:

$$r(k) \approx \frac{\Delta\psi(k)}{h} = \frac{\psi(k) - \psi(k-1)}{h} \tag{6.536}$$

Hence, (6.534) takes the form:

$$\Delta\psi(k) = \phi^T(k)\, \theta \tag{6.537}$$

with

$$\phi(k) = [\Delta\psi(k-1)\ \ \delta(k-1)]^T \tag{6.538}$$

$$\theta = [\exp(-h/T)\ \ hK(1-\exp(-h/T))]^T \tag{6.539}$$

The convergence of the RLS algorithm for the Nomoto model is illustrated by the following simple MATLAB example.

```
% Recursive Least Squares (RLS) with exponential forgetting applied
% to a 1st-order Nomoto model with T and K as unknown parameters

h  = 1.0;                          % sampling time (s)
Tf = 50;                           % final simulation time (s)
T  = 105;                          % time constant (s)
K  = 0.2;                          % gain          (1/s)
U  = 7.7;                          % forward speed (m/s)
L  = 160;                          % length of hull (m)
r  = 0; delta = 0; e = 0;          % initial states
error = 0;                         % output error (percent)

theta = [    exp(-h/T);            % ship model parameters
         K*(1 - exp(-h/T))];

T_hat  = 50;                       % initial estimate of T
K_hat  = 0.4;                      % initial estimate of K
theta_hat = [exp(-h/T_hat);        % initial parameter estimates
      K_hat*(1-exp(-h/T_hat))];
```

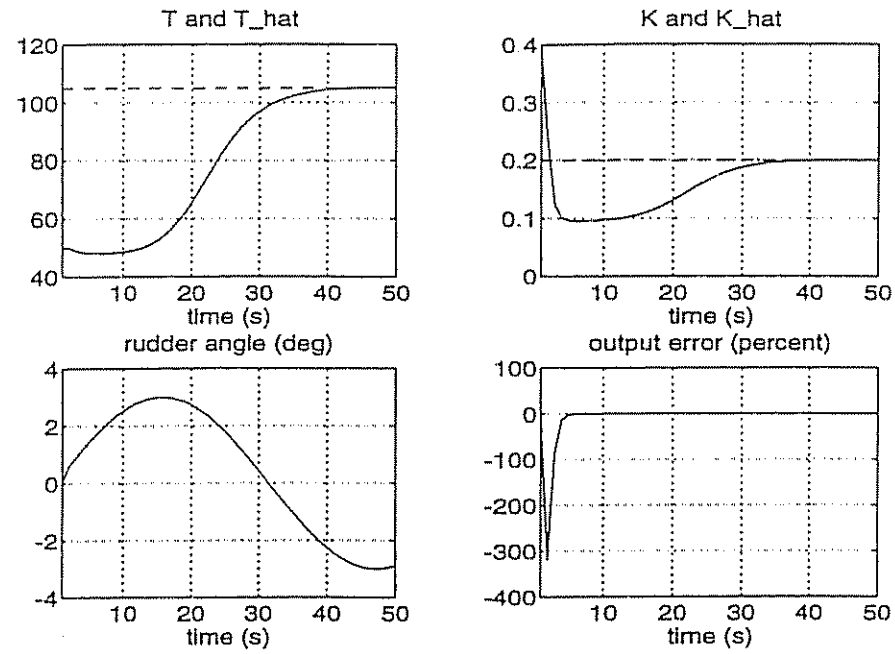

Figure 6.57: RLS parameter estimation applied to Nomoto's 1st-order model with regressor (6.535) utilizing yaw rate measurements. Similar results are obtained for the RLS algorithm for the yaw angle based regressor (6.538) under the assumption of no measurement noise.

```
P      = 5e3*diag([100 1]);      % initial covariance matrix
Phi    = [r delta]';             % initial regressor
lambda = 0.98;                   % forgetting factor

for k=2:h:Tf,
  delta(k) = 3*pi/180*sin(0.1*h*k);    % commanded rudder angle
  Phi    = [r(k-1) delta(k)]';         % regressor
  r(k) = Phi'*theta;                   % sway velocity
  e(k) = r(k) - Phi'*theta_hat;        % output error

  % parameter and covariance update
  theta_hat = theta_hat + P*Phi*e(k);
  P = inv(lambda)*(P - P*Phi*inv(lambda + Phi'*P*Phi)*Phi'*P);

  % data storage
  T_hat(k) = -inv(log(theta_hat(1)))*h;
  K_hat(k) = theta_hat(2)*inv(1 - exp(-h/(T_hat(k))));
  error(k) = 100*e(k)/r(k);
end

T_hat = T_hat*U/L;                     % scaling of estimates
K_hat = K_hat*L/U;
e     = e*180/pi;
time  = h*(1:k);                       % time vector
```

```
% graphics

subplot(221),plot(time,T_hat*L/U,'-',time,T*ones(Tf,1),'--'); grid;
title('T and T_hat'); xlabel('time (s)');
subplot(222); plot(time,K_hat*U/L,'-',time,K*ones(Tf,1),'--'); grid;
title('K and K_hat'); xlabel('time (s)');
subplot(223); plot(time,delta*180/pi); grid
title('rudder angle (deg)'); xlabel('time (s)');
subplot(224); plot(time,error); grid;
title('output error (percent)'); xlabel('time (s)');
```

□

The example shows how an ARX model can be used for RLS parameter estimation. However, this method cannot be used if the signals $r(k)$ and $\psi(k)$ are corrupted with colored noise (for instance 1st-order wave disturbances). In fact, a good wave filter will be crucial for success with the RLS estimation approach. Therefore, an alternative to wave filtering could be to use an ARMAX model where the 1st-order wave disturbances are estimated together with the model parameters. This requires that the noise term $C(z^{-1})$ is chosen properly. In the next section we will show how an RML estimation algorithm can be designed for this purpose.

6.8.5 Recursive Maximum Likelihood (RML) Estimation

The ARMAX model (6.516) cannot be converted directly to a regression model since the variable $e(k)$ is not known. However, a suitable approximation for $e(k)$ is the *prediction error*:

$$\varepsilon(k) = y(k) - \phi^T(k)\,\hat{\theta}(k) \tag{6.540}$$

where

$$\phi(k) = [-y(k-1), .., -y(k-n), u(k-1), .., u(k-m), \varepsilon(k-1), .., \varepsilon(k-r)]^T \tag{6.541}$$

$$\hat{\theta}(k) = [\hat{a}_1(k), .., \hat{a}_n(k), \hat{b}_1(k), .., \hat{b}_m(k), c_1(k), .., \hat{c}_r(k)]^T \tag{6.542}$$

Minimization of the criterion:

$$V_N(\theta) = \frac{1}{2N} \sum_{k=1}^{N} \lambda^{N-k}\, \varepsilon^2(k) \tag{6.543}$$

yields the following recursive algorithm:

Algorithm 6.2 (SISO Recursive Maximum Likelihood (RML))
The RML algorithm is (Ljung 1987):

$$\hat{\theta}(k) = \hat{\theta}(k-1) + K(k)\,[y(k) - \phi^T(k)\,\hat{\theta}(k-1)] \tag{6.544}$$

$$K(k) = \frac{P(k-1)\psi(k)}{\lambda + \psi^T(k)P(k-1)\psi(k)} \tag{6.545}$$

$$P(k) = \frac{1}{\lambda}[I - K(k)\psi^T(k)]\,P(k-1) \tag{6.546}$$

where the gradient vector $\psi(k)$ is defined as:

$$\phi(k) = \hat{C}(z^{-1})\psi(k) \quad \Longrightarrow \quad \psi(k) = \frac{\phi(k)}{\hat{C}(z^{-1})} \tag{6.547}$$

The method is not truly recursive since computation of $\psi(k)$ at time k requires the latest estimate $\hat{\theta}(k)$ to be known. This problem is usually solved by using the previous estimate $\hat{\theta}(k-1)$ to compute $\psi(k)$.
□

Example 6.11 (ARMAX Model for Ship–Wave Parameter Estimation)

Consider the ship model:

$$T\dot{r}_L(t) + r_L(t) = K\,\delta(t) \tag{6.548}$$

$$r_L(t) = \dot{\psi}_L(t) \tag{6.549}$$

with 1st-order wave disturbances:

$$\dot{\psi}_H(t) + 2\,\zeta\,\omega_n\,\psi_H(t) + \omega_n^2\,\xi_H(t) = K_w\,w(t) \tag{6.550}$$

$$\dot{\xi}_H(t) = \psi_H(t) \tag{6.551}$$

This system can be written in state-space form according to:

$$\dot{x}(t) = A\,x(t) + B\,u(t) + E\,e(t) \tag{6.552}$$

$$y(t) = C\,x(t) \tag{6.553}$$

where $y(t) = \psi_L(t) + \psi_H(t)$ is the measured heading, $u(t) = \delta(t)$ is the rudder angle and $e(t) = \dot{w}(t)$ is a zero-mean Gaussian white noise sequence. Next we have to transform this model representation to a discrete-time ARMAX model, that is:

$$A(z^{-1})\,y(k) = B(z^{-1})\,u(k) + C(z^{-1})\,e(k) \tag{6.554}$$

The polynomial $A(z^{-1})$, $B(z^{-1})$ and $C(z^{-1})$ will depend on what discretization procedure is used. One attractive solution is (see Appendix B.1):

$$x(k+1) = \Phi\, x(k) + \Delta\, u(k) + \Gamma\, e(k) \quad (6.555)$$
$$y(k) = C\, x(k) \quad (6.556)$$

where

$$\Phi = \exp(A\, h); \qquad \Delta = A^{-1}(\Phi - I)\, B; \qquad \Gamma = A^{-1}(\Phi - I)\, E \quad (6.557)$$

Hence,

$$y(k) = C\,(zI - \Phi)^{-1}\, \Delta\, u(k) + C\,(zI - \Phi)^{-1}\, \Gamma\, e(k) \quad (6.558)$$

Using the fact that:

$$(zI - \Phi)^{-1} = \frac{\mathrm{adj}(zI - \Phi)}{\det(zI - \Phi)} \quad (6.559)$$

yields

$$\det(zI - \Phi)\, y(k) = C\, \mathrm{adj}(zI - \Phi)\, \Delta\, u(k) + C\, \mathrm{adj}(zI - \Phi)\, \Gamma\, e(k) \quad (6.560)$$

which suggests that:

$$A(z^{-1}) = \det(zI - \Phi); \quad B(z^{-1}) = C\, \mathrm{adj}(zI - \Phi)\, \Delta; \quad C(z^{-1}) = C\, \mathrm{adj}(zI - \Phi)\, \Gamma$$

□

For details on RML applied to identification of ship dynamics see Källström and Åström (1981) and references therein. Other references discussing SI in terms of RLS and RML are Åström and Källström (1976), Holzhüter (1989), Källström (1979), Källström et al. (1979) and Källström and Åström (1981), Ohtsu et al. (1979) and Tiano and Volta (1978).

6.8.6 Recursive Prediction Error Method (RPEM)

In this section we will apply a *Gauss–Newton search direction* to derive an RPEM (Zhou 1987). The proposed estimation algorithm can be used together with a state estimator (Kalman filter) which implies that we do not have to measure all states. Another advantage with the combined use of the RPEM and the Kalman filter algorithm is that the wave filter states can be incorporated in the model as well; see Sælid and Jenssen (1983). This can be done by minimizing the quadratic criterion:

$$V_N(\theta) = \frac{1}{2N} \sum_{k=1}^{N} \varepsilon^T(\theta, k)\, \Lambda^{-1}(k)\, \varepsilon(\theta, k) \tag{6.561}$$

where $\varepsilon(k) = y(k) - \overline{y}(\theta, k) \in \mathbb{R}^m$ is the prediction error subject to the parameter vector $\theta \in \mathbb{R}^d$. Moreover, the Gauss–Newton search direction is defined as:

$$\hat{\theta}(k) = \hat{\theta}(k-1) - \boldsymbol{H}^{-1}(k-1)\, \nabla V_N(k-1) \tag{6.562}$$

where the $m \times m$ Hessian at time k is computed as:

$$\boldsymbol{H}(k) = \frac{\partial^2 V_N(\theta(k))}{\partial \varepsilon(k)\, \partial \varepsilon^T(k)} \tag{6.563}$$

The $d \times 1$ gradient of V at time k is given by:

$$\nabla V_N(\hat{\theta}(k)) = \left[\frac{\partial \varepsilon(k)}{\partial \hat{\theta}(k)}\right]^T \boldsymbol{\Lambda}^{-1}(k)\, \varepsilon(k) = -\boldsymbol{\Psi}(k)\, \boldsymbol{\Lambda}^{-1}(k)\, \varepsilon(k) \tag{6.564}$$

where $\boldsymbol{\Psi}(k)$ can be interpreted as a $d \times p$ *sensitivity matrix* defined as:

$$\boldsymbol{\Psi}^T(k) = -\frac{\partial \varepsilon(\theta(k))}{\partial \hat{\theta}(k)} = -\frac{\partial y(k)}{\partial \hat{\theta}(k)} + \frac{\partial \overline{y}(\hat{\theta}(k))}{\partial \hat{\theta}(k)} = \frac{\partial \overline{y}(\hat{\theta}(k))}{\partial \hat{\theta}(k)} \tag{6.565}$$

Hence, the following parameter update law is obtained:

$$\hat{\theta}(k) = \hat{\theta}(k-1) + \boldsymbol{H}^{-1}(k-1)\, \boldsymbol{\Psi}(k-1) \boldsymbol{\Lambda}^{-1}(k-1)\, \varepsilon(k-1) \tag{6.566}$$

In practical implementations of the prediction error method it is convenient to use a recursive version of this algorithm to approximate the Hessian and the sensitivity matrix.

MIMO Systems

The derivation of the recursive prediction error (RPE) method is found in Ljung and Söderström (1986) who propose the following standard equations when using the Gauss–Newton search direction:

$$\begin{aligned}
\varepsilon(k) &= y(k) - \overline{y}(k) && (6.567)\\
\dot{\boldsymbol{\Lambda}}(k) &= \dot{\boldsymbol{\Lambda}}(k-1) + \gamma(k)\, [\varepsilon(k)\varepsilon^T(k) - \dot{\boldsymbol{\Lambda}}(k-1)] && (6.568)\\
\boldsymbol{S}(k) &= \boldsymbol{\Psi}^T(k)\boldsymbol{P}(k-1)\boldsymbol{\Psi}(k) + \lambda(k)\dot{\boldsymbol{\Lambda}}(k-1) && (6.569)\\
\boldsymbol{L}(k) &= \boldsymbol{P}(k-1)\boldsymbol{\Psi}(k)\boldsymbol{S}^{-1}(k) && (6.570)\\
\hat{\theta}(k) &= \hat{\theta}(k-1) + \boldsymbol{L}(k)\varepsilon(k) && (6.571)\\
\boldsymbol{P}(k) &= \frac{1}{\lambda(k)} \left[\boldsymbol{P}(k-1) - \boldsymbol{L}(k)\boldsymbol{S}(k)\boldsymbol{L}^T(k)\right] && (6.572)
\end{aligned}$$

Here the gain sequence $\gamma(k)$ is defined as:

$$\gamma(k) = \frac{1}{1 + \lambda(k)/\gamma(k-1)} \tag{6.573}$$

where $\lambda(k)$ is the forgetting factor.

SISO Systems

For SISO systems $\boldsymbol{\Lambda}(k)$ will be a scalar scaling $\boldsymbol{P}(k)$ and $\boldsymbol{S}(k)$. For constant values of $\boldsymbol{\Lambda}(k)$ this scaling will not affect $\boldsymbol{L}(k)$ which implies that $\boldsymbol{\Lambda}(k)$ often is replaced by unity in the SISO case. This assumption suggests that the following SISO algorithm could be used:

$$\boldsymbol{L}(k) = \frac{\boldsymbol{P}(k-1)\boldsymbol{\Psi}(k)}{\lambda(k) + \boldsymbol{\Psi}^T(k)\boldsymbol{P}(k-1)\boldsymbol{\Psi}(k)} \tag{6.574}$$

$$\hat{\boldsymbol{\theta}}(k) = \hat{\boldsymbol{\theta}}(k-1) + \boldsymbol{L}(k)\,\varepsilon(k) \tag{6.575}$$

$$\boldsymbol{P}(k) = \frac{1}{\lambda(k)}\left[\boldsymbol{P}(k-1) - \frac{\boldsymbol{P}(k-1)\boldsymbol{\Psi}(k)\boldsymbol{\Psi}^T(k)\boldsymbol{P}(k-1)}{\lambda(k) + \boldsymbol{\Psi}^T(k)\boldsymbol{P}(k-1)\boldsymbol{\Psi}(k)}\right] \tag{6.576}$$

Application to Discrete-Time State-Space Models

Consider the discrete-time state-space model:

$$\boldsymbol{x}(k+1) = \boldsymbol{\Phi}(\boldsymbol{\theta})\,\boldsymbol{x}(k) + \boldsymbol{\Delta}(\boldsymbol{\theta})\,\boldsymbol{u}(k) + \boldsymbol{\Gamma}\,\boldsymbol{w}(k) \tag{6.577}$$

$$\boldsymbol{z}(k) = \boldsymbol{H}\,\boldsymbol{x}(k) + \boldsymbol{v}(k) \tag{6.578}$$

Let the state estimator (Kalman filter) equations be described by:

$$\overline{\boldsymbol{x}}(k+1) = \hat{\boldsymbol{\Phi}}(\hat{\boldsymbol{\theta}})\,\hat{\boldsymbol{x}}(k) + \hat{\boldsymbol{\Delta}}(\hat{\boldsymbol{\theta}})\,\boldsymbol{u}(k) + \boldsymbol{K}(\hat{\boldsymbol{\theta}})\,\varepsilon(k) \tag{6.579}$$

$$\hat{\boldsymbol{x}}(k) = \overline{\boldsymbol{x}}(k) + \boldsymbol{K}(\hat{\boldsymbol{\theta}})\,\varepsilon(k) \tag{6.580}$$

where $\hat{\boldsymbol{\Phi}}$ and $\hat{\boldsymbol{\Delta}}$ are the parameter estimate of the unknown matrices $\boldsymbol{\Phi}$ and $\boldsymbol{\Delta}$. The estimated parameter vector is denoted as $\hat{\boldsymbol{\theta}}$ while $\boldsymbol{K}(\hat{\boldsymbol{\theta}})$ is the Kalman gain matrix. Substituting (6.580) into (6.579) yields:

$$\overline{\boldsymbol{x}}(k+1) = \hat{\boldsymbol{\Phi}}(\hat{\boldsymbol{\theta}})\,\overline{\boldsymbol{x}}(k) + \hat{\boldsymbol{\Delta}}(\hat{\boldsymbol{\theta}})\,\boldsymbol{u}(k) + \hat{\boldsymbol{\Phi}}(\hat{\boldsymbol{\theta}})\boldsymbol{K}(\hat{\boldsymbol{\theta}})\,\varepsilon(k) \tag{6.581}$$

Sensitivity Equations for Discrete-Time State-Space Model

Let us introduce the notation:

$$\boldsymbol{x}_{\theta_i}(k) = \frac{\partial \overline{\boldsymbol{x}}(k)}{\partial \hat{\boldsymbol{\theta}}_i(k)} \qquad (i = 1...d) \tag{6.582}$$

which implies that:

$$\Psi^T(k) = \frac{\partial \overline{y}(\hat{\theta}(k))}{\partial \hat{\theta}(k)} = [H\, x_{\theta_i}(k), ..., H\, x_{\theta_d}(k)] \tag{6.583}$$

Hence, the *sensitivity equations* for parameter θ_i $(i = 1...d)$ can be found by differentiating (6.581) with respect to time, that is:

$$x_{\theta_i}(k+1) = \hat{\Phi}(\hat{\theta})[I - K(\hat{\theta})H]\, x_{\theta_i}(k) \tag{6.584}$$

$$+\frac{\partial \hat{\Phi}(\hat{\theta})}{\partial \hat{\theta}_i}\, \hat{x}(k) + \frac{\partial \hat{\Delta}(\hat{\theta})}{\partial \hat{\theta}_i}\, u(k) + \hat{\Phi}(\hat{\theta})\frac{\partial \hat{K}(\hat{\theta})}{\partial \hat{\theta}_i}\, \varepsilon(k) \tag{6.585}$$

We have here used the fact that:

$$\frac{\partial \varepsilon(k)}{\partial \hat{\theta}_i(k)} = -H\, x_{\theta_i}(k) \tag{6.586}$$

The computation of $K(\hat{\theta})$ requires a large number of differential equations to be solved on-line. The implementation of the RPEM algorithm is considerably simplified if constant values for $K(\hat{\theta})$ are used. This can be done by using a set of pre-computed steady-state Kalman gain matrices for different values of $\hat{\theta}$. Hence, the sensitivity equations reduce to:

$$x_{\theta_i}(k+1) = \hat{\Phi}(\hat{\theta})[I - K(\hat{\theta})H]\, x_{\theta_i}(k) + \frac{\partial \hat{\Phi}(\hat{\theta})}{\partial \hat{\theta}_i}\, \hat{x}(k) + \frac{\partial \hat{\Delta}(\hat{\theta})}{\partial \hat{\theta}_i}\, u(k) \tag{6.587}$$

A discussion on gain scheduling and the application of the RPEM method to identification to adaptive ship steering is found in Sælid and Jenssen (1983). Other useful references are Zhou (1987) and Zhou and Blanke (1989).

6.8.7 State Augmented Extended Kalman Filter (EKF)

An alternative to the RPEM is to apply a state augmented extended Kalman filter (EKF) to estimate the ship parameters. Consider a nonlinear system:

$$\dot{x} = f(x, u, \theta) + w_1 \tag{6.588}$$

$$\dot{\theta} = \eta \tag{6.589}$$

where $x \in \mathbb{R}^n$ is the state vector, $u \in \mathbb{R}^r$ is the input vector, $\theta \in \mathbb{R}^p$ is the unknown parameter vector and $w_1 \in \mathbb{R}^n$ and $\eta \in \mathbb{R}^n$ are zero-mean Gaussian white noise sequences. This model can be expressed in augmented state-space form as:

$$\boxed{\dot{\xi} = \mathcal{F}(\xi, u) + w} \tag{6.590}$$

Table 6.6: Summary of discrete-time extended Kalman filter (EKF).

System model Measurement	$x(k+1) = f(x(k), u(k)) + \Gamma\, w(k); \quad w(k) \sim N(0, Q(k))$ $z(k) = h(x(k)) + v(k); \quad v(k) \sim N(0, R(k))$
Initial conditions	$\hat{x}(0) = x_0; \qquad \hat{X}(0) = X_0$
State estimate propagation	$\overline{x}(k+1) = f(\hat{x}(k), u(t))$
Error covariance propagation	$\overline{X}(k+1) = \Phi(k)\, \hat{X}(k)\, \Phi^T(k) + \Gamma(k)\, Q(k)\, \Gamma^T(k)$
Gain matrix	$K(k) = \overline{X}(k) H^T(k) \left[H(k) \overline{X}(k) H^T(k) + R(k) \right]^{-1}$
State estimate update	$\hat{x}(k) = \overline{x}(k) + K(k)\, [z(k) - h(\overline{x}(k))]$
Error covariance update	$\hat{X}(k) = [I - K(k)H(k)]\, \overline{X}(k)\, [I - K(k)H(k)]^T + K(k)\, R(k)\, K^T(k)$
Definitions	$\Phi(k) = \left. \frac{\partial f(\cdot)}{\partial x(k)} \right\|_{x(k)=\hat{x}(k)} \qquad H(k) = \left. \frac{\partial h(\cdot)}{\partial x(k)} \right\|_{x(k)=\hat{x}(k)}$

where $\xi = [x^T, \theta^T]^T$ is the augmented state vector, $w = [w_1^T, \eta^T]^T$ and

$$\mathcal{F}(\xi, u) = \begin{pmatrix} f(x, u, \theta) \\ 0 \end{pmatrix} \tag{6.591}$$

Furthermore, we assume that the measurement equation can be written:

$$\boxed{z = \mathcal{H}(\xi) + v} \tag{6.592}$$

where $z \in \mathbb{R}^m$. The discrete-time extended Kalman filter algorithm in Table 6.6 can then be applied to estimate $\xi = [x^T, \theta^T]^T$ in (6.590) by means of the measurement (6.592). For details on the implementation issues see Gelb et al. (1988).

Off-Line Parallel Processing

In order to improve the performance of the parameter estimator we can measure the same quantity N times for different excitation sequences. Moreover, we assume that the input $u_i \in \mathbb{R}^r$ corresponds to the states $x_i \in \mathbb{R}^n$ and measurement $z_i \in \mathbb{R}^m$ for $(i = 1....N)$. Under the assumption of constant parameters, the parameter vector $\theta \in \mathbb{R}^p$ will be the same for all these subsystems. Moreover we can express this mathematically as:

$$\begin{aligned} \dot{x}_1 &= f(x_1, u_1, \theta) + w_1 \\ \dot{x}_2 &= f(x_2, u_2, \theta) + w_2 \\ &\vdots \\ \dot{x}_N &= f(x_N, u_N, \theta) + w_N \\ \dot{\theta} &= \eta \end{aligned} \tag{6.593}$$

with measurements:

$$\begin{aligned} z_1 &= h_1(x_1, \theta) + v_1 \\ z_2 &= h_2(x_2, \theta) + v_2 \\ &\vdots \\ z_N &= h_N(x_N, \theta) + v_N \end{aligned} \tag{6.594}$$

Hence, we can write this system in augmented state-space form as:

$$\dot{\xi} = \mathcal{F}(\xi, u) + w \tag{6.595}$$

$$z = \mathcal{H}(\xi) + v \tag{6.596}$$

where $\xi = [x_1^T, x_2^T, ..., x_N^T, \theta^T]^T$, $u = [u_1^T, u_2^T, ..., u_N^T]^T$, $z = [z_1^T, z_2^T, ..., z_N^T]^T$ and

$$\mathcal{F}(\xi, u) = \begin{pmatrix} f(x_1, u_1, \theta) \\ f(x_2, u_2, \theta) \\ \vdots \\ f(x_N, u_N, \theta) \\ 0 \end{pmatrix} \qquad \mathcal{H}(\xi) = \begin{pmatrix} h(x_1, \theta) \\ h(x_2, \theta) \\ \vdots \\ h(x_N, \theta) \end{pmatrix} \tag{6.597}$$

We now observe that dim $x = Nn + p$, dim $u = Nr$ and dim $z = Nm$. It is then clear that we have obtained more information about the system. Increased information improves parameter identifiability and reduces the possibility for parameter drift. However it should be noted that parallel processing implies that the parameters estimation must be performed off-line.

For most ship applications significant performance improvement is obtained already for $N = 2$, see Abkowitz (1975, 1980) and Hwang (1980). We will illustrate this by considering a case study of a dynamically positioned ship.

Case Study: Identification of a Dynamically Positioned Ship

Identification of a dynamically positioned ship is difficult since a low-speed model of the ship, that is $U \approx 0$, should be estimated. Low speed implies that the ship will not be persistently excited, which again results in parameter drift. If the speed is increased additional terms due to Coriolis, quadratic damping etc., must also be estimated. A dynamically positioned ship can be described by the following non-dimensional model (Bis-system) in surge, sway and yaw (see Section 6.7):

$$\boldsymbol{M}''\dot{\boldsymbol{\nu}}'' + \boldsymbol{D}''\boldsymbol{\nu}'' = \boldsymbol{T}''\boldsymbol{K}''\boldsymbol{u}'' \tag{6.598}$$

where $\boldsymbol{\nu}'' = [u'', v'', r'']^T$ and $\boldsymbol{u}''$ is a control vector of signed squared propeller pitch ratios, that is $u_i'' = |p_i'' - p_{i0}''|(p_i'' - p_{i0}'')$ $(i = 1...r)$ where p_{i0}'' is the propeller pitch ratio off-set. The structures of the matrices are:

$$\boldsymbol{M}'' = \begin{bmatrix} 1 - X_{\dot{u}}'' & 0 & 0 \\ 0 & 1 - Y_{\dot{v}}'' & x_G'' - Y_{\dot{r}}'' \\ 0 & x_G'' - Y_{\dot{r}}'' & k_z^2 - N_{\dot{r}}'' \end{bmatrix} \quad \boldsymbol{D}'' = \begin{bmatrix} -X_u'' & 0 & 0 \\ 0 & -Y_v'' & -Y_r'' \\ 0 & -N_v'' & -N_r'' \end{bmatrix} \tag{6.599}$$

where $\boldsymbol{M}'' = (\boldsymbol{M}'')^T > \boldsymbol{0}$ and $\boldsymbol{D}'' > \boldsymbol{0}$. In the case study we will consider a supply vessel with thruster configuration matrix:

$$\boldsymbol{T}'' = \begin{bmatrix} 1.0000 & 1.0000 & 0 & 0 & 0 & 0.0000 \\ 0 & 0 & 1.0000 & 1.0000 & 1.0000 & 1.0000 \\ 0.0472 & -0.0472 & -0.4108 & -0.3858 & 0.4554 & 0.3373 \end{bmatrix} \tag{6.600}$$

corresponding to two main propellers (u_1'' and u_2''), two aft tunnel thrusters (u_3'' and u_4''), one bow thruster (u_5'') and one azimuth thruster (u_6''). Hence, the thruster forces are given by:

$$\boldsymbol{K}'' = \text{diag}\{K_1'',\ K_2'',\ K_3'',\ K_4'',\ K_5'',\ K_6''\} \tag{6.601}$$

In order to improve the convergence of the parameter estimator Fossen et al. (1995) propose using several off-line measurement series generated by a number of predefined maneuvers. For instance, it is advantageous to decouple the surge mode from sway and yaw modes. This is motivated by the block diagonal structure of $\boldsymbol{M}''$ and $\boldsymbol{D}''$.

Sea Trials

The following two decoupled sea trials are proposed:

(1) **uncoupled surge:** the ship is only allowed to move in surge (constant heading) by means of the main propellers. Two maneuvers should be performed both satisfying ($|u| \leq u_{\max}$, and v and r small).

(2) coupled sway and yaw: the ship should perform two maneuvers; one in sway ($|v| \leq v_{\max}$ and r small) and one in yaw ($|r| \leq r_{\max}$ and v small) by means of the tunnel and the azimuth thrusters. It is important that u is kept small during both maneuvers. Moreover the coupling terms uv, ur and vr should all be small to obtain best results.

This implies that four sea trials must be performed. Hence, we first identify the surge dynamics:

$$(1 - X''_{\dot{u}})\dot{u}'' - X''_u u'' = K''_1 u''_1 + K''_2 u''_2 \tag{6.602}$$

$$\dot{x}'' = u'' \tag{6.603}$$

by means of two measurement series. The estimated parameters in surge are *frozen* and used as input for the second identification scheme, that is coupled sway and yaw identification. Since the ship is allowed to change heading during this maneuver we must include the kinematic equation:

$$\dot{\eta}'' = J''\,\nu'' \tag{6.604}$$

where $\eta'' = [x'', y'', \psi'']^T$ and:

$$J'' = \begin{bmatrix} \cos\psi'' & -\sin\psi'' & 0 \\ \sin\psi'' & \cos\psi'' & 0 \\ 0 & 0 & 1 \end{bmatrix} \tag{6.605}$$

Notice that $\psi'' = \psi$. It is convenient to rewrite this model in terms of the vessel *momentum*:

$$h'' = M''\,\nu'' \tag{6.606}$$

Based on this definition Fossen et al. (1995) propose using the following model for parameter estimation:

$$\dot{h}'' = A''_h(\theta'')\,h'' + T''\,K''(\theta'')u'' + b_h \tag{6.607}$$

$$\dot{\eta}'' = J''M''^{-1}_0\,h'' + w_\eta \tag{6.608}$$

$$\dot{b}_h = w_h \tag{6.609}$$

$$\dot{\theta}'' = w_\theta \tag{6.610}$$

where w_h, w_η and w_θ are zero-mean Gaussian white noise processes, b_h is a slowly-varying parameter representing unmodelled dynamics and disturbances, θ'' is the parameter vector to be estimated and M''_0 is an estimate of M''. Hence, we can write the resulting model in the form:

$$\dot{x}_1 = f(x_1, u_1, \theta) + w_1 \tag{6.611}$$
$$\dot{x}_2 = f(x_2, u_2, \theta) + w_2 \tag{6.612}$$
$$\dot{\theta} = w_\theta \tag{6.613}$$

where $x_i = [h_i^T, \eta_i^T, b_{hi}^T]^T$, $w_i = [G_i w_{\eta i}^T, w_{hi}^T]^T$ $(i = 1, 2)$ and with obvious definition of f. If we measure position (x, y) and heading (ψ), we can write:

$$z_1 = H_1 x_1 + v_1 \tag{6.614}$$
$$z_2 = H_2 x_2 + v_2 \tag{6.615}$$

The matrix M_0'' is a constant matrix based on *a priori* information. Several techniques can be used to estimate $X_{\dot{u}}'', Y_{\dot{v}}'', N_{\dot{r}}''$ and $Y_{\dot{r}}''$. For the supply ship in this case study M_0'' was estimated to be:

$$M_0'' = \begin{bmatrix} 1 - \hat{X}_{\dot{u}}'' & 0 & 0 \\ 0 & 1 - \hat{Y}_{\dot{v}}'' & x_G'' - \hat{Y}_{\dot{r}}'' \\ 0 & x_G'' - \hat{Y}_{\dot{r}}'' & (k_z'')^2 - \hat{N}_{\dot{r}}'' \end{bmatrix} \approx \begin{bmatrix} 1.1274 & 0 & 0 \\ 0 & 1.8902 & -0.0744 \\ 0 & -0.0744 & 0.1278 \end{bmatrix} \tag{6.616}$$

The unknown parameters $\theta'' = [\theta_1'', ..., \theta_9'']^T$ are defined according to:

$$A_h'' = \begin{bmatrix} \theta_1'' & 0 & 0 \\ 0 & \theta_2'' & \theta_3'' \\ 0 & \theta_4'' & \theta_5'' \end{bmatrix}; \qquad K'' = \text{diag}\{\theta_6'', \theta_6'', \theta_7'', \theta_7'', \theta_8'', \theta_9''\} \tag{6.617}$$

The system (6.607) can be related to a standard state-space model:

$$\dot{\nu}'' = A''\nu'' + Bu'' \tag{6.618}$$

by defining:

$$A'' = M_0''^{-1} A_h'' M_0''; \qquad B'' = M_0''^{-1} T'' K'' \tag{6.619}$$

The performance of the EKF is shown in Figures 6.58 and 6.59. The estimated model is:

Identified Momentum Equation:

$$\hat{A}_h'' = \begin{bmatrix} -0.0318 & 0 & 0 \\ 0 & -0.0602 & 0.0618 \\ 0 & -0.0075 & -0.2454 \end{bmatrix} \tag{6.620}$$

$$\hat{K}'' = \text{diag}\{0.0093, 0.0093, 0.0020, 0.0020, 0.0028, 0.0026\} \tag{6.621}$$

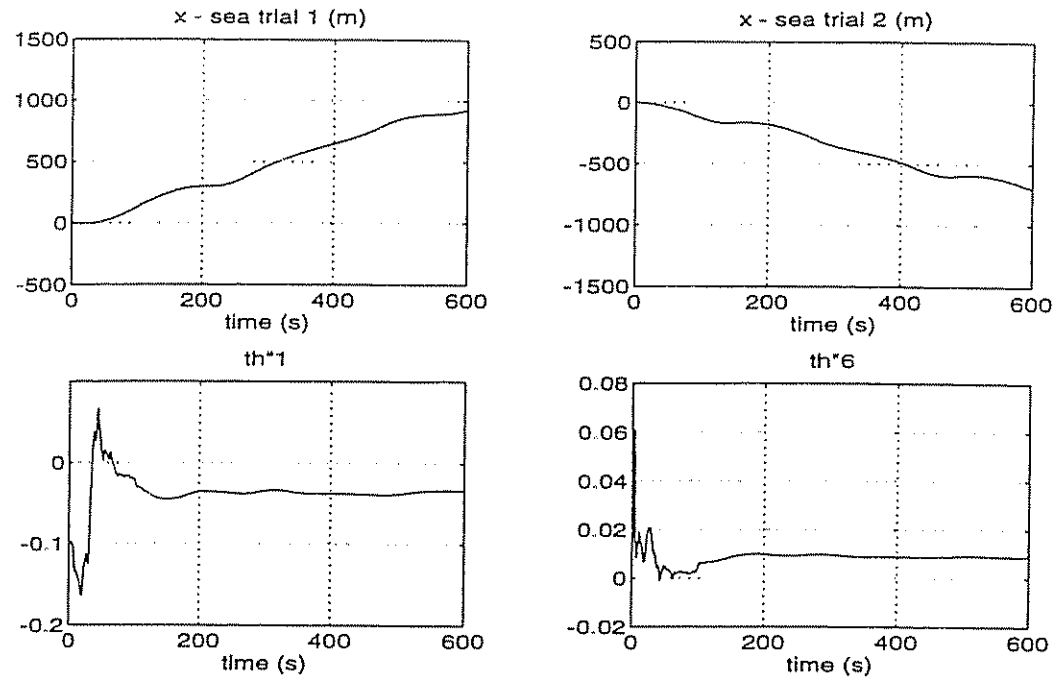

Figure 6.58: Full scale experiment with a supply vessel (uncoupled surge), reproduced by permission of ABB Industry, Oslo.

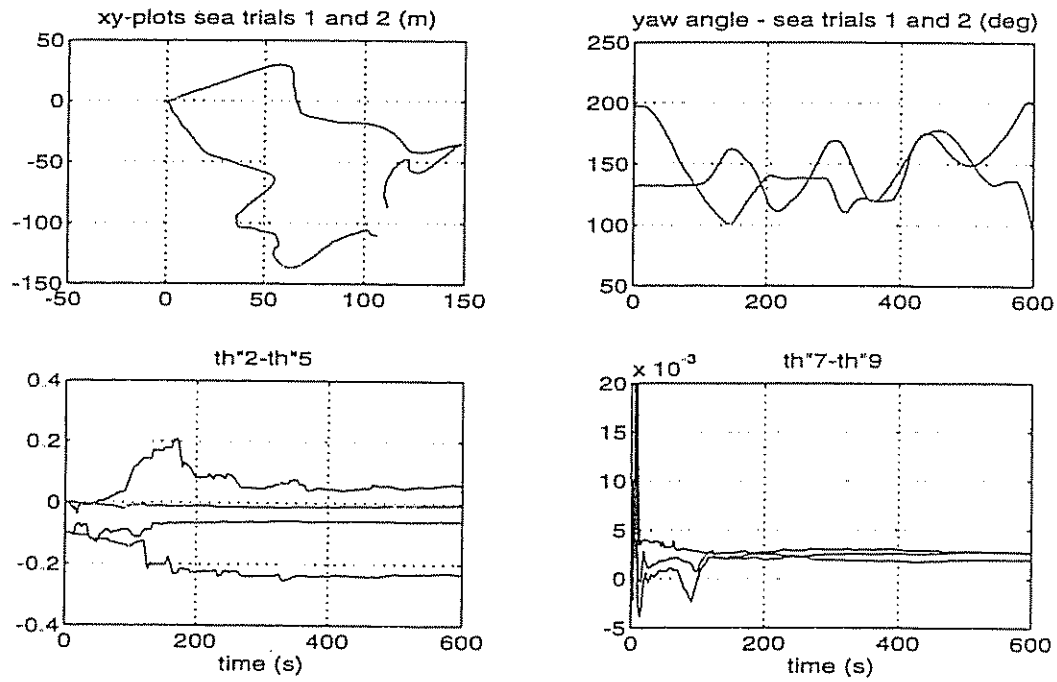

Figure 6.59: Full scale experiment with a supply vessel (coupled sway and yaw), reproduced by permission of ABB Industry, Oslo.

Identified State-Space Model:

$$\hat{A}'' = \begin{bmatrix} -0.0318 & 0 & 0 \\ 0 & -0.0628 & -0.0030 \\ 0 & -0.0045 & -0.2428 \end{bmatrix} \tag{6.622}$$

$$\hat{B}'' = \begin{bmatrix} 0.0082 & 0.0082 & 0 & 0 & 0 & 0 \\ 0.0001 & -0.0001 & 0.0008 & 0.0008 & 0.0020 & 0.0017 \\ 0.0035 & -0.0035 & -0.0059 & -0.0055 & 0.0113 & 0.0079 \end{bmatrix} \tag{6.623}$$

6.8.8 Biased Estimates: Slowly-Varying Disturbances

It is necessary to remove constant or slowly-varying disturbances from the model to ensure that the parameter estimates converge to their true values. This can be done by *high-pass filtering* of the signal vector (regressor), that is:

$$y(s) = H(s)\, u(s) + w(s) \quad \overset{\text{high-pass}}{\longrightarrow} \quad y_f(s) = H(s)\, u_f(s) \tag{6.624}$$

Here $w(s)$ is a slowly-varying disturbance and $y_f(s)$ and $u_f(s)$ are the high-pass filtered signal vectors. Another approach is to include an additional constant in the dynamic model to be estimated with the parameters. For instance,

$$T\dot{r}(t) + r(t) = K\,\delta(t) + r_b\,1 \tag{6.625}$$

Here r_b is an unknown constant parameter (rate bias) to be estimated together with T and K and 1 is a known signal to be included in the regression vector.

An attractive solution intended for discrete-time models is to rewrite the system model in terms of *differenced data*. Consider the discrete-time state-space model:

$$x(k+1) = \Phi\, x(k) + \Delta\, u(k) + \Gamma\, w(k) \tag{6.626}$$

where $w(k) = w(k-1)$ is assumed to be constant or at least slowly-varying compared to the x-dynamics. Hence, we can define the differenced data vectors:

$$\tilde{x}(k) = x(k) - x(k-1) \tag{6.627}$$

$$\tilde{u}(k) = u(k) - u(k-1) \tag{6.628}$$

which yields:

$$\tilde{x}(k+1) = \Phi\, \tilde{x}(k) + \Delta\, \tilde{u}(k) \tag{6.629}$$

This model describes the relation between the differenced data rather the original input and output data. We now notice that the disturbance term is eliminated in this model representation while the sampling time is unchanged, that is Φ and Δ are unchanged. For details see Söderström and Stoica (1989).

6.9 Conclusions

A brief introduction to automatic control systems design for ships has been given. Both model-based and conventional control systems design (PID-control) have been discussed, together with a large number of examples and full scale experiments. The emphasis has been on discussing systems for course control (course-keeping and turning), track-keeping systems, dynamic positioning (DP) systems, rudder-roll stabilization (RRS) and speed-propulsion control. Besides this an introduction to filtering of 1st-order wave disturbances (wave filtering) has been made. The last part of the chapter discusses system identification (SI) techniques intended for model-based and self-tuning ship control. This is particular useful when *a priori* information about the model parameters is difficult to obtain. Direct adaptive control is also discussed in some of the sections above.

References to articles discussing ship control systems design are included under each section to increase readability. The interested reader is, however, recommended to consult the proceedings of the *Ship Control Systems Symposium* (SCSS), the *IFAC Workshop on Control Applications in Marine Systems* (CAMS) and the *International Conference on Maneuvering and Control of Marine Craft* (MCMC) for applications in the field of ship control systems design.

6.10 Exercises

6.1 Speed control system design.

(a) Consider Figure 6.17. Compute estimates for $T_{|n|n}$, $T_{|n|V_a}$, $Q_{|n|n}$ and $Q_{|n|V_a}$ by using a linear approximation for K_T and K_Q. Assume that $\rho = 1025$ (kg/m^3) and $D = 6$ (m).

(b) Plot thrust T and torque Q as a function propeller revolution n (rps) for advance speeds $V_a = \{4, 8, 12\}$ (m/s).

(c) Let both the wake fraction number w and thrust deduction number t be 0.1. Consider a diesel engine given by:

$$\frac{Q_m}{Y}(s) = \frac{1.0 \cdot 10^7 \, \exp(-(0.5/n)s)}{1 + (5.7/n)s}$$

where n is in (rps). The inertia I_m (included added inertia) of all rotating parts including the propeller is $2.5 \cdot 10^5$ (kgm^2). The surge motion of the ship can be described by:

$$(m - X_{\dot{u}})\,\dot{u} = X_{|u|u}\,|u|u + (1 - t)\,T$$

where $m = 3.6 \cdot 10^8$ (kg), $X_{\dot{u}} = -0.05\,m$ (kg), $X_{|u|u} = -4.5 \cdot 10^3$ (kg/m). Design a governor for this system by using the estimated propeller thrust and torque from (a). Friction torques are assumed negligible. Assume that both n and Y are measured. Simulate the control law for set-point changes in n_d.

(d) Assume that n, Y and u are measured. Design a speed controller for the system under (c). Simulate the speed controller in the time-domain.

6.2 Show that the optimal solution to the criterion of Van Amerongen and Van Nauta Lempke implies that the controller gains should be chosen as:

$$\begin{aligned} K_p &= \sqrt{\frac{1}{\lambda_2}} \\ K_d &= \frac{L}{U}\,\frac{\sqrt{1+2K_pK'T'+K'^2(U/L)^2\,(\lambda_1/\lambda_2)}-1}{K'} \end{aligned}$$

by using the results of Appendix D.

6.3 Consider the combined optimal and feedforward controller in Section 6.4.2. Show that:

$$\ddot{e} = -\frac{1}{T}\dot{e} - \frac{K}{T}\,\delta_{LQ}$$

Derive an optimal control law:

$$\delta_{LQ} = K_p\, e + K_d\, \dot{e}$$

by minimizing:

$$\min J = \frac{1}{2}\int_0^T (e^2 + \lambda_1\, \dot{e}^2 + \lambda_2\, \delta_{LQ}^2)\, d\tau$$

where $\lambda_1 > 0$ and $\lambda_2 > 0$.

6.4 Show that the adaptive control law of Theorem 6.2 with the tracking error

$$s = \dot{\tilde{\psi}} + 2\,\lambda\,\tilde{\psi} + \lambda^2 \int_0^t \tilde{\psi}(\tau)\, d\tau$$

yields a stable system.

6.5 Use the results in Appendix D to derive the expressions for K_p and K_d which minimizes criterion (6.209).

6.6 The control bandwidth of a system with loop transfer function $l(s)$ is defined as the frequency ω_b (rad/s) at which:

$$|\, l(j\omega)\,|_{\omega=\omega_b} = \frac{\sqrt{2}}{2}$$

or equivalently,

$$20\log\,|\, l(j\omega)\,|_{\omega=\omega_b} = -3\ (\mathrm{dB})$$

Use this definition to show that the control bandwidth of a 2nd-order system:

$$l(s) = \frac{\omega_n^2}{s^2 + 2\,\zeta\,\omega_n\,s + \omega_n^2}$$

with natural frequency ω_n and relative damping ratio ζ is:

$$\omega_b = \omega_n \sqrt{1 - 2\,\zeta^2 + \sqrt{4\,\zeta^4 - 4\,\zeta^2 + 2}}$$

Compute the ratio ω_b/ω_n for ζ equal to $\sqrt{2}/2$, 0.8, 1.0 and 2.0.

6.7 Show that the steering criterion of Norrbin can be written:

$$\min J = \frac{\alpha}{T} \int_0^T T_{loss}\, d\tau$$

where $\alpha > 0$ and:

$$T_{loss} = \left[\frac{(m + X_{vr})K_v}{K} + X_{rr} + m x_G \right] \omega_r^2\, \varepsilon^2 + X_{cc\delta\delta} c^2 \delta^2$$

Define a weighting factor λ such that this criterion can be written as (6.177).

6.8 Consider a ship given by $T' = 0.5$ and $K' = 3.0$ (Nomoto's 1st-order model). The length of the ship is 150 (m) while the service speed is 5 (m/s).

(a) Design a PID-control law for the ship based on feedback from ψ_L and r_L (HF wave disturbances can be neglected). Simulate the control law in the time domain.

(b) Assume that the ship is exposed to 1st-order wave disturbances given by:

$$\psi_H(s) = \frac{K_w\, s}{s^2 + 2\,\zeta\,\omega_e\, s + \omega_e^2}\, w(s)$$

where $\zeta = 0.05$, $\omega_e = 0.6$ (rad/s), w is white noise and K_w is chosen such that $|\psi_H(t)| \leq 8$ (deg). Design a Kalman filter for the ship-wave system. Assume that the only measurement is $\psi = \psi_L + \psi_H + v$ where $|v(t)| \leq 0.1$ (deg) is white noise.

(c) Simulate the course-keeping controller under (a) with feedback from the Kalman filter estimates $\hat{\psi}_L$ and $\hat{r}_L$. Comment on the results.

(d) Design a 2nd-order reference model. Simulate turning responses for the PID-control by using the output from the 2nd-order reference model. The input to the reference model should be 5, 10 and 30 degrees. All course-changing maneuvers should be performed without overshoot.

(e) Include a rudder rate limiter in the control loop such that $\dot{\delta}_{\max} = 3$ (deg/s). Does this affect the simulation results ? If yes, modify your design to handle rudder rate saturation.

(f) Is the autopilot robust for variations in ζ, ω_e, U, K' and T' ?

6.9 Show that it is impossible to control both the roll and yaw modes of a ship with a single rudder if ϕ_d (desired roll angle) and ψ_d (desired yaw angle) are non-zero and constant.

6.10 Derive the symbolic expression for $A(z^{-1})$, $B(z^{-1})$ and $C(z^{-1})$ in Example 6.11. Write a simulation program for estimation of the model parameters in terms of RML.

Chapter 7

Control of High-Speed Craft

The development of high-speed marine vehicles for passenger and cargo transportation as well as naval applications is expected to be of increasing importance in the future. Already several ship builders have managed to produce high-speed vehicles capable of doing 50–60 knots with satisfactory passenger comfort in terms of wave-induced vibrations. Many new advanced concepts for vibration damping have been suggested in the last decades. However, we will restrict our discussion to two types of vessels:

- Surface Effect Ships
- Foilborne Catamarans

Modeling, maneuverability and control systems design of SES and foilborne catamarans will be discussed in Sections 7.1 and 7.2, respectively.

7.1 Ride Control of Surface Effect Ships

by Asgeir Sørensen[1]

Surface effect ships (SES) have a catamaran-type hull form which contains an air cushion with flexible structures called seals or skirts at the fore and aft ends of the air cushion. Pressurized air is supplied into the cushion by a lift fan system and is retained by rigid side-hulls and flexible skirt systems at the bow and the stern. The excess pressure lifts the craft and thereby reduces its calm water resistance. The major part of the craft weight (about 80 %) is supported by the excess air cushion pressure, while the rest of the weight is supported by the buoyancy of the side-hulls. The most common stern seal system is the flexible rear bag system, consisting of a loop of flexible material, open at both sides with one or two internal webs restraining the aft face of the loop into a two or three loop configuration. Pressurized air from the aft of the air cushion is supplied into the bag system. The bag pressure is about 10–15 % higher than the air cushion pressure. A major advantage of SES over hovercraft is that the rigid

[1] ABB Corporate Research, Oslo, Norway

side-hulls permit the use of water propulsion; either waterjets or propellers can be used. The small draft of the side-hulls in the water is also sufficient to produce the necessary lateral forces affecting the maneuverability and the stability of the craft in the horizontal plane. The side-hulls are designed with sufficient buoyancy for the SES to float with an airgap between the wetdeck and the free surface when the lift fan system is turned off, in the same way as conventional catamarans.

SES is known to offer a high-quality ride in heavy sea states, compared with conventional catamarans. However, in low and moderate sea states there are problems with discomfort due to high-frequency vertical accelerations induced by resonances in the pressurized air cushion. A high-performance ride control system is required in order to achieve satisfactory human comfort and crew workability. To develop such a ride control system it is essential to use a rational dynamic model containing the significant dynamics. Previous ride control systems have been based on the coupled equations of motion in heave and pitch as derived by Kaplan and Davis (1974, 1978) and Kaplan, Bentson and Davis (1981). Their work was based on the assumption that the major part of the wave-induced loads from the sea was imparted to the craft as dynamic uniform air pressure acting on the wetdeck, whereas a minor part of the wave-induced loads from the sea was imparted to the craft as dynamic water pressure acting on the side-hulls. This work was further extended by Sørensen, Steen and Faltinsen (1992, 1993), Sørensen (1993) and Steen (1993) who included the effect of spatial pressure variations in the air cushion. It was found that acoustic resonances in the air cushion caused by incident sea waves resulted in significant vertical vibrations. A distributed model was derived from a boundary value problem formulation where the air flow was represented by a velocity potential subject to appropriate boundary conditions on the surfaces enclosing the air cushion volume. A solution was found using the Helmholtz equation in the air cushion region. In Sørensen and Egeland (1993) and Sørensen (1993) a ride control system for active damping of the vertical accelerations induced by resonances of both the dynamic uniform and the spatially varying pressure in the air cushion has been proposed. The basic design principles of such a ride control system will now be presented.

7.1.1 Mathematical Modeling

The mathematical model of the heave and pitch motions of SES as presented in Sørensen (1993) is used to derive the ride control system, which provides active damping of both the dynamic uniform pressure and the acoustic resonances in the air cushion. A moving coordinate frame is defined so that the origin is located in the mean water plane below the center of gravity with the x-, y- and z-axes oriented positive forwards, to the port, and upwards, respectively (see Figure 7.1). This type of coordinate frame is commonly used in marine hydrodynamics to analyze vertical motions and accelerations (Faltinsen, Helmers, Minsaas and Zhao 1991). The equations of motion are formulated in this moving frame. Translation along the z-axis is called heave and is denoted $\eta_3(t)$. The rotation angle around

the y-axis is called pitch and is denoted $\eta_5(t)$. Heave is defined positive upwards, and pitch is defined positive with the bow down. We are mainly concerned with the high-frequency vertical vibrations. In this frequency range the hydrodynamic loads on the slender side-hulls are of minor importance. Strip theory is used and hydrodynamic memory effects are assumed to be negligible due to the high frequency of oscillation. Furthermore, infinite water depth is assumed.

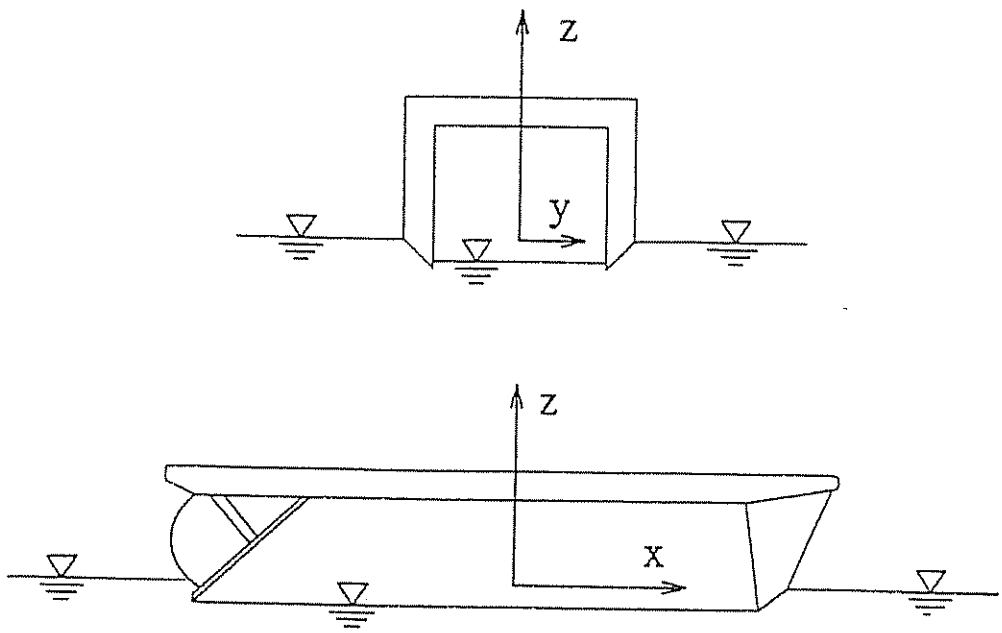

Figure 7.1: Surface effect ship (SES) - coordinate frame.

The craft is assumed to be advancing in regular head sea waves. The waves are assumed to have a small wave slope with circular frequency ω_0. For head sea ($\beta = 180^o$), Formula (3.63) for the circular frequency of encounter ω_e takes the form:

$$\omega_e = \omega_0 + k\,U \overset{\omega_0^2 = k\,g}{=} \omega_0 + k\,\frac{\omega_0^2\,U}{g} \tag{7.1}$$

Here $k = 2\pi/\lambda$ is the wave number, λ is the sea wave length and U is the craft speed. The circular frequency of encounter ω_e is the apparent wave frequency as experienced on the craft advancing at the speed U in head sea. The incident surface wave elevation $\zeta(x,t)$ for regular head sea is defined as:

$$\zeta(x,t) = \zeta_a \sin(\omega_e t + kx) \tag{7.2}$$

where ζ_a is the wave elevation amplitude. In the case of calm water the wave elevation amplitude is equal to zero. The water waves are assumed to pass through the air cushion undisturbed. For simplicity a rectangular cushion is considered at the equilibrium condition with height h_0 , beam b and length L, reaching from $x = -L/2$ at the stern to $x = L/2$ at the bow. The beam and the height of the air

cushion are assumed to be much less than the length. Hence, a one-dimensional ideal and compressible air flow in the x-direction is assumed. This means that the longitudinal position of the center of air cushion pressure is assumed to coincide with the origin of the coordinate frame. The air cushion area is then given by $A_c = Lb$. The total pressure $p_c(x,t)$ in the air cushion is represented by:

$$p_c(x,t) = p_a + p_u(t) + p_{sp}(x,t) \tag{7.3}$$

where p_a is the atmospheric pressure, $p_u(t)$ is the uniform excess pressure and $p_{sp}(x,t)$ is the spatially varying pressure. The basic thermodynamic variations in the air cushion are assumed to be adiabatic. When neglecting seal dynamics, aerodynamics and viscous effects, the external forces are given by the water pressure acting on the side-hulls and by the dynamic air cushion pressure acting on the wetdeck. It is assumed that the dynamic cushion pressure is excited by incoming sea wave disturbances. In the absence of waves, the stationary excess pressure in the air cushion is equal to the equilibrium excess pressure p_0. The non-dimensional uniform pressure variation $\mu_u(t)$ and the non-dimensional spatial pressure variation $\mu_{sp}(x,t)$ are defined according to:

$$\mu_u(t) = \frac{p_u(t) - p_0}{p_0} \qquad \mu_{sp}(x,t) = \frac{p_{sp}(x,t)}{p_0} \tag{7.4}$$

The volumetric air flow into the air cushion is given by a linearization of the fan characteristic curve about the craft equilibrium operating point. It is assumed that there are q fans with constant revolutions per minute feeding the cushion, where fan i is located at the longitudinal position x_{Fi}. The volumetric air flow out of the air cushion is proportional to the leakage area $A_L(t)$, which is defined as:

$$A_L(t) = A_0 + A^{RCS}(t) \tag{7.5}$$

Here $A_L(t)$ represents the total leakage area and is expressed as the sum of an equilibrium leakage area A_0 and a controlled variable leakage area $A^{RCS}(t)$. The equilibrium leakage area:

$$A_0 = A_0^{AP} + A_0^{FP} \tag{7.6}$$

will be divided into leakage areas under the bow and stern region or more precisely under the stern and bow seals. A_0^{AP} is the stern equilibrium leakage area at the aft perpendicular ($x = -L/2$) and A_0^{FP} is the bow equilibrium leakage area at the fore perpendicular ($x = L/2$). The controlled leakage area $A^{RCS}(t)$ of the ride control system is written:

$$A^{RCS}(t) = \sum_{i=1}^{r} \left(A_{0i}^{RCS} + \Delta A_i^{RCS}(x_{Si}, t) \right) \tag{7.7}$$

Here r is the number of louvers. The louvers are variable vent valves located at the longitudinal position $x = x_{Li}$, which change the area of openings in

the wetdeck for the purpose of leakage control. A_{0i}^{RCS} is defined as the mean operating value or bias of the leakage area and $\Delta A_i^{RCS}(x_{Si}, t)$ is defined as the commanded variable leakage area of louver i. Pressure sensors are used to measure the pressure variations in the air cushion. Sensor i is placed at the longitudinal position $x = x_{Si}$. Dynamic leakage areas under the side-hulls and the seals due to craft motion are assumed to be negligible in this analysis. This type of leakage is a hard nonlinearity and can be analyzed using describing functions (Gelb and Velde 1968). Computer simulations done by Sørensen et al. (1992) indicate that the dynamic leakage terms due to craft motion can be neglected for small amplitudes of sea wave disturbances and associated small amplitudes of heave and pitch motions, as long as the sealing ability is good.

Equations of Motion and Dynamic Cushion Pressure

The coupling between the spatially varying pressure and the dynamic uniform pressure is assumed to be negligible. For simplicity (without loss of generality), off-diagonal hydrodynamic and hydrostatic coupling terms like added mass A_{ij}, linear damping B_{ij} and restoring terms C_{ij} will be set to zero.

1. Uniform Pressure Equation

The uniform pressure equation is written:

$$K_1\,\dot{\mu}_u(t) + K_3\,\mu_u(t) + \rho_{c0}\,A_c\,\dot{\eta}_3(t) = K_2 \sum_{i=1}^{r} \Delta A_i^{RCS}(x_{Si}, t) + \rho_{c0}\,\dot{V}_0(t) \qquad (7.8)$$

where

$$\mathrm{K_1} = \frac{\rho_{c0}\,\mathrm{h_0}\,\mathrm{A_c}}{\gamma\left(1 + \frac{\mathrm{p_a}}{\mathrm{p_0}}\right)} \qquad \mathrm{K_2} = \rho_{c0}\,\mathrm{c_n}\sqrt{\frac{2\mathrm{p_0}}{\rho_a}} \qquad \mathrm{K_3} = \rho_{c0}\sum_{i=1}^{q}\left(\frac{\mathrm{Q_{0i}}}{2} - \mathrm{p_0}\left.\frac{\partial \mathrm{Q}}{\partial \mathrm{p}}\right|_{0i}\right) \qquad (7.9)$$

Here ρ_a is the air density at the atmospheric pressure p_a, ρ_{c0} is the density of the air at the equilibrium pressure p_0, γ is the ratio of specific heat for air, Q_{0i} is the equilibrium air flow rate of fan i when $p_u(t) = p_0$ and $(\partial Q/\partial p)\,|_{0i}$ is the corresponding linear fan slope about the craft equilibrium operating point Q_{0i} and p_0 of fan i. c_n is the orifice coefficient varying between 0.61 and 1 depending of the local shape on the edges of the leakage area. In the numerical simulations $c_n = 0.61$ is used.

The time derivative of $V_0(t)$ is the wave volume pumping, and it is found in the following way for regular head sea waves:

$$\dot{V}_0(t) = b\int_{-L/2}^{L/2} \zeta(x,t)\,dx = A_c\,\zeta_a\,\omega_e\,\frac{\sin(kL/2)}{kL/2}\,\cos(\omega_e t) \qquad (7.10)$$

2. Spatially Varying Pressure Equation

The effect of spatial pressure variations in the air cushion can be analyzed in terms of Helmholtz's equation. Sørensen (1993) has derived a distributed model from a boundary value formulation. It can be shown that the following mode shape function (eigenfunction) will satisfy the boundary conditions on the seals:

$$r_j(x) = \cos\frac{j}{\pi}\left(x + \frac{L}{2}\right) \qquad x \in [-L/2,\ L/2] \tag{7.11}$$

for $(j = 1, 2, 3, \ldots)$. This implies that we can define the corresponding eigenfrequency ω_j for mode j as:

$$\omega_j = c\,\frac{j\pi}{L} \tag{7.12}$$

Here c is the speed of sound in air. Hence, we can write the spatially varying pressure equation as:

$$\mu_{sp}(x,t) = \sum_{j=1}^{\infty} \dot{p}_j(t)\, r_j(x) \qquad x \in [-L/2,\ L/2] \tag{7.13}$$

Odd modes around the center of pressure are described by $(j = 1, 3, 5, \ldots)$,

$$\begin{aligned}\ddot{p}_j(t) + 2\xi_j\,\omega_j\,\dot{p}_j(t) + \omega_j^2\,p_j(t) \\ = -c_{2j}\,\dot{\eta}_5(t) + c_1 \sum_{i=1}^{r} r_j(x_{Li})\,\Delta A_i^{RCS}(x_{Si},t) + \rho_{c0}\,\dot{V}_j(t)\end{aligned} \tag{7.14}$$

where

$$c_1 = \frac{2\,K_2\,c^2}{p_0\,V_{c0}} \qquad c_{2j} = \frac{4\,\rho_{c0}\,L\,c^2}{p_0\,h_0\,(j\pi)^2} \tag{7.15}$$

The wave volume pumping for regular head sea $(j = 1, 3, 5, \ldots)$ is:

$$\dot{V}_j(t) = -\frac{4\,c^2}{p_0\,h_0 L}\,\frac{k\,\cos(kL/2)}{k^2 - (j\pi/L)^2}\,\omega_e\,\zeta_a \sin(\omega_e t) \tag{7.16}$$

Even modes around the center of pressure are described by $(j = 2, 4, 6, \ldots)$,

$$\begin{aligned}\ddot{p}_j(t) + 2\,\xi_j\,\omega_j\,\dot{p}_j(t) + \omega_j^2\,p_j(t) \\ = c_1 \sum_{i=1}^{r} r_j(x_{Li})\,\Delta A_i^{RCS}(x_{Si},t) + \rho_{c0}\,\dot{V}_j(t)\end{aligned} \tag{7.17}$$

where the wave volume pumping for regular head sea $(j = 2, 4, 6, \ldots)$ is:

$$\dot{V}_j(t) = \frac{4\,c^2}{p_0\,h_0\,L}\,\frac{k\,\sin(kL/2)}{k^2 - (j\pi/L)^2}\,\omega_e\,\zeta_a \cos(\omega_e t) \tag{7.18}$$

The relative damping ratio is ($j = 1, 2, 3, 4, \ldots$),

$$\xi_j = \frac{c}{j\pi\, h_0\, b}\left(\frac{K_2}{2\,p_0}A_0 + \frac{K_2}{2\,p_0}\sum_{i=1}^{r} A_{0i}^{RCS}\, r_j^2(x_{Li}) - \rho_{c0}\sum_{i=1}^{q}\left.\frac{\partial Q}{\partial p}\right|_{0i} r_j^2(x_{Fi})\right) \quad (7.19)$$

3. Heave Equation

The heave equation is written:

$$(m + A_{33})\,\ddot{\eta}(t) + B_{33}\,\dot{\eta}_3(t) + C_{33}\,\eta_3(t) - A_c\,p_0\,\mu_u(t) = F_3^e(t) \quad (7.20)$$

Here m is the craft mass and A_{33}, B_{33} and C_{33} are the added mass, damping and spring coefficients in heave. $F_3^e(t)$ represents the hydrodynamic excitation force in heave.

4. Pitch Equation

The pitch equation is written:

$$(I_{55} + A_{55})\,\ddot{\eta}_5(t) + B_{55}\,\dot{\eta}_5(t) + C_{55}\,\eta_5(t) - 2\,p_0\,b\sum_{j=1,3,\ldots}\left(\frac{L}{j\pi}\right)^2 \dot{p}_j(t) = F_5^e(t) \quad (7.21)$$

Here I_{55} is the moment of inertia about the y-axis and A_{55}, B_{55} and C_{55} are the added inertia moment, damping and spring coefficients in pitch. $F_5^e(t)$ represents the hydrodynamic excitation moment in pitch.

Computation of Heave and Pitch Excitations

The excitation force in heave $F_3^e(t)$ and moment in pitch $F_5^e(t)$ are derived from hydrodynamic load calculations on the side-hulls. This is described in more detail by Nestegård (1990), Faltinsen, Helmers, Minsaas and Zhao (1991), Faltinsen and Zhao (1991a, 1991b) and Hoff, Kvålsvold and Zhao (1992). Since we are most concerned with the high-frequency motions, we can simplify these calculations by applying strip theory (Salvesen et al. 1970). Neglecting the effects of transom stern and radiation damping, the hydrodynamic excitation forces on the side-hulls in heave and pitch can be written:

$$F_3^e(t) = 2\,\zeta_a\,\exp(-kd)\frac{\sin(kL/2)}{kL/2}\,(C_{33} - \omega_0\,\omega_e\,A_{33})\,\sin(\omega_e t) \quad (7.22)$$

$$F_5^e(t) = 2\,\zeta_a\,\exp(-kd)\left[\left(\frac{1}{k}\cos(kL/2) - \frac{2}{k^2 L}\sin(kL/2)\right)(C_{33} - \omega_0\,\omega_e\,A_{33}) - U\,\omega_0\,\frac{\sin(kL/2)}{kL/2}\,A_{33}\right]\cos(\omega_e t) \quad (7.23)$$

where d is the draft of the side-hulls. In the case studied here, the submerged parts of side-hulls are assumed to have constant cross-sectional area. Examples of two-dimensional frequency dependent added-mass and wave radiation damping coefficients are found in Chapter 2. However, the control system analysis is based on the assumption of constant 2-D values for A_{ii} and B_{ii}. Moreover, the high-frequency limit of the 2-D added mass coefficient found in Faltinsen (1990) is used. The selected wave radiation damping coefficient in pitch corresponds to the value at the pitch resonance frequency determined from structural mass forces acting on the craft and hydrodynamic forces on the side-hulls. For heave we have chosen the wave radiation damping coefficient at the resonance frequency that will exist without the presence of the excess air cushion pressure. These simplifications are motivated by the fact that the effect of damping is most pronounced around the corresponding resonance frequency.

Discussion of the Mathematical Model

It is evident from (7.20) and (7.21) that the heave and pitch motions are coupled to the dynamic excess pressure in the air cushion region. This is to be expected since the major part of the SES mass is supported by the air cushion excess pressure. The dynamic air cushion pressure is expressed as the sum of the dynamic uniform pressure and the spatially varying pressure. An important question is how many acoustic modes should be included in the mathematical model. Even if the solution is formally presented by an infinite number of acoustic modes, the modeling assumptions will not be valid in the high-frequency range when two- and three-dimensional effects become significant. Then a more detailed numerical analysis is required, like for instance a boundary element or a finite element method. In the following we will use a finite number k of acoustic modes in the mathematical model. The effect of higher order modes is assumed to be negligible.

It is important to note that the air cushion dimensions and the forward speed affect the energy level of the vertical accelerations caused by the acoustic resonances. The acoustic resonance frequencies are inversely proportional to the air cushion length as seen from (7.12). The wave excitation frequency which is given by the circular frequency of encounter $\omega_e = \omega_0 + kU$, increases with the forward speed U. Thus waves of relatively low circular frequency ω_0 may excite the craft in the frequency range of the acoustic resonances when the speed U is high. This may result in more energy in the sea wave excitation around the resonance frequencies, since the maximum sea wave height will tend to increase when the period of the sea waves increases.

The relative damping ratio ξ_j given by (7.19) is an important parameter. As expected the leakage terms and the fan inflow term contribute to increased damping. One should notice that the fan slope $(\partial Q/\partial p)|_{0i}$ is negative. We also observe that the longitudinal placement of the fan and the louver systems strongly affects the relative damping ratio. In the cases of a single-fan system and a single-louver system, it may seem natural to place the fan and the louver in the middle

of the air cushion, that is $x_F = x_L = 0$. However, from (7.19) we observe that the relative damping ratio for the odd modes will be reduced significantly if x_L and x_F are equal to 0. Maximum damping of both the odd and even acoustic resonance modes in the case of a single lift fan system and a single louver system is obtained for x_F and x_L equal to $-L/2$ or $L/2$. The relative damping ratio of the first odd acoustic mode on a 35 m SES will increase from about 0.05 to 0.2 by placing the lift fan system at one of the ends of the air cushion instead in the middle. This gives a significant improvement in ride quality even when the ride control system is turned off. In the same manner the active damping due to the ride control system is maximized by placing the louver system at one of the ends of the air cushion.

7.1.2 State-Space Model

The dynamic system presented in the previous section can be written in standard state-space form according to:

$$\begin{aligned} \dot{\boldsymbol{x}}(t) &= \boldsymbol{A}\,\boldsymbol{x}(t) + \boldsymbol{B}\,\boldsymbol{u}(t) + \boldsymbol{E}\,\boldsymbol{w}(t) \\ \boldsymbol{y}(t) &= \boldsymbol{C}\,\boldsymbol{x}(t) \end{aligned} \tag{7.24}$$

Here the state vector $\boldsymbol{x} \in \mathbb{R}^n$ is defined as:

$$\boldsymbol{x}(t) = [\eta_3,\ \eta_5,\ \dot{\eta}_3,\ \dot{\eta}_5,\ \mu_u,\ p_1,\ p_2, ...,\ p_k,\ \dot{p}_1,\ \dot{p}_2, ...,\ \dot{p}_k]^T \tag{7.25}$$

$\boldsymbol{w} \in \mathbb{R}^{3+k}$ is a disturbance vector defined as:

$$\boldsymbol{w}(t) = [F_3^e,\ F_5^e,\ \dot{V}_0,\ \dot{V}_1,\ \dot{V}_2, ...,\ \dot{V}_k]^T \tag{7.26}$$

Here the time derivatives of V_i for $(i = 0, 1, 2, ..., k)$, and F_3^e and F_5^e are given by (7.16), (7.18), (7.22) and (7.23) while k is the number of acoustic modes. $\boldsymbol{u} \in \mathbb{R}^r$ is the control input vector whereas r is the number of louvers. The elements of $\boldsymbol{u}$ for $(i = 1, 2, ..., r)$ are:

$$u_i(t) = \Delta A_i^{RCS}(x_{Si}, t) \tag{7.27}$$

where $\Delta A_i^{RCS}(x_{Si}, t)$ is defined in (7.7). $\boldsymbol{y} \in \mathbb{R}^m$ is the measurement vector whereas m is the number of pressure sensors. The matrices in the model are:

$$\boldsymbol{A} = \begin{bmatrix} \mathrm{A1}_{5\times5} & \mathrm{0}_{5\times k} & \mathrm{A2}_{5\times k} \\ \mathrm{0}_{5\times5} & \mathrm{0}_{k\times k} & \mathrm{I}_{k\times k} \\ \mathrm{A3}_{k\times5} & \mathrm{A4}_{k\times k} & \mathrm{A5}_{k\times k} \end{bmatrix} \tag{7.28}$$

where

$$\mathrm{A1}_{5\times5} = \begin{bmatrix} 0 & 0 & 1 & 0 & 0 \\ 0 & 0 & 0 & 1 & 0 \\ -\frac{C_{33}}{m+A_{33}} & 0 & -\frac{B_{33}}{m+A_{33}} & 0 & \frac{A_c p_0}{m+A_{33}} \\ 0 & -\frac{C_{55}}{I_{55}+A_{55}} & 0 & -\frac{B_{55}}{I_{55}+A_{55}} & 0 \\ 0 & 0 & -\frac{\rho_{c0} A_c}{K_1} & 0 & -\frac{K_3}{K_1} \end{bmatrix} \tag{7.29}$$

$$\mathrm{A2}_{5\times k} = \begin{bmatrix} 0 & 0 & 0 & 0 & 0 & \cdots & 0 \\ 0 & 0 & 0 & 0 & 0 & \cdots & 0 \\ 0 & 0 & 0 & 0 & 0 & \cdots & 0 \\ d_1 & 0 & d_3 & 0 & d_5 & \cdots & d_k \\ 0 & 0 & 0 & 0 & 0 & \cdots & 0 \end{bmatrix} \quad \text{where} \quad \mathrm{d_j} = \frac{2\,\mathrm{p_0\,b}}{\mathrm{I_{55}+A_{55}}} \left(\frac{\mathrm{L}}{\mathrm{j}\pi}\right)^2 \tag{7.30}$$

$$\mathrm{A3}_{k\times5} = \begin{bmatrix} 0 & 0 & 0 & g_1 & 0 \\ 0 & 0 & 0 & 0 & 0 \\ 0 & 0 & 0 & g_3 & 0 \\ \vdots & & & & \vdots \\ 0 & 0 & 0 & \cdot & 0 \end{bmatrix} \quad \text{where} \quad g_j = -\frac{4\rho_{c0} L c^2}{p_0 h_0 (j\pi)^2} \tag{7.31}$$

$$\mathrm{A4}_{k\times k} = \mathrm{diag}\{-\omega_j^2\} \tag{7.32}$$

$$\mathrm{A5}_{k\times k} = \mathrm{diag}\{-2\xi_j\omega_j\} \tag{7.33}$$

$$E_{n\times(3+k)} = \begin{bmatrix} 0 & 0 & 0 & 0 & 0 & \cdots & 0 \\ 0 & 0 & 0 & 0 & 0 & \cdots & 0 \\ \frac{1}{m+A_{33}} & 0 & 0 & 0 & 0 & \cdots & 0 \\ 0 & \frac{1}{I_{55}+A_{55}} & 0 & 0 & 0 & \cdots & 0 \\ 0 & 0 & \frac{\rho_{c0}}{K_1} & 0 & 0 & \cdots & 0 \\ & & & \mathbf{0}_{k\times(3+k)} & & & \\ & \mathbf{0}_{k\times3} & & & \rho_{c0}\,\mathbf{I}_{k\times k} & & \end{bmatrix} \tag{7.34}$$

$$C^T_{m\times n} = \begin{bmatrix} 0 & 0 & \cdots & 0 \\ 0 & 0 & \cdots & 0 \\ 0 & 0 & \cdots & 0 \\ 0 & 0 & \cdots & 0 \\ 1 & 1 & \cdots & 1 \\ & \mathbf{0}_{k\times m} & & \\ \cos\frac{\pi}{L}\left(x_{S1}+\frac{L}{2}\right) & \cos\frac{\pi}{L}\left(x_{S2}+\frac{L}{2}\right) & \cdots & \cos\frac{\pi}{L}\left(x_{Sm}+\frac{L}{2}\right) \\ \cos\frac{2\pi}{L}\left(x_{S1}+\frac{L}{2}\right) & \cos\frac{2\pi}{L}\left(x_{S2}+\frac{L}{2}\right) & \cdots & \cos\frac{2\pi}{L}\left(x_{Sm}+\frac{L}{2}\right) \\ \vdots & & & \vdots \\ \cos\frac{k\pi}{L}\left(x_{S1}+\frac{L}{2}\right) & \cos\frac{k\pi}{L}\left(x_{S2}+\frac{L}{2}\right) & \cdots & \cos\frac{k\pi}{L}\left(x_{Sm}+\frac{L}{2}\right) \end{bmatrix} \tag{7.35}$$

$$B_{n\times r} = \begin{bmatrix} 0 & 0 & \cdots & 0 \\ 0 & 0 & \cdots & 0 \\ 0 & 0 & \cdots & 0 \\ 0 & 0 & \cdots & 0 \\ \frac{K_2}{K_1} & \frac{K_2}{K_1} & \cdots & \frac{K_2}{K_1} \\ & 0_{k\times r} & & \\ c_1 \cos\frac{\pi}{L}\left(x_{L1}+\frac{L}{2}\right) & c_1 \cos\frac{\pi}{L}\left(x_{L2}+\frac{L}{2}\right) & \cdots & c_1 \cos\frac{\pi}{L}\left(x_{Lr}+\frac{L}{2}\right) \\ c_1 \cos\frac{2\pi}{L}\left(x_{L1}+\frac{L}{2}\right) & c_1 \cos\frac{2\pi}{L}\left(x_{L2}+\frac{L}{2}\right) & \cdots & c_1 \cos\frac{2\pi}{L}\left(x_{Lr}+\frac{L}{2}\right) \\ \vdots & & & \vdots \\ c_1 \cos\frac{k\pi}{L}\left(x_{L1}+\frac{L}{2}\right) & c_1 \cos\frac{k\pi}{L}\left(x_{L2}+\frac{L}{2}\right) & \cdots & c_1 \cos\frac{k\pi}{L}\left(x_{Lr}+\frac{L}{2}\right) \end{bmatrix} \tag{7.36}$$

where c_1 is defined in (7.15).

7.1.3 Robust Dissipative Control Design

We will now derive a ride control system based on the mathematical model discussed in the previous section. The control objective is to damp out pressure fluctuations around the equilibrium pressure p_0 in the presence of sea wave disturbances. This can be formulated in terms of the desired value of the non-dimensional dynamic uniform pressure $\mu_u^d(t) = 0$ and the non-dimensional spatially varying pressure $\mu_{sp}^d(x,t) = 0$, where the superscript d denotes the desired value. The number of modes to be damped depends on the requirements related to established criteria for crew workability and passenger comfort.

The mathematical model of the craft dynamics is of high order as it contains a high number of acoustic modes. A practical implementable controller has to be of reduced order. When designing a controller based on a reduced order model, it may happen that the truncated or residual modes result in a degradation of the performance, and even instability of the closed-loop system. This is analogous with the so-called spillover effect in active damping of vibrations in mechanical structures (Balas 1978). The inadvertent excitation of the residual modes has been termed control spillover, and the unwanted contribution of the residual modes to the sensed outputs has been termed observation-spillover, see Figure 7.2. This problem was also discussed by Gevarter (1970) in connection with control of flexible vehicles. Mode 0 in Figure 7.2 is related to the uniform pressure, whereas the higher order modes are related to the spatially varying pressure.

The controller must be robust with respect to modeling errors and parametric and non-parametric uncertainties, nonlinearities in sensors and actuators and component failure. The use of collocated compatible actuators and sensors pairs and strictly passive controllers provides a design technique for circumventing these problems. Then louver and sensor pairs are distributed along the air cushion, preferentially in the longitudinal direction. The problem described in this section is closely related to the problem of vibration damping in large flexible space structures. Inspired by the work of Joshi (1989) we propose to use dissipative control for vibration damping of SES.

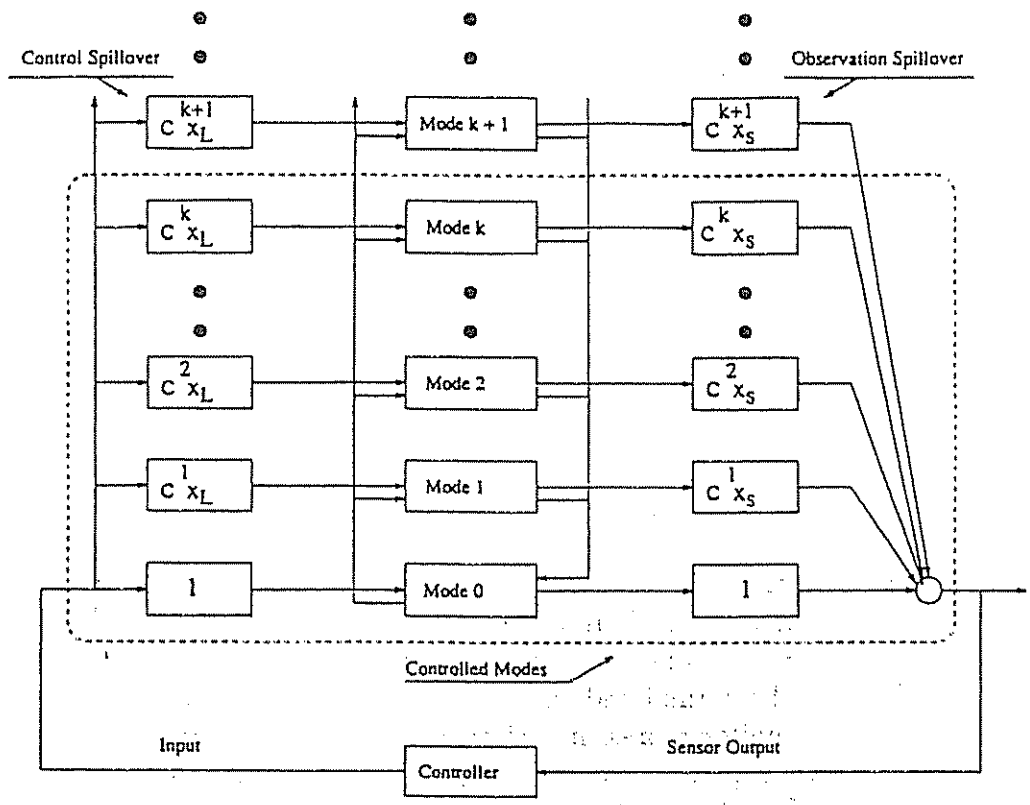

Figure 7.2: Observation and control spillover, where $C^k x_L = \cos k\pi(x_L + L/2)/L$ and $C^k x_S = \cos k\pi(x_S + L/2)/L$.

Perfect Collocation

Consider the case where sensors and actuators are ideal, that is linear and instantaneous with no noise. It is assumed that the control input matrix B can be related to the measurement matrix C so that:

$$C = B^T P \tag{7.37}$$

where $P = P^T > 0$ is an $n \times n$ symmetrical positive definite matrix providing correct scaling of B^T to the matrix C. This is the case when there is *perfect collocation* between the sensors and the louvers, that is $x_{Li} = x_{Si}$ for all i and $r = m$.

We can derive the linear time-invariant operators between the outputs and the inputs of the dynamic system given by (7.24). Let s denote the Laplace operator. Since the pair (A, B) is controllable and the pair (A, C) is observable, the dynamic system can be represented by:

$$y = y_u(s) + y_w(s) = H_p(s)\, u(s) + H_d(s)\, w(s) \tag{7.38}$$

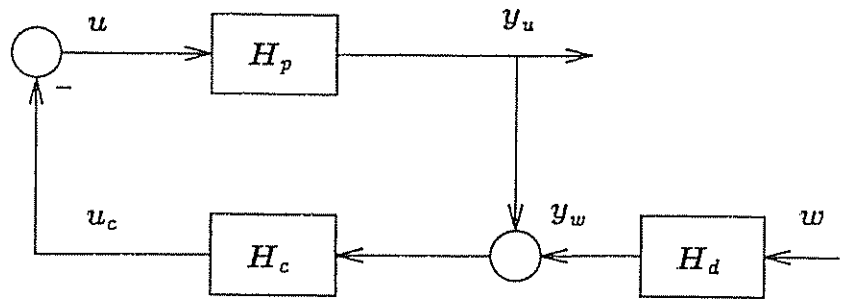

Figure 7.3: Feedback system; H_p, H_d and H_c represent the process, disturbance and control law, respectively.

where $H_p(s)$ and $H_d(s)$ are defined as:

$$\begin{aligned} H_p(s) &= C(sI - A)^{-1}B \\ H_d(s) &= C(sI - A)^{-1}E \end{aligned} \tag{7.39}$$

Input–Output Stability Analyses

Employing the definitions of passivity on an interconnected system consisting of two subsystems in a standard feedback configuration (see Figure 7.3), robust stability (RS) of the feedback system can be shown for certain input–output properties of the subsystems (Desoer and Vidyasagar 1975 and Vidyasagar 1993). The following lemma can be used to prove that the SES system matrix A is *Hurwitz*.

Lemma 7.1
Consider the system (7.24) with A defined in (7.28). The eigenvalues of the system matrix A have negative real parts.

Proof: *Consider the system (7.24) with $u(t) = w(t) = 0$. Define a Lyapunov function candidate:*

$$V(x) = \frac{1}{2}\, x^T\, P\, x > 0 \tag{7.40}$$

where $P = P^T > 0$ is an $n \times n$ diagonal positive definite matrix to be defined later. Hence, $V(x)$ must be positive definite. The time derivative of $V(x)$ is:

$$\dot{V}(x) = \frac{1}{2}\, x^T\, (A^T P + PA)x \triangleq -\frac{1}{2}\, x^T\, Q\, x \leq 0 \tag{7.41}$$

where $Q = Q^T \geq 0$. This implies that P must satisfy:

$$A^T P + PA = -Q \tag{7.42}$$

Let us choose Q diagonal and positive semi-definite, for instance:

$$\mathrm{Q} = \mathrm{diag}\{0_{2\times 2},\ \mathrm{Q1}_{3\times 3},\ 0_{k\times k},\ \mathrm{Q2}_{k\times k}\} \tag{7.43}$$

with $\mathrm{Q1}_{3\times 3}$ *defined as:*

$$\begin{gathered}\mathrm{Q1}_{3\times 3} = \mathrm{diag}\{Q_{ii}\} \qquad (i = 3,4,5)\\ Q_{33} = P_3\tfrac{2B_{33}}{m+A_{33}} \qquad Q_{44} = P_4\tfrac{2B_{55}}{I_{55}+A_{55}} \qquad Q_{55} = P_5\tfrac{2K_3}{K_1}\end{gathered} \tag{7.44}$$

and $\mathrm{Q2}_{k\times k}$ *defined as:*

$$\begin{gathered}\mathrm{Q2}_{k\times k} = \mathrm{diag}\{Q_{ii}\} \qquad (i = 5+k+1,\ 5+k+2,\ldots,\ 5+2k)\\ Q_{(5+k+j)(5+k+j)} = P_{(5+k+j)(5+k+j)}\ 4\,\xi_j\,\omega_j \qquad (j = 1,2,3,\ldots,k)\end{gathered} \tag{7.45}$$

Hence, we can compute $\boldsymbol{P}$ *from (7.42), that is:*

$$\boldsymbol{P}_{n\times n} = \mathrm{diag}\{P_{ii}\} \qquad (i = 1,2,3,\ldots,n) \tag{7.46}$$

where

$$\begin{gathered}P_{11} = P_{33}\tfrac{C_{33}}{m+A_{33}} \quad P_{22} = P_{44}\tfrac{C_{55}}{I_{55}+A_{55}} \quad P_{33} = P_{55}\tfrac{\rho_{c0}(m+A_{33})}{K_1 p_0} \quad P_{44} = -\tfrac{g_1}{d_1 c_1}\\ P_{55} = \tfrac{K_1}{\rho_{c0}K_2} \qquad P_{(5+j)(5+j)} = \omega_j^2 \qquad P_{(5+k+j)(5+k+j)} = \tfrac{1}{c_1}\end{gathered} \tag{7.47}$$

where $(j = 1,2,3,\ldots,k)$ *and* c_1 *is defined in (7.15). From (7.24) and (7.41) it is seen that* $\dot{V}(\boldsymbol{x}) = 0$ *implies that:*

$$\boldsymbol{x}(t) = [\eta_3,\ \eta_5,\ 0,\ 0,\ 0,\ p_1,\ p_2,\ldots,\ p_k,\ 0,\ 0,\ldots,0]^T \tag{7.48}$$

However, from (7.24) we have that:

$$\ddot{\eta}_3 = \ddot{\eta}_5 = \dot{\mu}_u = \ddot{p}_1 = \ddot{p}_2 = \ldots = \ddot{p}_k = 0 \tag{7.49}$$

which implies:

$$\eta_3 = \eta_5 = p_1 = p_2 = \ldots = p_k = 0 \tag{7.50}$$

Hence, application of the invariant set theorem, Vidyasagar (1993), the equilibrium point $\boldsymbol{x}(t) = 0$ *is asymptotically stable and the result of Lemma 7.1 follows.* □

Define the linear time-invariant operators $\boldsymbol{H}_p : L_{2e}^m \to L_{2e}^r$ $(r = m)$ and assume that $\boldsymbol{H}_d : L_2^{3+k} \to L_2^m$, such that $\boldsymbol{y}_w \in L_2^m$ whenever $\boldsymbol{w} \in L_2^{3+k}$, see Appendix C.2. In the following lemma it is shown that the process operator $\boldsymbol{H}_p$ is passive. This allows for the design of a robust, stable output feedback control law for ride control of SES.

Lemma 7.2
The process operator H_p is passive.

Proof: *Set $w(t) = 0$ in (7.24) and use the Lyapunov function candidate as given in (7.40). $V(x)$ is positive definite. The time derivative of $V(x)$ along the system trajectories is:*

$$\dot{V}(x) = \frac{1}{2} x^T (A^T P + P A) x + x^T P B u \tag{7.51}$$

If we assume perfect collocation between the sensor and actuator pairs, that is $C = B^T P$, (7.51) becomes:

$$\dot{V}(x) = x^T C^T u - \frac{1}{2} x^T Q x = y_u^T u - \frac{1}{2} x^T Q x \tag{7.52}$$

where Q is the diagonal positive semi-definite matrix given in (7.43). Integrating (7.52) from $t = 0$ to $t = T$ we obtain:

$$\langle y_u | u \rangle_T = V(t = T) - V(t = 0) + \frac{1}{2} \int_0^T x^T Q x \, dt \tag{7.53}$$

Since $Q \geq 0$ and $V(t = T) > 0$, (7.53) can be written:

$$\langle y_u | u \rangle_T \geq \beta \tag{7.54}$$

where $\beta = -V(t = 0)$. Hence, the result of Lemma 7.2 follows, see Appendix C.2.
□

Remark 7.1 *It is evident from (7.40) that if the initial conditions are equal to zero that is $x(t = 0) = 0$, then:*

$$\beta = -\frac{1}{2} x^T(t = 0) P x(t = 0) = 0 \tag{7.55}$$

□

Remark 7.2 *The transfer matrix $H_d(s)$ of the linear time-invariant operator H_d as defined by (7.39) is strictly proper and all the poles have negative real parts according to Lemma 7.1. Hence, if $w \in L_2^{3+k}$, then:*

$$y_w = H_d w \in L_2^m \cap L_\infty^m \tag{7.56}$$

□

Let the controller be defined as the linear time-invariant operator H_c between the input $y = y_u + y_w$ and the output u_c. Connecting the H_c operator with the H_p and H_d operators, we obtain the feedback system illustrated in Figure 7.3. The transfer matrix of H_c is denoted $H_c(s)$.

Proportional Feedback Control

A strictly u-passive proportional pressure feedback controller with finite gain is proposed according to:

$$u_c(s) = H_c(s)y(s) \qquad \text{with} \qquad H_c(s) = G_p \tag{7.57}$$

Here $G_p = \text{diag}\{g_{pi}\} > 0$ is a constant diagonal feedback gain matrix of dimension $r \times r$. This control law provides enhanced damping of the pressure variations around the resonance frequencies. The main result of this section is contained in the following theorem.

Theorem 7.1 (L_2^m and L_∞^m Stable Feedback Control)
Consider the following system, see Figure 7.3,

$$\begin{aligned} y_u &= H_p\, u \\ y_w &= H_d\, w \\ y &= y_u + y_w \end{aligned} \tag{7.58}$$

with feedback:

$$u = -u_c = -H_c\, y \tag{7.59}$$

Here H_p $H_c : L_{2e}^m \to L_{2e}^m$. Assume that $H_d : L_2^{3+k} \to L_2^m$, so that $y_w \in L_2^m$ whenever $w \in L_2^{3+k}$. The control law H_c is strictly u-passive with finite gain while the plant H_p is passive. Hence, the feedback system defined by (7.58) and (7.59) is L_2^m stable. Since the system H_p, H_p and H_c is linear, L_2^m stability is equivalent to L_∞^m (BIBO) stability. This implies that $y(t) \to 0$ in finite time.

Proof: *Set $w(t) = 0$ in (7.24) and use the Lyapunov function candidate as given in (7.40). $V(x)$ is positive definite. If we assume perfect collocation between the sensor and actuator pairs, that is $C = B^T P$, the time derivative of $V(x)$ along the closed-loop system trajectories becomes:*

$$\dot{V}(x) = -y_u^T\, G_p\, y_u - \frac{1}{2} x^T\, Q\, x = -x^T\, (C^T G_p\, C + \frac{1}{2}\, Q)\, x \tag{7.60}$$

where $Q = Q^T \geq 0$ is given in (7.43). Since the diagonal matrix $G_p = G_p^T > 0$ it follows that:

$$C^T\, G_p\, C + \frac{1}{2}\, Q \geq 0 \tag{7.61}$$

Hence, the time derivative of $V(x)$ is negative semi-definite. Using the invariant set theorem (Vidyasagar 1993), the equilibrium point of the closed-loop system is asymptotically stable and the result follows.
□

L_2^m and L_∞^m stability of the closed-loop system using collocated sensor and actuator pairs is maintained regardless of the number of modes, and regardless of the inaccuracy in the knowledge of the parameters. Thus the spillover problem is eliminated and the parameters do not have to be known in advance for stability to be obtained. Notice that there are no restrictions on the location of the collocated sensor and actuator pairs with respect to stability. However, optimizing the performance, the longitudinal location of the sensor actuator pairs is crucial as seen in (7.19). Robustness with respect to unmodelled dynamics and sector nonlinearities in the actuators are demonstrated in Sørensen (1993).

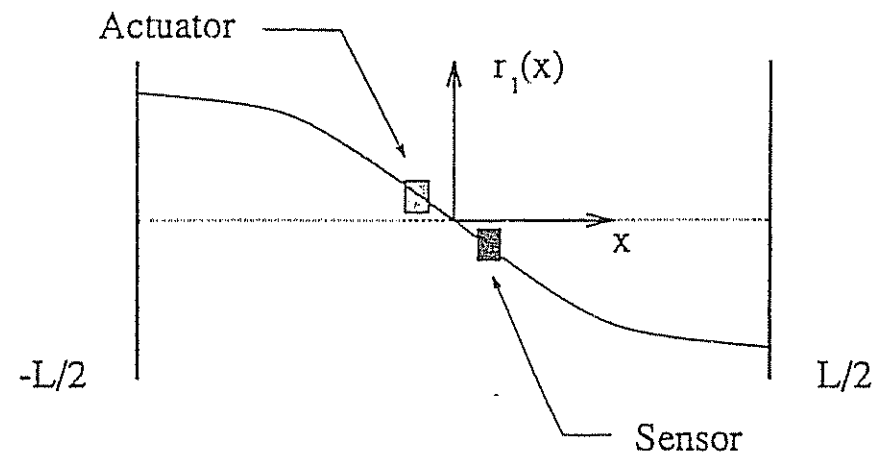

Figure 7.4: Non-collocated sensor and actuator pair.

The property of perfect collocation between the sensors and the actuators does not exist in practice. Since we do not want the measurements to be influenced by the local flow characteristics around the vent areas of the louvers, it is necessary to locate the sensors at some distance from the louvers. This means that the mode shape values at the louver and sensor locations will not be the same. For the acoustic resonance modes of practical interest this may not be of any problem due to the long acoustic wave lengths relative to the imperfection in collocation between the sensor and actuator pairs. However, this claims that the sensor and actuator pairs are located at some distance from a node, see Figure 7.4. If the vent valve and the sensor are located close to a node, the vent valve and the sensor may be located on either side of the node. This may lead to spillover problems, where the mode shape function associated with the sensor will have the opposite sign to the mode shape function associated to the actuator. This is similar to positive feedback. In Sørensen (1993) it is shown that some imperfection in the collocation will be tolerated without violating the stability properties of the closed-loop system.

7.1.4 Simulation and Full-Scale Results

In this section numerical simulations and results from full-scale trials with a 35 m SES advancing at high speed in head sea waves are presented. The effect of collocation and non-collocation of the sensor and actuator pairs for the 35 m SES is investigated. The SES is equipped with one single-fan and louver system. Main dimensions and data of the SES craft are given below. The number of acoustic modes considered in the simulation model is four, that is $k = 4$.

Figure 7.5 shows the Bode plot of $\boldsymbol{H}_p(j\omega_e)$ between the pressure sensor $y_u(s)$ and the louver $u(s)$ when the pressure sensor and actuator pair is fully collocated. The sensor and louver pair is located at the fore end of the air cushion. When the frequency of encounter goes to zero, the dynamic pressure tends to be a static value proportional to K_1/K_2. This indicates that the equilibrium pressure p_0 will decrease when the equilibrium leakage area increases, and vice versa.

SES Main Data				
Length overall	L_{oa}	=	35	m
Equilibrium fan flow rate	Q_{0i}	=	150	m^3/s
Linear fan slope	$\frac{\partial Q}{\partial p}\Big\|_{0i}$	=	−140	m^2/s
Cushion length	L	=	28	m
Nominal cushion pressure	p_0	=	500	mmWc
Cushion beam	b	=	8	m
Cushion height	h_0	=	2	m
Weight	W	=	150	ton
Maximum speed	U	=	50	knots

Numerical Simulations

Around 0.1 Hz the response is close to zero. This is related to the structural mass forces acting on the SES and the hydrodynamic forces acting on the side-hulls. The high value around 2 Hz is due to the resonance of the dynamic uniform pressure. The high values around 6 Hz, 12 Hz, 18 Hz and 24 Hz are related to the four acoustic resonance modes. From the phase plot we observe that the phase varies between 90^o and -90^o in the whole frequency range. This is to be expected when using collocated sensor and actuator pairs.

Figure 7.6 shows the Bode plots of $\boldsymbol{H}_p(j\omega_e)$ when the pressure sensor is located at the fore end of the air cushion and the louver is located at the aft end of the air cushion. From the phase plot we observe that the sensed pressure signal at the fore end for 6 Hz and upwards is more than 180^o out of phase with the pressure signal at the aft end where the louver is located. This is to be expected with non-collocated sensor and louver pairs. Non-collocated sensor and actuator pairs introduce negative phase and may lead to instability.

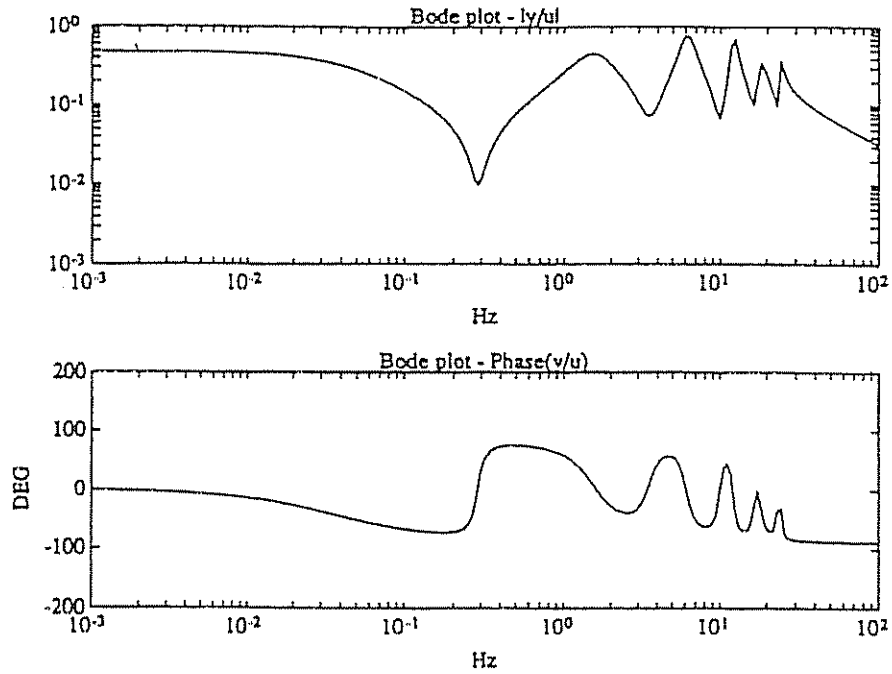

Figure 7.5: Bode plot of $\mathrm{H}_p(j\omega_e)$ for $x_L = x_S = 12$ m, $x_F = 6$ m, $U = 50$ knots and $p_0 = 500$ mmWc (mm water column).

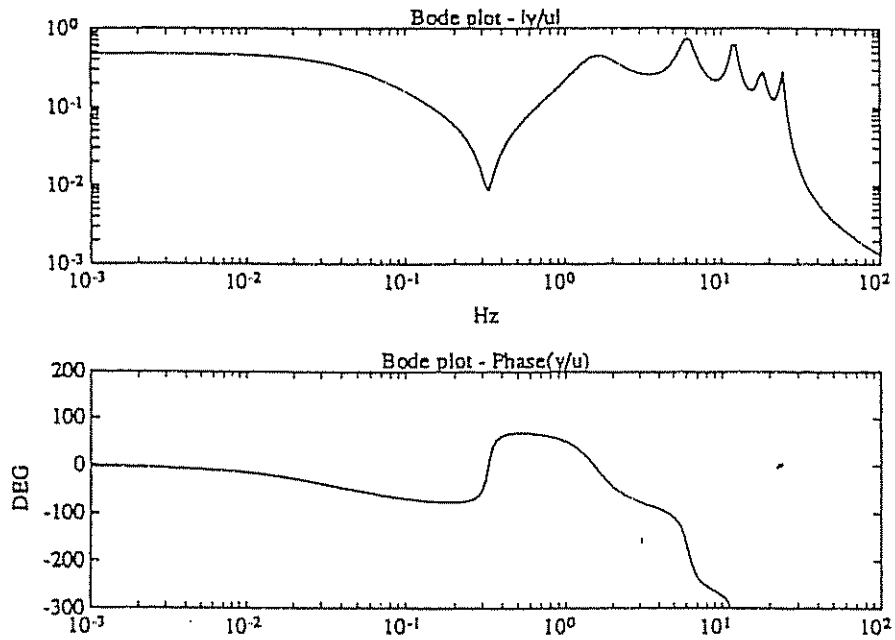

Figure 7.6: Bode plot of $\mathrm{H}_p(j\omega_e)$ for $x_S = 12$ m, $x_L = -12$ m, $x_F = 6$ m, $U = 50$ knots and $p_0 = 500$ mmWc (mm water column).

Experimental Results

The prototype ride control system used in the full-scale experiments was based on the passive controller presented in the previous section. The control algorithms in the ride control system were partly implemented on a personal computer (PC). Analog hardware devices were also used. An outer feedback loop was implemented on the PC, while a faster inner feedback loop around the electro- hydraulic louver system was implemented by means of analog hardware devices. The louver system consisted of two vent valves located side by side at the same longitudinal position $x_L = 8$ m. The two vent valves were operated in parallel in the outer feedback loop. Two pressure sensors located at $x_{S1} = 10$ m and $x_{S2} = -10$ m were used to measure the excess pressure variations in the air cushion. One accelerometer located about 5 m aft of the center of gravity was used to measure the vertical accelerations. The inner analog controller loop around the louver system provided the necessary opening and closing actions of the vent valves. The experimental arrangement is illustrated in Figure 7.7.

The full-scale measurements were carried out in sea states with significant wave heights estimated to vary between 0.3 and 0.6 m. The power spectra of the vertical accelerations with and without the ride control system are presented.

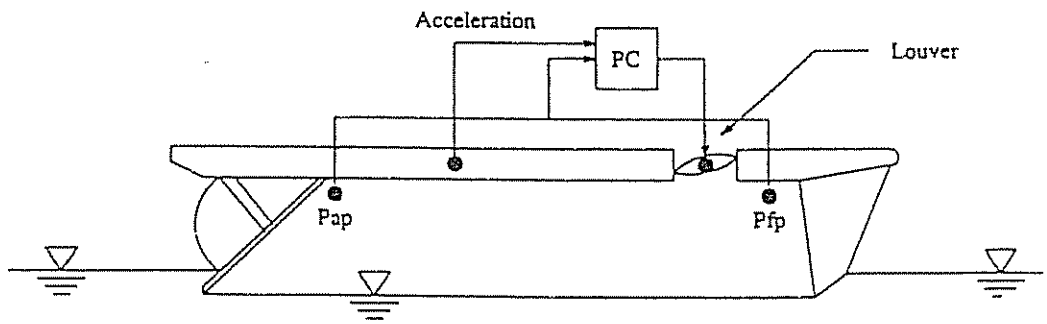

Figure 7.7: Experimental arrangement.

The upper plot in Figure 7.8 shows the full-scale power spectra of the vertical accelerations 5 m aft of the center of gravity with and without the ride control system activated. With the control system turned off, we observed significant responses around 2 Hz, 5 Hz and 8 Hz. The response around 2 Hz is related to the resonance of the dynamic uniform pressure, whereas the responses around 5 Hz and 8 Hz are related to the first odd and even resonance modes. Activating the control system the response around 5 Hz was significantly amplified, whereas the response around 2 Hz was only slightly reduced. The pressure signal at $x_{S2} = -10$ m was used in the feedback loop. In this case the actuator and sensor pair was non-collocated since the louver was located at $x_L = 8$ m. This means that for the first odd mode, the non-collocation resulted in positive feedback for this particular mode because the pressure at the sensor location was 180° out of

phase with the pressure at the actuator location in the frequency range dominated by the first odd acoustic resonance mode. The response around 8 Hz was more or less unchanged. Both time series were recorded when the craft was advancing with $U = 45$ knots in head seas with significant wave height $H_s = 0.3$ m.

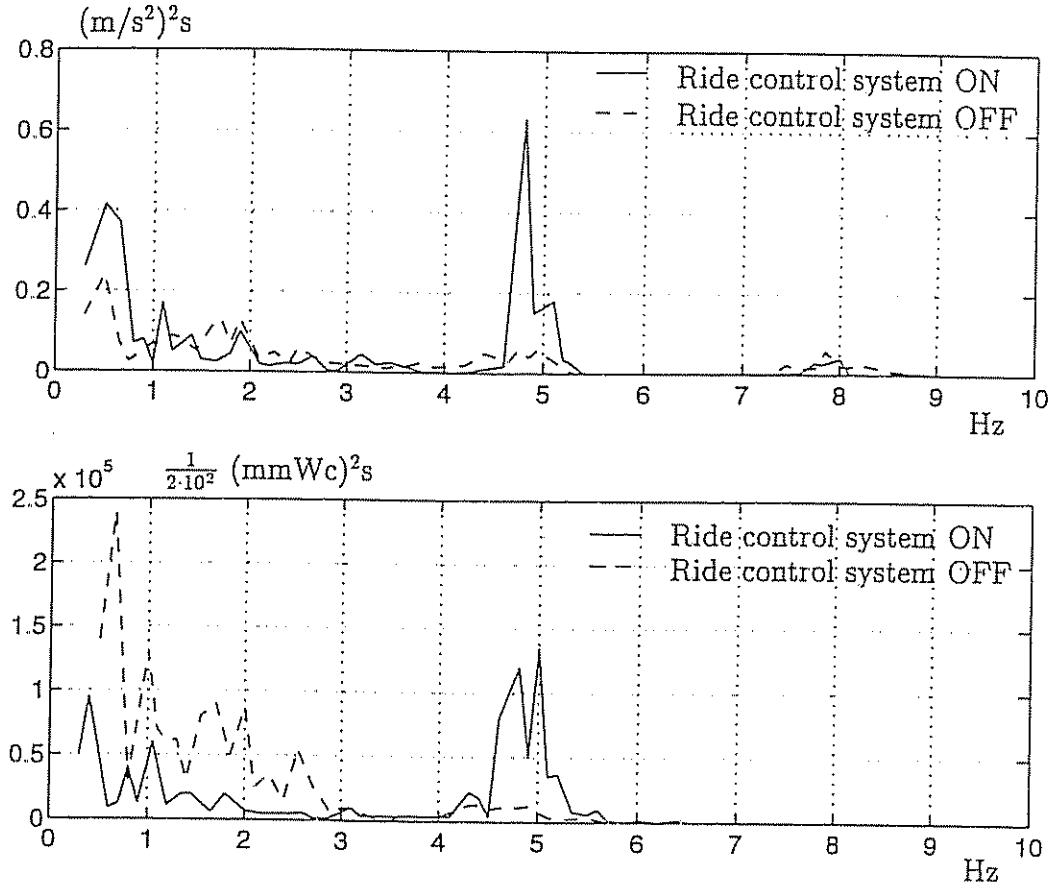

Figure 7.8: Non-collocated: full-scale power spectra of the vertical accelerations at $x = -5$ m (upper plot) and excess pressure at $x = 10$ m (lower plot) of a 35 m SES with ride control system on and off; $p_0 = 450$ mmWc (mm water column).

The lower plot in Figure 7.8 shows the full-scale power spectra of the excess pressure variations at $x_{S1} = 10$ m in the air cushion with and without the ride control system activated. The time series was taken from the same run as above. The pressure signal at $x_{S2} = -10$ m was used in the feedback loop. Hence, the louvers and sensors were non-collocated. With the control system turned off, we observed responses around 2 Hz and 5 Hz. Activating the ride control system, the response around 5 Hz was significantly amplified. At the resonance of the dynamic pressure around 2 Hz the response level was reduced by the ride control system.

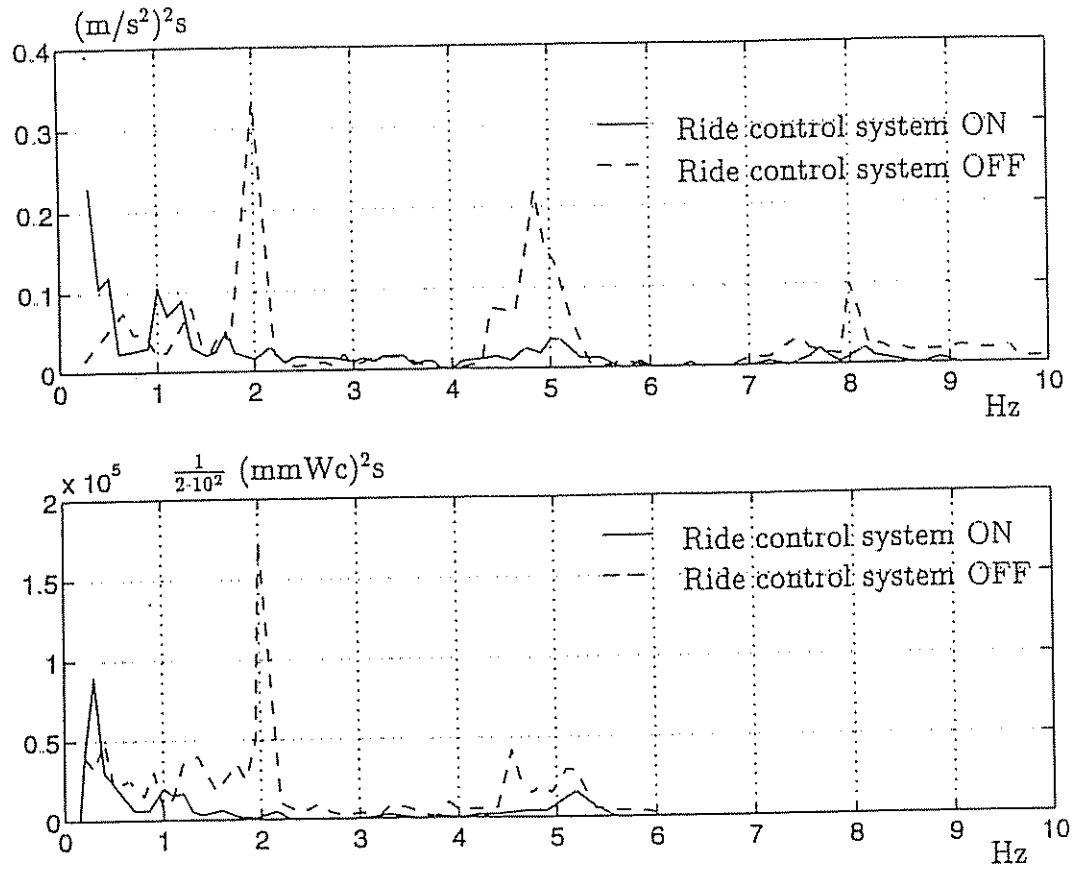

Figure 7.9: Collocated: full-scale power spectra of the vertical accelerations at $x = -5$ m (upper plot) and the excess pressure at $x = 10$ m (lower plot) of a 35 m SES with ride control system on and off; $p_0 = 430$ mmWc (mm water column).

The upper plot in Figure 7.9 shows the full-scale power spectra of the vertical accelerations 5 m aft of the center of gravity with and without the ride control system activated. In this case the pressure signal at $x_{S1} = 10$ m was used in the feedback loop. Hence, the louvers and sensors were "almost" collocated since the louvers were located at $x_L = 8$ m. With the ride control system turned off, we observed responses around 2 Hz, 5 Hz and 8 Hz. Activating the ride control system the responses around all three resonance frequencies were significantly reduced. These time series were recorded when the craft was advancing with the speed $U = 44$ knots in head sea waves with significant wave height estimated to be $H_s = 0.6$ m. The lower plot shows the full-scale power spectra of the excess pressure variations at $x_{S1} = 10$ m in the air cushion with and without the ride control system activated. The pressure signal at $x_{S1} = 10$ m was used in the feedback loop. Hence, the louvers and sensors were "almost" collocated. With

the ride control system turned off, we observed responses around 2 Hz and 5 Hz at the fore end of the air cushion. Activating the ride control system the response around all three resonance frequencies was significantly reduced.

Comparison of full-scale results with numerical simulations shows that the acoustic resonances occur at lower frequencies for the real system than in the mathematical model. This is due to the fact that flexibility in the seals results in a larger equivalent cushion length and hence a lower resonance frequency (Steen 1993).

7.1.5 Conclusions

The pressure variations in the pressurized air cushion of an SES have two fundamental characteristics; a dynamic uniform and a spatially varying pressure term. It has been demonstrated that the resonances of the dynamic uniform pressure and the spatially varying pressure cause excessive vertical accelerations when the craft is advancing in sea states which contain energy in the frequency domains corresponding to the resonance frequencies. In order to obtain high human comfort and crew workability, it is necessary to reduce these accelerations using a ride control system. A distributed ride control system has been developed based on the theory of passive systems in terms of a proportional pressure feedback controller. Full-scale experiments of a prototype ride control system showed a significant improvement in ride quality using a ride control system which provided dissipation of energy around the resonance frequencies. The full-scale experiments also showed the importance of using collocated sensor and actuator pairs in the acoustic-dominated frequency range. Spillover effects were avoided regardless of the number of modes considered and parameter values through the use of collocated sensor and actuator pairs.

7.2 Ride Control of Foilborne Catamarans

by Erling Lunde[2] *and William C. O'Neill*[3]

Developing the ride control of a foilborne catamaran involves generating the hydrodynamic forces on the foils necessary to counter the seaway-induced forces. Since these control forces can be relatively large, it is essential that they are generated in a stable manner and do not jeopardize the ship or its passengers in the case of a failure in the control system.

The development of foil supported naval vessels has been going on for several decades. At the same time, Norwegian shipyards have a long tradition in building catamarans. During the last years these two concepts have been combined into a new type of vessel called *FoilCat* (the generic name for a hydrofoil-supported

[2]Consultant for Dynamica AS, Trondheim, Norway.

[3]Consultant for Advanced Marine Vehicles, 852 Goshen Road, Newtown Square, PA 19073, USA.

catamaran) by two Norwegian ship builders: *Westamarin West* and *Kværner Fjellstrand*. Recently, the Japanese company *Mitsubishi* presented their foil catamaran. We will mainly use the concepts of the two Norwegian companies as reported in Svenneby and Minsaas (1992), RW (1992) and Instanes and Pedersen (1991) to illustrate the qualities and high performance of foil supported vessels.

In this section, an attempt is made to explain the design process required to develop a FoilCat control system which assures stability, maneuverability, sea kindliness (ride quality) and safety (even in the event of a gross control failure). This section will start with the development of the control designers essential tool, a mathematical computer model of the FoilCat and the seaway. This will be followed by discussions on stability, maneuverability and the safety considerations which dominate the basic structure of the control system.

7.2.1 FoilCat Modeling

A mathematical model of the ship for which one must design a control system is the most important tool available to the designer. It is used to establish the best available control algorithms and to predict the behavior of the ship in the various environments in which it must operate. Modeling should start early in the ship design process and be updated as the design matures. Developing the model early allows the results obtained from the model studies to be entered into the design when it is relatively easy to incorporate changes.

A major use of a computer model of the ship is to simulate the effects of control system failures, some of which may be dangerous or expensive to demonstrate on the real ship. The ability of such failure studies to mitigate the effects of failure can change the configuration of the control system, and are used to define where and how much redundancy is needed to assure safety.

Useful mathematical models can run from the most simple linear models to highly nonlinear detailed simulations. The choice depends on the degree of sophistication required for the end use. Fortunately, foilborne ships are far easier to model than hullborne ships, as the hydrodynamic forces on the struts and foils are relatively easily calculated and can be considered to act as point forces rather than distributed forces as is the case with hullborne ships.

Simplified Model of Foil-Supported Ship (O'Neill 1991)

The simplest model for a foilborne ship and its corresponding block diagram is shown in Figure 7.10. In this model it is assumed that each foil on the ship is individually controlled to maintain a constant inertial height and the vertical motion of each foil is representative of the vertical motion of the whole ship, particularly when investigating the statistical responses to a seaway.

Consider a FoilCat moving at *constant* forward speed $u \gg 0$. Furthermore, assume that $v = 0$ and that $\phi = \theta = 0$. For small angles the lift force F_L will be linear, that is:

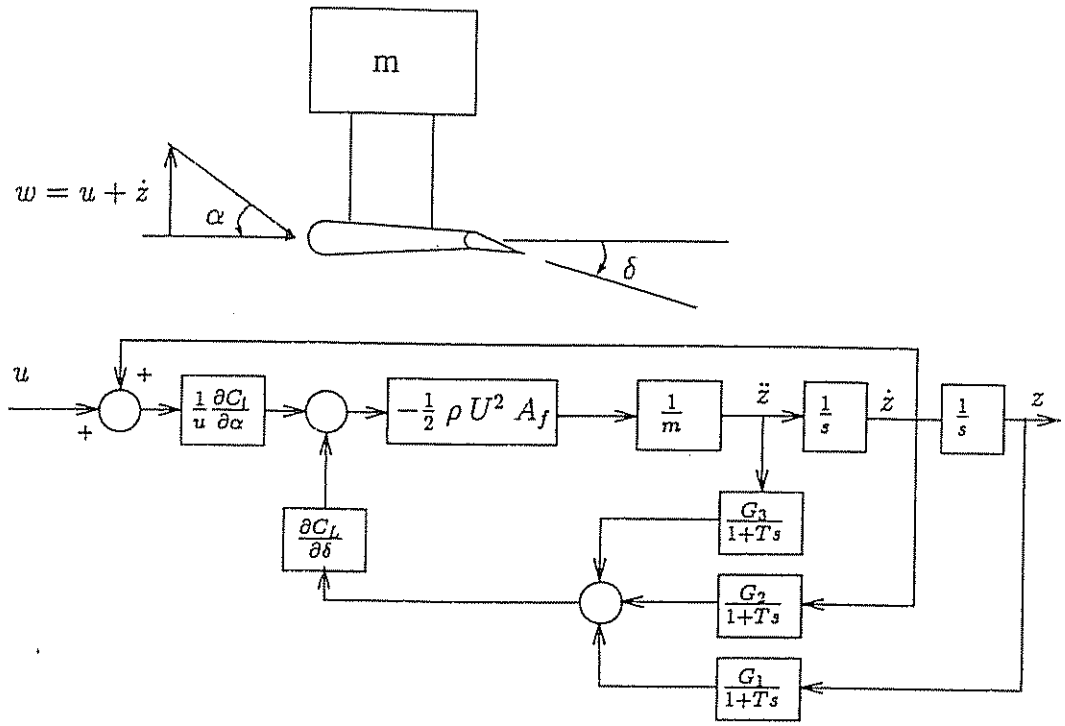

Figure 7.10: Simplified model of foil supported ship (O'Neill 1991).

$$F_L = -\frac{1}{2}\rho U^2 A_f \underbrace{\left(C_{L0} + \frac{\partial C_L}{\partial \alpha}\alpha + \frac{\partial C_L}{\partial \delta}\delta\right)}_{C_L} \tag{7.60}$$

where ρ is the water density, $U = \sqrt{u^2 + w^2}$ is the total speed, A_f is the foil area, C_L is the lift coefficient, C_{L0} is the lift due to camber (the lift at $\alpha = \delta = 0$), δ is the flap angle and α is the foil *angle of attack* defined as:

$$\alpha = \tan^{-1}\frac{w}{u} \approx \frac{w}{u} \tag{7.61}$$

If we assume that $C_{L0} = 0$, the heave motion is described by:

$$m\,\dot{w} = -\frac{1}{2}\rho U^2 A_f \left(\frac{\partial C_L}{\partial \alpha}\frac{w}{u} + \frac{\partial C_L}{\partial \delta}\delta\right) \tag{7.62}$$

$$\dot{z} = -u + w \tag{7.63}$$

or equivalently:

$$m\,\ddot{z} = -\frac{1}{2}\rho U^2 A_f \left(\frac{\partial C_L}{\partial \alpha}\frac{\dot{z}+u}{u} + \frac{\partial C_L}{\partial \delta}\delta\right) \tag{7.64}$$

The flap angle control system is taken to be:

$$\delta(s) = \left(G_1 + G_2\, s + G_3\, s^2\right) \frac{z(s)}{1+Ts} \tag{7.65}$$

where G_1, G_2 and G_3 are the controller gains and T is the effective time lag from sensors, control and actuators. In this model, the mass is considered to be that portion of the ship mass supported by that foil. Since this model is both simple and linear, all studies can be made easily in the frequency domain rather than in the time domain, simplifying how to obtain the statistical responses of the ship in a seaway. This model, which was used by O'Neill (1991), has proven remarkably accurate in determining the limiting gains in the control system for stability.

Modeling of Lift Coefficient

For small angles and at slow speed linearity holds up to separation, but at the speeds at which FoilCats must operate, cavitation greatly limits the lift that can be generated. Based on model tests and full-scale experience of the *Kværner Fjellstrand FoilCat*, the maximum foil-loading, $C_L\, q$ where $q = \rho\, U^2/2$ is the dynamic pressure, that can be generated by a flapped foil is about 150 kN/m^2. Another limit which must be modelled is the lift that can be generated by flap angle. This limit depends of the foil section and the ratio of flap chord to foil chord and can be determined from model tests in a cavitation tunnel. Without a model test one can use a maximum change in foil loading of 62 kN/m^2 due to positive flap angles and -70 kN/m^2 due to negative flap angles. These limits are typical for flapped foil systems on existing ships, see Figure 7.11.

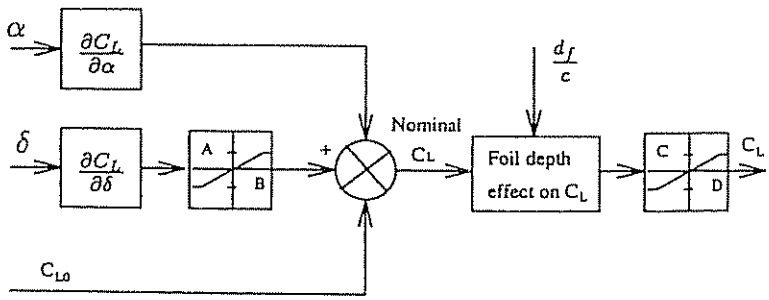

Figure 7.11: Block diagram showing lift coefficient C_L for the Kværner Fjellstrand FoilCat where the limits are $A = 62/q$ (kN/m^2), $B = -70/q$ (kN/m^2), $C = 150/q$ (kN/m^2) and $D = -150/q$ (kN/m^2). The dynamic pressure is $q = \rho\, U^2/2$.

The modeling of the foil lift coefficient is further complicated by the decrease in lift coefficient from its nominal value (no free surface effect) as the foil approaches the free surface. This depth effect can be approximately modeled by:

$$
\begin{array}{ll}
d_f/c < 0 & C_L = 0 \\
d_f/c = 0 & C_L = 0.5\, C_{L,\,\text{nominal}} \\
0 < d_f/c < 1 & C_L = 0.5\,(1 + d_f/c)\, C_{L,\,\text{nominal}} \\
d_f/c > 1 & C_L = C_{L,\,\text{nominal}}
\end{array}
$$

where d_f is the foil depth and c is the foil chord length. Modeling of the side face on the struts supporting the foils must take into account four factors. They are:

1. Strut area varies with foil depth.
2. Side force coefficient $\frac{\partial C_y}{\partial \beta}$ varies with foil depth.
3. Maximum side area force on strut is limited by cavitation.
4. Strut ventilation.

The first of these can be modelled directly from the strut geometry. The second and third can be obtained from model tests in a free surface cavitation tunnel and modelled similarly to the foil system. Lacking such a test, $\frac{\partial C_y}{\partial \beta}$ can be estimated from the literature of small aspect ratio surfaces such as rudders and a value of 70 kN/m^2 can be used as the maximum side load substainable, based on a typical strut section used on existing ships. This leaves strut ventilation, which is one of the most difficult phenomena to predict. Strut ventilation occurs when atmospheric air breaks through the surface to the low-pressure side of a strut operating under a side slip angle. When this occurs there is a sudden decrease (and even reversal) in the side force generated by the strut, which can result in serious stability problems. Once a vent takes place, it remains tenaciously in place until the path to atmospheric air is sealed, normally by the hull contacting the water surface. Although it is difficult to accurately predict the onset of ventilation, the following generalities based on experience on US hydrofoils can be made.

1. Local cavitation on the strut exists prior to ventilation in most cases.
2. Manufacturing a strut to accurate contours delays the onset of local cavitation and thus ventilation.
3. Keeping the side ship angle low (below 3 or 4 degrees) greatly reduces the chance of ventilation (the meeting of this criterion is one of the primary factors in selecting a steering method for a FoilCat which will be discussed later).
4. Debris in the water hitting the strut can trigger ventilation even under conditions where it normally would not occur.
5. When a strut ventilates, this results instantly in a decrease in total side force coefficient of about 0.14.

A natural extension of this simple model is to model the forces on each foil separately and tie them together through the geometry of the ship. Since the forces on each of the foils may differ from one another, we have now introduced pitch and roll moments to the ship. Once we have introduced pitch and roll into the model, it is necessary to include lateral forces on the ship and apply Euler's transformations from body axes to earth axes and vice versa. When this is done, the equations which model the ship take a quantum leap in complexity, which prior to the advent of computers drove control system engineers to seek simplifying assumptions. These simplifications which include uncoupling the longitudinal (surge, heave and pitch) from the lateral mode (sway, roll and yaw) are still useful for preliminary studies and give the designer a good sense of the effect of each feedback. Modern high-speed computers have now removed the need for such simplifications for studying the complete system and allow the use of the full 6 DOF equations of motion.

6 DOF FoilCat Equations of Motion

Consider the rigid-body dynamics in abbreviated form:

$$M_{RB}\,\dot{\nu} + C_{RB}(\nu)\,\nu + g(\eta) = \tau \tag{7.66}$$

$$\dot{\eta} = J(\eta)\,\nu \tag{7.67}$$

where $\tau = [X, Y, Z, K, M, N]^T$ is a vector of external hydrodynamics forces and moments to be interpreted later. It is reasonable to assume that the catamaran has a homogeneous mass distribution and that $I_{xy} = I_{yz} = 0$ (port/starboard symmetry). Furthermore, the origin of the body-fixed coordinate system is chosen to coincide with the CG, that is $x_G = y_G = z_G = 0$. Hence:

$$M_{RB} = \begin{bmatrix} m & 0 & 0 & 0 & 0 & 0 \\ 0 & m & 0 & 0 & 0 & 0 \\ 0 & 0 & m & 0 & 0 & 0 \\ 0 & 0 & 0 & I_x & 0 & -I_{xz} \\ 0 & 0 & 0 & 0 & I_y & 0 \\ 0 & 0 & 0 & -I_{xz} & 0 & I_z \end{bmatrix} \qquad g(\eta) = \begin{bmatrix} mg\,s\theta \\ -mg\,c\theta s\phi \\ -mg\,c\theta c\phi \\ 0 \\ 0 \\ 0 \end{bmatrix} \tag{7.68}$$

$$C_{RB}(\nu) = \begin{bmatrix} 0 & 0 & 0 & 0 & mw & -mv \\ 0 & 0 & 0 & -mw & 0 & mu \\ 0 & 0 & 0 & mv & -mu & 0 \\ 0 & mw & -mv & 0 & -I_{xz}p + I_z r & -I_y q \\ -mw & 0 & mu & I_{xz}p - I_z r & 0 & -I_{xz}r + I_x p \\ mv & -mu & 0 & I_y q & I_{xz}r - I_z p & 0 \end{bmatrix} \tag{7.69}$$

The full 6 DOF equations in component form are shown in Table 7.1 in the left hand column. These equations can be further simplified by assuming relatively small motions of the ship, which is true for any acceptable FoilCat. The simplified equations are shown in the right hand column of Table 7.1.

The equations shown in Table 7.1 have omitted the added mass terms since for foilborne ships there is very little of the ship in the water and therefore most added mass terms are very small. For forces in the z-direction, the added mass $A_{33} = -Z_{\dot{w}}$ may be large enough to warrant adding it to m in the expression

for $\dot{w}$. A_{33} can be approximated by the mass of the water enclosed in a body of revolution whose local diameter is equal to the local foil chord. This added mass can also be reflected in $A_{44} = -K_{\dot{p}}$ and $A_{55} = -M_{\dot{q}}$ and added to I_x and I_y in the expressions for $\dot{p}$ and $\dot{r}$, respectively.

Table 7.1: 6 DOF complete and simplified FoilCat equations of motion.

Complete equations	Simplified equations
$\dot{u} = \frac{1}{m}[X + vr - wq - mg\,s\theta]$ $\dot{v} = \frac{1}{m}[Y + wp - ur + mg\,c\theta s\phi]$ $\dot{w} = \frac{1}{m}[Z + uq - vp + mg\,c\theta c\phi]$ $\dot{p} = \frac{1}{I_x}[K - (I_z - I_y)qr + I_{xz}(\dot{r} + pq)]$ $\dot{q} = \frac{1}{I_y}[M - (I_y - I_z)pq - I_{xz}(p^2 - r^2)]$ $\dot{r} = \frac{1}{I_z}[N - (I_y - I_z)pq - I_{xz}(\dot{p} - qr)]$	$\dot{u} = \frac{1}{m}[X - wq - mg\,\theta]$ $\dot{v} = \frac{1}{m}[Y - ur + mg\,s\phi]$ $\dot{w} = \frac{1}{m}[Z + uq + mg\,c\phi]$ $\dot{p} = \frac{1}{I_x}K$ $\dot{q} = \frac{1}{I_y}M$ $\dot{r} = \frac{1}{I_z}N$
$\dot{x} = c\psi c\theta\,u + (c\psi s\theta s\phi - s\psi c\phi)\,v + (s\psi s\phi + c\psi c\phi s\theta)\,w$ $\dot{y} = (s\psi c\theta)\,u + (c\psi c\phi + s\phi s\theta s\psi)\,v + (s\theta s\psi c\phi - c\psi s\phi)\,w$ $\dot{z} = -s\theta\,u + c\theta s\phi\,v + c\theta c\phi\,w$ $\dot{\phi} = p + s\phi t\theta\,q + c\phi t\theta\,r$ $\dot{\theta} = c\phi\,q - s\phi\,r$ $\dot{\psi} = (s\phi/c\theta)\,q + (c\phi/c\theta)\,r$	Substitute $s\theta = \theta$ and $c\theta = 1$

The forces and moments X, Y, Z, K, M and N in Table 7.1 are derived from the hydrodynamic forces on the struts and foils and the thrust. They are:

$$X = \sum_{i=1}^{nf}(X_F)_i + \sum_{i=1}^{ns}(X_S)_i + T \tag{7.70}$$

$$Y = \sum_{i=1}^{ns}(Y_S)_i \tag{7.71}$$

$$Z = \sum_{i=1}^{nf}(Z_F)_i \tag{7.72}$$

$$K = \sum_{i=1}^{nf}(Z_F)_i\,(l_{y_F})_i - \sum_{i=1}^{ns}(Y_S)_i\,(l_{z_S})_i \tag{7.73}$$

$$M = -\sum_{i=1}^{nf}(Z_F)_i\,(l_{x_F})_i + \sum_{i=1}^{nf}(X_F)_i\,(l_{z_F})_i + \sum_{i=1}^{ns}(X_S)_i\,(l_{z_S})_i + T\,l_{z_T} \tag{7.74}$$

$$N = \sum_{i=1}^{ns} (Y_S)_i \, (l_{x_S})_i \tag{7.75}$$

where

T	=	forward thrust	$(l_{x_F})_i$	=	x-coordinate of foil i
$(X_F)_i$	=	x-force foil i	$(l_{x_S})_i$	=	x-coordinate of strut i
$(X_S)_i$	=	x-force strut i	$(l_{y_F})_i$	=	y-coordinate of foil i
$(Y_S)_i$	=	y-force strut i	$(l_{z_F})_i$	=	z-coordinate of foil i
$(Z_F)_i$	=	z-force foil i	$(l_{z_S})_i$	=	z-coordinate of strut i
			l_{z_T}	=	z-coordinate of forward thrust

A block diagram showing the relationship between the 6 DOF equations and the flow between body axes and earth axes is shown in Figure 7.12.

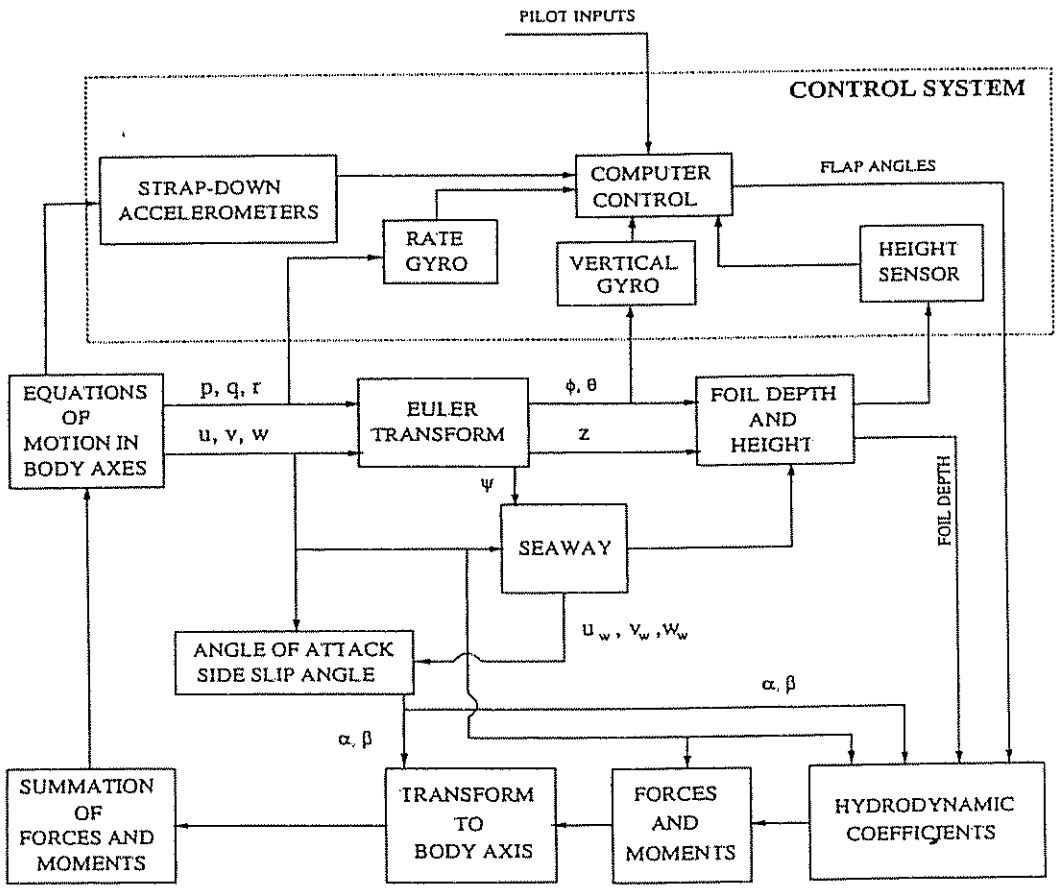

Figure 7.12: Block diagram of FoilCat and control modeling. In the figure angle of attack is defined as $\alpha = \tan^{-1}(w/u) \approx w/u$ and sideslip angle as $\beta = \sin^{-1}(v/U) \approx v/u$ under the assumption of no seaway.

Seaway Modeling

Since FoilCats must operate in the open seas, it is necessary to model the seaway in which it operates properly in order to design a control system which will give the ship a satisfactory ride. Whichever mathematical description of the seaway one chooses (see Section 3.2.1), it is necessary to model the height and orbital velocity both temporally and spacially (including depth). If one uses 8–12 frequencies of waves with weighted heights to represent the spectrum of the seaway (see Figure 3.1, Section 3.2) and attempts to model it both temporally and spacially at four different foil locations, an inordinate amount of computer time is soon being used. This makes it very time-consuming to run a simulation long enough in each heading to get good statistical data. If computational time is a problem, then it can be reduced by calculating the seaway at only one foil and assuming that exactly the same seaway reaches the other foils at a time delayed or advanced, determined by the foil separation, the ship speed and the group velocity (energy propagation velocity) of the propagating waves. An approximation could be to assume that the group velocity of the waves is equal to the velocity of the wave with dominant energy. This obviously is not correct but should give a reasonably good statistical representation of the ship's motion in a seaway.

7.2.2 Control Systems Design

The control system of a ship consists of the sensors, the computer and the force producers, see Figure 7.13.

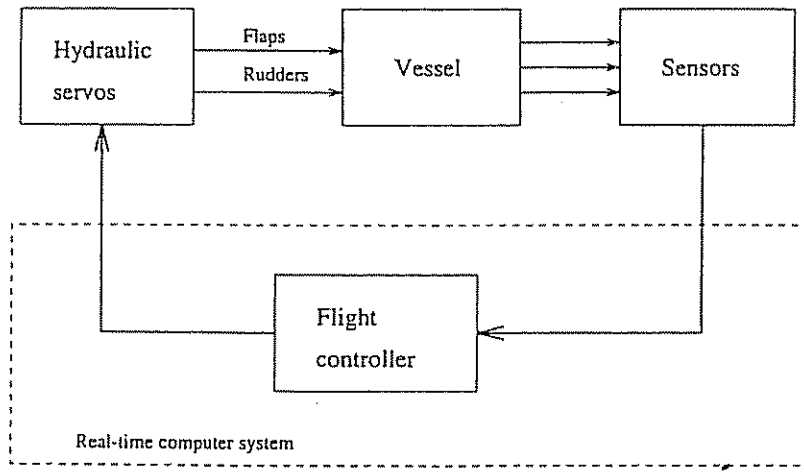

Figure 7.13: Block diagram showing the main functional elements of the control system.

The inputs to the system are pilot commands and seaway-induced disturbances. Using these three elements, a control system of a FoilCat must perform three functions. The first is to assure stability throughout its operating and maneuvering envelopes; the second is to attenuate seaway-induced motions; the third is to

assure the safety of the ship and its passengers at all times even if there is any failure in the control system. The first two functions are closely related, in that the first limits the gains that can be used in the control loop to attenuate the seaway-induced motions. Designing the control system for these two functions is a fairly straightforward problem for a control designer, particularly if a good computer model of the ship and seaway is used. The one factor that can complicate the design of a control system for stability and motion attenuation is a structural mode with a frequency low enough to be near the frequency at which one wishes to close the control loop. This rarely occurs for small and relatively stiff ships, but as the size of ships increases and their structural modal frequencies decrease it can be a limiting factor on the control gains and thus the motion attenuation It is the third function, safety, which should consume most of a control designer's effort and we will now direct our discussion to this issue. Inherent safety and a failure safe criterion in most cases determine the basic philosophy and architecture of the control system as well, as the selection of sensors and the degree of redundancy.

Control Objectives

A modern foil-supported vessel requires the solution to several complicated control system problems. Most relevant to the actual operation of the vessel are the following:

1. Flight control (attitude control, ride control, stabilization system) is needed to stabilize the vessel when foilborne, to ensure passenger comfort by compensating wave-induced disturbances, and to control the vessel attitude. Moreover, this system controls the *heave, pitch and roll* modes.

2. Steering by means of rudder control. This system controls the combined *sway and yaw* modes.

3. Forward speed (surge) control is achieved by adjustments of the thrust handle. This includes engine and propeller control.

The most important control variables associated with these sub-systems are as follows:

Flight Height: The captain will expect that the vessel runs steadily at the specified height. However, depending on the vessel speed, there will be maximum and minimum limitations to the flight height. At low speed the vessel cannot "take-off". At high speeds the vessel cannot go hullborne, that is it has to go foilborne. Figure 7.14 shows the possible flight height range for the *Westamarin West FoilCat 2900*. Several authors, like Johnson (1985), discuss the contouring (tracking the wave) and platforming (cutting through the wave) phenomena. Obviously, we prefer the vessel to keep a constant height regardless of the waves. Consequently, contouring should occur only as a result of the system's inability to achieve platforming.

Banked Turn: The roll angle should be held constant at zero except during turning maneuvers. At high speed the vessel should bank inwards when turning to reduce the impact of centrifugal forces on the passengers.

Constant Pitch Trim: The pitch angle will normally have an optimum value where the drag forces reach a minimum and propulsion forces reach their maximum, or as a trade-off between these two. This angle will be the constant pitch reference.

Heading Control: The yaw angle should be kept constant during course-keeping while steady-state turning is usually performed at constant yaw rate.

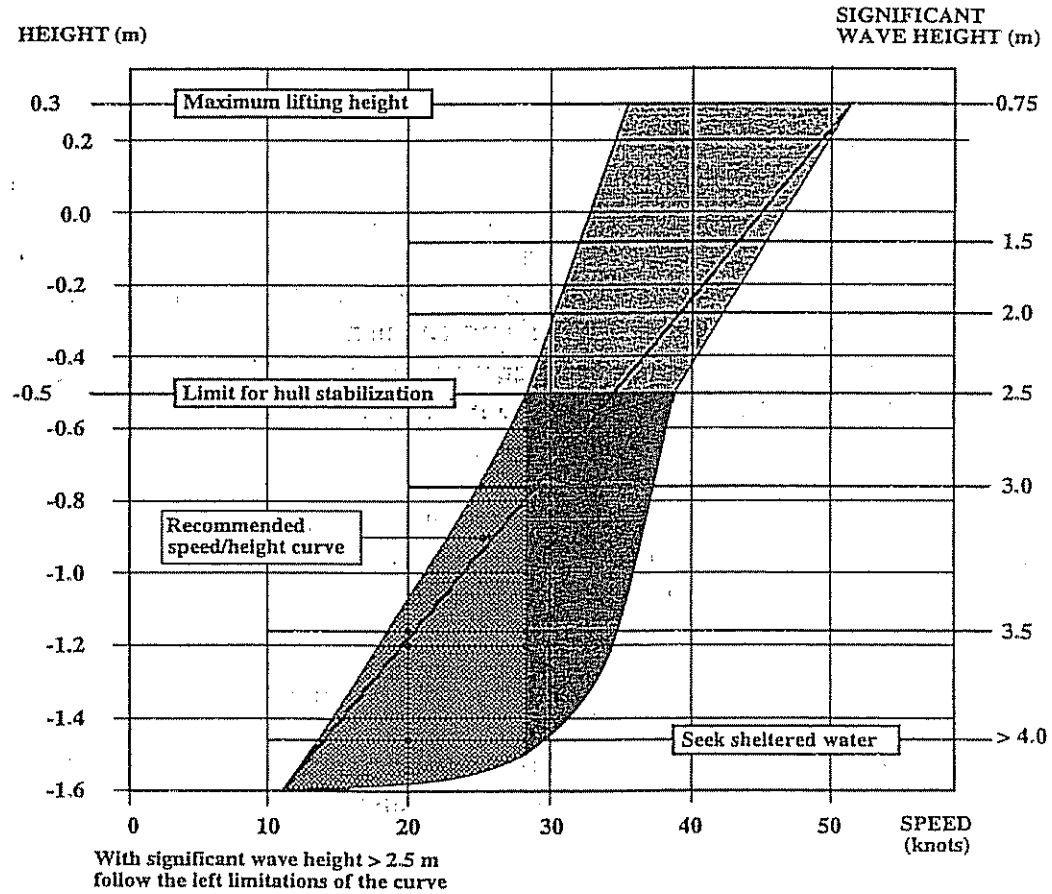

Figure 7.14: Height limitations versus speed for the Westamarin West FoilCat 2900. The height is defined as zero when the keels at the forward struts are at the mean water surface (Svenneby and Minsaas 1992).

FoilCats generally have two foils forward and one large foil which spans the whole beam aft. The rear foil has two sets of independently controlled flaps, one port and one starboard. Schematically the ship may be considered a rectangular box supported on its corners. Now if each foil is controlled by its own independent control system as shown in Figure 7.10, regardless of what failed in the control

system the worst that could happen is that one foil flap would go hard up and down.

Now if the control authority for roll and pitch was split equally between the forward and aft foils, then the large moment created by a hard over flap failure can be compensated for by the remaining three independently controlled foils. This has actually been demonstrated on an existing FoilCat. Such a control arrangement, however, requires an independent sensor package for each foil, which is expensive and leads perhaps to overkill. Splitting the control authority for pitch and roll between the forward and aft foils guards against many failures, the most important being a failure in a hydraulic servo valve.

If one assumes a control sensor package to sense roll, pitch and height and their respective derivatives that most foilborne craft have, then there are failures which can drive the FoilCat into a sudden and perhaps dangerous attitude. The most serious of these are a sudden failure of the vertical gyro, which gives the roll and pitch attitudes. It is therefore necessary to introduce redundancy in the form of two vertical gyros, to guard against such a failure. If you have two vertical gyros and one is used to control the forward foils and one is used to control the rear foils, then the split control authority mentioned in the previous paragraph mitigates the consequences of a failure in one vertical gyro. The failsafe thought process is carried through to all aspects and components of the control system.

Decentralized control of fully submerged foils has been discussed by several authors, Vogt (1969), Stark (1974) and O'Neill (1991) for instance.

Linear Multivariable Control

A linear multivariable control system can be designed by minimizing a quadratic performance index (Dixon 1976):

$$\min J = \frac{1}{2}\int_0^T (\nu^T Q_1 \nu + (\eta - \eta_d)^T Q_2 (\eta - \eta_d) + \tau^T P \tau)\, dt \qquad (7.76)$$

In this criterion the squared tracking error is weighted against the consumption of power. The optimal control gives feedback from all state variables can be written (see Appendix D):

$$\tau = G_1 \nu + G_2 \eta + G_3 \eta_d \qquad (7.77)$$

where G_1, G_2 and G_3 are three control gain matrices. Usually, all state variables cannot be measured directly, so we have to construct an estimator, for instance a Kalman filter, to produce estimates, $\hat{\eta}$ and $\hat{\nu}$, of the remaining variables; see Itoko, Higashino, Yamagami and Ikebuchi (1991).

The performance index can be formulated to minimize vertical acceleration for instance (Hsu 1975). Note, however, that the resulting optimal control will not include acceleration feedback. Wave-induced disturbances can be modelled and included in the performance index as well. This results in additional feedback

from wave measurements or estimates. This is, unfortunately, rather difficult to achieve.

A major drawback of this approach is that the optimal feedback is valid only for a neighborhood of the operating point ($\eta = \eta_d$, $\nu = 0$). One must make sure that the system is stable and has a certain performance in all other possible, or probable, operating points. If necessary, several optimal controllers for different operating points have to be calculated, and the flight controller will have to switch (or interpolate) between the different feedback gains according to some scheduling scheme. An alternative to gain scheduling could be to apply a nonlinear control law which can be designed for a large number of operating points. One such technique is feedback linearization.

Nonlinear Flap Control: Feedback Linearization

A multivariable nonlinear control system can be designed by considering the FoilCat model (7.66) and (7.67), that is:

$$M_{RB}\,\dot{\nu} + C_{RB}(\nu)\,\nu + g(\eta) = \tau \tag{7.78}$$

$$\dot{\eta} = J(\eta)\,\nu \tag{7.79}$$

with control input (forces and moments):

$$\tau = B(\nu)\,u \tag{7.80}$$

Here u is the new control variable usually specified in terms of volt signals in the computer and $B(\nu)$ is a control matrix given by the location of the flaps and rudder actuators. We recall from Section 4.5.2, Equation (4.223), that the nonlinear decoupling control law can be written:

$$\boxed{\tau = M_{RB}\,a_\nu + C_{RB}(\nu)\,\nu + g(\eta)} \tag{7.81}$$

where

$$a_\nu = J^{-1}(\eta)\,[a_\eta - \dot{J}(\eta)\,\nu] \tag{7.82}$$

and

$$a_\eta = \ddot{\eta}_d - K_d\,\dot{\tilde{\eta}} - K_p\,\tilde{\eta} \tag{7.83}$$

This yields the error dynamics:

$$\ddot{\tilde{\eta}} + K_d\,\dot{\tilde{\eta}} + K_p\,\tilde{\eta} = 0 \tag{7.84}$$

where K_p and K_d are two positive definite matrices specifying the closed-loop response.

Flap Servo Allocation

The control forces and moments can be distributed to the flap servos according to (see (4.24)):

$$\boxed{u = B_W^{\dagger}(\nu)\,\tau} \tag{7.85}$$

where

$$B_W^{\dagger}(\nu) = W^{-1}B^T(\nu)[B(\nu)W^{-1}B^T(\nu)]^{-1} \tag{7.86}$$

is the generalized pseudo inverse of B which exists if the matrix $BW^{-1}B^T$ is non-singular. W is usually taken to be a diagonal matrix weighting the different actuators. If all flaps are weighted equally and B is a square matrix with full rank we can replace $B_W^{\dagger}$ with B^{-1}.

Consider a FoilCat having 4 flaps which can be used to control 3 DOF (heave, roll and pitch). Consequently, we have flap redundancy. Let us assume that all 4 flaps are placed symmetrically around the vessel. Hence, the control matrix relating the heave, roll and pitch responses to the flap angles will be of dimension 3×4, that is:

$$B = \begin{bmatrix} b_1 & -b_1 & b_2 & -b_2 \\ b_3 & b_3 & b_4 & b_4 \\ b_5 & b_5 & b_6 & b_6 \end{bmatrix} \tag{7.87}$$

where the elements b_i $(i = 1...6)$ may be constants or nonlinear expressions. Now, note that for any value of Δ, the input vector:

$$u_0 = \begin{bmatrix} \Delta & -\Delta & -\frac{b_1}{b_2}\Delta & \frac{b_1}{b_2}\Delta \end{bmatrix} \tag{7.88}$$

has the property that:

$$B\,u_0 = 0 \tag{7.89}$$

That is, all inputs on the form u_0 will not affect any of the three degrees of freedom. The vector u_0 is said to lie in the *null space* of B. This redundancy phenomenon opens new perspectives to control: If we do not give this problem our full attention, we may end up with control algorithms that every now and then generate input vectors, u, in (or near) the null space of B, and for those moments the vessel will be uncontrolled. On the other hand, redundancy means that the vessel can still be controlled if we lose one actuator. Also note that we have the possibility of manipulating the inputs without degrading the vessel performance. For example, if one of the flaps is saturated, we can bring it back in operation with an additional input u_0 where Δ is properly chosen.

Sensors and Failure Detection

Several sensors are normally needed on a foil catamaran. An inertial platform or vertical gyros are usually used to measure the roll, pitch and yaw angles and also possible heave motion. In addition to these sensor units accelerometers can be used to give the vertical acceleration at different positions on the vessel, and a speed sensor (Doppler log, GPS etc.) is needed to calculate speed-dependent height and flap angle limitations.

The flight height is usually measured by some kind of range sensor (ultrasonic or laser) mounted in the vessel bow. The problem with the range sensor is that the sensor measures the distance to a disturbed sea surface while we actually need the distance to the mean sea level. However, an accurate mean level estimate can be obtained by comparing the disturbed height sensor signal with an accurate vertical acceleration measurement, preferably corrected for roll and pitch motion. This can be done by applying a Kalman filter as shown in Figure 7.15.

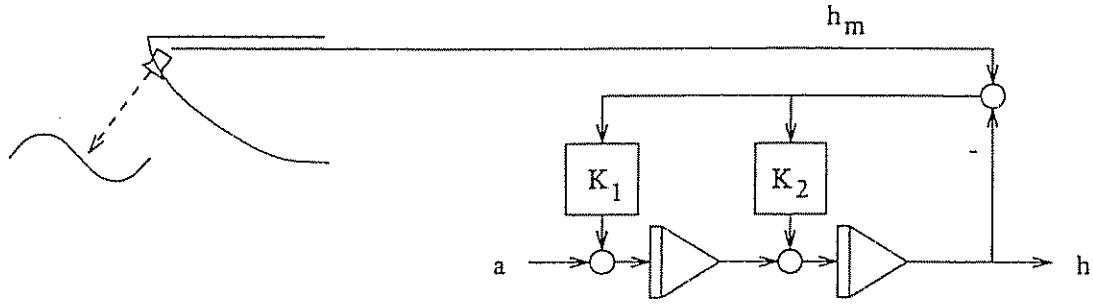

Figure 7.15: Integrating height sensor signal h_m and vertical acceleration measurement a.

The purpose of the estimator in Figure 7.15 is to use the information from the height sensor for mean level determination and the acceleration measurements for high-frequency motion estimates. By a proper tuning of the estimator gains we get transfer functions from the height sensor and the accelerometer, respectively, to the height estimate, as shown in Figure 7.16.
The low-frequency range (e.g. mean value) uses height sensor information, whereas the high-frequency estimate is essentially the double integral of the acceleration. The interesting frequency range can be found from local wave statistics, from typical frequencies of encounter. Moreover, the estimator should be tuned so that the typical frequency of encounter ω_e is above the cross frequency ω_c.

The consequences of component failures in flight control systems may be severe. To reduce the risk of single sensor errors causing serious accidents, one should design an on-line error detection and isolation algorithm (Clark 1978). Erroneous sensor signals should be detected before the control system governs the vessel into a dangerous situation. It is equally important to *isolate* the defect component so that the flight controller can still operate utilizing the functionality remaining in the system. A signal may be checked against max/min limits or a maximum rate of change. Dynamic relationships, for instance the transfer

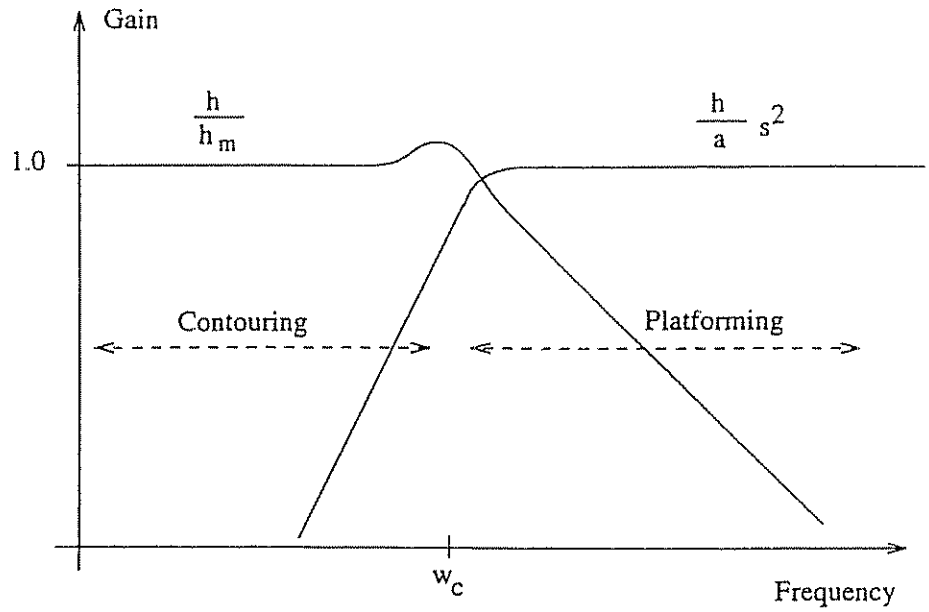

Figure 7.16: Transfer functions from height sensor signal, h_m, and vertical acceleration, a, to height estimate, h.

between position and acceleration, can be checked by means of a dynamic model in an estimator (Frank 1990).

The following lists control components and gives a short discussion of how they should be used to achieve failsafe or make failure detection easier, so that immediate steps can be taken to compensate for the failure.

Flap Position Sensor: The position of the flap is usually provided by a linear differential transformer (LVDT). Each flap usually has two LVDT position sensors and their output is summed. Most failures in the LVDT would result in zero output or high output. If for the maximum and minimum flap positions the normal range of the LVDT was above zero to below the maximum output, then any time the LVDT output was zero or above the maximum one would immediately know there has been a failure, and that LVDT is disconnected and the gain of the remaining doubled.

Servo Valves: Servo valves can be bought with a slight spring bias in them so that in case of no power to them, they will drift in a preferred direction. The designers determine which direction is the safest and order the servo valve biased accordingly. Servo valves also have two coils in them. They should be wired in parallel as the most likely failure is a break in one coil wire, in which case there is only a halving of the servo valve gain.

Vertical Gyros: Most rapid failures in vertical gyros are either to zero or they tumble and give a high angle output. Since FoilCats normally operate at low roll and pitch angles, any time one vertical gyro reads a very high angle and the other reads a reasonable angle, the one reading a very high angle is assumed to have failed and the system it was controlling is switched to the good gyro.

7.2.3 Stability and Maneuverability

Maneuvering Control

The side force required to maneuver or turn a FoilCat can be generated in three ways.

1. A stern rudder or in the case of water-jet driven ships by deflecting the jets with turning buckets.
2. Forward rudders.
3. Banking the ship and using the lateral component of the lift vector.

The turning effectiveness of the first two is inversely proportional to the degree of directional stability inherent in the ship. Reducing the directional stability in order to enhance maneuverability is a design trade-off study which must be done with care, particularly if the method of turning creates side-slip angles on the struts which may trigger ventilation.

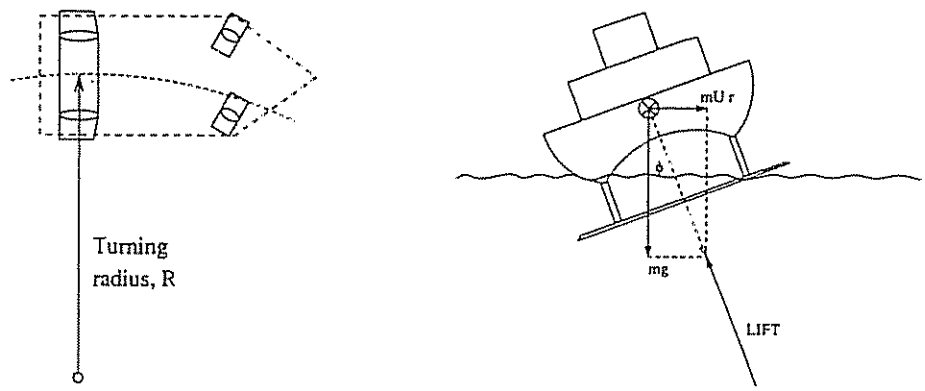

Figure 7.17: Banking of the ship by means of steerable forward struts. The bank (roll) angle during steady state turn is given by $\phi = \tan^{-1}(Ur/g) \approx Ur/g$ where U is the forward speed, r is the turning rate and g is the acceleration of gravity.

The third method, banking the ship in conjunction with steerable forward struts (see Figure 7.17) gives relatively high turn rates, independent of directional stability while keeping the sideslip angle of the struts close to zero. It is little wonder that this method of turning has evolved as the preferred way for foilborne ships. For FoilCats in which the length of the struts is relatively short compared to conventional hydrofoils, the bank angle is limited to 5 or 6 (deg) before the inboard hull touches the water. This limits the turn rate at which perfect coordination can be achieved to about 2.5 to 3.0 (deg/s). Holding the maximum bank at say 5 to 6 (deg), and increasing the angle on the forward struts, 5 (deg/s) can be achieved while still keeping the maximum side slip angle on the struts below one degree.

Stability

The two basic functions of a FoilCat control system are to assure stability and to attenuate seaway-induced motions. Just assuring stability is quite simple. The geometry of a FoilCat gives it a slight degree of inherent stability. The decrease in lift as the foil depth decreases gives a slight stabilizing force in both the roll and heave mode. The normally larger struts aft needed for propulsion give a degree of yaw stability, and the normally lower aspect ratio of the forward foils have the necessary lower lift curve slope to meet the criterion:

$$(C_{L\alpha}/C_{L0})_{\text{fore}} < (C_{L\alpha}/C_{L0})_{\text{aft}} \tag{7.90}$$

for inherent pitch stability. This inherent stability, however, is generally very slight and must be augmented by the control system.

The primary variables to be controlled are pitch, roll and heave. Pitch and roll are usually sensed by a vertical gyro, and height above the water surface is measured by a sonic or radar height sensor. The anticipation needed to damp the derivatives of pitch and roll can be obtained by simple pitch and roll rate gyroscopes. Heave rate is best achieved by integrating a vertical accelerometer. The vertical accelerometer output is also used directly in the control system to give the anticipation needed to attenuate the higher frequency seaway induced motion.

The height sensor measures the distance from a point on the ship to the water surface. In a seaway this can be quite a varying signal. The control system should not attempt to hold the height above the water surface constant (this would indeed be a tough ride) but should maintain the height above the mean surface constant. In other words, the height sensor output must be filtered sufficiently to give an approximate average of the height above the mean water surface. As is clearly demonstrated by O'Neill (1991), the height sensor controls low-frequency motions, the heave rate signal medium-frequency motions and the accelerometer high-frequency motions.

The degree of motion attenuation is a direct function of the control system gains, particularly the gains of the acceleration and heave rate feedback loops; that is, the higher these gains the better the motion attenuation. Unfortunately, there is a limit to the gains that are possible and still maintain adequate stability. The degree of stability needed to have a robust system, that is one which has sufficient margins to account for weight and speed variations, structural compliance and other unknown phenomena, is usually defined by the gain and phase margins. For most foilborne ships a minimum gain margin of 2 to 1 and a minimum phase margin of 60^o is used. Early in the design process a simplified linear model can be used with classical control techniques to design the control system and determine the feedback gains. Later, when the nonlinear computer model is available, the control system can be tuned to give the best performance while staying within the specified margins.

7.2.4 FoilCat Performance

Figure 7.18 shows the vertical vibrations experienced by passengers onboard the FoilCat 2900. For comparison, the response onboard a conventional catamaran is included. The diagram indicates that the FoilCat can run for more than 8 hours in heavy seas without having too many cases of sea sickness.

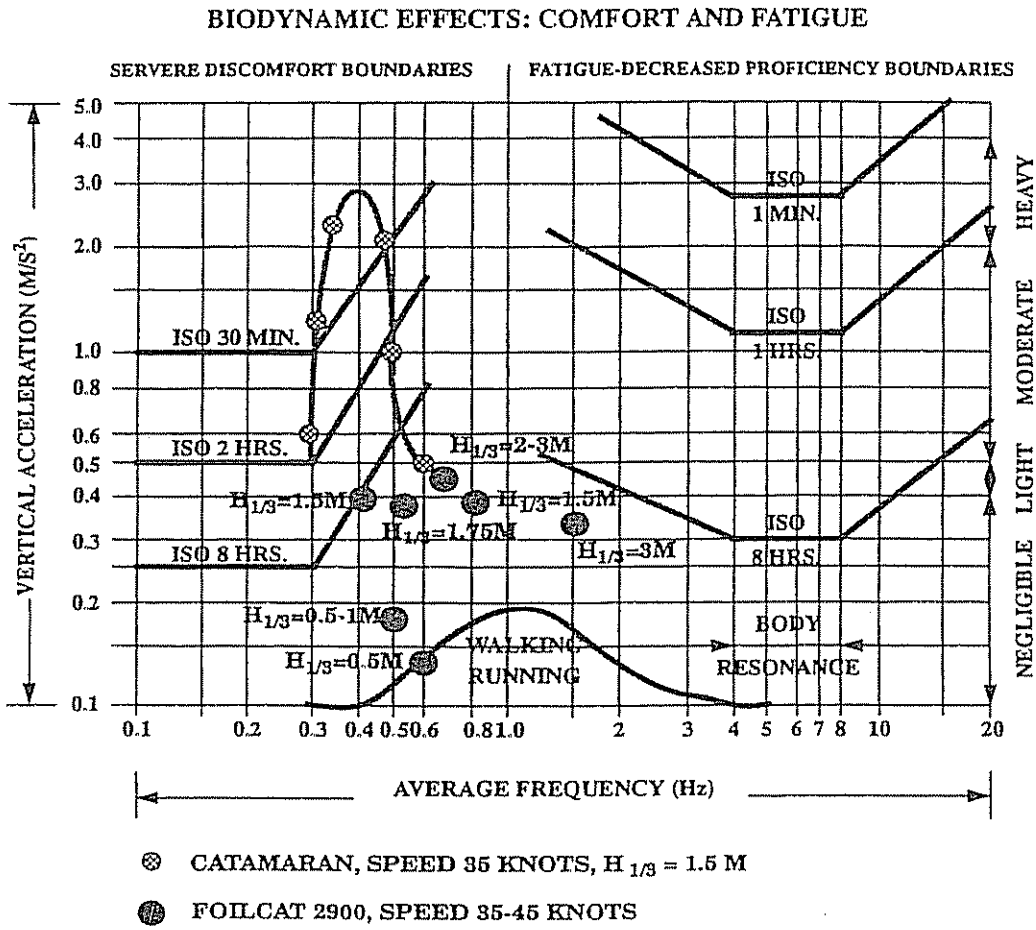

Figure 7.18: Comparison of dynamic load for the Westamarin FoilCat 2900 and a conventional catamaran: RMS value of vertical acceleration versus frequency. The curves show human discomfort boundaries for different exposure times (Svenneby and Minsaas 1992).

A simulation example comparing the response of a FoilCat and a conventional catamaran is shown in Figure 7.19. The catamaran model was obtained by removing all forces from the foil system in the FoilCat model. The FoilCat is foilborne with both hulls above the mean sea level. Comparable RMS values for vertical acceleration are 0.05 g for the FoilCat and 0.7 g for the catamaran.

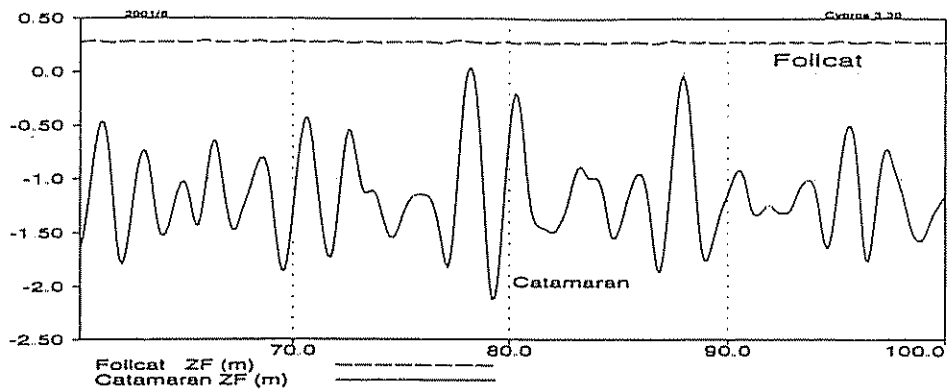

Figure 7.19: Comparison of heave response in m for the Westamarin FoilCat 2900 and a conventional catamaran at 37 knots in head seas with $H_{1/3} = 1.0$ m.

7.3 Conclusions

In this chapter a brief introduction to the control of high-speed craft has been made.

In Section 7.1 we have discussed mathematical modeling and control of surface effect ships (SES). This is done in the framework of passivity theory and by using collocated sensor and actuator pairs. Full-scale experiments have been used to verify the design. It was observed that perfect collocation increased the energy dissipation and thus the ride quality in rough seas.

In Section 7.2 we have discussed mathematical modeling, maneuvering and control of foilborne catamarans (FoilCats). This is done in terms of a simplified FoilCat model and a more general 6 DOF model. Nonlinear FoilCat control system design and flap servo allocation are also briefly discussed.

The interested reader is advised to study the proceedings of the *Conference on Fast Sea Transportation* (FAST) for articles discussing modeling and control of high-speed crafts.

Appendix A

Some Matrix Results

Let A be an $n \times n$ real matrix. Then we can make the following useful matrix definitions (Strang 1980):

Definition A.1 (Symmetric Matrix)
The real matrix A is symmetrical if:

$$A = A^T \tag{A.1}$$

□

Definition A.2 (Quadratic Form)
The scalar:

$$\alpha = x^T A x \quad \forall \ x \in \mathbb{R}^n \tag{A.2}$$

formed by the vector x and matrix A is a quadratic form.
□

Definition A.3 (Skew-Symmetric Matrix)
The real matrix A is skew-symmetrical if:

$$A = -A^T \tag{A.3}$$

Hence its quadratic form is zero, that is $\alpha = x^T A x = 0 \quad \forall \ x \in \mathbb{R}^n$.
□

Definition A.4 (Positive Matrix)
The real matrix A is positive if:

$$\alpha = x^T A x \geq 0 \quad \forall \ x \in \mathbb{R}^n \tag{A.4}$$

□

Definition A.5 (Strictly Positive Matrix)
The real matrix A is strictly positive if:

$$\alpha = x^T A x > 0 \quad \forall \ x \neq 0 \tag{A.5}$$

□

Definition A.6 (Positive Definite Matrix)
Each of the following tests is a necessary and sufficient condition for the real symmetric matrix $A = A^T$ to be positive definite:

1. $x^T A x > 0 \ \forall \ x \neq 0$
2. *All the eigenvalues of A satisfy:* $\lambda_i(A) > 0$
3. *All the upper left submatrices A_k have positive determinants*
4. *There exists a matrix W such that:* $A = W^T W$

Moreover, a positive definite matrix is both symmetrical and strictly positive.
□

Definition A.7 (Positive Semi-Definite Matrix)
The real symmetric matrix $A = A^T$ is positive semi-definite if it is quadratic form satisfies:

$$\alpha = x^T A x \geq 0 \quad \forall \ x \in \mathbb{R}^n \tag{A.6}$$

□

Remark A.1 (Strictly Positive Matrix)
A non-symmetric real matrix $A \neq A^T$ is strictly positive if $(A+A^T)/2$ is positive definite. Let A be written as:

$$A = \frac{1}{2}(A + A^T) + \frac{1}{2}(A - A^T) \tag{A.7}$$

where $(A+A^T)/2$ is a symmetric matrix and $(A-A^T)/2$ will be a skew-symmetric matrix. Consequently, the quadratic form $x^T A x = 1/2\, x^T (A + A^T) x$ must be positive for all $x \neq 0$ for A to be positive.
□

Notation Used for Positive Matrices

For notational simplicity both a positive definite (symmetric) and strictly positive (non-symmetric) matrix will be denoted by:

$$A > 0 \tag{A.8}$$

while a positive semi-definite (symmetric) and positive (non-symmetric) matrix is written as:

$$A \geq 0 \tag{A.9}$$

Appendix B

Numerical Methods

From a physical point of view the vehicle dynamics is most naturally derived in the continuous-time domain based on concepts from Newtonian or Lagrangian dynamics. In the implementation of the control law it is desirable to represent the nonlinear dynamics and kinematics in discrete time. We will briefly discuss discretization of linear and nonlinear systems in this chapter. In addition to this, we will discuss numerical integration and differentiation.

B.1 Discretization of Continuous-Time Systems

In this section we will first discuss discretization of linear state-space models before we discuss a method presented by Smith (1977) for nonlinear systems.

Notation Used for Discrete-Time Systems

For notational simplicity, we will denote $t_k = kt$ such that:

$$x(k) = x(t_k); \qquad x(k+1) = x(t_k + h) \tag{B.1}$$

where h is the sampling interval. Furthermore, the *forward shift operator* z defined by:

$$x(k+1) \triangleq z\, x(k) \tag{B.2}$$

will be used for stability analyses in the z-domain.

B.1.1 Linear State-Space Models

Consider the linear continuous-time model:

$$\dot{x} = A\, x + B\, u \tag{B.3}$$

Assume that u is piecewise constant over the sampling interval h and equal to $u(k)$. Hence, the solution of (B.3) can be written:

$$x(k+1) = \exp(Ah)\, x(k) + \int_{kh}^{(k+1)h} \exp(A\,[(k+1)h - \tau])\, B\, u(k)\, d\tau \qquad \text{(B.4)}$$

which after integration yields the linear discrete-time model:

$$x(k+1) = \Phi\, x(k) + \Delta\, u(k) \qquad \text{(B.5)}$$

where

$$\Phi = \exp(Ah) \qquad \text{(B.6)}$$
$$\Delta = A^{-1}(\Phi - I)\, B \qquad \text{(B.7)}$$

Φ is usually computed as:

$$\Phi = \exp(Ah) = I + A\,h + \frac{1}{2!}A^2\,h^2 + ... + \frac{1}{n!}\,A^n\,h^n + ... \qquad \text{(B.8)}$$

Hence, a 1st-order approximation (Euler discretization) will be:

$$\Phi \approx I + A\,h \qquad \text{(B.9)}$$
$$\Delta \approx B\,h \qquad \text{(B.10)}$$

Alternately, Φ can be computed by applying a similarity transformation, that is:

$$\Phi = \exp(Ah) = E\, \exp(\Lambda\, h)\, E^{-1} \qquad \text{(B.11)}$$

where

$$\exp(\Lambda\, h) = \mathrm{diag}\{\exp(\lambda_i\, h)\} \qquad \text{(B.12)}$$

is a diagonal matrix containing the eigenvalues λ_i of A and E is the corresponding eigenvector matrix.

Example B.1 (Discretization of a 1st-Order Linear System)
Consider the SISO linear system:

$$\dot{x} = a\,x + b\,u \qquad \text{(B.13)}$$
$$y = c\,x + d\,u \qquad \text{(B.14)}$$

Hence,

$$x(k+1) = \exp(ah)\, x(k) + \frac{b}{a}(\exp(ah) - 1)\, u(k) \qquad \text{(B.15)}$$
$$y(k) = c\,x(k) + d\,u(k) \qquad \text{(B.16)}$$

□

B.1.2 Nonlinear State-Space Models

Consider the nonlinear model:

$$M\,\dot{\nu} + C(\nu)\,\nu + D(\nu)\,\nu + g(\eta) = B\,u \tag{B.17}$$

$$\dot{\eta} = J(\eta)\,\nu \tag{B.18}$$

which can be expressed as a nonlinear time-invariant system:

$$\dot{x} = f(x,u) \tag{B.19}$$

where $x = [\eta^T, \nu^T]^T$ and:

$$f(x,u) = \begin{bmatrix} J(\eta)\,\nu \\ M^{-1}[B\,u - C(\nu)\,\nu - D(\nu)\,\nu - g(\eta)] \end{bmatrix} \tag{B.20}$$

Differentiating (B.19) with respect to time, yields:

$$\ddot{x} = \frac{\partial f(x,u)}{\partial x}\dot{x} + \frac{\partial f(x,u)}{\partial u}\dot{u} \tag{B.21}$$

The effect of a zero-order-hold in the digital-to-analog converter makes $\dot{u} = 0$ over the discrete-time interval. Furthermore, the definition of the Jacobian:

$$\mathcal{J}(x) = \frac{\partial f(x,u)}{\partial x} \tag{B.22}$$

implies that the nonlinear continuous equation (B.21) is reduced to a homogeneous equation:

$$\ddot{x} = \mathcal{J}(x)\,\dot{x} \tag{B.23}$$

Let $\mathcal{J}(x)$ evaluated at $x(k)$ be denoted by:

$$\mathcal{J}[x(k)] = \left.\frac{\partial f(x,u)}{\partial x}\right|_{x=x(k)} \tag{B.24}$$

Hence, the solution of the homogeneous differential equation is:

$$\dot{x} = \exp(\mathcal{J}[x(0)]\,(t - t_0))\,\dot{x}(0) \tag{B.25}$$

Integration of this expression over a sampling interval h, finally yields:

$$x(k+1) = x(k) + \int_0^h \exp(\mathcal{J}[x(k)]\,\tau)\,\dot{x}(k)\,d\tau \tag{B.26}$$

Example B.2 (Discretization of a 2nd-Order Nonlinear System)
Consider the SISO nonlinear system:

$$\dot{x}_1 = x_2 \tag{B.27}$$

$$\dot{x}_2 = f(x_2) + u \tag{B.28}$$

where $x = [x_1, x_2]^T$ is the state vector and u is the input. The Jacobian is found as:

$$\mathcal{J}(x) = \begin{bmatrix} 0 & 1 \\ 0 & a(x_2) \end{bmatrix}; \qquad a(x_2) = \frac{\partial f(x_2)}{\partial x_2} \tag{B.29}$$

Hence, applying a similarity transformation:

$$\exp(\mathcal{J}[x(k)]\, t) = \boldsymbol{E}^{-1} \exp(\boldsymbol{\Lambda}\, t)\, \boldsymbol{E} \tag{B.30}$$

where $\boldsymbol{\Lambda}$ is a diagonal matrix containing the eigenvectors of $\mathcal{J}$ and $\boldsymbol{E}$ is a matrix formed by the corresponding eigenvectors, yields:

$$\exp(J[x(k)]\, t) = \begin{bmatrix} 1 & \frac{1}{a_k}(1 - \exp(a_k t)) \\ 0 & \exp(a_k t) \end{bmatrix} \tag{B.31}$$

where $a_k = a(x_2(k))$. Hence,

$$\begin{bmatrix} x_1(k+1) \\ x_2(k+1) \end{bmatrix} = \begin{bmatrix} x_1(k) \\ x_2(k) \end{bmatrix} + \int_0^h \begin{bmatrix} 1 & \frac{1}{a_k}(1 - \exp(a_k \tau)) \\ 0 & \exp(a_k \tau) \end{bmatrix} \begin{bmatrix} x_2(k) \\ f(x_2(k)) + u(k) \end{bmatrix} d\tau \tag{B.32}$$

□

The discrete model (B.26) can be simplified by approximating the exponential function to the the first order, that is:

$$\exp(\mathcal{J}[x(k)]\, h) = I + \mathcal{J}[x(k)]\, h + O(h^2) \tag{B.33}$$

B.2 Numerical Integration

In this section we will briefly discuss numerical solutions to the nonlinear time-varying system:

$$\dot{x} = f(x, u, t) \tag{B.34}$$

where the control input u is assumed to be constant over the sampling interval h (zero-order hold). The stability properties of the different methods will be evaluated for a 2nd-order test system.

Test System

The test system used in the stability analyses is described by the following set of differential equations:

$$\dot{v} + 2\,\zeta\,\omega_0 v + \omega_0^2\, x = u \tag{B.35}$$

$$\dot{x} = v \tag{B.36}$$

where ζ is the relative damping factor and ω_0 is the natural frequency. An undamped harmonic oscillator is obtained for $\zeta = 0$. The undamped oscillator has two imaginary roots at $\lambda_{1,2} = \pm\, i\,\omega_0$. This system can be represented by the state-space model:

$$\dot{\boldsymbol{x}} = \boldsymbol{A}\,\boldsymbol{x} + \boldsymbol{B}\,\boldsymbol{u} \tag{B.37}$$

with obvious choices of $\boldsymbol{A}$ and $\boldsymbol{B}$. Applying a similarity transformation $\boldsymbol{x} = \boldsymbol{E}\,\boldsymbol{q}$ to this system, yields:

$$\dot{\boldsymbol{q}} = \boldsymbol{\Lambda}\,\boldsymbol{q} + \boldsymbol{E}^{-1}\boldsymbol{B}\,\boldsymbol{u} \tag{B.38}$$

where $\boldsymbol{\Lambda} = \mathrm{diag}\{\lambda_i\} = \boldsymbol{E}^{-1}\boldsymbol{A}\boldsymbol{E}$ is a diagonal matrix with the system eigenvalues on the diagonal and $\boldsymbol{E}$ is a matrix formed by the corresponding eigenvectors. The diagonal structure of (B.38) suggests that the *stability region* for most numerical integration routines can be derived by simply considering a 1st-order test system with eigenvalue λ, that is:

$$\dot{x} = \lambda\, x \tag{B.39}$$

This corresponds to choosing $f(x) = \lambda\, x$ in (B.34).

Stability Region

The stability region for a linear multistep integration method (LMIM):

$$\sum_{j=0}^{n} \alpha_j\, x(k+j) = h \sum_{j=0}^{n} \beta_j\, f(k+j) \tag{B.40}$$

where α_j and β_j $(j = 1...n)$ are two coefficients depending on what type of integration method which is used, is obtained through the following definition (see Lambert 1973):

Definition B.1 (Absolute Stability)
The LMIM (B.40) is said to have absolute stability for a given $\overline{h} = h\lambda$ if all roots r_s of the characteristic equation:

$$\pi(r, \overline{h}) = \sum_{j=0}^{n} (\alpha_j - \overline{h}\,\beta_j)\, r^j = 0 \tag{B.41}$$

satisfy

$$|r_s| < 1; \qquad s = 1...n \tag{B.42}$$

Otherwise, the LMIM is said to be absolutely unstable for that $\overline{h}$.
□

Consequently, the stability region for $\overline{h}$ in the complex plane is directly given by inequality (B.42).

B.2.1 Euler's Method

Euler proposed the algorithm:

$$x(k+1) = x(k) + h\, f(x(k), u(k), t_k) \tag{B.43}$$

The global truncation error for Euler's Method is of order $O(h)$. Applying Euler's method to the 2nd-order test system, yields:

$$\begin{aligned} v(k+1) &= v(k) + h\,[u(k) - 2\,\zeta\,\omega_0\,v(k) - \omega_0^2\,x(k)] && \text{(B.44)} \\ x(k+1) &= x(k) + h\,v(k) && \text{(B.45)} \end{aligned}$$

It should be noted that Euler's method should only be applied to a well-damped 2nd-order system. This can be seen by studying the 1st-order test system in the z-domain, that is:

$$x(k+1) = (1 + h\,\lambda)\,x(k) \tag{B.46}$$

which clearly is stable if $1 + h\lambda$ is inside the unit circle. The stability region for this system is shown in Figure B.1. Alternatively, the stability region can be derived by solving the characteristic equation (see (B.40) and (B.41)):

$$\pi(r, \overline{h}) = (1 - \overline{h} \cdot 0)\, r^1 + (-1 - \overline{h} \cdot 1)\, r = r - (1 + \overline{h}) = 0 \tag{B.47}$$

which yields:

$$|r_s| = |1 + \overline{h}| < 1 \tag{B.48}$$

Unfortunately (see the upper left plot in Figure B.1) this solution implies that systems with $\zeta = 0$ and thus $\lambda = \pm i\omega_0$ corresponding to an undamped oscillator will yield an unstable solution. However, a stable method for the undamped 2nd-order system can be obtained by combining the following two schemes:

$$\begin{aligned} &\text{Forward Euler:} && v(k+1) = v(k) + h\,[u(k) - 2\,\zeta\,\omega_0\,v(k) - \omega^2 x(k)] && \text{(B.49)} \\ &\text{Backward Euler:} && x(k+1) = x(k) + h\,v(k+1) && \text{(B.50)} \end{aligned}$$

The transfer function between $u(k)$ and $x(k)$ is:

$$\frac{x}{u}(z) = \frac{h^2}{z^2 + [(\omega_0 h)^2 + 2(\zeta\omega_0 h - 1)]\, z + (1 - 2\zeta\omega_0 h)} \tag{B.51}$$

The stability region for this test system can be found by application of Jury's stability test; see Ogata (1987).

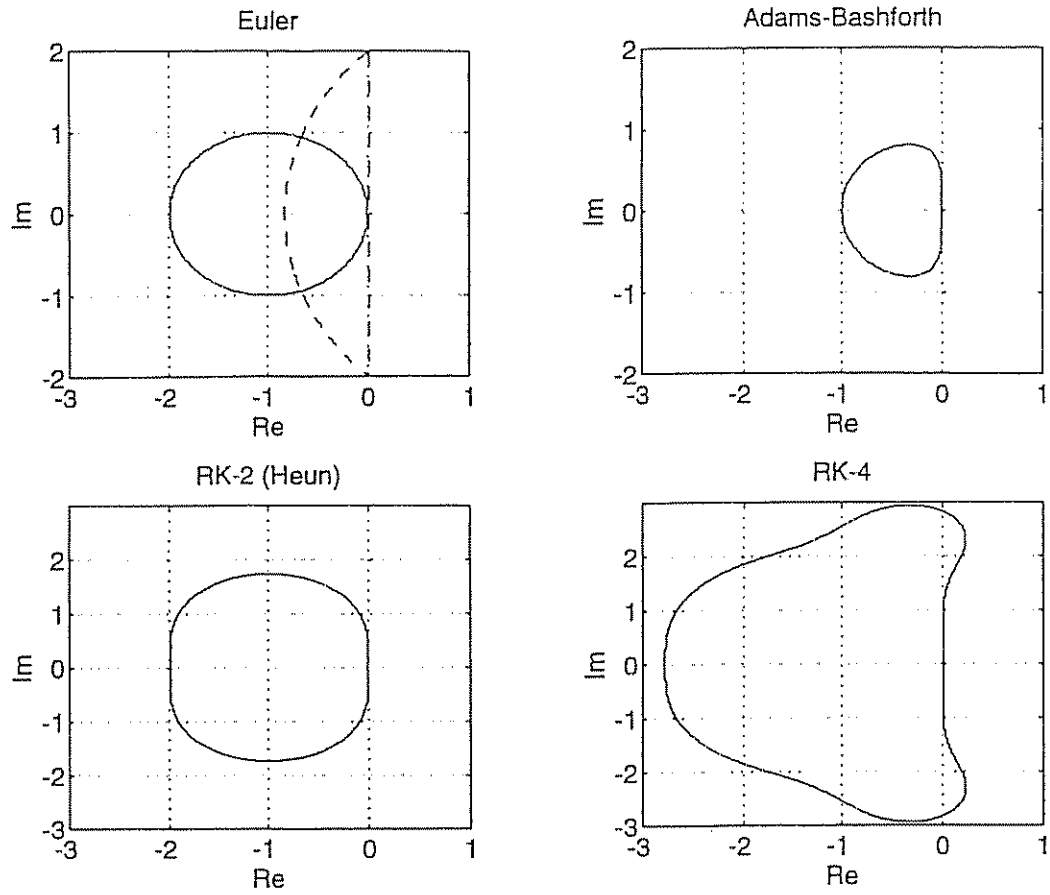

Figure B.1: Plots showing the stability regions for forward Euler (solid) and combined forward and backward Euler (dotted), Adams–Bashforth 2nd-order, Heun and Runge–Kutta 4th-order integration.

Definition B.2 (Stability Criterion by the Jury Test)
A 2nd-order system with characteristic polynomial:

$$P(z) = z^2 + a_1\, z + a_2 \tag{B.52}$$

where a_1 and a_2 are real coefficients, is stable if the following inequalities hold:

$$|a_2| < 1 \tag{B.53}$$
$$a_1 + a_2 + 1 > 0 \tag{B.54}$$
$$a_2 - a_1 + 1 > 0 \tag{B.55}$$

□

Hence, $a_1 = (\omega_0 h)^2 + 2(\zeta\omega_0 h - 1)$ and $a_2 = 1 - 2\zeta\omega_0 h$. According to Definition B.2 this implies that:

$$|1 - 2\zeta\omega_0 h| < 1 \quad \text{(B.56)}$$
$$\omega_0 h > 0 \quad \text{(B.57)}$$
$$(\omega_0\, h)^2 + 4\,(\zeta\,\omega_0\, h - 1) > 0 \quad \text{(B.58)}$$

The eigenvalues of the 2nd-order system are:

$$\lambda_{1,2} = (-\zeta \pm \sqrt{\zeta^2 - 1})\,\omega_0 \quad \text{(B.59)}$$

Since $h > 0$ and $\zeta \geq 0$, the first two conditions reduces to:

$$\omega_0 > 0 \quad \text{(B.60)}$$

and the last inequality can be written:

$$(h\,\lambda_{1,2})^2 + 4\,\gamma\,\zeta\,h\,\lambda_{1,2} - 4\,\gamma^2 > 0 \qquad \gamma = -\zeta \pm \sqrt{\zeta^2 - 1} \quad \text{(B.61)}$$

which simply reduces to $h < 2/\omega_0$ for the undamped system. The stability region for the combined method is shown in the upper left plot of Figure B.1.

Extension to Nonlinear Systems

The methods of Euler can be extended to the more general nonlinear system:

$$\dot{\nu} = M^{-1}\,[B\,u - C(\nu)\,\nu - D(\nu)\,\nu - g(\eta)] \quad \text{(B.62)}$$
$$\dot{\eta} = J(\eta)\,\nu \quad \text{(B.63)}$$

by the following set of discrete-time equations:

$$\nu(k+1) = \nu(k) + h\,M^{-1} [B\,u(k) - C(\nu(k))\,\nu(k) - D(\nu(k))\,\nu(k) - g(\eta(k))] \quad \text{(B.64)}$$
$$\eta(k+1) = \eta(k) + h\,[J(\eta(k))\,\nu(k+1)] \quad \text{(B.65)}$$

It should be noted that care should be taken in the nonlinear case since all stability regions presented are based on a purely linear analysis. However, computer simulations of 2nd-order nonlinear systems show good numerical behavior.

B.2.2 Adams–Bashforth's 2nd-Order Method

Adams-Bashforth integration is more computationally involved than the schemes of Euler. For instance, the two-step Adams–Bashforth integration:

$$x(k+1) = x(k) + h\left[\frac{3}{2}f(x(k), u(k), t_k) - \frac{1}{2}f(x(k-1), u(k-1), t_{k-1})\right] \quad \text{(B.66)}$$

implies that the old value:

$$\dot{x}(k-1) = f(x(k-1), u(k-1), t_{k-1}) \tag{B.67}$$

must be stored. The global truncation error for this method is of order $O(h^2)$. The advantage with this method compared to Euler integration is seen from Figure B.1. The stability region is obtained from:

$$\pi(r, \overline{h}) = r^2 - (1 + \frac{3}{2}\overline{h})\, r + \frac{1}{2}\overline{h} = 0 \tag{B.68}$$

which yields the following constraint:

$$|r_s| = \left| \frac{1}{2} \left((1 + \frac{3}{2}\overline{h}) \pm \sqrt{(1 + \frac{3}{2}\overline{h})^2 - 2\overline{h}} \right) \right| < 1 \tag{B.69}$$

B.2.3 Runge–Kutta 2nd-Order Method (Heun's Method)

Heun's integration method can be written:

$$\begin{aligned} k_1 &= f(x(k), u(k), t_k) && \text{(B.70)} \\ k_2 &= f\left(x(k) + hk_1, u(k), t_k + h\right) && \text{(B.71)} \end{aligned}$$

$$x(k+1) = x(k) + \frac{h}{2}\left(k_1 + k_2\right) \tag{B.72}$$

The global truncation error for Heun's Method is of order $O(h^2)$ while the stability region is given by:

$$|r_s| = \left| 1 + \overline{h} + \frac{1}{2}\overline{h}^2 \right| < 1 \tag{B.73}$$

B.2.4 Runge–Kutta 4th-Order Method

An extension of Heun's integration method to 4th-order is:

$$\begin{aligned} k_1 &= hf(x(k), u(k), t_k) && \text{(B.74)} \\ k_2 &= hf(x(k) + k_1/2, u(k), t_k + h/2) && \text{(B.75)} \\ k_3 &= hf(x(k) + k_2/2, u(k), t_k + h/2) && \text{(B.76)} \\ k_4 &= hf(x(k) + k_3/2, u(k), t_k + h) && \text{(B.77)} \end{aligned}$$

$$x(k+1) = x(k) + \frac{1}{6}\left(k_1 + 2k_2 + 2k_3 + k_4\right) \tag{B.78}$$

$$x(k+1) = x(k) + \frac{1}{6}\left(k_1 + 2k_2 + 2k_3 + k_4\right) \tag{B.79}$$

The global truncation error for the RK-4 Method is of order $O(h^4)$ and the stability region is given by:

$$|r_s| = \left|1 + \overline{h} + \frac{1}{2}\overline{h}^2 + \frac{1}{6}\overline{h}^3 + \frac{1}{24}\overline{h}^4\right| < 1 \tag{B.80}$$

B.3 Numerical Differentiation

Numerical differentiation is usually sensitive to noisy measurements. Nevertheless, a reasonable estimate of the time derivative $\dot{\eta}$ of a signal η can be obtained by using a *filtered differentiation*. The simplest filter is obtained by the 1st-order low-pass structure:

$$\dot{\eta}_f(s) = \frac{Ts}{1+Ts}\,\eta(s) \tag{B.81}$$

corresponding to the continuous-time system:

$$\dot{x} = a\,x + b\,u \tag{B.82}$$
$$y = c\,x + d\,u \tag{B.83}$$

with $u = \eta$, $y = \dot{\eta}_f$, $a = b = -1/T$ and $c = d = 1$. Using the results from Example B.1, we obtain the following filter equations:

$$x(k+1) = \exp(-h/T)\,x(k) + (\exp(-h/T) - 1)\,u(k) \tag{B.84}$$
$$y(k) = x(k) + u(k) \tag{B.85}$$

The advantage with this procedure to an observer or a Kalman filter is that no explicit model of the plant is required. A large number of alternative filter structures based on higher-order approximations can be derived. However, this will not be studied more closely in this text.

Appendix C

Stability Theory

In this chapter we will briefly review some useful results from linear and nonlinear stability theory. This includes Lyapunov theory, input–output stability in terms of L_p-stability, passivity and positive realness.

C.1 Lyapunov Stability Theory

Lyapunov stability theory can be applied to both autonomous and non-autonomous systems. A nonlinear system is said to be *autonomous* if the system's state equation can be expressed as

$$\dot{x} = f(x) \tag{C.1}$$

where the nonlinear function f does not explicitly depend on time. Similarly, *non-autonomous systems* can be described as systems where f explicitly depends on the time t, that is:

$$\dot{x} = f(x,t) \tag{C.2}$$

C.1.1 Lyapunov Stability for Autonomous Systems

Lyapunov' s direct method is only valid for autonomous systems (Lyapunov 1907). For such systems, a scalar Lyapunov function, often representing the energy of the system, can be applied to determine whether the system is stable or not. Lyapunov's direct method for autonomous systems simply states the following:

Theorem C.1 (Lyapunov's Direct Method for Autonomous Systems) *Assume that there is a scalar function $V(x)$ with continuous first derivatives satisfying:*

(1) $V(x) > 0$ *(positive definite)*

(2) $\dot{V}(x) < 0$ *(negative definite)*

(3) $V(x) \to \infty$ *as* $\|x\| \to \infty$ *(radially unbounded)*

then the equilibrium point x^* satisfying $f(x^*) = 0$ is globally asymptotically stable.
□

Conditions (1) and (2) imply that the system is *asymptotically stable*. For the system to be *globally asymptotically stable*, we must in addition require that $V(x)$ is radially unbounded, that is condition (3). The equilibrium point x^* satisfying $f(x^*) = 0$ is only *stable* if condition (2) is relaxed to $\dot{V}(x) \leq 0$.

Essentially, Lyapunov stability implies that the system trajectories can be kept arbitrarily close to the origin by starting sufficiently close to it. However, this only guarantees that the system stays at an equilibrium point. If the same system is exposed to disturbances, we usually require that the system states will go gradually back to their originally value and not only stay at rest. This type of stability is usually referred to as *asymptotic stability*.

C.1.2 Lyapunov Stability for Non-Autonomous Systems

Stability analysis techniques for non-autonomous systems can be used to study the *motion stability* of a system tracking a time-varying reference trajectory or for systems that are inherently non-autonomous in their nature.

It is well known that the motion stability problem can be transformed into an equivalent stability problem around an equilibrium point by considering the system's error dynamics instead of the system's state dynamics. Although the original system is autonomous, tracking of time-varying trajectories implies that the equivalent system will be non-autonomous. For non-autonomous systems the following Lyapunov theorem has proved to be quite useful:

Theorem C.2 (Lyapunov Theorem for Non-Autonomous Systems) *Assume that there is a scalar function $V(x,t)$ with continuous first derivatives satisfying:*

(1) $V(x,t) > 0$ *(positive definite)*

(2) $\dot{V}(x,t) < 0$ *(negative definite)*

(3) $V(x,t) \leq V_0(x) \quad \forall\, t \geq 0 \quad$ *where* $\quad V_0(x) > 0$ *(decrescent)*

(4) $V(x,t) \to \infty$ *as* $\|x\| \to \infty$ *(radially unbounded)*

then the equilibrium point x^* satisfying $f(x^*,t) = 0$ is globally asymptotically stable.
□

Lyapunov stability for non-autonomous systems imposes an additional requirement that $V(x,t)$ must be decrescent. The reason for this is that $V(x,t)$ explicitly depends on the time. Conditions (1), (2) and (3) imply that the system is *asymptotically stable*. For the system to be *globally asymptotically stable*, we must in addition require that $V(x,t)$ is radially unbounded.

Lyapunov-Like Theory

In many engineering applications conditions (1) to (4) of the previous Lyapunov theorem can be non-trivial to satisfy. Often these problems can be circumvented by applying a Lyapunov-like lemma (Popov 1973), which is based on the results of the Rumanian mathematician Barbălat (1959). However this lemma only guarantees *convergence* of the system trajectories to the origin. Unfortunately, convergence does not necessarily imply stability since it is possible that the system trajectories first move away from the origin before converging to the same point. Hence, the origin is unstable in the sense of Lyapunov, despite the state convergence. Nevertheless, the lemma has been shown to be highly applicable from an engineering point of view. The main results are as follows:

Lemma C.1 (Barbălat's Lemma)
If the function $g(t)$ has a finite limit as $t \to \infty$, is differentiable and $\dot{g}(t)$ is uniformly continuous, then $\dot{g}(t) \to 0$ as $t \to \infty$.
□

A Lyapunov-like version of Barbălat's lemma can be found in Slotine and Li (1991). This lemma states:

Lemma C.2 (Lyapunov-Like Lemma for Convergence)
Assume that there exists a scalar function $V(\boldsymbol{x}, t)$ satisfying:

(1) $V(\boldsymbol{x}, t)$ is lower bounded

(2) $\dot{V}(\boldsymbol{x}, t)$ is negative semi-definite

(3) $\dot{V}(\boldsymbol{x}, t)$ is uniformly continuous in time

then $\dot{V}(\boldsymbol{x}, t) \to 0$ as $t \to \infty$.
□

Sufficient conditions for the first and last condition are:

Remark C.1 (Lower boundness)
A sufficient condition for the scalar function $V(\boldsymbol{x}, t)$ to be lower bounded is that $V(\boldsymbol{x}, t)$ is positive semi-definite i.e.

$$V(\boldsymbol{x}, t) \geq 0 \qquad \forall\, t \geq t_0 \tag{C.3}$$

□

Remark C.2 (Uniform Continuity)
A sufficient condition for a differentiable function $\dot{V}(\boldsymbol{x}, t)$ to be uniformly continuous is that its derivative $\ddot{V}(\boldsymbol{x}, t)$ is bounded $\forall\, t \geq t_0$.
□

C.2 Input–Output Stability

The concepts of input–output stability require some brief introduction to *Lebesgue* theory. The following definitions are adopted from Naylor and Sell (1982):

C.2.1 Some Basic Definitions

Definition C.1 (L_p-Spaces)
Let $\mathcal{X}$ be a measurable set in $\mathbb{R}$ and let p satisfy $1 \leq p < \infty$. A function $x : \mathcal{X} \to \mathbb{R}$ is said to belong to the Lebesgue space L_p if:

$$L_p = \left\{ x : \mathcal{X} \to \mathbb{R} \;\middle|\; \int_0^\infty |x(t)|^p \, dt < \infty \right\} \tag{C.4}$$

□

Definition C.2 (Norms on L_p)
A norm is defined on L_p by:

$$\|x\|_p = \left[\int_0^\infty |x(t)|^p \, dt \right]^{1/p} \tag{C.5}$$

□

Furthermore let the inner product between two functions $x, y \in \mathcal{X}$ be written:

$$\langle x|y \rangle = \int_0^\infty x(t) \, y(t) \, dt \tag{C.6}$$

For $p = 2$, the norm $\| \cdot \|_2$ corresponds to the inner product:

$$\|x\|_2 = \langle x|x \rangle^{1/2} = \left[\int_0^\infty x^2(t) \, dt \right]^{1/2} \tag{C.7}$$

The following special cases are particularly useful:

$$L_1 = \left\{ x : \mathcal{X} \to \mathbb{R} \;\middle|\; \int_0^\infty |x(t)| \, dt < \infty \right\} \tag{C.8}$$

$$L_2 = \left\{ x : \mathcal{X} \to \mathbb{R} \;\middle|\; \int_0^\infty x^2(t) \, dt < \infty \right\} \tag{C.9}$$

$$L_\infty = \operatorname*{ess\,sup}_{t \in [0,\infty)} |x(t)| \tag{C.10}$$

Before we discuss input–output stability theory in terms of norms in the L_p-space we will consider the following simple example:

Example C.1 (Linear Homogeneous System)
Consider the linear homogeneous system:

$$\dot{x} = a \, x, \qquad x(0) = x_0 \tag{C.11}$$

where $a < 0$ for a stable system and $a > 0$ for an unstable system. Integration of (C.11), yields:

$$x(t) = \exp(at)\, x_0 \tag{C.12}$$

The $\|\cdot\|_2$-norm for this system is:

$$\|x\|_2 = \lim_{m\to\infty} \left[\int_0^m \exp(2at)\, x_0^2\, dt\right]^{1/2} = \frac{x_0}{\sqrt{2a}} \lim_{m\to\infty} (\exp(2am) - 1) \tag{C.13}$$

Hence, $x \in L_2$ for $a < 0$ and $\|x\|_2$ is undefined for $a > 0$. This shows that the norm $\|\cdot\|_p$ defined in L_p does not necessarily exist for unstable systems.
□

However, to study unstable systems we will introduce the *truncation* x_T of x on the interval $[0, T]$, defined as:

$$x_T(t) = \begin{cases} x(t) & 0 \le t \le T \\ 0 & T < t \end{cases} \tag{C.14}$$

Thus the extended Lebesgue-spaces L_{pe} can be defined as:

$$L_{pe} \triangleq \{x(t) \in \mathcal{X} \mid x_T(t) \in L_p \quad \forall \quad T\} \tag{C.15}$$

From this definition it is clear that $\|x_T\|_p \le \|x\|_p$, since:

$$\|x_T\|_p = \left[\int_0^\infty |x_T(t)|^p\, dt\right]^{1/p} = \left[\int_0^T |x(t)|^p\, dt\right]^{1/p} \le \left[\int_0^\infty |x(t)|^p\, dt\right]^{1/p} = \|x\|_p \tag{C.16}$$

Extension to Multivariable Systems

For MIMO systems we introduce the symbol L_p^n to denote the set of all n-tuples:

$$\boldsymbol{x} = [x_1, \ldots, x_n]^T \tag{C.17}$$

where $x_i \in L_p$ for $(i = 1 \ldots n)$. The norm on L_p^n of the vector $\boldsymbol{x}$ is defined as:

$$\|\boldsymbol{x}\|_p \triangleq \left[\sum_{i=1}^n \|x_i(t)\|_p^2\right]^{1/2} \tag{C.18}$$

which is simply the square root of the sum of the squares of the norms $\|x_i(t)\|_p$ of the component functions $x_i \in L_p$. A more detailed discussion of *Lebesgue* theory is found in Desoer and Vidyasagar (1975) and Vidyasagar (1978).

C.2.2 L_p-Stability

Consider the nonlinear system:

$$\dot{x} = f(x, u, t) \tag{C.19}$$
$$y = h(x, u, t) \tag{C.20}$$

where $u \in \mathbb{R}^r$ is the system input vector, $y \in \mathbb{R}^m$ is the system output vector and $x \in \mathbb{R}^n$ is the system state vector. For linear systems this model is usually written:

$$\dot{x} = Ax + Bu \tag{C.21}$$
$$y = Cx + Du \tag{C.22}$$

Independently of whether the linear or nonlinear model is used, we will denote the mapping from the input vector u to the output vector y by:

$$y = H\,u \tag{C.23}$$

where H is the operator. Example C.1 indicates that it is necessary to formulate the stability problem in the extended space L_{pe} to be able to study unstable systems with feedback. Motivated by this, the stability question can be formulated as: Given the input u in L_p^r and assume that there exist a solution in L_{pe}^m for y, does this solution actually belong to L_p^m ? The answer is yes, if the following definition is satisfied (Vidyasagar 1978).

Definition C.3 (L_p-Stability)
The system (C.23) is said to be L_p-stable if the solution $y \in L_{pe}^m$ actually belong to L_p^m whenever $u \in L_p^r$ and there exist two finite constants α and β such that:

$$\|y\|_p \leq \alpha \|u\|_p + \beta \tag{C.24}$$

□

Example C.2 (L_p-Stability)
Consider the system:

$$\dot{x} = x + u; \qquad x(0) = 0 \tag{C.25}$$

Hence,

$$x(t) = \int_0^t \exp(t - \tau)\, u(\tau)\, d\tau \tag{C.26}$$

For a bounded input $u \in L_{\infty e}$ satisfying:

$$\begin{array}{rl} 0 < |u(t)| \leq u_m & \text{if } t \leq T \\ u(t) = 0 & \text{if } t > T \end{array} \tag{C.27}$$

we have that:

$$x(t) = \int_0^t \exp(t-\tau)\, u(\tau)\, d\tau \leq u_m \int_0^T \exp(t-\tau)\, d\tau = u_m\,(\exp(T) - 1) \tag{C.28}$$

Consequently, x is finite for every finite T which proves that $x \in L_{\infty e}$ for every $u \in L_{\infty e}$. However, this mapping is not *L_p-stable since there exists at least one input in L_∞ whose corresponding output does not belong to L_∞. For instance $u(t) = 1\ \forall\ t$ is in L_∞, but:*

$$x(t) = \int_0^t \exp(t-\tau)\, d\tau = \exp(t) - 1 \tag{C.29}$$

does not belong to L_∞.
□

BIBO Stability

For $p = \infty$, the concept of L_p-stability becomes equivalent to what is commonly referred to as *bounded-input bounded-output* (BIBO) stability. Roughly speaking, if (C.24) holds and in addition the input u is bounded, that is $u \in L_\infty$, the input u will produce a bounded output[1] $y \in L_\infty$.

C.2.3 Feedback Stability

Theorem C.3 may be extended to an interconnected system describing a feedback control system by letting H_1 and H_2 be two operators satisfying:

$$y_1 = H_1\,(u_1 - y_2) \tag{C.30}$$
$$y_2 = H_2\,(u_2 + y_1) \tag{C.31}$$

A block diagram of this system is shown in Figure C.1. Feedback stability may be checked by applying the following definition of Vidyasagar (1978):

Definition C.4 (L_p-Stability for Feedback Systems)
The system (C.30) and (C.31) is said to be L_p-stable if the solution $y_1, y_2 \in L_{pe}^m$ actually belongs to L_p^m whenever $u_1, u_2 \in L_p^r$ and there exist two finite constants α and β such that:

[1] It should be noted that some authors prefer to define BIBO stability without the norm condition (C.24), that is all inputs in L_p produce outputs in L_p.

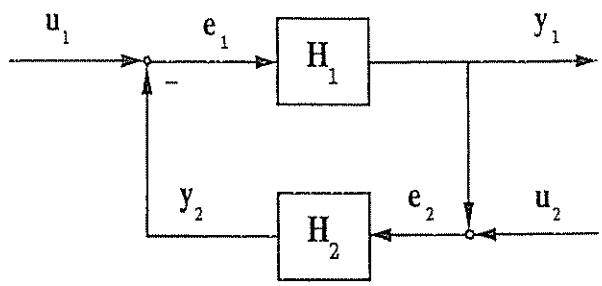

Figure C.1: Input–output representation of a feedback control system.

$$\|y_1\|_p \leq \alpha \left(\|u_1\|_p + \|u_2\|_p\right) + \beta \tag{C.32}$$
$$\|y_2\|_p \leq \alpha \left(\|u_1\|_p + \|u_2\|_p\right) + \beta \tag{C.33}$$

□

For systems where L_2-stability is the major concern, a unified framework referred to as *passivity theory* can be used to check whether the system is L_2-stable or not. The next section is devoted to this topic.

C.3 Passivity Theory

C.3.1 Passivity Interpretation of Mechanical Systems

A physical interpretation of passivity may be made by simply considering a mechanical system (plant and control system) with energy $V(t)$ at time t. The total energy of this system will be the sum of the kinetic and potential energy. Let the mechanical energy stored in the system at the initial time $t = t_0$ be denoted by $V(0) \geq 0$. Since the energy $V(T)$ must be positive and lower bounded, it makes sense to define the total system as passive if and only if the mechanical energy dissipated by the system is less than or equal to $V(0)$. This can be mathematically expressed as:

$$V(T) \leq V(0) + \int_0^T y^T(\tau) u(\tau)\, d\tau \tag{C.34}$$

where the integral represents the external energy inputs. Hence, the rate of change of energy in the system at time t is:

$$\dot{V}(t) \leq y^T(t)\, u(t) \tag{C.35}$$

where the vector product $y^T u$ simply represents the external power input.

Definition C.5 (Passive Mapping)
A mechanical system with input u and output y is a passive mapping from u to y if and only if there exists an energy function $V(t) \geq 0$ for all $t \geq 0$ such that:

$$\langle y|u\rangle_T = \int_0^T y^T(\tau)u(\tau)\,d\tau \geq \beta \tag{C.36}$$

for all $u \in L_{2e}^r$, all $T \geq 0$ and some constant $\beta > -\infty$. This simply states that there exists some lower bound on the energy function $V(t)$.
Proof: *From (C.34) we have that:*

$$\int_0^T y^T(\tau)u(\tau)\,d\tau \geq V(T) - V(0) \geq -V(0) \tag{C.37}$$

Hence, choosing $V(0) = -\beta \geq 0$ concludes the proof.
□

Furthermore, we say that a system with input u and output y is *strictly passive* and *strictly output passive* if the following holds:

Definition C.6 (Strictly Passive Mapping)
A mechanical system with input u and output y is input strictly passive (strictly u-passive) if and only if there exist an $\alpha > 0$ and some constant β such that:

$$\langle y|u\rangle_T \quad \geq \quad \alpha\|u_T\|_2 + \beta \tag{C.38}$$

for all $u \in L_{2e}^r$ and all $T \geq 0$.
□

Definition C.7 (Output Strictly Passive Mapping)
A mechanical system with input u and output y is output strictly passive (strictly y-passive) if and only if:

$$\langle y|u\rangle_T \quad \geq \quad \alpha\|y_T\|_2 + \beta \tag{C.39}$$

for all $u \in L_{2e}^r$ and all $T \geq 0$.
□

Internal Power Generation

In the case of internal power generation a more general description of passivity is required. For instance, a system with an energy source will not be passive if the energy supplied to the system by the energy source is larger than the energy which is dissipated by the system. More precisely (Slotine and Li 1991):

$$\underbrace{\dot{V}(t)}_{\substack{\text{change of}\\ \text{energy}}} \leq \underbrace{y^T(t)u(t)}_{\substack{\text{external}\\ \text{power}\\ \text{input}}} - \underbrace{g(t)}_{\substack{\text{internal}\\ \text{power}\\ \text{generation}}} \tag{C.40}$$

where the function $g(t)$ denotes the internal power generation. In this case the mapping from u to y is *passive* if and only if:

(1) $V(t)$ is lower bounded

(2) $g(t) \geq 0$

An even more harsh requirement is that no energy shall be generated in the system, that is:

(3) $\int_0^T y^T(\tau)u(\tau)d\tau \neq 0 \implies \int_0^T g(\tau)\,d\tau > 0$ for all $T \geq 0$.

Feedback Systems

For feedback systems the following passivity theorem is particularly useful (Popov 1973):

Theorem C.3 (Passivity Theorem)
Consider the feedback system in Figure C.1 described by:

$$y_1 = H_1(u_1 - y_2) \tag{C.41}$$
$$y_2 = H_2(u_2 + y_1) \tag{C.42}$$

where H_1 and H_2 are two appropriate mappings and:

$$e_1 = u_1 - y_2 \tag{C.43}$$
$$e_2 = u_2 + y_1 \tag{C.44}$$

Assume that there for any u_1 and u_2 in L_2^r there are solutions $e_1, e_2 \in L_{2e}^m$. Furthermore, assume that there exist constants α_i and β_i for $(i = 1...3)$, such that:

$$\|y_{1T}\|_2 \leq \alpha_1\|e_{1T}\|_2 + \beta_1 \tag{C.45}$$
$$\langle e_1|y_1\rangle_T \geq \alpha_2\|e_{1T}\|_2^2 + \beta_2 \tag{C.46}$$
$$\langle y_2|e_2\rangle_T \geq \alpha_3\|e_{2T}\|_2^2 + \beta_3 \tag{C.47}$$

for all $T \geq 0$. If in addition

$$\alpha_2 + \alpha_3 > 0 \tag{C.48}$$

then

$$u_1, u_2 \in L_2^r \implies e_1, e_2, y_1, y_2 \in L_2^m$$

Proof: *See Popov (1973).*
□

C.3.2 Feedback Stability in the Sense of Passivity

In this section, we will briefly present an important result from the previous section relating passivity to feedback stability. This result is well suited for design and analyses of L_2-stable control systems. Consider the feedback structure in Figure C.2:

$$\text{Plant:} \qquad y = H\,u = H(r - u_0) \tag{C.49}$$

$$\text{Control law:} \qquad u_0 = G\,y \tag{C.50}$$

where $y \in \mathbb{R}^m$ is the output vector, $u \in \mathbb{R}^r$ is the plant input vector and $r \in \mathbb{R}^r$ is a feedforward term. For linear systems, the operator H is simply the plant transfer matrix and G is the controller transfer matrix. Hence, we present the following useful theorem:

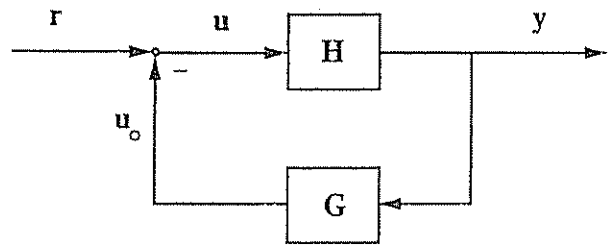

Figure C.2: Feedback System in terms of a passive and a strictly passive block.

Definition C.8 (Feedback Stability in the Sense of Passivity)
Assume that the mapping $H : u \to y$ is passive and that the mapping $G : y \to u_0$ is strictly passive, hence:

$$r \in L_2^r \quad \Longrightarrow \quad y \in L_2^m$$

This will also be true if $H : u \to y$ is strictly passive and that the mapping $G : y \to u_0$ is passive.
□

C.3.3 Passivity in Linear Systems

Consider the SISO system:

$$\dot{x} = A\,x + Bu; \qquad y = c^T\,x \tag{C.51}$$

with transfer function

$$h(s) = c^T(sI - A)^{-1}b \tag{C.52}$$

Hence, the following considerations can be made:

- **Passive:** If $h(s)$ is asymptotically stable the SISO linear system is *passive* if (and only if):

$$\mathrm{Re}\{h(j\omega)\} \geq 0 \quad \forall \quad \omega \geq 0 \tag{C.53}$$

  where Re refers to the real part of the transfer function.

- **Strictly Passive:** If $h(s)$ is asymptotically stable the SISO linear system is *strictly passive* if (and only if):

$$\mathrm{Re}\{h(s-\sigma)\} \geq 0 \quad \forall \quad \omega \geq 0 \tag{C.54}$$

  for some $\sigma > 0$.

Geometrically, these two conditions can be expressed in terms of the system *phase shift*, that is:

- **Passive:**

$$\angle h(j\omega) \leq 90^o \quad \forall \quad \omega \geq 0 \tag{C.55}$$

- **Strictly Passive:**

$$\angle h(j\omega) < 90^o \quad \forall \quad \omega \geq 0 \tag{C.56}$$

Similarly, it can be shown that for a asymptotically stable MIMO system, passivity is obtained by requiring that the transfer matrix:

$$\boldsymbol{H}(s) = \boldsymbol{C}(s\boldsymbol{I} - \boldsymbol{A})^{-1}\boldsymbol{B} \tag{C.57}$$

satisfies

$$\boldsymbol{H}(j\omega) + \boldsymbol{H}^T(-j\omega) \geq 0 \quad \forall \quad \omega \geq 0 \tag{C.58}$$

and the same system is strictly stable if (and only if):

$$\boldsymbol{H}(j\omega) + \boldsymbol{H}^T(-j\omega) > 0 \quad \forall \quad \omega \geq 0 \tag{C.59}$$

It should be noted that the passivity formalism achieves stability by restrictions on the phase shift, whereas standard L_p-stability gives stability by restricting the loop gain. For a more detailed discussion on L_p-stability and passivity see Popov (1973) and Desoer and Vidyasagar (1975).

C.3.4 Positive Real Systems

For linear systems the concepts of *positive realness* can be related to passivity by the Kalman–Yakubovich Lemma. This lemma simply states:

Lemma C.3 (Kalman–Yakubovich Lemma)
Consider a MIMO controllable linear time-invariant system:

$$\begin{aligned} \dot{x} &= Ax + Bu \\ y &= Cx \end{aligned} \tag{C.60}$$

with transfer matrix:

$$H(s) = C(sI - A)^{-1}B \tag{C.61}$$

is strictly positive real (SPR) if, and only if, there exists two positive definite matrices $P = P^T > 0$ and $Q = Q^T > 0$ such that:

$$A^T P + PA = -Q \tag{C.62}$$

$$B^T P = C \tag{C.63}$$

If the condition on the matrix Q is relaxed to positive semi-definiteness, that is $Q \geq 0$ the system is said to be positive real (PR).
□

Notice that a *PR* and *SPR* causal linear system will be passive. However, strictly positive realness is not sufficient for the system to be strictly passive. This is illustrated by considering the following Lyapunov function candidate:

$$V(x) = \frac{1}{2}\, x^T P\, x; \qquad P = P^T > 0 \tag{C.64}$$

Differentiating V with respect to time yields:

$$\dot{V} = \frac{1}{2}\, x(A^T P + PA)x + x^T PBu \tag{C.65}$$

Substituting (C.62) and (C.63) into the expression for $\dot{V}$ yields:

$$\dot{V} = y^T\, u - g(t) \tag{C.66}$$

where

$$g(t) = \frac{1}{2} x^T Q\, x \tag{C.67}$$

Hence, the system is *passive* if $Q = Q^T \geq 0$. However, we are not able to show that the system is *strictly passive*. By using the PR formalism to check passivity for the linear system (usually the error dynamics), we can design an L_2-stable

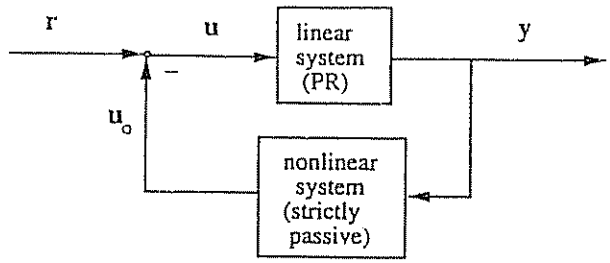

Figure C.3: Feedback System in terms of a linear PR (passive) and nonlinear strictly passive block.

system by simply requiring that the feedback control law to be *strictly passive*, see Figure C.3. For SISO systems positive realness implies that the transfer function:

$$h(s) = c^T(sI - A)^{-1}b \tag{C.68}$$

satisfies:

$$\mathrm{Re}\{h(s)\} \geq 0 \quad \forall \quad \mathrm{Re}\{s\} \tag{C.69}$$

The system is SPR if:

$$\mathrm{Re}\{h(s-\sigma)\} \geq 0 \quad \forall \quad \mathrm{Re}\{s\} \tag{C.70}$$

for some $\sigma > 0$.

Appendix D

Linear Quadratic Optimal Control

In this chapter, we will briefly review some results from Athans and Falb (1966) on linear quadratic (LQ) optimal control theory. Consider a linear controllable system with state $x(t) \in \mathbb{R}^n$, input $u(t) \in \mathbb{R}^r$, disturbance $w(t) \in \mathbb{R}^r$ and output $y(t) \in \mathbb{R}^m$. The system performance output y is given by:

$$\dot{x} = A\,x + B\,u + E\,w \tag{D.1}$$
$$y = C\,x + D\,u \tag{D.2}$$

Both $x(t)$ and $w(t)$ are assumed measured or at least obtained by state estimation. In order to design an optimal control law we must require that the above system is controllable. The controllability condition is given by the following theorem:

Definition D.1 (Controllability)
The state and input matrix (A, B) must satisfy the controllability condition *to ensure that there exists a control $u(t)$ which can drive any arbitrary state $x(t_0)$ to another arbitrary state $x(t_1)$ for $t_1 > t_0$. The* controllability condition *requires that the $n \times n$ matrix (Gelb 1988):*

$$\mathcal{C} = [B \mid AB \mid \ldots \mid (A)^{n-1}B] \tag{D.3}$$

must be of rank n. A sufficient and necessary condition is that $\mathcal{C}$ has an inverse (non-singular).
□

D.1 Solution of the LQ Tracker Problem

Our control objective is to design an "energy" optimal controller to track a time-varying reference trajectory $y_d(t)$. For this purpose, we will define an error vector:

$$\tilde{y} = y - y_d = C\,(x - x_d) \tag{D.4}$$

where $x_d(t)$ is the desired state. We will show that the optimal control law utilizing feedback from $x(t)$ and feedforward from both $w(t)$ and $y_d(t)$ can be obtained by minimalization of a quadratic performance index:

$$\min\ J = \frac{1}{2}\int_0^T (\tilde{y}^T Q \tilde{y} + u^T P u)\, d\tau \tag{D.5}$$

where $P > 0$ and $Q \geq 0$ are the weighting matrices. Substituting (D.2) into (D.5) yields the equivalent formulation:

$$\min\ J = \frac{1}{2}\int_0^T (\tilde{x}^T C^T Q C \tilde{x} + u^T P u)\, d\tau = \frac{1}{2}\int_0^T (\tilde{x}^T \tilde{Q} \tilde{x} + u^T P u)\, d\tau \tag{D.6}$$

where $\tilde{x} = x - x_d$ and

$$\tilde{Q} = C^T Q C \geq 0 \tag{D.7}$$

D.1.1 Linear Time-Varying Systems

The system Hamiltonian can be written as (see e.g. Athans and Falb 1966):

$$\mathcal{H} = \frac{1}{2}(\tilde{x}^T \tilde{Q} \tilde{x} + u^T P u) + p^T (Ax + Bu + Ew) \tag{D.8}$$

Differentiating H with respect to u yields:

$$\frac{\partial \mathcal{H}}{\partial u} = Pu + B^T p = 0 \quad \Longrightarrow \quad u = -P^{-1} B^T p \tag{D.9}$$

Assume that p can be expressed as a linear combination:

$$p = Rx + h_1 + h_2 \tag{D.10}$$

where R, h_1 and h_2 are unknown quantities to be determined. Differentiating p with respect to time, yields:

$$\dot{p} = \dot{R}x + R\dot{x} + \dot{h}_1 + \dot{h}_2 \tag{D.11}$$

From optimal control theory, we know that:

$$\dot{p} = -\frac{\partial \mathcal{H}}{\partial x} = -\tilde{Q}\tilde{x} - A^T p = \tilde{Q}x_d - \tilde{Q}x - A^T R x - A^T h_1 - A^T h_2 \tag{D.12}$$

Consequently, elimination of $\dot{p}$ from (D.11) and (D.12) yields:

$$\dot{R}x + R\dot{x} + \dot{h}_1 + \dot{h}_2 - \tilde{Q}x_d + \tilde{Q}x + A^T R x + A^T h_1 + A^T h_2 = 0 \tag{D.13}$$

Finally, substitution of the expressions for $\dot{x}$ and u into (D.13) yields:

$$(\dot{R} + RA + A^T R - RBP^{-1}B^T R + \tilde{Q})\, x = 0 \tag{D.14}$$

$$\dot{h}_1 + (A - BP^{-1}B^T R)^T h_1 - \tilde{Q}x_d = 0 \tag{D.15}$$

$$\dot{h}_2 + (A - BP^{-1}B^T R)^T h_2 + REw = 0 \tag{D.16}$$

This implies that R must be solved from the Riccati equation:

$$\dot{R} + RA + A^T R - RBP^{-1}B^T R + \tilde{Q} = 0 \tag{D.17}$$

The boundary conditions are derived from the so-called *transversality condition*, see Athans and Falb (1966), which simply yields:

$$h_1(T) = 0; \qquad h_2(T) = 0 \tag{D.18}$$

Since (D.10) must be valid for all $x(T)$, we have that:

$$R(T) = 0 \tag{D.19}$$

Hence, the differential equations for R, h_1 and h_2 can be solved for all $t \in [0, T]$ by backward integration.

D.1.2 Approximate Solution for Linear Time-Invariant Systems

MIMO Systems

Unfortunately, the theory dealing with the limiting case $T \to \infty$, that is:

$$\min\ J = \frac{1}{2} \lim_{T\to\infty} \int_0^T (\tilde{y}^T Q \tilde{y} + u^T P u)\, d\tau \tag{D.20}$$

is not available. This problem is usually circumvented by assuming that T is large but still limited. Moreover, we shall assume that:

$$0 \ll T_1 \ll T \ll \infty \tag{D.21}$$

where T_1 is a large constant. For $T \to \infty$ the solution of (D.17) will tend to the constant matrix R_∞ satisfying:

$$R_\infty A + A^T R_\infty - R_\infty B P^{-1} B^T R_\infty + \tilde{Q} = 0\ . \tag{D.22}$$

We will interpret this solution as the steady-state solution of (D.17). Since $T_1 \ll T$ we can approximate $R(t) \approx R_\infty$ for all $t \in [0, T_1]$. Furthermore, we will assume that x_d = constant and w = constant for all $t \in [0, T_1]$. In many applications this restriction can be relaxed to slowly-varying compared to the state dynamics. Provided that the eigenvalues of the matrix:

$$A_c = A + BG_1 \quad \text{where} \quad G_1 = -P^{-1}B^T R_\infty \tag{D.23}$$

have negative real parts, that is:

$$\lambda_i(A_c) < 0 \quad (i = 1...n) \tag{D.24}$$

we can approximate the steady-state solution for h_1 and h_2 on $[0, T_1]$ as:

$$h_{1\infty} = (A + BG_1)^{-T} \bar{Q} x_d \tag{D.25}$$

$$h_{2\infty} = -(A + BG_1)^{-T} R_\infty E w \tag{D.26}$$

Substituting of (D.10) into (D.9) yields the steady-state optimal control law:

$$u = G_1\, x + G_2\, y_d + G_3 w \tag{D.27}$$

where

$$G_1 = -P^{-1} B^T R_\infty \tag{D.28}$$
$$G_2 = -P^{-1} B^T (A + BG_1)^{-T} C^T Q \tag{D.29}$$
$$G_3 = P^{-1} B^T (A + BG_1)^{-T} R_\infty E \tag{D.30}$$

This solution is shown in Figure D.1.

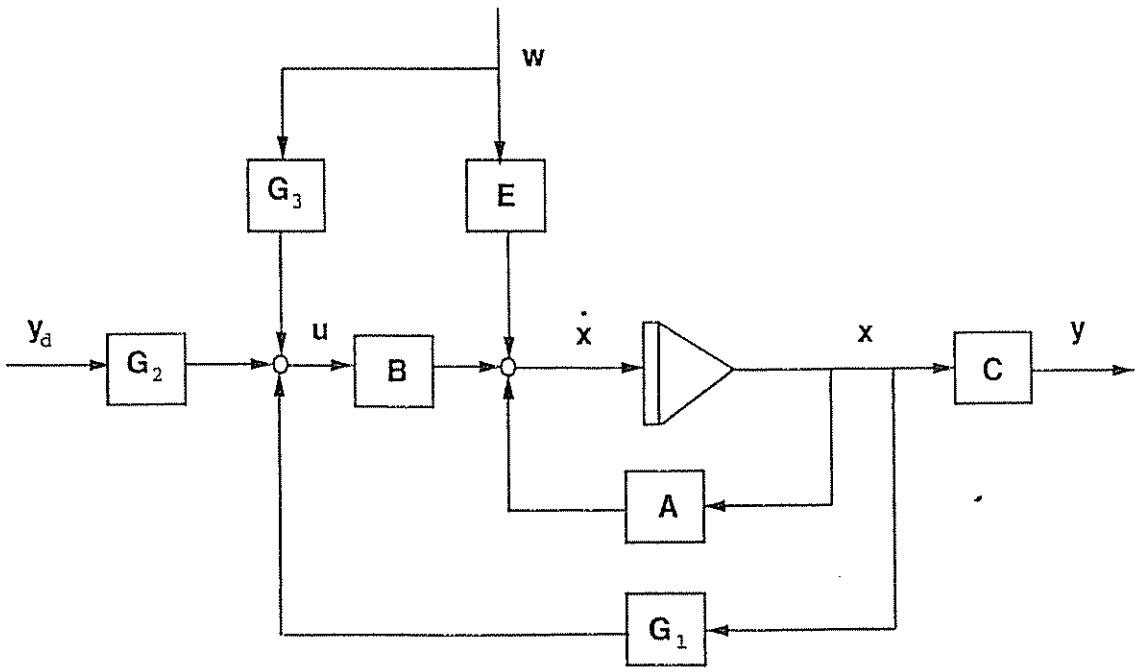

Figure D.1: Linear Quadratic Optimal Control

SISO Systems

For SISO systems, the performance index (D.5) simplifies to:

$$\min\ J = \frac{1}{2}\lim_{T\to\infty}\int_0^T (q\,\tilde{y}^2 + p\,u^2)\,d\tau = \frac{q}{2}\lim_{T\to\infty}\int_0^T (\tilde{y}^2 + \frac{p}{q}\,u^2)\,d\tau \qquad \text{(D 31)}$$

where p and q are two scalars. By choosing q as $q = 1$ and $\lambda = p/q > 0$, the performance index (D.31) reduces to:

$$\min\ J^* = \frac{1}{2}\lim_{T\to\infty}\int_0^T (\tilde{y}^2 + \lambda u^2) d\,\tau \qquad \text{(D.32)}$$

The corresponding state-space model is:

$$\dot{x} = Ax + bu + Ew \qquad \text{(D.33)}$$
$$y = c^T x \qquad \text{(D.34)}$$

Consequently, the steady-state optimal solution can be approximated as:

$$u = g_1^T\,x + g_2\,y_c + g_3^T\,w \qquad \text{(D.35)}$$

where

$$g_1^T = -\frac{1}{\lambda}b^T R_\infty \qquad \text{(D.36)}$$
$$g_2 = -\frac{1}{\lambda}b^T(A + bg_1^T)^{-T}c \qquad \text{(D.37)}$$
$$g_3^T = \frac{1}{\lambda}b^T(A + bg_1^T)^{-T}R_\infty E \qquad \text{(D.38)}$$

Here R_∞ is the solution of the algebraic Riccati equation (ARE):

$$R_\infty A + A^T R_\infty - \frac{1}{\lambda}R_\infty bb^T R_\infty + cc^T = 0 \qquad \text{(D.39)}$$

D.2 Linear Quadratic Regulator

A fundamental design problem is the regulator problem, where it is necessary to regulate the outputs of the system to zero while ensuring that they exhibit desirable time-response characteristics. A linear quadratic regulator (LQR) can be designed for this purpose by considering the state-space model:

$$\dot{x} = A\,x + B\,u + E\,w \qquad \text{(D.40)}$$
$$y = C\,x \qquad \text{(D.41)}$$

with performance index:

$$\min\ J = \frac{1}{2}\int_0^T (y^T Q y + u^T P u)\, d\tau = \frac{1}{2}\int_0^T (x^T C^T Q C x + u^T P u)\, d\tau \quad \text{(D.42)}$$

where $P > 0$ and $Q \geq 0$ are the weighting matrices. The steady-state solution to this problem is:

$$u = G\, x \quad \text{(D.43)}$$

where

$$G = -P^{-1} B^T R_\infty \quad \text{(D.44)}$$

and

$$R_\infty A + A^T R_\infty - R_\infty B P^{-1} B^T R_\infty + C^T Q C = 0 \quad \text{(D.45)}$$

Matlab Program for Computation of the LQR Feedback Gain Matrix

The steady-state LQR feedback control law can be computed in Matlab by applying the following commands:

```
Q = diag([q11,q22,...,qnn]);
P = diag([p11,p22,...,pnn]);

[K,R,E] = lqr(A,B,C'*Q*C,P);
G = -K;
```

where E contains the eigenvalues of the closed-loop system:

$$\dot{x} = (A + BG)\, x \quad \text{(D.46)}$$

Appendix E

Ship and ROV Models

In order to verify a good control design it is useful to simulate the control law against a realistic model of the vessel. The following motion parameters will be used to describe the different mathematical models:

$$\begin{array}{lll} u = u_0 + \Delta u; & p = p_0 + \Delta p; & \phi = \phi_0 + \Delta\phi \\ v = v_0 + \Delta v; & r = r_0 + \Delta r; & \delta = \delta_0 + \Delta\delta \end{array} \tag{E.1}$$

For instance, this definition implies that Δu is a small perturbation from a nominal (constant) surge velocity u_0 while u denotes the total surge velocity. The total speed of the vessel is defined according to:

$$U = \sqrt{u^2 + v^2} = \sqrt{(u_o + u)^2 + v^2} \tag{E.2}$$

E.1 Ship Models

E.1.1 Mariner Class Vessel

The hydro- and aerodynamics laboratory in Lyngby, Denmark, has performed both planar motion mechanism (PMM) tests and full-scale steering and maneuvering predictions for a *Mariner Class Vessel*. The main data and dimensions of the Mariner Class Vessel are (Chislett and Strøm-Tejsen 1965b):

Length overall (L_{oa})	171.80	(m)
Length between perpendiculars (L_{pp})	160.93	(m)
Maximum beam (B)	23.17	(m)
Design draft (T)	8.23	(m)
Design displacement (∇)	18541	(m^3)
Design speed (u_0)	15	(knots)

For this vessel the dynamic equations of motion in surge, sway and yaw are:

$$\begin{bmatrix} m' - X'_{\dot{u}} & 0 & 0 \\ 0 & m' - Y'_{\dot{v}} & m'x'_G - Y'_{\dot{r}} \\ 0 & m'x'_G - N'_{\dot{v}} & I'_z - N'_{\dot{r}} \end{bmatrix} \begin{bmatrix} \Delta\dot{u}' \\ \Delta\dot{v}' \\ \Delta\dot{r}' \end{bmatrix} = \begin{bmatrix} \Delta X' \\ \Delta Y' \\ \Delta N' \end{bmatrix} \tag{E.3}$$

where the nonlinear forces and moment $\Delta X'$, $\Delta Y'$ and $\Delta N'$ are defined as (Prime-System I with L_{pp} and U as normalization variables, see Section 5.3.3):

$$\begin{aligned}
\Delta X' &= X'_u\Delta u' + X'_{uu}\Delta u'^2 + X'_{uuu}\Delta u'^3 + X'_{vv}\Delta v'^2 + X'_{rr}\Delta r'^2 + X'_{rv}\Delta r'\Delta v' \\
&+ X'_{\delta\delta}\Delta\delta'^2 + X'_{u\delta\delta}\Delta u'\Delta\delta'^2 + X'_{v\delta}\Delta v'\Delta\delta' + X'_{uv\delta}\Delta u'\Delta v'\Delta\delta' \\
\Delta Y' &= Y'_v\Delta v' + Y'_r\Delta r' + Y'_{vvv}\Delta v'^3 + Y'_{vvr}\Delta v'^2\Delta r' + Y'_{vu}\Delta v'\Delta u' + Y'_{ru}\Delta r'\Delta u' \\
&+ Y'_\delta\Delta\delta' + Y'_{\delta\delta\delta}\Delta\delta'^3 + Y'_{u\delta}\Delta u'\Delta\delta' + Y'_{uu\delta}\Delta u'^2\Delta\delta' + Y'_{v\delta\delta}\Delta v'\Delta\delta'^2 \\
&+ Y'_{vv\delta}\Delta v'^2\Delta\delta' + (Y0' + Y0'_u\Delta u' + Y0'_{uu}\Delta u'^2) \\
\Delta N' &= N'_v\Delta v' + N'_r\Delta r' + N'_{vvv}\Delta v'^3 + N'_{vvr}\Delta v'^2\Delta r' + N'_{vu}\Delta v'\Delta u' + N'_{ru}\Delta r'\Delta u' \\
&+ N'_\delta\Delta\delta' + N'_{\delta\delta\delta}\Delta\delta'^3 + N'_{u\delta}\Delta u'\Delta\delta' + N'_{uu\delta}\Delta u'^2\Delta\delta' + N'_{v\delta\delta}\Delta v'\Delta\delta'^2 \\
&+ N'_{vv\delta}\Delta v'^2\Delta\delta' + (N0' + N0'_u\Delta u' + N0'_{uu}\Delta u'^2)
\end{aligned}$$

The non-dimensional coefficients in the model are:

$$m' = 798 \cdot 10^{-5}; \qquad I'_z = 39.2 \cdot 10^{-5}; \qquad x'_G = -0.023$$

Table E.1: Non-dimensional hydrodynamic coefficients for the Mariner Class Vessel (Chislett and Strøm-Tejsen 1965b).

X-equation		Y-equation		N-equation	
$-X'_{\dot u} + m' =$	$-840 \cdot 10^{-5}$	$-Y'_{\dot v} + m' =$	$-1546 \cdot 10^{-5}$	$-N'_{\dot v} + m'x'_G =$	$23 \cdot 10^{-5}$
		$-Y'_{\dot r} + m'x'_G =$	$9 \cdot 10^{-5}$	$-N'_{\dot r} + I'_z =$	$-83 \cdot 10^{-5}$
$X'_u =$	$-184 \cdot 10^{-5}$	$Y'_v =$	$-1160 \cdot 10^{-5}$	$N'_v =$	$-264 \cdot 10^{-5}$
$X'_{uu} =$	$-110 \cdot 10^{-5}$	$Y'_r =$	$-499 \cdot 10^{-5}$	$N'_r =$	$-166 \cdot 10^{-5}$
$X'_{uuu} =$	$-215 \cdot 10^{-5}$	$Y'_{vvv} =$	$-8078 \cdot 10^{-5}$	$N'_{vvv} =$	$1636 \cdot 10^{-5}$
$X'_{vv} =$	$-899 \cdot 10^{-5}$	$Y'_{vvr} =$	$15356 \cdot 10^{-5}$	$N'_{vvr} =$	$-5483 \cdot 10^{-5}$
$X'_{rr} =$	$18 \cdot 10^{-5}$	$Y'_{vu} =$	$-1160 \cdot 10^{-5}$	$N'_{vu} =$	$-264 \cdot 10^{-5}$
$X'_{\delta\delta} =$	$-95 \cdot 10^{-5}$	$Y'_{ru} =$	$-499 \cdot 10^{-5}$	$N'_{ru} =$	$-166 \cdot 10^{-5}$
$X'_{u\delta\delta} =$	$-190 \cdot 10^{-5}$	$Y'_\delta =$	$278 \cdot 10^{-5}$	$N'_\delta =$	$-139 \cdot 10^{-5}$
$X'_{rv} =$	$798 \cdot 10^{-5}$	$Y'_{\delta\delta\delta} =$	$-90 \cdot 10^{-5}$	$N'_{\delta\delta\delta} =$	$45 \cdot 10^{-5}$
$X'_{v\delta} =$	$93 \cdot 10^{-5}$	$Y'_{u\delta} =$	$556 \cdot 10^{-5}$	$N'_{u\delta} =$	$-278 \cdot 10^{-5}$
$X'_{uv\delta} =$	$93 \cdot 10^{-5}$	$Y'_{uu\delta} =$	$278 \cdot 10^{-5}$	$N'_{uu\delta} =$	$-139 \cdot 10^{-5}$
		$Y'_{v\delta\delta} =$	$-4 \cdot 10^{-5}$	$N'_{v\delta\delta} =$	$13 \cdot 10^{-5}$
		$Y'_{vv\delta} =$	$1190 \cdot 10^{-5}$	$N'_{vv\delta} =$	$-489 \cdot 10^{-5}$
		$Y0' =$	$-4 \cdot 10^{-5}$	$N0' =$	$3 \cdot 10^{-5}$
		$Y0'_u =$	$-8 \cdot 10^{-5}$	$N0'_u =$	$6 \cdot 10^{-5}$
		$Y0'_{uu} =$	$-4 \cdot 10^{-5}$	$N0'_{uu} =$	$3 \cdot 10^{-5}$

Matlab M-File for Nonlinear Model of Mariner Class Vessel

```
function xdot = mariner(x, ui)

% xdot = MARINER(x, u) returns the time derivated of the state vector:
%
% x   = [ u v r psi xpos ypos ]'  where
%
% u     = pertubed surge velocity (m/s)
% v     = pertubed sway velocity  (m/s)
% r     = pertubed yaw velocity   (rad/s)
% psi   = pertubed yaw angle      (rad)
% xpos  = position in x-direction (m)
% ypos  = position in y-direction (m)
% delta = actual rudder angle     (rad)
%
% The input is:
%
% u       = delta_c ,   where
%
% delta_c = commanded rudder angle (rad)
%
% Reference: M.S. Chislett and J. Stroem-Tejsen (1965)
%            Planar Motion Mechanism Tests and Full-Scale Steering and
%            Maneuvering Predictions for a Mariner Class Vessel, Technical
%            Report Hy-5, Hydro- and Aerodynamics Laboratory, Lyngby, Denmark.

% Check of input and state dimensions

if ~(length(x)  == 7),error('x-vector must have dimension 7 !');end
if ~(length(ui) == 1),error('u-vector must have dimension 1 !');end

% Normalization variables

U0 = 7.72;                            % cruise speed U0 = 7.72 m/s = 15 knots
U  = sqrt((U0 + x(1))^2 + x(2)^2);    % total speed U in m/s
L  = 160.93;                          % length of ship in m

% Non-dimensional states and inputs

delta_c = ui(1);

u     = x(1)/U;   v     = x(2)/U;  delta = x(7);
r     = x(3)*L/U; psi   = x(4);

% Parameters, hydrodynamic derivatives and main dimensions

delta_max  = 10;           % max rudder angle      (deg)
Ddelta_max = 5;            % max rudder derivative (deg/s)

m  = 798e-5; Iz = 39.2e-5; xG = -0.023;

Xudot = -840e-5;   Yvdot = -1546e-5;   Nvdot =    23e-5;
```

```
Xu    = -184e-5;   Yrdot =     9e-5;   Nrdot =   -83e-5;
Xuu   = -110e-5;   Yv    = -1160e-5;   Nv    =  -264e-5;
Xuuu  = -215e-5;   Yr    =  -499e-5;   Nr    =  -166e-5;
Xvv   = -899e-5;   Yvvv  = -8078e-5;   Nvvv  =  1636e-5;
Xrr   =   18e-5;   Yvvr  = 15356e-5;   Nvvr  = -5483e-5;
Xdd   =  -95e-5;   Yvu   = -1160e-5;   Nvu   =  -264e-5;
Xudd  = -190e-5;   Yru   =  -499e-5;   Nru   =  -166e-5;
Xrv   =  798e-5;   Yd    =   278e-5;   Nd    =  -139e-5;
Xvd   =   93e-5;   Yddd  =   -90e-5;   Nddd  =    45e-5;
Xuvd  =   93e-5;   Yud   =   556e-5;   Nud   =  -278e-5;
                   Yuud  =   278e-5;   Nuud  =  -139e-5;
                   Yvdd  =    -4e-5;   Nvdd  =    13e-5;
                   Yvvd  =  1190e-5;   Nvvd  =  -489e-5;
                   Y0    =    -4e-5;   N0    =     3e-5;
                   Y0u   =    -8e-5;   N0u   =     6e-5;
                   Y0uu  =    -4e-5;   N0uu  =     3e-5;

% Masses and moments of inertia

m11 = m-Xudot;   m23 = m*xG-Yrdot;   m33 = Iz-Nrdot;
m22 = m-Yvdot;   m32 = m*xG-Nvdot;

% Rudder saturation and dynamics

if abs(delta_c) >= delta_max*pi/180,
   delta_c = sign(delta_c)*delta_max*pi/180; end

delta_dot = delta_c - delta;
if abs(delta_dot) >= Ddelta_max*pi/180,
   delta_dot = sign(delta_dot)*Ddelta_max*pi/180; end

% Forces and moments

X = Xu*u + Xuu*u^2 + Xuuu*u^3 + Xvv*v^2 + Xrr*r^2 + Xrv*r*v + Xdd*delta^2 + ...
    Xudd*u*delta^2 + Xvd*v*delta + Xuvd*u*v*delta;

Y = Yv*v + Yr*r + Yvvv*v^3 + Yvvr*v^2*r + Yvu*v*u + Yru*r*u + Yd*delta + ...
    Yddd*delta^3 + Yud*u*delta + Yuud*u^2*delta + Yvdd*v*delta^2 + ...
    Yvvd*v^2*delta + (Y0 + Y0u*u + Y0uu*u^2);

N = Nv*v + Nr*r + Nvvv*v^3 + Nvvr*v^2*r + Nvu*v*u + Nru*r*u + Nd*delta + ...
    Nddd*delta^3 + Nud*u*delta + Nuud*u^2*delta + Nvdd*v*delta^2 + ...
    Nvvd*v^2*delta + (N0 + N0u*u + N0uu*u^2);

% Dimensional state derivative

xdot = [           X*(U^2/L)/m11
        -(-m33*Y+m23*N)/(m22*m33-m23*m32)*U^2/L
         (-m32*Y+m22*N)/(m22*m33-m23*m32)*U^2/L^2
                   r*U/L
           (cos(psi)*(U0/U+u)-sin(psi)*v)*U
           (sin(psi)*(U0/U+u)+cos(psi)*v)*U
                     delta_dot                ];
```

E.1.2 The ESSO 190000 dwt Tanker

Mathematical models describing the maneuverability of large tankers in deep and confined waters are found in Van Berlekom and Goddard (1972). One of these models, the ESSO 190000 dwt tanker, is listed below:

Length between perpendiculars (L_{pp})	304.8	(m)
Beam (B)	47.17	(m)
Draft to design waterline (T)	18.46	(m)
Displacement (∇)	220,000	(m^3)
L_{pp}/B	6.46	(-)
B/T	2.56	(-)
Block coefficient (C_B)	0.83	(-)
Design speed (u_0)	16	(knots)
Nominal propeller	80	(rpm)

Deep and confine waters are described by a *water depth parameter*:

$$\zeta = \frac{T}{h - T} \tag{E.4}$$

where T (m) is the ship draft and $h > T$ (m) is the water depth.

Speed and Steering Equations of Motion

The speed and steering equations of motion are (Bis-System):

$$\begin{aligned} \dot{u} - v r &= g\, X'' \\ \dot{v} + u r &= g\, Y'' \\ (L\, k_z'')^2\, \dot{r} + L\, x_G''\, u r &= g L\, N'' \end{aligned}$$

where $k_z'' = L^{-1}\sqrt{I_z/m}$ is the non-dimensional radius of gyration, $x_G'' = L^{-1} x_G$, and X'', Y'' and N'' are nonlinear non-dimensional functions:

$$\begin{aligned} X'' &= X''(\dot{u}, u, v, r, T, \zeta, c, \delta) \\ Y'' &= Y''(\dot{v}, u, v, r, T, \zeta, c, \delta) \\ N'' &= N''(\dot{r}, u, v, r, T, \zeta, c, \delta) \end{aligned}$$

The hydrodynamic derivatives corresponding to these expressions are given in the table on the next page. In addition to these equations, propeller thrust T and flow velocity c at the rudder are defined as (see Norrbin (1970) for details):

$$\begin{aligned} g\, T'' &= L^{-1}\, T_{uu}'' u^2 + T_{un}'' u n + L\, T_{|n|n}'' |n| n \\ c^2 &= c_{un}^2 u n + c_{nn}^2 n^2 \end{aligned}$$

For details on the Bis-System normalization procedure see Section 5.3.3.

Non-Dimensional Hydrodynamic Derivatives (Bis-System)

X-equation			
$1 - X''_{\dot{u}}$	1.050		
X''_{uu}	−0.0377		
$1 + X''_{vr}$	2.020		
X''_{vv}	0.300		
$X''_{c/c/\delta\delta}$	−0.093		
$X''_{c/c/\beta\delta}$	0.152		$(\beta = v/u)$
t	0.22		(thrust deduction)
$X''_{\dot{u}\zeta}$	−0.05		
$X''_{uu\zeta}$	−0.0061		additional terms
$X''_{vr\zeta}$	0.387		in shallow water
$X''_{vv\zeta\zeta}$	0.0125		$\zeta \neq 0$
Y-equation			
$1 - Y''_{\dot{v}}$	2.020		
$Y''_{ur} - 1$	−0.752		
Y''_{uv}	−1.205		
$Y_{v/v/}$	−2.400		
$Y''_{c/c/\delta}$	0.208		
$Y''_{c/c/\beta/\beta//\delta/}$	−2.16		
Y''_T	0.04		(propeller side force)
$Y''_{\dot{v}\zeta}$	−0.387		additional
$Y''_{ur\zeta}$	0.182		terms in
$Y''_{uv\zeta}$	$-0.85\ (1 - \frac{0.8}{\zeta})$	$\zeta \geq 0.8$	shallow water
$Y''_{uv\zeta}$	0.0	$\zeta < 0.8$	$\zeta \neq 0$
$Y''_{v/v/\zeta}$	−1.50		
$Y''_{c/c/\beta/\beta//\delta/\zeta}$	−0.191		
N-equation			
$(k''_x)^2 - N''_{\dot{r}}$	0.1232		
$N''_{ur} - x''_G$	−0.231		
N''_{uv}	−0.451		
$N''_{/v/r}$	−0.300		
$N''_{c/c/\delta}$	−0.098		
$N''_{c/c/\beta/\beta/\delta/}$	0.688		
N''_T	−0.02		(propeller yaw moment)
$N''_{\dot{r}\zeta}$	−0.0045		
$N''_{ur\zeta}$	−0.047		additional terms
$N''_{uv\zeta}$	−0.241		in shallow water
$N''_{/v/r\zeta}$	−0.120		$\zeta \neq 0$
$N''_{c/c/\beta/\beta//\delta/\zeta}$	0.344		

T-equation		
T''_{uu}	-0.00695	
T''_{un}	-0.000630	
$T''_{\|n\|n}$	0.0000354	
c-equation		
c_{un}	0.605	$n \geq 0$
c_{nn}	38.2	
$c = 0$		$n < 0$

The hydrodynamic derivatives in the table follow standard hydrodynamic notation. For instance, the non-dimensional surge force is written:

$$\begin{aligned} g\,X'' &= X''_{\dot{u}}\dot{u} + L^{-1}X''_{uu}u^2 + X''_{vr}vr + L^{-1}X''_{vv}v^2 + L^{-1}X''_{c|c|\delta\delta}\,|c|c\delta^2 \\ &+ L^{-1}X''_{c|c|\beta\delta}\,|c|c\beta\delta + gT''(1-t) \\ &+ X''_{\dot{u}\zeta}\dot{u}\zeta + L^{-1}X''_{uu\zeta}u^2\zeta + X''_{vr\zeta}vr\zeta + L^{-1}X''_{vv\zeta\zeta}v^2\zeta^2 \end{aligned}$$

where the first two lines are deep water effects and the last line is confinement effects. Hence, we can write the resulting surge dynamics according to:

$$\begin{aligned} (1 - X''_{\dot{u}} - X''_{\dot{u}\zeta}\zeta)\,\dot{u} &= L^{-1}\,(X''_{uu} + X''_{uu\zeta}\zeta)u^2 + (1 + X''_{vr} + X''_{vr\zeta}\zeta)vr \\ &+ L^{-1}\,(X''_{vv} + X''_{vv\zeta\zeta}\zeta^2)v^2 + L^{-1}X''_{c|c|\delta\delta}\,|c|c\delta^2 + L^{-1}X''_{c|c|\beta\delta}\,|c|c\beta\delta + g\,T''\,(1-t) \end{aligned}$$

The expressions for the sway and yaw dynamics are derived in a similar manner.

Matlab M-File for Nonlinear Model of Tanker

```
function xdot = tanker(x, u)

% xdot = TANKER(x, u) returns the time derivative of the state vector
%
% x   = [ u v r psi xpos ypos delta n ]'  where
%
% u     = surge velocity                (m/s)
% v     = sway velocity                 (m/s)
% r     = yaw velocity                  (rad/s)
% xpos  = position in x-direction       (m)
% ypos  = position in y-direction       (m)
% psi   = yaw angle                     (rad)
% delta = actual rudder angle           (rad)
% n     = actual shaft velocity         (rpm)
%
% The input vector is:
%
% u       = [ delta_c  n_c  h ]'  where
```

```
%
% delta_c = commanded rudder angle      (rad)
% n_c     = commanded shaft velocity    (rpm)
% h       = water depth                 (m)
%
% Reference : W.B. Van Berlekom and T.A. Goddard (1972)
%             Maneuvering of Large Tankers,
%             Transaction of SNAME, 80:264-298

% Check of input and state dimensions

if ~(length(x) == 8),error('x-vector must have dimension 8 !');end
if ~(length(u) == 3),error('u-vector must have dimension 3 !');end

L   =  304.8;          % Length of ship (m)
T   =  18.46;          % Draft to design waterline (m)

% Dimensional states and inputs

delta_c = u(1);
n_c     = u(2)/60;
h       = u(3);

u     = x(1);    v = x(2);
r     = x(3);
psi   = x(4);
delta = x(7);
n     = x(8)/60;

delta_max  = 20;       % max rudder angle   (deg)
Ddelta_max = 2.33;     % max rudder rate    (deg/s)
n_max      = 80;       % max shaft velocity (rpm)

% Parameters, hydrodynamic derivatives and main dimensions

g   =  9.8;
t   =  0.22;
Tm  =  50;

cun =  0.605;
cnn =  38.2;

Tuu = -0.00695;
Tun = -0.00063;
Tnn =  0.0000354;

m11 =  1.050;          % 1 - Xudot
m22 =  2.020;          % 1 - Yvdot
m33 =  0.1232;         % kz^2 - Nrdot

d11 =  2.020;          % 1 + Xvr
d22 = -0.752;          % Yur - 1
d33 = -0.231;          % Nur - xG
```

```
Xuuz   = -0.0061;   YT      =  0.04;   NT      = -0.02;
Xuu    = -0.0377;   Yvv     = -2.400;  Nvr     = -0.300;
Xvv    =  0.3;      Yuv     = -1.205;  Nuv     = -0.451;
Xudotz = -0.05;     Yvdotz  = -0.387;  Nrdotz  = -0.0045;
Xuuz   = -0.0061;   Yurz    =  0.182;  Nurz    = -0.047;
Xvrz   =  0.387;    Yvvz    = -1.5;    Nvrz    = -0.120;
Xccdd  = -0.093;    Yuvz    =  0;      Nuvz    = -0.241;
Xccbd  =  0.152;    Yccd    =  0.208;  Nccd    = -0.098;
Xvvzz  =  0.0125;   Yccbbd  = -2.16;   Nccbbd  =  0.688;

% Additional terms in shallow water

z = T/(h - T);
if z >= 0.8, Yuvz = -0.85*(1-0.8/z);end

% Rudder saturation and dynamics

if abs(delta_c) >= delta_max*pi/180,
   delta_c = sign(delta_c)*delta_max*pi/180;
end

delta_dot = delta_c - delta;
if abs(delta_dot) >= Ddelta_max*pi/180,
   delta_dot = sign(delta_dot)*Ddelta_max*pi/180;
end

% Shaft velocity saturation and dynamics

if abs(n_c) >= n_max,
   n_c = sign(n_c)*n_max
end

n_dot = 1/Tm*(n_c-n)*60;

% Forces and moments

beta = v/u;
gT   = (1/L*Tuu*u^2 + Tun*u*n + L*Tnn*abs(n)*n);
c    = sqrt(cun^2*u*n + cnn^2*n^2);

gX   = 1/L*(Xuu*u^2 + L*d11*v*r + Xvv*v^2 + Xccdd*abs(c)*c*delta^2 ...
     + Xccbd*abs(c)*c*beta*delta + L*gT*(1-t) + Xuuz*u^2*z ...
     + L*Xvrz*v*r*z + Xvvzz*v^2*z^2);

gY   = 1/L*(Yuv*u*v + Yvv*abs(v)*v + Yccd*abs(c)*c*delta + L*d22*u*r ...
     + Yccbbd*abs(c)*c*abs(beta)*beta*abs(delta) + YI*gI*L ...
     + L*Yurz*u*r*z + Yuvz*u*v*z + Yvvz*abs(v)*v*z  ...
     + Yccbbdz*abs(c)*c*abs(beta)*beta*abs(delta)*z);

gLN  = 1/L^2*(Nuv*u*v + L*Nvr*abs(v)*r + Nccd*abs(c)*c*delta +L*d33*u*r ...
     + Nccbbd*abs(c)*c*abs(beta)*beta*abs(delta) + L*NT*gT ...
     + L*Nurz*u*r*z + Nuvz*u*v*z + L*Nvrz*abs(v)*r*z ...
```

```
     + Nccbbdz*abs(c)*c*abs(beta)*beta*abs(delta)*z);

m11 = (m11 - Xudotz*z);
m22 = (m22 - Yvdotz*z);
m33 = (m33 - Nrdotz*z);

% Dimensional state derivative

xdot = [        gX/m11
                gY/m22
                gLN/m33
                   r
          cos(psi)*u-sin(psi)*v
          sin(psi)*u+cos(psi)*v
                delta_dot
                 n_dot       ];
```

E.1.3 Container Ship

A mathematical model for a single-screw high-speed container ship in surge, sway, roll and yaw have been presented by Son and Nomoto (1981, 1982). The main results of this work are presented below as three mathematical models, all describing the couplings in sway, roll and yaw. The models are:

1) Nonlinear equations of motion in surge, sway, roll and yaw.

2) Nonlinear course-keeping equations of motion (sway, roll and yaw).

3) Linearized course-keeping equations of motion (sway, roll and yaw).

The container ship is given by the following set of data:

Length	(L)	175.00	m
Breadth	(B)	25.40	m
Draft ..... fore	(d_F)	8.00	m
aft	(d_A)	9.00	m
mean	(d)	8.50	m
Displacement volume		21,222	m^3
Height from keel to transverse metacenter	(KM)	10.39	m
Height from keel to center of buoyancy	(KB)	4.6154	m
Block coefficient	(C_B)	0.559	
Rudder area	(A_R)	33.0376	m^2
Aspect ratio	(Λ)	1.8219	
Propeller diameter	(D)	6.533	m

1. Nonlinear Equations of Motion (Surge, Sway, Roll and Yaw)

$$\begin{aligned}
(m' + m'_x)\dot{u}' - (m' + m'_y)v'r' &= X' \\
(m' + m'_y)\dot{v}' + (m' + m'_x)u'r' + m'_y\alpha'_y\dot{r}' - m'_y l'_y\dot{p}' &= Y' \\
(I'_x + J'_x)\dot{p}' - m'_y l'_y\dot{v}' - m'_x l'_x u'r' + W'\overline{GM}'\phi' &= K' \\
(I'_z + J'_z)\dot{r}' + m'_y\alpha'_y\dot{v}' &= N' - Y'x'_G
\end{aligned} \tag{E.5}$$

Here m'_x, m'_y, J'_z and J'_x denote the added mass and added moment of inertia in the x and y directions and about the z and x axes, respectively. Furthermore, α'_y denotes the x-coordinates of the center of m'_y, and I'_x and I'_y the z-coordinates of the centers of m'_x and m'_y, respectively. The hydrodynamic forces and moment are:

$$\begin{aligned}
X' &= X'(u') + (1-t)T'(J) + X'_{vr}v'r' + X'_{vv}v'^2 \\
&\quad + X'_{rr}r'^2 + X'_{\phi\phi}\phi'^2 + c_{RX}F'_N\sin\delta' \\
K' &= K'_v v' + K'_r r' + K'_p p' + K'_\phi\phi' + K'_{vvv}v'^3 + K'_{rrr}r'^3 \\
&\quad + K'_{vvr}v'^2r' + K'_{vrr}v'r'^2 + K'_{vv\phi}v'^2\phi' + K'_{v\phi\phi}v'\phi'^2 \\
&\quad + K'_{rr\phi}r'^2\phi' + K'_{r\phi\phi}r'\phi'^2 - (1+a_H)z'_R F'_N\cos\delta' \\
Y' &= Y'_v v' + Y'_r r' + Y'_p p' + Y'_\phi\phi' + Y'_{vvv}v'^3 + Y'_{rrr}r'^3 \\
&\quad + Y'_{vvr}v'^2r' + Y'_{vrr}v'r'^2 + Y'_{vv\phi}v'^2\phi' + Y'_{v\phi\phi}v'\phi'^2 \\
&\quad + Y'_{rr\phi}r'^2\phi' + Y'_{r\phi\phi}r'\phi'^2 + (1+a_H)F'_N\cos\delta' \\
N' &= N'_v v' + N'_r r' + N'_p p' + N'_\phi\phi' + N'_{vvv}v'^3 + N'_{rrr}r'^3 \\
&\quad + N'_{vvr}v'^2r' + N'_{vrr}v'r'^2 + N_{vv\phi}v'^2\phi' + N'_{v\phi\phi}v'\phi'^2 \\
&\quad + N'_{rr\phi}r'^2\phi' + N'_{r\phi\phi}r'\phi'^2 + (x'_R + a_H x'_H)F'_N\cos\delta'
\end{aligned} \tag{E.6}$$

where $X'(u)$ is a velocity-dependent damping function, e.g. $X'(u) = X'_{|u|u}\,|u|u$. The rudder force F'_N can be resolved as:

$$\begin{aligned}
F'_N &= -\tfrac{6.13\Lambda}{\Lambda+2.25}\cdot\tfrac{A_R}{L^2}(u'^2_R + v'^2_R)\sin\alpha_R \\
\alpha_R &= \delta + \tan^{-1}(v'_R/u'_R) \\
u'_R &= u'_P\varepsilon\sqrt{1 + 8kK_T/(\pi J^2)} \\
v'_R &= \gamma v' + c_{Rr}r' + c_{Rrrr}r'^3 + c_{Rrrv}r'^2v'
\end{aligned} \tag{E.7}$$

where

$$\begin{aligned}
J &= u'_P\,U/(nD) \\
u'_P &= \cos v'\left[(1-w_p) + \tau\{(v' + x'_p r')^2 + c_{pv}v' + c_{pr}r'\}\right]
\end{aligned} \tag{E.8}$$

The different parameters in the model are given below.

Model Parameters

(a) Hull only:

m'	0.00792	Y'_p	0.0	$N'_{vv\phi}$	-0.019058
m'_x	0.000238	Y'_ϕ	-0.000063	$N'_{v\phi\phi}$	-0.0053766
m'_y	0.007049	Y'_{vvv}	-0.109	$N'_{rr\phi}$	-0.0038592
I'_x	0.0000176	Y'_{rrr}	0.00177	$N'_{r\phi\phi}$	0.0024195
J'_x	0.0000034	Y'_{rvv}	0.0214	K'_v	0.0003026
I'_z	0.000456	Y'_{rrv}	-0.0405	K'_r	-0.0003026
J'_z	0.000419	$Y'_{vv\phi}$	0.04605	κ_ϕ 0.1	$(F_n \leq 0.1)$
α'_y	0.05	$Y'_{v\phi\phi}$	0.00304	0.2	$(F_n \geq 0.2)$
l'_x	0.0313	$Y'_{rr\phi}$	0.009325	F_n	$(0.1 < F_n < 0.2)$
l'_y	0.0313	$Y'_{r\phi\phi}$	-0.001368	K'_ϕ	-0.000021
K_T	$0.527 - 0.455J$	N'_v	-0.0038545	K'_p	-0.0000075
X'_{uu}	-0.0004226	N'_r	-0.00222	K'_{vvv}	0.002843
X'_{vr}	-0.00311	N'_p	0.000213	K'_{rrr}	-0.0000462
X'_{vv}	-0.00386	N'_ϕ	-0.0001424	K'_{rvv}	-0.000558
X'_{rr}	0.00020	N'_{vvv}	0.001492	K'_{rrv}	0.0010565
$X'_{\phi\phi}$	-0.00020	N'_{rrr}	-0.00229	$K'_{vv\phi}$	-0.0012012
Y'_v	-0.0116	N'_{rvv}	-0.0424	$K'_{v\phi\phi}$	-0.0000793
Y'_r	0.00242	N'_{rrv}	0.00156	$K'_{rr\phi}$	-0.000243
				$K'_{r\phi\phi}$	0.00003569

(b) Propeller and rudder:

N_p (rpm)	79.10 $(Fn\ 0.2)$	a_H	0.237	ϵ	0.921
	118.64 $(Fn\ 0.3)$	x'_H	-0.48	k	0.631
	158.19 $(Fn\ 0.4)$	c_{RX}	0.71	γ	0.088 $(v' > 0)$
$(1-t)$	0.825	z'_R	0.033		0.193 $(v' \leq 0)$
$(1-w_p)$	0.816	c_{pv}	0.0	c_{Rr}	-0.156
x'_R	-0.5	c_{pr}	0.0	c_{Rrrr}	-0.275
x'_p	-0.526	τ	1.09	c_{Rrrv}	1.96

2. Nonlinear Course-Keeping Equations of Motion (Sway, Roll and Yaw)

Consider a ship sailing nearly straight with an automatic course-keeping device in operation. Hence, we can assume constant forward speed ($u' = 1$) which implies that the above equations of motion can be approximated by:

$$\begin{bmatrix} (m' + m'_y) & -m'_y l'_y & 0 \\ -m'_y l'_y & I'_x + J'_x & 0 \\ 0 & 0 & I'_z + J'_z \end{bmatrix} \begin{bmatrix} \dot{v}' \\ \dot{p}' \\ \dot{r}' \end{bmatrix} = \begin{bmatrix} Y' \\ K' \\ N' \end{bmatrix} \tag{E.9}$$

where

$$
\begin{aligned}
Y' &= Y'_v v' - (m' + m'_x - Y'_r) r' + Y'_p p' + Y'_\phi \phi' + Y'_{vv\phi} v'^2 \phi' + Y'_{v\phi\phi} v' \phi'^2 \\
&+ Y'_{rr\phi} r'^2 \phi' + Y'_{r\phi\phi} r' \phi'^2 + Y'_\delta \delta' \\
K' &= K'_\phi p' - (W' \overline{GM}' - K'_\phi) \phi' + K'_v v' + (m'_x l'_x + K'_r) r' + K'_{vv\phi} v'^2 \phi' \\
&+ K'_{v\phi\phi} v' \phi'^2 + K'_{rr\phi} r'^2 \phi' + K'_{r\phi\phi} r' \phi'^2 + K'_\delta \delta' \\
N' &= N'_r r' + N'_v v' + N'_p p' + N'_\phi \phi' + N'_{vv\phi} v'^2 \phi' + N'_{v\phi\phi} v' \phi'^2 + N'_{rr\phi} r'^2 \phi' \\
&+ N'_{r\phi\phi} r' \phi'^2 + N'_\delta \delta'
\end{aligned}
\tag{E.10}
$$

with $p' = \dot{\phi}' = \dot{\phi}\,(L/U)$. The non-dimensional hydrodynamic derivatives for the course-keeping model with $\overline{KG} = 10.09$ m and $\overline{GM} = 0.3$ m are given below:

$(m' + m'_y)$	0.01497	N'_p	0.000213
$(I'_z + J'_z)$	0.000875	N'_ϕ	−0.0001468
$(I'_x + J'_x)$	0.000021	$N'_{vv\phi}$	−0.018191
$m'_y \alpha'_y$	0.0003525	$N'_{v\phi\phi}$	−0.005299
$m'_y l'_y$	0.0002205	$N'_{rr\phi}$	−0.003684
Y'_y	−0.012035	$N'_{r\phi\phi}$	0.0023843
$(m' + m'_x - Y'_r)$	0.00522	N'_δ	0.00126
Y'_p	0.0	κ_ϕ	0.2
Y'_ϕ	−0.0000704	K'_ϕ	−0.000021
$Y'_{vv\phi}$	0.046364	K'_v	0.000314
$Y'_{v\phi\phi}$	0.003005	$(m'_x l'_x + K'_r)$	−0.0000692
$Y'_{rr\phi}$	0.0093887	$K'_{vv\phi}$	−0.0012094
$Y'_{r\phi\phi}$	−0.0013523	$K'_{v\phi\phi}$	−0.0000784
Y'_δ	−0.002578	$K'_{rr\phi}$	−0.0002449
N'_r	−0.00243	$K'_{r\phi\phi}$	0.00003528
N'_v	−0.0038436	K'_δ	0.0000855

3. Linearized Course-Keeping Equations of Motion (Sway, Roll and Yaw)

The linearized course-keeping equations of motion are:

$$
\begin{bmatrix} m'_{11} & m'_{12} & 0 & 0 \\ m'_{21} & m'_{22} & 0 & 0 \\ 0 & 0 & m'_{33} & 0 \\ 0 & 0 & 0 & 1 \end{bmatrix} \begin{bmatrix} \Delta\dot{v}' \\ \Delta\dot{p}' \\ \Delta\dot{r}' \\ \Delta\dot{\phi}' \end{bmatrix} + \begin{bmatrix} d'_{11} & d'_{12} & d'_{13} & d'_{14} \\ d'_{21} & d'_{22} & d'_{23} & d'_{24} \\ d'_{31} & d'_{32} & d'_{33} & d'_{34} \\ 0 & -\frac{U}{L} & 0 & 0 \end{bmatrix} \begin{bmatrix} \Delta v' \\ \Delta p' \\ \Delta r' \\ \Delta\phi' \end{bmatrix} = \begin{bmatrix} b'_1 \\ b'_2 \\ b'_3 \\ 0 \end{bmatrix} \Delta\delta
$$

where

$$
\begin{aligned}
m'_{11} &= m' + m'_y \\
m'_{12} &= -m'_y l'_y \\
m'_{21} &= m_{12} \\
m'_{22} &= I'_x + J'_x \\
m'_{33} &= I'_z + J'_z \\
d'_{11} &= -Y'_v - 2Y'_{vv\phi} v'_0 \phi'_0 - Y'_{v\phi\phi} \phi'^2_0 \\
d'_{12} &= -Y'_p \\
d'_{13} &= (m' + m'_x - Y'_r) - 2Y'_{rr\phi} r'_0 \phi'_0 - Y'_{r\phi\phi} \phi'^2_0 \\
d'_{14} &= -Y'_\phi - Y'_{vv\phi} v'^2_0 - 2Y'_{v\phi\phi} v'_0 \phi'_0 - Y'_{rr\phi} r'^2 - 2Y'_{r\phi\phi} r'_0 \phi'_0 \\
d'_{21} &= -K'_v - 2K'_{vv\phi} v'_0 \phi'_0 - K'_{v\phi\phi} \phi'^2_0 \\
d'_{22} &= -K'_p \\
d'_{23} &= -(m'_x l'_x + K'_r) - 2K'_{rr\phi} r'_0 \phi'_0 - K'_{r\phi\phi} \phi'^2_0 \\
d'_{24} &= (W'\overline{GM}' - K'_\phi) - K'_{vv\phi} v'^2_0 - 2K'_{v\phi\phi} v'_0 \phi'_0 - K'_{rr\phi} r'^2_0 - 2K'_{r\phi\phi} r'_0 \phi'_0 \\
d'_{31} &= -N'_v - 2N'_{vv\phi} v'_0 \phi'_0 - N'_{v\phi\phi} \phi'^2_0 \\
d'_{32} &= -N'_p \\
d'_{33} &= -N'_r - 2N'_{rr\phi} r'_0 \phi'_0 - N'_{r\phi\phi} \phi'^2_0 \\
d'_{34} &= -N'_\phi - N'_{vv\phi} v'^2_0 - 2N'_{v\phi\phi} v'_0 \phi'_0 - N'_{rr\phi} r'^2_0 - 2N'_{r\phi\phi} r'_0 \phi'_0 \\
b'_1 &= Y'_\delta \\
b'_2 &= K'_\delta \\
b'_3 &= N'_\delta
\end{aligned}
\tag{E.11}
$$

Matlab M-File for Nonlinear Model of Container Ship

```
function xdot = contship(x, u)

% xdot = CONTSHIP(x, u) returns the time derivated of the state vector:
%
% x   = [ u v p r phi psi xpos ypos delta n ]'  where
%
% u     = surge velocity          (m/s)
% v     = sway velocity           (m/s)
% p     = roll velocity           (rad/s)
% r     = yaw velocity            (rad/s)
% phi   = roll angle              (rad)
% psi   = yaw angle               (rad)
% xpos  = position in x-direction (m)
% ypos  = position in y-direction (m)
% delta = actual rudder angle     (rad)
% n     = actual shaft velocity   (rpm)
%
% The input vector is:
%
% u       = [ delta_c n_c ]'  where
%
% delta_c = commanded rudder angle   (rad)
% n_c     = commanded shaft velocity (rpm)
%
% Reference : Son og Nomoto (1982).
```

```
%             On the Coupled Motion of Steering and
%             Rolling of a High Speed Container Ship,
%             Naval Architect of Ocean Engineering,
%             20: 73-83. From J.S.N.A. , Japan, Vol. 150, 1981.

% Check of input and state dimensions

if ~(length(x) == 10),error('x-vector must have dimension 10 !');end
if ~(length(u) ==  2),error('u-vector must have dimension  2 !');end

L = 175;                        % length of ship (m)
V = sqrt(x(1)~2 + x(2)~2);      % service speed (m/s)

% Check of service speed

if V == 0,error('The ship must have speed greater than zero');end

delta_max  = 10;                % max rudder angle (deg)
Ddelta_max = 5;                 % max rudder rate (deg/s)
n_max      = 160;               % max shaft velocity (rpm)

% Non-dimensional states and inputs

delta_c = u(1);
n_c     = u(2)/60*L/V;

u     = x(1)/V;   v   = x(2)/V;
p     = x(3)*L/V; r   = x(4)*L/V;
phi   = x(5);     psi = x(6);
delta = x(9);     n   = x(10)/60*L/V;

% Parameters, hydrodynamic derivatives and main dimensions

m  = 0.00792;    mx     = 0.000238;   my = 0.007049;
Ix = 0.0000176;  alphay = 0.05;       lx = 0.0313;
ly = 0.0313;     Ix     = 0.0000176;  Iz = 0.000456;
Jx = 0.0000034;  Jz     = 0.000419;   xG = 0;

B     = 25.40;   dF = 8.00;    g     = 9.81;
dA    = 9.00;    d  = 8.50;    nabla = 21222;
KM    = 10.39;   KB = 4.6154;  AR    = 33.0376;
Delta = 1.8219;  D  = 6.533;   GM    = .3/L;
rho   = 1000;    t  = 0.175;   T     = 0.0005;

W     = rho*g*nabla/(rho*L~2*V~2/2);

Xuu      = -0.0004226;  Xvr    = -0.00311;    Xrr      = 0.00020;
Xphiphi  = -0.00020;    Xvv    = -0.00386;

Kv       =  0.0003026;  Kr     = -0.000063;   Kp       = -0.0000075;
Kphi     = -0.000021;   Kvvv   =  0.002843;   Krrr     = -0.0000462;
Kvvr     = -0.000588;   Kvrr   =  0.0010565;  Kvvphi   = -0.0012012;
Kvphiphi = -0.0000793;  Krrphi = -0.000243;   Krphiphi =  0.00003569;
```

```
Yv       = -0.0116;     Yr      =  0.00242;    Yp       =  0;
Yphi     = -0.000063;   Yvvv    = -0.109;      Yrrr     =  0.00177;
Yvvr     =  0.0214;     Yvrr    = -0.0405;     Yvvphi   =  0.04605;
Yvphiphi =  0.00304;    Yrrphi  =  0.009325;   Yrphiphi = -0.001368;

Nv       = -0.0038545;  Nr      = -0.00222;    Np       =  0.000213;
Nphi     = -0.0001424;  Nvvv    =  0.001492;   Nrrr     = -0.00229;
Nvvr     = -0.0424;     Nvrr    =  0.00156;    Nvvphi   = -0.019058;
Nvphiphi = -0.0053766;  Nrrphi  = -0.0038592;  Nrphiphi =  0.0024195;

kk     =  0.631;  epsilon =  0.921;  xR    = -0.5;
wp     =  0.184;  tau     =  1.09;   xp    = -0.526;
cpv    =  0.0;    cpr     =  0.0;    ga    =  0.088;
cRr    = -0.156;  cRrrr   = -0.275;  cRrrv =  1.96;
cRX    =  0.71;   aH      =  0.237;  zR    =  0.033;
xH     = -0.48;

% Masses and moments of inertia

m11 = (m+mx);
m22 = (m+my);
m32 = -my*ly;
m42 = my*alphay;
m33 = (Ix+Jx);
m44 = (Iz+Jz);

% Rudder saturation and dynamics

if abs(delta_c) >= delta_max*pi/180,
   delta_c = sign(delta_c)*delta_max*pi/180;
end

delta_dot = delta_c - delta;
if abs(delta_dot) >= Ddelta_max*pi/180,
   delta_dot = sign(delta_dot)*Ddelta_max*pi/180;
end

% Shaft velocity saturation and dynamics

n_c = n_c*V/L;
n   = n*V/L;
if abs(n_c) >= n_max/60,
   n_c = sign(n_c)*n_max/60;
end

if n > 0.3,Tm=5.65/n;else,Tm=18.83;end
n_dot = 1/Tm*(n_c-n)*60;

% Calculation of state derivatives

  vR     = ga*v + cRr*r + cRrrr*r^3 + cRrrv*r^2*v;
  uP     = cos(v)*((1 - wp) + tau*((v + xp*r)^2 + cpv*v + cpr*r));
```

```
   J      = uP*V/(n*D);
  KT      = 0.527 - 0.455*J;
  uR      = uP*epsilon*sqrt(1 + 8*kk*KT/(pi*J^2));
  alphaR  = delta + atan(vR/uR);
  FN      = - ((6.13*Delta)/(Delta + 2.25))*(AR/L^2)*(uR^2 + vR^2)*sin(alphaR);
  T       = 2*rho*D^4/(V^2*L^2*rho)*KT*n*abs(n);

% Forces and moments

  X     = Xuu*u^2 + (1-t)*T + Xvr*v*r + Xvv*v^2 + Xrr*r^2 + Xphiphi*phi^2 + ...
          cRX*FN*sin(delta) + (m + my)*v*r;

  Y     = Yv*v + Yr*r + Yp*p + Yphi*phi + Yvvv*v^3 + Yrrr*r^3 + Yvvr*v^2*r + ...
          Yvrr*v*r^2 + Yvvphi*v^2*phi + Yvphiphi*v*phi^2 + Yrrphi*r^2*phi + ...
          Yrphiphi*r*phi^2 + (1 + aH)*FN*cos(delta) - (m + mx)*u*r;

  K     = Kv*v + Kr*r + Kp*p + Kphi*phi + Kvvv*v^3 + Krrr*r^3 + Kvvr*v^2*r + ...
          Kvrr*v*r^2 + Kvvphi*v^2*phi + Kvphiphi*v*phi^2 + Krrphi*r^2*phi + ...
          Krphiphi*r*phi^2 - (1 + aH)*zR*FN*cos(delta) + mx*lx*u*r - W*GM*phi;


  N     = Nv*v + Nr*r + Np*p + Nphi*phi + Nvvv*v^3 + Nrrr*r^3 + Nvvr*v^2*r + ...
          Nvrr*v*r^2 + Nvvphi*v^2*phi + Nvphiphi*v*phi^2 + Nrrphi*r^2*phi + ...
          Nrphiphi*r*phi^2 + (xR + aH*xH)*FN*cos(delta);

% Dimensional state derivatives

xdot =[                          1/m11*X*V^2/L
     -(-m33*m44*Y+m32*m44*K+m42*m33*N)/(m22*m33*m44-m32^2*m44-m42^2*m33)*V^2/L
(-m32*m44*Y+K*m22*m44-K*m42^2+m32*m42*N)/(m22*m33*m44-m32^2*m44-m42^2*m33)*V^2/L^2
(-m42*m33*Y+m32*m42*K+N*m22*m33-N*m32^2)/(m22*m33*m44-m32^2*m44-m42^2*m33)*V^2/L^2
                                   p*V/L
                                cos(phi)*r*V/L
                      (cos(psi)*u-sin(psi)*cos(phi)*v)*V
                      (sin(psi)*u+cos(psi)*cos(phi)*v)*V
                                 delta_dot
                                   n_dot                 ];
```

E.2 Underwater Vehicle Models

This section contains three underwater vehicle models intended for computer simulations.

E.2.1 Linear Model of a Deep Submergence Rescue Vehicle (DSRV)

The non-dimensional hydrodynamic derivatives for a DSRV are given below (Healey 1992). This model uses the stern plane δ_S for depth changing maneuvers.

I'_x	=	0.000118	$M'_{\dot{q}}$	=	−0.001573	Z'_q	=	−0.017455
I'_z	=	$I'_y = 0.001925$	M'_w	=	0.011175	$Z'_{\dot{q}}$	=	−0.000130
m'	=	0.036391	$M'_{\dot{w}}$	=	−0.000146	Z'_w	=	−0.043938
u_0	=	13.5 (ft/s)	M_δ	=	−0.012797	Z'_δ	=	−0.027695
M'_q	=	−0.01131	M'_θ	=	$-0.156276/U^2$	$Z'_{\dot{w}}$	=	−0.031545

Here the non-dimensional hydrodynamic derivatives are defined according to Prime-system I in Table 5.1 with u_0 in (ft/s) and L in (ft); see Section 5.3.3 (1 ft = 0.30 m). Assume that $x'_G = 0$. The total speed of the vehicle is:

$$U = \sqrt{(u_0 + \Delta u)^2 + (v_0 + \Delta v)^2 + (w_0 + \Delta w)^2} = \sqrt{u_0^2 + (\Delta w)^2}$$

E.2.2 Linear Model of a Swimmer Delivery Vehicle (SDV)

The non-dimensional hydrodynamic derivatives for a SDV are given below (Healey 1992). This model uses the rudder δ_R to control the heading.

Sway and Yaw Modes

I'_x		= 0.000949	Y'_v	=	$-1.0 \cdot 10^{-1}$	$Y'_{\dot{v}}$	=	$-5.5 \cdot 10^{-2}$
I'_z	$= I'_y$	= 0.006326	Y'_r	=	$3.0 \cdot 10^{-2}$	$Y'_{\dot{r}}$	=	0
m'		= 0.1415	N'_v	=	$-7.4 \cdot 10^{-3}$	$N'_{\dot{v}}$	=	0
u_0		= 13.5 (ft/s)	N'_r	=	$-1.6 \cdot 10^{-2}$	$N'_{\dot{r}}$	=	$-3.4 \cdot 10^{-3}$
W'	$= B'$	= 0.2175	Y'_δ	=	$2.7 \cdot 10^{-2}$	N'_δ	=	$-1.3 \cdot 10^{-2}$

Notice that the non-dimensional hydrodynamic derivatives are defined according to Prime-system I in Table 5.1 with u_0 in (ft/s) and L in (ft); see Section 5.3.3. In addition to this, we have $x_G = y_G = 0$ and $z_G = 0.2$ (ft). The length of the vehicle is $L = 17.4$ (ft). The total speed of the vehicle is:

$$U = \sqrt{(u_0 + \Delta u)^2 + (v_0 + \Delta v)^2 + (w_0 + \Delta w)^2} = \sqrt{u_0^2 + (\Delta v)^2}$$

Furthermore, we can include the roll mode by using:

Roll Mode

$K'_{\dot{p}} = -1.0 \cdot 10^{-3}$	$K'_p = -1.1 \cdot 10^{-2}$	$K'_v = 1.3 \cdot 10^{-4}$	$K'_{\dot{v}} = 3.1 \cdot 10^{-3}$
$K'_{\dot{r}} = -3.4 \cdot 10^{-5}$	$K'_r = -8.4 \cdot 10^{-4}$	$K'_\delta = 0$	$N'_{\dot{p}} = K'_{\dot{r}}$

E.2.3 Nonlinear Model of the Naval Postgraduate School AUV II

The 6 DOF nonlinear equations of motion for the Naval Postgraduate School (NPS) AUV II are given below (Healey and Lienhard 1993):

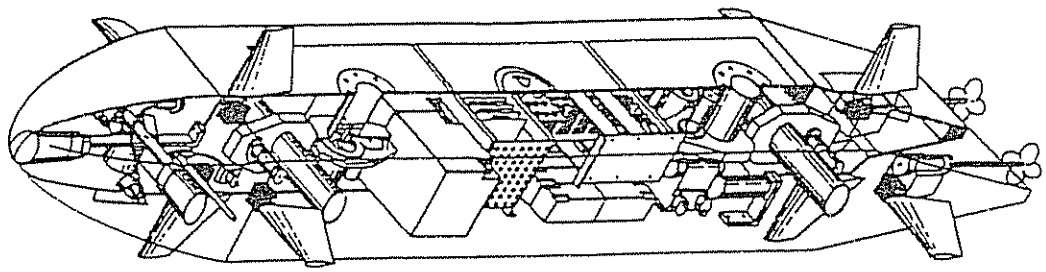

Figure E.1: Schematic drawing of the NPS AUV II (Healey and Lienhard 1993).

Surge Motion Equation

$$
\begin{aligned}
&m\left[\dot{u} - vr + wq - x_G(q^2 + r^2) + y_G(pq - \dot{r}) + z_G(pr + \dot{q})\right] \\
&\quad = \frac{\rho}{2}L^4\left[X'_{pp}p^2 + X'_{qq}q^2 + X'_{rr}r^2 + X'_{pr}pr\right] + \frac{\rho}{2}L^3\left[X'_{\dot{u}}\dot{u} + X'_{wq}wq\right. \\
&\quad \left. + X'_{vp}vp + X'_{vr}vr + uq(X'_{q\delta s}\delta_s + X'_{q\delta b/2}\delta_{bp} + X'_{q\delta b/2}\delta_{bs}) + X'_{r\delta r}ur\delta_r\right] \\
&\quad + \frac{\rho}{2}L^2\left[X'_{vv}v^2 + X'_{ww}w^2 + X'_{v\delta r}uv\delta_r + uw(X'_{w\delta s}\delta_s + X'_{w\delta b/2}\delta_{bs} + X'_{w\delta b/2}\delta_{bp})\right. \\
&\quad \left. + u^2(X'_{\delta s\delta s}\delta_s^2 + X'_{\delta b\delta b/2}\delta_{\delta b}^2 + X'_{\delta r\delta r}\delta_r^2)\right] - (W - B)\sin\theta + \frac{\rho}{2}L^3X'_{q\delta_{sn}}uq\delta_s\epsilon(n) \\
&\quad + \frac{\rho}{2}L^2\left[X'_{w\delta_{sn}}uw\delta_{sn} + X'_{\delta s\delta sn}u^2\delta_s^2\right]\cdot\epsilon(n) + \frac{\rho}{2}L^2u^2X_{prop}
\end{aligned}
$$

Sway Motion Equation

$$
\begin{aligned}
&m\left[\dot{v} + ur - wp + x_G(pq + \dot{r}) - y_G(p^2 + r^2) + z_G(qr - \dot{p})\right] \\
&\quad = \frac{\rho}{2}L^4\left[Y'_{\dot{p}}\dot{p} + Y'_{\dot{r}}\dot{r} + Y'_{pq}pq + Y'_{qr}qr\right] + \frac{\rho}{2}L^3\left[Y'_{\dot{v}}\dot{v} + Y'_{p}up\right. \\
&\quad \left. + Y'_{r}ur + Y'_{vq}vq + Y'_{wp}wp + Y'_{wr}wr\right] + \frac{\rho}{2}L^2\left[Y'_{v}uv + Y'_{vw}vw + Y'_{\delta r}u^2\delta_r\right] \\
&\quad - \frac{\rho}{2}\int_{x_{tail}}^{x_{nose}}\left[C_{dy}h(x)(v + xr)^2 + C_{dz}b(x)(w - xq)^2\right]\cdot\frac{(v + xr)}{U_{cf}(x)}dx \\
&\quad + (W - B)\cos\theta\sin\phi
\end{aligned}
$$

Heave Motion Equation

$$
\begin{aligned}
&m\left[\dot{w} - uq + vp + x_G(pr - \dot{q}) + y_G(qr + \dot{p}) - z_G(p^2 + q^2)\right] \\
&\quad = \frac{\rho}{2}L^4\left[Z'_{\dot{q}}\dot{q} + Z'_{pp}p^2 + Z'_{pr}pr + Z'_{rr}r^2\right] + \frac{\rho}{2}L^3\left[Z'_{\dot{w}}\dot{w} + Z'_{q}uq\right. \\
&\quad \left. + Z'_{vp}vp + Z'_{vr}vr\right] + \frac{\rho}{2}L^2\left[Z'_{w}uw + Z'_{vv}v^2 + u^2(Z'_{\delta s}\delta_s + Z'_{\delta b/2}\delta_{bs}\right.
\end{aligned}
$$

$$+ Z'_{\delta b/2}\delta_{bp})\Big] + \frac{\rho}{2}\int_{x_{tail}}^{x_{nose}} \left[C_{dy}h(x)(v+xr)^2 + C_{dz}b(x)(w-xq)^2\right]\frac{(w-xq)}{U_{cf}(x)}dx$$
$$+ (W-B)\cos\theta\cos\phi + \frac{\rho}{2}L^3 Z'_{qn}uq\epsilon(n) + \frac{\rho}{2}L^2\left[Z'_{wn}uw + Z'_{\delta sn}u^2\delta_s\right]\epsilon(n)$$

Roll Motion Equation

$$I_x\dot{p} + (I_z - I_y)qr + I_{xy}(pr - \dot{q}) - I_{yz}(q^2 - r^2) - I_{xz}(pq + \dot{r})$$
$$+ m\left[y_G(\dot{w} - uq + vp) - z_G(\dot{v} + ur - wp)\right] = \frac{\rho}{2}L^5\left[K'_{\dot{p}}\dot{p} + K'_{\dot{r}}\dot{r}\right.$$
$$\left.+K'_{pq}pq + K'_{qr}qr\right] + \frac{\rho}{2}L^4\left[K'_{\dot{v}}\dot{v} + K'_{p}up + K'_{r}ur + K'_{vq}vq\right.$$
$$\left.+K'_{wp}wp + K'_{wr}wr\right] + \frac{\rho}{2}L^3\left[K'_{v}uv + K'_{vw}vw + u^2(K'_{\delta b/2}\delta_{bp} + K'_{\delta b/2}\delta_{bs})\right]$$
$$+ (y_G W - y_B B)\cos\theta\cos\phi - (z_G W - z_B B)\cos\theta\sin\phi$$
$$+ \frac{\rho}{2}L^4 K'_{pn}up\epsilon(n) + \frac{\rho}{2}L^3u^3K'_{prop}$$

Pitch Motion Equation

$$I_y\dot{q} + (I_x - I_z)pr - I_{xy}(qr + \dot{p}) + I_{yz}(pq - \dot{r}) + I_{xz}(p^2 - r^2)$$
$$- m\left[x_G(\dot{w} - uq + vp) - z_G(\dot{u} - vr + wq)\right] = \frac{\rho}{2}L^5\left[M'_{\dot{q}}\dot{q} + M'_{pp}p^2\right.$$
$$\left.+ M'_{pr}pr + M'_{rr}r^2\right] + \frac{\rho}{2}L^4\left[M'_{\dot{w}}\dot{w} + M'_{uq}uq + M'_{vp}vp + M'_{vr}vr\right]$$
$$+ \frac{\rho}{2}L^3\left[M'_{uw}uw + M'_{vv}v^2 + u^2(M'_{\delta s}\delta_s + M'_{\delta b/2}\delta_{bp} + M'_{\delta b/2}\delta_{bs})\right]$$
$$- \frac{\rho}{2}\int_{x_{tail}}^{x_{nose}}\left[C_{dy}h(x)(v+xr)^2 + C_{dz}b(x)(w-xq)^2\right]\cdot\frac{(w+xq)}{U_{cf}(x)}xdx$$
$$- (x_G W - x_B B)\cos\theta\cos\phi - (z_G W - z_B B)\sin\theta$$
$$+ \frac{\rho}{2}L^4 M_{qn}uq\epsilon(n) + \frac{\rho}{2}L^3\left[M'_{wn}uw + M'_{\delta sn}u^2\delta_s\right]\epsilon(n)$$

Yaw Motion Equation

$$I_z\dot{r} + (I_y - I_x)pq - I_{xy}(p^2 - q^2) - I_{yz}(pr + \dot{q}) + I_{xz}(qr - \dot{p})$$
$$+ m\left[x_G(\dot{v} + ur - wp) - y_G(\dot{u} - vr + wq)\right]$$
$$= \frac{\rho}{2}L^5\left[N'_{\dot{p}}\dot{p} + N'_{\dot{r}}\dot{r} + N'_{pq}pq + N'_{qr}qr\right] + \frac{\rho}{2}L^4\left[N'_{\dot{v}}\dot{v} + N'_{p}up + N'_{r}ur\right.$$
$$\left.+N'_{vq}vq + N'_{wp}wp + N'_{wr}wr\right] + \frac{\rho}{2}L^3\left[N'_{v}uv + N'_{vw}vw + N'_{\delta r}u^2\delta_r\right]$$
$$- \frac{\rho}{2}\int_{x_{tail}}^{x_{nose}}\left[C_{dy}h(x)(v+xr)^2 + C_{dz}b(x)(w-xq)^2\right]\cdot\frac{(v+xr)}{U_{cf}(x)}xdx$$
$$+ (x_G W - x_B B)\cos\theta\sin\phi + (y_G W - y_B B)\sin\theta + \frac{\rho}{2}L^3u^2N'_{prop}$$

Main Data

$W = 53.4$ kN	$B = 53.4$ kN	$L = 5.3m$	$I_z = 13587$ Nms^2
$I_{xy} = -13.58$ Nms^2	$I_{yz} = -13.58$ Nms^2	$I_{xz} = -13.58$ Nms^2	$I_y = 13587$ Nms^2
$I_x = 2038$ Nms^2	$x_G = 0.0$	$x_B = 0.0$	$y_G = 0.0$
$y_B = 0.0$	$z_G = 6.1$ cm	$z_B = 0.0$	$g = 9.81$ m/s^2
$\rho = 1000$ kg/m^3	$m = 5454.54$ kg	$b(x) =$ hull breadth	$h(x) =$ hull height

Non-Dimensional Hydrodynamic Derivatives

$$
\begin{array}{llllllll}
X'_{pp} = 7.0\cdot10^{-3} & X'_{qq} = -1.5\cdot10^{-2} & X'_{rr} = 4.0\cdot10^{-3} & X'_{pr} = 7.5\cdot10^{-4} \\
X'_{\dot{u}} = -7.6\cdot10^{-3} & X'_{wq} = -2.0\cdot10^{-1} & X'_{vp} = -3.0\cdot10^{-3} & X'_{vr} = 2.0\cdot10^{-2} \\
X'_{q\delta_s} = 2.5\cdot10^{-2} & X'_{q\delta b/2} = -1.3\cdot10^{-3} & X'_{r\delta_r} = -1\cdot10^{-3} & X'_{vv} = 5.3\cdot10^{-2} \\
X'_{ww} = 1.7\cdot10^{-1} & X'_{v\delta_r} = 1.7\cdot10^{-3} & X'_{w\delta_s} = 4.6\cdot10^{-2} & X'_{w\delta b/2} = 0.5\cdot10^{-2} \\
X'_{\delta s\delta s} = -1\cdot10^{-2} & X'_{\delta b\delta b/2} = -4\cdot10^{-3} & X'_{\delta r\delta r} = -1\cdot10^{-2} & X'_{q\delta sn} = 2.0\cdot10^{-3} \\
X'_{w\delta_{sn}} = 3.5\cdot10^{-3} & X'_{\delta s\delta sn} = -1.6\cdot10^{-3} & & \\
\\
Y'_{\dot{p}} = 1.2\cdot10^{-4} & Y'_{\dot{r}} = 1.2\cdot10^{-3} & Y'_{pq} = 4\cdot10^{-3} & Y'_{qr} = -6.5\cdot10^{-3} \\
Y'_{\dot{v}} = -5.5\cdot10^{-2} & Y'_{p} = 3.0\cdot10^{-3} & Y'_{r} = 3.0\cdot10^{-2} & Y'_{vq} = 2.4\cdot10^{-2} \\
Y'_{wp} = 2.3\cdot10^{-1} & Y'_{wr} = -1.9\cdot10^{-2} & Y'_{v} = -1.0\cdot10^{-1} & Y'_{vw} = 6.8\ 10^{-2} \\
Y'_{\delta r} = 2.7\cdot10^{-2} & & & \\
\\
Z'_{\dot{q}} = -6.8\cdot10^{-3} & Z'_{pp} = 1.3\cdot10^{-4} & Z'_{pr} = 6.7\cdot10^{-3} & Z'_{rr} = -7.4\cdot10^{-3} \\
Z'_{\dot{w}} = -2.4\cdot10^{-1} & Z'_{q} = -1.4\cdot10^{-1} & Z'_{vp} = -4.8\cdot10^{-2} & Z'_{vr} = 4.5\cdot10^{-2} \\
Z'_{w} = -3.0\cdot10^{-1} & Z'_{vv} = -6.8\cdot10^{-2} & Z'_{\delta s} = -7.3\cdot10^{-2} & Z'_{\delta b/2} = -1.3\cdot10^{-2} \\
Z'_{qn} = -2.9\cdot10^{-3} & Z'_{wn} = -5.1\cdot10^{-3} & Z'_{\delta sn} = -1.0\cdot10^{-2} & \\
\\
K'_{\dot{p}} = -1.0\cdot10^{-3} & K'_{\dot{r}} = -3.4\cdot10^{-5} & K'_{pq} = -6.9\cdot10^{-5} & K'_{qr} = 1.7\cdot10^{-2} \\
K'_{\dot{v}} = 1.2\cdot10^{-4} & K'_{p} = -1.1\cdot10^{-2} & K'_{r} = -8.4\cdot10^{-4} & K'_{vq} = -5.1\cdot10^{-3} \\
K'_{wp} = -1.3\cdot10^{-4} & K'_{wr} = 1.4\cdot10^{-2} & K'_{v} = 3.1\cdot10^{-3} & K'_{vw} = -1.9\cdot10^{-1} \\
K'_{\delta b/2} = 0.0 & K'_{pn} = -5.7\cdot10^{-4} & K'_{prop} = 0.0 & \\
\\
M'_{\dot{q}} = -1.7\cdot10^{-2} & M'_{pp} = 5.3\cdot10^{-5} & M'_{pr} = 5.0\cdot10^{-3} & M'_{rr} = 2.9\cdot10^{-3} \\
M'_{\dot{w}} = -6.8\cdot10^{-3} & M'_{uq} = -6.8\cdot10^{-2} & M'_{vp} = 1.2\cdot10^{-3} & M'_{vr} = 1.7\cdot10^{-2} \\
M'_{uw} = 1.0\cdot10^{-1} & M'_{vv} = -2.6\cdot10^{-2} & M'_{\delta s} = -4.1\cdot10^{-2} & M'_{\delta b/2} = 3.5\cdot10^{-3} \\
M'_{qn} = -1.6\cdot10^{-3} & M'_{wn} = -2.9\cdot10^{-3} & M'_{\delta sn} = -5.2\cdot10^{-3} & \\
\\
N'_{\dot{p}} = -3.4\cdot10^{-5} & N'_{\dot{r}} = -3.4\cdot10^{-3} & N'_{pq} = -2.1\cdot10^{-2} & N'_{qr} = 2.7\cdot10^{-3} \\
N'_{\dot{v}} = 1.2\cdot10^{-3} & N'_{p} = -8.4\cdot10^{-4} & N'_{r} = -1.6\cdot10^{-2} & N'_{vq} = -1.0\cdot10^{-2} \\
N'_{wp} = -1.7\cdot10^{-2} & N'_{wr} = 7.4\cdot10^{-3} & N'_{v} = -7.4\cdot10^{-3} & N'_{vw} = -2.7\cdot10^{-2} \\
N'_{\delta r} = -1.3\cdot10^{-2} & N'_{prop} = 0.0 & &
\end{array}
$$

Crossflow Velocity, Drag Coefficients and Propulsion Terms

$$
\begin{aligned}
U_{cf}(x) &= \left[(v + x_T)^2 + (w - xq)^2\right]^{1/2} \\
X'_{prop} &= C_{d0}(\eta|\eta| - 1); \qquad \eta = 0.012\, n/u \\
C_{d0} &= 0.00385
\end{aligned}
$$

$$
\begin{aligned}
\epsilon(n) &= -1 + \text{sign}(n)/\text{sign}(u) \cdot (\sqrt{C_t + 1} - 1)/(\sqrt{C_{t1} + 1} - 1) \\
C_t &= 0.008L^2\eta|\eta|/2.0; \qquad C_{t1} = 0.008L^2/2.0 \\
C_{dy} &= 0.5 \\
C_{dz} &= 0.6
\end{aligned}
$$

Appendix F

Conversion Factors

In marine applications the following conversion factors are frequently used for linear measure, velocity, temperature and density.

Conversion of Linear Measure

The relationship between some commonly used linear measures is given in the table below.

Table F.1: Conversion of linear measure.

	meters	feet	nautical miles	kilometers	land miles
meters (m)	1.0	3.2808	0.000540	0.001	0.000621
feet (ft)	0.3048	1.0	0.000165	0.0003	0.000189
nautical miles	1852.0	6076.1	1.0	1.852	1.1508
kilometers (km)	1000.0	3280.8	0.5400	1.0	0.6214
land miles	1609.4	5280.0	0.8690	1.6094	1.0

Velocity Conversion

The following table can be used to convert velocity in terms of knots, meters per second (m/s) and feet per second (ft/s).

Table F.2: Velocity conversion.

	knots	m/s	ft/s
knots	1.0	0.5145	1.6835
m/s	1.9438	1.0	3.2808
ft/s	0.5940	0.3048	1.0

Temperature Conversion

The relationship between Celsius (C) and Fahrenheit (F) is given by:

$$C = \frac{5}{9}(F - 32)$$
$$F = \frac{9}{5}C + 32$$

Air and Water Densities

The air and water densities in kg/m^3 as a function of temperature are given in the following table.

Table F.3: Air and water density ρ.

medium	$0^o\,C$	$10^o\,C$	$20^o\,C$	$30^o\,C$	$40^o\,C$
air	1.310	1.264	1.224	1.170	1.124
fresh water	1002.680	1005.525	998.560	994.930	-
sea water (3.5% salinity)	1028.480	1026.911	1024.851	1021.810	-

Kinematic Viscosity

The kinematic viscosity in m^2/s as a function of temperature is given in the following table.

Table F.4: Kinematic viscosity $\nu \cdot 10^6$ of water and air.

medium	$0^o\,C$	$5^o\,C$	$10^o\,C$	$15^o\,C$	$20^o\,C$
air	13.2	13.6	14.1	14.5	15.0
fresh water	1.79	1.52	1.31	1.14	1.00
sea water (3.5% salinity)	1.83	1.56	1.35	1.19	1.05

Bibliography

2nd ISSC (1964). Report of the Seakeeping Committee, *Proceedings of the 2nd International Ship and Offshore Structures Congress*, Delft, August 1964, p. 19.

10th ISSC (1988). Volume 1, *Proceedings of the 10th International Ship and Offshore Structures Congress*, Lyngby, Denmark, August 1988.

12th ITTC (1969a). A Review of Methods of Defining and Measuring the Maneuverability of Ships, *Proceedings of the 12th International Towing Tank Conference*, Rome, September 1969, pp. 1–19.

12th ITTC (1969b). Report of the Seakeeping Committee, *Proceedings of the 12th International Towing Tank Conference*, Rome, September 1969, pp. 775–779.

14th ITTC (1975). Discussion and Recommendations for an ITTC 1975 Maneuvering Trial Code, *Proceedings of the 14th International Towing Tank Conference*, Ottawa, September 1975, pp. 348–365.

15th ITTC (1978). Report of the Seakeeping Committee, *Proceedings of the 15th International Towing Tank Conference*, The Hague, September 1978, pp. 55–70.

17th ITTC (1984). Report of the Seakeeping Committee, *Proceedings of the 17th International Towing Tank Conference*, The Hague, September 1984, pp. 531–534.

Abkowitz, M. A. (1964). Lectures on Ship Hydrodynamics - Steering and Maneuverability, *Technical Report Hy-5*, Hydro- and Aerodynamic's Laboratory, Lyngby, Denmark.

Abkowitz, M. A. (1975). System Identification Techniques for Ship Maneuvering Trials, *Proceeding of Symposium on Control Theory and Navy Applications*, Monterey, CA, pp. 337–393.

Abkowitz, M. A. (1980). Measurement of Hydrodynamic Characteristics from Ship Maneuvring Trials by System Identification, *Transactions on SNAME, 88:283–318*.

Albert, A. E. and Gardner, L. A. (1967). *Stochastic Approximation and Nonlinear Regression*, MIT Press, Boston, Massachusetts.

Allmendinger, E. E. (ed.) (1990). *Submersible Vehicle Systems Design*, The Society of Naval Architects and Marine Engineers, 601 Pavonia Avenue, Jersey City, N. J. 07306.

Andersen, T. E. (1974). *On Dynamics of Large Diesel Engines*, PhD thesis, Technical University of Denmark.

Arimoto, S. and Miyazaki, F. (1984). Stability and Robustness of PID Feedback Control for Robot Manipulators of Sensory Capability, *in* **M. Brady and R. Paul** (eds), *1st International Symposium on Robotics Research*, MIT Press, pp. 783–799.

Asare, H. and Wilson, D. (1986). *Design of Computed Torque Model Reference Adaptive Control for Space-Based Robotic Manipulators*, ASME, Winter Annual Meeting (WAM), pp. 195–204.

Athans, M. and Falb, P. L. (eds) (1966). *Optimal Control*, McGraw-Hill Book Company, New York.

Baitis, A. E. (1980). The Development and Evaluation of a Rudder Roll Stabilization System for the WHEC Hamiltonian Class, *Technical Report DTNSRDC*, Naval Ship Research and Development Center, Bethesda, Md.

Baitis, E., Woolaver, D. A. and Beck, T. A. (1983). Rudder Roll Stabilization for Coast Guards Cutters and Frigates, *Naval Engineers Journal*, pp. 267–282.

Baitis, E., Woolaver, D. A. and Beck, T. A. (1989). Ship Roll Stabilization in the U. S. Navy, *Naval Engineers Journal*, pp. 43–53.

Balas, M. (1978). Feedback Control of Flexible Systems", *IEEE Transactions on Automatic Control* **AC-23**(4): 673–679.

Balchen, J. G. (1991). Ship Positioning: Adaptive Control, *in* **M. Papageorgiou** (ed.), *Concise Encyclopedia of Traffic and Transportation Systems*, Pergamon Press, UK, pp. 308–331.

Balchen, J. G., Jenssen, N. A. and Sælid, S. (1976). Dynamic Positioning Using Kalman Filtering and Optimal Control Theory, *IFAC/IFIP Symposium on Automation in Offshore Oil Field Operation*, Holland, Amsterdam, pp. 183–186.

Balchen, J. G., Jenssen, N. A. and Sælid, S. (1980a). Dynamic Positioning of Floating Vessels Based on Kalman Filtering and Optimal Control., *Proceedings of the 19th IEEE Conference on Decision and Control*, New York, NY, pp. 852–864.

Balchen, J. G., Jenssen, N. A., Mathisen, E. and Sælid, S. (1980b). Dynamic Positioning System Based on Kalman Filtering and Optimal Control., *Modeling, Identification and Control* **MIC-1**(3): 135–163.

Barbălat (1959). Systèmes d'Équations Différentielles d'Oscillations Non Linéaires, *Revue de Mathématiques Pures et Appliquées* **Vol. 4**(2): 267–270. Académie de la République Populaire Roumaine (in French).

Bardal, J. and Ørpen, O. (1983). GPS Performance in Marine Applications, *Modeling, Identification and Control* **MIC-4**(1): 1–23.

Bech, M. I. (1968). The Reversed Spiral Test as Applied to Large Ships, *Shipping World and Shipbuilder*, pp. 1753–1754.

Bech, M. I. and Wagner Smith, L. (1969). Analogue Simulation of Ship Maneuvers, *Technical Report Hy-14*, Hydro- and Aerodynamics Laboratory, Lyngby, Denmark.

Bennett, S. (1991). Ship Stabilization: History, *in* M. Papageorgiou (ed.), *Concise Encyclopedia of Traffic and Transportation Systems*, Pergamon Press, pp. 454–459.

Berghuis, H. (1993). *Model-Based Robot Control: From Theory to Practice*, PhD thesis, University of Twente, Enschede, The Netherlands.

Bhattacharyya, R. (1978). *Dynamics of Marine Vehicles*, John Wiley & Sons Ltd., New York, NY.

Blanke, M. (1981). *Ship Propulsion Losses Related to Automated Steering and Prime Mover Control*, PhD thesis, The Technical University of Denmark, Lyngby.

Blanke, M. (1986). Requirements of Adaptive Techniques for Enhanced Control of Large Diesel Engines, *Proceedings of IFAC Workshop on Adaptive Systems for Control and Signal Processing*, Lund, Sweden, pp. 197–202.

Blanke, M. (1994). *Optimal Speed Control for Cruising*, The 3rd Conference on Marine Craft Maneuvering and Control (MCMC'94), Southampton, UK.

Blanke, M. and Andersen, J. S. (1984). On Modelling Large Two-Stroke Diesel Engines: New Results from Identification, *Proceedings of the 9th IFAC World Congress*, Hungary, pp. 2015–2020.

Blanke, M. and Christensen, A. (1993). Rudder-Roll Damping Autopilot Robustness due to Sway-Yaw-Roll Couplings, *10th International Ship Control Systems Symposium (SCSS'93)*, Ottawa, Canada, pp. A.93–A.119.

Blanke, M. and Nielsen, P. B. (1990). *The Marine Engine Governor*, Proceedings from Conference on Maritime Communications and Control. The Institute of Marine Engineers, London 21–23 November 1990. Published by Marine Management Ltd, London.

Blanke, M., Haals, P. and Andreasen, K. K. (1989). Rudder Roll Damping Experience in Denmark, *IFAC Workshop on Expert Systems and Signal Processing in Marine Automation*, Lyngby, Denmark, pp. 149–160.

Bretschneider, C. L. (1959). Wave Variability and Wave Spectra for Wind Generated Gravity Waves, *Technical report*, Beach Erosion Board, Corps. of Engineers. 118 (Technical Memo).

Bretschneider, C. L. (1969). *Wave and Wind Loads. Section 12 of Handbook of Ocean and Underwater Engineering.*, McGraw-Hill., New York, NY.

Brogliato, B. and Landau, I. D. (1991). Adaptive Motion Control of Robot Manipulators: A Unified Approach Based on Passivity, *International Journal of Robust and Nonlinear Control* 1(1): 187–202.

Burger, W. and Corbet, A. G. (1960). *Ship Stabilizers. Their Design and Operation in Correcting the Rolling of Ships. A Handbook for Merchant Navy Officers*, Pergamon Press Ltd., London.

Butler, H., Honderd, G. and Van Amerongen, J. (1991). Reference Model Decomposition in Direct Adaptive Control, *International Journal of Adaptive Control and Signal Processing* **5**(1): 199–217.

Carley, J. B. (1975). Feasibility Study of Steering and Stabilizing by Rudder, *Proceedings of the 4th International Ship Control Systems Symposium (SCSS'75)*, The Hague, The Netherlands.

Chislett, M. S. and Strøm-Tejsen, J. (1965a). Planar Motion Mechanism Tests and Full-Scale Steering and Maneuvering Predictions for a Mariner Class Vessel, *Technical Report Hy-5*, Hydro- and Aerodynamics Laboratory, Lyngby, Denmark.

Chislett, M. S. and Strøm-Tejsen, J. (1965b). Planar Motion Mechanism Tests and Full-Scale Steering and Maneuvering Predictions for a Mariner Class Vessel, *Technical Report Hy-6*, Hydro- and Aerodynamics Laboratory, Lyngby, Denmark.

Chou, J. C. K. (1992). Quaternion Kinematic and Dynamic Differential Equations, *IEEE Transactions on Robotics and Automation* **RA-8**(1): 53–64.

Christensen, A. (1992). *Models of Control Design - Modelling and Validation in Ship Control*, PhD thesis, Institute of Automatic Control Systems, Technical University of Denmark.

Christensen, A. and Blanke, M. (1986). A Linearized State-Space Model in Steering and Roll of a High-Speed Container Ship, *Technical Report 86-D-574*, Servolaboratoriet, Technical University of Denmark, Denmark.

Clark, R. N. (1978). Instrument Fault Detection, *IEEE Transactions on Aerospace and Electronic Systems* **AES-14**: 456–465.

Collar, P. G. (1986). Measurement of Surface Currents, *Journal of Navigation* **Vol. 39**: 327–340.

Comstock, J. P. (ed.) (1967). *Principles of Naval Architecture*, The Society of Naval Architects and Marine Engineers, 601 Pavonia Avenue, Jersey City, NJ 07306.

Cowley, W. E. and Lambert, T. H. (1972). The Use of Rudder as a Roll Stabilizer, *Proceedings of the 3rd International Ship Control Systems Symposium (SCSS'72)*, Bath, UK.

Cowley, W. E. and Lambert, T. H. (1975). Sea Trials on a Roll Stabilizer Using the Ship's Rudder, *Proceedings of the 4th International Ship Control Systems Symposium (SCSS'75)*, The Hague, The Netherlands.

Craig, J. J. (1989). *Introduction to Robotics*, Addison-Wesley, Reading, Massachusetts.

Cristi, R., Papoulias, F. A. and Healey, A. J. (1990). Adaptive Sliding Mode Control of Autonomous Underwater Vehicles in the Dive Plane , *IEEE Journal of Oceanic Engineering* OE-15(3): 152–160.

Davenport, A. G. (1961). The Spectrum of Horizontal Gustiness Near the Ground in High Winds, *Quarterly Journal of the Royal Meterological Society* 87: 194–211.

Davidson, K. S. M. and Schiff, L. I. (1946). Turning and Course Keeping Qualities, *Transactions of SNAME, vol. 54*.

Defant, A. (1961). *Physical Oceanography*, Pergamon Press, London.

De Kat, J. O. and Wichers, J. E. W. (1991). Behavior of a Moored Ship in Unsteady Current, Wind and Waves, *Marine Technology* 28(5): 251–264.

Desoer, C. A. and Vidyasagar, M. (1975). *Feedback Systems: Input–Output Properties*, Academic Press.

Dieudonné, J. (1953). Collected French Papers on the Stability of Route of Ships at Sea, 1949-1950. (Translated by H. E. Saunders and E. N. Labouvie), *Technical Report DTMB-246*, Naval Ship Research and Development Center, Washington D.C.

Dixon, M. (1976). Linear Multivariable Control: Its Development, Computer Implementation and Application to Hydrofoil Motion Control Problems, *Proceedings of the Hovercraft Conference*, pp. 369–391.

DnV (1990). *Rules for Classification of Steel Ships: Dynamic Positioning Systems, Part 6, Chapter 7*, Det norske Vertitas, Veritasveien 1, N-1322 Høvik, Norway.

Dougherty, F. and Woolweaver, G. (1990). At-Sea Testing of an Unmanned Underwater Vehicle Flight Control System, *Symposium on Autonomous Underwater Technology*, Washington, DC, pp. 65–68.

Dougherty, F., Sherman, T., Woolweaver, G. and Lovell, G. (1988). An Autonomous Underwater Vehicle (AUV) Flight Control System Using Sliding Mode Control, *Ocean'88*, Baltimore, MD, pp. 1265–1270.

Dyne, G. and Trägårdh, P. (1975). Simuleringsmodell för 350000 tdw tanker i fullast- och ballastkonditioner på djupt vatten, *Report 2075-1*, Swedish State Shipbuilding Experimental Tank (SSPA), Gothenburg, Sweden (in Swedish).

Eda, H. and Crane, C. L. (1965). Steering Characteristics of Ships in Calm Water and in Waves, *Transactions on SNAME*.

Eykhoff, P. (1988). *A Bird's Eye View on Parameter Estimation and System Identification*, Automatisierungstechnik at, 36. Jahrgang, Heft 12.

Faltinsen, O. M. (1990). *Sea Loads on Ships and Offshore Structures*, Cambridge University Press.

Faltinsen, O. M. and Zhao, R. (1991a). Flow Predictions Around High-Speed Ships in Waves, *Mathematical Approaches in Hydrodynamics, SIAM*.

Faltinsen, O. M. and Zhao, R. (1991b). Numerical Predictions of Ship Motions at High Forward Speed, *Philosophical Transaction of the Royal Society, Series A*.

Faltinsen, O. M., Helmers, J. B., Minsaas, K. J. and Zhao, R. (1991). Speed Loss and Operability of Catamarans and SES in a Seaway, *Proceedings of the 1st International Conference on Fast Sea Transportation (FAST'91)*, The Norwegian Institute of Technology, Trondheim.

Feldman, J. (1979). DTMSRDC Revised Standard Submarine Equations of Motion, *Technical Report DTNSRDC-SPD-0393-09*, Naval Ship Research and Development Center, Washington D.C.

Fjellstad, O. E. and Fossen, T. I. (1994a). *Position and Attitude Tracking of AUVs: A Quaternion Feedback Approach*, Submitted to the IEEE Journal of Oceanic Engineering: Special Issue On Advanced Control and Signal Processing.

Fjellstad, O. E. and Fossen, T. I. (1994b). Quaternion Feedback Regulation of Underwater Vehicles, *Proceedings of the 3rd IEEE Conference on Control Applications (CCA'94)*, Glasgow.

Fjellstad, O. E., Fossen, T. I. and Egeland, O. (1992). Adaptive Control of ROVs with Actuator Dynamics and Saturation, *Proceedings of the 2nd International Offshore and Polar Engineering Conference (ISOPE)*, San Francisco, CA.

Flobakk, T. (1983). *Parameter Estimation Techniques Applied to Ship Maneuvering Tests in Model Scale*, Dr.ing. thesis, Dept. of Engineering Cybernetics, The Norwegian Institute of Technology, Trondheim, Norway.

Forssell, B. (1991). *Radio Navigation Systems*, Prentice Hall, Englewood Cliffs, NJ.

Fossen, T. I. (1991). *Nonlinear Modelling and Control of Underwater Vehicles*, Dr.ing. thesis, Dept. of Engineering Cybernetics, The Norwegian Institute of Technology, Trondheim.

Fossen, T. I. (1993a). Comments on "Hamiltonian Adaptive Control of Spacecraft", *IEEE Transactions on Automatic Control* **AC-38**(4): 671–672.

Fossen, T. I. (1993b). High Performance Ship Autopilot With Wave Filter, *Proceedings of the 10th International Ship Control Systems Symposium (SCSS'93)*, Ottawa, Canada, pp. 2.271–2.285.

Fossen, T. I. and Fjellstad, O. E. (1993). Cascaded Adaptive Control of Ocean Vehicles with Significant Actuator Dynamics, *Proceedings of the 12th IFAC World Congress*, Vol. 9, Sydney, Australia, pp. 517–522.

Fossen, T. I. and Fjellstad, O. E. (1994). Methods for Parameterization of Inertia, Coriolis and Centrifugal Forces for Marine Vehicles in 6 DOF: A Passive Control Approach, *Submitted to the Journal of Robust and Nonlinear Control*.

Fossen, T. I. and Fjellstad, O. E. (1995). Robust Adaptive Control of Underwater Vehicles: A Comparative Study, *Submitted to the IFAC Workshop on Control Applications in Marine Systems (CAMS'95)*, Trondheim, Norway.

Fossen, T. I. and Foss, B. A. (1991). Sliding Control of MIMO Nonlinear Systems, *Proceedings of the 1991 European Control Conference*, Grenoble, France, pp. 1855–1860.

Fossen, T. I. and Lauvdal, T. (1994). Nonlinear Stability Analysis of Ship Autopilots in Sway, Roll and Yaw, *The 3rd Conference on Marine Craft Maneuvering and Control (MCMC'94)*, Southampton, UK.

Fossen, T. I. and Paulsen, M. (1992). Adaptive Feedback Linearization Applied to Steering of Ships, *Proceedings of the 1st IEEE Conference on Control Applications*, Dayton, Ohio, pp. 1088–1093.

Fossen, T. I. and Sagatun, S. I. (1991a). Adaptive Control of Nonlinear Systems: A Case Study of Underwater Robotic Systems, *Journal of Robotic Systems* JRS-8(3): 393–412.

Fossen, T. I. and Sagatun, S. I. (1991b). Adaptive Control of Nonlinear Underwater Robotic Systems, *Proceedings of the IEEE Conference on Robotics and Automation*, Sacramento, California, pp. 1687–1695.

Fossen, T. I., Sagatun, S. I. and Sørensen, A. (1995). Identification of Dynamically Positioned Ships, *Submitted to the IFAC Workshop on Control Applications in Marine Systems (CAMS'95)*, Trondheim, Norway.

Fotakis, J., Grimble, M. J. and Kouvaritakis, B. (1982). A Comparison of Characteristic Locus and Optimal Designs for Dynamic Ship Positioning Systems, *IEEE Transactions on Automatic Control* AC-27(6): 1143–1157.

Frank, P. M. (1990). Fault Diagnosis in Dynamic Systems Using Analytical and Knowledge-Based Redundancy: A Survey and Some New Results, *Automatica* **26**: 459–474.

Freund, E. (1973). Decoupling and Pole Assignment in Nonlinear Systems, *Electronics Letters*.

Fung, P. T.-K. and Grimble, M. J. (1981). Self-tuning Control of Ship Positioning Systems, *in* **C. J. Harris and S. A. Billings** (eds), *Self-tuning and adaptive control: theory and applications*, Peter Peregrinus Ltd. on behalf of IEE, pp. 308–331.

Fung, P. T.-K. and Grimble, M. J. (1983). Dynamic Ship Positioning Using a Self Tuning Kalman Filter, *IEEE Transactions on Automatic Control* AC-28(3): 339–349.

Gallardo, K. (1986). *Design of a Sliding Mode Control System for a Remotely Operated Underwater Vehicle*, Master's thesis, Massachusetts Institute of Technology.

Gelb, A. and Velde, W. E. V. (1968). *Multiple-Input Describing Functions and Nonlinear System Design*, McGraw-Hill Book Company.

Gelb, A., Kasper, Jr., J. F., Nash, Jr., R. A., Price, C. F. and Sutherland, Jr., A. A. (1988). *Applied Optimal Estimation*, MIT Press, Boston, Massachusetts.

Gertler, M. (1959). The DTMB Planar Motion Mechanism System, *Proceedings of Symposium on Towing Tank Facilities, Instrumentation and Measuring Techniques*, Zagreb, Yugoslavia.

Gertler, M. and Hagen, G. R. (1967). Standard Equations of Motion for Submarine Simulation, *Technical Report DTMB-2510*, Naval Ship Research and Development Center, Washington D.C.

Gertler, M. and Hagen, S. C. (1960). Handling Criteria for Surface Ships, *Technical Report DTMB-1461*, Naval Ship Research and Development Center, Washington D.C.

Gevarter, W. B. (1970). Basic Relations for Control of Flexible Vehicles, *AIAA Journal, Vol 8, No. 4*.

Goheen, K. R. (1986). *The Modelling and Control of Remotely Underwater Operated Vehicles*, PhD thesis, Dept. of Mechanical Eng.,University College London.

Goldstein, H. (1980). *Classical Mechanics*, Addison-Wesley, Reading, MA.

Grimble, M. J. (1978). Relationship Between Kalman and Notch Filters Used in Dynamic Ship Positioning Systems, *Electronics Letters* 14(13): 399–400.

Grimble, M. J. and Johnson, M. A. (1989). *Optimal Control and Stochastic Estimation. Theory and Applications*, John Wiley & Sons Ltd.

Grimble, M. J., Patton, R. J. and Wise, D. A. (1980a). The Design of Dynamic Positioning Control Systems Using Stochastic Optimal Control Theory, *Optimal Control Applications and Methods* 1: 167–202.

Grimble, M. J., Patton, R. J. and Wise, D. A. (1980b). Use of Kalman Filtering Techniques in Dynamic Ship Positioning Systems, *IEE Proceedings* Vol. 127, Pt. D, No. 3, pp. 93–102.

Grimble, M. J., Van der Molen, G. and Liceaga-Castro, E. (1993). Submarine Depth and Pitch Control, *2nd IEEE Conference of Control Applications (CCA '93)*.

Harris, C. J. and Billings, S. (eds) (1981). *Self-Tuning and Adaptive Control: Theory and Applications*, The Institute of Electrical Engineers, Peter Peregrinus Ltd., Stevenage, UK.

Harris, R. I. (1971). *The Nature of the Wind, the Modern Design of Wind-Sensitive Structures*, Construction Industry Research and Information Association, London, pp. 29–55.

Hasselmann et al. (1973). Measurements of Wind-Wave Growth and Swell Decay during the Joint North Sea Wave Project (JONSWAP), *Deutschen Hydrografischen Zeitschrift*.

Healey, A. J. (1992) *Marine Vehicle Dynamics Lecture Notes and Problem Sets*, Naval Postgraduate School (NPS), Monterey, CA.

Healey, A. J. and Lienard, D. (1993). Multivariable Sliding Mode Control for Autonomous Diving and Steering of Unmanned Underwater Vehicles, *IEEE Journal of Ocean Engineering* OE-18(3): 327–339.

Healey, A. J. and Marco, D. B. (1992). Slow Speed Flight Control of Autonomous Underwater Vehicles: Experimental Results with the NPS AUV II, *Proceedings of the 2nd International Offshore and Polar Engineering Conference (ISOPE)*, San Francisco, CA, pp. 523–532.

Healey, A. J., Papoulias, F. A. and Cristi, R. (1989). Design and Experimental Verification of a Model Based Compensator for Rapid AUV Depth Control, *Proceedings of the 7th International Symposium on Unmanned Untethered Submersible Technology*, MSEL-UNH, Durham NH, pp. 458–474.

Hino, M. (1971). Spectrum of Gusty Wind, *Proceedings of the 3rd Conference on Wind Effect on Buildings and Structures*, pp. 69–77.

Hoff, O. M. F. J., Kvålsvold, J. and Zhao, R. (1992). Global Loads on High-Speed Cat Catamarans, *PRADS'92*, Newcastle, UK.

Holzhüter, T. (1989). Robust Identification Scheme in an Adaptive Track-Controller for Ships, *Proceedings of the 3rd IFAC Symposium on Adaptive Systems in Control and Signal Processing*, Glasgow, pp. 461–466.

Holzhüter, T. (1990). A High Precision Track Controller for Ships, *Preprints of the 11th IFAC World Congress*, Tallinn, Estonia, pp. 118–123.

Holzhüter, T. (1992). On the Robustness of Course Keeping Autopilots, *Proceedings of IFAC Workshop on Control Applications in Marine Systems (CAMS'92)*, Genova, Italy, pp. 235–244.

Holzhüter, T. and Strauch, H. (1987). A Commercial Adaptive Autopilot for Ships: Design and Experimental Experience, *Proceedings of the 10th IFAC World Congress*, July 27-31, Munich, Germany, pp. 226–230.

Horigome, M., Hara, M., Hotta, T. and Ohtsu, K. (1990). Computer Control of Main Diesel Engine Speed for Merchant Ships, *Proceedings of ISME Kobe90, Vol. 2.*

Horowitz, R. and Tomizuka, M. (1986). An Adaptive Control Scheme for Mechanical Manipulators-Compensation of Nonlinearity and Decoupling Control, *Technical Report No. 80-WA/DSC-6*, ASME.

Hsu, S. K. (1975). Application of Optimal Control Theory to a Large Hydrofoil Craft, *Proceedings of the 4th International Ship Control Systems Symposium (SCSS'75)*, Royal Netherlands Naval College, pp. 46–57.

Hughes, P. C. (1986). *Spacecraft Attitude Dynamics*, John Wiley & Sons Ltd., NY.

Humphreys, D. E. and Watkinson, K. W. (1978). Prediction of the Acceleration Hydrodynamic Coefficients for Underwater Vehicles from Geometric Parameters, *Technical Report NCSL-TR-327-78*, Naval Coastal System Center, Panama City, Florida.

Humphreys, D. E. and Watkinson, K. W. (1982). Hydrodynamic Stability and Control Analyses of the UNH-EAVE Autonomous Underwater Vehicle, *Technical Report A.R.A.P. Tech. Memo. No. 82-2*. University of New Hampshire, Marine Systems Engineering Laboratory, Durham, New Hampshire 03824.

Hunt, K. J. (1986). *A Survey of Recursive Identification Algorithms*, Trans. Inst. MC Vol. 8, No 5, Oct.–Dec.

Hwang, W.-Y. (1980). *Application of System Identification to Ship Maneuvering*, Master's thesis, Massachusetts Institute of Technology.

Imlay, F. H. (1961). The Complete Expressions for Added Mass of a Rigid Body Moving in an Ideal Fluid, *Technical Report DTMB 1528*, David Taylor Model Basin, Washington D.C.

Instanes, E. and Pedersen, J. T. (1991). Safe and Comfortable Operation of Foil-catamarans, *Proceedings of the 1st International Conference on Fast Sea Transportation (FAST'91)*, The Norwegian Institute of Technology, Trondheim, Norway, pp. 1093–1112.

Ioannou, P. A. and Kokotovic, P. V. (1983). *Adaptive Systems with Reduced Models*, Springer Verlag, New York, NY.

Isherwood, R. M. (1972). Wind Resistance of Merchant Ships, *RINA Trans. Vol. 115*, pp. 327–338.

Itoko, T., Higashino, S., Yamagami, Y. and Ikebuchi, T. (1991). The Development of an Automatic Control System for a Submerged Hull and Foil Hybrid Super-High-Speed Liner, *Proceedings of the 1st International Conference on Fast Sea Transportation (FAST'91)*, The Norwegian Institute of Technology, Trondheim, Norway, pp. 997–1012.

Jalving, B. and Størkersen, N. (1994). The Control System of an Autonomous Underwater Vehicle, *Proceedings of the 3rd IEEE Conference on Control Applications (CCA'94)*, Glasgow.

Jenssen, N. A. (1980). *Estimation and Control in Dynamic Positioning of Vessels*, Dr.ing. thesis, Dept. of Engineering Cybernetics, The Norwegian Institute of Technology, Trondheim, Norway.

Johnson, R. J. (1985). *Hydrofoils*, Naval Engineers Journal, February, pp. 142–199.

Joshi, S. M. (1989). *Control of Large Flexible Space Structures*, Springer Verlag.

Kaasen, K. E. (1986). *Estimation of Parameters in Ship Maneuvering Models From Full-Scale Measurements*, Dr.ing. thesis, Dept. of Engineering Cybernetics, The Norwegian Institute of Technology, Trondheim, Norway.

Kaimal et al., J. C. (1972). Spectral Characteristics of Surface Layer Turbulence, *Quarterly Journal of the Royal Meterological Society* 98: 563–589.

Kalske, S. (1989). Motion Dynamics of Subsea Vehicles, *Technical report*, Technical Research Centre of Finland, Vuorimiehentie 5, SF-02150 Espoo, Finland.

Kane, T. R., Likins, P. W. and Levinson, D. A. (1983). *Spacecraft Dynamics*, McGraw-Hill, NY, NY.

Kaplan, P. and Davis, S. (1974). A Simplified Representation of the Vertical Plane Dynamics of SES Craft, *AIAA Paper No 74-314, AIAA/SNAME Advanced Marine Vehicle Conference*, San Diego, CA.

Kaplan, P. and Davis, S. (1978). System Analysis Techniques for Designing Ride Control System for SES Craft in Waves, *Proceedings of the 5th International Ship Control Systems Symposium (SCSS'78)*, Annapolis, MD.

Kaplan, P., Bentson, J. and Davis, S. (1981). Dynamics and Hydrodynamics of Surface Effect Ships, *Trans. SNAME, Vol. 89*.

Kareem, A. (1985). Structure of Wind Field over the Ocean, *Proceedings Int. Workshop on Offshore Winds and Icing*, pp. 224–235.

Katebi, M. R., Wong, D. K. K. and Grimble, M. J. (1987). LQG Autopilot and Rudder Roll Stabilization Control System Design, *Proceedings of the 8th International Ship Control Systems Symposium (SCSS'87)*, The Hague, The Netherlands, pp. 3.69–3.84.

Källström, C. G. (1979). *Identification and Adaptive Control Applied to Ship Steering*, PhD thesis, Dept. of Automatic Control, Lund Institute of Technology, Sweden.

Källström, C. G. (1981). Control of Yaw and Roll by Rudder/Fin Stabilization System, *Proceedings of the 6th International Ship Control Systems Symposium (SCSS'81), Vol 2, Paper F2 3-1*, Ottawa, Canada.

Källström, C. G. (1987). Improved Operational Effectiveness of Naval Ships by Rudder Roll Stabilization, *NAVAL'87, Asian Pacific Naval Exhibition and Conference*, Singapore.

Källström, C. G. and Åström, K. J. (1981). Experiences of System Identification Applied to Ship Steering, *Automatica* 17: 187–198.

Källström, C. G. and Schultz, W. L. (1990). An Integrated Rudder Control System for Roll Damping and Maintenance, *9th International Ship Control Systems Symposium (SCSS'90)*, Bethesda, MD, pp. 3.278–3.296.

Källström, C. G. and Theorén, K. (1992). Turning Controller for Ships, *Proceedings of IFAC Workshop on Control Applications in Marine Systems (CAMS'92)*, Genoa, Italy.

Källström, C. G., Åstrøm, K. J., Thorell, N. E., Eriksson, J. and Sten, L. (1979). Adaptive Autopilot for Tankers, *Automatica* 15: 241–254.

Källström, C. G., Wessel, P. and Sjölander, S. (1988). Roll Reduction by Rudder Control, *SNAME Spring Meeting/STAR Symposium*, Pittsburg, Pennsylvania, pp. 67–76.

Kempf, G. (1932). Measurements of the Propulsive and Structural Characteristic of Ships, *Transactions of SNAME, vol. 40*, pp. 42–57.

Kempf, G. (1944). Manöveriernorm für Schiffe, *Hansa, Deutsche Schiffahrtszeitschrift, Heft 27/28*, pp. 372–276. (in German).

Kirchhoff, G. (1869). *Über die Bewegung eines Rotationskorpers in einer Flussigkeit*, Crelle's Journal, No. 71, pp. 237–273 (in German).

Koyama, T. (1967). *On the Optimum Automatic Steering System of Ships at Sea*, J.S.N.A., Vol. 122.

Kresselmeier, G. and Narendra, K. S. (1982). Stable Model Reference Adaptive Control in the Presence of Bounded Disturbances, *IEEE Transactions on Automatic Control* AC-27: 1169–1175.

Lambert, J. D. (1973). *Computional Methods in Ordinary Differential Equations*, John Wiley and Sons, New York, NY.

Lamb, H. (1932). *Hydrodynamics*, Cambridge University Press, London.

Landau, Y. D. (1979). *Adaptive Control: The Model Reference Approach*, Marcel Dekker Inc., New York, NY.

Lewis, D. J., Lipscombe, J. M. and Thomasson, P. C. (1984). The Simulation of Remotely Operated Vehicles, *Proceedings of ROV'84*, pp. 245–251.

Lewis, F. M. (1967). The Motion of Ships in Waves, *in* J. P. Comstock (ed.), *Principles of Naval Architecture*, The Society of Naval Architects and Marine Engineers, 601 Pavonia Avenue, Jersey City, NJ 07306, pp. 669–692.

Lin, C.-F. (1992). *Modern Navigation, Guidance and Control Processing*, Prentice-Hall Inc., Englewood Cliffs, New Jersey 07632.

Lindfors, I. (1993). Thrust Allocation Method for the Dynamic Positioning System, *10th International Ship Control Systems Symposium (SCSS'93)*, Ottawa, Canada, pp. 3.93–3.106.

Ljung, L. (1987). *System Identification: Theory for the User*, Prentice Hall, Inc, Englewood Cliffs, New Jersey.

Ljung, L. and Söderström, T. (1986). *Theory and Practice of Recursive Identification*, MIT Press, Cambridge, Massachusetts.

Lloyd, A. E. J. M. (1975). Roll Stabilization by Rudder, *Proceedings of the 4th International Ship Control Systems Symposium (SCSS'75)*, The Hague, The Netherlands.

Lyapunov, M. A. (1907). Probléme Générale de la Stabilité de Mouvement, *Ann. Fac. Sci. Toulouse* Vol. 9: 203–474. (Translation of a paper published in Comm. Soc. math. Kharkow 1893, reprinted in Ann. math Studies, Vol. 17, Princeton 1949).

Maciejowski, J. M. (ed.) (1989). *Multivariable Feedback Design*, Addison-Wesley, Wokingham, England.

Mahesh, H., Yuh, J. and Lakshmi, R. (1991). Control of Underwater Robots in Working Mode, *Proceedings of IEEE International Conference on Robotics and Automation*, Sacramento, California, pp. 2630–2635.

Marco, D. B. and Healey, A. J. (1992). Sliding Mode Acoustic Servoing for an Autonomous Underwater Vehicle, *24th Offshore Technology Conference (OTC'92)*, Houston, Texas, pp. 257–267.

Marshfield, W. B. (1991). Submarine Depth Keeping Control Using an H_∞ Controller Together With Sea-Noise Reduction Notch Filters, *Trans. Inst. MC* 13: 233–240.

McGookin, E. W. (1993). *Sliding Mode Control of a Submarine*, Master's thesis, Department of Electronic and Electrical Engineering, University of Glasgow.

Meirovitch, L. (1990). *Dynamics and Control of Structures*, Wiley Interscience, NY.

Meirovitch, L. and Kwak, M. K. (1989). State Equations for a Spacecraft With Flexible Appendages in Terms of Quasi-Coordinates, *Applied Mechanics Reviews* 42(11): 161–170.

Milliken, L. G. (1984). *Multivariable Control of an Underwater Vehicles*, Master's thesis, Massachusetts Institute of Technology.

Milne-Thomson, L. M. (1968). *Theoretical Hydrodynamics*, MacMillan Education Ltd., London.

Morgan, J. M. (ed.) (1978). *Dynamic Positioning of Offshore Vessels*, Petroleum, Tulsa, OK.

MTS (1986). *Operational Guidelines for ROVs*, Marine Technology Society.

Nagumo, J. I. and Noda, A. (1967). A Learning Method for System Identification, *IEEE Transactions on Automatic Control* AC-12(3): 282–287.

Narendra, K. S. and Annaswamy, A. M. (1987). A New Adaptive Law for Robust Adaption Without Persistent Excitation, *IEEE Transactions on Automatic Control* AC-32(2): 134–145.

Narendra, K. S. and Annaswamy, A. M. (1989). *Stable Adaptive Systems*, Prentice Hall Inc., Boston, MA.

Naylor, A. W. and Sell, G. R. (1982). *Linear Operator Theory in Engineering and Science*, Springer Verlag, New York, NY.

Nestegård, A. (1990). Motions of Surface Effect Ships, *Det norkse Veritas (DnV) Report No: 90-2011*.

Neumann, G. (1952). *On Wind-Generated Ocean Waves with Special Reference to the Problem of Wave Forecasting*, New York University, College of Eng. Res. Div., Dept. of Meteorology and Oceanography, Prepared for the Naval Res.

Newman, J. N. (1977). *Marine Hydrodynamics*, MIT Press, Cambridge, MA.

Niemeyer, G. and Slotine, J. J. E. (1991). Performance in Adaptive Manipulator Control, *The International Journal of Robotic Research* **JRS-10**: 149–161.

Nomoto, K., Taguchi, T., Honda, K. and Hirano, S. (1957). On the Steering Qualities of Ships, *Technical report*, International Shipbuilding Progress, Vol. 4.

Norrbin, N. H. (1963). On the Design and Analyses of the Zig-Zag Test on Base of Quasi Linear Frequency Response, *Technical Report B 104-3*, The Swedish State Shipbuilding Experimental Tank (SSPA), Gothenburg, Sweden.

Norrbin, N. H. (1965). Zig-Zag Provets Teknik och Analys, *Technical Report no. 12*, The Swedish State Shipbuilding Experimental Tank (SSPA), Gothenburg, Sweden. (in Swedish).

Norrbin, N. H. (1970). Theory and Observation on the use of a Mathematical Model for Ship Maneuvering in Deep and Confined Waters, *8th Symposium on Naval Hydrodynamics*, Pasadena, California.

Norrbin, N. H. (1972). On the Added Resistance due to Steering on a Straight Course, *Proceedings of the 13th ITTC*, Berlin, Hamburg, Germany.

Ochi, M. K. and Bales, S. L. (1977). Effect of Various Spectral Formulations in Predicting Responses of Marine Vehicles and Ocean Structures, *9th Annual OTC*, Houston, TX.

Ochi, M. K. and Shin, Y. S. (1988). Wind Turbulent Spectra for Design Considerations of Offshore Structures, *20th Annual OTC*, Houston, TX, pp. 461–476.

OCIMF (1977). *Prediction of Wind and Current Loads on VLCCs*, Oil Companies International Marine Forum, London, pp. 1–77.

Oda et al., H. (1992). Rudder Roll Stabilization Control System through Multivariable Auto Regressive Model, *Proceedings of IFAC Workshop on Control Applications in Marine Systems (CAMS'92)*, Genoa, Italy, pp. 113–127.

Ogata, K. (1987). *Discrete-Time Control Systems*, Prentice-Hall, Inc., London.

Ohtsu, K. and Ishizuka, M. (1992). Statistical Identification and Optimal Control of Marine Engine, *Proceedings of IFAC Workshop on Control Applications in Marine Systems (CAMS'92)*, Genoa, Italy.

Ohtsu, K., Horigome, M. and Kitagawa, G. (1979). A New Ship's Autopilot Design Through a Stochastic Model, *Automatica* 15: 255–268.

O'Neill, W. C. (1991). The Maximum Attenuation of Seaway Induced Motions, Within a Given Set of Design Constraints, Possible for Hydrofoil Supported Ships, *Proceedings of the 1st International Conference on Fast Sea Transportation (FAST'91)*, The Norwegian Institute of Technology, Trondheim, Norway, pp. 1215–1231.

Ortega, R. and Spong, M. W. (1988). Adaptive Motion Control of Rigid Robots: A Tutorial, *Proceedings of the 27th Conference on Decision and Control*, Austin, TX, pp. 1575–1584.

Peterson, B. B. and Narendra, K. S. (1982). Bounded Error Adaptive Control, *IEEE Transactions of Automatic Control* AC-27: 1161–1168.

Phillips, O. M. (1958). The Equilibrium Range in the Spectrum of Wind Generated Waves., *Journal of Fluid Mechanics* JFM-4(4): 426–434.

Pierson, W. J. and Moskowitz, L. (1963). *A Proposed Spectral Form for Fully Developed Wind Seas Based on the Similarity Theory of S. A. Kitaigorodsku*, U. S. Naval Oceanograhic Office Contract 62306-1042.

Popov, V. M. (1973). *Hyperstability of Control Systems*, Springer-Verlag, Berlin.

Price, W. G. and Bishop, R. E. D. (1974). *Probalistic Theory of Ship Dynamics*, Chapman and Hall, London.

Reid, R. E., Tugcu, A. K. and Mears, B. C. (1984). The Use of Wave Filter Design in Kalman Filter State Estimation of the Automatic Steering Problem of a Tanker in a Seaway, *IEEE Transaction on Automatic Control* AC-29(7): 577–584.

Rios-Neto, A. and Da Cruz, J. J. (1985). A Stochastic Rudder Control Law for Ship Path-Following Autopilots, *Automatica* 21(4): 371–384.

Roberts, G. N. (1992). Ship Roll Damping Using Rudder and Stabilizing Fins, *Proceedings of IFAC Workshop on Control Applications in Marine Systems (CAMS'92)*, Genoa, Italy, pp. 129–138.

Roberts, G. N. and Braham, S. W. (1990). Warship Roll Stabilization Using Integrated Rudder and Fins, *9th International Ship Control Systems Symposium (SCSS'90)*, Bethesda, MD, pp. 1.234–1.248.

Routh, E. J. (1877). *A Treatise on The Stability on Motion*, Macmillan, London.

RW (1992). *Foilcat Ready for Service*, Ship & Boat International, July/August, pp. 31–34.

Sadegh, N. and Horowitz, R. (1990). Stability and Robustness Analysis of a Class of Adptive Controllers for Robotic Manipultaors, *Int. Journal of Robotics Research* 9: 74–94.

Sagatun, S. I. (1992). *Modeling and Control of Underwater Vehicles: A Lagrangian Approach*, Dr.ing. thesis, Dept. of Engineering Cybernetics, The Norwegian Institute of Technology, Trondheim, Norway.

Sagatun, S. I. and Fossen, T. (1991). Lagrangian Formulation of Underwater Vehicles' Dynamics, *Proceedings of the IEEE International Conference on Systems, Man and Cybernetics*, Charlottesville, VA, pp. 1029–1034.

Sagatun, S. I., Sørensen, A. and Fossen, T. I. (1994a). *Dynamic Positioning of Marine Vessels*, Submitted to the IEEE Transactions on Control Systems Technology.

Sagatun, S. I., Sørensen, A. and Fossen, T. I. (1994b). *The ABB Dynamic Positioning System*, Submitted to ABB Review.

Salvesen, N., Tuck, E. O. and Faltinsen, O. M. (1970). *Ship Motions and Sea Loads*, Trans. SNAME, vol. 78, pp. 250–287.

Sargent, J. S. and Cowgill, P. N. (1976). Design Considerations for Dynamically Positioned Utility Vessels, *Proceedings of the 8th Offshore Technology Conference*, Dallas.

Sarpkaya, T. (1981). *Mechanics of Wave Forces on Offshore Structures*, Van Nostrand Reinhold Company, New York, NY.

Sælid, S. and Jenssen, N. A. (1983). Adaptive Ship Autopilot with Wave Filter, *Modeling, Identification and Control* **MIC-4**(1): 33–46.

Sælid, S., Jenssen, N. A. and Balchen, J. G. (1983). Design and Analysis of a Dynamic Positioning System Based on Kalman Filtering and Optimal Control, *IEEE Transaction on Automatic Control* **AC-28**(3): 331–339.

Sellars, F. H. and Martin, J. P. (1992). Selection and Evaluation of Ship Roll Stabilization Systems, *Marine Technology* **29**(2): 84–101.

Shepperd, S. W. (1978). Quaternion from Rotation Matrix, *Journal of Guidance and Control* Vol. 1(3): 223–224.

Simiu, E. and Leigh, S. D. (1983). *Turbulent Wind Effects on Tension Leg Platform Surge*, Nat. Bur. Stand., Building Sci. Ser. 151.

Slotine, J. J. E. and Benedetto, M. D. D. (1990). Hamiltonian Adaptive Control of Spacecraft, *IEEE Transactions on Automatic Control* **AC-35**(7): 848–852.

Slotine, J. J. E. and Li, W. (1987). Adaptive Manipulator Control. A Case Study., *Proceedings of the 1987 IEEE Conference on Robotics and Automation*, Raleigh, North Carolina, pp. 1392–1400.

Slotine, J. J. E. and Li, W. (1991). *Applied Nonlinear Control*, Prentice-Hall Int., Englewood Cliffs, New Jersey 07632.

J. E. Smith (1977). *Mathematical Modeling and Digital Simulation for Engineers and Scientists*, John Wiley and Sons, New York, NY.

SNAME (1950). The Society of Naval Architects and Marine Engineers. Nomenclature for Treating the Motion of a Submerged Body Through a Fluid, *Technical and Research Bulletin No. 1-5*.

SNAME (1989). The Society of Naval Architects and Marine Engineers. Guide For Sea Trials, *Technical and Research Bulletin No. 3-47*.

Son, K. H. and Nomoto, K. (1981). *On the Coupled Motion of Steering and Rolling of a High Speed Container Ship*, J.S.N.A., Japan, Vol. 150, pp. 232–244 (in Japanese).

Son, K. H. and Nomoto, K. (1982). On the Coupled Motion of Steering and Rolling of a High Speed Container Ship, *Naval Architect of Ocean Engineering* 20: 73–83. From J.S.N.A., Japan, Vol. 150, 1981.

Stark, D. R. (1974). The PHM Hydrofoil Automatic Control System, *Proceedings of National Aerospace and Manufacturing Meeting*, pp. 1–15.

Steen, S. (1993). *Cobbelstone Effect on SES*, Dr.ing. thesis, Dept. of Marine Hydrodynamics, The Norwegian Institute of Technology. Trondheim.

Strang, G. (1980). *Linear Algebra and Its Applications*, Academic Press, NY.

Svenneby, E. J. and Minsaas, K. J. (1992). Foilcat 2900 - Design and Performance, *Proceedings of 3rd Conference on High Speed Marine Craft*, Kristiansand, Norway.

Söderström, T. and Stoica, P. (1989). *System Identification*, Prentice Hall, Englewood Cliffs, NJ.

Sørensen, A. J. (1993). *Modelling and Control of SES Dynamics in the Vertical Plane*, Dr.ing. thesis, Dept. of Engineering Cybernetics, The Norwegian Institute of Technology, Trondheim, Norway.

Sørensen, A. J. and Egeland, O. (1993). Ride Control of Surface Effect Ships Using Distributed Control, *Proceedings of the 12th IFAC World Congress*, Vol. 4, Sydney, Australia, pp. 81–88.

Sørensen, A. J., Steen, S. and Faltinsen, O. M. (1992). Cobblestone Effect on SES, *High Performance Marine Vehicle Conference (HPMV'92), ASNE*, Washington D.C.

Sørensen, A. J., Steen, S. and Faltinsen, O. M. (1993). SES Dynamics in the Vertical Plane, *Journal of Ship Technology Research, Vol. 40, No. 2*.

Sørensen, A., Sagatun, S. I. and Fossen, T. I. (1995). The Design of the ABB Dynamic Positioning System Using Model Based Control, *Submitted to the IFAC Workshop on Control Applications in Marine Systems (CAMS'95)*, Trondheim, Norway.

Tagegaki, M. and Arimoto, S. (1981). A New Feedback Method for Dynamic Control of Manipulators, *Transactions of ASME, Journal of Dynamic Systems, Measurement and Control* 102: 119–125.

Tiano, A. and Volta, E. (1978). Application of the Identification Techniques to the Ship System, *Proceedings of the 7th IFAC World Congress*, Helsinki, Finland.

Triantafyllou, M. S. and Amzallag, A. M. (1984). A New Generation of Underwater Unmanned Tethered Vehicles Carrying Heavy Equipment at Large Depths, *Technical Report MITSG 85-30TN*, MIT Sea Grant, Boston, Massachusetts.

Triantafyllou, M. S. and Grosenbaugh, M. A. (1991). Robust Control For Underwater Vehicle Systems With Time Delays, *IEEE Journal of Oceanic Engineering* OE-16(1): 146–152.

Triantafyllou, M. S., Bodson, M. and Athans, M. (1983). Real Time Estimation of Ship Motions Using Kalman Filtering Techniques, *IEEE Journal of Ocean Engineering* OE-8(1): 9–20.

Van Amerongen, J. (1982). *Adaptive Steering of Ships - A Model Reference Approach to Improved Maneuvering and Economical Course Keeping*, PhD thesis, Delft University of Technology, The Netherlands.

Van Amerongen, J. (1984). Adaptive Steering of Ships - A Model Reference Approach, *Automatica* 20(1): 3–14.

Van Amerongen, J. and ten Cate, A. J. U. (1975). Model Reference Adaptive Autopilots for Ships, *Automatica* 11(1): 441–449.

Van Amerongen, J. and Van Cappelle, J. C. (1981). Mathematical Modelling for Rudder Roll Stabilization, *Proceedings of the 6th International Ship Control Systems Symposium (SCSS'81)*, Ottawa, Canada.

Van Amerongen, J. and Van Nauta Lemke, H. R. (1978). Optimum Steering of Ships with an Adaptive Autopilot, *Proceedings of the 5th Ship Control Systems Symposium*, Annapolis, Md, USA.

Van Amerongen, J. and Van Nauta Lemke, H. R. (1980). Criteria for Optimum Steering of Ships, *Proceedings of Symposium on Ship Steering Automatic Control*, Genoa, Italy.

Van Amerongen, J. and Van Nauta Lempke, H. R. (1987). Adaptive Control Aspects of a Rudder Roll Stabilization System, *Proceedings of the 10th IFAC World Congress*, Munich, Germany, pp. 215–219.

Van Amerongen, J., Van der Klugt, P. G. M. and Pieffers, J. B. M. (1987). Rudder Roll Stabilization - Controller Design and Experimental Results, *Proceedings of the 8th International Ship Control Systems Symposium (SCSS'87)*, The Hague, The Netherlands, pp. 1.120–1.142.

Van Amerongen, J., Van der Klugt, P. G. M. and Van Nauta Lempke, H. R. (1990). Rudder Roll Stabilization for Ships, *Automatica* AUT-26(4): 679–690.

Van Berlekom, W. B. (1975). Effects of Propeller Loading on Rudder Efficiency, *Proceedings of the 4th International Ship Control Systems Symposium (SCSS'75)*, Haag, Netherlands, pp. 5.83–5.98.

Van Berlekom, W. B. and Goddard, T. A. (1972). Maneuvering of Large Tankers, *Transactions of SNAME, 80:264–298.*

Van Berlekom, W. B., Trägårdh, P. and Dellhag, A. (1974). Large Tankers: Wind Coefficients and Speed Loss Due to Wind and Sea, *Meeting at the Royal Institution of Naval Architects, April 25, 1974, London*, pp. 41–58.

Van der Klugt, P. G. M. (1987). *Rudder Roll Stabilization*, PhD thesis, Delft University of Technology, The Netherlands.

Van Lammern, W. P. A., Van Manen, J. D. and Oosterveld, M. W. C. (1969). *The Wageningen B-Screw Series*, Presented at the Annual Meeting, New York, NY, Nov. 12–14, 1969, SNAME.

Van Nauta Lemke, H. R. and De-Zhao, W. (1985). Fuzzy PID Supervisor, *Proceedings of the 24th Conference on Decision and Control (CDC'85)*, Fort Lauderdale, Florida, pp. 602–608.

Venkatachalam, R., Limbert, D. E. and Jalbert, J. C. (1985). Design and Simulation of a Crab-Wise Motion Controller for the EAVE-EAST Submersible, *ROV'85.*

Vidyasagar, M. (1978). *Nonlinear Systems Analysis*, Prentice-Hall, Englewood Cliffs, NJ.

Vidyasagar, M. (1993). *Nonlinear Systems Analysis. Second Edition*, Prentice-Hall, Englewood Cliffs, NJ.

Vogt, J. E. (1969). Automatic Control of the Hydrofoil Gunboat, *Proceedings of AIAA 2nd Advanced Marine Vehicles*, pp. 1–10.

Wagner, V. B. (1967) Windkräfte an Überwasserschiffen, *Schiff und Hafen, Heft 12, 19. Jahrgang*, pp. 894–900. (in German).

Webster, W. C. (ed.) (1992). *Shiphandling Simulation. Application to Waterway Design*, National Academy Press, Washington, D.C.

Wendel, K. (1956). Hydrodynamic Masses and Hydrodynamic Moments of Inertia, *Technical report*, TMB Translation 260.

Williams, S. J. and Marshfield, W. B. (1990). H_∞ Multivariable Design of a Submarine Depth Control System, *Inst. of Measurement and Control, Symp. on Applications of Multivariable System Techniques.*

Williams, S. J. and Marshfield, W. B. (1991). A Full Envelope Submarine Depth Control System Incorporating Switched H_∞ Controllers, *Proceedings of the American Control Conference (ACC'91)*, pp. 583–588.

Yoerger, D. R. and Slotine, J. J. E. (1984). Nonlinear Trajectory Control of Autonomous Underwater Vehicles using the Sliding Methodology, *Proceedings of the ROV' 84 Conference*, pp. 245–251.

Yoerger, D. R. and Slotine, J. J. E. (1985). Robust Trajectory Control of Underwater Vehicles, *IEEE Journal of Oceanic Engineering* OE-10(4): 462–470.

Yoerger, D. R. and Slotine, J. J. E. (1991). Adaptive Sliding Control of an Experimental Underwater Vehicle, *Proceedings of IEEE International Conference on Robotics and Automation*, Sacramento, California, pp. 2746–2751.

Yoerger, D. R., Cooke, J. G. and Slotine, J. J. E. (1990). The Influence on Thruster Dynamics on Underwater Vehicle Behavior and Their Incorporation Into Control Systems Design, *IEEE Journal of Oceanic Engineering* OE-15(3): 167–179.

Yoerger, D. R., Newman, J. B. and Slotine, J. J. E. (1986). Supervisory Control System for the JASON ROV, *IEEE Oceanic Engineering* OE-11(3): 392–400.

Yuh, J. (1990). Modeling and Control of Underwater Robotic Vehicles, *IEEE Transactions on Systems, Man and Cybernetics* TSMC-20(6): 1475–1483.

Zhou, W. W. (1987). *Identification of Nonlinear Marine Systems*, PhD thesis, Servolaboratoriet, The Technical University of Denmark, Lyngby, Denmark.

Zhou, W. W. (1990). A New Approach for Adaptive Rudder Roll Stabilization Control, *9th International Ship Control Systems Symposium (SCSS'90)*, Bethesda, MD, pp. 1.115–1.125.

Zhou, W. W. and Blanke, M. (1989). Identification of a class of Nonlinear State-space Models Using RPE Techniques", *IEEE Transactions on Automatic Control* AC-34(3): 312–316.

Zuidweg, J. K. (1970). *Automatic Guidance of Ships as a Control Problem*, PhD thesis, Delft University of Technology, The Netherlands.

Åström, K. J. and Eklund, K. (1971). A Simplified Nonlinear Model of a Drum Boiler-Turbine Unit, *Technical Report 7104*, Lund Institute of Technology.

Åström, K. J. and Källström, C. G. (1976). Identification of Ship Steering Dynamics, *Automatica* AUT-12(9): 9–22.

Åström, K. J. and Wittenmark, B. (1989). *Adaptive Control*, Addison-Wesley Publishing Company, Reading, Massachusetts.

Index